ACTIVITY-BASED PROTEIN PROFILING (ABPP)

BY SMALL MOLECULES LABELING APPROACH

CHENG XIAMIN

NATIONAL UNIVERSITY OF SINGAPORE
2014

ACTIVITY-BASED PROTEIN PROFILING (ABPP) BY SMALL MOLECULES LABELING APPROACH

CHENG XIAMIN

(M.Sc., NANYANG TECHNOLOGICAL UNIVERSITY)

A THESIS SUBMITTED

FOR THE DEGREE OF DOCTOR OF PHILOSOPHY

DEPARTMENT OF CHEMISTRY

NATIONAL UNIVERSITY OF SINGAPORE

2014

Declaration

I hereby declare that the thesis is my original work and it has been written by me in its entirety. Under the supervision of Prof. Yao Shao Q., (in the laboratory S5-03-18), Department of Chemistry, National University of Singapore, between Aug 2009 and Jan 2014.

I have duly acknowledged all the sources of information which have been used in the thesis.

This thesis has also not been submitted for any degree in any university previously.

The content of the thesis has been partly published in:

1) **Cheng, X**.; Li, L.; Uttamchandani, M.; Yao, S. Q.*, *In situ* Proteome Profiling of C75, a Covalent Bioactive Compound with Potential Anti-cancer Activities. *Org. Lett.* (2014), 16, 1414-1417.

2) **Cheng, X**.; Li, L.; Uttamchandani, M.; Yao, S. Q.*, A Tuned Affinity-based Staurosporine Probe for *in situ* Profiling of Protein Kinases. *Chem. Commun.,* (2014), 50, 2851–2853.

Cheng Xiamin		Feb, 2014
Name	Signature	Date

Acknowledgements

First of all, I would like to thank my supervisor and mentor - *Prof. Yao Shao Qin* for giving me the opportunity to work in his lab and always highly supporting my works. Because of his critical and comprehensive thinking, research is taking shape in my mind. He let me know the passion and aspiration on discovering things and pursuing ideas. His enthusiasm and guidance have led me to my accomplishments. And I would like to thank *Dr Mahesh* help me to revise the manuscripts especially.

I would like to thank all members in Prof. Yao group — both past and present, Grace, Lay Pheng, Pengyu, Wu Hao, Kalesh, Liu Kai, Candy, Mingyu, Haibin, Jingyan, Liqian, Dr. Li Lin, Dr. Li Zhengqiu, Dr. Jiang Bo, Dr. Yu Changmin, Zhenkun, Su Ying, Chongjing, Biwei, Jiaqi, Jigang, Sijun, Linghui, ,Peng Bo, Danyang, Farhana, Cindy, Pei Xin, Chelsea, Xiaoyuan, Rajesh, Yu Min, Joo Leng, Yuhui, Choon Meng, Liang Xian, who made this time so special and enjoyable. I thank particularly the following people: Haibin, Pengyu, and Wu Hao who taught me biological experiments; Dr Li Lin who help me do the bioimaging; Xiaoyuan help me do bioexperiments; Jigang taught me how to deal with mass samples.; Zhengqiu, Chongjing and Jingyan kindly provide intermediates. Thank all of you for helping and accompanying these years, providing me a nice and friendly home - Yao lab in Singapore.

I would like to thank Prof Lu Yixin, Zeng Huaqiang and Wang Jian as my oral QE examiners when doing my PhD conversion; Prof Tan Choon Hong wrote recommendation letter. Thanks to my collaborators for their excellent work including: Prof. Siu Kwan Sze (Nanyang Technological University, Singapore) for his support for LC-MS/MS experiments; Allan, Licheng and Prof. Zhao Yu. for their patience and support.

I appreciate the support from *National University of Singapore* for providing me research scholarship. Thanks also go to Department of

Chemistry administrative staffs for their supports, especially Ms Suriawati and Ms Chia Siew Ing for their help on all kinds of issues.

Finally, I would like to thank my parents, my wife and my sister for their unconditional understanding, supports and encouragement throughout these years.

Big thanks to all of you!

Table of Contents

Summary

Natural products are becoming an important source of drug discovery with the advances in the natural product identification and organic synthesis. The identification of unknown potential targets of the bioactive compounds remains an urgent challenge. However, there is a lack of strategy which is capable of large-scale investigation of small molecule-protein interaction comprehensively under its native cellular environments. The interactions, including on and off, are very important at the early stage of drug discovery because they are closely relevant to predict the true biological activities of the drug candidates.

There's about 2% of human gene encoding a large family of protein kinase (500+), which reversibly phosphorylated about 30% of all human proteins, including biomolecules that regulate every complex cellular processes and pathway. Dysregulation and mutation of kinase (more than 180) is a very important pathogeny in human disease such as cancer, diabetes, hypertension and other disease, therefore, kinase is becoming the interesting targets in the therapy. However, it is difficult to design a kinase inhibitor to recognize a kinase from the huge family (500+) which possesses the highly conserved sequence and structure of the ATP-binding pocket. And in the native cellular environment, the interaction between the small molecule and kinase was also interfered by other bioactive molecules (such as ATP/ADP/AMP and etc.) distributing ubiquitously and other functional proteins containing the similar nucleotide-binding site, which are much more than kinases.

In this thesis, firstly, we describe a click-based *in situ* profiling approach to identify the targets of natural product derivative—C75. (Chapter 2) Secondly, a new approach to develop covalent irreversible inhibitors of kinase from a natural product —staurosporine, as a reversible general binding core, is introduced. (Chapter 3) By this strategy, the probe-like inhibitor could also be tested and evaluated by a comprehensive proteome profiling. The native cellular targets of the probe were identified and localized with the probe by subsequent biological experiment in the live cancer cell. The following few projects

were unfinished works. Thirdly, this click-based *in situ* profiling approach was applied to Lymphostin (covalent inhibitor) and Ammosamide analogues (affinity inhibitor) (Chapter 4). Fourthly, a novel approach about cancer cell targeting cell-specific drug delivery of protein kinase inhibitors by cell penetrating peptide (CPP) is described (Chapter 5). Finally, this project is about cancer cell targeting delivery of regenerated wortmannin by Folic acid and protein target profiling of wortmannin (Chapter 6).

List of Tables

List of Figures

List of Schemes

List of Symbols

Å	angstrom
°C	degree celsius
cal	calorie
g	gram
h	hour
k	kilo
K_d	dissociation constant
L	liter
λ	wavelength
m	milli
µ	micro
M	molar
min	minutes
mol	mole
n	nano
p	pico
s	seconds

List of publications (2009-2014)

1. **Cheng, X**.; Li, L.; Uttamchandani, M.; Yao, S. Q.*, *In situ* Proteome Profiling of C75, a Covalent Bioactive Compound with Potential Anti-cancer Activities. *Org. Lett.* (2014), *DOI 10.1021/ol500206w*.

2. **Cheng, X**.; Li, L.; Uttamchandani, M.; Yao, S. Q.*, A Tuned Affinity-based Staurosporine Probe for *in situ* Profiling of Protein Kinases. *Chem. Commun.,* (2014), 50, 2851–2853.

3. Ravindran, M.S.; Rao, S.; **Cheng, X.**; Shukla, A.; Cazenave-Gassiot, A.; Yao, S.Q.; Wenk, M.R.*, Targeting Lipid Metabolism in Mycobacteria under Different Physiological Conditions Using Activity-based Profiling with Tetrahydrolipstatin. (2013), *Mol. Cell Proteomics*, in press.

4. Tam, E. K. W.; Li, Z.; Goh, Y. L.; **Cheng, X.**; Wong, S. Y. Wong, Santhanakrishnan, S.; Chai, C. L. L.*; Yao, S. Q.*, Cell-Based Proteome Profiling Using an Affinity-Based Probe (AfBP) Derived from 3-Deazaneplanocin A (DzNep). *Chem. Asian. J*., (2013), 8, 1818-1828.

5. Li, Z.; Hao, P.; Li, L.; Tan, C.Y.J.; **Cheng, X.**; Chen, G.Y.J.; Sze, S.K.; Shen, H.-M.; Yao, S.Q.*, Design and Synthesis of “Minimalist” Terminal Alkyne-Containing Diazirine Photo-Cross-Linkers and Their Incorporation into Kinase Inhibitors for Cell- and Tissue-Based Proteome Profiling. *Angew. Chem. Int. Ed.*, (2013), 52, 8551-8556.

6. Ge, J.; **Cheng, X.**; Tan, L.P.; Yao, S.Q.*, Ugi Reaction-Assisted Rapid Assembly of Affinity-Based Probes against Potential Protein Tyrosine Phosphatases. *Chem. Commun.*, (2012), 48, 4453-4455.

7. Shi, H.; **Cheng, X.**; Sze, S.K.; Yao, S.Q.*, Proteome Profiling Reveals Potential Cellular Targets of Staurosporine Using a “Clickable” Cell-Permeable Probe. *Chem. Commun.,* (2011), 47, 11306-11308.

List of Abbreviations

AA	Amino acid
ADP	Adenosine diphosphate
AMP	Adenosine monophosphate
ATP	Adenosine triphosphate
Boc	*t*-butoxycarbonyl
BSA	Bovine serum albumin
CoA	Coenzyme A
C-terminus	Carboxy terminus
Da	Dalton
DCC	*N*, *N*'-dicyclohexylcarbodiimide
DCM	Dichloromethane
2D-DIGE	Two-dimensional difference gel electrophoresis
DIC	*N*, *N*'-diisopropylcarbodiimide
DIEA	*N*, *N*'-diisopropylethylamine
DMAP	4-Dimethylaminopyridine
DMF	*N*,*N*-dimethylformamide
DMSO	Dimethylsulfoxide
DNA	Deoxyribonucleic
dNTP	Deoxy Nucleotide Triphosphate
DTT	Dithiothreitol
EA	Ethyl acetate
E. coli	*Escherichia coli*
EDC	1-Ethyl-3-(3-dimethylaminopropyl) carbodiimide HCl

EDTA	Ethylenediamine tetraacetic acid
ESI	Electrospray ionization
Et	ethyl
Fmoc	9-Fluorenylmethoxycarbonyl
GST	Glutathione-S-transferase
HATU	(1-[Bis(dimethylamino)methylene]-1*H*-1,2,3-triazolo[4,5-b]pyridinium 3-oxid hexafluorophosphate)
HBTU	*O*-Benzotriazole-*N,N,N',N'*-tetramethyl-uronium-hexafluorophosphate
HCl	Hydrochloric acid
HEPES	4-(2-Hydroxyethyl)-1-piperazineethanesulfonic acid
HOAT	1-Hydroxy-7-azabenzotriazole
HOBT	*N*-Hydroxybenzotriazole
HPLC	High performance liquid chromatography
IC_{50}	Half the maximal inhibitory concentration
IT	Ion trap
kD	kilodalton
LB	Luria-bertani
$LiAlH_4$	Lithium aluminium hydride
Me	Methyl
MS	Mass spectrometry
MW	Molucular weight
N-terminus	Amino terminus
NHS	*N*-hydroxy succinimide
NMR	Nuclear magnetic resonance

PAGE	Polyacrylamide gel electrophoresis
PBS	Phosphate buffered saline
PCC	Pyridinium chlorochromate
PDB ID	Protein data bank identification code
PEG	Polyethylene glycol
pH	Negative logarithm of the hydroxonium ion concentration
Ph	Phenyl
PMB	*p*-Methoxybenzyl
PPs	Protein Phosphatases
PSSM	Position-specific scoring matrix
PTKs	Protein tyrosine kinases
PTPs	Protein tyrosine phosphatases
PVDF	Polyvinylidene fluoride
PyBOP	Benzotriazole-1-yl-oxy-tris-pyrrolidino-phosphoniumhexafluorophosphate
RNA	Ribonucleic acid
RF	Relative fluorescence
RP	Reverse-phase
SDS	Sodium dodecyl sulfate
SAR	Structure-activity relationship
TBTA	Tris[(1-benzyl-1*H*-1,2,3-triazol-4-yl)methyl]amine
TCEP	Tris(2-carboxyethyl)phosphine
TFA	Trifluoroacetic acid
THF	Tetrahydrofuran
TIS	Triisopropylsilane

TMS	Trimethylsilyl
TOF	Time of flight
Tris	Trishydroxymethyl amino methane
Ts	*p*-Toluenesulfonyl
TsOH	*p*-Toluenesulfonic acid
UV	Ultra-violet
WB	Western blotting

List of 20 Natural Amino acids

Single Letter	Three Letter	Full Name
A	Ala	Alanine
C	Cys	Cysteine
D	Asp	Aspartic acid
E	Glu	Glutamic acid
F	Phe	Phenylalanine
G	Gly	Glycine
H	His	Histidine
I	Ile	Isoleucine
K	Lys	Lysine
L	Leu	Leucine
M	Met	Methionine
N	Asn	Asparagine
P	Pro	Proline
Q	Gln	Glutamine
R	Arg	Arginine
S	Ser	Serine
T	Thr	Threonine
V	Val	Valine
W	Trp	Tryptophan
Y	Tyr	Tyrosine

Chapter 1

Introduction

1.1 Activity-based Protein Profiling (ABPP) and Affinity-based Protein Profiling

1.2 Development of Kinase Inhibitor Drugs (an overview)

1.1 Activity-based Protein Profiling (ABPP) and Affinity-Based Protein Profiling

1.1.1 Introduction

Proteins are the main components of physiological metabolites of cells and execute almost all of the cell's function.[1] Genome sequencing projects provide a platform to identify the protein encoded by the genomes in prokaryotic and eukaryotic organisms.[2] However, in the subsequent study of biological systems, assigning the functions for the entire set of proteins (proteome) contained in a living organism remains an ongoing challenge in the post-genomic era. Proteomics (the study of proteome) is more complicated than genomics (the study of genome) because an organism's genome is relatively constant, whereas the regulation of proteome is dynamic, which may not be directly encoded in the genome. Proteome is not only regulated by translation, but also a complex array of post-translational modifications and protein-protein interactions.

Proteomics is able to dissect the behaviour of the living system at the molecular level by many methods to analyze the presence of the proteins and their quantities. Conventional proteomics methods provide informations about expression patterns, interactions, and *in vitro* functions of proteins, including liquid chromatography–mass spectroscopy (LC-MS) analysis,[3] yeast two-hybrid assays[4] and protein microarrays[5]. However, these methods are limited because they do not reflect the activity of proteins in their native environments. As an important sub-filed of proteomics, a chemical proteomics dubbed as "activity-based protein profiling" (ABPP) has been systematically explored and has become a standard approach for the identification and functional characterization of proteins in the native complex proteomes.[6]

According to the ABPP strategy, a typical activity–based probe (ABP)[6a] normally possesses three elements: 1) a binding group with a reactive warhead, which directs ABP to its targets and simulate

structure and function of natural substrate or ligand. The warhead very close to the affinity binding group therefore is ready to react in the active site to form a covalent bonding between ABP and protein; 2) a proper spacer, linked the binding group with warhead to tags and avoid other parts to disturb the interactions formed; 3) a tag, which allows visualization and/ or purification of bound target protein. The tags normally could be fluorescent dyes, radioactive tags for visualization and/or biotin for affinity purification. Normally, the approach is cooperated with Liquid chromatography coupled to tandem mass spectrometry (LC–MS/MS) for protein identification. (Figure. 1.1)

A number of analytical platforms have been developed to specifically visualize and identify the labeled protein targets by ABPP probe in complex proteomic mixtures. According to the informations intended to obtain, the platform is chosen in consideration of its advantages and disadvantages in throughput, sensitivity, target identification, and sample amount required. As a most mature standard high-throughput technique, gel-based analysis is simple and fast to visualize the proteins by either in-gel fluorescence scanning or avidin blotting, for fluorescent and biotinylated ABPP probes, respectively.[7] However, it does not provide enough informations (only molecular weights indicated by 1D electrophoresis and isoelectric points indicated by 2D electrophoresis) to reveal the identity of the labeled target enzymes. To further identify the probe pulled down proteomes, multiple LC-MS strategies[8] with high resolution and sensitivity have been developed normally after the sample preparation including biotin–(strept)avidin enrichment and trypsin digest. Subsequent computer-based database match searching of peptide informations reveals the identity of the protein labelled. Microarrays is applied in ABPP by combination of the isolation, detection, and identification of probe-labeled enzymes into one step.[9]

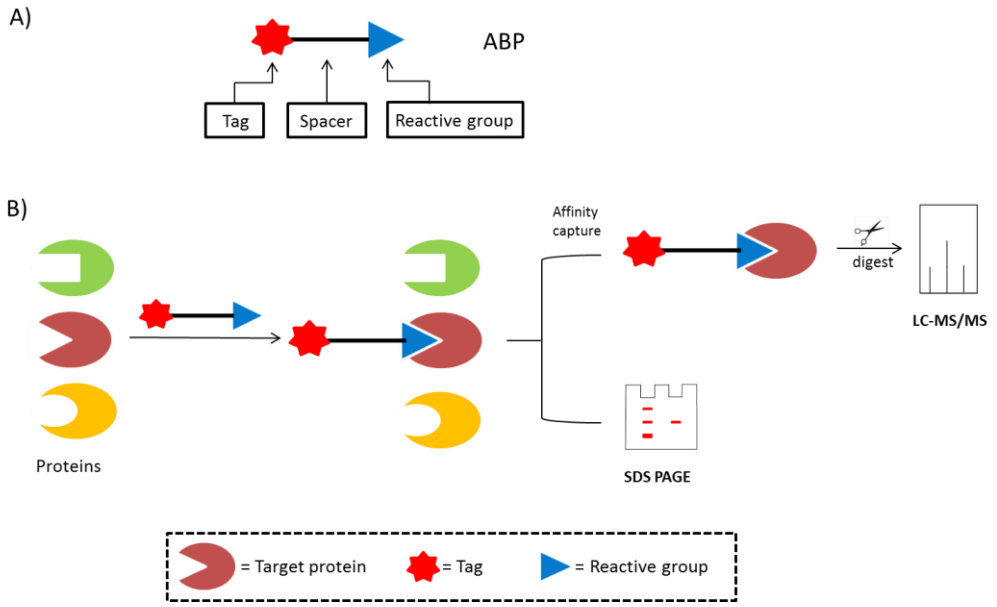

Figure 1.1 (A) The typical stucture of an activity-based probe (ABP); **(B)** the strategy of activity-based protein profiling (ABPP), consisting of a labeling step in complex proteomes and an analytical step to visualize and characterize activity-dependent labeled proteins.

Using chemically-modified probe, ABPP as a powerful and mature functional proteomic technology has been successfully used to study the mechanistically-related classes of enzymes including serine hydrolase,[10] cysteine protease,[11] tyrosine phosphatase[12] and kinase[13]. In the ABPP strategy, after the ABP is used in the target labeling, the tagged protein could be visulized by flurorescent detection with fluorscent tags and/or identification by LC-MS/MS with biotin tag. First of all, the warhead based-on the enzymatic mechanism is the key of specificity. A variety of electrophiles is introduced as warheads. For example, fluorophosphonate (FP) served as mechanism-based reactive groups is successfully used to speifically profile the serine hydrolases family,[10] which shows selective reactivity to the enzymes in active form and minimal cross-reactivity with other classes of hydrolases based on distinct mechanism.[14] Other warheads are also introduced including epoxide,[11] Michael acceptor, haloacetamide,[15] acyl phosphate[16], α-bromophosphate,[12] vinyl sulfone,[17] quinone methide[18] and so on. (Figure 1.2)

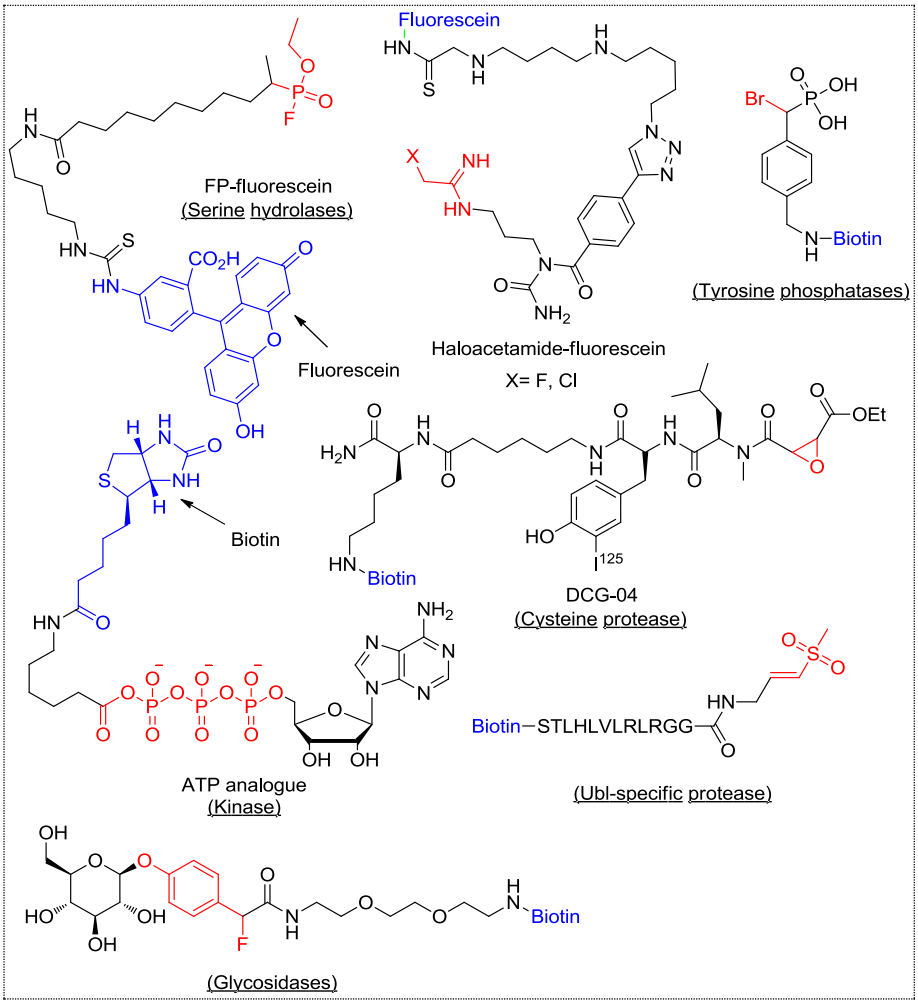

Figure 1.2 Typical instances of activity-base probes (ABPs).

As a complementery for ABP, affinity-based probe (A*f*BP) is used in the target proteome profiling of the affinity-based inhibitor. Unlike the mechanism of the suicide-based inhibitor which forms a stable covalent bond, the inhibition between the affintiy-based inhibitor and its targets is based on the strong affinity. The inhibition of the latter is probably not tolerate in the cellular exposure and subsequent affinity-based protein profiling process including harsh washing, denauration and so on. For example, the beads-immobilized inhibitors is used in the proteome profiling of the inhibitors intended. However, the method is limited to *in vitro* assay including recominbant protein and lysates with the problems of target missing and false targets, and thereby can't reflect the the true relationship between the inhititors and its celluar targets.[19] To

overcome the shortcomings, in this approach, a photo-labile group was typically incorporated into A*f*BP. After A*f*BP binds its targets reversibley including noncovalent interactions or reversible covalent bonds, the colvalent binding between the probe and targeted protein, upon activation of light, is formed. (Figure. 1.3)

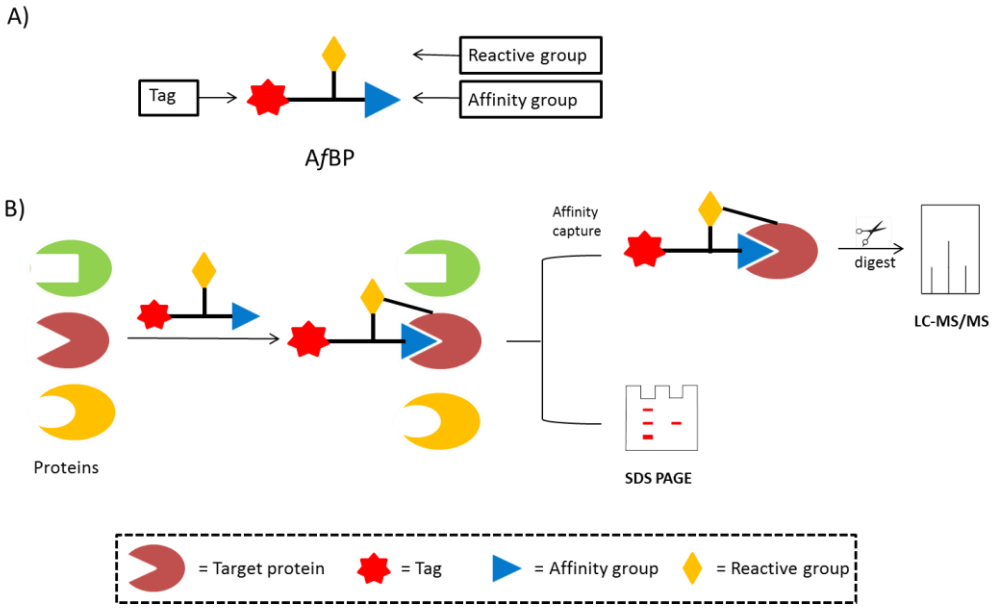

Figure 1.3 (A) The stucture of a typical affinity-based probe (A*f*BP); **(B)** the strategy of affinity-based protein profiling.

In the strategy of affinity-based protein profiling, the most important difference between A*f*BP and ABP is the additional reactive groups, which established the irreversible covalent binding to form a stable protein-probe complex. In order to use an A*f*BP for labeling of (active) enzymes in biological environments, the photo-crossing groups should fulfil some requirements. The groups should be inert to the environments and activated under a bio-safe light in a specific wavelength. The generated species should have a short lifetime to fix the enzyme-probe complex with less nonspecific labeling. The size of the groups should be small to avoid influences on the interactions between the target and probe.[20] Upon activation with appropriate light,

an aryl azide would generate active species which could react with C–H bonds and nucleophiles nearby in the ligand binding pocket of proteins to form a stable covalent protein-ligand complex. Photolysis of diazirine generates active carbenes which react with C–H bonds, C–N bonds and hydroxyl groups nearby to covalent adducts. Photolysis of benzophenone gives triplet diradical which subsequently reacts with C–H bonds available in all amino acids.[6d] The representing examples of affinity-based probes (A*f*BPs) using the photoreactive groups including aryl azide,[21] benzophenone[22] and diazirine[23] are introduced in Figure 1.4.

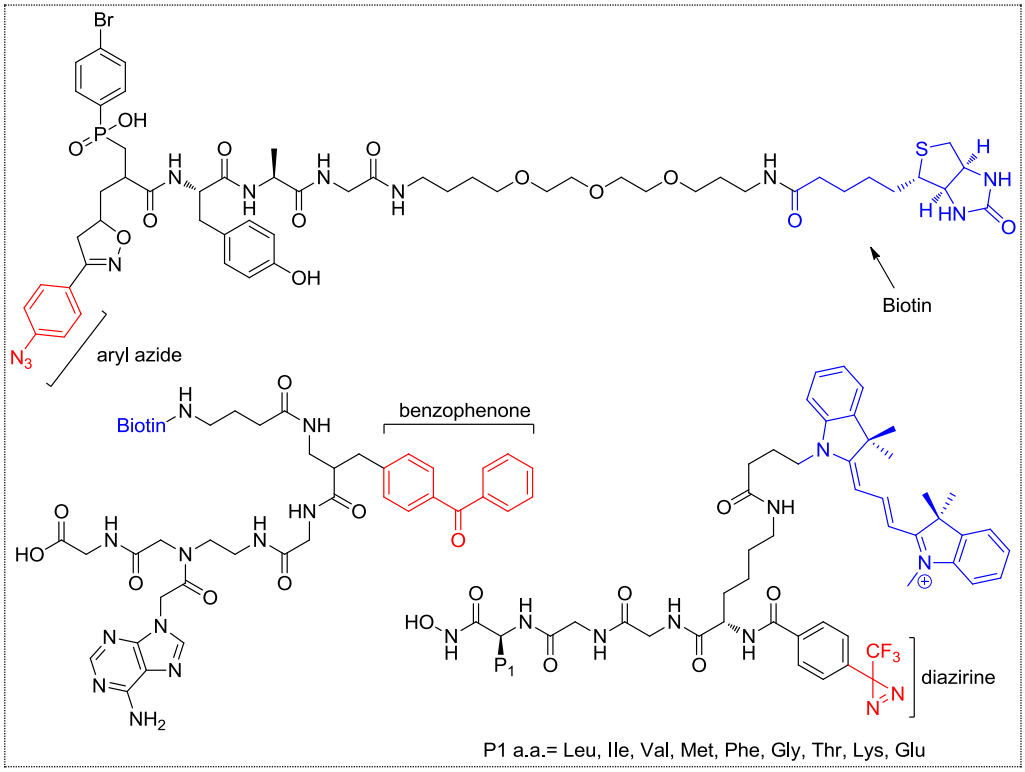

Figure 1.4 The representing examples of affinity-based probes (A*f*BPs)

1.1.2 Bioorthogonal Chemistry in ABPP

In the application of ABP, some typical drawbacks were encountered. For example, tag-conjugated modification makes the probe too bulky, which probably affects its uptake by the live cell, in

terms of cell penetration, drug distribution and disturbance of the reactivity by the reporter. To resolve the problems, a new trend of the ABP design is developed by separation of the probe from the reporter. The advantages of the minimum-modified design include maintaining the original reactivity, less bulky and flexible option of reporters. To complete the ABPP strategy, the warhead tethered with the target proteins should be linked to the reporter for visualization or affinity purification, by bioorthogonal chemistry. Typically, a reaction as bioorthogonal chemistry which neither interacts with nor interferer with a biological system, should fulfill the requirements: 1) the two groups used to form a stable linkage should be bioinert and ideally nontoxic; 2) the reaction should occurs between each other of the two functional groups specifically; 3) have fast kinetics at low concentration under physiological conditions such as pH, temperature and biological media; and 4) the groups should be small as well.[24]

So far, only a few types of reactions fulfilled the requisite qualities of biocompatibility and selective reactivity to function as bioorthogonal chemical groups in living cells. The Staudinger ligation can be used to covalently attach probes to azide-bearing biomolecules.[25] The reaction proceeds at pH 7 with no apparent toxic effects and the size of azide is small, but suffers from low kinetics and the side reaction of the slow oxidation of phosphine.[24] The typical click chemistry between the terminal alkyne and azide group was used widely in ABPP.[26] The reaction is fast and the reaction groups are small, but the Cu (I) as a necessary catalyst is cytotoxic. To overcome this shortcoming, the stained-promoted copper-free click chemistry between azide and cyclooctyne was developed.[27] In the reaction, azide group is small and kinetics is faster than unmodified alkyne, but the cyclooctyne part is difficult to synthesize and the rate is relatively low. To pursue nontoxicity and high kinetics, tetrazine cycloadditions was developed. Comparably, the starting material is easy to synthesize and the reaction is extremely fast without catalyst. But tetrazine is much larger than azide and the reaction is not region/stereoselectivity.[28] A tetracysteine motif (CCXXCC) chemical reporter can be fused to target

proteins at the genetic level and covalently labeled in living cells with membrane-permeable dyes (FlAsH and ReAsH).[29] The modification is small comparing to GFP, but is not tolerated to biosynthetic enzyme.[24] Ketones and aldehydes as bioorthogonal chemical reporters could react with hydrazide and aminoxyl groups to form stable Schiff base under physiological conditions.[30] (Figure 1.5)

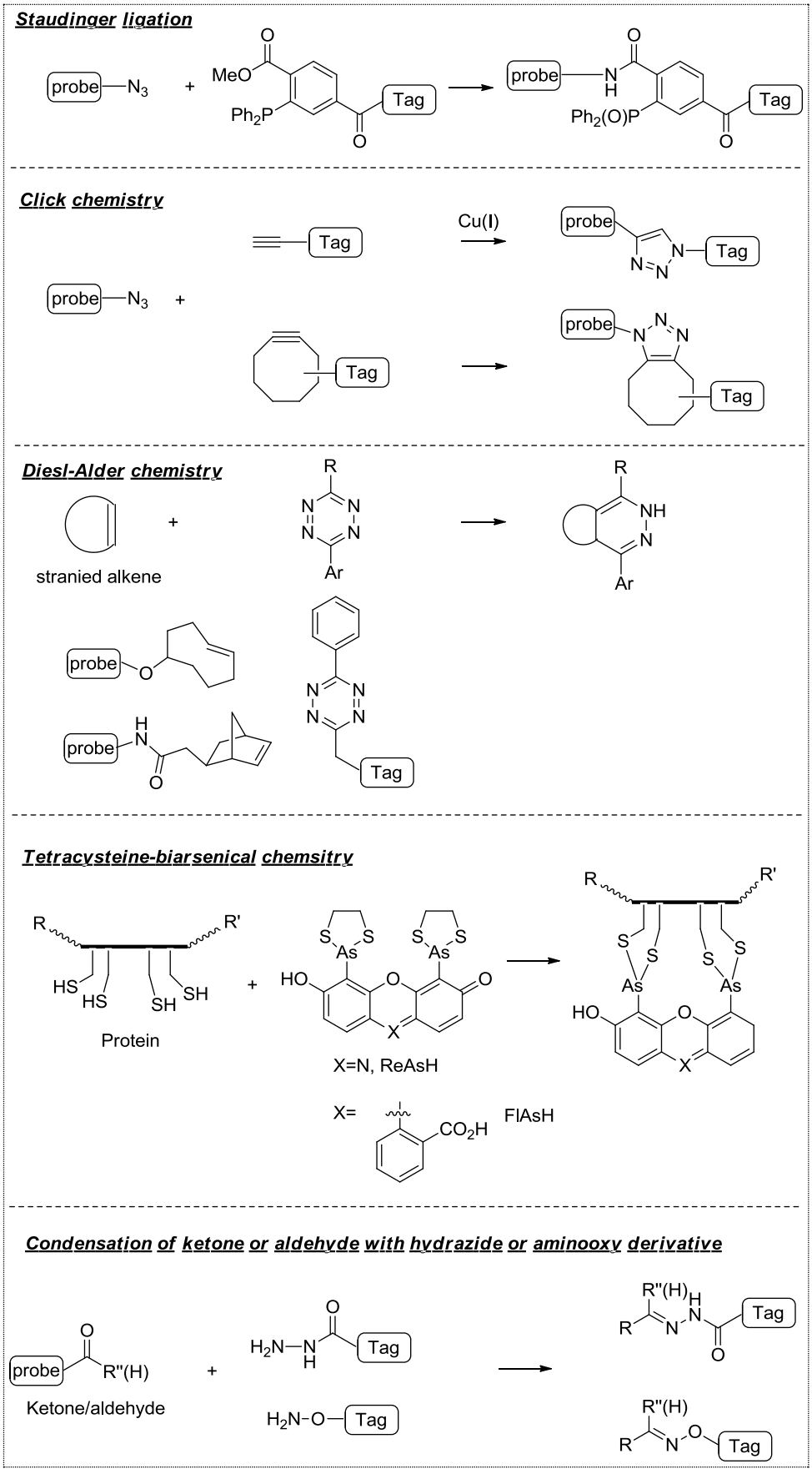

Figure 1.5 Reaction types of bioorthogonal chemistry

With the development of the high efficient and biocompatible bioorthogonal chemistry, ABP and A*f*BP in tag-conjugated manner are evolved to tag-free manner. Therefore, the probe gets smaller with less influence on the drug activity and better cell permeability. The activity-based protein profiling (ABPP) was broken into two steps and then joined together with bioorthogonal chemistry (typically as click chemistry). (Figure 1.6) The tag-free design was applied to ABP to facilitate the *in situ* target identification efficiently. (Figure 1.7) The "clickable" version of epoxide compound (MJE3) could specifically label the glycolytic enzyme phosphoglycerate mutase B (PGAM1) *in situ*.[31] "Clickable" SAM analogs are used for labeling protein methyltransferase substrates which are linked to various human diseases.[32] A library of *β*-lactones also is used to screen the bacterial proteome.[33] Sieber et al. adopted a library of *β*-lactam probes (CephN, Azt and AmpN) derived from natural or synthetic sources for comparative *in situ* profiling experiments in non-resistant and resistant strains of S. aureus (SA and MRSA) and identified uncharacterised MRSA enzymes which hydrolyse *β*-lactam antibiotics.[34] The traceless labeling of glycoprotein with BA-tosyl was reported latest.[35]

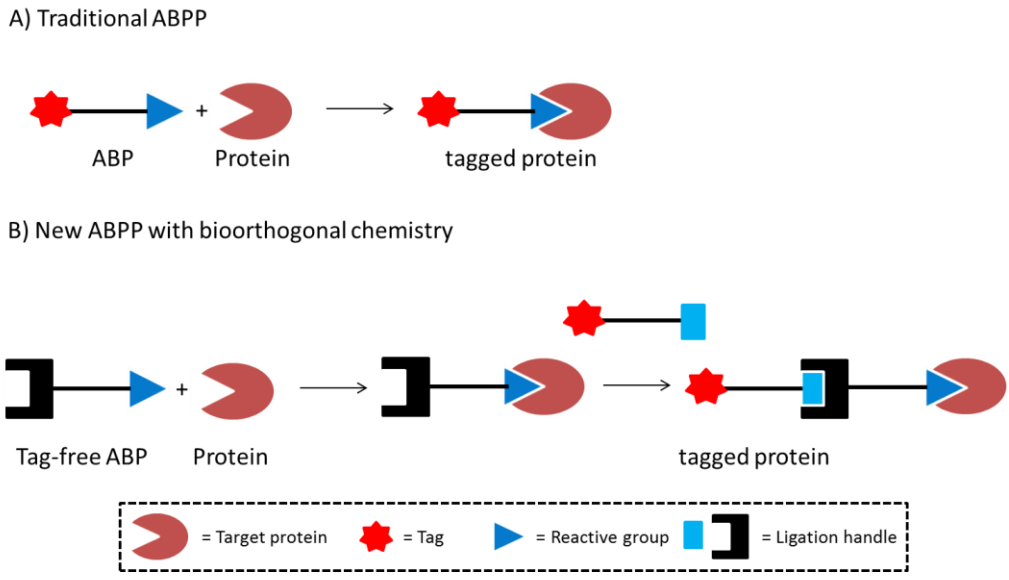

Figure 1.6 Traditional one-step ABPP and the two-step ABPP assisted with bioorthogonal chemistry

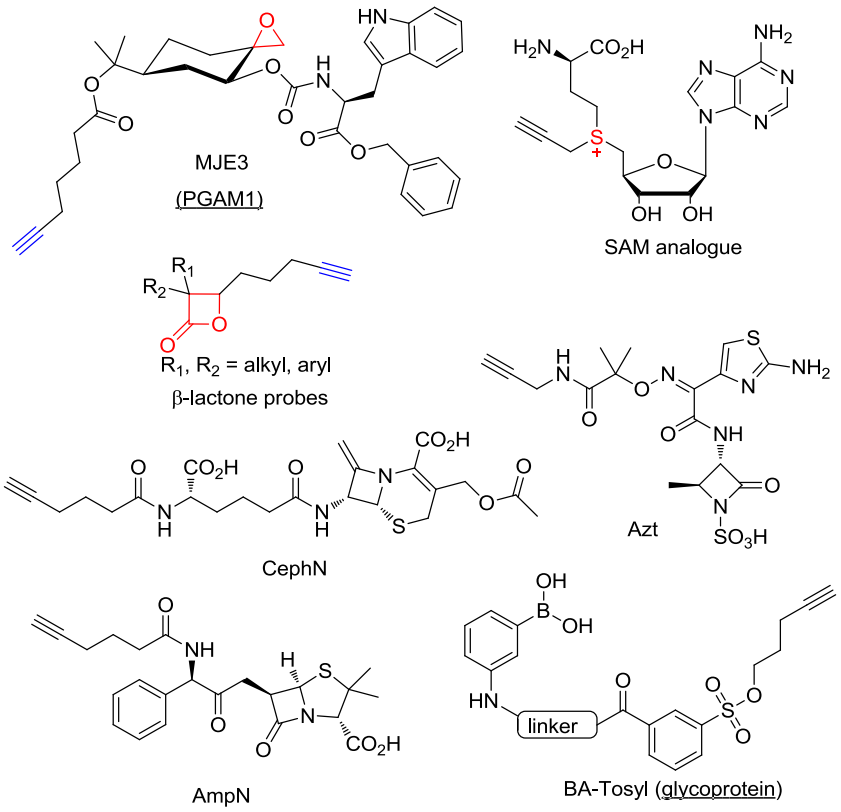

Figure 1.7 The representing examples of tag-free activity-based probes (ABPs)

For the tag-free manner of A*f*BP, there're many interesting instances to achieve the investigation. Similarly to tag-free ABP, a ligation handle was introduced to A*f*BP in the place of tags to make the probe smaller. (Figure 1.8) Recently, tag-free A*f*BP was used in the on and off-target identification of Dasatinib,[36] Staurosporine and other kinase inhibitors by *in situ* proteome profiling. [36b, 37] The clickable handle and photo-labile group are introduced to the suitable positions on the kinase inhibitors to minimally affect their activities. (Figure 1.9)

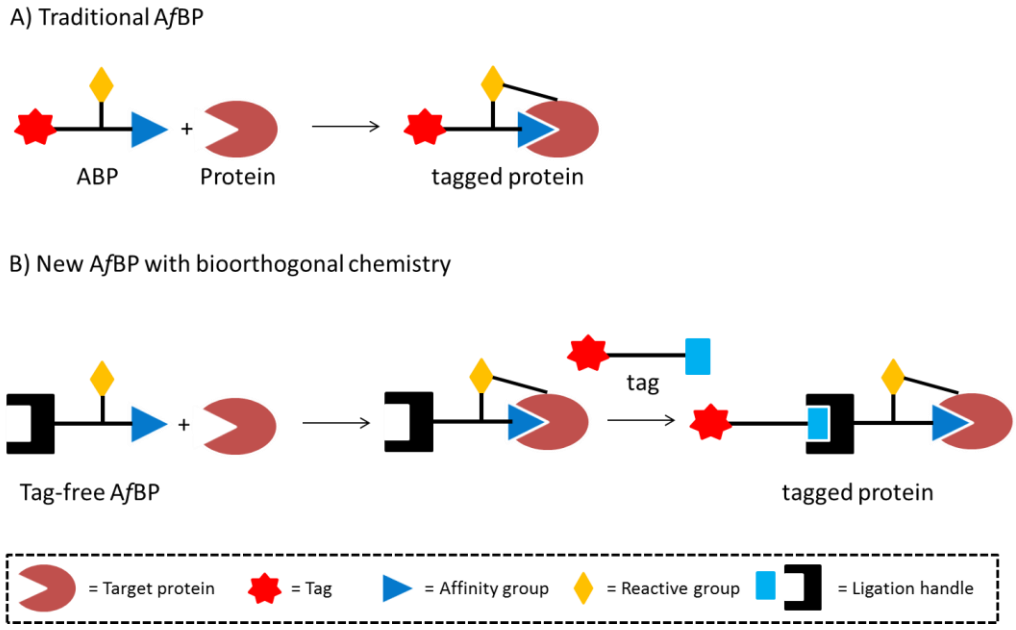

Figure 1.8 Traditional A*f*BP and new type of affinity-based protein profiling assisted with bioorthogonal chemistry

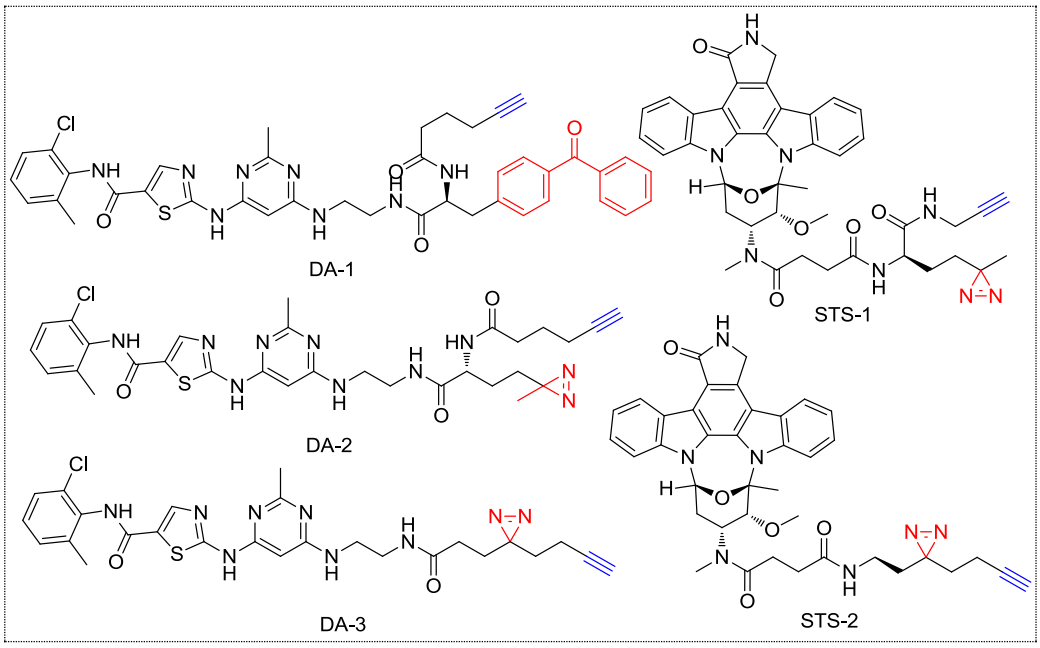

Figure 1.9 The representing examples of tag-free affinity-based probes (A*f*BPs)

1.1.3 Application of ABPP in target identification of bioactive molecules including natural product and drug

A large number of bioactive molecules including natural product, drug and etc. emerge in the sight of scientist. Natural products are becoming one of the most important sources of modern drug discovery because the privileged structure and biological function of natural product must bind to some enzymes to fulfill the inherent purpose of their biosynthesis and origin in the organisms.[38] Fast development in techniques of the modern isolation, purification and identification, provides more and more natural product candidates from fungi, metabolite, plants, marine source and etc.[38a] However, the current innovation is deficient in the identification of compounds with the desired activity.[39] In other words, there're limitations of techniques in drug targets identification of natural products. Furthermore, even for those FDA-approved drugs, the side-targets remain unknown, which result the safety issue and the drug withdrawn from the market.[40]

There're few approaches developed to fulfill the purpose. Firstly, identification of an active natural product from the traditional medicine against certain disease is a shortcut to establish the relationship between natural product and proteins which results the disease in the known mechanistic hypotheses. However it does not provide the comprehensive information about drug effect. Secondly, high-throughput screening techniques allow the fast screening over a large library of compounds in protein or cell-based assay. Thirdly, comparing the phenotype caused by the compound with by gene knockout, RNA interference or other chemicals, provide the protein target of the compound. Then, the affinity capture by the immobilized natural product incorporated with 2D SDS-PAGE and LC-MS/MS analysis is applied to identify its targets. It is limited in *in vitro* assay. Finally, ABPP as a powerful tool is applied to target identification of the bioactive molecules (e.g. natural product) by establishing a covalent linkage with the probe derived from the bioactive molecules and its targets in the native state.[6d, 10, 41] The probe could be in tag-conjugated or tag-free manner.[6c, 38b, 42] Based on the nature of interactions between the bioactive molecules (e.g. natural product) and targets, the drug-like

designs of the probes could be classified into ABP for covalent molecule and A*f*BP for non-covalent molecule.

For those bioactive molecules containing a reactive group served as warhead to recognize and then bind the protein targets covalently, their corresponding ABPs are designed with a terminal alkyne group (or other tags) at a suitable position. The stable protein-probe complex is tolerable to the subsequent enrichment and identification process. The representative examples include AX7574[43] and wortmannin[13] in tag-conjuated manner. Compared to the probe tagged with TMR and Biotin that are only capable to labeling targets *in vitro*, the probe tagged with smaller-size BODIPY shows the improved ability of proteome profiling *in vivo*. Therefore, design of ABP further evolves into the tag-free manner because of many advantages.(described in section 1.1.1) The drug-like probe derived from Showdomycin as a potent nucleoside antibiotic is modified minmally with a 5-hexynoic acid tag and shows identical MIC value with the parent drug.[44] It is applied in the proteome profiling and identify 13 potential targets including MurA1 and MurA2, which are important enzymes in bacterial cell wall biosynthesis. THL (an FDA-approved anti-obesity drug) derived probes (THL-L, THL-R, THL-T and other analogues) have identified the cellular off-targets and side effects except the the known target fatty acid synthase (FASN) by *in situ* proteome profiling.[45] The “clickable” probes (VS-1, diazomethyl ketone and azanitrile probe) derived from anti-parasitic compound K11777 help to identify its cellular targets in live parasites.[46] (Figure 1.10)

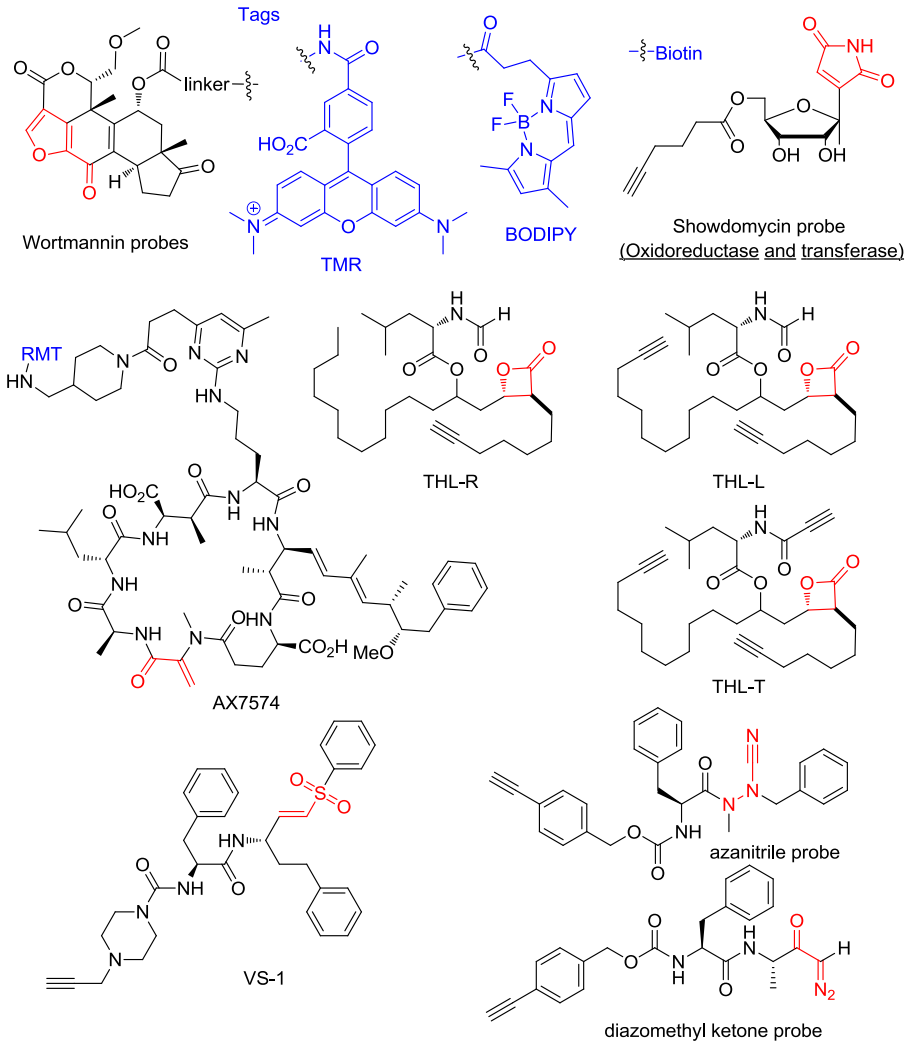

Figure 1.10 ABPs based-on natural products and drugs with warhead

However, most bioactive compounds bind to their protein targets non-covalently and therefore the transient protein–small molecule complex may not survive the following enrichment process. The design of A*f*BPs derived from such molecules is applied to identify the cellular targets by the proteome profiling. The key is the formation of stable protein-probe complex *in situ* by incorporation of additional photo-labile group. Yao group has reported a series of “clickable” probes derived from kinase inhibitors incorperating with photo-labile groups, which are incapable of *in situ* target identification. (Structures of partial probes listed in Figure 1.9) Trimodular probes are developed to label type I methionine aminopeptidase (MetAP) in *E. coli* cell lysate. Apparently, the probe in tag-free manner is much more selective than the biotin-conjugated probe in this case.[47] Probe **1-1** and **1-2** derived from type-II

kinase inhibitors allow to label protein kinases in the DFG-out inactive conformation by a trifluoromethylphenyl diazarine group.[48] Dasatinib probe **1-3** could be used to rapid and quantitative profiling of kinase active sites in both lysates and live cells.[49] In this probe, benzopheone is used for photo-linking with targets and hexylchloride tag is served for ligation with protein Halo tag. Recently, a clickable cell-permeable DzNep probe is developed from a global histone methylation inhibitor (3-Deazaneplanocin A) to identify its *in situ* cellular targets.[50] (Figure 1.11)

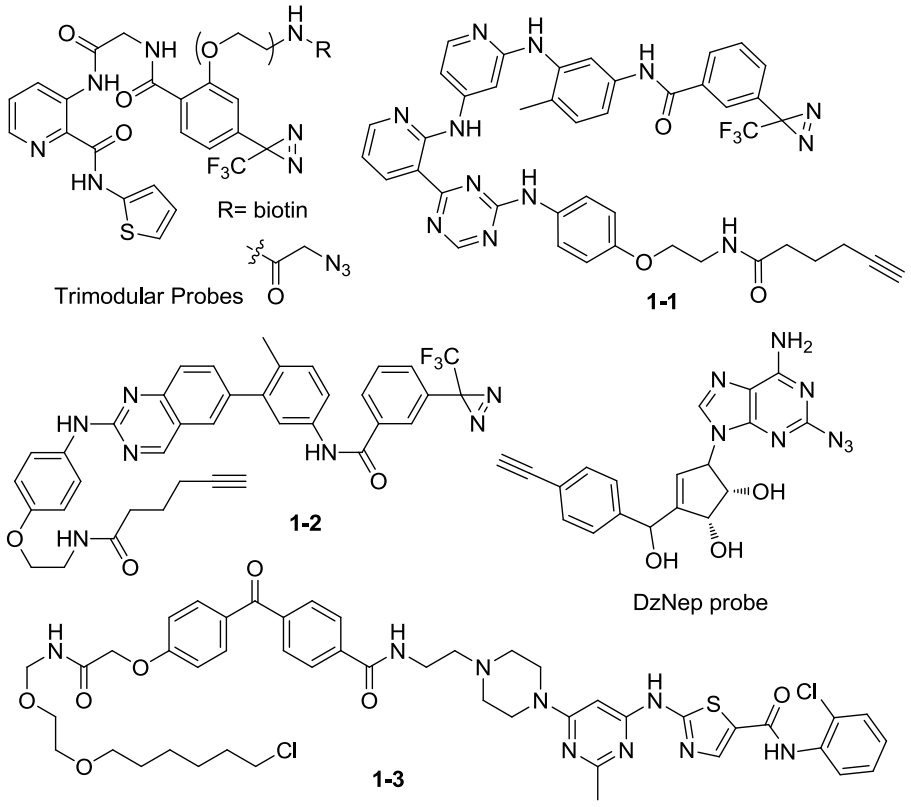

Figure 1.11 A*f*BPs based-on natural products and drugs via affinity interactions

1.1.4 Application of ABPP in Protein Inhibitor Design and Enzyme Activity Detection

Enzyme activity inside cells is regulated by many factors including posttranslational modification, small molecules, or cofactor binding. Molecular imaging is one of method to monitor the dynamics of

distributions of enzyme and bioorganic molecules. Unlike GFP-fusion protein, ABPP have the advantages of smaller size and convenience to real-time monitor the enzyme function and activity in living cell or organism. Several challenges still remain for researchers interested in using ABPP to investigate biological processes.[6a] For example, the common ABP conjugated a fluorescent tag served for imaging, have the limitation that the permanent fluorescent signal is obtained regardless whether the probe is bound to targets or free in the cell. As a new concept, a fluorescently quenched Activity-based probe(qABP) (GB117) was developed by Bogyo and colleagues for the visualization of cathepsin activities in living cells.[51] In the probe, BODIPY fluorophore was OFF by the interaction with the quencher. Based on its mechanism, once the quencher was replaced by cathepsin, the fluorophore was turned ON with the strong fluorescence and thereby ready for real-time imaging of cathepsin activity in live cell. Hu et al. reported a new class of qABPs (P1, P6) which were based on quinine methide chemistry and conjugated with 1-photo and 2-photo fluorophores for imaging of enzyme activity in live cells.[52] (Figure 1.12)

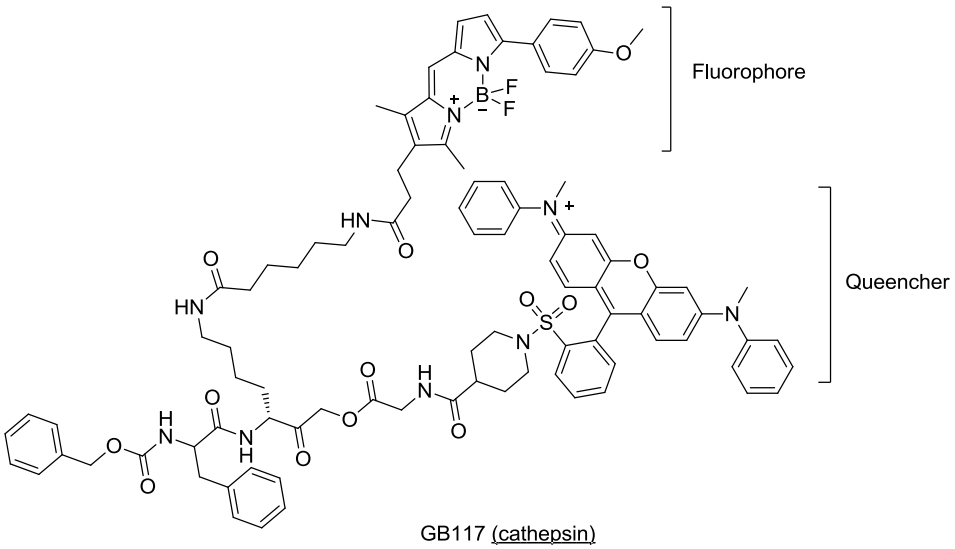

GB117 (cathepsin)

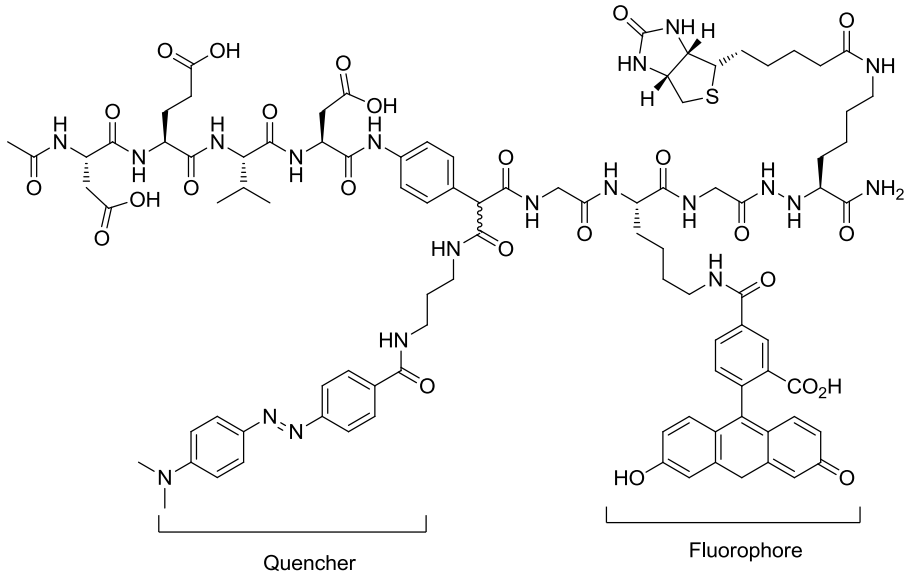

P1 (cysteine proteases)

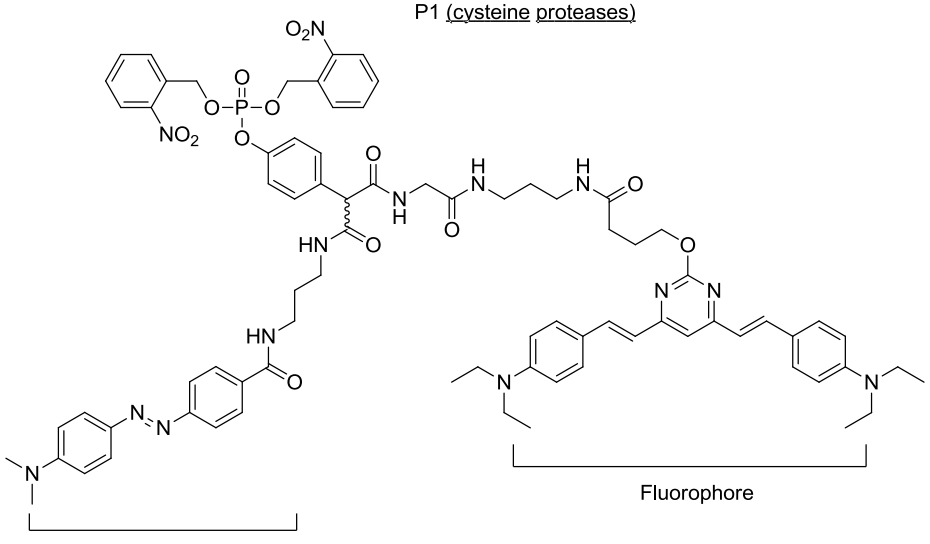

P6 (phosphatases)

Figure 1.12 qABPs in the activity detection and imaging

1.2 Development of Kinase Inhibitor Drugs

2% of human gene encodes a large family of protein kinases (500+), which reversibly phosphorylated about 30% of all human proteins, including biomolecules that regulate every complex cellular processes and pathway, such as growth, differentiation, proliferation, apoptosis and cellular signal transduction.[53]

1.2.1 Kinase and Its Catalytic Mechanism

The Nobel Prize in Physiology or Medicine for 1992 was awarded jointly to Edmond H. Fischer and Edwin G. Krebs for their discoveries concerning "*reversible protein phosphorylation as a biological regulatory mechanism*".[54] Phosphorylation and dephosphorylation of protein are a pair of reversible contrary processes which plays a very important role in regulation of the transformation, charge, activity, cellular location of protein and interaction with other cooperating protein in living organisms.[53] Kinase is a type of protein which could modify its specific substrate including small molecule and protein, by transferring the terminal phosphate group from the high energy molecule—ATP. The process is defined as phosphorylation. Simultaneously, the conformation and function of the substrate was changed. Contrariwise, phosphatase removes the phosphate group from the phosphorylated target and releases an inorganic species—phosphate ion. Accordingly, the process is defined as dephosphorylation. Consequently, in the process, the conformation and function of the substrate is recovered to the starting point in the phosphorylation process. (Figure 1.13)

Apart from the kinase named after the small molecular as the substrate, protein kinase named after the protein as the substrate, could be also classified by types of the residue as acceptor in substrate proteins, as serine/threonine-specific kinase and tyrosine-specific kinase. From the structure point of view, all of kinases share a catalytic

domain including ATP-binding pocket, substrate-bind pocket and catalytic loop. ATP-binding pocket serves to coordinate and orient the ATP. Substrate pocket is the capacity for substrate pocket. Catalytic loop nearby was involved to anchor the substrate and phosphate transferring.[55] (Figure 1.14A)

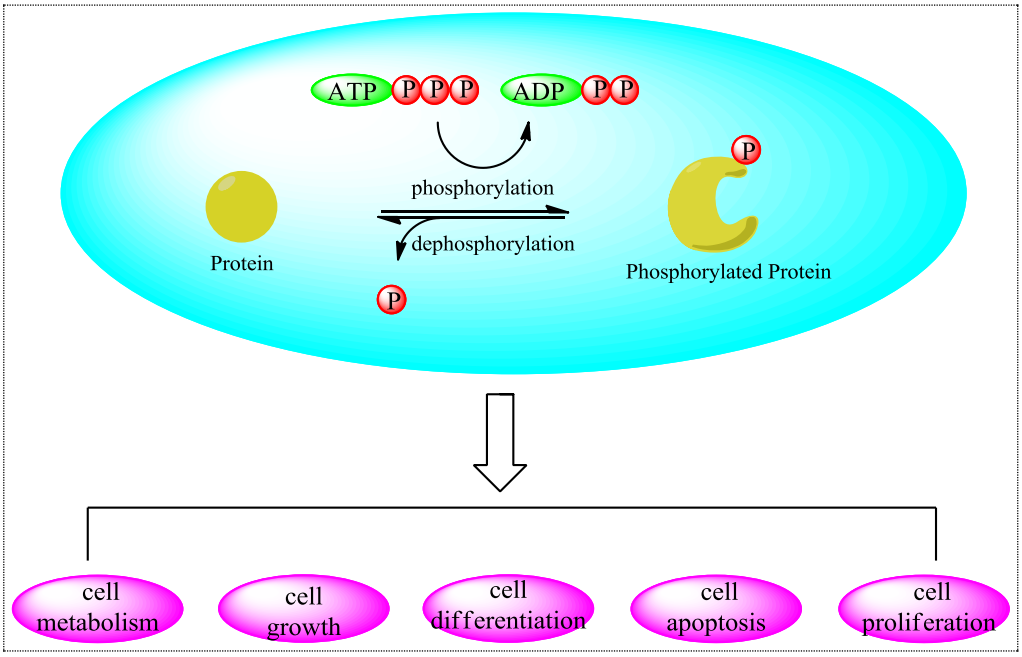

Figure 1.13 Phosphorylation by kinase and dephosphorylation by phosphatase

1.2.2 Development of Kinase Inhibitors

In normal state, kinase as part of the larger family of phosphotransferase would cooperate nicely with phosphatase to regulate the enzymes to complete the cellular process in the complex living system. However, in disease state, dysregulation and mutation of kinase (more than 180) is a very important pathogeny in human disease such as cancer, diabetes, hypertension and other disease. Therefore, kinase is becoming the interesting targets in the therapy.[56] Most of FDA (the U.S. Food and Drug Administration)-approved kinase inhibitor drugs are especially targeting different types of cancer.

There're several typical ways to inhibit the activity of kinase targeting ATP-binding pocket, substrate-binding pocket, allosteric sites and other upstream regulation with small molecules and antibodies.[57] Until now, most small molecule kinase inhibitors are ATP competitive, which form few hydrogen bonds with ATP pocket and prevent the phosphate donor ATP from binding to kinase in order to terminate the subsequent phosphorylation. The X-ray diagram of PKA with Staurosporine as an ATP competitive inhibitor represents the inhibition model in Figure 1.13B. Staurosporine occupies ATP pocket and prevents the subsequent phosphorylation of the peptide substrate

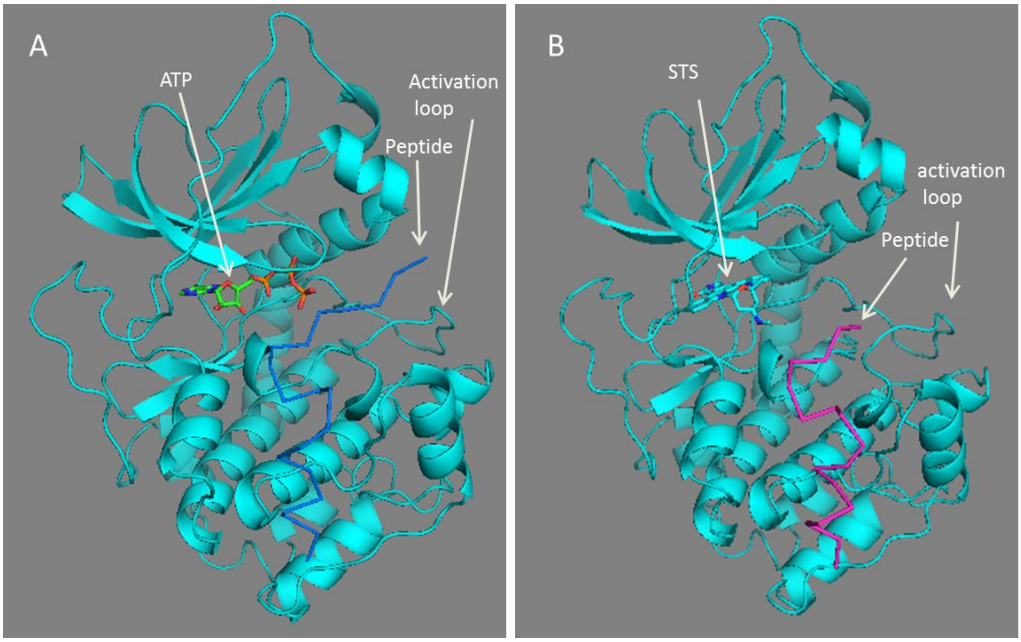

Figure 1.14 Ribbon representation of PKA c-α in complex with **(A)** ATP, and a peptide inhibitor (PDB ID: 1ATP); and **(B)** Staurosporine (STS) and a peptide inhibitor (PDB ID: 1STC).

In the past decade, a great progress in the development of small molecule kinase inhibitors has been achieved. Many of them are used in clinical trials with different types of cancer and some are successfully approved in clinic protein kinase inhibitors.[56b, 58] (Table 1.1) However, comparing to the large family (500+) of kinase and their complicated interaction network involved in the therapy, an urgent need occurs to develop efficient and specific inhibitors. The strategy is normally a combination of methods including analogue synthesis, structure-

informed design and fragment-based assembly strategies.[58a] To date, by the nature of binding, inhibition model is typically classified to reversible and irreversible inhibition. The reversible inhibitor is the majority as the ATP competitive inhibitor. This type of inhibitor typically occupies the pocket of ATP bonding region including “type I” and “type II” binding modes. The binding comes from the nature of interactions between kinase and inhibitor, including hydrogen bond and hydrophobic interaction. The typical instances include staurosporine (Figure 1.14B), Imatinib, Dasatinib and so on. (Figure 1.15) This type of inhibitor has the advantage in terms of safety as the binding to the off-targets could be released.

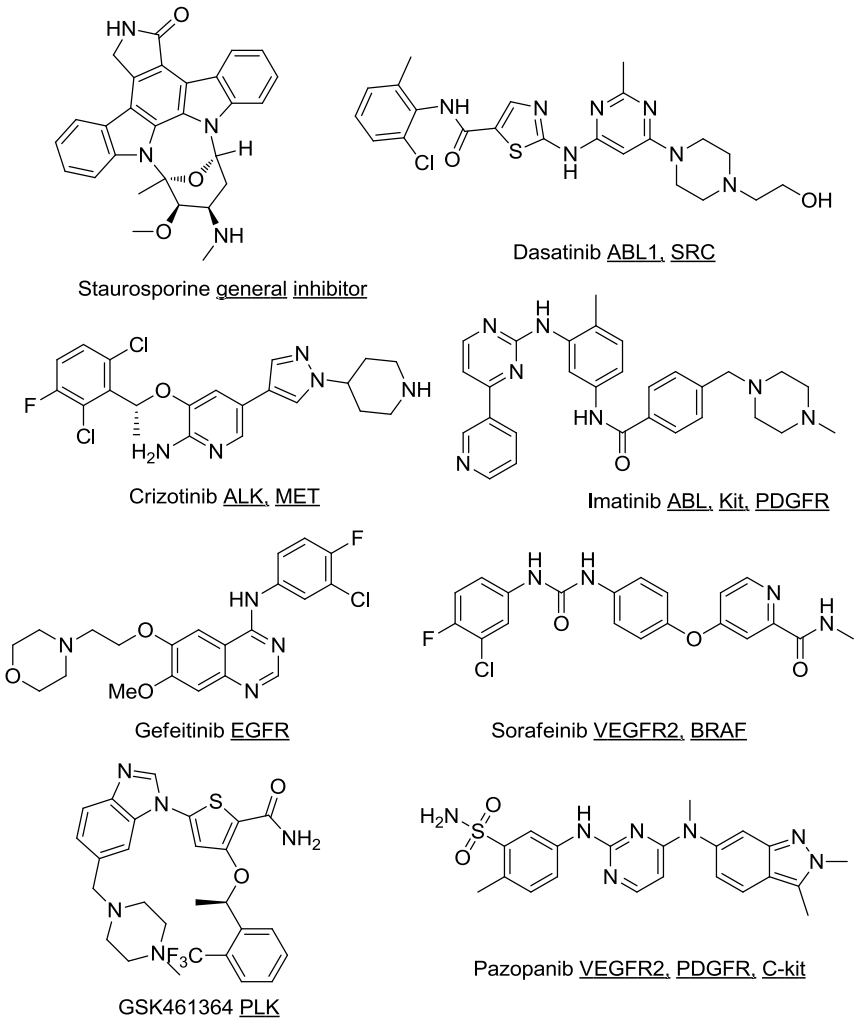

Figure 1.15. Structures of representative reversible kinase inhibitors

Table 1.1 FDA approved kinase small molecule inhibitors

Entry	First approval year	Agent	Target kinases	US FDA-approved indication
1	1999	Rapamycin	FKBP12/mTOR	Immunosuppression
2	2001	Imatinib	ABL, PDGFR, KIT	CML, GIST
3	2003	Gefitinib	EGFR	NSCLC
4	2005	Erlotinib	EGFR	NSCLC, PC
5	2005	Sorafenib	VEGFR2, PDGFR, RAF, etc.	RCC, HC
6	2006	Dasatinib	ABL, SRC	CML, ALL
7	2006	Sunitinib	VEGFR2, PDGFR, KIT	RCC, GIST
8	2007	Nilotinib	ABL	CML
9	2007	Lapatinib	EGFR, ERBB2 (HER2)	Breast cancer
10	2007	Temsirolimus	FKBP12/mTOR	RCC
11	2009	Everolimus	FKBP12/mTOR	Immunosuppression, RCC, etc.
12	2009	Pazopanib	VEGFR2, PDGFR, KIT	RCC, STS
13	2011	Crizotinib	ALK, MET	NSCLC
14	2011	Vemurafenib	BRAF	Melanoma
15	2011	Ruxolitinib	JAK1/2	Myelofibrosis
16	2011	Vandetanib	VEGFR2, EGFR, RET	MTC
17	2012	Bosutinib	ABL	CML
18	2012	Ponatinib	ABL, SRC	CML, ALL
19	2012	Tofacitinib	JAK3	RA
20	2012	Axitinib	VEGFR1/2/3, PDGFR, KIT	RCC
21	2012	Cabozantinib	VEGFR2, RET, MET	MTC
22	2012	Regorafenib	VEGFR2, TIE2, etc	Colorectal cancer, GIST
23	2013	Dabrafenib	BRAF	Melanoma with BRAF(V600E)
24	2013	Trametinib	MEK	Melanoma with BRAF(V600E/V600K)
25	2013	Afatinib	EGFR	NSCLC with EGFR (exon 19 deletion and L858R)

ALL (acute lymphoblastic leukemia)
AMD (Age-related macular degeneration)
CML (chronic myelogenous leukemia)
DME (diabetic macular edema)
GIST (gastrointestinal stromal tumors)
HC (hepatocellular carcinoma)
HNC (head and neck cancer)
MTC (medullary thyroid cancer)
NSCLC (non-small cell lung cancer)
PC (pancreatic cancer)
RCC (renal cell carcinoma)
RA (rheumatoid arthritis)
STS (advanced soft tissue sarcoma

However, it becomes difficult to design a kinase inhibitor to recognize a kinase from the huge family which possesses the highly conserved sequence and structure of the ATP-binding pocket. Additionally, many cellular biological important molecules like ATP, ADP, AMP and etc., may ubiquitously distribute considerable interactions to compete with the inhibitor. On the other hand, a sum of the functional proteins which is much larger than of kinases, containing the similar nucleotide-binding site, makes the screening much more complicated.[2, 59] Therefore, there's the opportunity for the irreversible covalent inhibitor as another important type. The interactions between the irreversible covalent inhibitor and kinase include affinity binding and subsequent covalent binding. The potency for toxicity of covalent inhibitor is the unredeemable binding to unanticipated targets. Although the disadvantages including toxicity come of the irreversible covalent kinase inhibitors, many valuable advantages are owing to them, including high potency, high specificity, prolonged pharmacodynamics, identification of the active site, flexibility of introduction of warhead and other fragment. On the other hand, because of the nature of irreversibility and high potency, durable target suppression without the necessity of keeping high continuous drug exposure like reversible drug is the advantage of safety.

Balancing the promising benefits and the potential risk, the irreversible covalent inhibitor becomes an increasing type in the last decade.[58d] Typically, an electrophile as the warhead targeting the unique nucleophilic residue in the ATP pocket is incorporated to a scaffold, which is already an affinity-based inhibitor with the decent potency and specify. The higher selectivity comes from the cumulation of the non-covalent and covalent binding. From the structure point of view, the majority type of the nucleophilic residues targeted by the inhibitors is cysteine in the ATP pocket. According to the relative positions, Zhang et al. gave a pioneering system that classified cysteines into four groups in the ATP pocket, and additional two groups in the gateway or the activation loop near the ATP pocket.[58a] The

representing crystal structures illustrate how the inhibitors target the cysteine in the different locations. (Figure 1.16)

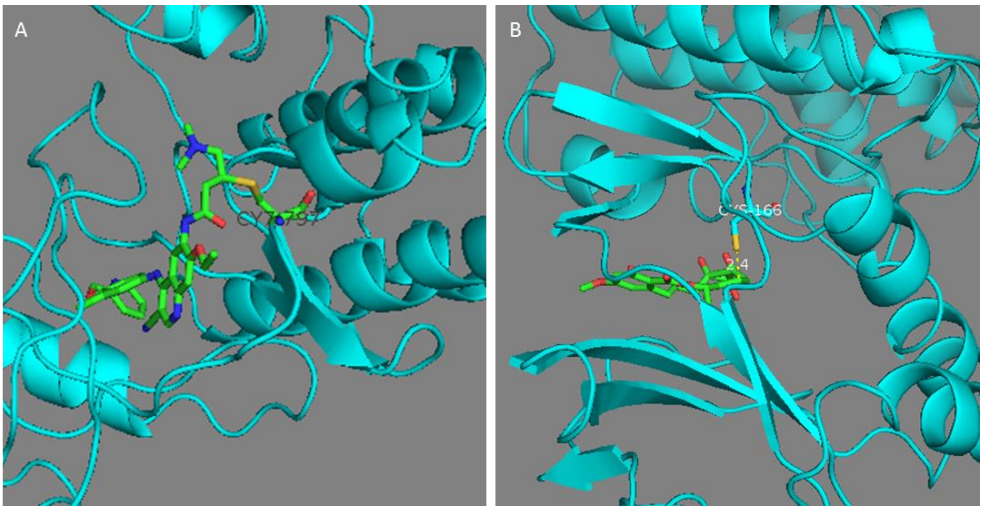

Figure 1.16 The representing modes of irreversible inhibition targeting the cysteine in the ATP pocket. **(A)** EGFR with HKI-272 (PDB ID: 2JIV) at Cys 797 in Group 3; **(B)** ERK with hypothemycin (PDB ID: 3W55) at Cys 166 in Group 4.

A number of electrophiles as ‘‘warheads’’ that can react with nucleophiles such as cysteine, lysine, or tyrosine within the active sites have been investigated in the design of irreversible kinase inhibitors. Michael addition reaction is widely utilized to achieve irreversible binding, which involves the typical functional groups: vinyl ketone (E6201),[60] vinyl sulfonates,[61] acrylamides (PCI-32765,[62] BIBW-2992,[63] EKB-569,[64] JNK-IN-8,[65] FIIN-1,[66] PF-00299804[67] and PD168393[68]), alkynyl amides (JH295)[69] and quinones[70]. There are also other functional groups which take place nucleophilic displacement or addition, including α-haloketones (**1-4**,[71] FMK,[72] **1-5**[73]), thiocyanates,[74] alkynes,[75] epoxides[76] and sulfonyl fluoride[77]. The representative irreversible inhibitors are shown in Figure 1.17.

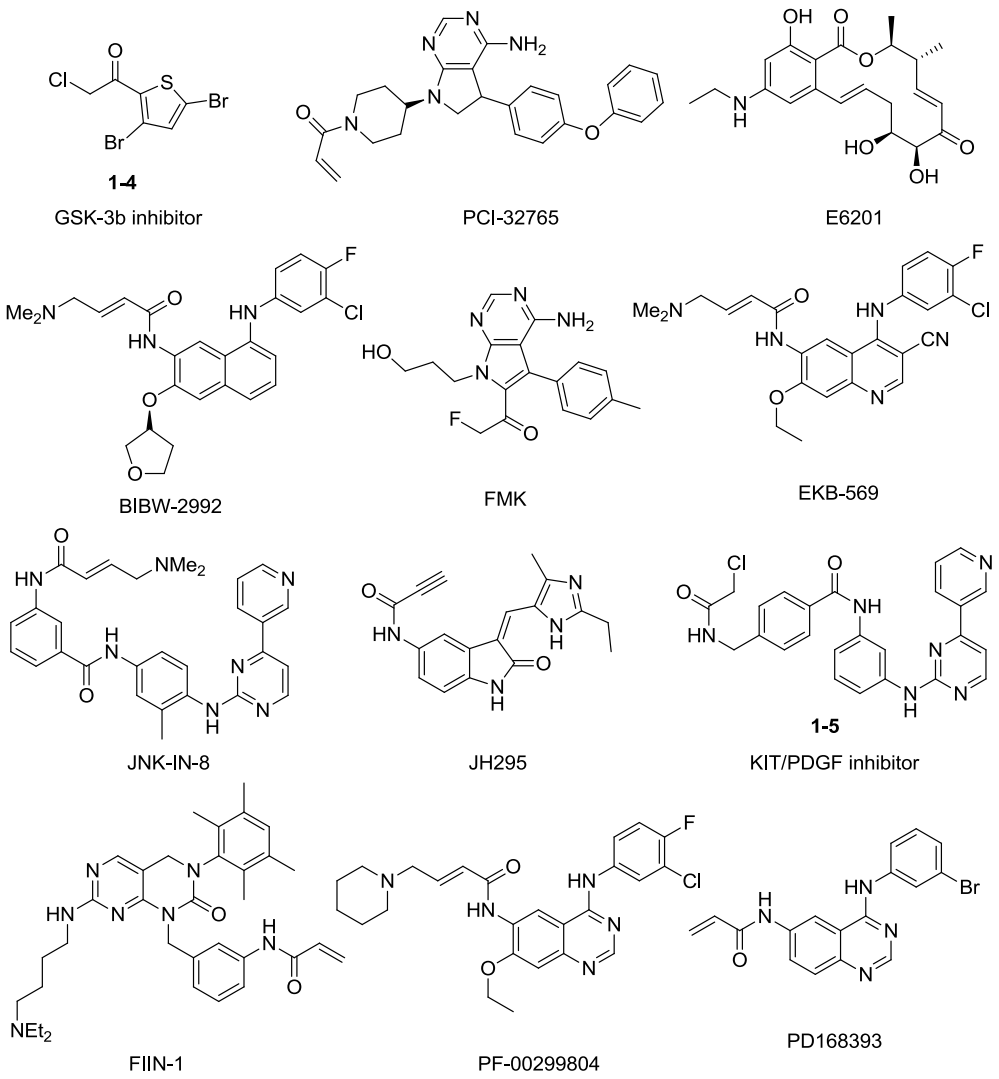

Figure 1.17 Structures of representative irreversible kinase inhibitors

In conclusion, although a dramatic development has been accomplished in the last decade, there're still some challenges including the inhibition mechanism of target and off-target, drug metabolic mechanism, drug-resistant of tumour and efficient biomarker for tumour.

1.3 Research Objective

Assigning the cellular targets of bioactive small molecules is still a big challenge in the drug discovery, including the unknown side effects of drugs. It is the aim of this thesis to develop a convenient chemical

proteomic method to unravel the global target spectrum for the bioactive small molecules, using a click-based in situ profiling approach. This method should enable the repertoire of drug-target interactions to be probed within living systems.

On the other hand, to study the interactions of kinase inhibitor with protein targets in the cancer cell, we also intend to develop a specific drug delivery targeting cancer cell together with the proteome profiling method.

Chapter 2

In situ Proteome Profiling of C75, a Covalent Bioactive Compound with Potential Anti-cancer Activities

Part of the chapter has been distilled and submitted for publication

2.1 Summary

This chapter describes a library of C75-based ABPs for investigate the cellular targets of C75 in cancer cell. C75, a covalent bioactive compound, has been particularly promising as a weight-loss and anti-cancer agent through its ability to modulate fatty acid oxidation. Various pathways have been found to be modulated by C75, including inhibition of fatty acid synthase (FASN) and activation of carnitine O-palmitoyltransferase-1 (CPT1). In the current study, we set out to identify unknown cellular targets (on and off) of C75 at its early stages of development as a potential therapeutic agent. A small library of eight activity-based probes (ABPs) was first designed from the C75 scaffold. One probe called **2-9g**, was shown to be active in live cancer cells, capable of covalent targeting of both known C75 targets including FASN and CPT-1A, as well as previously unknown targets including PDIA3, TFRC and GAPDH. Further studies could elucidate the mechanism of C75 binding against these newly identified targets.

2.2 Introduction

Despite recent success with the use of covalent drugs, for example, Orlistat (weight-loss), Clopidogrel (anti-platelet) and Esomeprazole (peptic ulcer), there remain significant safety concerns over the large-scale development of covalent-based therapeutics.[78] Besides the fear that in modifying proteins, such drugs could trigger an idiosyncratic immune response. Such concerns are in part attributed to the difficulty in establishing the spectrum of 'off-target' binding events which can cause many undesirable side-effects.[42b]

To address this problem, we have recently developed a convenient chemical proteomic method to unravel the global target spectrum for any given covalent drug, using a click-based in situ profiling approach.[6a, 45] This method enables the repertoire of drug-target interactions to be probed within living systems. By introducing a very conservative modification onto the lead molecule (namely, an alkyne

tag), at solvent accessible sites (to retain pharmacodynamic properties), observations can be reliably made to determine molecular behaviour and interactions within complex and dynamic cellular environments (Figure. 2.1).[42b]

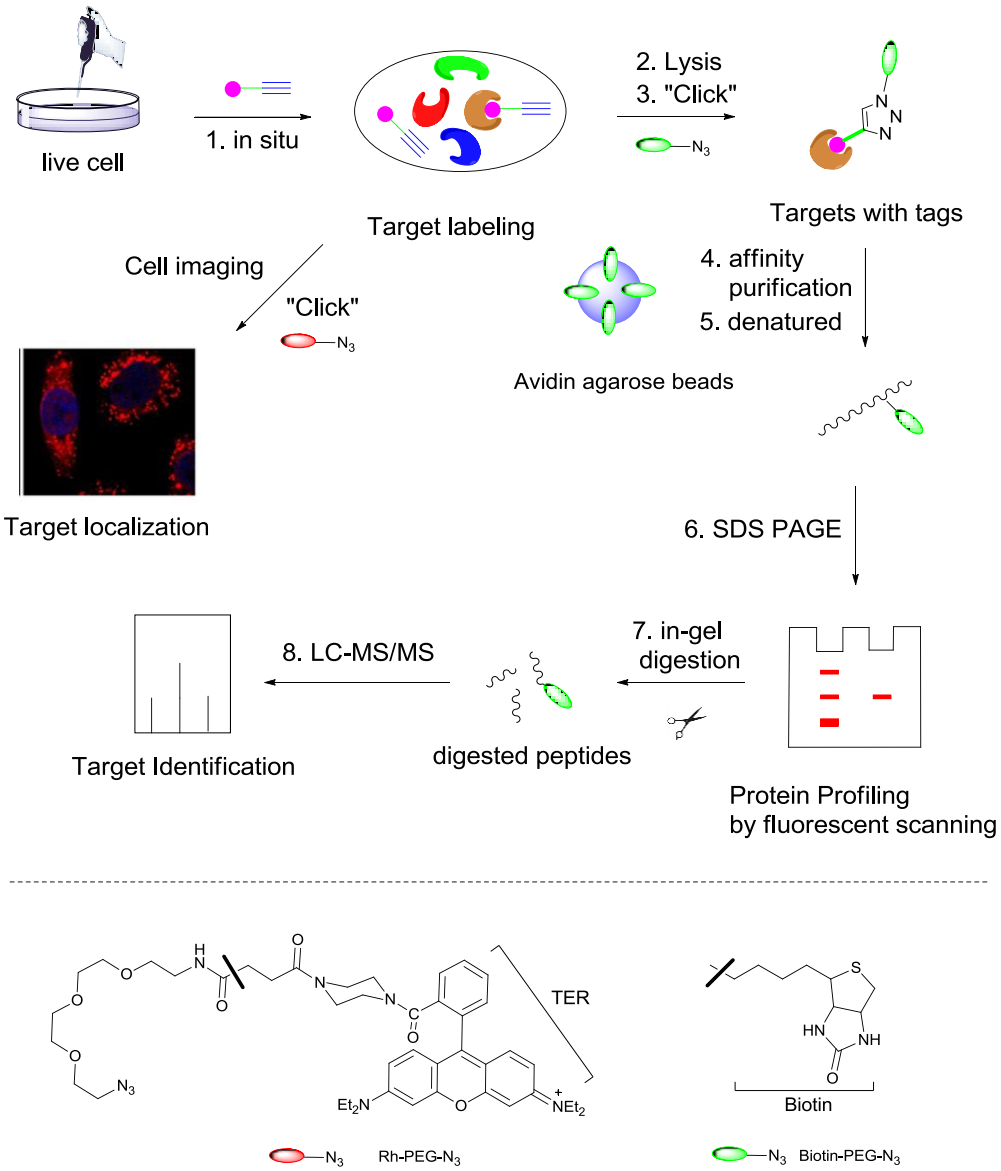

Figure 2.1 Flow chart of in situ proteome profiling. In the approach, after in situ labeling with "clickable" probe, the labeled proteins were clicked with reporters to facilitate the identification by fluorescent scanning and pull-down/LCMS analysis.

We had previously applied this strategy to successfully profile the on- and off- targets of Orlistat,[45] as well as those of various kinase inhibitors.[26, 36a] Here we extend the strategy by building a library of a covalent bioactive compound, C75, which has been particularly promising as a weight-loss and anti-cancer agent through its ability to modulate fatty acid oxidation.[79] C75 is a more stable synthetic mimic of cerulenin (a fungal metabolite), and belongs to a class of α-methylene-γ-butyrolactones.[79a, b] (Figure 2.2) Various pathways have been found to be modulated by C75, including inhibition of fatty acid synthase (FASN) and activation of carnitine *O*-palmitoyltransferase-1 (CPT1).[79c, d] The compound is also known to alter the level of neuropeptide Y and AMP-activated protein kinase (AMPK) activity in the hypothalamus, reducing food intake.[79d] Many common human cancers, including breast, ovarian, prostate and colon, express high levels of FASN. So decreased fatty acid production through FASN inhibition is seen as a viable anti-cancer strategy.[79a, b] Prior work using isotopic labeling and immunoprecipitation validated FASN as the cellular target of C75.[79b] In a separate study, a very similar butyrolactone scaffold was shown to bind histone acetyltransferase GCN5, with a weak IC_{50} of approximately 100 μM, highlighting that other proteins may have affinity to C75 as well.[80]

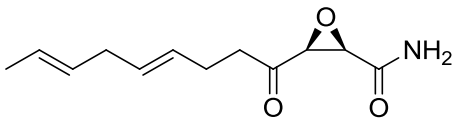

Cerulenin

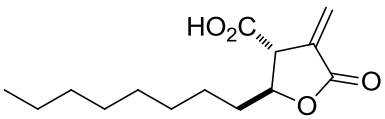

C75

Figure 2.2 Structures of Cerulenin and C75

To identify unknown cellular targets (on and off) of C75 at its early stages of development as a potential therapeutic agent, a small library of eight activity-based probes (ABPs) was first designed from the C75 scaffold. The 5-member-ring (4-methylene-2-octyl-5-oxo-tetrahydro-

furan-3-carboxylic acid) nucleophilic acceptor was retained as the pharmacophore, for binding to its respective targets. The linker lengths were varied between 2 and 10 carbon chains. The terminal alkyne as a ligation handle was introduced to the linker side chain. Compared to the tag-conjugated manner, the minimized modification was to avoid altering the drug activity and available for the *in situ* proteome profiling. (Figure 2.3)

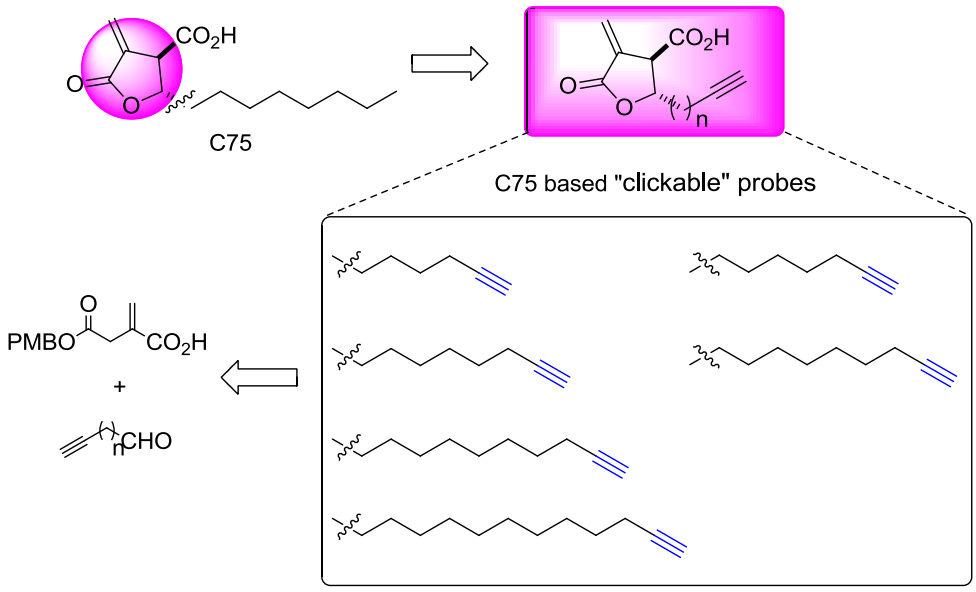

Figure 2.3 Synthetic plan of C75-based probes

2.3 Results and Discussion

2.3.1 Synthesis of C75-based Probes

To perform the following biological evaluation, the “clickable” probes based on C75 were established first. The synthesis of important fragment of alkynal **3** was outlined in Scheme 2.1. Bromocarboxylic acid **2-1d** (or **2-1e**, **2-1g**) was treated with lithium acetylide, which was prepared from trimethylsiliylacetylene with *n*-butyllithlium, to give the intermediate **2-2d** (or **2-2e**, **2-2g**). After deprotection of trimethylsiliyl group and subsequent reduction, alkynol **2-4d** (or **2-4e**, **2-4g**) was obtained. . 6-Bromohexanoic acid was treated with ethylide lithium to

give **2-6c**. Then **2-6b** (or **2-6c**, **2-6f**) was reduced with lithium aluminumhydride to give **2-4b** (or **2-4c**, **2-4f**). The final oxidation of alkynols **2-4a-g** in presence of PCC and sodium acetate proceeded smoothly to provide the smelly alkynals **2-5a-g**. Due to the high volatility, the purification of alkynals **2-5a-g** should be handled fast and carefully.

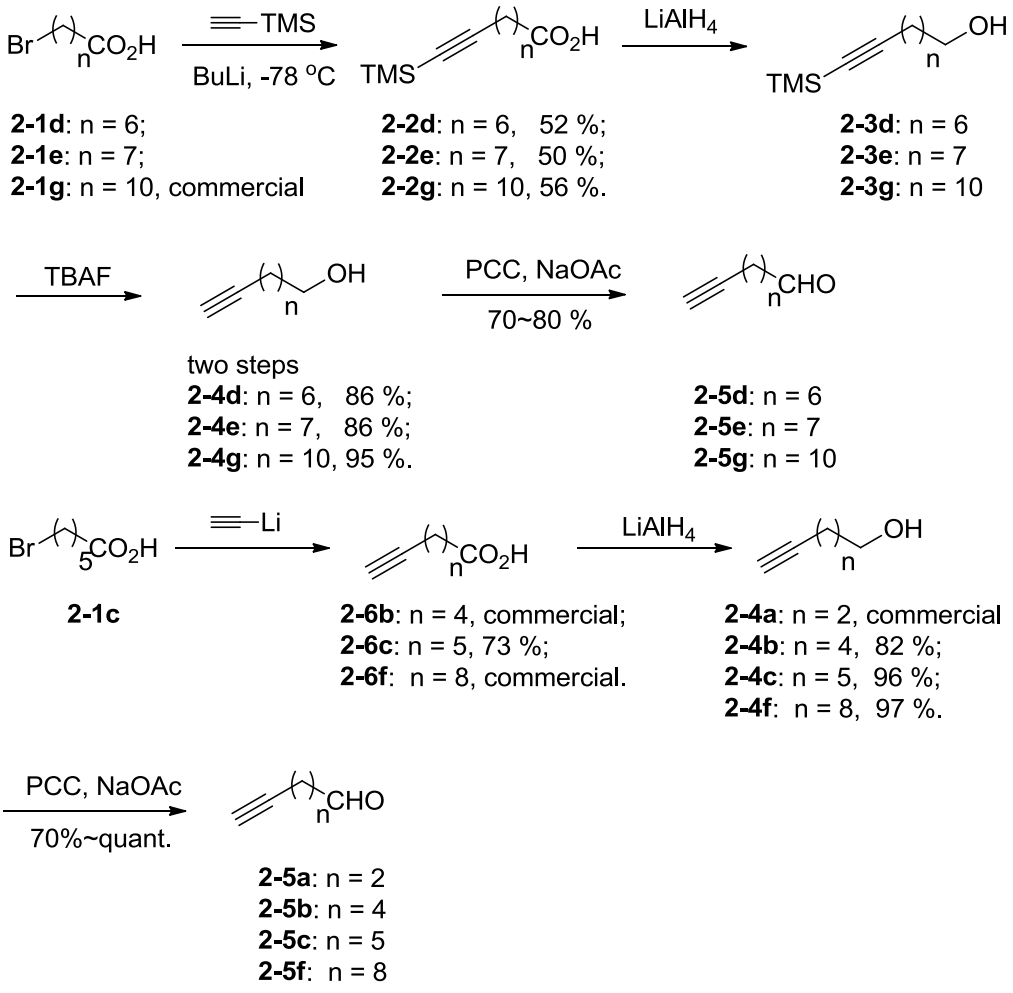

2-1d: n = 6;
2-1e: n = 7;
2-1g: n = 10, commercial

2-2d: n = 6, 52 %;
2-2e: n = 7, 50 %;
2-2g: n = 10, 56 %.

2-3d: n = 6
2-3e: n = 7
2-3g: n = 10

2-4d: n = 6, 86 %;
2-4e: n = 7, 86 %;
2-4g: n = 10, 95 %.

2-5d: n = 6
2-5e: n = 7
2-5g: n = 10

2-1c

2-6b: n = 4, commercial;
2-6c: n = 5, 73 %;
2-6f: n = 8, commercial.

2-4a: n = 2, commercial
2-4b: n = 4, 82 %;
2-4c: n = 5, 96 %;
2-4f: n = 8, 97 %.

2-5a: n = 2
2-5b: n = 4
2-5c: n = 5
2-5f: n = 8

Scheme 2.1 Synthesis of alkynal **2-5a-g**

With alkynals **2-5a-g** in hand, we pushed forward to the synthesis of C75-based probes **2-9a-g** as shown in Scheme 2.2. Itaconic anhydride reacted with 4-methoxybenzyl alcohol (PMB-OH) to give intermediate **2-7**. The cyclization of compound **2-7** with alkynals **2-5a-g** in presence

of LDA and subsequent acidification provided compounds **2-8a-g**, which were unstable in air at room temperature. The final deprotection of compounds **2-8a-g** with phenol at 60 ^{o}C provided the desired probes **2-9a-g**. (Scheme 2.2)

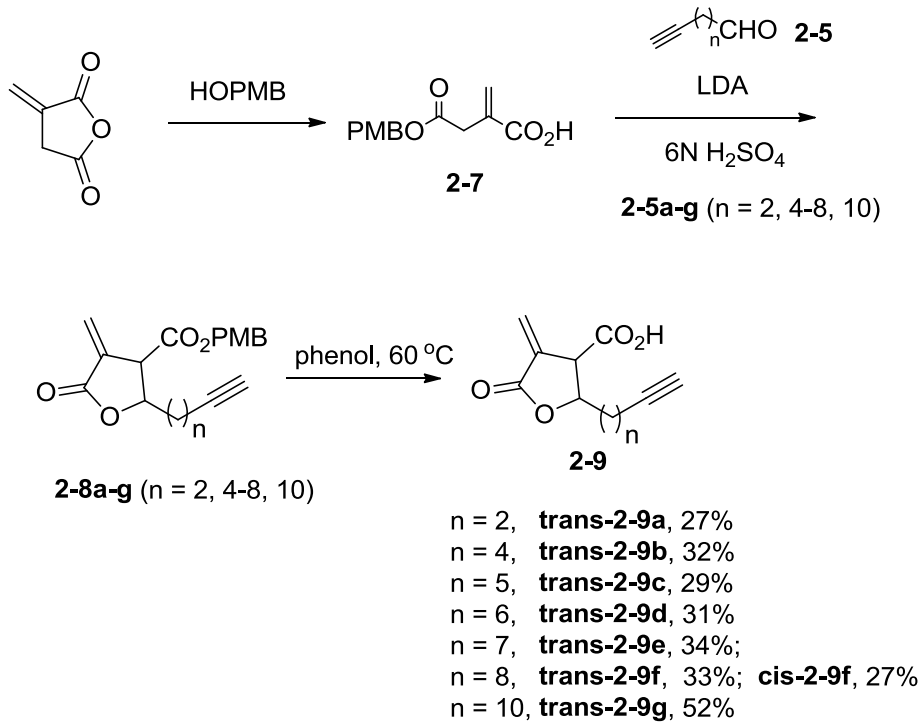

Scheme 2.2 Synthesis of **2-9a-g**

2.3.2 Design and Synthesis of Tri-functional Tag

Rhodamine B and Biotin are common tags which are widely used to label protein in azide-conjugated manner. (Figure 2.4) Azide group is partner of alkyne in Cu(I)-catalyzed Huisgen 1,3-dipolar cycloaddition reaction (Click chemistry). PEG is incorporated as a hydrophilic linker, which is compatible to physiological conditions. Rhodamine B as a fluorescent dye could be detected easily and inexpensively with instruments. Biotin binds to avidin (also streptavidin and neutravidin) very tightly as one of the strongest known protein-ligand interactions.

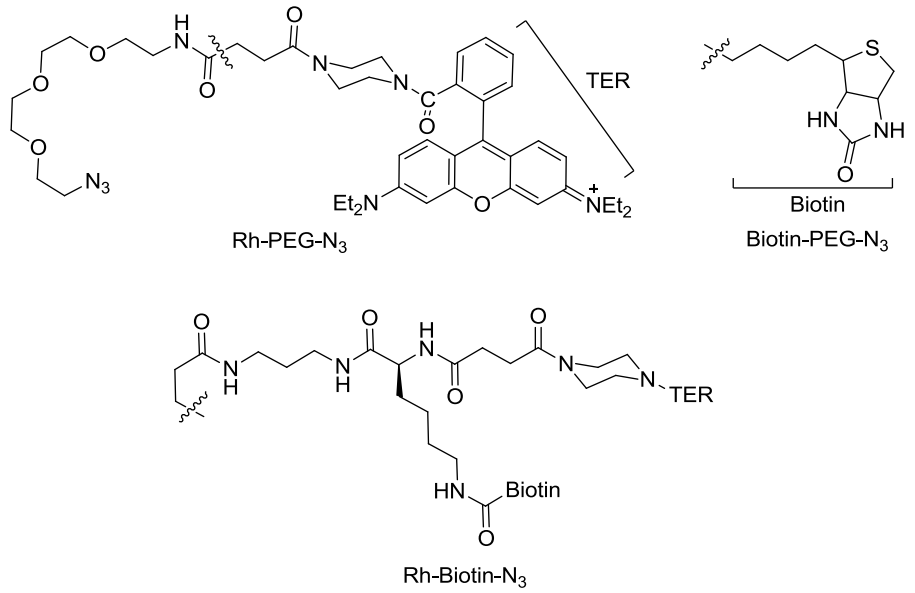

Figure 2.4 Structures of Rh-PEG-N_3, Biotin-PEG-N_3 and trifunctional tag Rh-Biotin-N_3

Although the two tags are used widely, it's not convenient to compare the results from fluorescent detection and pull-down experiment. Herein, we reported a trifunctional tag (Rh-Biotin-N_3), which could be used both for fluorescent detection and avidin affinity-based capture. Two tags Rhodamine and Biotin would be incorporated to azide group with proper linkers. The design would facilitate the sample preparation for fluorescent detection and affinity-based capture by biotin-avidin interaction. (Figure 2.4)

The synthetic route of trifunctional tag Rh-Biotin-N_3 was shown in Scheme 2.3. The PEG linker **2-14** was synthesized from **2-10** by four steps.[81] Biotin **2-15** was activated by NHS and then the resulted product **2-16** Biotin-NHS was coupled with deBoc version of Fmoc-Lys(Boc)-OH **2-17** to give lysine-biotin **2-18**.[82] Lysine-biotin **2-18** was coupled with mono-Boc protected 3-propanediamine **2-19**[52] to give compound **2-20**. Deprotection of compound **2-20** with 20 % piperidine and subsequent coupling with Rh-acid **2-21**,[83] provided product **2-22**. After Boc deprotection of compound **2-22**, the final amide coupling with PEG linker **2-14** provided the desired Rh-Biotin-N_3.

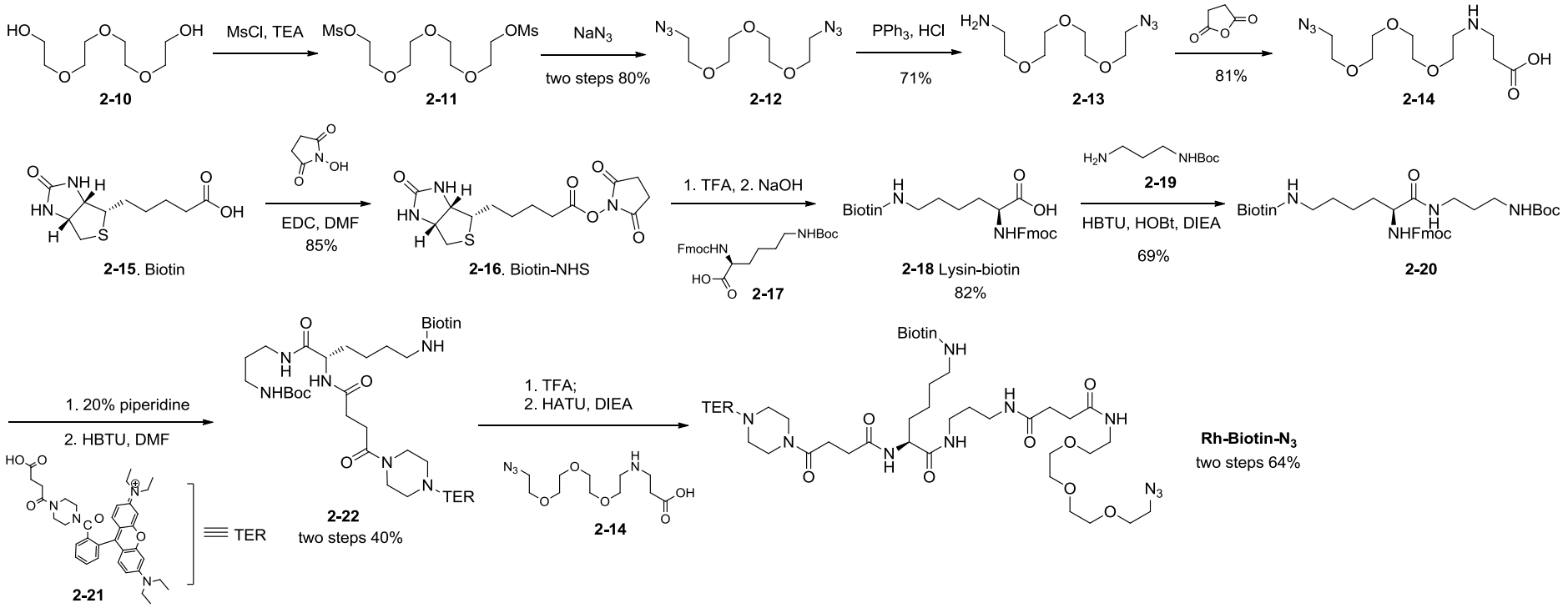

Scheme 2.3 The synthesis of trifunctional tag Rh-Biotin-N_3

2.3.3 Cell Anti-proliferation Assay and Proteome Profiling of HepG2 Cancer Cell with C75-based Probes

After the library of eight probes was established, anti-proliferation and proteome profiling were performed. Firstly, anti-proliferation assay was used to evaluate activities of C75 analogues at a concentration range of 0-100 μM against C75 (positive control) by XTT assay on HepG2 cell line (a human hepatocellular liver carcinoma cell line). (Figure 2.5) Compared to the parent drug C75, **2-9g** produced the best anti-proliferation activity amongst the various C75 analogs. The longer hydrophobic side chain in **2-9g** might have afforded better cell permeability of this compound, giving rise to its improved cellular activities. The stereoisomers of *trans*-**2-9f** and *cis*-**2-9f** did not show significant activity differences. Subsequently, **2-9g** was used for further biological studies.

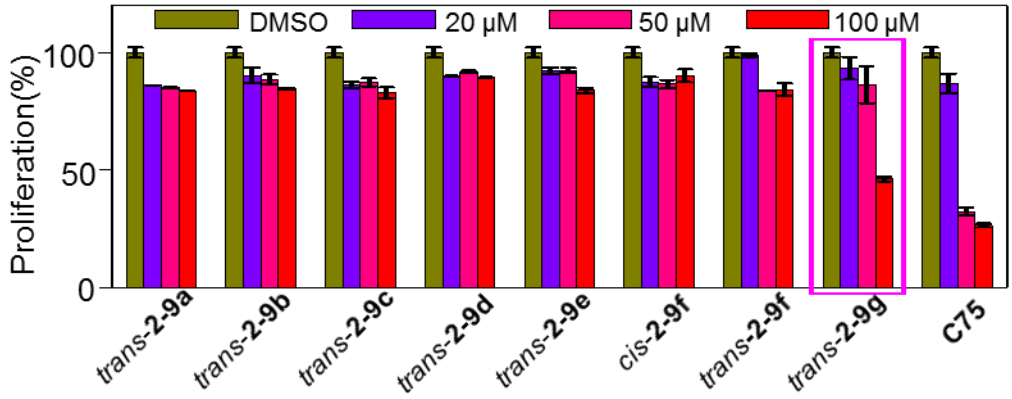

Figure 2.5 Dose dependent inhibition of HepG2 proliferation by C75 and its analogues **2-9a-g** (0, 20, 50, 100 μM) by XTT assay.

Next, *in vitro* and in situ labelling experiments were performed to test the proteome reactivity profiles of all probes (**2-9a-g**) by using mammalian cell lysates and live cells, respectively. To *in vitro* labeling experiment, the probes were first incubated at a concentration range of 5-20 μM with HepG2 cells lysates and clicked with the fluorescent reporter Rh-PEG-N_3. Then the tag-conjugated proteins were separated by SDS-PAGE gel, and analyzed by in-gel fluorescence scanning. Results from the in-gel fluorescence scanning showed that even 5 μM

of the probes were able to produce numerous significant fluorescent bands, in a dose-dependent manner. The labeled bands could be competed away by pre-treatment of C75, indicating that the corresponding labeled proteins were likely true cellular targets of C75. (Figure 2.6)

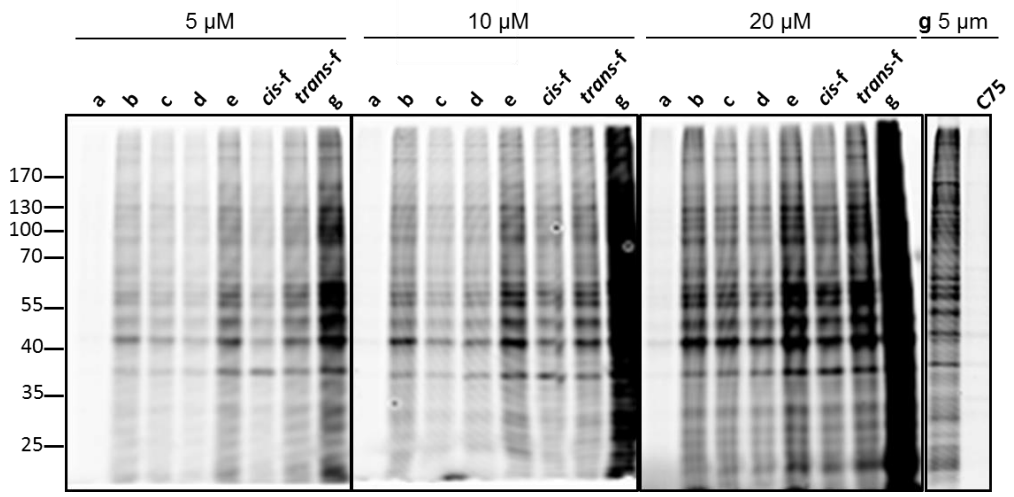

Figure 2.6 *in vitro* labeling of HepG2 proteomes with C75 based probes. The lysate was treated with **2-9a-g** (5, 10, 20 μM, here abbreviated as **a-g**) in presence or absence of C75 (25 μM).

Further the library was tested *in situ* at a higher 20 μM concentration with each of the **2-9a-g** analogs. The probes were first incubated with live HepG2 cancer cells, where its targets were labeled *in situ* covalently. After lysis, the labeled proteins were then clicked with and clicked with Rh-PEG-N_3. Then labeled proteins were subjected to subsequent analysis similar to previous *in vitro* proteome labeling. This provided a compartmentalized living system in which to test the binding activities of these scaffolds. The in-gel fluorescence scanning showed that probe **2-9g** remained the compound with the most intense proteome labelling profiles. (Figure 2.7)

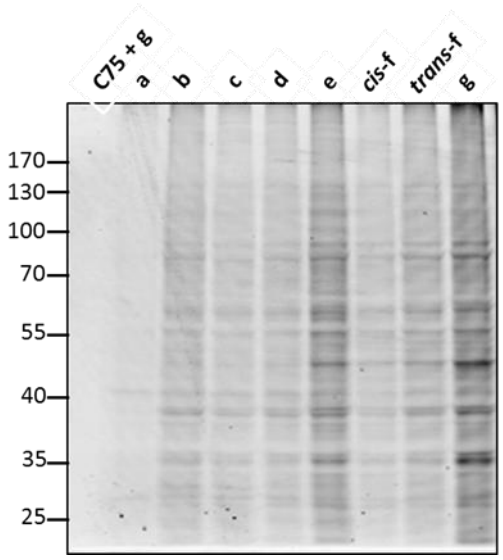

Figure 2.7 *In situ* labeling of HepG2 proteomes with C75 based probes. The lysate was treated with **2-9a-g** (20 μM, here abbreviated as **a-g**) with pretreatment in presence or absence of C75 (25 μM)

2.3.4 Target Identification and Validation

To positively identify some of the putative protein targets visualized on the gels, a large-scale pull-down experiment was performed. Live HepG2 cancer cells were incubated with the representative probe **2-9g**, where its targets were labeled *in situ* covalently. After lysis, the labeled proteins were then clicked with Rh-Biotin-N_3 under the same conditions as previous labeling experiment. Then the biotinylated proteins were captured by Avidin-immobilized agarose beads via affinity interaction, subsequently washed and eluted, the pulled-down samples were separated by SDS-PAGE. The separated proteins were transferred to PVDF membrane and analysed with Western Blotting by corresponding antibodies. The results unambiguously confirmed the existence of FASN and CPT1A, which were previously identified as targets of C75.[79] (Figure 2.8B) There results indicated that our newly develop "clickable" C75 analogues, e.g. **2-9g**, were indeed suitable small molecule probes for large scale, cell-based proteome profiling of potential targets of C75 in cancer cells.

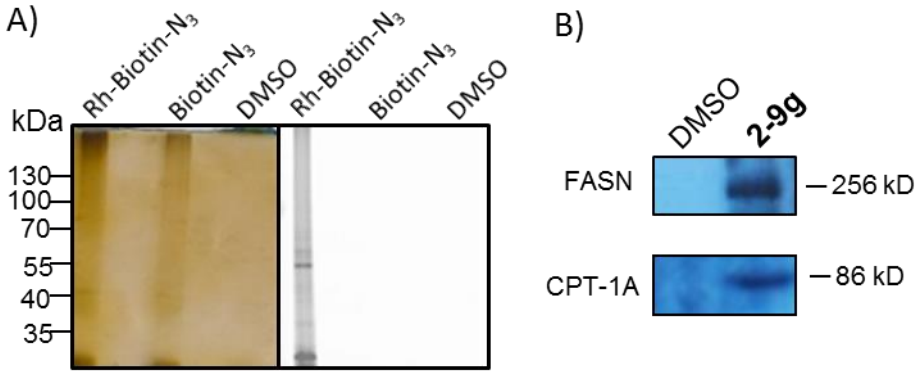

Figure 2.8 (A) *In situ* pull-down experiment treated with 20 μM of **2-9g**, clicked with Rh-Biotin-N_3 or Biotin-N_3. Silver stain (left), fluorescent scanning (right); (B) Validation of known targets of C75 by *in situ* pull-down experiment over HepG2 treated with DMSO (negative control) and **2-9g**.

After confirmation of the existence of interactions between C75 and know targets in live HepG2 cancer cell, we proceeded with pull-down/LCMS experiments to identify the putative cellular targets of C75. The same pulled-down samples were separated by SDS-PAGE and visualized with fluorescent scanning and silver stain. (Figure 2.8A) The entire gel lane for the pull-down sample was then cut into small particles and processed for in-gel trypsin digestion as standard procedure. As negative control, a large-scale proteomic experiment was also carried out with cells treated by DMSO instead of **2-9g**. The fragmented peptides were extracted from gel particles and subjected to LC-MS/MS analysis. Fragmentation analysis and database match searching was performed for protein identification against human protein database using an in-house MASCOT server. By the aid of the high-throughput technology (LC-MS/MS), the global information of the potential targets could be uncovered. A list of the hits, which was potential targets of C75, was generated. (Chapter 9 Appendix, Table S1)

We focused our attention on those candidates which possess known nucleophilic residues and play important roles in cancer cells (Figure 2.9A). FASN and CPT1A again emerged as top candidates on this list, as should be expected.[79a-c, 84] A number of lipid- and/or fatty-acid-metabolism-related proteins were also identified, including acyl-CoA dehydrogenase (ACADVL) and sterol O-acyltransferase (SOAT1).

Proteins possessing a cysteine active-site residue, including protein disulfide-isomerase A3 (PDIA3), glyceraldehyde-3-phosphate dehydrogenase (GAPDH), transferrin receptor protein 1 (TFRC), asparagine synthetase (ASNS), cytoskeleton-associated protein 4 (CKAP4), protein disulfide-isomerase (P4HB), thioredoxin reductase 1 (TXNRD1) and double-stranded RNA-specific adenosine deaminase (ADAR), were identified as potential C75 targets. Other proteins, including fructose-bisphosphatealdolase A (ALDOA), heat shock protein 90 β(HSP90AB2P), L-lactate dehydrogenase A chain (LDHA) and methyl crotonoyl-CoA carboxylase (MCCC1), were also identified as potential targets and they all contained an active-site lysine residue. Based on antibody availability, we validated several of these hits, including PDIA3, TFRC and GAPDH, by **2-9g** labelling/pull-down/ western blotting; all three proteins were positively labelled by **2-9g** and successfully pulled-down, indicating they are likely true cellular targets of C75 which had not been identified previously. (Figure 2.9B)

A)

Gene symbol	Localization	Protein function*
FASN	Cytoplasm	Fatty acid synthase
CPT1A	Mitochondria outter membrane	Carnitine O-palmitoyltransferase activity
PDIA3	ER	Catalyzing the rearrangement of -S-S bonds in proteins
TFRC	Cell membrane	Cellular uptake of iron
GAPDH	Cytoplasm Membrane Nucleus	glyceraldehyde-3-phosphate dehydrogenase and nitrosylase
ASNS	Cytosol	Asparagine biosynthesis
HSP90AB2P	Cytoplasm	Molecular chaperone.
ALDOA	Cytosol	Glycolysis
LDHA	Cytoplasm	Glycolysis
CKAP4	Membrane	Receptor for Surfactant protein-A
MCCC1	Mitochondrion	Catalyzing carboxylation of 3-methylcrotonyl-CoA to 3-methylglutaconyl-CoA
ACADVL	Mitochondrion inner membrane	acyl-CoA dehydrogenases
TXNRD1	ER membrane	Formation of cell membrane protrusions
SOAT1	Nucleus	Catalyzing the formation of fatty acid-cholesterol esters
P4HB	Cell membrane ER membrane	Catalyzing the formation, breakage and rearrangement of disulfide bond
ADAR	Cytoplasm	Double stranded RNA specific adenosine deaminase

B)

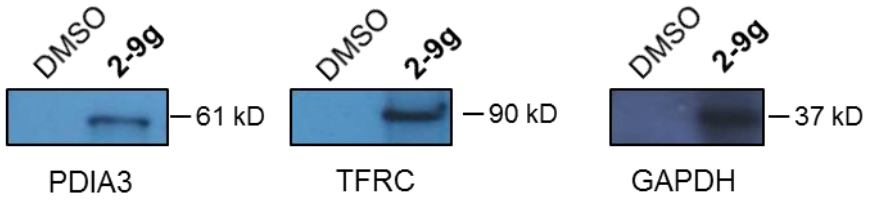

Figure 2.9 (A) Proteins identified by pull-down and subsequent mass spectrometry; **B**) Western Blotting validation of pull-down experiment with DMSO (DMSO-treated cell proteome as negative control, left) and **2-9g** (20 μM, right).

2.3.5 Target Localization by Cell Fluorescent Imaging

Finally, our probes could also be used as small molecular imaging probe to assess the cellular uptake of C75 and detect its cellular localization. To do this, the probe **2-9g** was selected as a representative example. Live HepG2 cancer cell was incubated with **2-9g** for 2 h, fixed with 3.7% formaldehyde, permeabilized with Triton X-

100 and then clicked with Rh-PEG-N_3 *in situ*. The fluorescent imaging experiment was performed to visualize the distribution of targets of the probe in the cell. Compared with the nucleus visualized by the blue fluorescence (Hoechst as a commercial available nucleus tracker), the red fluorescence (Rhodamine B) showed most of the targets of **2-9g** were located in cytosol, indicating this is where most of C75's cellular target reside. (Figure. 2.10)

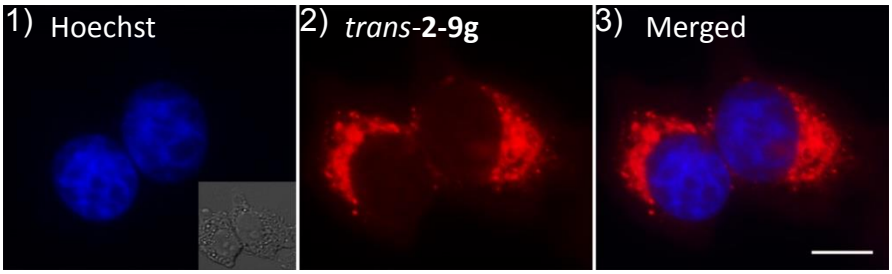

Figure 2.10 Fluorescence imaging of HepG2 cell probed with probe **2-9g** (20 μM). HepG2 cell was incubated with probe for 2 h and click with Rh-PEG-N_3 (Rodamine B channel, colored in red); the cell was stained with Nucleus tracker (Hoechst, colored in blue). Bright filed images (DIC) of the corresponding cells were shown. Overlay of probe and nucleus channels were shown Merged. Scale bar = 20 μm.

2.4 Conclusion

In conclusion, we have successfully designed and synthesized a library of C75 analogues with linker lengths varied between 2 and 10 carbon chains. As ABPs derived from C75, 5-member-ring (4-methylene-2-octyl-5-oxo-tetrahydro-furan-3-carboxylic acid) nucleophilic acceptor was retained as the pharmacophore, for binding to its respective targets and the terminal alkyne as a ligation handle was introduced to the linker side chain. The probes are suitable for the *in situ* proteome profiling for the minimal modification design. The known targets including FASN, CPT-1A were validated and other new potential targets including PDIA3, TFRC and GAPDH were identified by ABPPs approach including proteome profiling, labeled protein enrichment, LC-MS/MS analysis and validation. The cell-peneatrating probe **2-9g** as a representative sample has been explored in the

fluorescent imaging experiment to monitor the activity and localization of the cellular drug targets *in situ*. Therefore, the structure-effect relationship of C75 over cancer cell could give useful implications to design more efficient anti-tumor agent. Further study will enable extensive study of drug discovery based on the proteome results by *in situ* living cell profile, such as potential pharmacological effect, pharmacokinetic effects including absorption, distribution, even metabolism and excretion.

Chapter 3

Staurosporine-directed Labeling of Kinase and Specific Labeling of PDI in Live Cancer Cell with Chemically Tuned Electrophiles

Part of the chapter has been distilled and submitted for publication

3.1. Summary

In this chapter, we describe a new approach to design irreversible inhibitors of protein kinase from a general inhibitor—Staurosporine (STS). Three “clickable” probes based on STS have been successfully synthesized by introducing different electrophiles (chloroacetamide, sulfonate ester and acrylamide). This new STS-tagging configuration has minimized non-specific labeling, by preferentially gearing selectivity towards a range of kinases (or the so-called kinase cysteinome), which possess potentially targetable cysteine residues near the ATP-binding pocket of the enzyme. In the biological test, it was found that the inhibitor could irreversibly label protein kinases c-Src *in vitro*. By the ABPP approach, large scaled *in situ* and *in vitro* pull-down in cancer cell and subsequent LC-MS/MS analysis showed **STS-C1** could label 31 kinases *in vitro* (cell lysate) and 8 kinases in live cancer cell. Imaging experiment showed the probe was cell-permeable and predominantly cytosolic in HepG2 cells. On the other hand, by *in situ* proteome profiling and pull-down/WB validation, human PDI was identified as the major cellular target of **STS-T1** in the live cancer cell MCF-7.

3.2. Introduction

The brief introduction of kinase and kinase inhibitors was summarized in Chapter 1. Although small molecule inhibitor is rising as a hotspot to regulate the activity of kinase, it is still a big challenge in the drug discovery today.[58a] Only 25 small molecules were approved as kinase inhibitors by FDA (Food and Drug Administration, USA) until mid-2013.[58e] Compared the large number of disease-associated kinases with the limited successful instances, discovery of more specific kinase inhibitor drugs to the according kinases is becoming urgent now.

Most small molecule kinase inhibitors suffer from broad reactivities. For example, it was reported that the reversible drug—Dasitinib may

have many off-targets including dozen of kinases.[37] The highly conserved sequence of ATP-binding pocket and large number of kinases (500+) made it difficult to screen out kinase inhibitors, especially for reversible manner. Additionally, the interactions between the inhibitor and kinase were interfered by many nucleotide analogs such as ATP/ADP/AMP and etc, and a great number of nucleotide-pocket-holding proteins distributed ubiquitously in the cell.[2, 59] Therefore, it remains a challenge to design therapeutics that are able to specifically target the disease-causing kinase, and thus minimize toxicity and undesirable side effects. One proven strategy to enhance the selectivity of kinases inhibitors is through the development of novel kinase-targeting small molecule probes capable of interrogating endogenous kinase-drug interactions in an *in vivo* setting.[72]

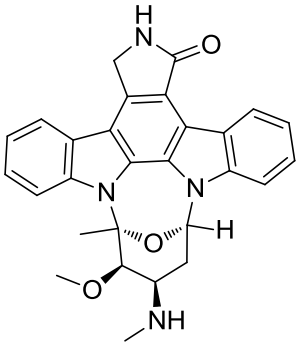

Figure 3.1 Structure of Staurosporine (STS)

Staurosporine (STS) is a natural product alkaloid isolated from *Streptomyces staurosporeus*, and is the most potent broad spectrum kinase inhibitor known.[19c, 85] (Figure 3.1) It has been applied as a tool to study the binding and inhibition spectrums of various kinases. Of the approximately 518 kinases in humans, a sizeable number (at least 253) are inhibited by staurosporine.[19c, 85] We and others have sought to modify and develop probes from STS, to better profile and understand its binding spectrum of kinases in vivo.[37, 86] In previous examples, other groups have developed biotin tagged STS,[86] which is too bulky and not cell permeable. We have separately designed cell-permeable diazirine-containing STS probes capable of large-scale kinase profiling experiments in live mammalian cells.[26, 37] Due to need to introduce a

photo-reactive diazirine moiety into such probes, they have intrinsically strong background labeling toward high-abundance endogenous proteins.

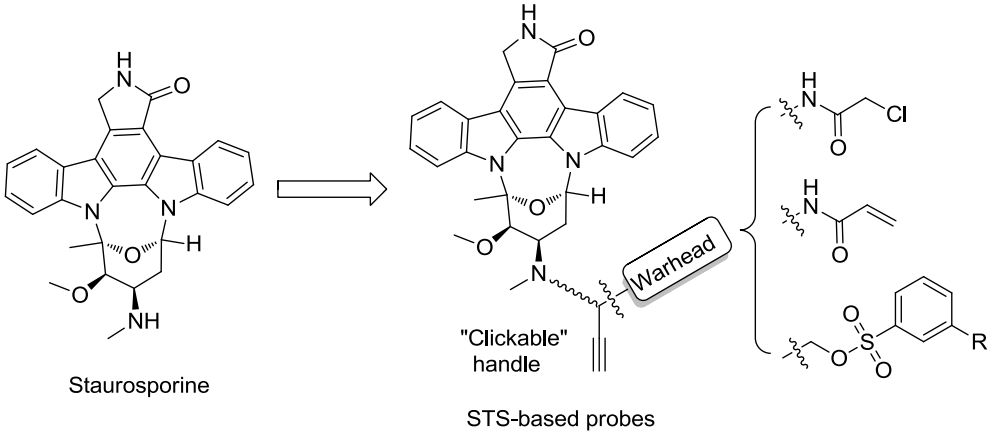

Figure 3.2 Proposed "clickable" STS-based probes

Herein, we report a method to convert STS into an irreversible covalent kinase probe by incorporation of electrophilic warheads (chloroacetamide, acrylamide and sulfonate ester) into STS (Figure 3.2). The modification commenced at the secondary amine of STS (a position previously shown to be highly tolerant to structural changes[87]) with a small handle containing the warhead and a terminal alkyne. The subtle modification was aimed to retain its biological function and activity in live cells. The design of the probe would enable *in vitro* and *in situ* proteome profiling for the convenience of investigation of the interactions between the probe and its targets.(Figure 3.3) We hypothesized that this new STS-tagging configuration may minimize non-specific labeling observed in previously developed STS probes,[26, 37, 86] by preferentially gearing selectivity towards a range of kinases (or the so-called kinase cysteinome[56b]), which possess potentially targetable cysteine residues near the ATP-binding pocket of the enzyme. In so doing, such a strategy could prove useful in lead development, and tune potencies of kinase inhibitors (i.e. enhance on- and minimize off-target interactions).

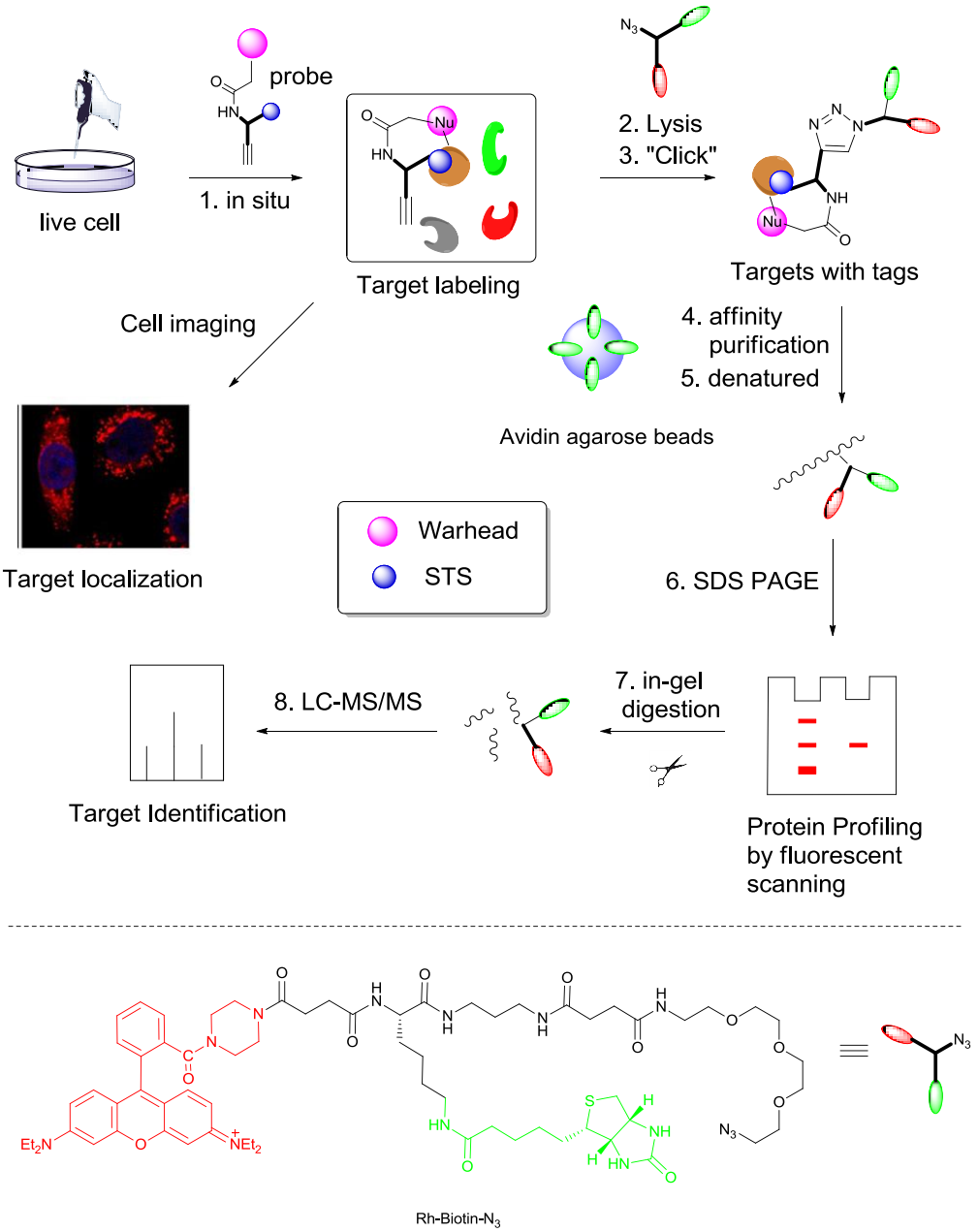

Figure 3.3 The flow chart of *in situ* proteome profiling strategy with Staurosporine derived probes. After the probe was incubated with live cell, the labelled protein was clicked with azide-conjugated tags and purified by Avidin-biotin binding. The pulled-down sample was subjected to SDS-PAGE/digestion/LCMS for the target identification.

3.3. Results and Discussion

3.3.1. The Synthesis of STS-derived Probes

Three STS derived probes have been synthesized successfully by introduction of different electrophiles together with terminal alkyne to STS, which would be described in details subsequently.

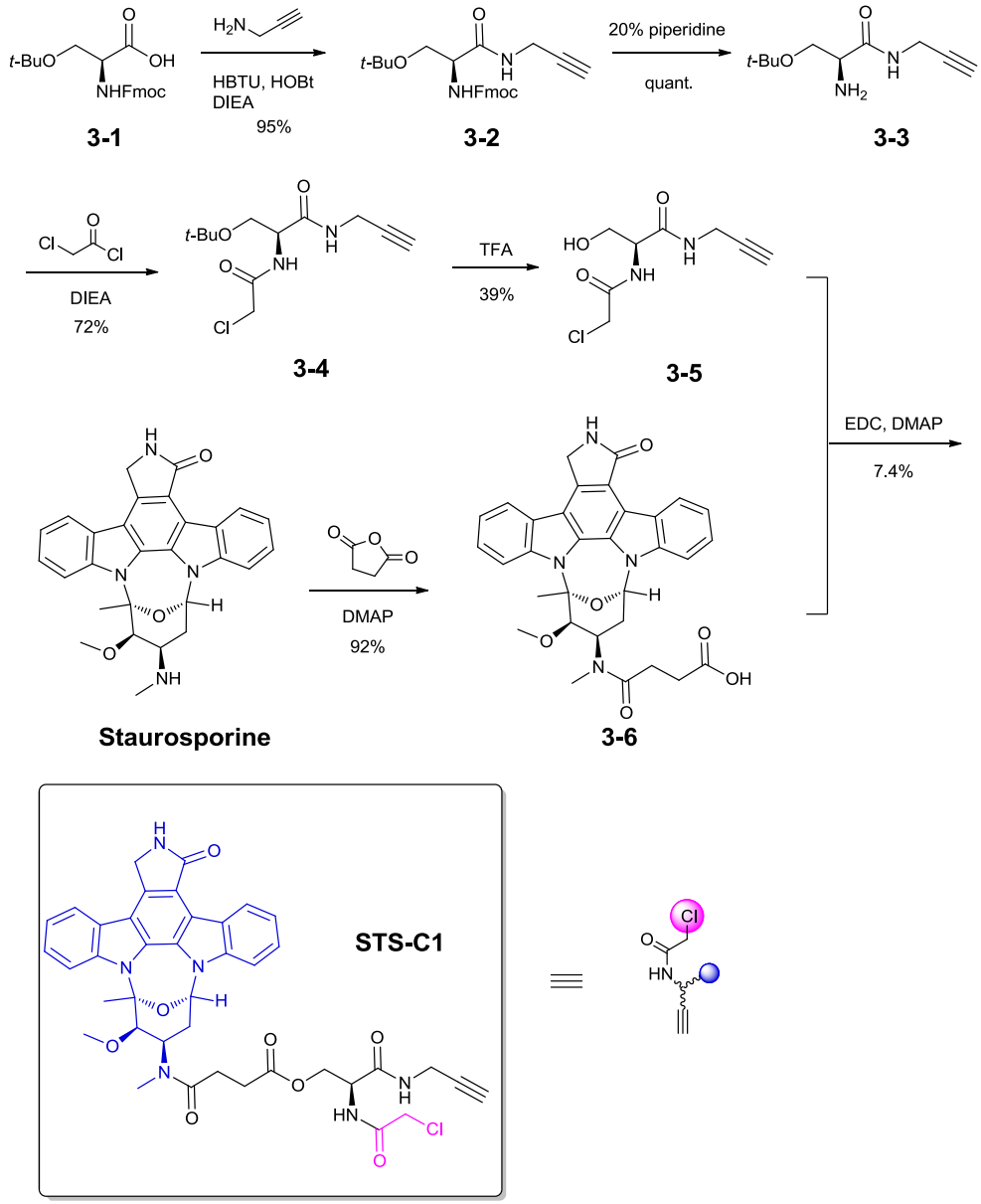

Scheme 3.1 Synthesis of **STS-C1**

The synthesis of probe **STS-C1** was outlined in Scheme 3.1. Fmoc-O-*tert*-Butyl-L-serine was coupled with propargylamine to give compound **3-2**. After deprotection of Fmoc group, the resulted compound **3-3** was reacted with 2-chloroacetyl chloride to give compound **3-4**. The intermediate **3-4** was treated with TFA for deprotection of t-butyl group to give compound **3-5**. STS was treated with succinic anhydride to provide the key intermediate **3-6**, which was subjected to coupling with compound **3-5** to afford the desired probe **STS-C1**. In the solution phase synthesis of chloroacetamide-containing probe, the functional group shows highly reactivity to the free amine. So the scaffold was changed from lysine to serine.

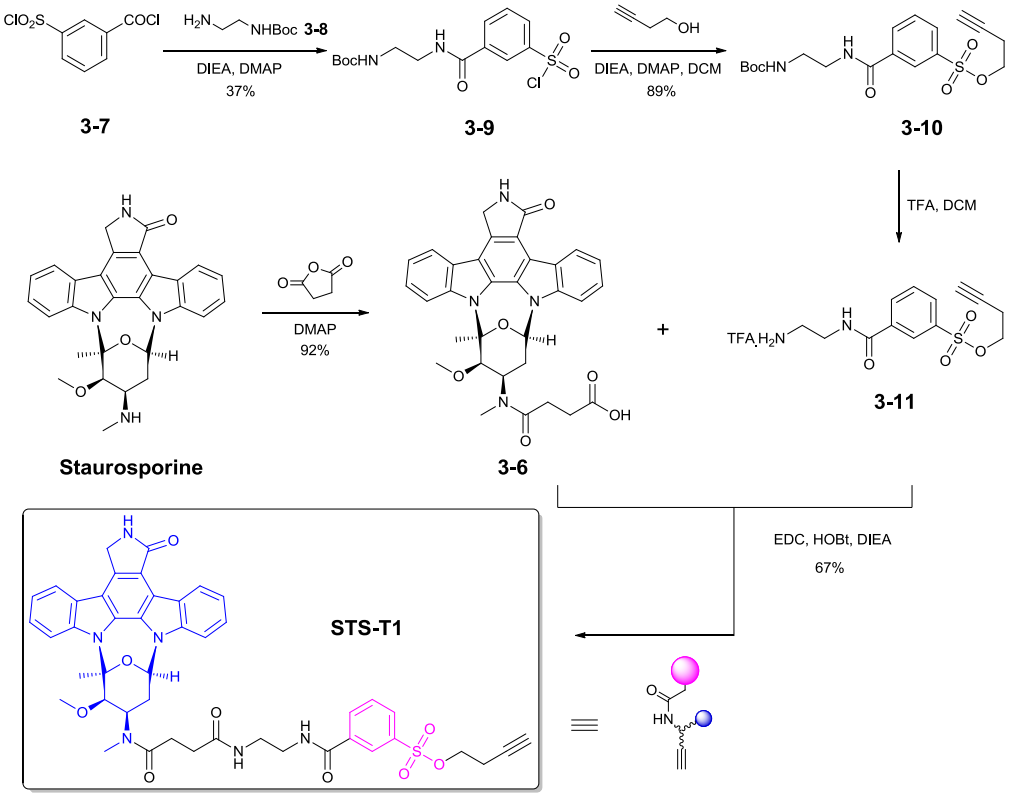

Scheme 3.2 Synthesis of **STS-T1**

The synthesis of probe **STS-T1** was outlined in Scheme 3.2. Benzoyl chloride **3-7** was reacted with *N*-Boc-ethylenediamine **3-8** to give sulfonyl chloride **3-9**, which was reacted with but-3-yn-1-ol to afford sulfonate ester **3-10**. After Boc-deproteciton with TFA, the

resulted amine **3-11** was coupled with intermediate **3-6** to give the desired product **STS-T1**.

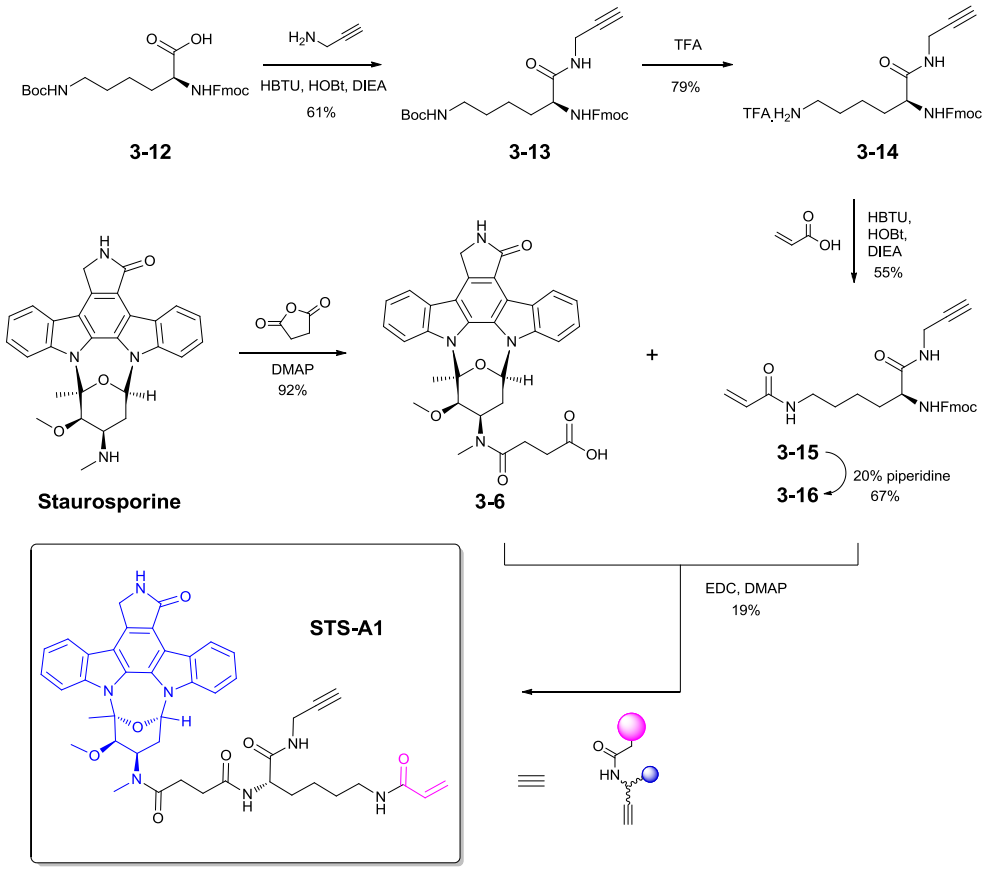

Scheme 3.3 Synthesis of **STS-A1**

The synthesis of probe **STS-A1** was outlined in Scheme 3.3. Fmoc-D-Lys (Boc)-OH **3-12** was coupled with propargyl amine to give compound **3-13**. Then deprotection of Boc of compound **3-13** with TFA to obtain compound **3-14**, which was coupled with acyl acid to give compound **3-14**. After removal of Fmoc with piperidine, compound **3-14** was coupled with compound **3-6** to give product **STS-A1**.

3.3.2. Preliminary biological activities screening with STS-derived probes

It was hypothesized that the newly synthesized STS-derived probes targeted the ATP-pocket-holding proteins (especially kinases). In order to evaluate reactivity of the probes, we carried out screening in live cancer cells including HepG2, MCF-7, MDA-MB-231 and T47D by the well-established proteome profiling approach. (Figure 3.4) In *in situ* labelling experiment, it was found that several representatives possessed interesting *in situ* proteome reactivity profiles. **STS-C1** showed distinct and strong labeling signals over four cancer cell lines. **STS-T1** showed strong and unique band over T47D, MDA-MB-231 and MCF-7, which potentially indicated the major target of **STS-T1** in the live cancer lines.

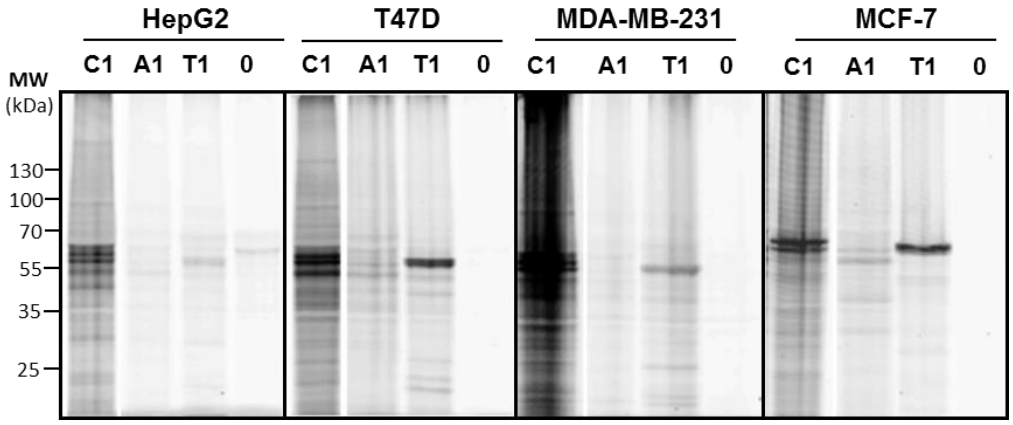

Figure 3.4 *In situ* proteome reactivity profiles of various electrophilic probes in live cancer cells (5 μM: T1, A1; 1 μM: C1) for 2 h. Then Cancer cells were lysed and clicked with Rh-PEG-N_3, separated by SDS-PAGE gels followed by in-gel fluorescence scanning (FL)

Many protein kinases, including c-Src, have potentially reactive cysteine residues near their ATP-binding pockets.[88] In the current study, we chose c-Src as one of our intended targets due to its obvious biological importance. In addition, few irreversible inhibitors of c-Src are known. One very recent report, however, has already indicated that it is possible to irreversibly target Cys277 (a residue near the ATP pocket of c-Src) by using an aminopyrazole based kinase inhibitor decorated with a suitable electrophilic moiety.[61] To test the labeling of STS derived probes against desired targets — protein kinases *in vitro*, five recombinant kinases including c-Src were selected. (Figure 3.5) The

proteins were incubated with the probes, followed by the formation of covalent bond. The stable probe-protein complex was ready for click reaction with Rh-Biotin-N_3 and then detected by in-gel fluorescence scanning. The labeling test showed **STS-C1** and **STS-A1** strongly labeled c-Src compared to other kinases. The results directed the following investigation.

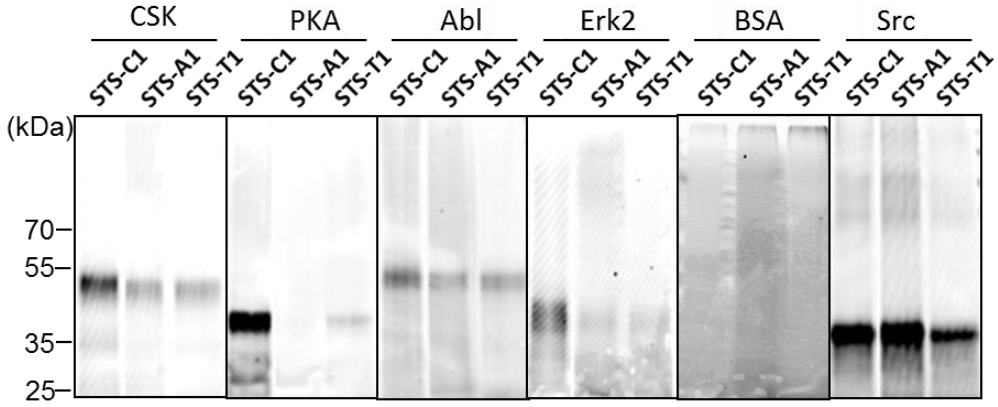

Figure 3.5 In vitro labeling of recombinant protein kinases (CSK, PKA, Abl, Erk2, Src) and BSA (as a negative control) with **STS-C1** **STS-A1** and **STS-T1** (1 μM). The intensity of Src was reduced. PMT of others was normal (600).

3.3.3. **STS-C1** targeting kinases *in vitro* and in live cell

Based on the preliminary screening results, **STS-C1** showed the possibility to target the kinase cysteinome including c-Src. Following experiments would be performed to evaluate the selectivity of the probe and in-vivo labeling reactivity. By the proteome profiling approach, the cellular targets of **STS-C1** could be identified comprehensively.

Molecule modeling and IC_{50} assay against c-Src

We performed docking experiments to guide the design of linker size and configuration in **STS-C1**. The binding mode of **STS-C1** with c-Src was simulated by molecular docking with AutoDock Vina (Figure 3.6).[89] After the probe **STS-C1** was docked into the ATP pocket of c-Src (PDB code: 3F6X),[61] Cys277 in c-Src was found to be located ~5.2

Å from the chloroacetamide moiety of **STS-C1**. In addition, the alkyne handle of **STS-C1** in the docked complex was shown to project toward the protein surface, thus making it accessible for subsequent click conjugation. The result showed the importance of the affinity-driven induction by STS core.

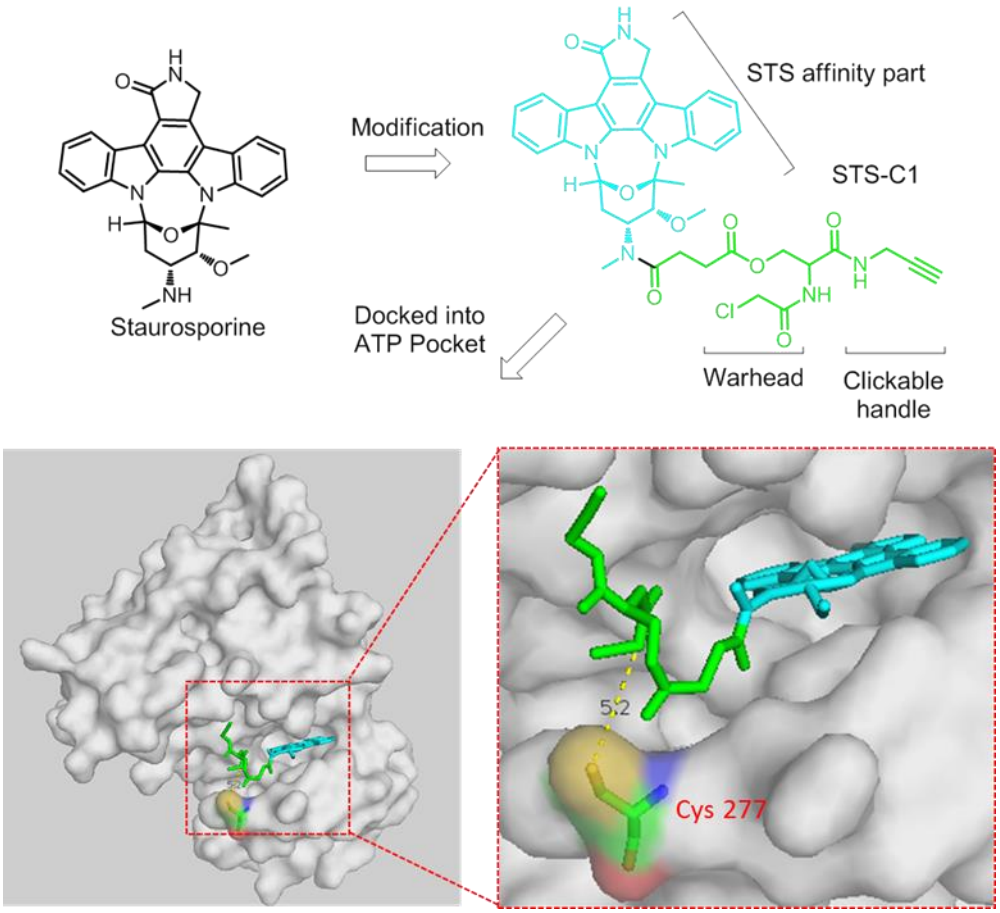

Figure 3.6 Docking of **STS-C1** into the ATP pocket of *c*-Src (PDB code: 3F6X), Cys 277 near to the warhead of the probe

IC_{50} assay against c-Src

To establish inhibition profiles of **STS-C1** against kinases, enzyme activity assays were tested. Compared to STS, the IC_{50} of **STS-C1** against recombinant c-Src in an *in vitro* kinase inhibition assay was approximately 2-fold lower. Interestingly, a 4-fold increase in IC_{50} value was observed for **STS-C1** against PKA (also a known target of STS). This suggests that while introduction of linker moiety in STS in general

negates the kinase/inhibitor interaction,[26] suitable positioning of the electrophilic moiety near Cys277 in c-Src actually promote such interactions, presumably via the formation of an irreversible covalent complex. (Figure 3.7)

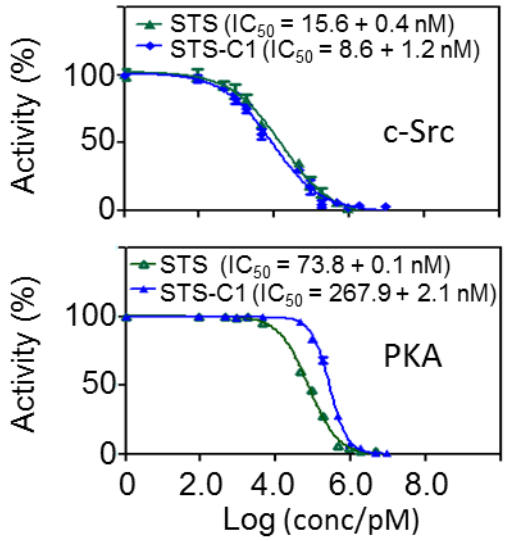

Figure 3.7 IC_{50} value of **STS-C1** against recombinant PKA and c-Src.

In vitro labeling of purified kinases

We next tested the covalent labeling of **STS-C1** against recombinantly purified proteins including BSA (not a kinase) and several kinases (ERK2, CSK, Abl, PKA and c-Src). As shown in Figure. 3.8, only c-Src was prominently labeled. Interestingly, even PKA was not positively labeled by **STS-C1** despite a relative potent inhibition (e.g. IC_{50} = 267.9 + 2.1 nM). This clearly showed that in order for the probe to covalently label the target protein, a proximal reactive cysteine residue, e.g. Cys277 in c-Src, is essential. We also compared the labeling profile of **STS-C1** with that of our previous developed photo-reactive probe **STS-2**.[26] The results further confirmed that these profiles are indeed distinctly different.

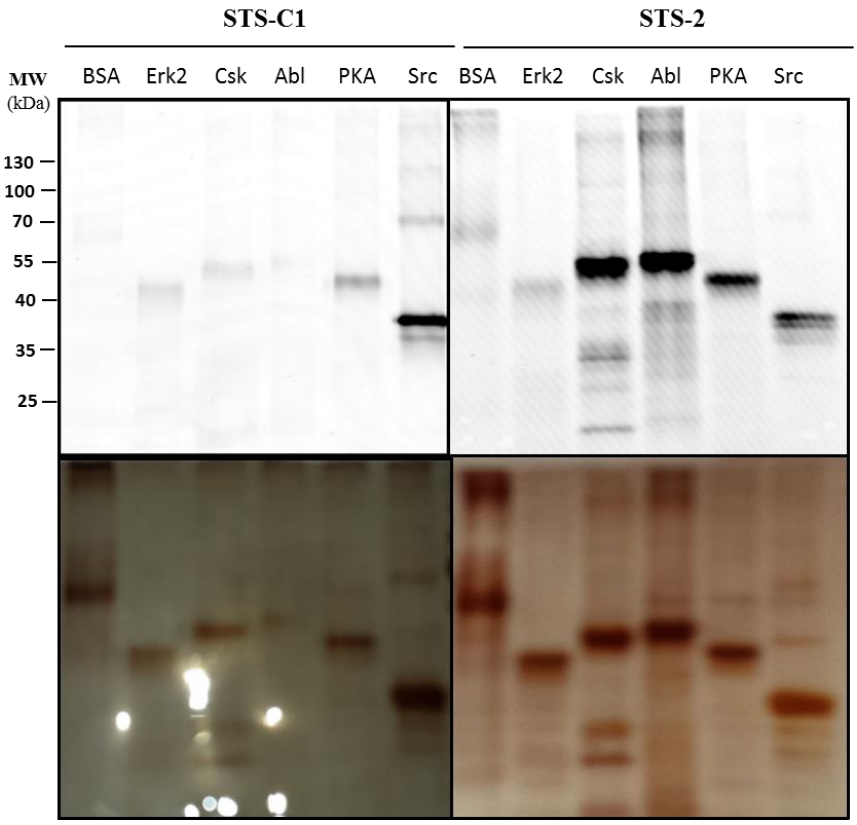

Figure 3.8 *In vitro* labeling of recombinant protein kinases and BSA with (A) **STS-C1** (200 nM) and **STS-2** (1 μM).

In vitro labeling of Bacterial proteome overexpressed c-Src

We next performed labeling of c-Src in a more complex environment by using bacterial lysates that overexpress c-Src (Figure 3.9); with different amounts of **STS-C1** (0 to 200 nM) being used to label 20 μg (each lane) of the lysates, it was observed that selective c-Src labeling could be readily detected with as little as 10 nM of the probe. (Figure 3.9A) In a separate experiment with 200 nM of **STS-C1**, c-Src labeling was clearly detected in as little as 1 μg of the bacterial lysate, indicating a good detection sensitivity of the probe. (Figure 3.9B) Competitive labeling experiment was also carried to confirm the covalent labeling of c-Src by **STS-C1** was activity-based (Figure.3.9C); the presence of excessive STS (2 μM; 10x of **STS-C1**) was able to significantly attenuate c-Src labeling.

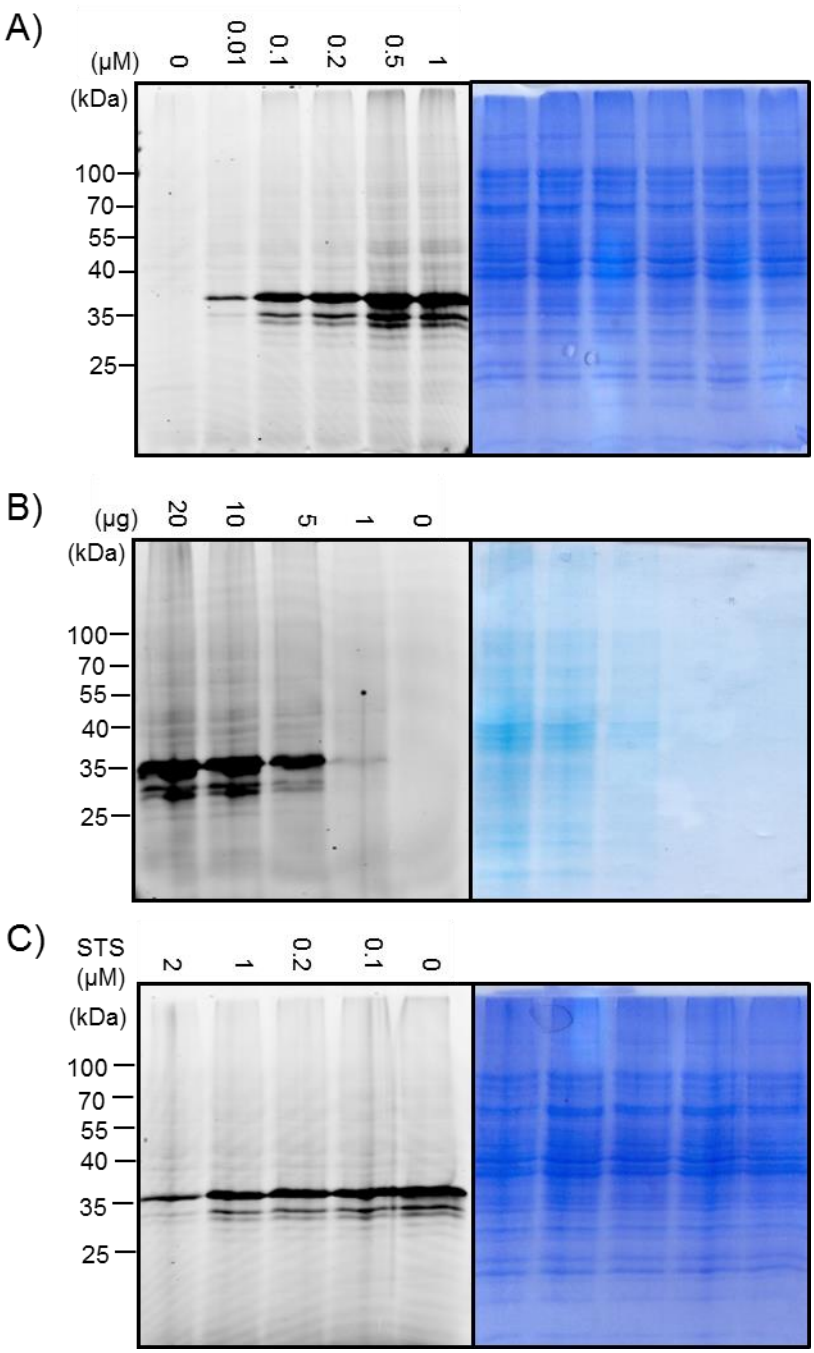

Figure 3.9 (A) *in vitro* labeling of bacterial lysate expressing c-Src (20 μg) with **STS-C1**; (B) Dose-depending labeling of bacterial lysate expressing c-Src with **STS-C1** (0.2 μM); (C) The labeling of bacterial lysate expressing c-Src with **STS-C1** (0.2 μM) was competed with STS.

Anti-proliferation and

After a series of experiments show **STS-C1** could specifically label c-Src in bacterial proteome, we further evaluated the anti-proliferative effects of STS and **STS-C1** on HepG2 cell lines (a human liver cancer cell line). The anti-proliferation by XTT assay showed the cell toxicity of **STS-C1** comparing with the parent drug-staurosporine (STS). (Figure 3.10) The profiles demonstrated very similar toxicity profiles, and indicated retention of STS function in **STS-C1**.

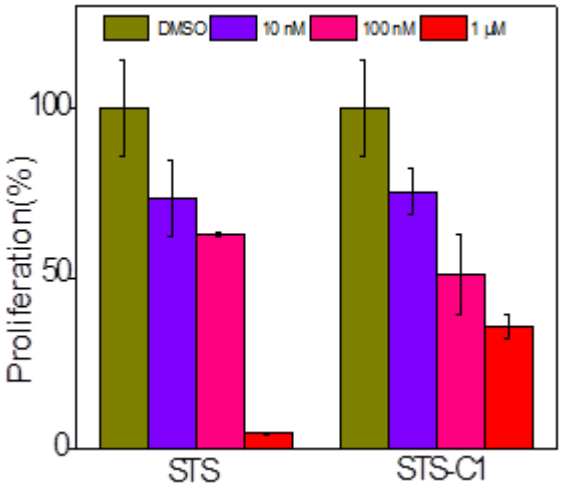

Figure 3.10 Anti-proliferation result by **STS-C1** and STS as determined by the XTT assay.

Cancer cell proteome profiling

Encouraged by these results, we went on to test the labeling of **STS-C1** in endogenous mammalian proteomes. HepG2 liver cancer cells were used and the labeling reactions were carried out both *in vitro* (cell lysates) and *in situ* (live cells) (Figure. 3.11); results from the in-gel fluorescence scanning of the labeled proteomes showed multiple fluorescent bands, highlighting the presence of many potential cellular targets of this probe.

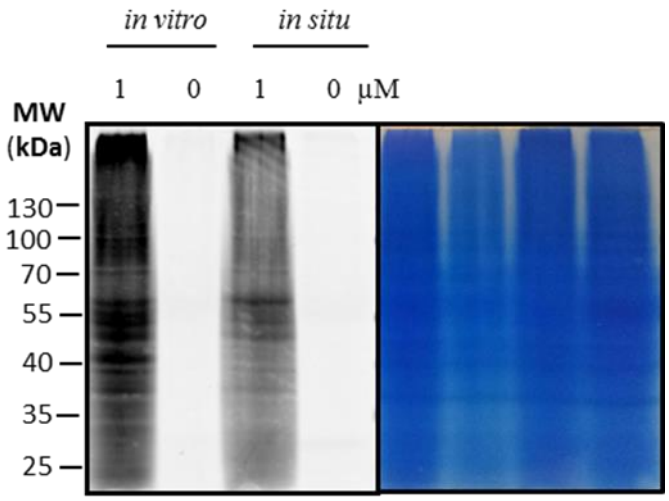

Figure 3.11 Labeling of HepG2 proteome with **STS-C1** *in vitro* and *in situ*.

Pull-down experiment of HepG2 proteome and LC-MS/MS analysis

In order to confirm that endogenous c-Src present in the HepG2 proteomes was indeed one of the labeled targets, these labeled proteomes were clicked with Rh-Biotin-N_3, pulled down with avidin beads followed by Western blotting analysis with anti-c-Src antibody; labeled c-Src was successfully detected in probe-treated proteomes, but not in negative controls (e.g. DMSO-treated proteomes), under both *in vitro* and *in situ* settings. (Figure 3.12)

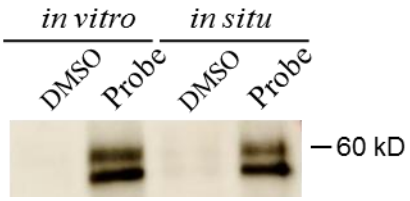

Figure 3.12 Target Identified of **STS-C1** by Western Blotting (*anti*-Src)

We further subjected the labeled proteomes to pull-down/LC-MS/MS analysis for large-scale identification of putative labeled protein targets and the results are summarized, with selected candidate proteins listed. As should be expected, kinases formed the bulk of the

most highly ranked hits. In total 35 kinases were identified from the *in vitro* pull-down and 11 kinases from the *in situ* pull-down, with 7 kinases that overlapped across both experimental sets (Fig. 3.13B). Full list of kinases identified from these experiments are provided in Chapter 9 Appendix Table S3. Compared to proteins identified from earlier-generation probes (e.g. diazirine-containing STS probes[26, 37]), **STS-C1** provided a different range of targets. In Figure 3.13A, by focusing our analysis on the 11 kinases identified from the *in situ* pull-down experiments we found some interesting hits. For example, both CDK1 and CDK2 were previously predicted to possess targetable cysteine near their ATP binding pockets,[56b] and they were positively puled-down/identified from our experiments. These findings further indicate that our newly developed probe might be a suitable chemical for future identification of unknown proteins in kinase cysteinome.

A)

ID	Gene Name	Score	Peptides Matched
H3BTN5	PKM	127	6
P60891	PRPS1	46	2
E5RIU6	CDK1	40	2
E7EUY0	PRKDC	52	5
B2R5T5	PRKAR1A	34	1
G3V5T9	CDK2	29	2
Q5R3A8	FYN	25	2
Q05655	PRKCD	39	1
Q8IWB6	TEX14	36	1
H7C175	AATK	32	1
Q4LE51	PIK3CA variant protein	16	1

B)

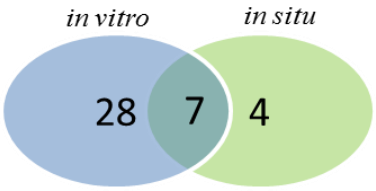

Figure. 3.13 (A) Kinases identified from *in situ* pull-down/LC-MS/MS; (B) Venn diagram illustrating the numbers of kinases identified from HepG2 cell lysates and live cells.

Target validation of STS-C1 by Western Blotting

The target identified by LC-MS/MS could be validated by Western Blotting. (Figure 3.14)

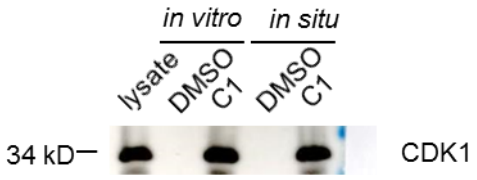

Figure 3.14 Western Blotting (*anti*-CDK1) validation of large scale pull-down samples (*in vitro* and *in situ*) with **STS-C1** (1 μM).

Localization of Targets STS-C1 in HepG2 by fluorescent imaging experiment

The probe could also be used as small molecular probe to detect the distribution of target and enzymatic activity. The cells seeded on glass-bottom dish were treated with DMSO and three gradually increasing concentration (DMSO, 200 nM, 500 nM and 1 μM). After fixation, permeabilization and clicked with Rh-PEG-N_3, the confocal fluorescence imaging showed the real signal of targets start to appear. (Figure 3.15) Results showed the probe was cell-permeable and predominantly cytosolic in HepG2 cells.

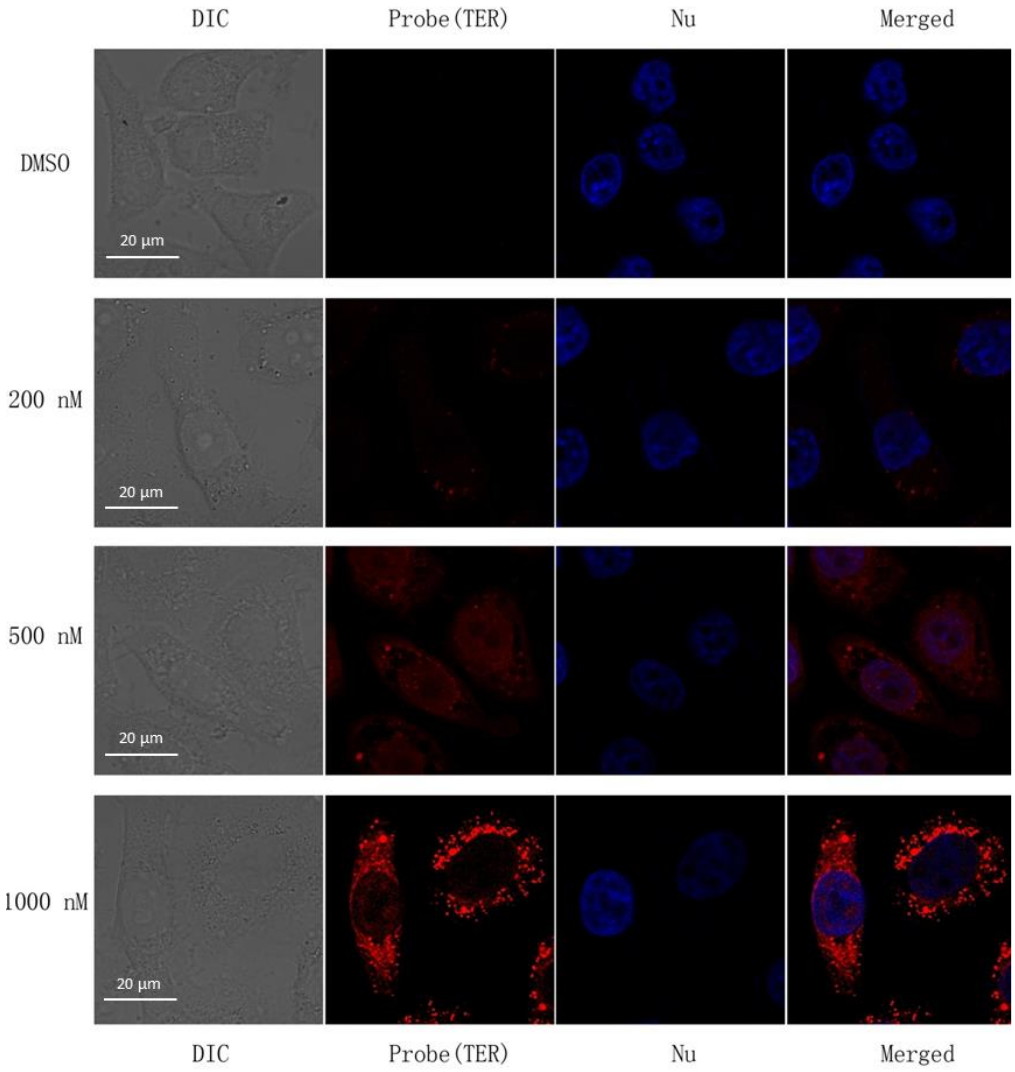

Figure 3.15 Fluorescence imaging of HepG2 cell probed with and different concentration of probe **STS-C1** (DMSO, 200, 500, 1000 nM). HepG2 cell was incubated with probe for 2 h and click with Rh-PEG-N_3 (Rodamine B channel, colored in red, Column 2); the cell was stained with Nucleus tracker (Hoechst, colored in blue, Column 3). Bright filed images (DIC) of the corresponding cells were shown in column 1. Overlay of probe and nucleus channels were shown in column 4.

3.3.4. Unexpected **STS-T1** targeting PDI in live cancer cell

Protein disulfide isomerase (PDI) as a chaperone protein plays very important roles in cell life, which catalyses disulfide bond breakage (reduction), formation (oxidation) and rearrangement (isomerization) in endoplasmic reticulum (ER).[90] The covalent bonding to form disulfide bridge between two cysteine residues is involved in the protein folding, which is the key process to assume the functional shape or

conformation of protein. PDIA1 (normally abbreviated as PDI, encoded by the P4HB gene)[91], is the well-known member of the PDIs family (at least 21 PDI family members known in human). The 57-kDa protein locating mostly in the ER, contains four thioredoxin-like domains (a, b, b' and a'), two of which have a canonical CGHC motif with two active sites within the catalytic domains (a and a'). The other two non-catalytic domains (b and b') are essential for docking the incompletely folded protein substrates by the non-covalent binding.[92] In recent years, PDI has been found to be involved in the apoptosis of cells in several neurological disorders including Huntington's disease, Alzhiemer's diseases and Parkinson's disease;[93] elevated PDI expression levels in a variety of human cancers;[92, 94] regulation of HIV infection of lymphocytes and monocytes.[92]

Traditional drug candidate screening requests a huge library synthesized by huge manpower consumed works such as peptide solid phase synthesis and therefore it is always a time and cost consumed program in the drug discovery. Staurosporine (**STS**) is a well-known general protein kinases inhibitor targeting ATP pocket of protein kinases. The irreversible inhibitor by introducing an electrophile on the pharmacophore may help to find the ATP-chaperone relationship in the live cell. It may even give the possibility to design a specific inhibitor to some ATP-pocket-holding enzyme by proper modification. The design may help to recognize the target under the slightly different environment in the pocket, from which possess particular nucleophilic residue specifically reacting with chemically tuned electrophiles of the probe.

It is reported that ATP has high affinity to PDI (K_d = 9.66 μM) and PDI has the ability of an ATP-dependent auto-phosphorylation.[95] In this section, we report a specific inhibitor **STS-T1** against human PDI in live cancer cell developed by proteome profiling approach, which allowed us to study the active targets in the complex cell environment.

In situ Cancer cell proteome profiling

Cravett et al reported phenyl sulfonate ester probes tageting PDI (~57 kD) together with ECH-2, GST, VLCAD and other proteins.[96] In section 3.3.2, preliminary results showed there're a unique strong band (~57 kD) resulted by **STS-T1** used sulfonate ester as warhead in the *in situ* labeling experiment over MCF-7 and T47D. These results suggested that the protein labeled may be the major cellular target of **STS-T1**. The concentration- and time-dependent labeling experiments were performed to confirm the band as the putative cellular target of **STS-T1**. (Figure 3.16) In the concentration-dependent labeling experiment, signal of the target (~57 kD) increased obviously with the increasing concentration of **STS-T1** from 0 to 10 μM. In the time-dependent labeling experiment, longer incubation time gave stronger and more distinct signal at ~57 kD. The band could be competed by STS (the parent drug) and 16F16 (a known PDI inhibitor[97]). Results showed the protein indicated by the fluorescent band was true cellular target of **STS-T1**.

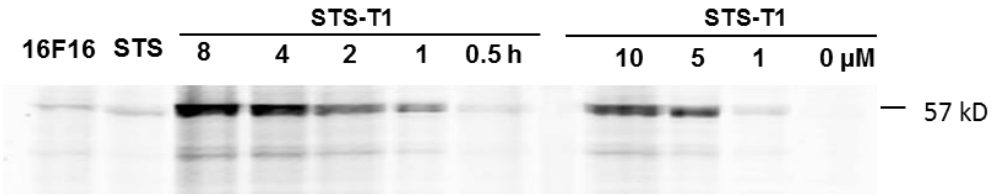

Figure 3.16 In-gel fluorescence protein profiling of concentration- (0, 1, 5, 10 μM for 2 h) and time-dependent (10 μM: 0.5, 1, 2, 4, 8 h) *in situ* labelling of MCF-7 cells treated with **STS-T1**.

Pull-down experiment of MCF-7 proteome and Target validation of STS-T1 by Western Blotting

To identify the cellular targets of **STS-T1**, large-scale pull-down experiment was performed in Figure. 3.17. The live cell MCF-7 was incubated with the probe, lysed and clicked with Rh-Biotin-N_3. After the biotinylated proteins were purified by affinity capture with Avidin beads. The protein detected as unique band (~57 kDa) by in-gel fluorescent

scanning was identified as human PDI by Western Blotting (anti-PDI). The results of Western Blotting against anti-biotin also supported PDI as the major target of **STS-T1** in live MCF-7 cell. Compared with the phenyl sulfonate ester probes mentioned previously,[96] **STS-T1** showed more specificity. The reason probably resided in the additional affinity interaction between STS and PDI, which proved the rationality of the probe design.

A)

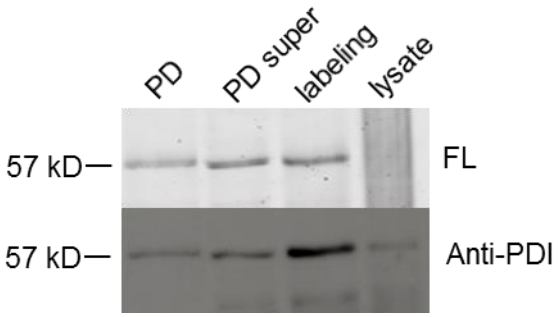

B)

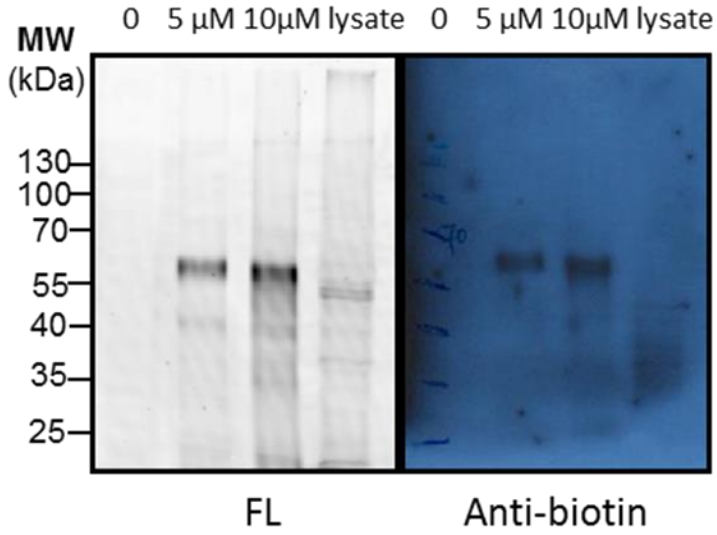

Figure 3.17 Validation of targets of **STS-T1** by Western Blotting. *In situ* labeling of MCF-7 cells by **STS-T1**, followed by click chemistry with Rh-Biotin-N_3, pulled-down (PD) by avidin agarose beads, then gel-separated before in-gel fluorescence scanning (FL) and Western blotting (WB) with **(A)** anti-PDI and **(B)** anti-biotin.

Pure enzyme labeling with STS-T1

Since the major target of **STS-T1** in live cancer cell MCF-7 was confirmed as PDI by Western Blotting, the subsequent pure enzyme

labeling was performed to evaluate the inhibition of **STS-T1** over PDI. In the experiment, recombinant bovine PDI, which shares > 95% sequence homology with human PDI, was used. Dose- and concentration-dependent labeling experiment showed the labeling efficiency of **STS-T1** is quite low. The possible reason is not clear. Compared to reported inhibitor P1, 100 ng of dose amount is higher than 25 ng which give strong enough signal in the labeling with P1.[98] (Figure 3.18)

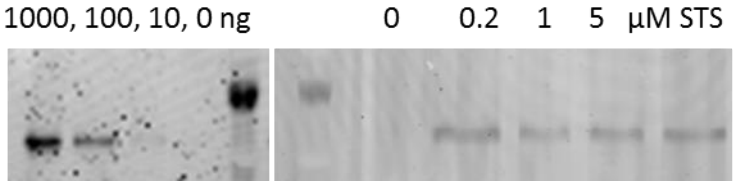

Figure 3.18 Concentration-dependent and dose-dependent labeling of recombinant bovine PDI by **STS-T1**.

Localization of Targets STS-T1 in MCF-7 by fluorescent imaging experiment

Although our probe **STS-T1** did not show good labeling activity to the recombinant bovine *in vitro* for some unknown reason, it could be used to visualize the localization of endogenous human PDI in mammalian cells. Live MCF-7 was treated with **STS-T1**, then clicked by Rh-PEG-N_3 and imaged. The same cells were subsequently treated with anti-PDI antibodies following standard immunofluorescence (IF) protocols, and imaged again. Merged channels indicated nearly complete co-localization of the fluorescence signals to the expected endoplasmic reticulum (ER). It showed a strong evidence to prove the human PDI as the major target of **STS-T1**. (Figure 3.19)

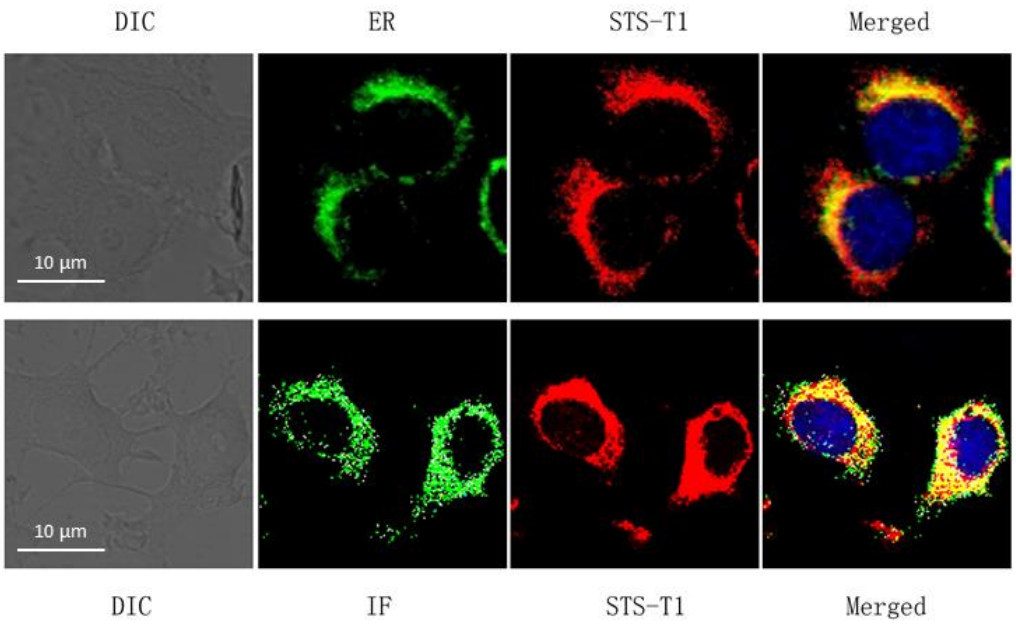

Figure 3.19. Cellular imaging of live MCF-7 cells was probed with **STS-T1** (5 μM; 2-h treatment, then clicked with Rh-PEG-N_3 (543 nm Channel, colored in red). Bright filed images (DIC) of the corresponding cells were shown in the first column. Co-localization experiments were performed with ER and Nucleus tracker. (A) co-localization with ER Tracker (colored in green), Overlay of probe, ER and nucleus channels were shown in last column. (Top) (B) Immunofluorescence (IF) was performed with anti-PDI (colored in green). Overlay of probe, IF and nucleus channels were shown in last column. (Bottom)

3.4. Conclusion

Three “clickable” probes have been successfully synthesized by introducing different electrophiles (chloroacetamide, sulfonate ester and acrylamide). Among of them, STS was successfully converted into an irreversible covalent probe, **STS-C1**, in an effort to minimize non-specific labeling from earlier-generation photoaffinity-based probes. We found **STS-C1** was able to preferentially target the protein kinase cysteinome both *in vitro* and *in situ*, by using c-Src as a representative example. Through the course of our study, we have tentatively identified previously unknown proteins in the kinase cysteinome, and they will be further validated in due course. The probe **STS-C1** also could be used as small molecular probe to detect the distribution of target and enzymatic activity *in situ* by fluorescent imaging experiment. On the other hand, human PDI was identified as the major cellular

target of **STS-T1** in the breast cancer cell MCF-7 by *in situ* proteome profiling. The reactive group sulfonate ester on the probe was served as a warhead which shows high reactivity to PDI.[96] However, in our design, the probe was incorporated with STS as the affinity binding to the ATP pocket and therefore a better specificity was achieved. The probe could be potentially applied to indicate the enzyme activity and cellular localization to facilitate the diagnoses and therapy of the PDI related diseases. There're also some questions need to be further investigated. The inhibition mechanism is essential to be clarified including active site. Side-target identification as another issue related its specificity *in situ* is needed to further address by LC-MS/MS and validation. Totally, the approach provides a new way to design the inhibitor of PDI. The approach about the probe design and has more flexibility for other general affinity scaffolds. It may give us efficient way to design a series of whole inhibition picture of protein kinases or other nucleotide-pocket-holding proteins like PDI.

Chapter 4

Protein Target Profiling of Lymphostin and Ammosamide B by Activity-Based Protein Profilings (ABPPs) in Live Cell

4.1 Summary

4.2 Introduction

4.3 Results and discussion

4.4 Conclusion

Mr. Allan and Licheng under Prof. Zhao Yu contributed the investigation of Probes based on Lymphostin; Ms Xiaoyuan contributed the preliminary biological tests.

4.1. Summary

In this chapter, we try to develop the activity-based probes (ABPs) based on Lymphostin and affinity-based probes (A*f*BPs) based on Ammosamide scaffold to identify their cellular targets.

4.2. Introduction

Marine natural products with a variety of unique structural classes are now very important sources for the candidate of synthesis and medicine.[39, 99] As one of marine natural product, Lymphostin could be used as an immunosuppressant which shows potential inhibitory activity against lymphocyte kinase (LCK) and phosphoinositide 3-kinase (PI3K).[100] Additionally, Ammosamide A and B were isolated from Streptomyces strain CNR-698 by cytotoxicity-guided (HCT-116) fractionation.[101] (Figure 4.1A) Because their novel mechanism of action impinged on a crucial biological cascade, the interactions between the natural products with protein targets have drawn the attention of medicinal scientists. Many approaches were developed to identify the cellular targets of natural products, including target-based screening of molecules library, cell-based phenotypic, affinity-based proteome profiling/LC-MS and so on.[6d] At a further stage, a promising *in situ* method emerged, which could reflect the small molecule–protein interactions in live cells.[6a, 42a, b]

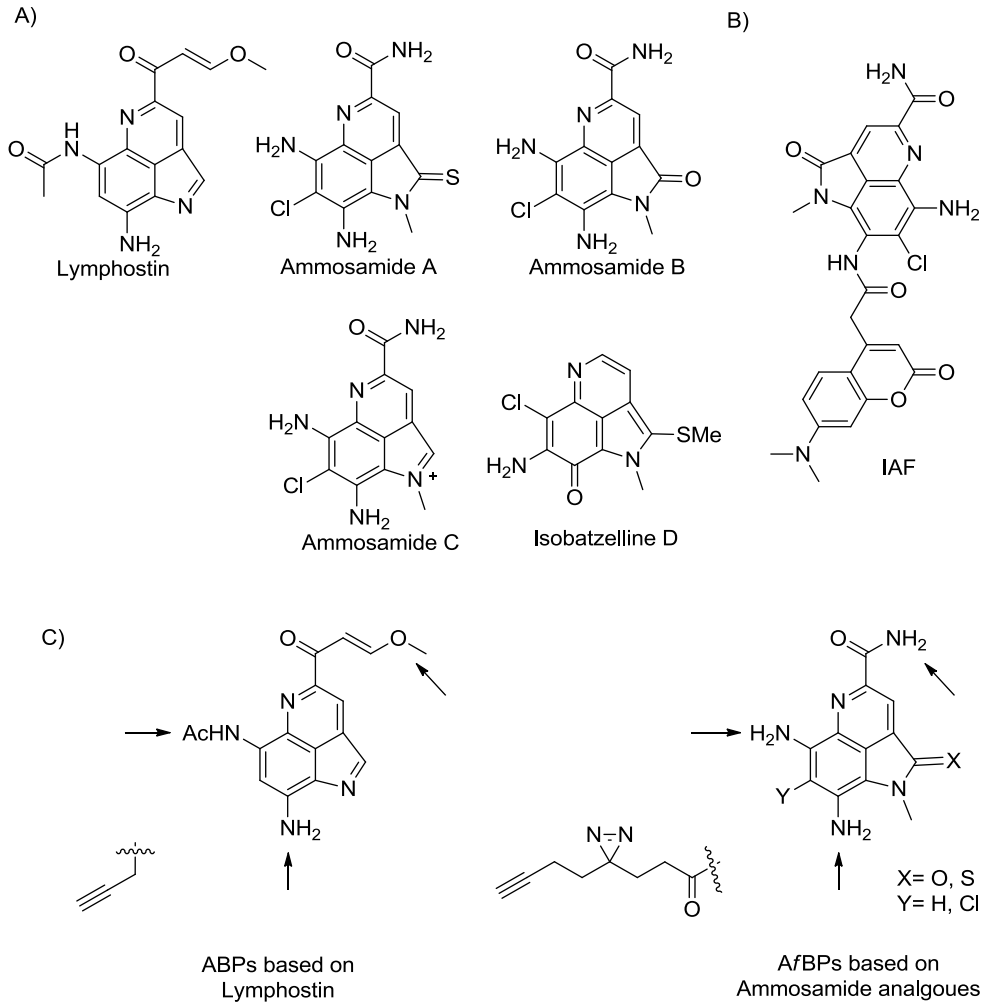

Figure 4.1 (A) Structure of Lymphostin and analogues of Ammosamide; and (B) The immunoaffinity fluorescence probe (IAF) of Ammosamide B; C) sites of chemical modification denoted by arrow.

By the affinity proteome profiling approach, Myosin was claimed the as the main target of Ammosamide A and B with an immunoaffinity fluorescence probe (IAF).[102] (Figure 4.1B) However the limitation of IAF is obvious. Firstly, the tag-conjugated manner makes the probe too big to maintain the original activity of parent drug. For example, the experiment indicated that cytotoxicity of IAF (IC_{50} = 17 μM) is much lower than of Ammosamide A and B (IC_{50} = 320 nM) for HCT-116 cells. Secondly, the interaction between IAF probe and protein is reversible as IAF is an affinity based probe. The targets could be lost in the process. Finally, the most possible reason is that Myosin as a high abundant protein has saturated the channel for other potential targets with low-expressed level. Therefore, this reversible tag-conjugated

approach using IAF probably has lost other interesting protein targets while at low expressed level.

To overcome the shortcomings of tag-conjugated and reversible probe design, the “clickable” probes based on Lymphostin and Ammosamide analogues was proposed. In our design, the typical modification sites and installed functional group were shown in Figure 4.1C. The nature of binding between ammosamide analogues and their targets is non-covalent. The transient protein–small molecule complex may not survive the *in vitro* affinity-based target enrichment process. Based on our successful design of affinity-based probes (A*f*BPs),[26, 36a, 37] the affinity scaffold incorporated with photo-labile linker (diazirine) could be facilitated to perform *in situ* proteome-based profiling of marine natural products, combined with downstream LCMS-based target identification. Diazirine as a photo-labile group, which could produce highly reactive species upon UV irradiation, could react with the molecules nearby. Of course, the size of the linker is as small as possible to avoid the additional influence over drug activity. Terminal alkyne as click handle was introduced with minimized modification. A variety of potentially bioactive functional groups would be included, such as chlorine, sulfur and carbonyl groups appeared in the ammosamide analogues. On the other hand, Lymphostin as covalent inhibitor would be converted to activity-based probes (ABPs) directly incorporated with a terminal alkyne group at suitable positions. While covalently bound with the “clickable” probes (A*f*BPs and ABPs) derived from the natural products, cellular targets would be investigated comprehensively by *in situ* proteome profiling/pull-down/target-identification to facilitate the drug discovery.

4.3. Results and discussion

4.3.1. A*f*BP based on Ammosamide analogues

Since our A*f*BPs are based on the scaffold of Ammosamide, the first step is to establish Ammosamide B as the pharmacophore template. In

the first synthetic route of Ammoamide B, intermediate **4-3** was made from 2-Oxoglutaric Acid **4-1** through esterification, bromination and elimination reactions subsequently.[103] Following the literature,[104] compound **4-11** was made from 1,3-dichlorobenzene **4-4** by seven steps of reactions. However, Boc deprotection of compound **4-11** did not proceed well to give the desired product **4-12** with the starting compound **4-11** decomposed. (Scheme 4.1) Compound **4-10** and **4-11** have poor solubility in common organic solvents.

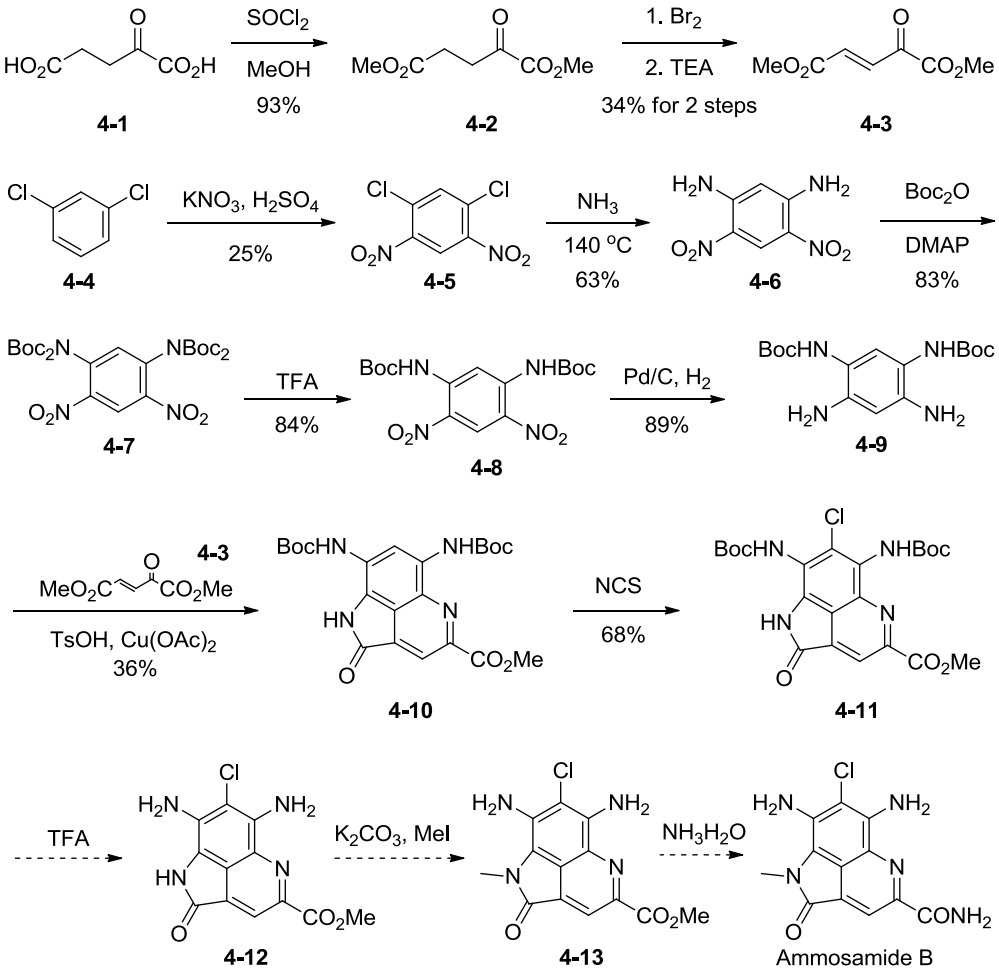

Scheme 4.1 The first synthetic route of Ammosamide B

So the alternative route was considered as shown in Scheme 4.2.[105] The synthesis was pushed forward to Ammosamide B through seven steps from 1,3-dichlorobenzene **4-4** and intermediate **4-3**. The cyclization reaction to compound **4-14** led to low yield as the product is unstable in the process of reaction and column purification. The longer

time in the purification, the more side-product appeared which was very close to the desired product **4-14**. The chlorination of compound **4-16** gave low yield as the starting material **4-16** decomposed under the condition and the reaction gets lousy and difficult to purify. The intermediates from compound **4-15** to Ammosamide B have poor solubility in common organic solvents.

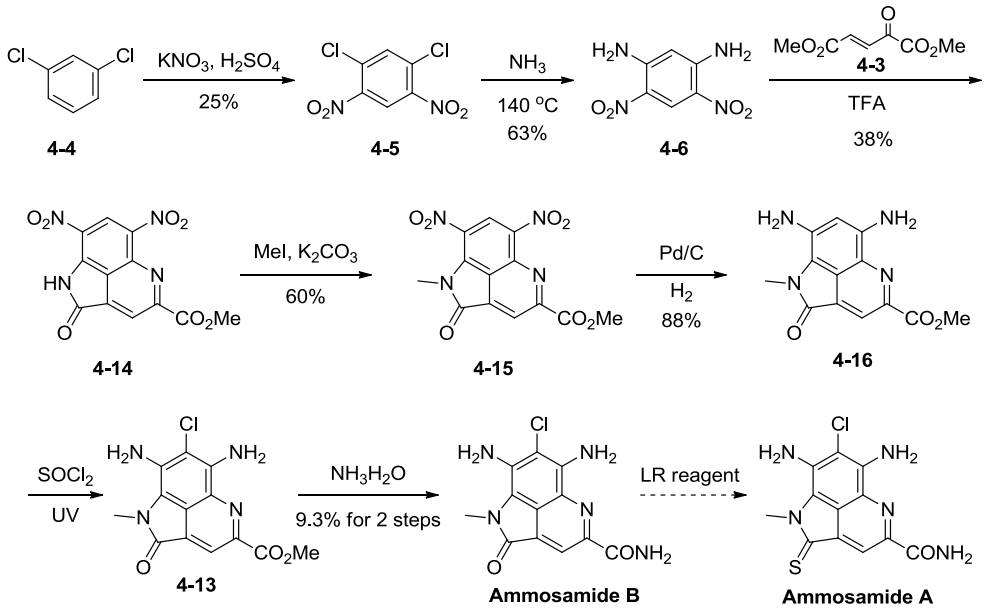

Scheme 4.2 The second synthetic route of Ammosamide A and B

In Scheme 4.3, to extend the library of the analogues, two probes **4-17** and **4-19** were obtained by coupling with photo-labile linker.[26] However, the desired product **4-20** was not obtained from Ammosamide B under the same condition. The reactivity of amine on Ammosamide B was deactivated by chlorine atom as electron-withdrawing group.

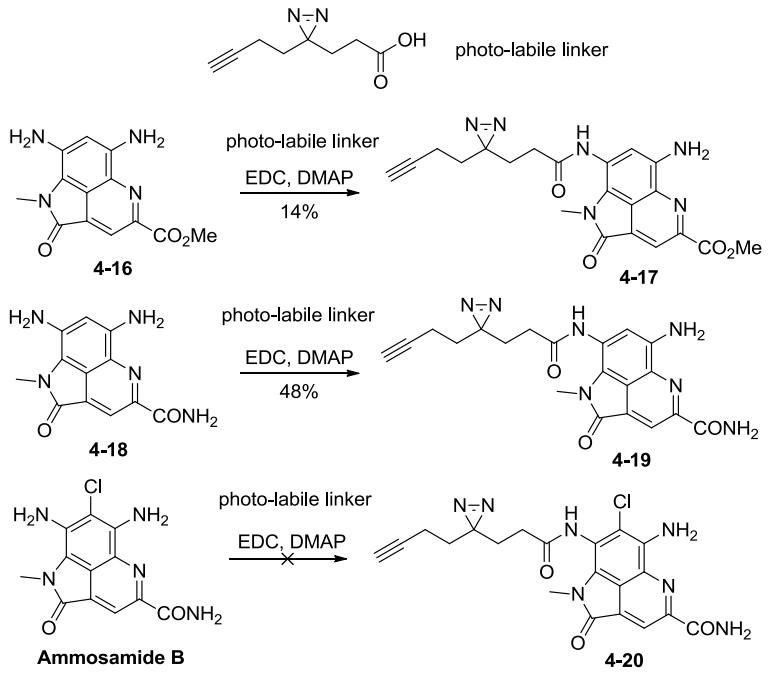

Scheme 4.3 The synthesis of the A*f*BPs

In order to get enough Ammoamide B, we have to continue optimizing synthetic route. Comparing with second route in Scheme 4.2, the reactions in the first route (Scheme 4.1) proceeded smoothly except the Boc-deprotection of compound **4-11**. So the Boc-deprotection of model compound **4-10** was optimized further by using thermolysis. Different solvents and temperature under microwave irradiation had been optimized. It was found that solvent system played key role in thermolysis reaction. No product was obtained by only DMSO as solvent. Only one Boc group was removed by DMF as solvent at 185 ^{o}C. The mixture of DMF-H_2O (1:1 by v/v) solvent system was found to be most efficient. Then the optimized condition was applied into the Boc-deprotection of compound **4-11**. This reaction proceeded well to provide compound **4-12** well. (Scheme 4.4)

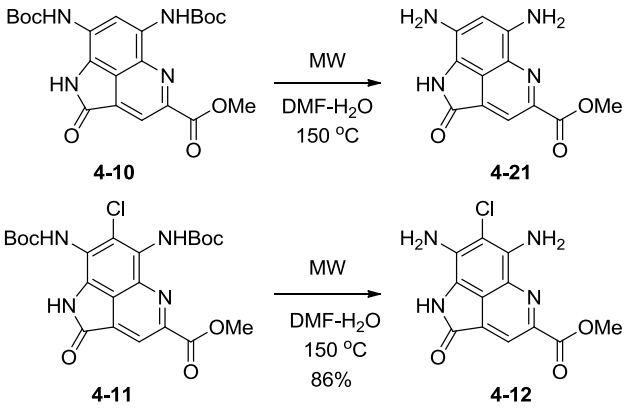

Scheme 4.4 Thermolysis of Boc group

With compound **4-12** in hand, we pushed forward the synthesis of Ammosamide B by the first synthetic route. The methylation of compound **4-12** did not work well. Then the third synthetic route was proposed as shown in Scheme 4.5. The methylation led to a mixture of starting material **4-11** and desired product **4-22**. The reaction was not complete even with longer time and high temperature. The two compound **4-11** and **4-22** were very difficult to be separated because of the same R_f value on TLC and same retention time on HPLC analysis. Then we forwarded the mixture to thermolysis of Boc-group. The Boc-deprotection proceeded well and the ratio of compound **4-13** to **4-12** was found to be 2:1. Due to the poor solubility, the two compound **4-13** and **4-12** were also difficult to be separated and then used as a mixture to next step.

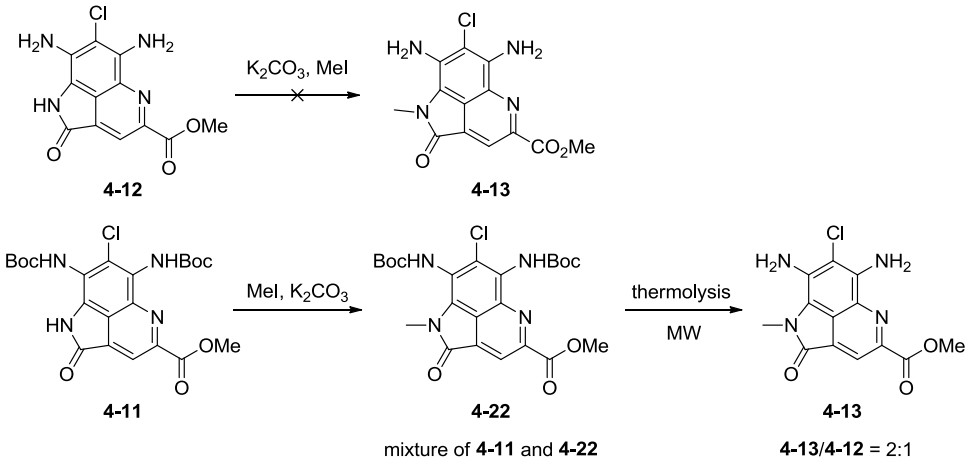

Scheme 4.5 Methylation and thermolysis of Boc group

Since the coupling reaction of Ammosamide B with photo-labile linker did not work (Scheme 4.3), the reactivity of compound **4-13** with photo-labile linker was tested. It was found that no product **4-23** was observed, once the adjacent amide was methylated. However pure compound **4-24** was isolated after purification from the same pot of reaction. The stereohindrance of *N*-methyl group may be the possible reason to prevent the reaction from proceeding. (Scheme 4.6)

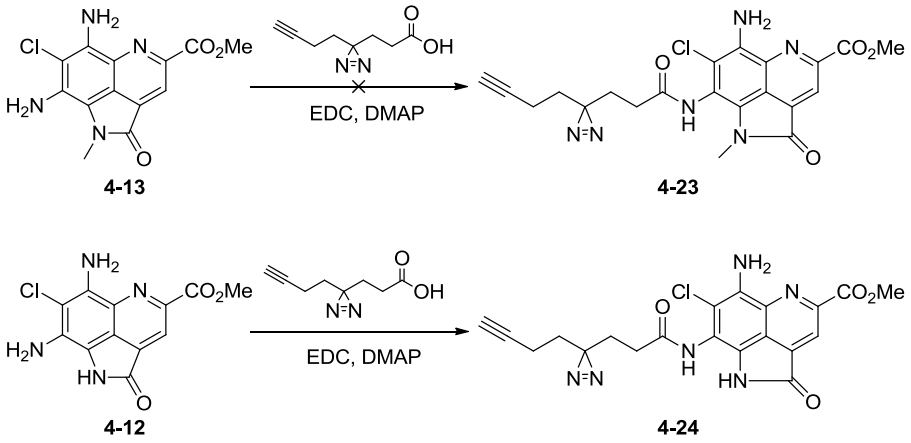

Scheme 4.6 Coupling reaction with photo-labile linker (diazirine)

4.3.2. ABP based on Lymphostin

Another mission is to synthesize ABPs based on Lymphostin. Three ABPs based on Lymphostin was proposed with the modification at different sites with “clickable” handle.

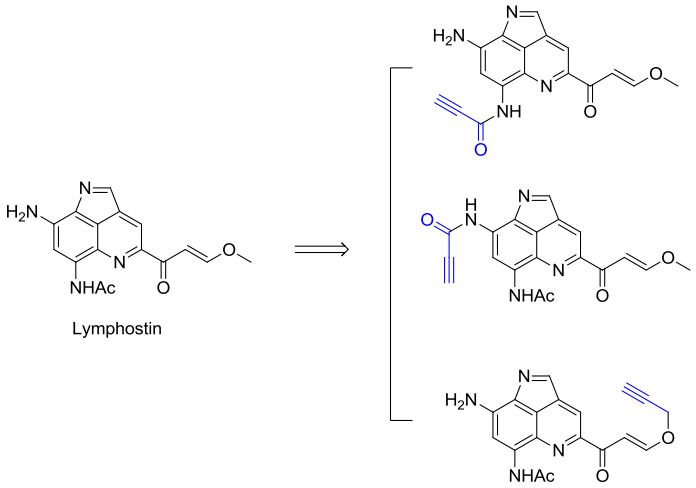

Figure 4.2 Chemical modification sites on Lymphostin

Since the total synthesis of Lymphostin in literature is complicated with up to 21 steps of linear multistep reactions, [106] we reconsidered the synthetic plan of ABP based on Lymphostin as shown in Scheme 4.7. With valuable experience on the synthesis of Ammosamide B (section 4.3.1), the key intermediate **4-10** would be employed as starting point to pursue the efficient synthesis of Lymphostin scaffold for further modifications to ABPs. Three key steps would be involved in this synthetic plan. First is the formation of cyclic imine **4-25**. And second is introduction of Michael accepter in compound **4-27** and **4-28**. The third is the selective formation of propiolamide **4-29** and **4-30**. Some research work in details has been done based on these three aspects.

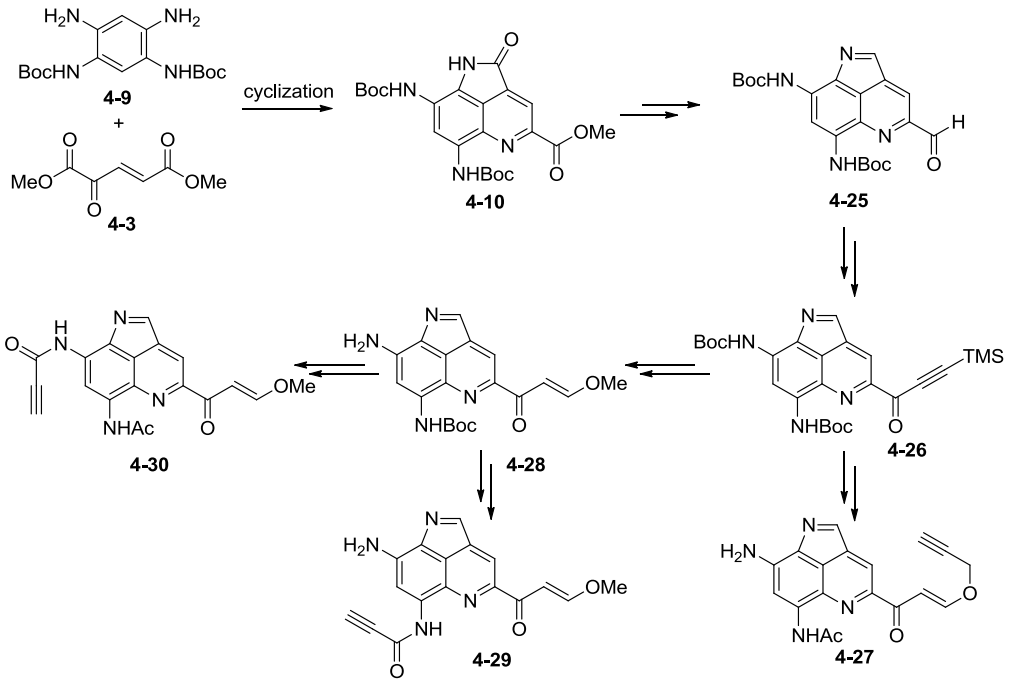

Scheme 4.7 Synthetic plan of ABPs based on Lymphostin

In the synthesis of cyclic imine starting from intermediate **4-10**, several conditions were employed.[107] The transformation of amide to triflate **4-31** proceeded well, followed by elimination. However, no desired product **4-32** was obtained but starting material **4-10** was recovered. Schwartz reagent and DIBAL-H were also employed. It was found that the desired product **4-32** was successfully synthesized by both reduction methods. The following synthesis of Weinreb amide **4-33** encountered problem as the cyclic imine is unstable in the process. (Scheme 4.8)

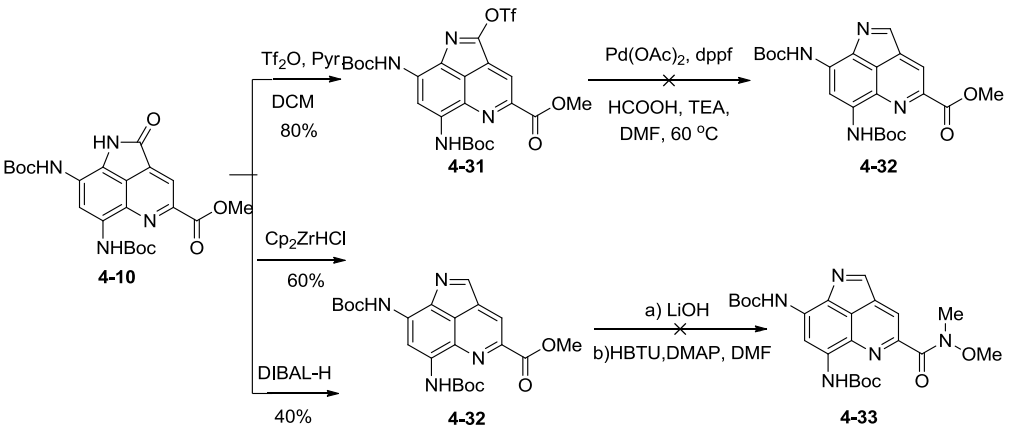

Scheme 4.8 Preparation of cyclic imine and Weinreb amide

Since the intermediate with cyclic imine was difficult to handle, the amide **4-10** was used as starting material to explore the second key step to introduce α, β-unsaturated alkyne. The synthesis of Weinreb amide **4-24** had been optimized by using aminolysis with Weinreb amine hydrochloride. No product was observed even using Grignard reagent or high temperature. The combination of hydrolysis with LiOH and amide coupling successfully provided Weinreb amide **4-34** in good yield. The following alkynlation encountered problem. Grignard reagent or Butyl lithium condition failed to give the desired product. The synthetic route would be modified by converting methyl ester to aldehyde, which would be subjected to Grignard reaction followed by oxidation. (Scheme 4.9)

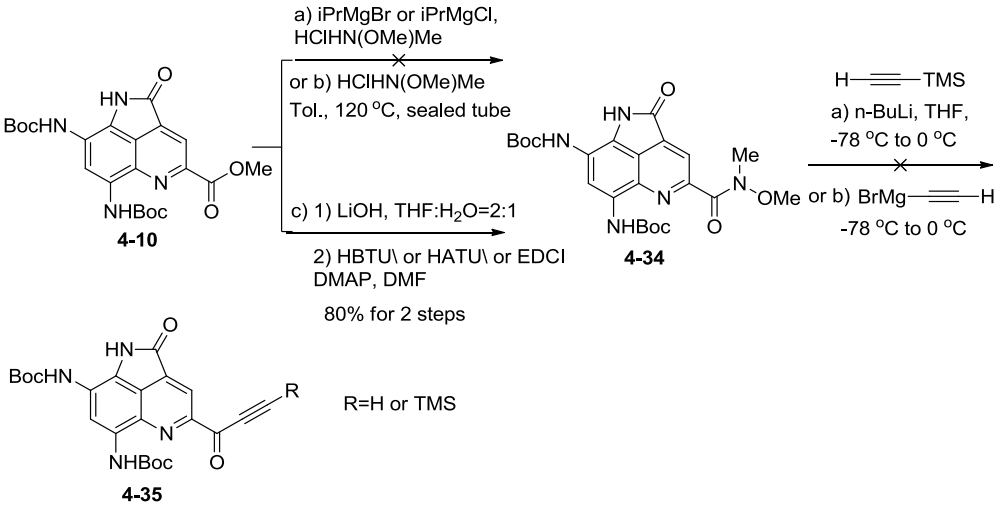

Scheme 4.9, Synthesis of Weinreb amide and subsequent alkynlation

4.3.3. Preliminary biological test

Two A*f*BPs (**Am-1** and **Am-2**) are ready in hand as shown in Figure 4.3. Some preliminary experiments were explored, including pure enzyme labeling over kinases, bacterial lysate labeling, mammalian lysate labeling and Jurkat cell lysate pull-down.

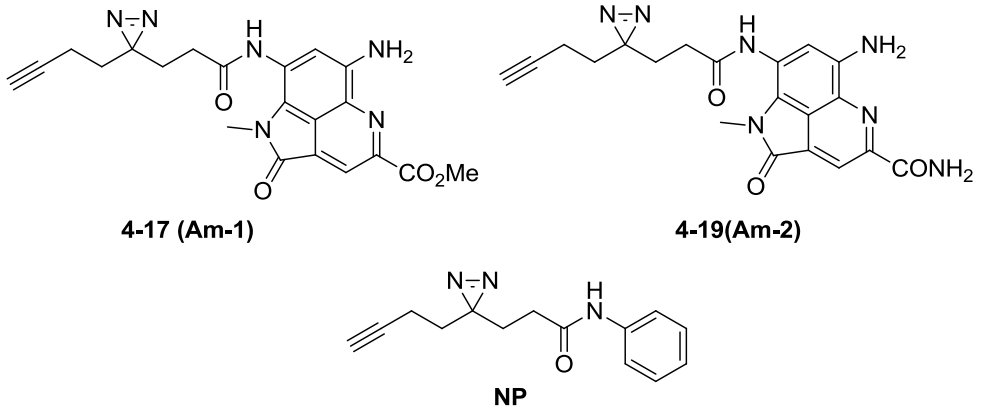

Figure 4.3 Structure of two A*f*BPs and control

To evaluate the potential activity with protein kinases, *in vitro* labeling of pure recombinant kinases was performed. **Am-1** and **Am-2** showed weak labeling with c-Src and Abl and no labeling with PKA and Lck. (Figure 4.4) while, in the labeling of bacterial lysates overexpressing

kinases, no obvious labeling by **Am-1** and **Am-2** was obtained comparing to the positive control (Figure 4.5), and even in the dose-dependent labeling (**STS-2**). (Figure 4.6)

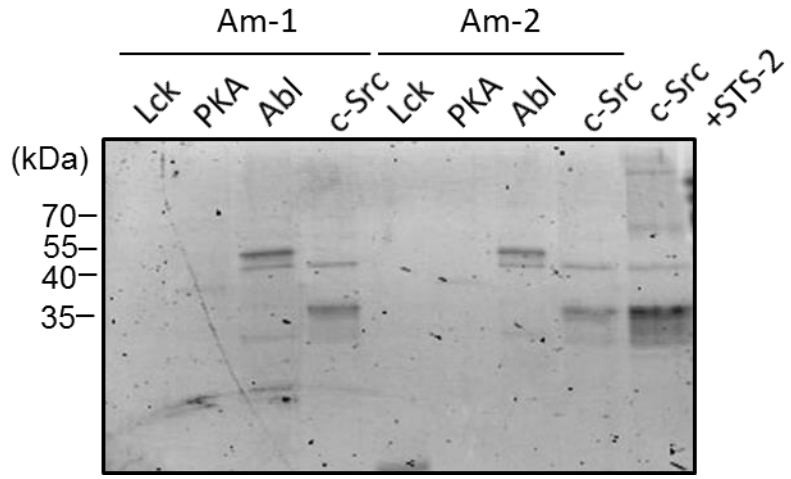

Figure 4.4 *in vitro* labeling of pure recombinant kinases. Recombinant kinases were incubated with **STS-2**, **Am-1** and **Am-2** (20 μM) at rt for 30 min and irradiate for 20 min (UV).

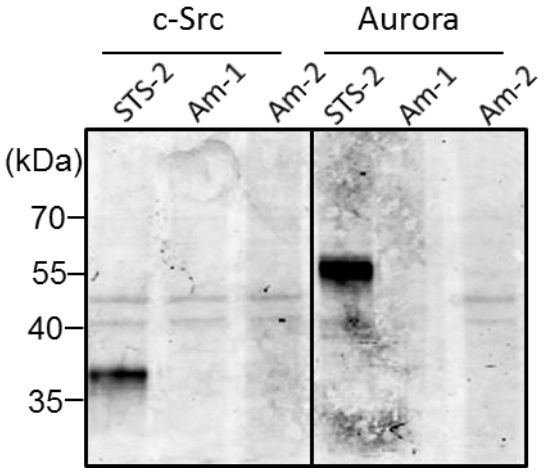

Figure 4.5, Bacterial lysate labeling. Cell lysates were incubated with **STS-2**, **Am-1** and **Am-2** (20 μM) at rt for 30 min and irradiate for 20 min (UV).

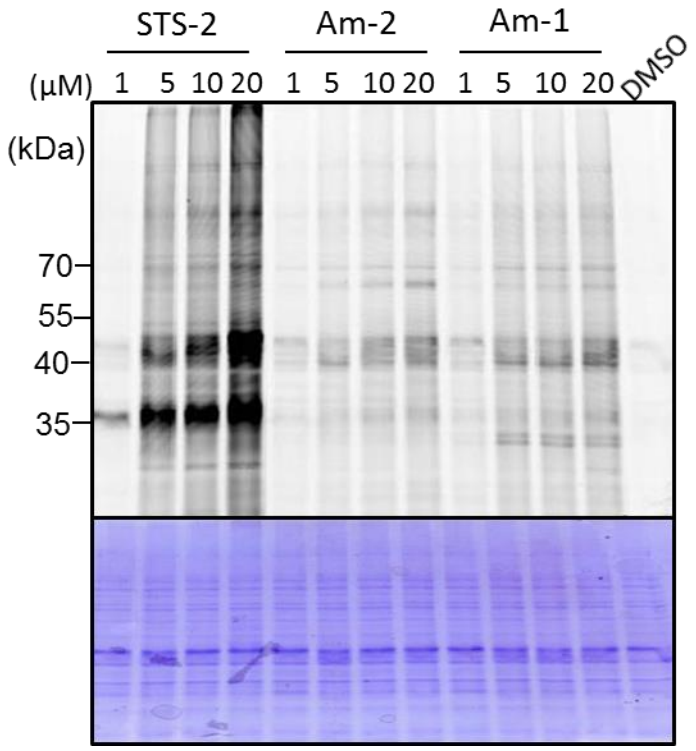

Figure 4.6 Bacterial lysate over-expressing c-Src was incubated with **STS-2**, **Am-1** and **Am-2** at rt for 30min and irradiate for 20 min (UV). DMSO was used as negative control.

Then, the next experiment is *in vitro* mammalian cell lysate labeling. Among of the three cell lines, jurkat cell shows distinctive bands with other two cell line (Figure 4.7). So the *in vitro* concentration-dependent labeling was studied in Figure 4.8. The results showed the labeling increased with the progressive concentration of **Am-2** from 1 to 10 μM. To identify the putative cellular targets of **Am-2**, the large scale pull-down experiment was performed as shown in Figure 9. The distinctive band circled by red rectangle was cut and submitted to MS analysis. Those non-specific binding proteins were deducted, which also appeared in negative control (treated with NP). After other operations of filtration, a list of the potential protein targets was obtained. (Chapter 9 Appendix, Table S3) We focused our attention on those candidates which play important roles in cancer cells including Myosin, PKM2, GAPDH, LDHB, HNRNPA2B1 and ECH1. GAPDH was a therapeutic target in deregulation of glycolysis in cancer.[108] (Table 4.1) Myosin appeared in the list without surprise, which was also identified by the tag-conjugated probe (IAF).[102] PKM2 was involved in the proliferation

of cancer cell.[109] LDHB was used as tumor marker.[110] HNRNPA2B1 was related to cell proliferation and carcinogenesis.[111] ECH1 was involved in the lymphatic metastasis of tumors.[112]

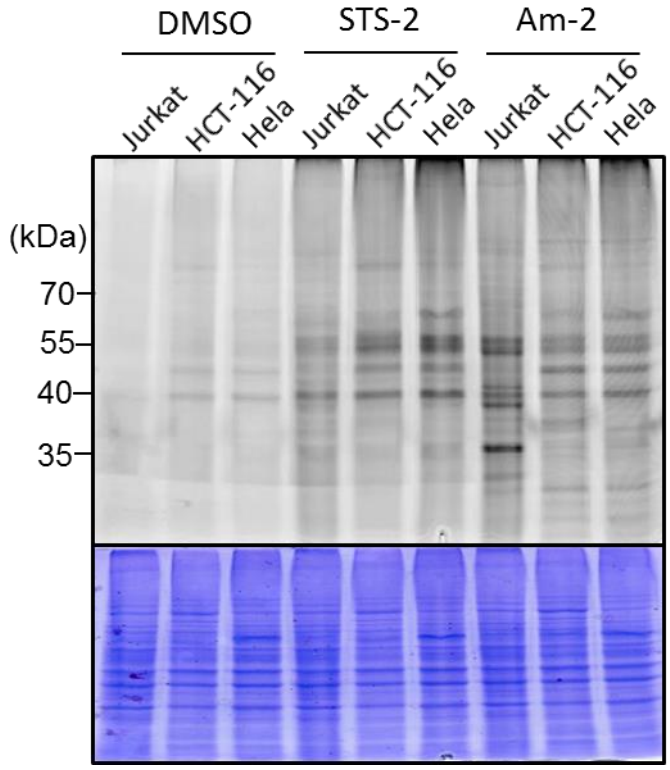

Figure 4.7 *In vitro* labeling of mammalian cell lysate. 20 μg of cell lysate was incubated with **STS-2** and **Am-2** (5 μM) at rt for 30 min and irradiate for 20 min (UV).

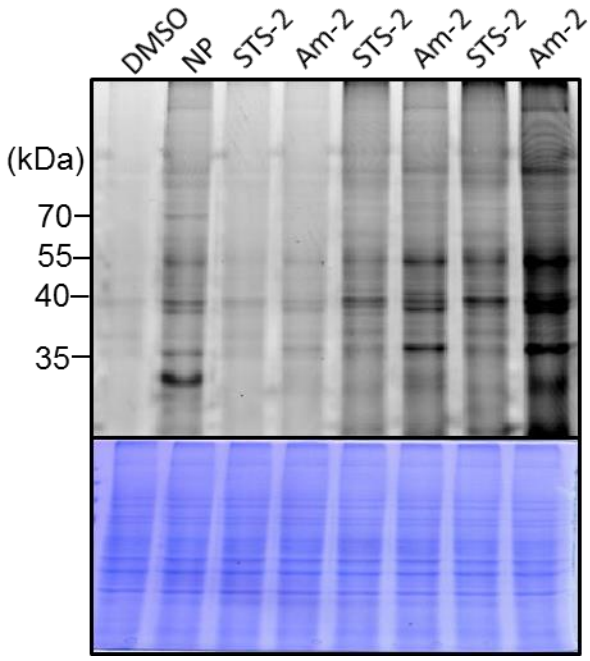

Figure 4.8 Concentration dependent mammalian cell lysate labeling. 20 µg of cell lysate was incubated with **STS-2**, **Am-2** (1, 5 and 10 µM) and **NP** (10 µM) as the negative control at rt for 30 min and irradiate for 20 min (UV).

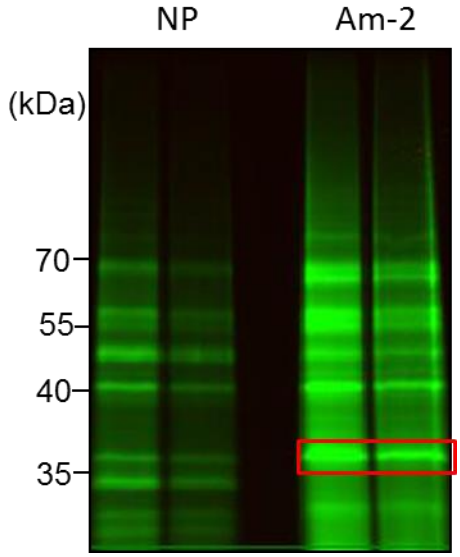

Figure 4.9 Pull-down experiment over Jurkat cell lysate. Cell lysate was incubated with **Am-2** (5 µM) for 1 h and UV irradiation for 30 min.

Table 4.1 The list of the potential protein targets of **Am-2**

Gene code	Description	MS	score	Peptides matched
PKM2	Pyruvate kinase isozymes M1/M2	30929	34	7
MYO10	Unconventionnal myosin-X (Fragment)	96861	17	3
GAPDH	Glyceraldehyde-3-phosphate dehydrogenase	36201	189	19
LDHB	L-lactate dehydrogenase B chain	36900	118	10
HNRNPA2B1	Isoform A2 of Heterogeneous nuclear ribonucleoproteins A2/B1	36041	91	7
ECH1	Delta(3,5)-Delta(2,4)-dienoyl-CoA isomerase, mitochondrial OS=Homo sapiens	36136	30	7

4.4. Conclusion

In the project, we have tried to develop a library of ABPs and A*f*BPs based on nature marine product-Lymphostin and Ammosamide analogues. Three A*f*BPs based on the bioactive scaffold of Ammosamide B have been successfully synthesized and the library of probes would be expanded with other bioactive elements. The efforts to construct ABPs based on Lymphostin have afforded some progress including methodologies in three key steps including the formation of cyclic imine **4-25**, introduction of Michael accepter in compound **4-27** and **4-28** and the selective formation of propiolamide **4-29** and **4-30**. Continuing with the investigationes, the synthesis would put forward in the further study. With the probes (**Am-1** & **Am-2**) in hand, some progress in proteome profiling of bacterial and mammalian cell lysate has given some interesting preliminary results. By the ABPP approach, Myosin was validated as a reported target of Ammoamide A and B, and other unknown targets were newly identified including PKM2, GAPDH, LDHB, HNRNPA2B1 and ECH1, which play important roles in cancer

cells. The preliminary results promote us to do comprehensive study further with more ABPs and A*f*BPs probes derived from Lymphostin and Ammosamides. Further study will enable extensive study of the library of the marine products by *in situ* living cell profile, such as potential pharmacological effect, pharmacokinetic effects including absorption, distribution, even metabolism and excretion especially in the cancer cell. The approach would further expand the sight over the cellular targets of the natural products by the novel systematic chemical proteome study.

Chapter 5

Cancer Cell Targeted Drug Delivery of Protein Kinase Inhibitors by Cell Penetrating Peptide (CPP)

5.1. Summary

We described a drug delivery of protein kinase inhibitors into the cancer cell by the aid of biomarker and cell penetrating peptide (CPP). It was expected that cancer cell would be regulated or killed specifically.

5.2. Introduction

Protein kinases (500+) play very important roles in cell life including cell signalling regulating the cellular pathway and are regulated as therapeutic targets by kinase inhibitors in many diseases especially for cancer.[53, 58] However, in the development of new therapeutic kinase inhibitors as anticancer drugs, the low biocompatibility of hydrophilic substances and the nonspecific toxicity toward healthy tissues are major obstacles. Firstly, in the regulation of the import and export of substances, cell membrane is selectively permeable to ions and organic molecules including peptides, proteins, DNA oligonucleotides and etc.[113] Secondly, drug-safety-related issues have been a major contributing factor to embarrass the development of new kinase inhibitor drug. At the early stage of drug discovery, there's a big challenge in the drug-target interactions optimization. Most small molecule kinase inhibitors suffer from broad reactivities because ATP pockets as their targets are high conserved, even across distantly related kinases. At the later stage, the lack of tumor-specific treatments limits the clinical applications of chemotherapy. Traditional chemotherapy relies on the cytotoxic agents to kill the rapidly proliferating cancer cells, however, cytotoxic agents have very little or no specificity and result systemic toxicity to healthy tissues, causing undesirable severe side effects, such as hair loss and damage to other tissues including liver, kidney, and bone marrow.[114] Therefore, there is an urgent need for the innovative and efficient tumor-specific drug delivery methods.

Although pharmacologists have paid a lot of efforts to develop the kinase inhibitor drugs which could specifically inhibit their targets as nosogenesis, limited outcome of the drug discovery and the difficulty inside push them to extend the scope to other fields. A rapidly growing tumor overexpress many tumor-specific receptors to get various nutrients and vitamins, which could be used as cancer biomarkers for cancer diagnosis, prognosis, epidemiology and treatment.[115] Those receptor proteins on the surface of cancer cell could be used as targets to deliver cytotoxic agents into tumors.[116] For example, monoclonal antibodies,[117] polyunsaturated fatty acids,[118] folic acid,[119] aptamers,[120] oligopeptides[121] and hyaluronic acid[122] has been applied to conjugate cytotoxic agents toward tumor-specific delivery. Unlike the endocytosis by the aid of specific receptors, cell-penetrating peptides (CPPs) have been developed to achieve the internalization of large therapeutic molecules, which is capable of crossing the membrane barrier.[123] In addition, the conjugated cytotoxic drug in prodrug manner could be released under control by different mechanisms.[124]

Herein, we try to develop an efficient approach which could specifically deliver cytotoxic kinase inhibitors into cancer cells to improve therapeutical effect. Many cancer cell lines overexpress matrix metalloproteinases (MMPs).[125] It is the key that triggers the cancer cell-specific recognition, where.the specific peptide as MMP substrate between CPP and its mask could be cleaved enzymatically to give the active CPP in drug conjugated manner (Figure 5.1**)** The enzymatic reaction takes place on surface of the cancer cell and therefore CPP is attached on the cell membrane and absorbed into the internalization of the cancer cells. The masked peptide by cation-anion pair (structure seen in Figure 5.2) is inactive for cell absorption and therefore the conjugated drug outside is safe for the normal cell. After absorption, the conjugated drug would be released by UV cleavage[126] or thiol cleavage by intracellular Glutathione (GSH)[127]. Then the life of cancer cells would be interrupted and even induced to apoptosis as the kinases are inhibited. (Figure 5.3)

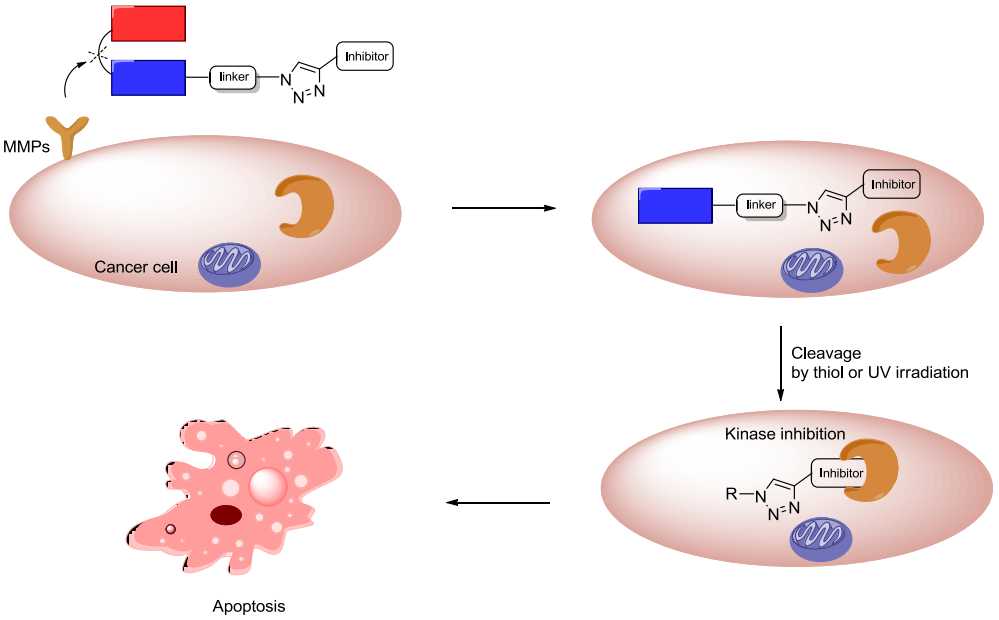

Figure 5.1 Concept study of drug delivery. A polycationic CPP peptide (in blue) fused to a polyanionic masking peptide (in red) through a linker cleavable by matrix metalloproteases (MMPs) which are overexpressed on the surface of numerous cancer cells.

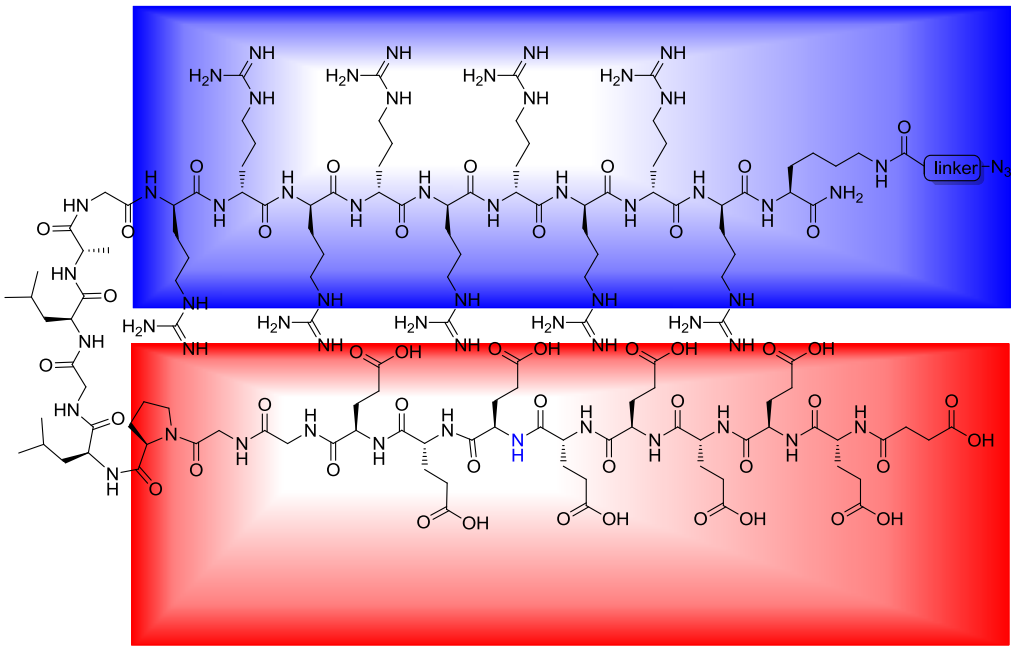

Figure 5.2 CPP masked with ions pair linked with peptide substrate (GGPLGLAG)

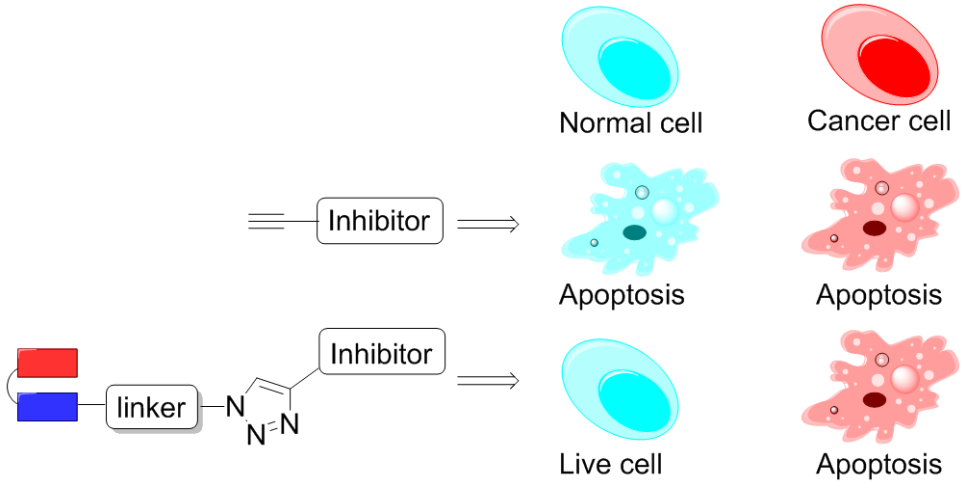

Figure 5.3 Strategy of cell specific delivery study

To control the release of the cytotoxic kinase inhibitor from a conjugated, the cleavable linkers would be introduced. The synthetic plan of lead probes is shown in Scheme 5.1. STS would be incorporated with CPP through different linkers such as photo-cleavable and disulfur inker, by which the controlled release of drugs could be triggered by different mechanism. Stable alkyl linker is used as control. TER would be used as a fluorescent tag in the paralleled imaging experiment. The clickable kinase inhibitors listed in the Figure 5.4 are the candidates in the place of STS, which provide a wide-range inhibition map over cancer cell through the molecular transporting approach.

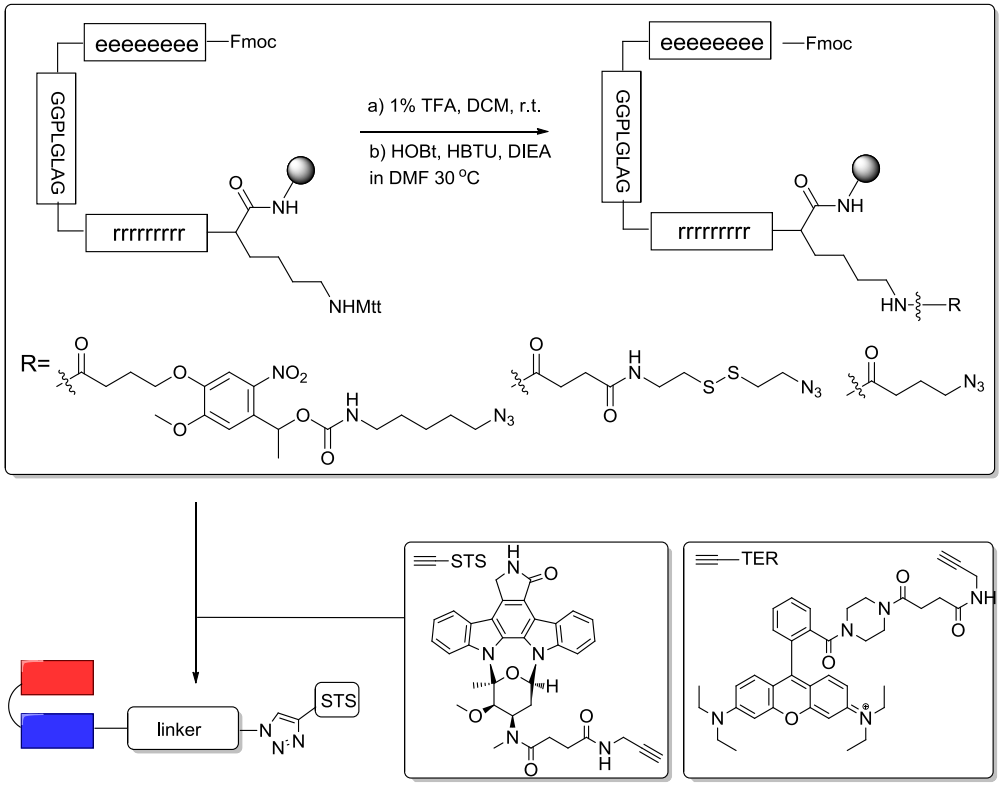

Scheme 5.1. Synthesis of the probes for the concept study of drug delivery

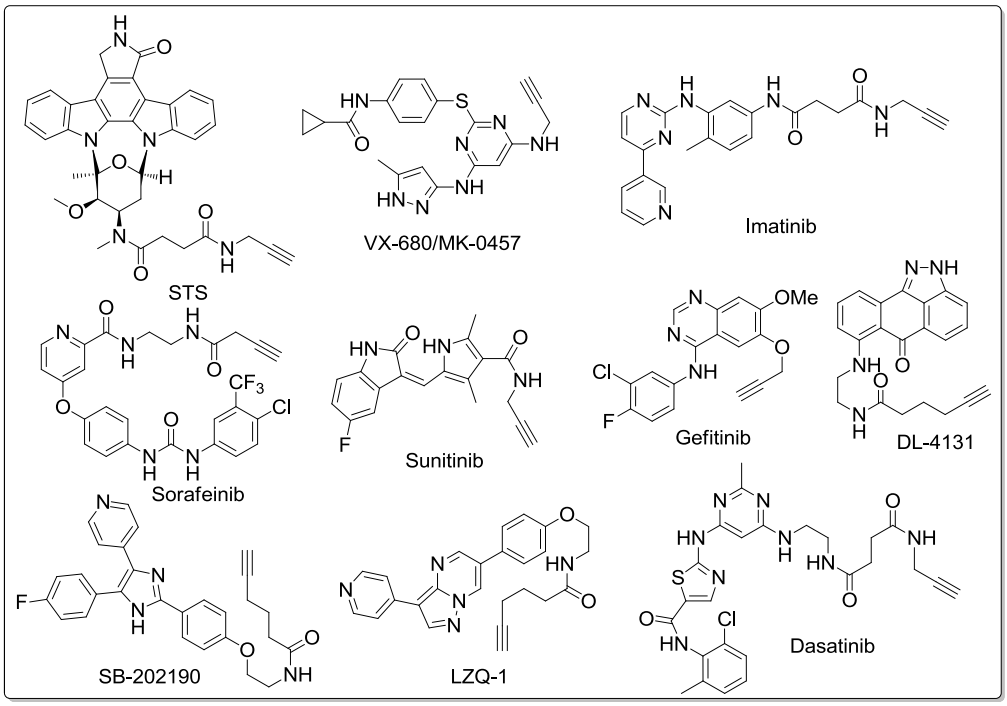

Figure 5.4 Candidates of kinase inhibitors

5.3. Results and discussion

The linkers were synthesized as shown in Scheme 5.2. In the synthesis of alkyl linker, 4-azidobutanoic acid **5-6** was synthesized from 4-bromobutanoic acid **5-5** by 3 steps of reactions. The di-sulfur linker **5-4** was synthesized from cystamine dihydrochloride **5-1** by mono-protection with Boc group, azidation and extension with succinic acid.

In the synthesis of photo-cleavable linker, protection of compound **5-7** with Bn group was proceed well to afford compound **5-8**, which was subjected to nitration to give compound **5-9** in good yield. After deprotection of Bn group with TFA, phenol **5-10** was obtained, which was subjected to the reaction with methyl 4-bromobutanoate to give compound **5-11**. Reaction with sodium borohydride and activation with carbonyl imidazole provided compound **5-13** in good yield, which was stable to be stored in -20 ^{o}C. Compound **5-13** was refluxed with amine to give carmbamate **5-14**, which was hydrolysed with LiOH to give compound **5-15**.

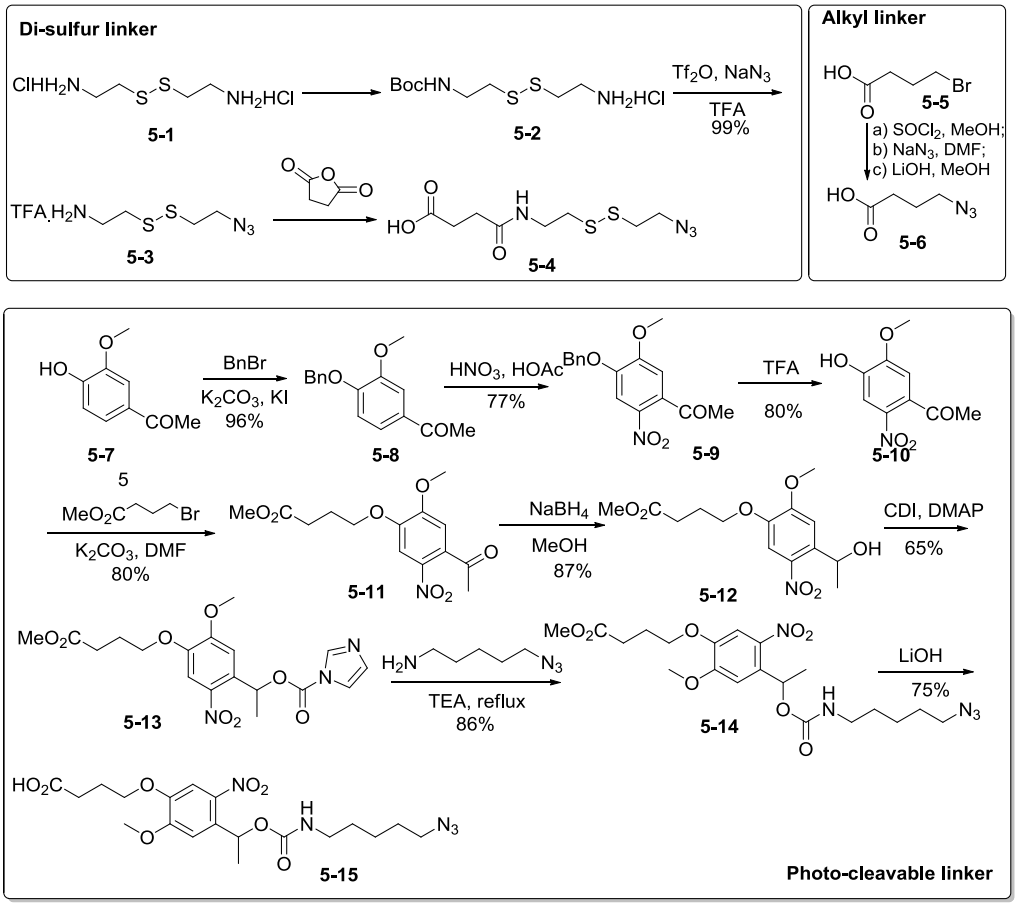

Scheme 5.2 The synthesis of linkers

In the synthesis of coupling of CPP with di-sulfur **5-4** and photo-cleavable linker **5-15**, no product was detected by LC-MS as shown in Scheme 5.1. Compound **5-15** is unstable in the LC-MS probably as the photo-cleavable group is very sensitive in the UV detector. Mild reaction condition and process should be considered.

5.4. Conclusion

This chapter has described an approach to design a probe by specific delivering the cell toxic kinase inhibitors into the cancer cell by CPP. The ion pair of CPP would be cleaved by MMPs overexpressed on some cancer cell surface through the specific substrate recognition. Then the inhibitors were supposed to be released after transported into the cell specifically by the trigger action with UV irradiation or cellular Glutathione (GSH). Therefore, it was hypothesized that kinases in targeted cancer cell would be regulated. In the efforts to synthesize the CPP probes, some progress has been obtained. Uncleavable alkyl linker **5-6**, di-sulfur linker **5-4** cleaved by GSH and photo-cleavable linker **5-15** were successfully synthesized. The synthesis of the probes would push forward in the further study.

Chapter 6

Cancer Cell Targeted Delivery of Regenerable Wortmannin by Folic Acid and Protein Target Profiling of Wortmannin

6.1. Summary

A novel approach was introduced to deliver specifically Wortmannin-based probes into target cancer cell by molecular transporter and then regenerate Wortmannin in active form inside. And its intracellular targets would be identified by activity-based protein profiling (ABPP).

6.2. Introduction

Wortmannin has been studied for many years as an irreversible inhibitor of phosphoinositide 3-kinase (PI3K),[128] which is involved in many types of cancer.[129] Wortmannin is also a potential inhibitor for PLK1, which plays critical roles throughout mitosis.[130] Unlike those kinase inhibitors targeting the cysteinome, as a special example, the active furan ring on Wortmannin targets the unique K833 as the active site in PI3K ATP pocket to form a covalent binding.[131] (Figure 6.1) To evaluate the interactions between Wortmannin and its cellular targets, Cimprich et al developed tag-conjugated probes of Wortmannin, in which the activities of the tag-conjugated probe were affected obviously by its modification mode.[13] At same time, similar work has been done by Liu et al[130, 132] and Lee et al[133]. However, the comprehensive identification of the cellular targets under the native environment is not performed, which could potentially reveal the pharmacodynamic events of Wortmannin *in situ* and benefit the further investigation of drug design.

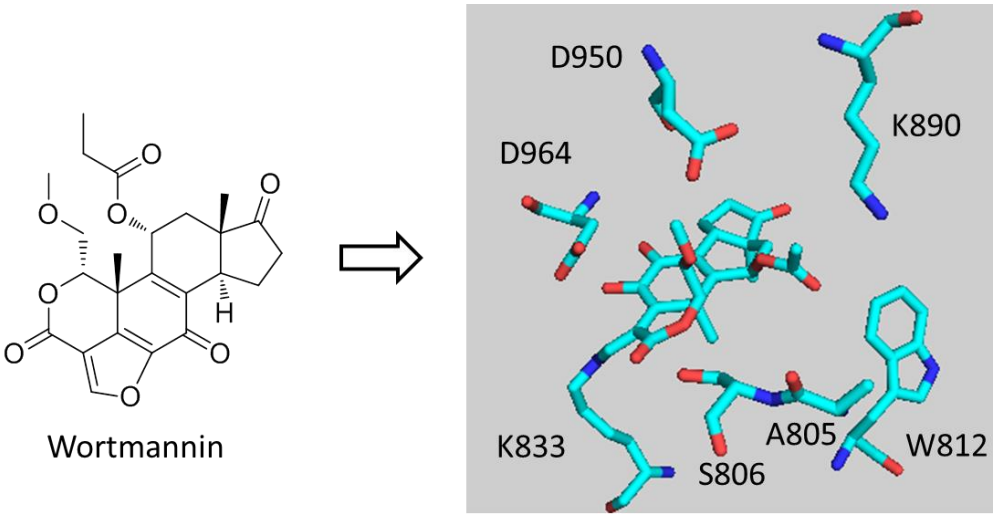

Figure 6.1 Interactions between Wormannin and the PI3K active site. (PDB ID: 1E7U)[131b] K833 as a nucleophile reacts with Wortmannin on the furan ring.

However the stability and toxicity issue of Wortmannin limited its further application in the therapy.[134] As an interesting example, PX-866 derived from Wortmannin with better stability and less toxicity, has been involved in a phase 1 clinical trial.[135] (Figure 6.2) The mechanism that Wortmannin-C20 conjugates could generate Wortmannin was well studied.[136] (Figure 6.3) Compared to the stable adduct from a primary amine with Wortmannin, the reversible adduct from a secondary amine with Wortmannin could regenerate Wortmannin through an intramolecular attack. This phenomenon provides possibility to design safer PI3K inhibitors in slow release form without additional consideration of influence of the modification on C20 position between inhibitor and PI3K.

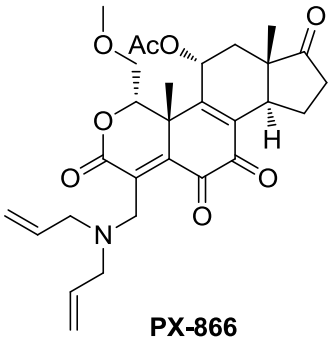

Figure 6.2 Structure of PX-886

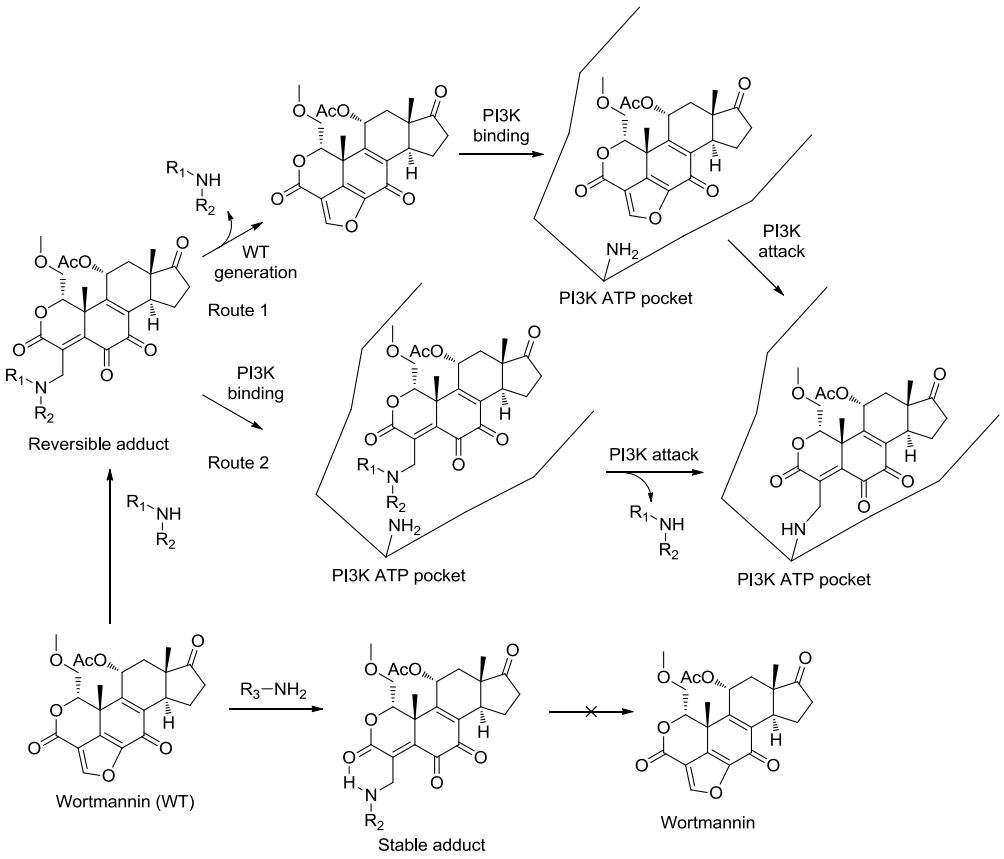

Figure 6.3 Possible mechanisms of Wortmannin (WT) C20 Derivatives.[136] For the reversible adduct from secondary amine with WT, in route 1, it was hypothesized that WT C20 derivatives generate WT and then inhibits PI3K; in route 2, WT C20 derivatives could also bind to PI3K by replacement of secondary amine by lysine as proposed. For the stable adduct from primary amine with WT, no WT is regenerated and no substitution of amine occurs.

To further overcome the toxicity issue, receptor-mediated endocytosis was also developed to allow selective intracellular delivery of therapeutic biomolecules into the cell membrane.[137] This drug delivery approach helps to achieve a better status about safety issue by reducing the drug exposure time and concentration while maintain the same drug effect. For example, the folate receptor (FR) for folic acid and reduced folic acid derivatives is a well-known tumour-associated receptor that is overexpressed on ~40% of human cancers, including those of the breast, lung, kidney brain and so on,[138] whereas in normal tissues and organs its distribution is highly limited.[139] Folic acid (known as vitamin B_9), in itself, shows low risk of toxicity and

therefore is suitable for the conjugating drug design.[140] Folate receptors on the cell membrane bind folate or its derivatives specifically and subsequently mediate delivery into the interior of cells. Based on the natural mechanism of folate uptake by folate receptor protein (FR), folate in drug-conjugated manner also binds tightly to the FR and trigger cellular uptake via endocytosis.[138d, 141] After delivery inside the cell, with the use of proper linkers, folate-conjugated drugs can be released inside the targeted cells where they can perform their desired activity including cytotoxicity. Like folic acid, Biotin was also adopted to deliver drug targeting cancer cell.[142]

Incorporating the advantages above, we try to design a cell permeable, specific and efficient probe, which is capable of the proteomic study of cellular Wortmannin targets. The probe targeting the cancer cells will be delivered by FR, and regenerate the “clickable” Wortmannin probe with minimum modification compared to its parent drug—Wortmannin. The typical format of the probe fulfilling the requirements is shown in Figure 6.4. C11 modified site is to click with reporter and C20 site is for transporter conjugating. Secondary amine is needed to form an adduct other than primary amine because the former could form a reversible adduct, while the latter could form a stable uncleavable adduct.[136] The folic acid conjugated probe will be delivered into cancer cell by FR, and then Wortmannin part will be regenerated through the reversible mechanism at C20. Then the regenerated “clickable” probe of Wortmannin will be available for proteomic study by the well-known activity-based protein profiling (ABPP).[6a](Figure 6.5)

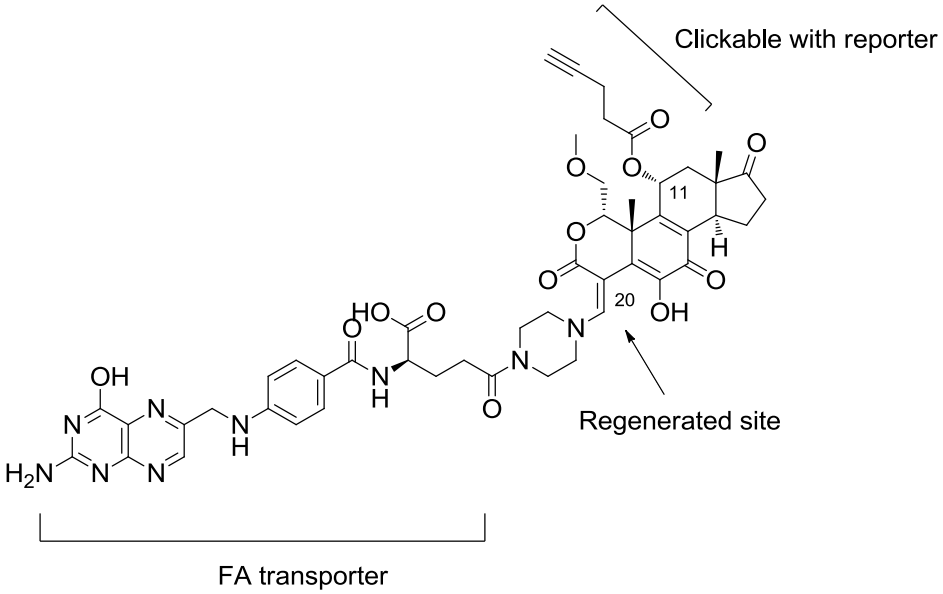

Figure 6.4 A typical probe containing transporter, regenerating group and “clickable” handle

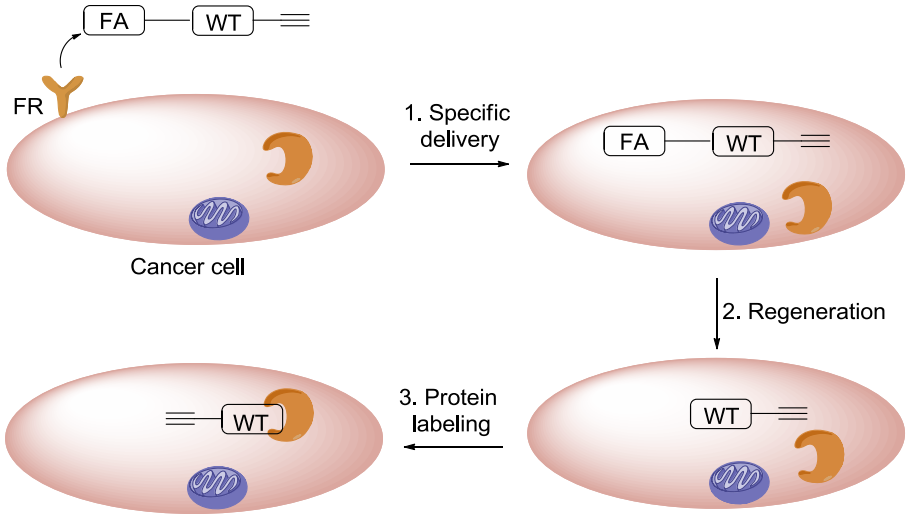

Figure 6.5 Specific delivery of Folic acid (FA) conjugated Wortmannin probe into cancer cell. In the first step, the probe was delivered into cancer cell specifically. Then in the second step, the uptaken probe regenerates “clickable” Wortmannin (WT) probe *in situ*. In the final step, the drug-like probe could labels the protein targets *in situ*.

6.3. Results and discussion

The synthetic route to the regenerated probe **6-7** was outlined in Scheme 6.1. Wortmannin was deacetylated successfully through two steps to give compound **6-2**.[13] The following esterification of compound **6-2** proceeded well to introduce terminal alkyne group, which is clickable with reporter. The modification of folic acid part also worked well to form compound **6-6** through two steps without further purification as the poor solubility of folate. Since Wortmannin was costly, the final step to form the regenerated site was first tested by model reaction.

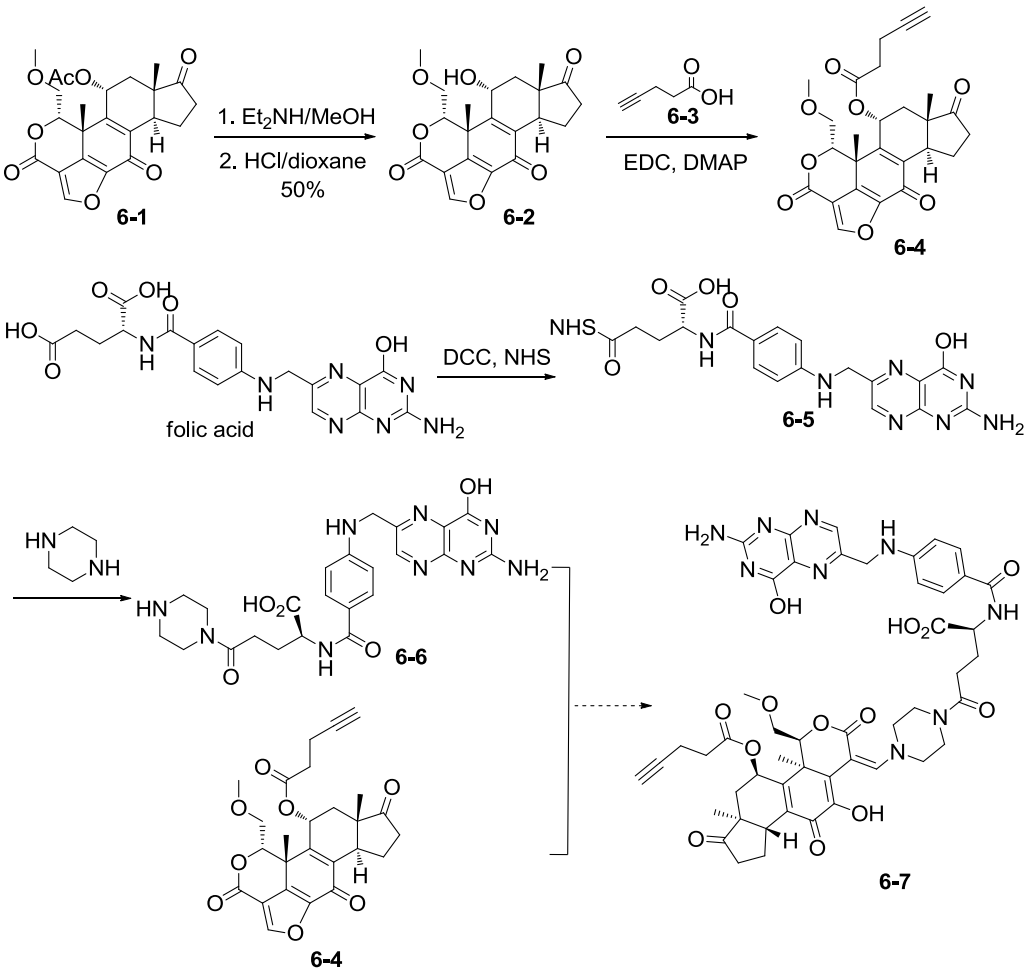

Scheme 6.1 Synthesis of the probe

In the model reaction of Wortmannin **6-1** with cyclic amine **6-6**,

product of **6-8** was detected by LC-MS analysis. (Scheme 6.2). Because of the poor solubility of folic acid moiety even in DMSO or DMF (insoluble in other solvents), we tried to isolate the product by HPLC. Unfortunately, the product as green fractions was decomposed in 30 min. The product **6-7** was too unstable to be handled. The stability of the conjugation adduct should be tuned by the different types of substituted amine. The uncyclic secondary amine conjugated product should be more stable according to the literatures.[136] And *in situ* generation of the ring-opening product **6-7** will be a better choice since the reaction is very fast to complete in few minutes.

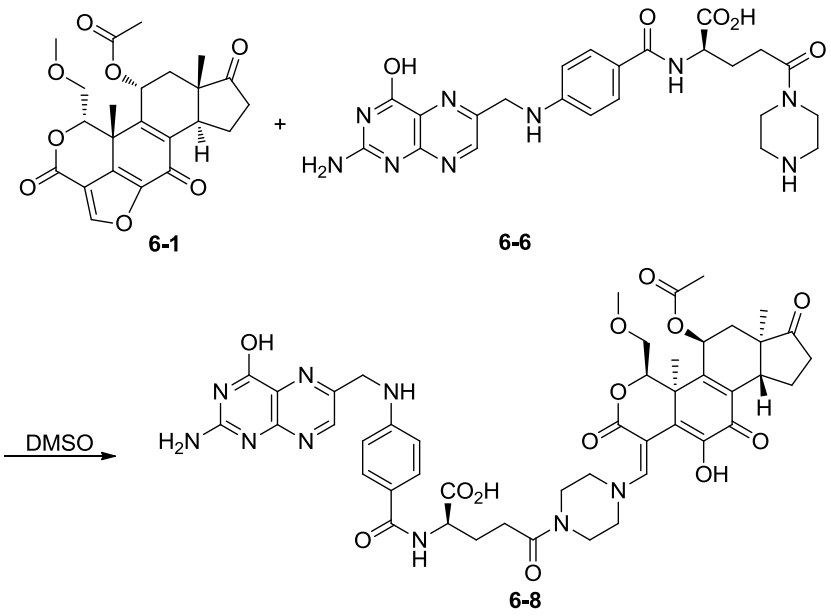

Scheme 6.2 The coupling of the amine with Wortmannin

6.4. Conclusion

This project has described an approach to design a prodrug-like probe **6-7** which delivers a cell toxic inhibitor-Wortmannin into the cancer cell by receptor-ligand based endocytosis. Based on the reversible mechanism of the C-20 conjugated adduct, the probe as a prodrug will re-generate a “clickable” Wortmannin probe **6-4** *in situ* after

being transported into cancer cells specifically by aid of folate receptor (FR)-triggered cellular uptake via endocytosis. This drug delivery approach would help to reduce the drug exposure time and concentration to achieve a better status about safety issue by “protecting” the drug in a prodrug manner. Combined with the LC-MS/validation experiment, the approach also would facilitate the subsequent protein profiling of the potential cellular targets *in situ* comprehensively. The key intermediate **6-4** which is the true probe used in the proteome labeling was successfully synthesized. This work is still under investigation to overcome the synthetic problems described before. Biotin as a ligand for the tumor-related receptor would be a better alternative due to its better solubility than folic acid.

Chapter 7

Experimental section

7.1. General

All chemicals were purchased from commercial vendors and used without further purification, unless indicated otherwise. All reaction requiring anhydrous conditions were carried out under argon or nitrogen atmosphere using oven-dried glassware. HPLC-grade solvents were used for all reactions. Reaction progress was monitored by TLC on pre-coated silica plates (Merck 60 F254, 0.25 µm) and spots were visualized by UV or iodine stain. Flash column chromatography was carried out using Merck 60 F254, 0.040-0.063 µm silica gel. All NMR spectra (^{1}H-NMR, ^{13}C-NMR) were recorded on a Bruker NMR spectrometer (300 MHz for ^{1}H and 75 MHz for ^{13}C). Chemical shifts were reported in parts per million referenced with respect to appropriate internal standards or residual solvent peaks ($CDCl_3$ = 7.26 ppm, CD_3OD = 3.31 ppm, DMSO-d_6 = 2.50 ppm). The following abbreviations were used in reporting spectra, s = singlet, d = doublet, t = triplet, q = quartet, m = multiplet, dd = doublet of doublets, br = broad. All analytical HPLC were carried out on Shimadzu LCMS (IT-TOF) system or Shimadzu LCMS-2010EV system equipped with an auto-sampler using reverse-phase Phenomenex Luna 5 µm C18(2) 100 Å 50 × 3.0 mm columns. Water with 0.1% TFA and acetonitrile with 0.1% TFA were used as eluents and the flow rate was 0.6 mL/min. For enzyme inhibition and IC_{50} measurements, Tecan microplate reader (Multimode Reader, Infinite®200) in luminescence mode with i-controlTM software was used. Fluorescence scanning of the SDS-PAGE gels was carried out with Typhoon 9410 fluorescence gel scanner (Amersham Biosciences), and where applicable, the bands were quantified with ImageQuant 3.3 (Molecular Dynamics) software installed on the scanner. Imaging was done with the Leica TCS SP5X confocal microscope system equipped with Leica HCX PL APO 63×/1.20 W CORR CS, 405 nm diode laser, white laser (470−670 nm, with 1 nm increments, with eight channels AOTF for simultaneous control of eight laser lines, each excitation wavelength provides 1.5 mV), and a photomultipliertube (PMT) detector ranging from 410 to 700

nm for steady state fluorescence. Images were processed with Leica Application Suite Advanced Fluorescence (LAS AF). All enzymes used were expressed in *E. coli* strain BL21-DE3 and purified as described previously.1 Staurosporine (98%) were purchased from LC Lab. Tris(2-carboxyethyl) phosphine (TCEP), and the click chemistry ligand, tris[(1-benzyl- 1H-1,2,3-triazol-4-yl)methyl]amine (TBTA) were purchased from Sigma-Aldrich.

7.2. Chapter 2

7.2.1. Procedures for the syntheses of probe C75 analogues 2-9a-g and trifunctional tag (Rh-Biotin-N_3)

General procedure of the synthesis of alkynoic acid 2-2d, 2-2e, 2-2g: To a solution of ethynyltrimethylsilane (5.1 mL, 36 mmol) in dry THF (45 mL) was added dropwise BuLi (23 mL, 37 mmol) at -78 °C. After 15 min of stirring, dry DMPU (28 mL) was added and the reaction was stirred for 1 h at -78 °C. The solution of bromoalkanoic acid **2-1** (14 mmol) in THF (2.0 mL) was added dropwise. The reaction was slowly warm to rt and stirred overnight. The reaction was quenched with 1 *N* HCl to pH=1~2 and extracted with ethyl acetate (10 mL × 3). The combined organic layers were dried over anhyd sodium sulfate, concentrated *in vacuo* to give the residue which was purified by comlumn chromatography.

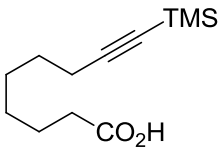

9-(Trimethylsilyl)non-8-ynoic acid (**2-2d)**, as a colorless liquid (52%). ^{1}H NMR (300 MHz, $CDCl_3$) δ 10.02 (*br*s, 1H), 2.34 (t, *J* = 7.5 Hz, 2H), 2.20 (t, *J* = 6.9 Hz, 2H), 1.70 – 1.56 (m, 2H), 1.56 – 1.45 (m, 2H), 1.45 – 1.28 (m, 4H), 0.15 – 0.06 (m, 9H);^{13}C NMR (75 MHz, $CDCl_3$) δ 180.27, 107.37, 84.44, 33.97, 28.44, 28.29, 24.46, 19.71, 0.12; ^{13}C NMR (DEPT 135, up(+), down(-), 75 MHz, $CDCl_3$) δ 33.97(-), 28.44(-), 28.29(-), 24.46(-), 19.71(-), 0.12(+).

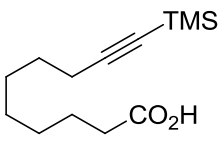

10-(Trimethylsilyl)dec-9-ynoic acid (**2-2e)**, as a colorless liquid (50%). ^{1}H NMR (300 MHz, $CDCl_3$) δ 10.34 (s, 1H), 2.32 (t, *J* = 7.4 Hz, 2H), 2.18 (t, *J* = 6.9 Hz, 2H), 1.60 (dd, *J* = 13.7, 6.8 Hz, 2H), 1.54 – 1.42 (m, 2H), 1.42 – 1.17 (m, 6H), 0.12 (s, 9H); ^{13}C NMR (75 MHz, $CDCl_3$) δ 180.34, 107.49, 84.30, 34.02, 28.82, 28.62, 28.47, 28.44, 24.52, 19.73, 0.10; ^{13}C NMR (DEPT 135, up(+), down(-), 75 MHz, $CDCl_3$) δ 34.02(-), 28.82(-), 28.62(-), 28.47(-), 28.44(-), 24.52(-), 19.73(-), 0.10(+).

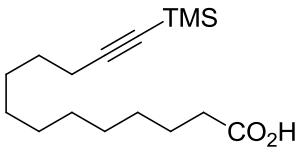

13-(Trimethylsilyl)tridec-12-ynoic acid (2-2g), as a white solid (56%). ^{1}H NMR (300 MHz, $CDCl_3$) δ 9.98 (s, 1H), 2.33 (t, *J* = 7.5 Hz, 2H), 2.19 (t, *J* = 7.1 Hz, 2H), 1.73 – 1.55 (m, 2H), 1.48 (dd, *J* = 14.6, 7.2 Hz, 2H), 1.31 (d, *J* = 23.3 Hz, 12H), 0.13 (s, 9H); ^{13}C NMR (75 MHz, $CDCl_3$) δ 180.35, 107.71, 84.22, 34.07, 29.37, 29.31, 29.18, 29.02, 29.00, 28.73, 28.59, 24.64, 19.81, 0.15.

General procedure for the syntheses of alkynol 2-4d, 2-4e, 2-4g: To the suspension of $LiAlH_4$ (1.1 g, 7.4 mmol) in THF (30 mL) was added dropwise the solution of alkynoic acid **2-2d** (**2-2e**, **2-2g**) in THF (2 mL) at 0 °C. The reaction was slowly warm to rt and stirred at r.t for 3 h. The reaction was quenched with aq NH_4Cl and filtered. After the precipitated solid was refluxed with THF (30 mL) for 30 min and filtered, the combined filtrates were concentrated, dissolved in the solution of TBAF (1.0 M, 15 mmol) and stirred at rt for further 3 h. After the reaction was complete, the reaction mixture was proportion with aq NH_4Cl (20 mL) and ethyl acetate (10 mL). The aq layer was extracted with ethyl acetate (10 mL × 3). The combined ethyl acetate was washed with brine, dried over anhyd sodium sulfate and concentrated

in vacuo. The residue was purified by column chromatography to give the desired product.

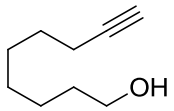

Non-8-yn-1-ol (2-4d), (86%). ^{1}H NMR (300 MHz, $CDCl_3$) δ 3.54 (t, J = 6.6 Hz, 2H), 2.28 (s, 1H), 2.11 (td, J = 6.9, 2.6 Hz, 2H), 1.88 (t, J = 2.6 Hz, 1H), 1.64 – 1.40 (m, 4H), 1.40 – 1.23 (m, 6H); ^{13}C NMR (75 MHz, $CDCl_3$) δ 84.47, 68.03, 62.54, 32.50, 28.74, 28.52, 28.23, 25.48, 18.18.

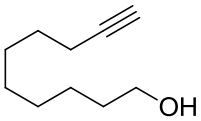

Dec-9-yn-1-ol (2-4e), (86%). ^{1}H NMR (300 MHz, $CDCl_3$) δ 3.58 (t, J = 6.6 Hz, 2H), 2.14 (td, J = 7.0, 2.6 Hz, 2H), 1.96 (br, 1H), 1.91 (t, J = 2.7 Hz, 1H), 1.63 – 1.43 (m, 4H), 1.42 – 1.24 (m, 8H); ^{13}C NMR (75 MHz, $CDCl_3$) δ 84.63, 68.04, 62.76, 32.61, 29.18, 28.96, 28.57, 28.35, 25.60, 18.27.

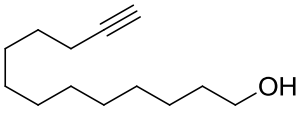

Tridec-12-yn-1-ol (**2-4g)**, (95%). ^{1}H NMR (300 MHz, $CDCl_3$) δ 3.58 (t, J = 6.6 Hz, 2H), 2.14 (td, J = 7.0, 2.5 Hz, 2H), 1.97 – 1.84 (m, 1H), 1.60 – 1.42 (m, 4H), 1.36 – 1.17 (m, 14H); ^{13}C NMR (75 MHz, $CDCl_3$) δ 84.48, 67.96, 62.43, 32.51, 29.42, 29.36, 29.31, 29.29, 28.92, 28.56, 28.30, 25.61, 18.19.

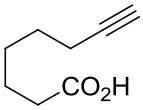

The synthesis of oct-7-ynoic acid (2-6c): To the mixture of ethane-1,2-diamine-ethynyllithium complex (2.0 g, 20 mmol) in THF (25 mL) was added 6-bromohexanoic acid **2-1c** (2.0 g, 10 mmol) in 1,3-Dimethyl-3,4,5,6-tetrahydro-2(1H)-pyrimidinone (DMPU,13 mL) at 0 °C. The reaction was allowed to warm to r. t. and stirred overnight. The reaction was quenched with aq NH_4Cl, extracted with ethyl acetate (30 mL × 3). The combined organic layers were dried over anhyd sodium sulfate, concentrated to give the residue purified by column chromatography to give **2-6c**. (73%) ^{1}H NMR (300 MHz, $CDCl_3$) δ 11.54 (s, 1H), 2.33 (t, J = 7.4 Hz, 2H), 2.15 (td, J = 6.8, 2.6 Hz, 2H), 1.91 (t, J = 2.6 Hz, 1H), 1.61 (dt, J = 11.4, 7.4 Hz, 2H), 1.56 – 1.34 (m, 4H); ^{13}C NMR (75 MHz, $CDCl_3$) δ 180.24, 84.09, 68.35, 33.82, 27.96, 27.92, 24.00, 18.08.

General procedure of the synthesis of alkynol 2-4b, 2-4c, 2-4f: To the suspension of $LiAlH_4$ (1.13 g, 7.4 mmol) in THF (30 mL) was added dropwise the solution of alkynoic acid **2-6** (7.4 mmol) in THF (2 mL) at 0 °C. The reaction was slowly warm to rt and stirred at rt for 3 h. The reaction was quenched with aq NH_4Cl and filtered. After the precipitated solid was refluxed with THF for 30 min and filtered, the combined filtrates were concentrated to give the residue which was purified by column chromatography.

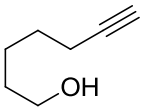

Hept-6-yn-1-ol (**2-4b),** (82%). ^{1}H NMR (300 MHz, $CDCl_3$) δ 3.55 (t, J = 6.3 Hz, 2H), 2.46 (s, 1H), 2.14 (td, J = 6.7, 2.5 Hz, 2H), 1.90 (t, J = 2.6

Hz, 1H), 1.57 – 1.35 (m, 6H); ^{3}C NMR (75 MHz, $CDCl_3$) δ 84.30, 68.20, 62.32, 31.99, 28.09, 24.78, 18.20.

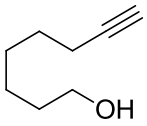

Oct-7-yn-1-ol (2-4c), (96%). ^{1}H NMR (500 MHz, $CDCl_3$) δ 3.56 (t, J = 6.6 Hz, 2H), 2.33 (s, 1H), 2.15 – 2.12 (m, 2H), 1.90 (s, 1H), 1.53 – 1.39 (m, 4H), 1.42 – 1.28 (m, 4H); ^{13}C NMR (126 MHz, $CDCl_3$) δ 84.47, 68.12, 62.50, 32.39, 28.35, 28.25, 25.12, 18.17.

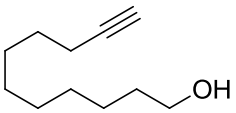

Undec-10-yn-1-ol (2-4f), (97%). ^{1}H NMR (300 MHz, $CDCl_3$) δ 3.56 (t, J = 6.6 Hz, 2H), 2.16 – 2.01 (m, 1H), 1.90 (t, J = 2.6 Hz, 1H), 1.52 – 1.44 (m, 1H), 1.40 – 1.05 (m, 5H); ^{13}C NMR (75 MHz, $CDCl_3$) δ 84.61, 68.00, 62.70, 32.60, 29.32, 29.25, 28.90, 28.59, 28.34, 25.61, 18.25.

General procedure of the synthesis of alkynal 2-5a-g: To the mixture of PCC (3.8 g, 18 mmol) and sodium acetate (0.15 g, 1.8 mmol) in dry DCM (15 mL) was added alkynol **4** (12 mmol) at 0 °C. After the reaction was complete, diethyl ether (15 mL) was added to the reaction. The mixture was loaded to silica gel column chromatography eluted with diethyl ether. The desired aldehyde was concentrated carefully and used in next step because most of the aldehydes are volatiles. ^{1}H NMR was used to detect proton of aldehyde (~9.7 ppm) in presence of residual solvent if any. (70%~quant.)

The representing ^{1}H NMR data for **2-5C**, ^{1}H NMR (300 MHz, $CDCl_3$) δ 9.77 (s, 1H), 2.55 – 2.38 (m, 2H), 2.20 (td, J = 6.8, 2.7 Hz, 2H), 1.94 (t, J = 2.6 Hz, 1H), 1.70-1.61 (m, 2H), 1.57 – 1.35 (m, 4H).

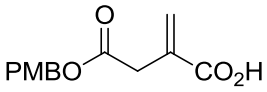

The synthesis of 4-((4-methoxybenzyl)oxy)-2-methylene-4-oxobutanoic acid (2-7)[80] Itaconic anhydride (10 g, 89 mmol) and 4-methoxybenzyl alcohol (12.30 g, 85 mmol) were suspended in 100 mL of a mixture of toluene/n-hexane = 1/1 (v/v) and stirred at 60 °C for 36 h. After cooling down, the formed precipitate was collected, washed with n-hexane and dried *in vacuo* to give **2-7** (100%)

General procedure for the synthesis of PMB-C75 analogues 2-8a-g: LDA (8.2 mL of 1 M solution in THF, 8.2 mmol) was added to a solution of **2-7** (1 g, 4 mmol), dissolved in 10 mL of dry THF and cooled to –78 °C in a dry ice-acetone bath. After 1 h, the aldehyde **2-5g** (5.2 mmol) was added and the mixture was stirred for additional 4 h at low temperature. To the reaction was added cold 6 *N* H_2SO_4. After 5 min, the reaction mixture was extracted with ethyl acetate. The organic layer was separated, dried with anhyd sodium sulfate and concentrated *in vacuo*. The resulted oily residue was purified through column chromatography with n-hexane, ethyl acetate (3/1 = v/v) as eluent.

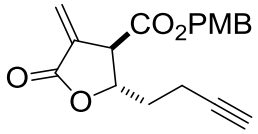

***trans*-4-Methoxybenzyl 2-(but-3-yn-1-yl)-4-methylene-5-oxotetrahydrofuran-3-carboxylate (2-8a)**, as a colorless oil (19%). ^{1}H NMR (300 MHz, $CDCl_3$) δ 7.27 (d, J = 8.6 Hz, 2H), 6.88 (d, J = 8.5 Hz, 2H),

6.35 (d, *J* = 2.9 Hz, 1H), 5.86 (d, *J* = 2.6 Hz, 1H), 5.14 (q, *J* = 11.8 Hz, 2H), 4.92 (dd, *J* = 13.2, 5.8 Hz, 1H), 3.79 (s, 3H), 3.65 (dt, *J* = 5.6, 2.7 Hz, 1H), 2.37 (t, *J* = 6.2 Hz, 2H), 1.99 – 1.83 (m, 3H); ^{13}C NMR (75 MHz, $CDCl_3$) *δ* 168.59, 167.88, 159.89, 132.41, 130.27, 126.91, 125.52, 114.01, 82.09, 69.62, 67.57, 55.19, 49.47, 34.27, 14.54.

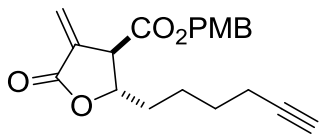

***trans*-4-Methoxybenzyl 2-(hex-5-yn-1-yl)-4-methylene-5-oxotetrahydrofuran-3-carboxylate (2-8b)**, as a colorless oil (58%). ^{1}H NMR (500 MHz, $CDCl_3$) *δ* 7.28 (d, *J* = 8.6 Hz, 2H), 6.89 (d, *J* = 8.6 Hz, 2H), 6.34 (d, *J* = 2.9 Hz, 1H), 5.84 (d, *J* = 2.7 Hz, 1H), 5.14 (dd, *J* = 27.6, 11.8 Hz, 2H), 4.78 (dd, *J* = 12.6, 6.2 Hz, 1H), 3.80 (s, 3H), 3.59 (dt, *J* = 5.8, 2.9 Hz, 1H), 2.17 (td, *J* = 6.5, 2.6 Hz, 2H), 1.95 (t, *J* = 2.7 Hz, 1H), 1.80 – 1.68 (m, 2H), 1.61 – 1.48 (m, 4H); ^{13}C NMR (126 MHz, $CDCl_3$) *δ* 168.74, 167.96, 159.75, 132.74, 130.10, 126.87, 124.92, 113.89, 83.66, 78.50, 68.59, 67.34, 55.04, 49.58, 34.85, 27.62, 23.67, 17.92.

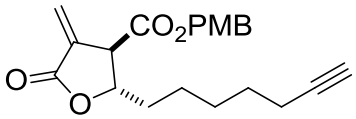

***trans*-4-Methoxybenzyl 2-(hept-6-yn-1-yl)-4-methylene-5-oxotetrahydrofuran-3-carboxylate (2-8c)**, as a colorless oil (29%). ^{1}H NMR (300 MHz, $CDCl_3$) *δ* 7.27 (d, *J* = 8.7 Hz, 2H), 6.89 (d, *J* = 8.7 Hz, 2H), 6.34 (d, *J* = 3.1 Hz, 1H), 5.83 (d, *J* = 2.7 Hz, 1H), 5.14 (q, *J* = 11.8 Hz, 2H), 4.78 (dd, *J* = 12.8, 6.0 Hz, 1H), 3.81 (s, 3H), 3.55 (dt, *J* = 5.8, 2.9 Hz, 1H), 2.19 – 2.12 (m, 2H), 1.93 (t, *J* = 2.6 Hz, 1H), 1.76 – 1.63 (m, 2H), 1.54 – 1.39 (m, 6H); ^{13}C NMR (75 MHz, $CDCl_3$) *δ* 168.97, 168.23, 159.96, 132.93, 130.31, 127.02, 125.14, 114.09, 84.25, 78.79, 68.38, 67.56, 55.26, 49.86, 35.52, 28.16, 28.10, 24.27, 18.21.

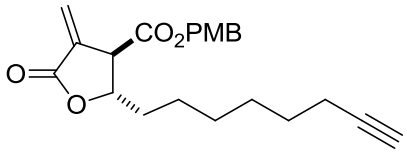

***trans*-4-Methoxybenzyl 4-methylene-2-(oct-7-yn-1-yl)-5-oxotetrahydrofuran-3-carboxylate (2-8d)**, as a colorless oil (11%). ^{1}H NMR (300 MHz, $CDCl_3$) δ 7.27 (d, J = 8.6 Hz, 2H), 6.89 (d, J = 8.7 Hz, 2H), 6.34 (d, J = 3.1 Hz, 1H), 5.82 (d, J = 2.7 Hz, 1H), 5.14 (q, J = 11.8 Hz, 2H), 4.77 (dd, J = 12.9, 5.9 Hz, 1H), 3.80 (s, 3H), 3.55 (dt, J = 5.8, 2.9 Hz, 1H), 2.22 – 2.08 (m, 2H), 1.93 (t, J = 2.6 Hz, 1H), 1.78 – 1.62 (m, 2H), 1.57 – 1.44 (m, 2H), 1.38 (m, 6H); ^{13}C NMR (75 MHz, $CDCl_3$) δ 168.97, 168.19, 159.92, 132.97, 130.26, 127.01, 125.02, 114.04, 84.40, 78.81, 68.23, 67.50, 55.22, 49.83, 35.52, 28.52, 28.33, 28.15, 24.54, 18.22.

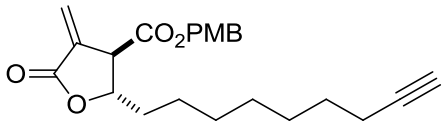

***trans*-4-Methoxybenzyl 4-methylene-2-(non-8-yn-1-yl)-5-oxotetrahydrofuran-3-carboxylate (2-8e)**, as a colorless oil (14%). ^{1}H NMR (300 MHz, $CDCl_3$) δ 7.27 (d, J = 8.4 Hz, 2H), 6.90 (d, J = 8.6 Hz, 2H), 6.34 (d, J = 3.0 Hz, 1H), 5.81 (d, J = 2.6 Hz, 1H), 5.15 (q, J = 11.9 Hz, 2H), 4.76 (dd, J = 12.4, 6.2 Hz, 1H), 3.81 (s, 3H), 3.55 (dt, J = 5.7, 2.8 Hz, 1H), 2.20 – 2.13 (m, 2H), 1.92 (t, J = 2.6 Hz, 1H), 1.79 – 1.64 (m, 2H), 1.56 – 1.48 (m, 2H), 1.46 – 1.29 (m, 8H); ^{13}C NMR (75 MHz, $CDCl_3$) δ 169.01, 168.25, 159.93, 132.99, 130.29, 127.02, 125.05, 114.06, 84.56, 78.88, 68.15, 67.53, 55.25, 49.85, 35.60, 28.94, 28.77, 28.46, 28.30, 24.62, 18.29.

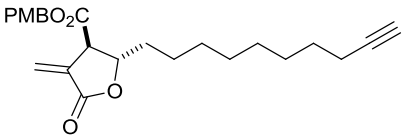

***trans*-4-Methoxybenzyl 2-(dec-9-yn-1-yl)-4-methylene-5-oxotetra-hydrofuran-3-carboxylate (*trans*-2-8f)**, as a colorless oil (26%). ^{1}H NMR (500 MHz, $CDCl_3$) δ 7.29 (d, J = 8.6 Hz, 2H), 6.90 (d, J = 8.6 Hz, 2H), 6.35 (d, J = 3.0 Hz, 1H), 5.83 (d, J = 2.7 Hz, 1H), 5.15 (dd, J = 30.0, 11.8 Hz, 2H), 4.79 (dt, J = 7.4, 5.7 Hz, 1H), 3.82 (s, 3H), 3.56 (dt, J = 5.8, 2.8 Hz, 1H), 2.18 (td, J = 7.1, 2.6 Hz, 2H), 1.94 (t, J = 2.6 Hz, 1H), 1.76 – 1.64 (m, 2H), 1.56 – 1.47 (m, 2H), 1.47 – 1.22 (m, 12H); ^{13}C NMR (75 MHz, $CDCl_3$) δ 168.98, 168.20, 159.89, 133.00, 130.22, 127.01, 124.96, 114.01, 84.58, 78.86 , 68.08, 67.46, 55.19, 49.80, 35.56, 29.11, 28.98, 28.81, 28.53, 28.31, 24.60, 18.26.

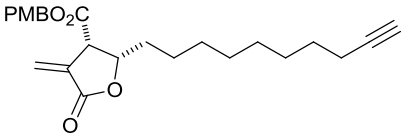

cis*-4-Methoxybenzyl 2-(dec-9-yn-1-yl)-4-methylene-5-oxotetra-hydrofuran-3-carboxylate** (cis*-2-8f)**, as a colorless oil (24%). ^{1}H NMR (300 MHz, $CDCl_3$) δ 7.27 (d, J = 8.7 Hz, 2H), 6.86 (d, J = 8.7 Hz, 2H), 6.36 (d, J = 2.4 Hz, 1H), 5.78 (d, J = 2.1 Hz, 1H), 5.17 – 5.02 (m, 2H), 4.62 – 4.51 (m, 1H), 3.96 (dt, J = 7.7, 2.2 Hz, 1H), 3.79 (d, J = 6.3 Hz, 3H), 2.16 (td, J = 7.0, 2.6 Hz, 2H), 1.92 (t, J = 2.6 Hz, 1H), 1.55 – 1.43 (m, 4H), 1.34 (dd, J = 12.2, 3.6 Hz, 2H), 1.29 – 1.14 (m, 8H); ^{13}C NMR (75 MHz, $CDCl_3$) δ 168.74, 168.66, 159.85, 133.57, 130.47, 127.02, 124.88, 113.91, 84.58, 78.26, 68.08, 66.95, 55.16, 48.88, 31.25, 29.04, 28.97, 28.80, 28.52, 28.33, 25.30, 18.25, -0.11.

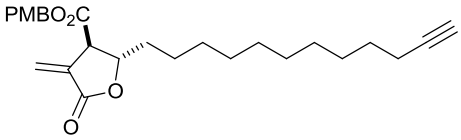

***trans*-4-Methoxybenzyl 2-(dodec-11-yn-1-yl)-4-methylene-5-oxotetrahydrofuran-3-carboxylate (2-8g)**, as a colorless oil (22%). ^{1}H NMR (300 MHz, $CDCl_3$) δ 7.27 (d, J = 8.7 Hz, 2H), 6.89 (d, J = 8.6 Hz, 2H), 6.34 (d, J = 3.0 Hz, 1H), 5.82 (d, J = 2.6 Hz, 1H), 5.14 (q, J = 11.8 Hz, 2H), 4.78 (dd, J = 12.7, 6.0 Hz, 1H), 3.81 (s, 3H), 3.56 (dt, J = 5.7, 2.8 Hz, 1H), 2.17 (td, J = 7.0, 2.5 Hz, 2H), 1.93 (t, J = 2.6 Hz, 1H), 1.77 – 1.59 (m, 2H), 1.54 – 1.45 (m, 2H), 1.40 – 1.22 (m, 14H); ^{13}C NMR (75 MHz, $CDCl_3$) δ 169.04, 168.27, 159.94, 133.05, 130.27, 127.05, 125.01, 114.07, 84.72, 78.94, 68.03, 67.52, 55.24, 49.87, 35.64, 29.35, 29.29, 29.10, 29.01, 28.68, 28.43, 24.67, 18.34.

General procedure for the synthesis of C75 analogues 2-9a-g: The 4-methoxybenzyl protected lactones **2-8a-g** were stirred together with phenol (7.5 g, 80 mmol) and acetic acid (0.37 mL, 6.5 mmol) for 3 h at 60 °C. The reaction mixture was loaded to column chromatography with hexane/ethyl acetate/acetic acid = 7/4/1 (v/v) as eluent.

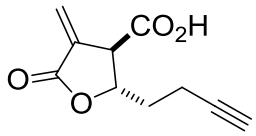

***trans*-2-(But-3-yn-1-yl)-4-methylene-5-oxotetrahydrofuran-3-carboxylic acid (2-9a)**, as a white solid (27%). ^{1}H NMR (300 MHz, $CDCl_3$) δ 6.45 (s, 1H), 6.02 (s, 1H), 4.81 (d, J = 5.3 Hz, 1H), 3.62 (s, 1H), 2.21 (s, 2H), 1.95 (s, 1H), 1.76 (d, J = 5.6 Hz, 2H), 1.58 (s, 4H); ^{13}C NMR (75 MHz, $CDCl_3$) δ 173.44, 168.09, 132.01, 126.36, 82.07, 77.50, 69.84, 49.30, 34.31, 14.59; RMS m/z calcd for $C_{10}H_{10}O_4$ 194.1, $[M-H]^-$ 193.1, found 193.0 (ESI); HRMS m/z calcd for $C_{10}H_{10}O_4$ 194.0579, $[M-H]^-$ 193.0506, found 193.0508 (ESI).

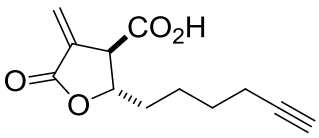

***trans*-2-(Hex-5-yn-1-yl)-4-methylene-5-oxotetrahydrofuran-3-carboxylic acid (2-9b)**, as a white solid, (32%). ^{1}H NMR (300 MHz, $CDCl_3$) δ 6.45 (s, 1H), 6.02 (s, 1H), 4.81 (d, J = 5.3 Hz, 1H), 3.62 (s, 1H), 2.21 (s, 2H), 1.95 (s, 1H), 1.76 (d, J = 5.6 Hz, 2H), 1.58 (s, 4H); ^{13}C NMR (75 MHz, $CDCl_3$) δ 173.97, 168.34, 132.37, 126.03, 83.80, 78.80, 68.78, 49.54, 35.12, 27.79, 23.85, 18.14;LRMS m/z calcd for $C_{12}H_{14}O_4$ 222.1, $[M-H]^-$ 221.1, found 221.0 (ESI); HRMS m/z calcd for $C_{12}H_{14}O_4$ 222.0892, $[M-H]^-$ 221.0819, found 221.0819 (ESI).

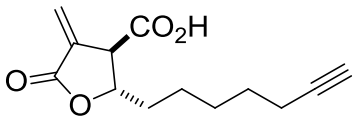

***trans*-2-(Hept-6-yn-1-yl)-4-methylene-5-oxotetrahydrofuran-3-carboxylic acid (2-9c)**, as a white solid (29%). ^{1}H NMR (300 MHz, $CDCl_3$) δ 6.44 (d, J = 2.9 Hz, 1H), 6.01 (d, J = 2.5 Hz, 1H), 4.80 (q, J = 6.2 Hz, 1H), 3.69 – 3.50 (m, 1H), 2.27 – 2.12 (m, 2H), 1.94 (t, J = 2.6 Hz, 1H), 1.74 (t, J = 6.7 Hz, 2H), 1.63 – 1.36 (m, 6H); ^{13}C NMR (75 MHz, $CDCl_3$) δ 173.89, 168.41, 132.39, 125.99, 84.25, 78.89, 68.44, 49.59, 35.54, 28.15, 28.08, 24.30, 18.21; LRMS m/z calcd for $C_{13}H_{16}O_4$ 236.1, $[M-H]^-$ 235.1, found 234.9 (ESI); HRMS m/z calcd for $C_{13}H_{16}O_4$ 236.1049, $[M-H]^-$ 235.0976, found 235.0971 (ESI).

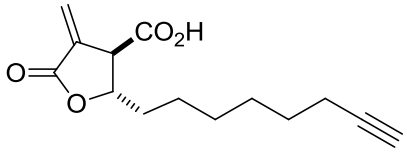

***trans*-4-Methylene-2-(oct-7-yn-1-yl)-5-oxotetrahydrofuran-3-carboxylic acid (2-9d)**, as a white solid (31%). ^{1}H NMR (300 MHz, $CDCl_3$) δ 6.43 (d, J = 2.9 Hz, 1H), 6.00 (d, J = 2.5 Hz, 1H), 4.79 (dd, J = 12.3,

6.1 Hz, 1H), 3.60 (dt, *J* = 5.3, 2.5 Hz, 1H), 2.19 – 2.11 (m, 2H), 1.92 (t, *J* = 2.6 Hz, 1H), 1.76 – 1.69 (m, 2H), 1.56 – 1.48 (m, 2H), 1.43 – 1.30 (m, 6H); ^{13}C NMR (75 MHz, $CDCl_3$) *δ* 173.93, 168.50, 132.50, 125.88, 84.42, 79.02, 68.27, 49.57, 35.55, 28.55, 28.33, 28.14, 24.58, 18.23; LRMS m/z calcd for $C_{14}H_{18}O_4$ 250.1, $[M-H]^-$ 249.1, found 249.0 (ESI); HRMS m/z calcd for $C_{14}H_{18}O_4$ 250.1205, $[M-H]^-$ 249.1132, found 249.1135 (ESI).

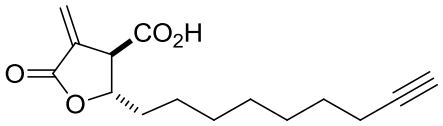

***trans*-4-Methylene-2-(non-8-yn-1-yl)-5-oxotetrahydrofuran-3-carboxylic acid (2-9e)**, as a white solid (34%). ^{1}H NMR (300 MHz, $CDCl_3$) *δ* 6.45 (d, *J* = 2.9 Hz, 1H), 6.01 (d, *J* = 2.5 Hz, 1H), 4.80 (dd, *J* = 12.3, 6.1 Hz, 1H), 3.68 – 3.55 (m, 1H), 2.18 (td, *J* = 7.0, 2.7 Hz, 2H), 1.93 (t, *J* = 2.6 Hz, 1H), 1.81 – 1.65 (m, 2H), 1.50 (m, *J* = 7.0 Hz, 2H), 1.44 – 1.29 (m, 8H); ^{13}C NMR (75 MHz, $CDCl_3$) *δ* 174.14, 168.35, 132.51, 125.86, 84.59, 78.95, 68.19, 49.59, 35.66, 28.97, 28.78, 28.47, 28.30, 24.67, 18.30; LRMS m/z calcd for $C_{15}H_{20}O_4$ 264.1, $[M-H]^-$ 263.1, found 263.0 (ESI); HRMS m/z calcd for $C_{15}H_{20}O_4$ 264.1362, $[M-H]^-$ 263.1289, found263.1296 (ESI).

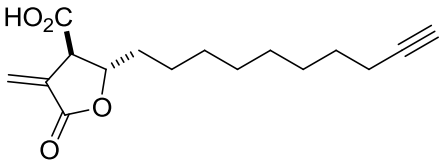

***trans*-2-(Dec-9-yn-1-yl)-4-methylene-5-oxotetrahydrofuran-3-carboxylic acid (*trans*-2-9f)**, as a white solid (33%). ^{1}H NMR (300 MHz, $CDCl_3$) *δ* 6.43 (d, *J* = 2.8 Hz, 1H), 6.00 (d, *J* = 2.5 Hz, 1H), 4.79 (q, *J* = 6.1 Hz, 1H), 3.66 – 3.53 (m, 1H), 2.16 (td, *J* = 7.0, 2.6 Hz, 2H), 1.92 (t, *J* = 2.6 Hz, 1H), 1.78 – 1.65 (m, 2H), 1.49 (dd, *J* = 14.2, 7.0 Hz, 2H), 1.44 – 1.19 (m, 10H); ^{13}C NMR (75 MHz, $CDCl_3$) *δ* 174.23, 168.48,

132.49, 125.85, 84.64, 79.01, 68.10, 49.56, 35.62, 29.14, 29.02, 28.83, 28.55, 28.32, 24.65, 18.28; LRMS m/z calcd for $C_{15}H_{20}O_4$ 278.2, $[M-H]^-$ 277.1, found 277.1 (ESI);HRMS m/z calcd for $C_{15}H_{20}O_4$ 278.1518, $[M-H]^-$ 277.1445, found 277.1443 (ESI).

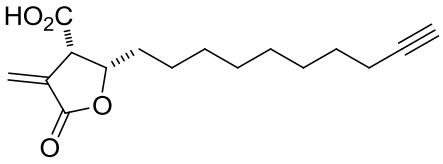

cis*-2-(Dec-9-yn-1-yl)-4-methylene-5-oxotetrahydrofuran-3-carboxylic acid** (cis*-2-9f)**, as a white solid (27%). ^{1}H NMR (300 MHz, $CDCl_3$) δ 6.41 (d, J = 1.8 Hz, 1H), 5.87 (d, J = 1.5 Hz, 1H), 4.64 (dd, J = 13.7, 7.3 Hz, 1H), 4.00 (d, J = 7.5 Hz, 1H), 2.21 – 2.12 (m, 2H), 1.93 (t, J = 2.6 Hz, 1H), 1.72 – 1.68 (m, 2H), 1.55 – 1.46 (m, 2H), 1.44 – 1.26 (m, 10H); ^{13}C NMR (75 MHz, $CDCl_3$) δ 173.72, 169.02, 133.51, 125.45, 84.67, 78.22, 68.13, 48.98, 31.30, 29.20, 29.06, 28.87, 28.58, 28.35, 25.52, 18.31;LRMS m/z calcd for $C_{16}H_{22}O_4$ 278.2, $[M-H]^-$ 277.1, found 277.1 (ESI);HRMS m/z calcd for $C_{16}H_{22}O_4$ 278.1518, $[M-H]^-$ 277.1445, found 277.1435 (ESI).

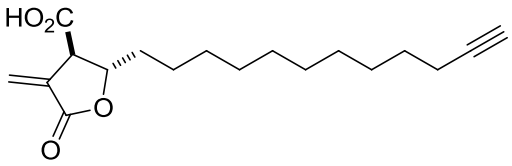

***trans*-2-(Dodec-11-yn-1-yl)-4-methylene-5-oxotetrahydrofuran-3-carboxylic acid (2-9g)**, as a white solid (52%). ^{1}H NMR (300 MHz, $CDCl_3$) δ 6.44 (d, J = 2.6 Hz, 1H), 6.00 (d, J = 1.9 Hz, 1H), 4.80 (dd, J = 11.9, 6.0 Hz, 1H), 3.61 (s, 1H), 2.18 (td, J = 7.0, 2.6 Hz, 2H), 1.93 (t, J = 2.6 Hz, 1H), 1.79 – 1.65 (m, 2H), 1.54 – 1.47 (m, 2H), 1.42 – 1.25 (m, 14H); ^{13}C NMR (75 MHz, $CDCl_3$) δ 174.37, 168.43, 132.64, 125.78, 84.77, 79.09, 68.06, 49.60, 35.72, 29.67, 29.39, 29.34, 29.16, 29.03, 28.70, 28.44, 24.74, 18.37;LRMS m/z calcd for $C_{18}H_{26}O_4$ 306.2, $[M-H]^-$

305.2, $[2M - H]^-$ 611.4, found 305.2, 611.3 (ESI);HRMS m/z calcd for $C_{18}H_{26}O_4$ 306.1831, $[2M - H]^-$ 611.3589, found 611.3606 (ESI).

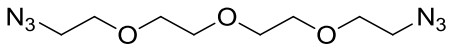

1-Azido-2-(2-(2-(2-azidoethoxy)ethoxy)ethoxy)ethane (4-12)[81a] To a solution of 1,2-Bis(2-hydroxyethoxy)ethane **2-10** (10 g, 52 mmol) and triethylamine (44 mL, 319 mmol) in diethyl ether (40 mL) was added MsCl (8.9 g, 115 mmol) at 0 ^oC. The reaction mixture was concentrated to give the residue containing compound **4-11** which was dissolve in ethanol (60 mL). The ethanolic solution was then refluxed with sodium azide (7.2 g, 112 mmol) for 1 d. The reaction mixture was concentrated, dissolved in diethyl ether (80 mL) and washed with brine. The oganic solution was dried over anhyd sodium sulfate, concentrated to give the product **2-12** as a yellowish oil. (10 g, 80%) ^1H NMR (300 MHz, $CDCl_3$) δ 3.69 – 3.62 (m, 12H), 3.37 (t, *J* = 5.1 Hz, 4H); ^{13}C NMR (75 MHz, $CDCl_3$) δ 70.62, 70.58, 69.94, 50.62.

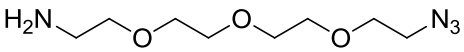

2-(2-(2-(2-Azidoethoxy)ethoxy)ethoxy)ethanamine (2-13)[81a] To a solution of compound **2-12** (4.9 g, 20 mmol) in diethyl ether (70 mL) and THF (10 mL) was added aq HCl (1 M, 89 mL). The solution of triphenylphosphine (5.3 g, 20 mmol) in diethyl ether (50 mL) was added dropwise at rt and the reaction was stirred at rt for 2 h. The aq layer was separated, saturated with sodium chloride and basified with NaOH (1 N, to pH = 14). Then the solution was extracted with toluene (50 mL X 3). The extract was washed with brine and dried over dry potassium hydroxide and concentrated to give the product. (3.1 g, 71%) ^1H NMR (300 MHz, $CDCl_3$) *δ* 3.70 – 3.49 (m, 10H), 3.48 – 3.37 (m, 2H), 3.37 – 3.10 (m, 2H), 2.95 – 2.63 (m, 2H); ^{13}C NMR (75 MHz, $CDCl_3$) *δ* 73.20, 70.52, 70.47, 70.45, 70.10, 69.85, 50.49, 41.58.

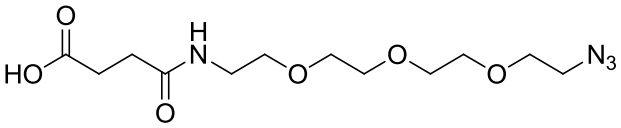

1-Azido-13-oxo-3,6,9-trioxa-12-azahexadecan-16-oic acid (2-14) The solution of compound 12 (0.80 g, 3.7 mmol) and succinic anhydride (0.44 g, 4.4 mmol) in THF (100 mL) was stirred overnight at rt. The solution was concentrated and the residue was dissolved in chloroform (100 mL) followed by washing with 1 N HCl (20 mL) and drying over anhyd sodium sulfate. After concentration *in vacuo*, the product was used in next step without further purification. (0.95 g, 81%) ^{1}H NMR (300 MHz, $CDCl_3$) δ 6.67 (s, 1H), 3.79 – 3.59 (m, 12H), 3.55 – 3.52 (m, 2H), 3.43 – 3.38 (m, 4H), 2.66 (t, J = 6.5 Hz, 2H), 2.51 (t, J = 6.5 Hz, 2H); ^{13}C NMR (75 MHz, $CDCl_3$) δ 175.5, 172.4, 70.5, 70.4, 70.1, 69.9, 69.5, 50.6, 39.4, 30.8, 29.9.

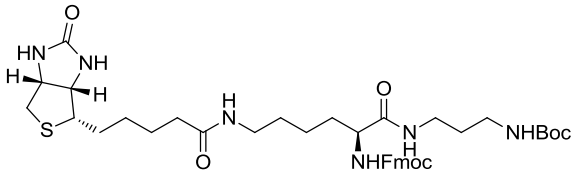

Synthesis of compound 2-20 After the solution of Fmoc-Lys(Biotin)-OH (4.0 g, 6.7 mmol), HBTU (3.0 g, 8.0 mmol) and HOBt (1.1 g, 8.0 mmol) was stirred at rt for 10 min, *N*-boc-propyldiamine[52] (1.8 g, 10 mmol) and DIEA (2.4 mL, 14mmol) were added. After the reaction was stirred overnight at rt, the product was precipitated with water as yellowish solid. (3.5 g, 69%) ^{1}H NMR (300 MHz, DMSO-d_6) δ 7.95-7.85 (m, 3H), 7.74 (s, 3H), 7.44-7.39 (m, 3H), 7.32 (t, J = 7.3 Hz, 2H), 6.76 (s, 1H), 6.42 (s, 1H), 6.35 (s, 1H), 4.49-4.22 (m, 4H), 4.11-4.09 (m, 1H), 3.92-3.85 (m, 1H), 3.15 – 2.75 (m, 9H), 2.04 (t, J = 6.8 Hz, 2H), 1.68 – 1.10 (m, 23H); ^{13}C NMR (75 MHz, DMSO-d_6) δ 171.8, 162.7, 155.9, 155.6, 143.9, 143.8, 140.7, 127.6, 127.0, 125.3, 120.1, 108.4, 77.4, 65.6, 61.0, 59.2, 55.4, 54.7, 46.7, 38.3, 37.4, 36.2, 35.8, 35.2, 31.6, 30.8, 29.5, 28.9, 28.2, 28.0, 25.3, 23.0.

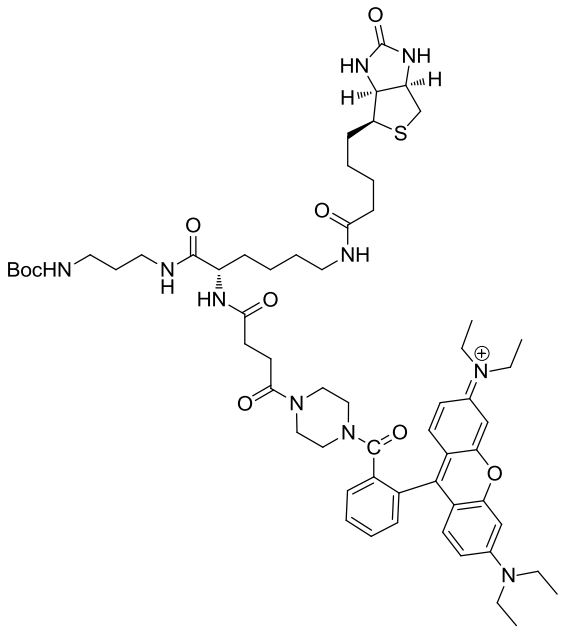

Synthesis of compound 2-22 A solution of compound **2-20** (3.5 g, 4.7 mmol) in piperidine-DMF (1:4, 15 mL) was stirred at rt for 1 h. After the volatiles were removed under reduced pressure, to the solution was added water (40 mL) until no more precipitate formed. The precipitate was filtered and the filtrate was concentrated under reduced pressure to give the product as a yellowish oil which was slowly changed to yellowish solid. (2.2 g, 89%) The product was pure enough to use in next step.

After the solution of TER acid (1.6 g, 2.2 mmol), HBTU (1.0 g, 2.6 mmol) and HOBt (0.36 g, 2.8 mmol) in DMF (18 mL) was stirred at rt for 10 min, crude product above (1.8 g, 3.4 mmol) and DIEA (0.74 mL) were added. After the reaction was stirred at rt overnight, the compound **2-22** (IT-TOF 1121.3252) was purified by prepHPLC (ACN-Water). (1.2 g, 45%)

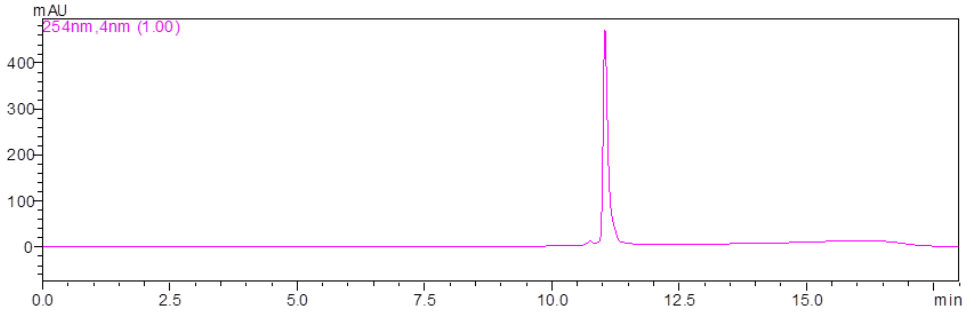

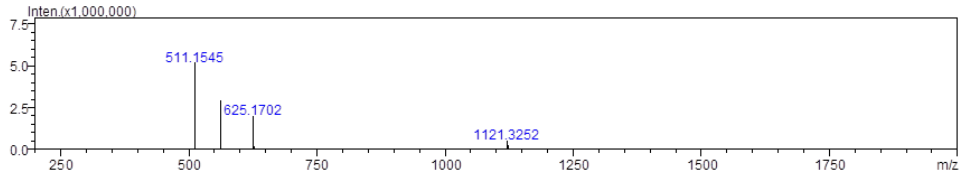

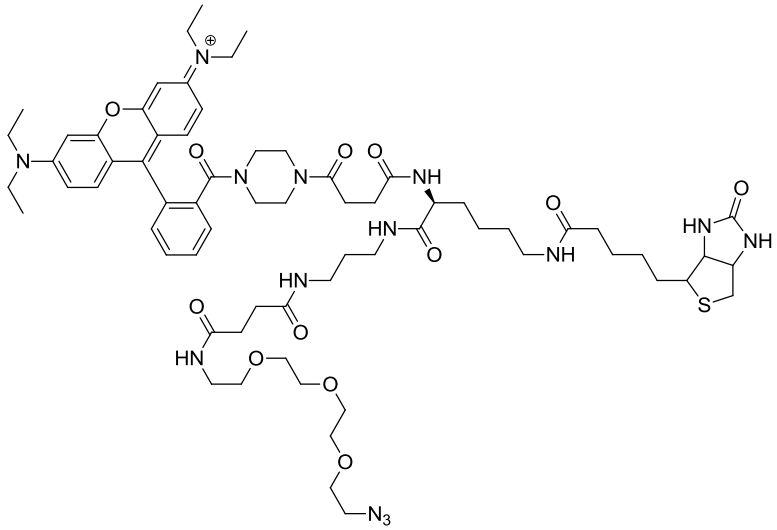

Synthesis of Rh-Biotin-N_3 To a solution compound **2-22** (300 mg, 0.27 mmol) in DCM (10 mL) was added TFA (0.5 mL) and the reaction was stirred at rt for 1 h. The volatiles were removed under reduced pressure. The residual TFA was removed by azeotropy with toluene. After the solution of the residue above, DIEA (400 µL), HATU (137 mg, 0.36 mmol) and compound **2-14** (0.11 g, 0.35 mmol) in DMF (10 mL) was stirred at rt overnight, the desired product (IT-TOF 661.3368) was purified by PrepHPLC (ACN-Water).(0.22 g, 64%)

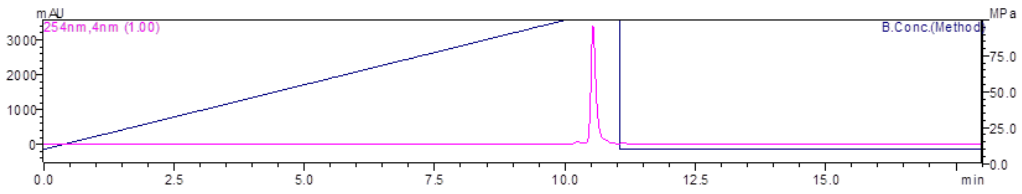

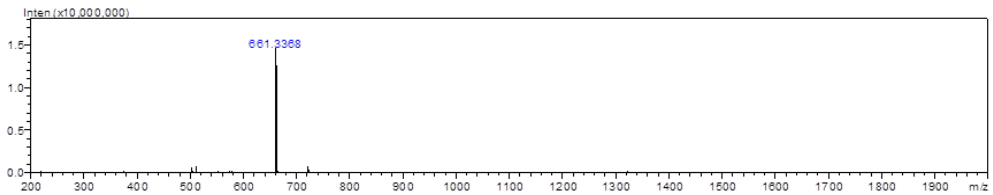

7.2.2. Cell culture and anti-proliferation

HepG2 were maintained in DMEM medium supplemented with 10% FBS and 1% P/S. The cells (0.2-0.4 × 10^6 per mL) were plated in duplicate in 96-well plates containing three different concentrations (20, 50 and 100 μM) of the 8 inhibitors and C75. After incubation at 37 °C in 5% CO_2 for 48 h, the effect of the compounds on the cell proliferation was determined by the XTT (sodium 3' – [1- (phenylaminocarbonyl)-3, 4-tetrazolium]-bis (4-methoxy-6-nitro) benzene sulfonic acid hydrate) colorimetric dye reduction method. Briefly, the procedure for the assay was as follows. The XTT was dissolved in hot DMEM media (37 °C) at a concentration of 1 mg/mL. Immediately before use, the electron coupling reagent PMS (*N*-methyl dibenzopyrazine methyl sulfate) was added to the XTT solution giving a PMS concentration of 125 μM (The PMS was stored as 100 mM stock solution in saline at 4 °C). 25 μL of this XTT/PMS solution was added to each well in the 96-well plate containing ~ 100 μL per well culture giving a final concentration of 0.2 mg/mL XTT and 25 μM PMS. After incubation at 37 °C in 5% CO_2 for 6 h the absorbance of each well was measured at a wavelength of 450 nm using Tecan microplate reader and effect of the compounds on the cell proliferation was determined by comparing with the DMSO (no inhibitor) controls.

7.2.3. Preparation of proteomes and proteomes labeling (*in vitro* and *in situ*)

HepG2 was grown in DMEM (Invitrogen, Carlsbad, CA) containing 10% heat-inactivated fetal bovine serum (FBS, Gibco Invitrogen), 100 U/mL penicillin and 100 μg/mL streptomycin (Thermo Scientific, Rockford, IL) and maintained in a humidified 37 °C incubator with 5% CO_2. To generate protein lysates, cells were washed twice with cold

phosphate buffered saline (1 × PBS), and harvested with a cell scraper, and collected by centrifugation. Cell pellets were re-suspended in 1 × PBS (0.1% SDS) and lysed by sonication (few seconds). Protein concentration was determined by the Bradford assay. Cell lysates were diluted with PBS to achieve final concentration of ~1 mg/mL for labeling reactions.

For *in vitro* proteome labeling, probes were added to cell lysates (100 µg) in 100 *µ*L of PBS (0.1% SDS) at a final concentration of 5-20 µM in the presence or absence of excess C75 (a final concentration of 50 µM). Unless indicated otherwise, samples were incubated for 2 h with varying concentrations of probe at room temperature. After incubation, 20 µL of the freshly premixed click chemistry reaction cocktail in 1 × PBS [Rhodamine-azide (100 µM, 10 mM stock solution in DMSO), tris(2-carboxyethyl)phosphine hydrochloride (TCEP) (1 mM, 50 mM freshly prepared stock solution in deionized water), tris[(1-benzyl-1*H*-1,2,3-triazol-4-yl)methyl] amine (TBTA) (100 µM, 10 mM stock solution in DMSO) and $CuSO_4$ (1 mM, 50 mM freshly prepared stock solution in deionized water)] was added and vortexed, then incubated for 2 h at room temperature with gentle mixing. The reactions were terminated by the addition of pre-chilled acetone (0.5 mL), placed at -20 °C for 30 min and centrifuged at 13000 rpm for 10 min at 4 °C to precipitate proteins. The supernatant was discarded and the pellet washed two times with 200 µL of prechilled methanol. The protein pellets were allowed to air-dry for 10 min, re-suspended in 50 µL 1 × standard reducing SDS-loading buffer and heated for 10 min at 95 °C; ~20 µg of protein was loaded per gel lane for separation by SDS-PAGE (10%), then visualized by in-gel fluorescence scanning using a Typhoon 9410 Variable Mode Imager scanner.

For *in situ* labeling, cells were grown to 80-90% confluence in 24-well plates under the conditions described above. The medium was removed, and then cells were washed twice with cold PBS, and treated with 0.5 mL of DMEM-containing probe (0, 20 µM) in the presence or absence of excess C75. Probes were applied from DMSO stocks whereby DMSO never exceeded 1% in the final solution. The same

volume of DMSO was used as a negative control. After 24 h of incubation at 37 °C/5% CO_2, the growth medium was aspirated, and cells were washed twice with 1 × PBS to remove the excessive probe, trypsined, and pelleted by centrifugation. The cell pellet was re-suspended in 1 × PBS (50 μL), homogenized by sonication, and diluted to ~1 mg/mL with PBS. Probe targets were detected by click chemistry with Rhodamine-azide, SDS-PAGE analysis, and in-gel fluorescence scanning.

7.2.4. Proteomes pull-down, LC/MS-MS and Western blotting experiments

In situ pull-down experiment on HepG2 cell line and sample preparation for MS analysis was carried out as described below. HepG2 cell was incubated with **2-9g** (0, 20 μM) in grow medium DMEM with 10% FBS and 1% P/S for 12 h at 37 °C, then lysed with 0.1% SDS and PMSF (100 μM) in 1 × PBS, and the lysate was adjusted to 5 mg/ 5 mL with 1 × PBS. Click chemistry was performed over lysate with $CuSO_4$ (1 mM), TBTA (100 μM), TCEP (1 mM), Rh-Biotin-N_3 or Biotin-N_3 (100 μM) overnight at rt. After cold acetone (20 mL) precipitation at –20 °C overnight and washed with cold methanol (1 mL × 3), the protein pellet was re-dissolved in 1% SDS-PBS solution. After centrifugation, the clear supernatant was incubated with Avidin beads (200 μL) with gentle shaking for 1 d at rt After the mixture was centrifuged at 1000 rpm for 10 min and the supernatant was removed, the beads were washed with 1% SDS-PBS solution (5 mL × 8); To the beads were added 1 × SDS loading buffer (100 μL), the protein was denatured at 95 °C and released into the buffer;

After SDS-PAGE, the whole lanes of samples treated with Rh-Biotin-N_3 and DMSO were processed and submitted to LC-MS/MS. The digestion process was introduced as following: the collected gel cut into small paritcles was washed twice with ~400 μl of 25 mM ammonium

bicarbonate/50% acetonitrile and vortex for 10 min; gel pieces was then washed with 400 µl of 100 mM ammonium bicarbonate at pH = 8 for 10 min while vortexing, and dehydrated with ~400 µl of 100% acetonitrile. After repeating rehydration and dehydration and Removing the solution, gel particles was incubated with 300 µL of 0.05 mg/mL trypsin solution for 16 h at 37 ºC; the solution was combined with two additional extractions using 2 vol of 5% FA/50% acetonitrile and concentrated *in vacuo*. The peptides were separated and analyzed on a Shimadzu UFLC system (Shimadzu, Japan) coupled to an LTQ-FT Ultra (Thermo Electron, Germany). Mobile phase A (0.1% formic acid in H2O) and mobile phase B (0.1% formic acid in acetonitrile) were used to establish the 60 min gradient comprising 45 min of 5−35% B, 8 min of 35−50% B, and 2 min of 80% B, followed by re-equilibrating at 5% B for 5 min. Peptides were then analyzed on LTQ-FT with an Advance CaptiveSpray Source (Michrom Bio Resources) at an electrospray potential of 1.5 kV. A gas flow of 2 L/min, iontransfer tube temperature of 180 °C, and collision gas pressure of 0.85 mTorr were used. The LTQ-FT was set to perform data acquisition in the positive-ion mode as previously described, except that the m/z range of 350−1600 was used in the full MS scan. The raw data were converted to mgf format. The database search was performed with an in-house Mascot server (version 2.2.07, Matrix Science) with MS tolerance of 10 ppm and MS/MS tolerance of 0.8 Da. Two missed cleavage sites of trypsin were allowed. Carbamidome-thylation (C) was set as a fixed modification, and oxidation (M) and phosphorylation (S, T, and Y) were set as variable modifications. The LC-MS/MS data were searched against the IPI (International Protein Index) human protein database using an in-house MASCOT server. All proteins were identified by a minimum score of 40 and at least one unique peptides. Based on these criteria, a list of the hits, which was potential targets of C75, was generated in Table S1. Some “sticky” or contaminated protein such as keratin, actin, and tubulin were deleted. “False” hits that appeared in negative control pull-down/LCMS experiments were further eliminated. The informations of structure and function of proteins could be searched on website of

UniProt.[91]

For Western blotting analysis, the PVDF membrane was blocked with 3% BSA-TBST (Tween-20, 0.1%) at 4 ºC overnight after the proteins on gel was transferred. Then PVDF membrane was incubated with primary antibody in 3% BSA-TBST (tween-20, 0.1%) at rt for 1 h followed by washing with TBST (Tween-20, 0.1%) for 10 min × 4. The PVDF membrane was further incubated with corresponding secondary antibody at rt for 1 h followed by washing with TBST (tween-20, 0.1%) for 10 min × 4. SuperSignal West Dura Kit (Thermo Scientific) was used to develop the blot.

7.2.5. Fluorescent imaging microscopy

HepG2 grow in DMEM in 12-well dish and incubated in **2-9g** (20 μM) at 37 °C for 6 h. The cells were washed with cold 1 × PBS (200 μL) and fixed with 3.7% formaldehyde in 1 × PBS (200 μL) for 2 h; Then cells were penetrated with 0.1% Triton in PBS at rt for 10 min; Click chemistry was performed with $CuSO_4$ (1 mM), TBTA (100 μM), TCEP (1 mM), TER-azide (10 μM) for 1 h at rt; After washed with PBS (0.5 mL × 8), the salts were washed with 0.5 mM EDTA-1% tween-20-PBS for 1 h twice at rt. The cells were stained with Hochest for 10 min at rt and washed with 1 × PBS.

7.3. Chapter 3

7.3.1. The procedure for the synthesis of STS probes

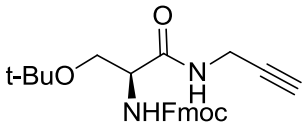

(9H-Fluoren-9-yl)methyl (3-(*tert*-butoxy)-1-oxo-1-(prop-2-yn-1-ylamino)propan-2-yl)carbamate (3-2) To a solution of Fmoc-O-*tert*-Butyl-L-serine (3.8 g, 10 mmol), HBTU (5.7 g, 15 mmol) and HOBt (2.7 g, 20 mmol) in dry DMF (150 mL) was added propargyl amine (0.96 mL, 15 mmol) and DIEA (3.5 mL, 20 mmol) at room temperature after 10 min of stirring. The reaction mixture was stirred at room temperature for 2 h. Solvent was removed *in vacuo* to give the residue which was purified by column chromatography to give white solid. (4.0 g, 95%) ^{1}H NMR (300 MHz, $CDCl_3$) δ 7.77 (d, J = 7.5 Hz, 1H), 7.60 (d, J = 7.3 Hz, 1H), 7.41 (t, J = 7.2 Hz, 1H), 7.32 (t, J = 7.4 Hz, 1H), 6.89 (s, 1H), 5.72 (s, 1H), 4.42 (d, J = 7.0 Hz, 1H), 4.23 (t, J = 6.8 Hz, 1H), 4.05 (dd, J = 5.1, 2.6 Hz, 1H), 3.81 (s, 1H), 3.37 (t, J = 8.4 Hz, 1H), 2.24 (t, J = 2.5 Hz, 1H), 1.22 (s, 5H); ^{13}C NMR (75 MHz, $CDCl_3$) δ 170.06, 156.01, 143.72, 141.32, 127.73, 127.06, 125.07, 120.00, 85.88, 79.13, 74.41, 71.72, 67.06, 61.65, 54.30, 47.17, 29.22, 27.40.

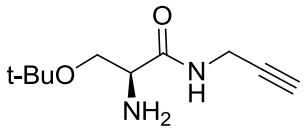

2-Amino-3-(*tert*-butoxy)-N-(prop-2-yn-1-yl)propanamide (3-3) The solution of compound **3-2** (2.0 g, 4.8 mmol) in piperidine-DCM (1:4, 50 mL) was stirred at room temperature for 30 min. The reaction was concentrated *in vacuo* to give white solid which was purified by column chromatography to give compound **3-3** as colorless oil. (0.94 g, quantatitive) ^{1}H NMR (300 MHz, $CDCl_3$) δ 7.66 (s, 1H), 4.29 – 3.79 (m, 2H), 3.66 – 3.20 (m, 3H), 2.21 (t, J = 2.5 Hz, 1H), 1.14 (s, 9H); ^{13}C

NMR (75 MHz, $CDCl_3$) δ 172.74, 79.46, 73.36, 71.19, 63.57, 54.88, 28.60, 27.25.

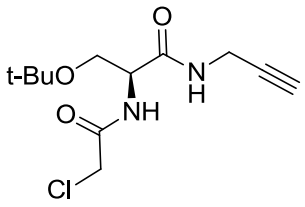

3-(*tert*-Butoxy)-2-(2-chloroacetamido)-N-(prop-2-yn-1-yl)propanamide (3-4) To a solution of 2-chloroacetyl chloride (1.1 g, 10 mmol) and DIEA (2.6 mL, 15 mmol) in dry DCM (10 mL) was added a solution of compound **3-3** (0.94 g, 5 mmol) in dry DCM (5 mL) at 0 ^{o}C. After 30 min of stirred at 0 ^{o}C, then the reaction was allowed to warm to room temperature. After the reaction mixture was concentrated *in vacuo*, the residue was re-dissolved in DCM (10 mL), washed with aq sat. sodium bicarbonate solution. The organic layer was dried over anhydrous sodium sulfate and concentrated to give residue which was purified by column chromatography to give compound **3-4** as a white solid. (1.0 g, 72%) ^{1}H NMR (300 MHz, $CDCl_3$) δ 7.49 (d, J = 6.5 Hz, 1H), 7.12 (s, 1H), 4.40 (td, J = 7.4, 4.4 Hz, 1H), 4.12 – 3.84 (m, 4H), 3.72 (dd, J = 8.7, 4.2 Hz, 1H), 3.35 (t, J = 8.3 Hz, 1H), 2.21 (t, J = 2.2 Hz, 1H), 1.14 (s, 9H); ^{13}C NMR (75 MHz, $CDCl_3$) δ 169.43, 166.24, 78.97, 74.26, 71.56, 60.98, 52.86, 42.36, 29.02, 27.16.

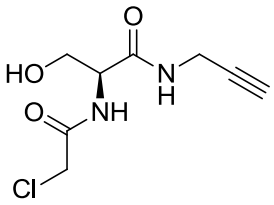

2-(2-Chloroacetamido)-3-hydroxy-N-(prop-2-yn-1-yl)propanamide (3-5) To a solution of compound **3-4** (0.80 g, 2.9 mmol) at room temperature was added TFA (15 mL). After 45 min of stirring, the reaction was concentrated to remove volatiles. The residue was re-

dissolved in ethyl acetate (10 mL) and washed with aq sat. sodium bicarbonate. The aq layer was extracted with ethyl acetate (10 mL X 3). The combined organic layers were dried over anhyd sodium sulfate and concentrated to give residue, which was purified by column chromatography to give compound **3-5** as a white solid. (0.25 g, 39%) ^{1}H NMR (500 MHz, MeOD) δ 4.44 (t, J = 5.1 Hz, 1H), 4.24 – 4.08 (m, 2H), 4.08 – 3.92 (m, 2H), 3.80 (qd, J = 11.2, 5.2 Hz, 2H), 2.58 (t, J = 2.5 Hz, 1H); ^{13}C NMR (75 MHz, MeOD) δ 171.57, 169.28, 80.29, 72.34, 62.85, 56.89, 43.20, 29.61.

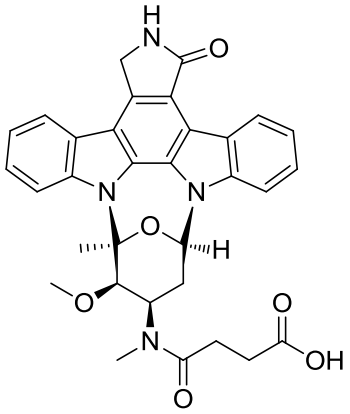

4-(((5S,6R,7R,9R)-6-Methoxy-5-methyl-14-oxo-5,6,7,8,9,14,15,16-octahydro-17-oxa-4b,9a,15-triaza-5,9-methanodibenzo[b,h] cyclonona[jkl]cyclopenta[e]-as-indacen-7-yl)(methyl)amino)-4-oxobutanoic acid (3-6) To a solution of Staurosporine (**STS**) (5.0 mg, 10 µmol) in DMSO, succinic anhydride (1.5 mg, 15 µmol) and DMAP (61 µg, 20 µmol) were added under dark. After 30 h stirring, the mixture was precipitated with 0.1 % TFA in water, and the precipitate was triturated twice with 0.1 % TFA in water to afford compound **3-6**. (5.6 mg, 92%). ^{1}H NMR (300 MHz, DMSO-d_6) δ 12.06 (s, 1H), 9.29 (d, J = 7.9 Hz, 1H), 8.59 (s, 1H), 8.05 (d, J = 7.7 Hz, 1H), 7.99 (d, J = 8.5 Hz, 1H), 7.67 (d, J = 8.2 Hz, 1H), 7.48 (t, J = 7.7 Hz, 2H), 7.35 (t, J = 7.5 Hz, 1H), 7.29 (t, J = 7.5 Hz, 1H), 7.03 (t, J = 7.5 Hz, 1H), 5.00 (s, 3H), 4.22 (s, 1H), 2.81 (s, 3H), 2.77 (s, 3H), 2.68 (d, J = 5.6 Hz, 1H), 2.60-2.56 (m, 2H), 2.33 (s, 3H), 2.28-2.17 (m, 1H). LCMS m/z calcd for $C_{32}H_{30}N_4O_6$ $[M+H]^+$ 567.220, found 567.199 (IT-TOF).

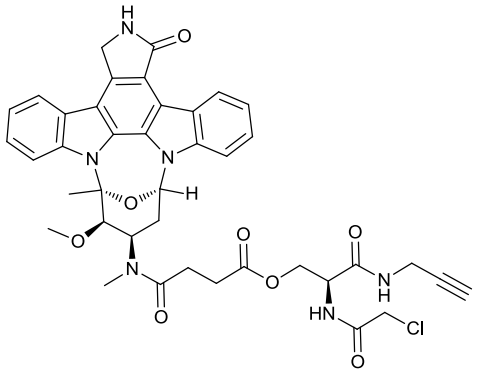

2-(2-Chloroacetamido)-3-oxo-3-(prop-2-yn-1-ylamino)propyl 4-(((5S,6R,7R,9R)-6-methoxy-5-methyl-14-oxo-5,6,7,8,9,14,15,16-octahydro-17-oxa-4b,9a,15-triaza-5,9-methanodibenzo[b,h] cyclonona[jkl]cyclopenta[e]-as-indacen-7-yl)(methyl)amino)-4-oxobutanoate (STS-C1) To a solution of STS-acid **3-6** (5.0 mg, 8.8 μmol) in DMSO (0. 5 mL) was added compound **3-5** (3.9 mg, 17.8 pmol), EDC (15 mg, 80 μmol) and DMAP (2.4 mg, 20 μmol) at 0 ^{o}C. Then the reaction was allowed to warm to rt and stirred at rt overnight until no more product formed monitored by LC-MS. Product was purified by HPLC (10% - 95% ACN/H_2O). (0. 50 mg, 7.4%) ^{1}H NMR (300 MHz, DMSO-d_6) *δ* 9.28 (d, *J* = 8.2 Hz, 1H), 8.67 (t, *J* = 5.1 Hz, 1H), 8.60 (s, 1H), 8.55 (d, *J* = 8.1 Hz, 1H), 8.05 (d, *J* = 7.9 Hz, 1H), 7.99 (d, *J* = 8.6 Hz, 1H), 7.67 (d, *J* = 8.5 Hz, 1H), 7.49 (t, *J* = 7.9 Hz, 2H), 7.41 – 7.33 (m, 1H), 7.29 (t, *J* = 7.4 Hz, 1H), 7.03 (t, *J* = 6.9 Hz, 1H), 5.00 (s, 3H), 4.64 – 4.57 (m, *J* = 14.1, 5.9 Hz, 2H), 4.33 – 4.15 (m, 5H), 3.92 (s, 2H), 2.82 (s, 3H), 2.78 (s, 3H), 2.73 (s, 1H), 2.68 (s, 1H), 2.54 (s, 1H), 2.33 (s, 3H), 2.21 (m, 1H); LCMS m/z calcd. for $C_{40}H_{40}ClN_6O_8$ $[M+H]^+$ 767.2596, found 767.244; $C_{40}H_{39}ClN_6NaO_8$ $[M+Na]^+$ 789.2416, found 789.224 (IT-TOF).

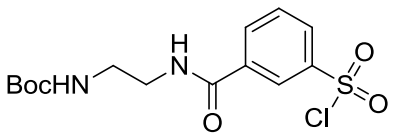

***tert*-Butyl (2-(3-(chlorosulfonyl)benzamido)ethyl)carbamate (3-9)** To a solution of 3-(chlorosulfonyl)benzoyl chloride **3-7** (1.9 mL, 12

mmol) in dry DCM (7.5 mL) was added dropwise the solution of *N*-Boc-ethylenediamine **3-8** (0.96 g, 6 mmol) and DIEA (2.6 mL, 15 mmol) in dry DCM (7.5 mL) at 0 ^{o}C. The reaction was stirred at r.t overnight. Solvent was evaporated under reduced pressure to give the residue which was purified by column chromatography. The solid was stored at -20 ^{o}C. (1.7 g, 40%) ^{1}H NMR (300 MHz, $CDCl_3$) δ 8.49 (s, 1H), 8.23 (d, *J* = 7.8 Hz, 1H), 8.10 – 8.02 (m, 1H), 7.63 (t, *J* = 7.9 Hz, 1H), 5.49 (s, 1H), 3.58 – 3.48 (m, 2H), 3.43 – 3.31 (m, 2H), 1.36 (s, 9H); ^{13}C NMR (75 MHz, $CDCl_3$) δ 164.96, 144.39, 136.02, 133.81, 129.90, 129.06, 125.69, 79.91, 54.08, 28.19, 18.42, 17.13.

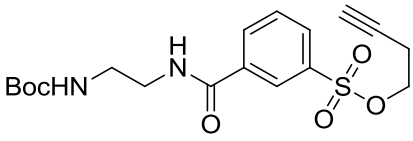

But-3-yn-1-yl 3-((2-((*tert*-butoxycarbonyl)amino)ethyl)carbamoyl) benzenesulfonate (3-10) To a solution of **3-7** (218 mg, 0.60 mmol) in dry DCM (3 mL) was added a solution of but-3-yn-1-ol (54 µL, 0.72 mmol), DIEA (208 µL, 1.2 mmol) and DMAP (14.5 mg, 0.12 mmol) in dry DCM (2 mL) at 0 ^{o}C. The reaction was stirred at r.t overnight. Solvent was evaporated under reduced pressure to give the residue which was purified by column chromatography. (212 mg, 89%) ^{1}H NMR (300 MHz, $CDCl_3$) δ 8.35 (s, 1H), 8.12 (d, *J* = 7.8 Hz, 1H), 7.98 (d, *J* = 7.9 Hz, 1H), 7.89 (s, 1H), 7.59 (t, *J* = 7.8 Hz, 1H), 5.30 (s, 1H), 4.10 (t, *J* = 6.8 Hz, 2H), 3.54 (dd, *J* = 10.6, 5.1 Hz, 2H), 3.43 – 3.26 (m, 2H), 2.52 (td, *J* = 6.8, 2.6 Hz, 2H), 1.95 (t, *J* = 2.6 Hz, 1H), 1.38 (s, 9H); ^{13}C NMR (75 MHz, $CDCl_3$) δ 165.58, 157.63, 136.26, 135.59, 132.52, 130.28, 129.56, 126.47, 80.00, 78.18, 70.92, 67.97, 42.22, 39.84, 28.23(3C), 19.35.

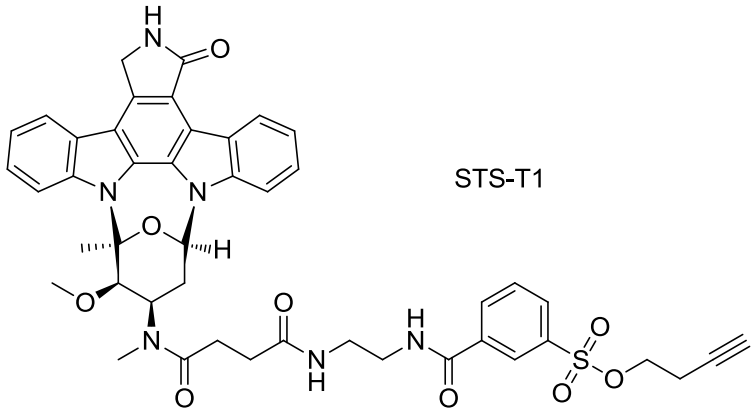

STS-T1

Synthesis of compound STS-T1 To a solution of compound **3-10** (40 mg) in DCM (3 mL) was added TFA (1 mL) at rt. The reaction mixture was allowed to warm to rt and stirred for 6 h. TFA and solvent were removed by azeotropy with toluene. The residue was re-dissolved in dry DMF (1 mL). To the solution was added compound **3-6** (5.0 mg), HOBt (4.8 mg), DIEA (2 µL) and EDC (6.0 mg) at rt and stirred overnight. The final product was purified by HPLC. (5.0 mg, 67%) ^{1}H NMR (300 MHz, DMSO-d_6) δ 9.29 (d, *J* = 8.3 Hz, 1H), 8.87 (s, 1H), 8.60 (s, 1H), 8.37 (s, 1H), 8.26 (d, *J* = 7.5 Hz, 1H), 8.07 (t, *J* = 6.9 Hz, 3H), 7.97 (d, *J* = 8.3 Hz, 1H), 7.81 (t, *J* = 7.9 Hz, 1H), 7.66 (d, *J* = 8.4 Hz, 1H), 7.48 (t, *J* = 7.7 Hz, 2H), 7.41 – 7.21 (m, 2H), 7.02 (t, *J* = 7.2 Hz, 1H), 5.00 (s, 3H), 4.20 (s, 1H), 4.12 (t, *J* = 6.1 Hz, 2H), 3.38-3.34 (m, 2H), 3.30-3.26 (s, 2H), 2.85 (t, *J* = 2.5 Hz, 1H), 2.80(s, 3H), 2.76 (s, 3H), 2.66 (d, *J* = 8.3 Hz, 1H), 2.57-2.54 (m, 2H), 2.42-2.38 (m, 2H), 2.30 (s, 3H), 2.25-2.17 (m, 1H). LCMS m/z calcd for $C_{45}H_{45}N_6O_9S$ $[M+H]^+$ 845.2969, found 845.2415.

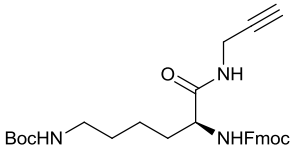

(9H-Fluoren-9-yl)methyl *tert*-butyl (6-oxo-6-(prop-2-yn-1-ylamino) hexane-1,5-diyl)dicarbamate (3-13) To a solution of Fmoc-L-Lys(Boc)-OH (4.7 g, 10 mmol), HBTU (4.6 g, 12 mmol) and HOBt (1.6 g, 12 mmol) in dry DMF (10 mL), propargyl amine (1 mL, 15 mmol) and DIEA (3.5 mL) were added at r.t and the reaction was stirred at rt

overnight. After reaction was complete, the reaction mixture was poured into cold water. The collected precipitate was re-crystallized in ethyl acetate to give compound **3-13** as a white solid. (3.1 g, 61%) ^{1}H NMR (300 MHz, MeOD) δ 7.79 (d, J = 7.4 Hz, 2H), 7.65 (d, J = 5.4 Hz, 2H), 7.35 (dt, J = 23.6, 7.3 Hz, 2H), 6.55 (s, 1H), 4.38 (d, J = 6.8 Hz, 2H), 4.21 (t, J = 6.4 Hz, 1H), 4.03 (d, J = 5.7 Hz, 1H), 3.95 (s, 2H), 3.03 (d, J = 5.9 Hz, 2H), 2.58 (s, 1H), 1.83 – 1.57 (m, 2H), 1.56-1.28 (m, 4H), 1.42 (s, 9H); ^{13}C NMR (75 MHz, MeOD) δ 174.61, 158.63, 158.46, 145.33, 145.16, 142.60, 128.79, 128.17, 126.21, 120.92, 80.45, 79.88, 72.28, 67.88, 56.31, 41.18, 41.07, 32.92, 30.52, 29.48, 28.79, 24.12.

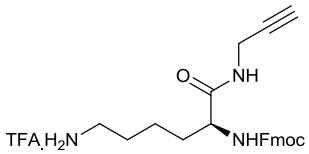

(9H-Fluoren-9-yl)methyl (6-amino-1-oxo-1-(prop-2-yn-1-ylamino) hexan-2-yl)carbamate (3-14) The solution of compound **3-13** (1.0 g, 2 mmol) was stirred in TFA-DCM (1:19, 20 mL) at rt overnight. Then the reaction mixture was concentrated *in vacuo* to give oily redidue. Add ether until no more precipitate formed, the white solid **3-14** was collected by filtration and washed with ether until no more TFA. (0.78 g, 79%) ^{1}H NMR (300 MHz, $CDCl_3$) δ 11.02 (s, 1H), 7.68 (d, J = 7.4 Hz, 1H), 7.48 (d, J = 6.8 Hz, 1H), 7.38 – 7.30 (m, 1H), 7.25 (d, J = 7.3 Hz, 1H), 6.17 (s, 1H), 4.31 (d, J = 4.8 Hz, 1H), 4.11 (d, J = 5.9 Hz, 1H), 3.89 (s, 1H), 2.97 (s, 1H), 2.12 (s, 1H), 1.87 – 1.46 (m, 1H), 1.30 (dd, J = 29.7, 9.2 Hz, 1H); ^{13}C NMR (75 MHz, $CDCl_3$) δ 173.07, 160.99, 160.47, 156.98, 143.34, 143.22, 141.18, 127.86, 127.09, 124.85, 120.94, 119.99, 117.10, 113.31, 109.53, 77.97, 72.00, 67.94, 54.52, 46.77, 39.98, 31.21, 29.33, 26.36, 21.87.

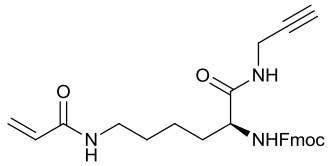

(9H-Fluoren-9-yl)methyl (6-acrylamido-1-oxo-1-(prop-2-yn-1-ylamino)hexan-2-yl)carbamate (3-15) To a solution of compound **3-14** (0.20 g, 0.4 mmol) and DIEA (0.21 mL) in THF (4 mL) was added acryloyl chloride (29 µL, 0.48 mmol) dropwise at 0 ^{o}C. Then the reaction was warm to rt and stirred at rt overnight. The reaction was concentrated *in vacuo* to give residue which was purified by column chromatography to give the product **3-15** as a white solid. (0.10 g, 55%) ^{1}H NMR (300 MHz, $CDCl_3$) δ 7.76 (d, *J* = 7.5 Hz, 2H), 7.58 (d, *J* = 6.8 Hz, 2H), 7.40 (t, *J* = 7.3 Hz, 2H), 7.30 (t, *J* = 7.4 Hz, 2H), 6.77 (s, 1H), 6.28 (d, *J* = 16.9 Hz, 1H), 6.07 (dd, *J* = 16.9, 10.2 Hz, 1H), 5.93 (s, 1H), 5.72-5.58 (m, 2H), 4.41 (d, *J* = 6.5 Hz, 2H), 4.20 (t, *J* = 6.7 Hz, 2H), 4.01 (s, 2H), 3.40 – 3.21 (m, 2H), 2.17 (t, *J* = 2.5 Hz, 1H) 1.90-1.82 (m, 1H), 1.64 – 1.48 (m, 2H), 1.44-1.31 (m, 3H).; ^{13}C NMR (75 MHz, MeOD) δ 174.57, 168.13, 158.45, 145.15, 142.59, 132.04, 128.79, 128.16, 126.60, 126.19, 120.92, 80.44, 72.27, 67.87, 56.28, 40.12, 32.84, 29.90, 29.48, 24.22.

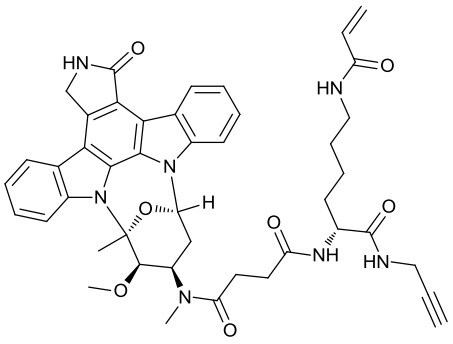

Synthesis of compound STS-A1 The solution of compound **3-15** was stirred in 20 % piperidine-DCM solution (5 mL) at rt for 2 h. After the reaction was complete, it was concentrated to remove valotiles to give the residue which was purified by column chromatography to give product. (52 mg, 67 %)

To a solution of STS acid (5.0 mg, 8.8 μmol), EDCI (15 mg, 90 μmol) and DMAP (2.4 mg, 19.7 μmol) in DMSO (1 mL) at 0 ^{o}C was added amine (4.2 mg, 17.7 μmol) above, then the reaction was allowed to warm to rt and stirred at r.t overnight. Product **STS-A1** was purified by HPLC as a white solid. (1.3 mg, 19%)) ^{1}H NMR (300 MHz, DMSO-d_6) δ 9.27 (d, *J* = 7.8 Hz, 1H), 8.58 (s, 1H), 8.34-8.30 (m, 1H), 8.14-8.04 (m, 3H), 7.99-7.95 (d, *J* = 8.3 Hz, 1H), 7.66 (d, *J* = 7.9 Hz, 1H), 7.49 (t, *J* = 7.4 Hz, 2H), 7.36 (d, *J* = 7.4, 1H), 7.29 (d, *J* = 7.4, 1H), 7.03-6.98 (m, 1H), 6.21 (dd, *J* = 17.0, 10.0 Hz, 1H), 6.06 (dd, *J* = 17.0, 2.2 Hz, 1H), 5.57 (dd, *J* = 9.7, 2.4 Hz, 1H), 4.99 (s, 3H), 4.21 (s, 2H), 3.92 – 3.90 (m, 2H), 3.33 (s, 4H), 3.25 (s, 1H), 3.16 (s, 7H), 2.81 (s, 3H), 2.75 (s, 3H), 2.67 – 2.61(m, 3H), 2.41 (s, 1H), 2.34 (s, 2H), 2.24 (s, 1H), 2.07 (d, *J* = 5.1 Hz, 1H), 1.78 – 1.67 (m, 1H), 1.62 – 1.20 (m, 4H). LCMS m/z calcd for $C_{44}H_{48}N_7O_7$ $[M+H]^+$ 786.3615, found 786.340.

7.3.2. Anti-proliferation

Cell viability was determined using the XTT colorimetric cell proliferation kit (Roche) following manufacturer's guidelines. Briefly, cells were grown to 20-30% confluence (since they will reach ~90% confluence within 48 to 72 h in the absence of drugs) in 96-well plates under the conditions described above. The medium was aspirated, and then washed with PBS, and treated in duplicate, with 0.1 mL of the medium containing different concentrations of probes (0-1 μM) or drug (0-1 μM, as a positive control). Probes were applied from DMSO stocks whereby DMSO never exceeded 1% in the final solution. The same volume of DMSO was used as a negative control. Fresh medium, along with two probes and one corresponding drug, were added every 24 h. After a total treatment time of 72 h, proliferations were assayed using the XTT colorimetric cell proliferation kit (Roche) following manufacturer's guidelines (read at 450 nm). Data represent the average (s.d. for two trials)

7.3.3. Pure enzyme labeling

To investigate the labeling specificity of our probes, pure enzyme labeling experiments were performed. Briefly, different proteins (a final concentration of 100 nM) were incubated with **STS-C1** and **STS-2** (a final concentration of 200 nM), respectively, in above reaction buffer for 2 h at rt and UV (365 nm, 20 min) for **STS-2**, followed by click-chemistry with Rhodamine azide (Rh-PEG-N_3). After 2 h of click reaction, 6×SDS loading dye was added and the mixture was heated to 95 ºC for 10 min. The resulting proteins were resolved by SDS-PAGE. In-gel fluorescence scanning was used to visualize the labelled protein bands. Both in-gel fluorescence scanning (FL) and silver staining was always carried out on the gels upon SDS-PAGE separation of labeled samples.

7.3.4. Pure enzyme activity assay

Concentration-dependent experiments were performed to determine the inhibition potency and the binding affinity of the probes towards the catalytic domain of the kinases. The inhibition assay was performed with Kinase-Glo® Plus Luminescent Kinase assay kit from Promega following the manufactures instructions. Recombinant kinase, ATP and the probe were mixed in the HEPES buffer (25 mM HEPES, pH 7.5, 150 mM NaCl, 2 mM $MgCl_2$) at a volume of 27.5 µL in a flat-bottom solid white 384-well plate. The incubation was allowed to continue for 20 min at 37 °C and the reaction was subsequently quenched by the addition of an equal volume of the Kinase-Glo reagent. After 5 min of incubation, the luminescence readouts from the wells were measured using Tecan microplate reader with i-control software. The ATP and substrate peptide concentrations used in the assay were 10 µM and 50 µM, respectively. Dose-dependent inhibition assays were performed by varying the concentration of the probes under optimized enzyme concentration of ~50 nM. The IC_{50} values of the

probes were calculated from the percentage activity vs. log [concentration of probe] curves generated using GraphPad Prism software.

7.3.5. Bacterial lysate labeling

Bacterial lysates were prepared using modified procedures based on previous reports. The cultures of LB (100 mL) with a single colony containing c-Src were grown at 37 ºC with shaking to reach OD_{600} = 1.2. Subsequently, IPTG (0.2 mM) was added to induce protein expression and incubated for further 18 h at 18 ºC with shaking (230 rpm). 5 mL LB was taken out before and after inducing, respectively, and harvested by centrifugation at 4000 rpm for 10 min at 4 ºC. The resulting pellets were resuspended in the lysis buffer (25 mM HEPES, pH 7.5, 150 mM NaCl, 2 mM $MgCl_2$, 50 µM PMSF) and sonicated (to complete lysis, 10 rounds of 3 s on and 3 s off, at 28 % amplitude) followed by centrifugation for 15 min (13,000 rpm at 4 ^{o}C). The total protein concentrations of these lysates were then quantified by Bio-Rad protein assay (Bio-Rad USA), and stored in -20 ^{o}C, and used for all subsequent labeling experiments.

For concentration-dependent *in vitro* labeling, to 20 µg of above bacterial lysates, the probe in different concentration were added and the reactions were incubated for 2h at r. t., followed by click-chemistry with Rhodamine azide (TER-N_3). After 2 h of click reaction, 6 X SDS loading dye (4 µL) was added and the mixture was heated to 95 ^{o}C for 10 min. The resulting proteins were resolved by SDS-PAGE. In-gel fluorescence scanning was used to visualize the labelled protein bands. Both in-gel fluorescence scanning (FL) and coomassie Brilliant Blue staining (CBB) were always carried out on the gels upon SDS-PAGE separation of labeled samples.

For dose-dependent *in vitro* labeling, to different amount of above bacterial lysates, the probe was added and the reactions were

incubated for 2h at r. t., followed by the same procedure as the previous labeling experiment.

For competing *in vitro* labeling, to 20 µg of above bacterial lysates, after different concentration of staurosporine was incubated at rt for 30 min, the probe were added and the reactions were incubated for 2 h at rt, followed by the same procedure as the previous labeling experiment.

7.3.6. *in vitro* and *in situ* labeling over cancer cell lines

For *in vitro* proteome labeling, the probes was added to 100 µg fresh HepG2 cell lysates (prepared as previously described) in 100 µL of HEPES buffer at a desired concentration. Samples incubated with probe were incubated for 2 h at room temperature. Four microliters of a freshly premixed click chemistry reaction cocktail (100 µM Rh-PEG-N_3 from 10 mM stock solution in DMSO, 100 µM TBTA from 10 mM freshly prepared stock solution in deionized water, 1 mM TCEP from 100 mM freshly prepared stock solution in deionized water, and 1 mM $CuSO_4$ from 100 mM freshly prepared stock solution in deionized water) was added. The reaction was further incubated for 2 h with gentle mixing, before being terminated by addition of pre-chilled acetone (0.4 mL; 30 min incubation at -20 ^{o}C). Precipitated proteins were subsequently collected by centrifugation (13000 rpm X 10 min at 4 ^{o}C). The supernatant was discarded and the pellet was washed with 200 µL of pre-chilled methanol. The air-dried pellet was added 2 X loading buffer and heated for 10 min at 95 ^{o}C. Around 20 µg (per gel lane) of proteins were separated by SDS-PAGE (10% gel) and then visualized by in-gel fluorescence scanning.

For *in situ* labeling, HepG2 cells were grown to 80~90% confluency in 24-well plates under conditions described above. The medium was removed, and cells were washed twice with cold PBS and then treated with 0.5 mL of the DMEM-containing probe (diluted from DMSO stocks whereby DMSO never exceeded 1% in the final solution). After 2 h of

incubation at 37 ^{o}C/5% CO_2, the medium was aspirated. The cells were trypsinized and pelleted by centrifugation. Eventually, the cell pellets were re-suspended in HEPES buffer (0.5% NP-40, 100 µL), homogenized by sonication, and diluted to 1 mg/mL with HEPES buffer. All subsequent procedures were similar to those from *in vitro* experiments. The protein pellets were then re-suspended in 20 µL of 1 X SDS- loading buffer and heated for 10 min at 95 ^{o}C. Around 20 µg (per gel lane) of proteins were separated by SDS-PAGE (10% gel) and then visualized by in-gel fluorescence scanning.

7.3.7. Pull-down experiment and validation

To identify potential cellular targets of the probes, pull-down (PD) experiments were carried out, and followed by Western blotting (WB) and LC-MS/MS, where applicable. The general pull-down procedure was based on previously reported procedures with the following optimizations. Fresh cell lysates were prepared and their protein concentrations determined, as described earlier. For *in vitro* pull-down experiment, cellular lysates (5 mg) were supplemented with 200 µL 5× HEPES buffer (125 mM HEPES, pH 7.5; 750 mM NaCl; 10 mM $MgCl_2$), the reaction volume was adjusted to 1 mL with milli-Q water. Subsequently, a solution of probe **STS-C1** (final 1µM) was added, and equilibration was carried out for 2 h at rt. Subsequently, the reaction was reacted by click chemistry with Rh-biotin-N_3 under the conditions described before, acetone precipitated, and resolubilized in 1% SDS in PBS with brief sonication. This re-suspended sample was then incubated with avidin-agarose beads (100 µL/mg protein) at rt overnight. After centrifugation, supernatant was removed and the beads were washed with 0.1% SDS once and PBS for 1 times, then washed with buffer A (8M Urea 200 mM NaCl 2% SDS 100 mM Tris pH 8), buffer B (8 M Urea 1.2 M NaCl 0.2% SDS 100 mM Tris 10% Ethanol 10% Isopropanol pH 8), buffer C (8 M Urea 100 mM Tris pH 8) and PBS. After washing, the beads were boiled in 1× SDS loading

buffer (200 mM Tris pH 6.8, 400 mM DTT, 8% SDS) for 15 min. Control PD using DMSO was carried out concurrently.

For *in situ* PD, the probe **STS-C1** (1 μM) was directly added to live cells, followed by incubation for 2 h. DMSO should never exceed 1% in the final solution. After 2 h of incubation at 37 ºC/5% CO_2, the medium was aspirated, and cells were washed twice gently with PBS to remove the excessive probe. The cells were then trypsined and pelleted by centrifugation. Eventually, the cell pellets were resuspended in PBS (50 μL), homogenized by sonication, and diluted to 1 mg/mL with PBS. The labeled lysates were then subjected to click reaction with Rh-biotin-N_3, and all subsequent experiments were carried out as above described. Control PD using DMSO were carried out concurrently with live cells. WB experiments were carried out as previously described using the corresponding antibodies.

After SDS-PAGE, digestion process was introduced as following: the collected gel cut into small particles was washed twice with ~400 μl of 25 mM ammonium bicarbonate/50% acetonitrile and vortex for 10 min; Gel pieces was then washed with 400 μl of 100 mM ammonium bicarbonate at pH= 8 for 10 min while vortexing, and dehydrated with ~400 μl of 100% acetonitrile. After repeating rehydration and dehydration and Removing the solution, gel particles was incubated with 300 μL of 0.05 mg/mL trypsin solution for 16 h at 37 ºC; the solution was combined with two additional extractions using 2 vol of 5% FA/50% acetonitrile and concentrated *in vacuo*. The peptides were separated and analyzed on a Shimadzu UFLC system (Shimadzu, Japan) coupled to an LTQ-FT Ultra (Thermo Electron, Germany). Mobile phase A (0.1% formic acid in H_2O) and mobile phase B (0.1% formic acid in acetonitrile) were used to establish the 60 min gradient comprising 45 min of 5−35% B, 8 min of 35−50% B, and 2 min of 80% B, followed by re-equilibrating at 5% B for 5 min. Peptides were then analyzed on LTQ-FT with an Advance Captive Spray Source (Michrom Bio Resources) at an electrospray potential of 1.5 kV. A gas flow of 2 L/min, ion transfer tube temperature of 180 °C, and collision gas

pressure of 0.85 mTorr were used. The LTQ-FT was set to perform data acquisition in the positive-ion mode as previously described, except that the m/z range of 350−1600 was used in the full MS scan. The raw data were converted to mgf format. The database search was performed with an in-house Mascot server (version 2.2.07, Matrix Science) with MS tolerance of 10 ppm and MS/MS tolerance of 0.8 Da. Two missed cleavage sites of trypsin were allowed. Carbamidome-thylation(C) was set as a fixed modification, and oxidation (M) and phosphorylation (S, T, and Y) were set as variable modifications. “False” hits that appeared in negative control pull-down/LCMS experiments were further eliminated. All proteins were identified by a minimum score of 40 and at least one unique peptides. Based on these criteria, a list of the hits, which was potential targets of **STS-C1**, was generated. Some “sticky” or contaminated proteins such as keratin, actin, and tubulin have been deleted. “False” hits that appeared in negative control pull-down/LCMS experiments have been further eliminated. The kinases were extracted into Table S2.

For Western blotting analysis, the PVDF membrane was blocked with 3% BSA-TBST (Tween-20, 0.1%) at 4 ºC overnight after the proteins on gel was transferred. Then PVDF membrane was incubated with primary antibody in 3% BSA-TBST (Tween-20, 0.1%) at rt for 1 h followed by washing with TBST (Tween-20, 0.1%) for 10 min × 4. The PVDF membrane was further incubated with corresponding secondary antibody at rt for 1 h followed by washing with TBST (tween-20, 0.1%) for 10 min × 4. SuperSignal West Dura Kit (Thermo Scientific) was used to develop the blot.

7.3.8. Imaging experiment with STS probes

a) Colocalization of STS-T1 over MCF-7

MCF-7 cells were seeded in glass bottom dishes (CELLview^{TM}, Cat. No. 627861) and grown till ~ 60% confluence. The cells were incubated with 1, 5, 10 µM of **STS-T1** in fresh growth medium (200 µL). The cells

were further incubated for 1 h at 37°C/CO_2. Then the cells were washed with PBS three times. Subsequently, cells were fixed with 3.7% formaldehyde in PBS for 20 min at 37°C/CO_2, washed twice again and permeabilized with 0.1% Triton X-100 in PBS for 15 min at 37°C/CO_2, washed twice again. Cell were then blocked with 2% BSA, 0.05% Tween-20 in PBS for 30 min at room temperature, washed twice with PBS and then subsequently treated with a freshly premixed click chemistry reaction in a 200 µL (10 µM Rh-PEG-N_3, 200 µM TBTA 2 mM TCEP, 2 mM $CuSO_4$) for 1 h at room temperature with gentle shaking. Cells were washed with 2x PBS, several times PBS containing 1% Tween-20 and 0.5 mM EDTA (until there was no small crystal under microscopy), 2x PBS, 2x methanol, 2x PBS. For ER-localization experiments, cells were further incubated with ER tracker™ Green (glibenclamide BODIPY® FL, Invitrogen, 0.3 µM in final concentration) for 2 h, washed with PBS twice. For immunofluorescent experiments, cells were further incubated with PDI primary antibody (1 : 200 in 2% BSA, Santa Cruz, sc-166474) for 1 h at room temperature, washed once with 2% BSA and twice with PBS, and then incubated with FITC-conjugated anti-mouse IgG secondary antibody (1 : 100 in 2% BSA, Santa Cruz, sc-2010), washed once with 2% BSA and twice with PBS. For both experiments the cells were incubated with nucleus stain (Hoechst, 0.2 µg/mL as final concentration) for 20 min and washed twice with PBS. Finally, the cells were washed imaged.

b) Colocalization of STS-C1 over HepG2

HepG2 cells were seeded in glass bottom dishes (CELLviewTM, Cat. No. 627861) and grown till ~ 60% confluence. The cells were incubated with 0, 200 nM, 500 nM, 1 µM of **STS-C1** in fresh growth medium (200 µL). The cells were further incubated for 2 h at 37°C/CO_2. Then the cells were washed with PBS three times. Subsequently, cells were fixed with 3.7% formaldehyde in PBS for 20 min at 37°C/CO_2, washed twice again and permeabilized with 0.1% Triton X-100 in PBS for 15 min at 37°C/CO_2, washed twice again. Cell were then blocked

with 2% BSA, 0.05% Tween-20 in PBS for 30 min at room temperature, washed twice with PBS and then subsequently treated with a freshly premixed click chemistry reaction in a 200 µL (10 µM Rh-PEG-N_3, 200 µM TBTA 2 mM TCEP, 2 mM $CuSO_4$) for 1 h at room temperature with gentle shaking. Cells were washed with 2 x PBS, several times PBS containing 1% Tween-20 and 0.5 mM EDTA (until there was no small crystal under microscopy), 2 x PBS, 2 x methanol, 2 x PBS. The cells were incubated with nucleus stain (Hoechst, 0.2 µg/mL as the final concentration) for 10 min and washed twice with PBS. Finally, the cells were washed imaged.

7.4. Chapter 4

7.4.1. The procedure for synthesis of intermediates and probes

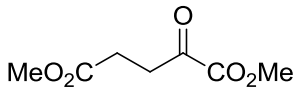

Dimethyl 2-oxopentanedioate (4-2) To a solution of 2-oxoglutaric Acid **4-1** (10 g, 68 mmol) in dry MeOH (100 mL) was added thionyl chloride (10 mL) dropwise at 0 ^{o}C. After addition was complete, the reaction was stirred at rt overnight. The reaction mixture was concentratined to give the product as colorless oil, which was used in next step without further purification. (11 g, 93%) ^{1}H NMR (300 MHz, $CDCl_3$) δ 3.81 (s, 3H), 3.61 (s, 3H), 3.09 (t, J = 6.5 Hz, 2H), 2.60 (t, J = 6.5 Hz, 2H).

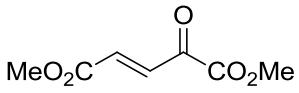

(*E*)-Dimethyl 4-oxopent-2-enedioate (4-3) To a solution of compound **4-2** (8.0 g, 46 mmol) in DCM (120 mL) was added bromine (4.0 mL) at refluxing and the reaction was refluxed for 3 h. Then the mixture was concentrated to give an orange oil. The resulted residue was dissolved in diethyl ether (200 mL) and TEA (7.2 mL) was added dropwise at rt with large of precipitated formed. The mixture was filtered through a pad of siliga gel and the filtrate was concentrated to give residue which was further purified by column chromatography to give the desired product **4-3** as a bright yellow solid. (2.7 g, 34%) ^{1}H NMR (300 MHz, $CDCl_3$) δ 7.62 (d, J = 16.0 Hz, 1H), 6.97 (d, J = 16.0 Hz, 1H), 3.93 (s, 3H), 3.84 (s, 3H).

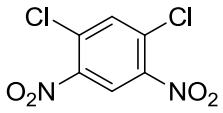

1,5-Dichloro-2,4-dinitrobenzene (4-5) To a clear solution of potassium nitrate (14 g, 140 mmol) and sulfuric acid (50 mL) at 60 ^{o}C, was added 1,3-dichlorobenzene **4-4** (10 g, 68 mmol). The the reaction was heated at 125 ^{o}C for 1 h. After cooled to 90 ^{o}C, the reaction mixture was poured into ice-water. The solid was collected by filtration and recrystallized in ethanol (60.0 mL) to give the product **4-5** as a yellow crystal. (4.0 g, 25%) ^{1}H NMR (500 MHz, $CDCl_3$) δ 8.57 (s, 1H), 7.84 (s, 1H).

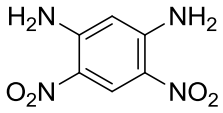

4,6-Dinitrobenzene-1,3-diamine (4-6) [143] A solution of compound **4-5** (4.0 g, 17 mmol) in ethylene glycol (30 mL) was heated to 140 ^{o}C under ammomium atmosphere with large of precipitate formed. After no more precipitated formed, the reaction was cooled down. Solid was collected by filtration followed by washing with boiling water and boiling ethanol to give product **4-6** as a yellow powder. (2.1g, 63%) ^{1}H NMR (300 MHz, $CDCl_3$) δ 9.01 (s, 1H), 6.99 (s, 1H).

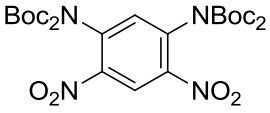

Di-*tert*-butyl (4,6-dinitro-1,3-phenylene)bis(*tert*-butoxycarbonyl carbamate) (4-7) To a solution of compound **4-6** (1.0 g, 5 mmol) and DMAP (0.30 g, 2.5 mmol), was added dropwise Boc_2O (5.7 g, 26 mmol) at 0 ^{o}C. After addition was complete, the reaction was allowed to warm to r.t .and stirred at rt overnight. The reaction was proportioned

with water (10 mL) and diethyl ether (10 mL). Aq layer was extracted with ether (10 mL X 3). The combined organic layers were dried over anhyd sodium sulfate and concentrated to give residue which was purified by column chromatography to give the product **4-7** as a white solid. (2.5 g, 83%) ^{1}H NMR (300 MHz, $CDCl_3$) δ 8.73 (s, 1H), 7.21 (s, 1H), 1.36 (s, 36H); ^{13}C NMR (75 MHz, $CDCl_3$) δ 148.99, 143.91, 137.49, 134.70, 122.04, 84.99, 27.71.

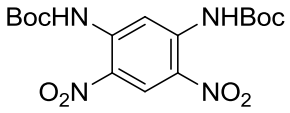

Di-*tert*-butyl (4,6-dinitro-1,3-phenylene)dicarbamate (4-8) To a solution of compound **4-7** in DCM (10 mL) at 0 ^{o}C, was added TFA (1.9 mL) dropwise and the reaction was stirred at 0 ^{o}C for 2 h. Then the reaction was quenched with sat. sodium bicabornate and extracted with DCM (20 mL X 3). The combined organic layers were dried over anhyd sodium sulfate and concentrated to give the residue which was purified by column chromatography to afford the product **4-8** as a white solid. (1.4 g, 84%) ^{1}H NMR (300 MHz, $CDCl_3$) δ 10.07 (s, 2H), 9.81 (s, 1H), 9.22 (s, 1H), 1.57 (s, 18H).

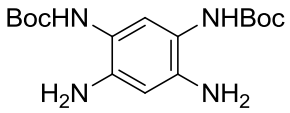

Di-*tert*-butyl (4,6-diamino-1,3-phenylene)dicarbamate (4-9) Dinitro compound **4-8** (3.0 g, 7.5 mmol) was subjected to catalytic hydrogenation over 10% Pd/C (0.50 g) at 30 psi in EtOAc (40 mL) for 12 h. The reaction mixture was filtrated through celite and the filtrate was concentrated to yield compound **4-9** as a light brown solid. (2.15 g, 84%) ^{1}H NMR (500 MHz, $CDCl_3$) δ 7.03 (s, 1H), 6.17 (s, 1H), 5.98 (br s, 1H), 3.71 (br s, 4H), 1.50 (s, 18H).

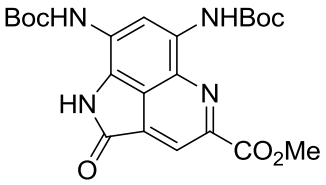

Methyl 6,8-bis((*tert*-butoxycarbonyl)amino)-2-oxo-1,2-dihydropyrrolo[4,3,2-de]quinoline-4-carboxylate (4-10) To a stirring solution of compound **4-9** (100 mg, 0.3 mmol) in chloroform (5 mL) was added comound **4-3** (65 mg, 0.38 mmol) at rt After 30 min, TsOH (5.3 mg) and $Cu(OAc)_2$ (5.6 mg) was added and the reaction was refluxed for 8 h. Then the reaction was quenched with sat. sodium bicarbonate solution. The mixture was extracted with chloroform (10 mL X 3). The combined extracts were dried over anhyd sodium sulfate and concentrated *in vacuo* to give the residue which was purified by column chromatography to afford the desired product **4-10** as a red solid. (50 mg, 36%) ^{1}H NMR (500 MHz, $CDCl_3$) δ 9.48 (s, 1H), 8.69 (s, 1H), 8.37 (s, 1H), 7.98 (s, 1H), 7.24 (s, 1H), 4.10 (s, 3H), 1.57 (s, 9H), 1.53 (s, 9H).

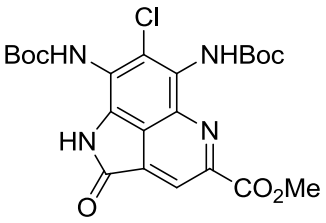

Methyl 6,8-bis((*tert*-butoxycarbonyl)amino)-7-chloro-2-oxo-1,2-dihydropyrrolo[4,3,2-de]quinoline-4-carboxylate (4-11) Pyrroloquinoline **4-10** (200 mg, 0.44 mmol) was subjected to chlorination with NCS (68 mg, 0.51 mmol) in anhyd DMF (2 mL) at 60 °C for 30 min. The reaction mixture poured into water. Solid was collected with filtration and purified by silica gel column chromatography to provide the product **4-11** as a yellow solid. (145.0 mg, 68%) ^{1}H NMR (300 MHz, $CDCl_3$) δ 9.47 (s, 1H), 8.61 (s, 1H), 7.49

(s, 1H), 7.29 (s, 1H), 4.06 (s, 4H), 1.55 (s, 9H), 1.49 (s, 9H); ^{13}C NMR (75 MHz, $CDCl_3$) δ 165.75, 164.97, 152.82, 152.27, 149.29, 138.55, 135.05, 129.12, 127.62, 122.02, 121.85, 119.21, 117.98, 83.51, 81.54, 53.26, 28.09, 28.04.

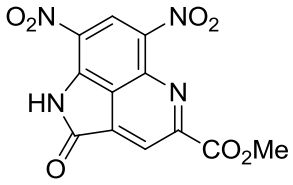

Methyl 6,8-dinitro-2-oxo-1,2-dihydropyrrolo[4,3,2-de]quinoline-4-carboxylate (4-14) A mixture of 1,3-diamin-6-dinitrobenzene **4-6** (100 mg, 0.51 mmol) and dimethyl 2-oxoglutaconate **4-3** (44 mg,0.25 mmol) in 20 mL of TFA was refluxed for 8 h, after which TFA was chilled out.The residue was purified by flash chromatography to yield the product **4-14** as a yellow solid (30 mg, 38%) ^{1}H NMR (300 MHz, DMSO-d_6) *δ* 9.01 (s, 1H), 8.53 (s, 1H), 4.01 (s, 3H).

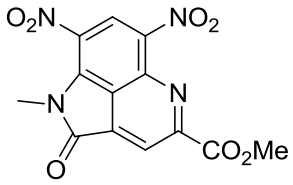

Methyl 1-methyl-6,8-dinitro-2-oxo-1,2-dihydropyrrolo[4,3,2-de]quinolone-4-carboxylate (4-15) To a stirring mixture of compound **4-14** (0.50 g, 1.5 mmol), potassium carbonate (0.45 g, 3 mmol) and molecular sieve (4Å, 0.20 g), was added methiodide (0.37 mL, 6 mmol) at rt. After overnight of stirring, the reaction mixture was concentrated *in vacuo* to give residue which was purified by column chromatography to give the desired product **4-15** as a dark solid. (0.31 g, 60%) ^{1}H NMR (300 MHz, DMSO-d_6) *δ* 9.03 (s, 1H), 8.64 (s, 1H), 4.02 (s, 3H), 3.52 (s, 3H).

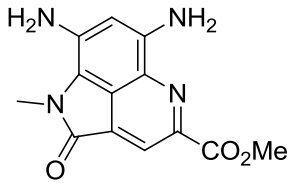

Methyl 6,8-diamino-1-methyl-2-oxo-1,2-dihydropyrrolo[4,3,2-de]quinoline-4-carboxylate (4-16) A solution of compound **4-15** (0.31 g, 0.93 mmol) in DMF (5.0 mL) was stirred with Pd/C (10%, 0.10 mg) under hydrogen atmosphere (5 bar) at rt overnight. Catalyst was filtrated off and washed with DMF. The filtrate was concentrated *in vacuo* to give the product **4-16** as a purple solid. (0.22 g, 88%) ^{1}H NMR (300 MHz, DMSO-d_6) δ 8.33 (s, 1H), 6.35 (s, 2H), 6.24 (s, 1H), 6.03 (s, 2H), 3.93 (s, 3H), 3.54 (s, 4H).

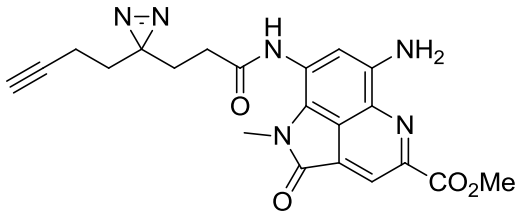

Methyl 6-amino-8-(3-(3-(but-3-yn-1-yl)-3*H*-diazirin-3-yl)propanamido)-1-methyl-2-oxo-1,2-dihydropyrrolo[4,3,2-de]quinoline-4-carboxylate (4-17) A solution of 3-(3-(but-3-yn-1-yl)-3*H*-diazirin-3-yl)propanoic acid (3.0 mg, 0.018 mmol), DMAP (2.2 mg, 0.018 mmol) and EDCI (13.8 mg, 0.072 mmol) in DMF (0.60 mL) was stirred at 0 ^{o}C for 10 min in dark. To above solution was added a solution of compound **4-16** (5.0 mg, 0.018 mmol) in DMF (0.50 mL) at 0 ^{o}C. Then the reaction was allowed to warm to rt and stirred at rt overnight. After 1 equiv. of the photo-labile linker and 4 equiv. of EDCI were added at 0 ^{o}C, the reaction was stirred at rt overnight until LC-MS analysis showed the product peak (m/z: 421.1) stopped increasing. The reaction mixture was concentrated to give residue which was purified by column chromatography to give the product **4-17** as purple solid. (1.1 mg, 14%)

^{1}H NMR (300 MHz, $CDCl_3$) δ 9.61 (s, 1H), 8.66 (s, 2H), 8.31 (s, 1H), 4.50 (s, 1H), 4.08 (s, 3H), 3.69 (s, 3H), 2.45 (t, *J* = 7.5 Hz, 2H), 2.12 – 2.06 (m, 2H), 1.97 (t, *J* = 7.6 Hz, 2H), 1.72 (d, *J* = 7.2 Hz, 2H).

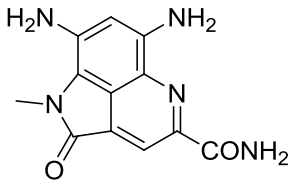

6,8-diamino-1-methyl-2-oxo-1,2-dihydropyrrolo[4,3,2-de]quinoline-4-carboxamide (4-18) A mixture of compound **4-16**[105] (89 mg, 0.32 mmol) in ammonium solution (10.0 mL) was stirred at rt overnight. Sovent was removed *in vacuo* to give desired product as a purple solid. (73 mg, 87%) ^{1}H NMR (300 MHz, DMSO-d_6) δ 8.70 (s, 1H), 8.29 (s, 1H), 7.69 (d, *J* = 3.8 Hz, 1H), 7.55 (s, 1H), 6.40 (s, 2H), 6.16 (s, 2H), 3.53 (s, 3H).

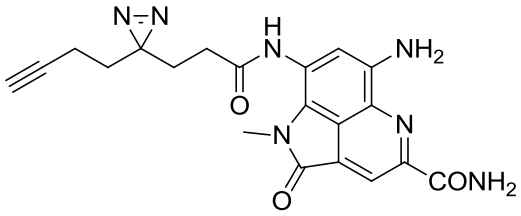

***N*-(6-Amino-4-((aminooxy)carbonyl)-1-methyl-2-oxo-1,2-dihydro pyrrolo[4,3,2-de]quinolin-8-yl)-3-(3-(but-3-yn-1-yl)-3*H*-diazirin-3-yl)propanamide (4-19)** A solution of 3-(3-(but-3-yn-1-yl)-3*H*-diazirin-3-yl) propanoic acid (6.5 mg, 0.039 mmol), DMAP (4.8 mg, 0.039 mmol) and EDCI (30 mg, 0.16 mmol) in DMF (1.3 mL) was stirred at 0 ^{o}C for 10 min in dark. To above solution was added a solution of compound **4-18** (100 mg, 0.039 mmol) in DMF (1.0 mL) at 0 ^{o}C. Then the reaction was allowed to warm to rt and stirred at rt overnight until LC-MS analysis showed the product peak ($[M+H]^+$, m/z: 421.1) stopped increasing. The reaction mixture was concentrated to give residue

which was purified by column chromatography to give the product as purple solid. (7.8 mg, 48%) ^{1}H NMR (300 MHz, MeOD) δ 8.59 (s, 1H), 8.31 (s, 1H), 5.49 (s, 2H), 3.66 (s, 3H), 2.52 – 2.47 (m, 2H), 2.08 (td, *J* = 7.4, 2.6 Hz, 2H), 1.97 – 1.92 (m, 2H), 1.71 (t, *J* = 7.4 Hz, 2H).

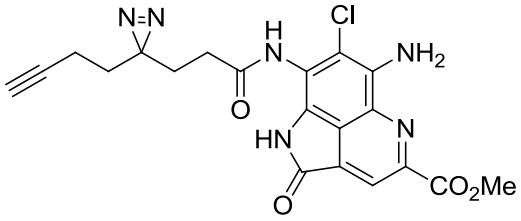

Methyl 6-amino-8-(3-(3-(but-3-yn-1-yl)-3*H*-diazirin-3-yl)propanamido)-7-chloro-2-oxo-1,2-dihydropyrrolo[4,3,2-de]quinoline-4-carboxylate (4-24) To a solution of the mixture of compound **4-12** and **4-17** (10 mg) and 3-(3-(but-3-yn-1-yl)-3*H*-diazirin-3-yl) propanoic acid (6.0 mg, 0.036 mmol) in DMF (1 mL), was added EDCI (42 mg, 0.22 mmol) and DMAP (7.2 mg, 0.059 mmol) at 0 ^{o}C. Then the reaction was allowed to warm to rt and stirred at rt overnight until LC-MS analysis showed the product peak ([M+H]$^+$, m/z: 440.9) stopped increasing. The mixture was loaded to column chromatography to give product. (3.4 mg) ^{1}H NMR (300 MHz, DMSO-d$_6$) δ 8.39 (s, 1H), 7.16 (s, 2H), 6.41 (s, 2H), 3.96 (s, 3H), 3.04 – 2.99 (s, 2H), 2.84 (s, 1H), 2.18 – 2.03 (m, 2H), 1.90 – 1.85 (m, 2H), 1.67 (t, *J* = 7.4 Hz, 2H).

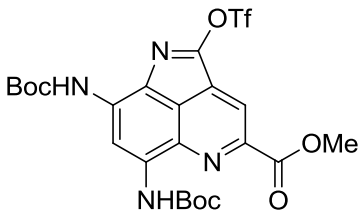

Methyl 6,8-*bis*((*tert*-butoxycarbonyl)amino)-2-(((trifluoromethyl)sulfonyl)oxy)pyrrolo[4,3,2-de]quinoline-4-carboxylate (4-31) To a stirred solution of compound **4-10** (33 mg, 0.072 mmol) and pyridine

(29 mg, 0.36 mmol) in DCM (1 mL) was added Tf_2O (28.5 mg, 0.36 mmol) at 0 °C. After stirring at rt for 1 h, the solution was treated with water. Then the mixture was extracted with DCM (5 mL x 3). The organic layer was washed with brine, dried over anhyd sodium sulfate, and concentrated to give the residue which was purified by preparative TLC (eluent: Hexanes/EA = 4/1) to afford as reddish solid. (34 mg, 80%) ^{1}H NMR (300 MHz, $CDCl_3$) δ 9.35 (s, 1H), 8.74 (s, 1H), 8.74 (s, 1H), 8.65 (s, 1H), 8.04 (s, 1H), 4.15 (s, 3H), 1.65 (s, 9H), 1.63 (s, 9H).

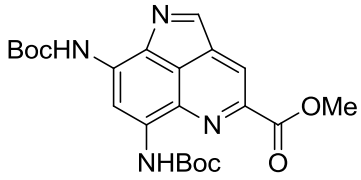

a) Reduced by Schwartz's reagent

Methyl 6,8-*bis*((*tert*-butoxycarbonyl)amino)pyrrolo[4,3,2-de]quino line -4-carboxylate (4-32) To a stirred solution of compound **4-10** (25 mg, 0.054 mmol) in dry THF (1 mL) was added Schwartz's reagent (28 mg, 0.11 mmol) at -30 ^{o}C under argon atmosphere. The solution was stirred at that temperature for 2 h before sat. brine was added into the solution. The mixture was extracted with ethyl acetate (5 mL x 3). Then the combined extracts were dried over anhyd sodium sulfate and concentrated to give the residue which was purified by column chromatography (Hexanes:EA = 4:1) to get the desired product as orange solid. (14 mg, 60%)

b) Reduced by DIBAL-H

Methyl 6,8-*bis*((*tert*-butoxycarbonyl)amino)pyrrolo[4,3,2-de]quino line-4-carboxylate (4-32) To a stirred solution of compound **4-10** (20 mg, 0.044 mmol) in dry THF was added DIBAL-H (1.0 M, 87 µL) at -78 ^{o}C under argon atmosphere, the reaction was slowly warmed up until the starting material was all consumed monitored by TLC analysis.

Then 1 mL of sat. sodium bicarbonate solution was added and the mixture was extracted with EA (5 mL x 3). After the extracts were dried over anhyd sodium sulfate and concentrated under reduced pressure, the residue was purified by column chromatography (Hexane:EA=4:1) to give the desired product as orange solid. (7.7 mg, 40%) ^{1}H NMR (300 MHz, $CDCl_3$) δ 9.46 (s, 1H), 8.70 (s, 1H), 8.42 (s, 1H), 7.92 (s, 1H), 6.91 (s, 1H), 4.09 (s, 3H), 1.57 (s, 9H), 1.54 (s, 9H).

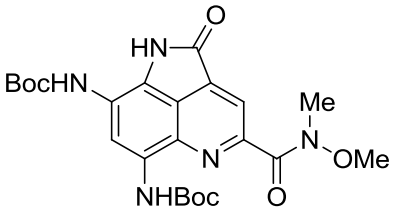

Di-*tert*-butyl (4-(methoxy(methyl)carbamoyl)-2-oxo-1,2-dihydropyrrolo[4,3,2-de]quinoline-6,8-diyl)dicarbamate (4-34) To a stirred mixture of THF (2 mL) and H_2O (1 mL) was added LiOH (7.2 mg, 0.30 mmol), and the solution was stirred for 10 min., before compound **4-10** (69 mg, 0.15 mmol) was added. After 1 h of stirring, 3 mL of sat. citric acid solution was added. The organic layer was separated and the aq layer was extracted with EA (5 mL x 3). The combined organic layer was dried over anhyd sodium sulfate and concentrated under the reduced pressure. The residue as crude product was used directly in next step without further purification as an organic solid. (59 mg, 89%) To a solution of the resulted acid (57 mg, 0.13 mmol) above and *N,O*-dimethylhydroxylamine hydrochloride(25 mg, 0.26 mmol) in THF (1 mL) was added EDCI (49 mg 0.26 mmol) and DMAP (52 mg, 0.51 mmol). The reaction was allowed to be stirred for 2 h before 1 mL sat. sodium bicarbonate solution was added. The organic layer was separated and the aq layer was extracted with EA (5 mL x 3), dried with anhyd sodium sulfate and concentrated under reduced pressure. The residue was purified with flash chromatography (Hexanes:EA = 2:1) to afford the desired product as orange solid (90%). ^{1}H NMR (300 MHz, $CDCl_3$) δ 9.50 (s, 1H), 8.22 (s, 1H), 8.17 (s, 1H), 7.89 (s, 1H), 7.05 (s, 1H), 3.65

(s, 3H), 3.47 (s, 3H), 3.25 (s, 3H), 1.55 (s, 9H), 1.53 (s, 9H); ^{13}C NMR (75 MHz, $CDCl_3$) δ 166.03, 152.65, 152.53, 151.98, 134.50, 132.34, 122.28, 120.40, 118.12, 115.84, 110.75, 82.61, 81.55, 61.58, 28.26, 28.10.

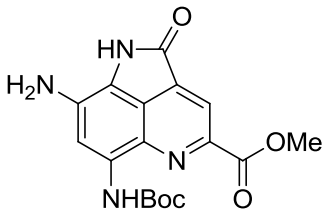

Methyl 8-amino-6-((*tert*-butoxycarbonyl)amino)-2-oxo-1,2-dihydro pyrrolo[4,3,2-de]quinoline-4-carboxylate (4-36) The compound **4-10** (0.20 g, 0.44 mmol) was dissoloved in DMF (5.0 mL) and the reaction was stirred under microwave at 150 ^{o}C for 1 h. Then the reaction was cooled to rt and concentrated *in vacuo* to give product **4-36** as a purple solid. (0.14 g, 90%) ^{1}H NMR (300 MHz, DMSO-d_6) δ 10.32 (s, 1H), 8.42 (s, 1H), 8.35 (s, 1H), 7.79 (s, 1H), 7.70 (s, 1H), 6.45 (s, 2H), 3.96 (s, 4H), 1.54 (s, 9H).

7.4.2. Pure enzyme labeling

To investigate the labeling specificity of our probes, pure enzyme labeling experiments were performed. Briefly, different proteins (a final concentration of 100 nM) were incubated with probes respectively, in above reaction buffer for 30 min at rt followed by UV irradiation (365 nm, 20 min). After 2 h of click reaction, 6×SDS loading dye was added and the mixture was heated to 95 ºC for 10 min. The resulting proteins were resolved by SDS-PAGE. In-gel fluorescence scanning was used to visualize the labelled protein bands. Both in-gel fluorescence scanning (FL) and silver staining was always carried out on the gels upon SDS-PAGE separation of labeled samples.

7.4.3. Bacterial lysate labeling

Bacterial lysates were prepared using modified procedures based on previous reports. To 20 μg of above bacterial lysates, the probes were added and the reactions were incubated for 30 min at rt followed by UV irradiation (365 nm, 20 min). After 2 h of click reaction, 6 X SDS loading dye (4 μL) was added and the mixture was heated to 95 ^{o}C for 10 min. The resulting proteins were resolved by SDS-PAGE. In-gel fluorescence scanning was used to visualize the labelled protein bands. Both in-gel fluorescence scanning (FL) and coomassie Brilliant Blue staining (CBB) were always carried out on the gels upon SDS-PAGE separation of labeled samples.

7.4.4. *In vitro* labeling over cancer cell lysate

The probes was added to 100 μg fresh cancer cell lysates (prepared as previously described) in 100 μL of HEPES buffer at a desired concentration. Samples incubated with probes were incubated for 30 min at rt followed by UV irradiation (365 nm, 20 min). After 2 h of click reaction, 4 μL of a freshly premixed click chemistry reaction cocktail (100 μM Rh-PEG-N_3 from 10 mM stock solution in DMSO, 100 μM TBTA from 10 mM freshly prepared stock solution in deionized water, 1 mM TCEP from 100 mM freshly prepared stock solution in deionized water, and 1 mM $CuSO_4$ from 100 mM freshly prepared stock solution in deionized water) was added. The reaction was further incubated for 2 h with gentle mixing, before being terminated by addition of pre-chilled acetone (0.4 mL; 30 min incubation at -20 ^{o}C). Precipitated proteins were subsequently collected by centrifugation (13000 rpm X 10 min at 4 ^{o}C). The supernatant was discarded and the pellet was washed with 200 μL of pre-chilled methanol. The air-dried pellet was added 2 X loading buffer and heated for 10 min at 95 ^{o}C. Around 20 μg (per gel lane) of proteins were separated by SDS-PAGE (10% gel) and then visualized by in-gel fluorescence scanning.

7.4.5. Pull-down experiment

To identify potential cellular targets of the probes, pull-down (PD) experiments were carried out, and followed by and LC-MS/MS. The general pull-down procedure was based on previously reported procedures with the following optimizations.[26] Fresh cell lysates were prepared and their protein concentrations determined, as described earlier. For *in vitro* pull-down experiment, cellular lysates (5 mg) were supplemented with 200 µL 5× HEPES buffer (125 mM HEPES, pH 7.5; 750 mM NaCl; 10 mM $MgCl_2$), the reaction volume was adjusted to 1 mL with milli-Q water. Subsequently, **Am-2** were added, and equilibration was carried out for 1 h at rt followed by UV irradiation (365 nm, 30 min). Subsequently, the reaction was reacted by click chemistry with Rh-biotin-N_3 under the conditions described before, acetone precipitated, and re-solubilized in 1% SDS in PBS with brief sonication. This re-suspended sample was then incubated with avidin-agarose beads (100 µL/mg protein) at rt for 2 h. After centrifugation, supernatant was removed and the beads were washed with 0.1% SDS once and PBS for 1 time, then washed with buffer A (8 M Urea 200 mM NaCl 2% SDS 100 mM Tris pH 8), buffer B (8 M Urea 1.2 M NaCl 0.2% SDS 100 mM Tris 10% Ethanol 10% Isopropanol pH 8), buffer C (8M Urea 100 mM Tris pH 8) and PBS. After washing, the beads were boiled in 1× SDS loading buffer (200 mM Tris pH 6.8, 400 mM DTT, 8% SDS) for 15 min. Control PD using NP was carried out concurrently.

After SDS-PAGE, digestion process was introduced as following: the collected gel cut into small particles was washed twice with ~400 µl of 25 mM ammonium bicarbonate/50% acetonitrile and vortex for 10 min; Gel pieces was then washed with 400 µl of 100 mM ammonium bicarbonate at pH= 8 for 10 min while vortexing, and dehydrated with ~400 µl of 100% acetonitrile. After repeating rehydration and dehydration and Removing the solution, gel particles was incubated with 300 µL of 0.05 mg/mL trypsin solution for 16 h at 37 ºC; the solution was combined with two additional extractions using 2 vol of 5% FA/50% acetonitrile and concentrated *in vacuo*. The peptides were separated and analyzed on a Shimadzu UFLC system (Shimadzu,

Japan) coupled to an LTQ-FT Ultra (Thermo Electron, Germany). Mobile phase A (0.1% formic acid in H_2O) and mobile phase B (0.1% formic acid in acetonitrile) were used to establish the 60 min gradient comprising 45 min of 5−35% B, 8 min of 35−50% B, and 2 min of 80% B, followed by re-equilibrating at 5% B for 5 min. Peptides were then analyzed on LTQ-FT with an Advance Captive Spray Source (Michrom Bio Resources) at an electrospray potential of 1.5 kV. A gas flow of 2 L/min, ion transfer tube temperature of 180 °C, and collision gas pressure of 0.85 mTorr were used. The LTQ-FT was set to perform data acquisition in the positive-ion mode as previously described, except that the m/z range of 350−1600 was used in the full MS scan. The raw data were converted to mgf format. The database search was performed with an in-house Mascot server (version 2.2.07, Matrix Science) with MS tolerance of 10 ppm and MS/MS tolerance of 0.8 Da. Two missed cleavage sites of trypsin were allowed. Carbamidome-thylation(C) was set as a fixed modification, and oxidation (M) and phosphorylation (S, T, and Y) were set as variable modifications. “False” hits that appeared in negative control pull-down/LCMS experiments were further eliminated. Some “sticky” or contaminated proteins such as keratin, actin, and tubulin have been deleted. “False” hits that appeared in negative control pull-down/LCMS experiments have been further eliminated. The list of potential targets was listed in Table S3. (See in Chapter 9 Appendix)

7.5. Chapter 5

Procedure for the synthesis of linkers

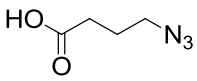

4-azidobutanoic acid (5-6) To a solution of compound **5-5** (5.0 g, 30 mmol) in dry MeOH (50 mL) was added thionyl chloride (4.4 mL, 60 mmol) dropwise at 0 ^{o}C. After the addition was complete, the reaction was allowed to warm to rt and stirred at r.t overnight. The reaction mixture was concentrated to give residue. To the residue was added sat. $NaHCO_3$, then the mixture was extracted with ethyl acetate (EA, 50 mL X 3). The combined extracts were dried over anhyd Sodium sulfate and concentrated to give liquid which was used in next step without further purification. ^{1}H NMR (300 MHz, $CDCl_3$) δ 3.63 (s, 1H), 3.30 (t, *J* = 6.6 Hz, 1H), 2.37 (t, *J* = 7.2 Hz, 1H), 1.85 (p, *J* = 6.9 Hz, 1H); ^{13}C NMR (75 MHz, $CDCl_3$) δ 172.95, 51.52, 50.44, 30.72, 24.06.

To a solution of the above product methyl 4-bromobutanoate in DMF (10 mL) was added NaN_3. The mixture was heated at 80 ^{o}C for 40 min by microwave. Then the reaction mixture was proportioned with water and EA. The organic layer was washed with aq $NaHCO_3$, brine and dried over anhyd sodium sulfate. The organic layer was concentrated to give the residue used in next step without purification. (4.1 g) ^{1}H NMR (500 MHz, $CDCl_3$) δ 4.31 (t, *J* = 7.1 Hz, 1H), 2.42 (dt, *J* = 14.0, 7.5 Hz, 1H), 2.28 – 2.12 (m, 1H).

To a solution of above product methyl 4-azidobutanoate in MeOH (40 mL) was added the solution of LiOH (1.4 g, 58 mmol) in H_2O (10 mL). After the stirring of overnight at rt, the mixture was concentrated to residue which was dissolved in EA (20 mL) and acidified to pH = 1 by 1 *N* HCl. After extraction with EA (20 mL X 30, the combined extracts were dried over anhyd sodium sulfate and concentrated to give product **5-6** as a colourless liquid without purification. (3.3 g, 89%) ^{1}H NMR (500 MHz, $CDCl_3$) δ 4.31 (t, *J* = 7.1 Hz, 2H), 2.53 – 2.33 (m, 2H), 2.30 – 2.12 (m, 2H).

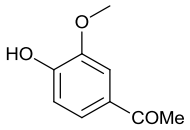

1-(4-Hydroxy-3-methoxyphenyl)ethanone (5-8) To the mixture of apocynin (15 g, 90 mmol), KI (0.6 g, 0.36 mmol) and K_2CO_3 (24 g, 174 mmol) in acetonitrile (100 mL) was added benzyl bromide (BnBr, 12 mL) and the reaction was refluxed overnight. After filtration, the filtrate was concentrated to give residue which was purified by column chromatography to give product **5-8** as a white solid. (22.1 g, 96%) ^{1}H NMR (500 MHz, $CDCl_3$) δ 7.55 (d, J = 1.9 Hz, 1H), 7.50 (dd, J = 8.3, 2.0 Hz, 1H), 7.44 (dd, J = 4.4, 3.8 Hz, 2H), 7.41 – 7.35 (m, 2H), 7.32 (d, J = 7.0 Hz, 1H), 6.93 – 6.86 (m, 1H), 5.23 (s, 2H), 3.94 (s, 3H), 2.54 (s, 3H).

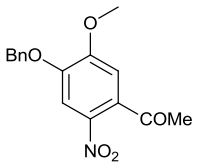

1-(4-(Benzyloxy)-5-methoxy-2-nitrophenyl)ethanone (5-9) To a solution of compound **5-8** (22 g, 86 mmol) was added nitric acid (HNO_3, 30 mL) dropwise at 0 ^{o}C and the reaction was stirred overnight at rt. The reaction mixture was poured into ice and the precipitate was collected by filtration. The solid was dissolved in DCM and precipitated by addition of MeOH. The product **5-9** was dried *in vacuo*. (20 g, 77%) ^{1}H NMR (300 MHz, $CDCl_3$) δ 7.67 (s, 1H), 7.41 (ddd, J = 15.0, 10.0, 7.2 Hz, 4H), 6.76 (s, 1H), 5.22 (s, 1H), 3.98 (s, 2H), 2.49 (s, 2H).

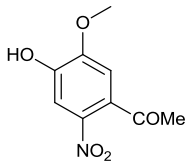

1-(4-Hydroxy-5-methoxy-2-nitrophenyl)ethanone (5-10) After compound **5-9** (6.0 g, 20 mmol) was dissolved in TFA (10 mL), the reaction was refluxed for 40 min. The reaction mixture was poured into ice-water. The product as yellow solid was collected by filtration. After filtration, the filtrate was basified by 1 *N* NaOH to pH = 10 and extracted with EA (50 mL X 3).Then the aq layer was acidified to pH = 2~3 by 1 *N* HCl and extracted with EA (50 mL X 3). The combined extracts were dried over anhyd sodium sulfate and concentrated to product **5-10** as a white solid. (3.4 g, 80%) ^{1}H NMR (300 MHz, $CDCl_3$) *δ* 7.67 (s, 1H), 7.40 (s, 1H), 6.80 (s, 1H), 4.02 (s, 1H), 2.49 (s, 1H).

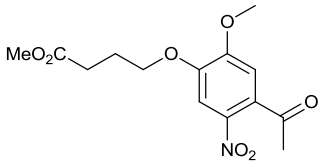

Methyl 4-(4-acetyl-2-methoxy-5-nitrophenoxy)butanoate (5-11) The mixture of **5-10** (2.5 g, 12 mmol), methyl 4-bromobutanoate (3.0 g, 17 mmol) and K_2CO_3 (3.3 g, 24 mmol) in DMF (40 mL) was heated at 80 ^{o}C overnight. After DMF was removed *in vacuo*, the desired residue was proportioned with DCM (20 mL) and water (20 mL). The aq layer was extracted with DCM (10 X 3). The combined organic layer was dried over anhyd sodium sulfate and concentrated to give the residue which was purified by column chromatography to give product **5-11** as a white solid. (1.5 g, 41%) ^{1}H NMR (300 MHz, $CDCl_3$) *δ* 7.58 (s, 1H), 6.73 (s, 1H), 4.13 (t, *J* = 6.2 Hz, 2H), 3.93 (s, 3H), 3.67 (s, 3H), 2.54 (t, *J* = 7.2 Hz, 2H), 2.47 (s, 3H), 2.22 - 2.13 (m, 2H); ^{13}C NMR (75 MHz, $CDCl_3$) *δ* 200.04, 173.18, 154.21, 148.74, 138.22, 132.76, 108.65, 107.89, 68.32, 56.51, 51.68, 30.30, 30.17, 24.06.

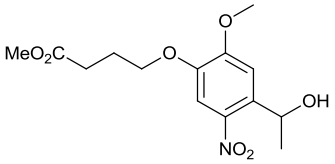

Methyl 4-(4-(1-hydroxyethyl)-2-methoxy-5-nitrophenoxy)butanoate (5-12) To the mixture of **5-11** (1.5 g, 4.8 mmol) in MeOH (100 mL) was added $NaBH_4$ in portions at 0 ^oC and stirred for 3 h at 0 ^oC. After the reaction was complete, the reaction was quenched with water and concentrated to give residue which was purified by column chromatography to yield product **5-12** a yellowish solid. (1.3 g, 87%) ^1H NMR (300 MHz, $CDCl_3$) δ 7.44 (s, 1H), 7.23 (s, 1H), 5.44 (q, J = 6.1 Hz, 1H), 4.01 (t, J = 6.1 Hz, 2H), 3.88 (s, 3H), 3.62 (s, 3H), 3.06 (broad, 1H), 2.48 (t, J = 7.2 Hz, 2H), 2.16 – 2.01 (m, 2H), 1.43 (d, J = 6.2 Hz, 3H); ^{13}C NMR (75 MHz, $CDCl_3$) δ 173.32, 153.87, 146.53, 139.06, 137.23, 108.75, 108.51, 68.00, 65.35, 56.08, 51.52, 30.18, 24.22, 24.05.

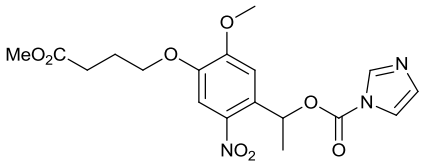

1-(5-Methoxy-4-(4-methoxy-4-oxobutoxy)-2-nitrophenyl)ethyl 1*H*-imidazole-1-carboxylate (5-13) The solution of **5-12** (1.0 g, 32 mmol), 1,1'-Carbonyldiimidazole (CDI) (0.53 g, 35 mmo) and 4-Dimethylaminopyridine (DMAP) (1.2 mg, 0.3 mol%) was stirred at rt for 4 h under protection from light. After the reaction was complete, the reaction mixture was concentrated and purified by column chromatography to give the desired product **5-13**. (0.85 g, 65%) ^1H NMR (500 MHz, $CDCl_3$) δ 8.04 (s, 1H), 7.48 (s, 1H), 7.33 (s, 1H), 6.94 (s, 1H), 6.57 (q, J = 6.4 Hz, 1H), 4.02 (t, J = 6.2 Hz, 2H), 3.83 (s, 3H), 3.56 (s, 3H), 2.43 (t, J = 7.2 Hz, 2H), 2.05 (dd, J = 13.4, 6.7 Hz, 2H), 1.70 (d, J = 6.4 Hz, 3H); ^{13}C NMR (126 MHz, $CDCl_3$) δ 172.85, 153.79,

147.47, 147.21, 139.59, 136.56, 130.42, 130.41, 116.69, 108.61, 107.63, 72.48, 67.89, 56.01, 51.26, 29.88, 23.81, 21.38.

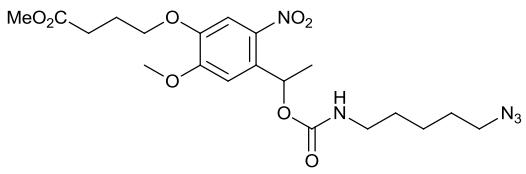

Methyl 4-(4-(1-(((5-azidopentyl)carbamoyl)oxy)ethyl)-2-methoxy-5-nitrophenoxy)butanoate (5-14) The reaction mixture of **5-14** (0.80 g, 2 mmol), 5-azidopentan-1-amine (0.64 g, 5 mmol), triethylamine (TEA, 0.83 g) and DMAP (12 mg, 5 mol%) in DMC (10 mL) was refluxed for 3 d. The mixture was concentrated to give residue which was purified by column chromatography to give the product **5-14**. (0.81 g, 85%) ^{1}H NMR (300 MHz, $CDCl_3$) δ 7.43 (s, 1H), 6.93 (s, 1H), 6.19 (q, *J* = 6.1 Hz, 1H), 5.34 (t, *J* = 5.7 Hz, 1H), 3.80 (s, 3H), 3.55 (s, 3H), 3.10 (t, *J* = 6.7 Hz, 2H), 2.98 (dd, *J* = 12.5, 6.2 Hz, 2H), 2.41 (t, *J* = 7.1 Hz, 2H), 2.11 – 1.98 (m, 2H), 1.52 – 1.14 (m, 9H); ^{13}C NMR (75 MHz, $CDCl_3$) δ 172.88, 155.03, 153.66, 146.54, 138.96, 133.99, 108.45, 107.67, 68.05, 67.69, 55.76, 51.12, 50.71, 40.17, 29.81, 28.95, 27.94, 23.78, 23.32, 21.61.

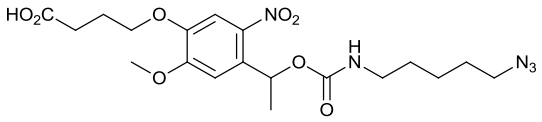

4-(4-(1-(((5-azidopentyl)carbamoyl)oxy)ethyl)-2-methoxy-5-nitro phenoxy)butanoic acid (5-15) To a solution of **5-14** (0.80 g, 1.7 mmol) in THF-H_2O (4:1, 40 mL) was added LiOH (0.50 g) and the reaction was then stirred at rt overnight. The reaction was quenched with aq NH_4Cl and concentrated to remove THF. The aq phase was acidified by 1 *N* HCl to pH 3~4 and extracted with EA (10 mL X 3). The combined extracts were dried over anhyd sodium sulfate and concentrated to give residue which was purified by column

chromatography to give product **5-15** as a white solid. (0.71 g, 91%) ^{1}H NMR (300 MHz, $CDCl_3$) δ 7.53 (s, 1H), 6.97 (s, 1H), 6.29 (dd, J = 12.5, 6.1 Hz, 1H), 5.09 (t, J = 5.7 Hz, 1H), 4.06 (t, J = 6.1 Hz, 2H), 3.89 (s, 3H), 3.20 (t, J = 6.7 Hz, 2H), 3.09 (d, J = 6.3 Hz, 1H), 2.53 (t, J = 7.1 Hz, 1H), 2.12 (p, J = 6.6 Hz, 1H), 1.66 – 1.26 (m, 9H); ^{13}C NMR (75 MHz, $CDCl_3$) δ 177.64, 155.35, 153.83, 146.82, 139.33, 134.00, 108.82, 107.94, 68.63, 67.88, 56.07, 51.01, 40.51, 30.04, 29.22, 28.21, 23.80, 23.60, 21.95.

7.6. Chapter 6

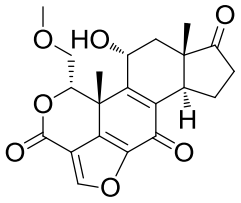

(1S,6b*R*,9a*S*,11*R*,11b*R*)-11-hydroxy-1-(methoxymethyl)-9a,11b-dimethyl-7,8,10,11-tetrahydro-1*H*-furo[4,3,2-de]indeno[4,5-h]isochromene-3,6,9(6b*H*,9a*H*,11b*H*)-trione (6-2) Wortmannin (20 mg, 47 µmol) was suspended in 0.50 mL of methanol, and diethylamine (12 µL, 112 µmol) was added. The solution turned orange immediately, and the wortmannin dissolved completely within a few minutes. The reaction was allowed to stir at r.t overnight. The solution was concentrated to remove the methanol. The residue was dissolved in 1.5 mL of distilled dioxane. Aq 1 M HCl (1.3 mL) was added and the solution was allowed to stir overnight. The solution was concentrated, and the resultant residue was purified by column chromatography to give the desired desacetyl wortmannin (9.0 mg, 50%) ^{1}H NMR (300 MHz, $CDCl_3$) δ 8.24 (s, 1H), 5.59 (dd, *J* = 9.1, 3.9 Hz, 1H), 4.95 – 4.5 (m, 1H), 3.55 – 3.42 (m, 3H), 3.15 (s, 3H), 2.91-2.85 (m, 1H), 2.84 – 2.80 (m, 1H), 2.58 (dd, *J* = 19.3, 8.2 Hz, 1H), 2.44 (dd, *J* = 12.7, 6.5 Hz, 1H), 2.30 – 2.14 (m, 1H), 2.12 – 1.96 (m, 1H), 1.79 (s, 3H), 1.54 (dd, *J* = 12.6, 10.1 Hz, 2H), 1.40 (d, *J* = 5.7 Hz, 1H), 0.95 (s, 3H).

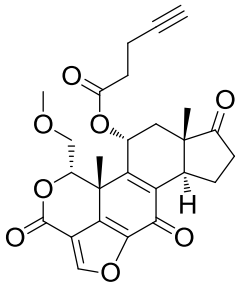

(1*S*,6b*R*,9a*S*,11*R*,11b*R*)-1-(methoxymethyl)-9a,11b-dimethyl-3,6,9-trioxo-3,6,6b,7,8,9,9a,10,11,11b-decahydro-1*H*-furo[4,3,2-de]indeno[4,5-h]isochromen-11-yl pent-4-ynoate (**6-4**) A solution of 11-deacetyl wortmannin (**6-2**) and pent-4-ynoic acid (**6-3**) (5.0 mg, 13 µmol), EDCI

(22 mg, 12 μmol) and DMAP (3.6 mg, 30 μmol) in DCM (1 mL) and DMF (1 mL) was stirred at rt overnight. The reaction mixture was concentrated *in vacuo* to give the residue which was purified by column chromatography to give the product as white solid. (4.0 mg, 67%) ^{1}H NMR (500 MHz, $CDCl_3$) δ 8.24 (s, 1H), 6.33 – 6.13 (m, 1H), 4.85 (dd, *J* = 6.7, 1.9 Hz, 1H), 3.45 (dd, *J* = 11.3, 1.9 Hz, 1H), 3.18 (s, 3H), 3.02 (dd, *J* = 11.2, 6.7 Hz, 1H), 2.90 (ddd, *J* = 12.6, 5.9, 2.7 Hz, 1H), 2.73 – 2.45 (m, 6H), 2.33 – 2.20 (m, 1H), 2.17 (s, 1H), 1.74 (s, 3H), 1.68 – 1.61 (m, 2H), 1.25 (s, 3H), 0.97 (s, 3H), 0.93 – 0.80 (m, 3H).

Chapter 8

References

1. B. Alberts, A. Johnson, J. Lewis, M. Raff, K. Roberts and P. Walter, eds., *Molecular Biology of the Cell*, Fifth edn., 2007.
2. J. C. Venter, M. D. Adams, E. W. Myers, P. W. Li, R. J. Mural, G. G. Sutton, H. O. Smith, M. Yandell, C. A. Evans, R. A. Holt, et al., *Science*, 2001, **291**, 1304-1351.
3. (a) S. Gygi, B. Rist, S. Gerber, F. Turecek, M. Gelb and R. Aebersold, *Nat. Biotechnol.*, 1999, **17**, 994-999; (b) M. Washburn, D. Wolters and J. Yates, *Nat. Biotechnol.*, 2001, **19**, 242-247.
4. (a) H. Zhu, M. Bilgin and M. Snyder, *Annu. Rev. Biochem*, 2003, **72**, 783-812; (b) T. Ito, K. Ota, H. Kubota, Y. Yamaguchi, T. Chiba, K. Sakuraba and M. Yoshida, *Mol. Cell. Proteomics*, 2002, **1**, 561-566.
5. G. MacBeath, *Nat. Genet.*, 2002, **32 Suppl**, 526-532.
6. (a) M. J. Evans and B. F. Cravatt, *Chem. Rev.*, 2006, **106**, 3279-3301; (b) A. Saghatelian and B. F. Cravatt, *Nat Chem Biol*, 2005, **1**, 130-142; (c) W. P. Heal, T. H. T. Dang and E. W. Tate, *Chem. Soc. Rev.*, 2011, **40**, 246-257; (d) M. Nodwell and S. Sieber, in *Activity-Based Protein Profiling*, ed. S. A. Sieber, Springer Berlin Heidelberg, 2012, vol. 324, pp. 1-41.
7. M. P. Patricelli, D. K. Giang, L. M. Stamp and J. J. Burbaum, *Proteomics*, 2001, **1**, 1067-1071.
8. M. P. Washburn, D. Wolters and J. R. Yates, *Nat Biotech*, 2001, **19**, 242-247.
9. S. Sieber, T. Mondala, S. Head and B. Cravatt, *J. Am. Chem. Soc.*, 2004, **126**, 15640-15641.
10. Y. S. Liu, M. P. Patricelli and B. F. Cravatt, *Proc. Natl. Acad. Sci. U. S. A.*, 1999, **96**, 14694-14699.
11. D. Greenbaum, K. F. Medzihradszky, A. Burlingame and M. Bogyo, *Chem. Biol.*, 2000, **7**, 569-581.
12. S. Kumar, B. Zhou, F. Liang, W.-Q. Wang, Z. Huang and Z.-Y. Zhang, *Proc. Natl. Acad. Sci. U. S. A.*, 2004, **101**, 7943-7948.
13. M. Yee, S. C. Fas, M. M. Stohlmeyer, T. J. Wandless and K. A. Cimprich, *J. Biol. Chem.*, 2005, **280**, 29053-29059.
14. B. N. Bouma, L. A. Miles, G. Beretta and J. H. Griffin, *Biochemistry (Mosc).* 1980, **19**, 1151-1160.
15. J. L. Slack, C. P. Causey, Y. Luo and P. R. Thompson, *ACS Chem. Biol.*, 2011, **6**, 466-476.

16. M. P. Patricelli, A. K. Szardenings, M. Liyanage, T. K. Nomanbhoy, M. Wu, H. Weissig, A. Aban, D. Chun, S. Tanner and J. W. Kozarich, *Biochemistry (Mosc).* 2006, **46**, 350-358.

17. (a) A. Borodovsky, H. Ovaa, W. J. N. Meester, E. S. Venanzi, M. S. Bogyo, B. G. Hekking, H. L. Ploegh, B. M. Kessler and H. S. Overkleeft, *ChemBioChem*, 2005, **6**, 287-291; (b) A. Borodovsky, H. Ovaa, N. Kolli, T. Gan-Erdene, K. D. Wilkinson, H. L. Ploegh and B. M. Kessler, *Chem. Biol.*, 2002, **9**, 1149-1159.

18. C.-S. Tsai, Y.-K. Li and L.-C. Lo, *Org. Lett.*, 2002, **4**, 3607-3610.

19. (a) M. A. Fabian, W. H. Biggs, D. K. Treiber, C. E. Atteridge, M. D. Azimioara, M. G. Benedetti, T. A. Carter, P. Ciceri, P. T. Edeen, M. Floyd, et al., *Nat. Biotechnol.*, 2005, **23**, 329-336; (b) M. Bantscheff, D. Eberhard, Y. Abraham, S. Bastuck, M. Boesche, S. Hobson, T. Mathieson, J. Perrin, M. Raida, C. Rau, et al., *Nat. Biotechnol.*, 2007, **25**, 1035-1044; (c) M. W. Karaman, S. Herrgard, D. K. Treiber, P. Gallant, C. E. Atteridge, B. T. Campbell, K. W. Chan, P. Ciceri, M. I. Davis, P. T. Edeen, et al., *Nat. Biotechnol.*, 2008, **26**, 127-132; (d) J. Fischer, O. Graebner and M. Dreger, in *Kinase Inhibitors*, ed. B. Kuster, Humana Press, 2012, vol. 795, pp. 135-147.

20. E. Vodovozova, *Biochemistry. Biokhimiia*, 2007, **72**, 1-20.

21. S. Bregant, C. l. Huillet, L. Devel, A.-S. Dabert-Gay, F. Beau, R. Thai, B. Czarny, A. Yiotakis and V. Dive, *J Proteome Res*, 2009, **8**, 2484-2494.

22. S. Hindi, H. Deng, L. James and A. Kawamura, *Bioorg. Med. Chem. Lett.*, 2006, **16**, 5625-5628.

23. E. W. S. Chan, S. Chattopadhaya, R. C. Panicker, X. Huang and S. Q. Yao, *J. Am. Chem. Soc.*, 2004, **126**, 14435-14446.

24. E. M. Sletten and C. R. Bertozzi, *Acc. Chem. Res.*, 2011, **44**, 666-676.

25. E. Saxon and C. R. Bertozzi, *Science*, 2000, **287**, 2007-2010.

26. Z. Li, P. Hao, L. Li, C. Y. Tan, X. Cheng, G. Y. Chen, S. K. Sze, H. M. Shen and S. Q. Yao, *Angew. Chem. Int. Ed.*, 2013, **52**, 8551-8556.

27. T. Plass, S. Milles, C. Koehler, C. Schultz and E. A. Lemke, *Angew. Chem. Int. Ed.*, 2011, **50**, 3878-3881.

28. N. K. Devaraj, R. Upadhyay, J. B. Haun, S. A. Hilderbrand and R. Weissleder, *Angew. Chem. Int. Ed.*, 2009, **48**, 7013-7016.

29. B. A. Griffin, S. R. Adams and R. Y. Tsien, *Science*, 1998, **281**, 269-272.

30. (a) S. A. Rotenberg, T. Calogeropoulou, J. S. Jaworski, I. B. Weinstein and D. Rideout, *Proceedings of the National Academy of Sciences*, 1991, **88**, 2490-2494; (b) Z. Zhang, B. A. C. Smith, L. Wang, A. Brock, C. Cho and P. G. Schultz, *Biochemistry (Mosc).* 2003, **42**, 6735-6746; (c) I. Chen, M. Howarth, W. Lin and A. Y. Ting, *Nat. Methods*, 2005, **2**, 99-104; (d) N. Amara, R. Mashiach, D. Amar, P. Krief, S. p. A. H. Spieser, M. J. Bottomley, A. Aharoni and M. M. Meijler, *J. Am. Chem. Soc.*, 2009, **131**, 10610-10619.

31. M. J. Evans, A. Saghatelian, E. J. Sorensen and B. F. Cravatt, *Nat. Biotechnol.*, 2005, **23**, 1303-1307.

32. (a) W. Peters, S. Willnow, M. Duisken, H. Kleine, T. Macherey, K. Duncan, D. Litchfield, B. Lüscher and E. Weinhold, *Angewandte Chemie (International ed. in English)*, 2010, **49**, 5170-5173; (b) K. Islam, W. Zheng, H. Yu, H. Deng and M. Luo, *Acs Chem Biol*, 2011, **6**, 679-684; (c) O. Binda, M. Boyce, J. Rush, K. Palaniappan, C. Bertozzi and O. Gozani, *Chembiochem : a European journal of chemical biology*, 2011, **12**, 330-334.

33. T. Böttcher and S. A. Sieber, *Angew. Chem. Int. Ed.*, 2008, **47**, 4600-4603.

34. I. Staub and S. A. Sieber, *J. Am. Chem. Soc.*, 2009, **131**, 6271-6276.

35. Y.-L. Yang, Y.-P. Lee, Y.-L. Yang and P.-C. Lin, *Acs Chem Biol*, 2013, ASAP.

36. (a) H. Shi, C.-J. Zhang, G. Y. J. Chen and S. Q. Yao, *J. Am. Chem. Soc.*, 2012, **134**, 3001-3014; (b) Z. Li, P. Hao, L. Li, C. Y. J. Tan, X. Cheng, G. Y. J. Chen, S. K. Sze, H.-M. Shen and S. Q. Yao, *Angew. Chem. Int. Ed.*, 2013, **52**, 8551-8556.

37. H. Shi, X. Cheng, S. K. Sze and S. Q. Yao, *Chem. Commun.*, 2011, **47**, 11306-11308.

38. (a) D. A. Dias, S. Urban and U. Roessner, *Metabolites*, 2012, **2**, 303-336; (b) R. Breinbauer, I. R. Vetter and H. Waldmann, *Angew. Chem. Int. Ed.*, 2002, **41**, 2878-2890; (c) D. J. Newman and G. M. Cragg, *J. Nat. Prod.*, 2007, **70**, 461-477.

39. J. W.-H. Li and J. C. Vederas, *Science*, 2009, **325**, 161-165.

40. K. M. Giacomini, R. M. Krauss, D. M. Roden, M. Eichelbaum, M. R. Hayden and Y. Nakamura, *Nature*, 2007, **446**, 975-977.

41. M. Fonović and M. Bogyo, *Expert Rev Proteomic*, 2008, **5**, 721-730.

42. (a) T. Böttcher, M. Pitscheider and S. A. Sieber, *Angew. Chem. Int. Ed.*, 2010, **49**, 2680-2698; (b) Y. Su, J. Ge, B. Zhu, Y.-G. Zheng, Q. Zhu and S. Q. Yao, *Curr.*

Opin. Chem. Biol., 2013, **17**, 768-775; (c) T. Boettcher, M. Pitscheider and S. A. Sieber, *Angew. Chem., Int. Ed.*, 2010, **49**, 2680-2698.

43. K. R. Shreder, Y. Liu, T. Nomanhboy, S. R. Fuller, M. S. Wong, W. Z. Gai, J. Wu, P. S. Leventhal, J. R. Lill and S. Corral, *Bioconjugate Chem.*, 2004, **15**, 790-798.
44. T. Böttcher and S. A. Sieber, *J. Am. Chem. Soc.*, 2010, **132**, 6964-6972.
45. P. Y. Yang, K. Liu, M. H. Ngai, M. J. Lear, M. R. Wenk and S. Q. Yao, *J. Am. Chem. Soc.*, 2010, **132**, 656-666.
46. (a) P.-Y. Yang, M. Wang, L. Li, H. Wu, C. He and S. Yao, *Chem. Eur. J.*, 2012, **18**, 6528-6541; (b) P.-Y. Yang, M. Wang, C. He and S. Yao, *Chem. Commun.*, 2012, **48**, 835-837.
47. W.-W. Qiu, J. Xu, J.-Y. Li, J. Li and F.-J. Nan, *ChemBioChem*, 2007, **8**, 1351-1358.
48. P. Ranjitkar, B. G. K. Perera, D. L. Swaney, S. B. Hari, E. T. Larson, R. Krishnamurty, E. A. Merritt, J. Villén and D. J. Maly, *J. Am. Chem. Soc.*, 2012, **134**, 19017-19025.
49. R. Krishnamurty, J. Brigham, S. Leonard, P. Ranjitkar, E. Larson, E. Dale, E. Merritt and D. Maly, *Nat. Chem. Biol.*, 2013, **9**, 43-50.
50. E. K. W. Tam, Z. Li, Y. L. Goh, X. Cheng, S. Y. Wong, S. Santhanakrishnan, C. L. L. Chai and S. Q. Yao, *Chem. Asian J.*, 2013, **8**, 1818-1828.
51. G. Blum, S. R. Mullins, K. Keren, M. Fonovic, C. Jedeszko, M. J. Rice, B. F. Sloane and M. Bogyo, *Nat Chem Biol*, 2005, **1**, 203-209.
52. M. Hu, L. Li, H. Wu, Y. Su, P.-Y. Yang, M. Uttamchandani, Q.-H. Xu and S. Q. Yao, *J. Am. Chem. Soc.*, 2011, **133**, 12009-12020.
53. G. Manning, D. B. Whyte, R. Martinez, T. Hunter and S. Sudarsanam, *Science*, 2002, **298**, 1912-1934.
54. , http://www.nobelprize.org/.
55. A. C. Dar, L. E. Wybenga-Groot and F. Sicheri, in *Modular Protein Domains*, Wiley-VCH Verlag GmbH & Co. KGaA, 2005, pp. 181-209.
56. (a) P. Lahiry, A. Torkamani, N. J. Schork and R. A. Hegele, *Nat. Rev. Genet.*, 2010, **11**, 60-74; (b) Q. Liu, Y. Sabnis, Z. Zhao, T. Zhang, S. J. Buhrlage, L. H. Jones and N. S. Gray, *Chem. Biol.*, 2013, **20**, 146-159; (c) http://www.cellsignal.com/; (d) P. Lahiry, A. Torkamani, N. J. Schork and R. A. Hegele, *Nat Rev Genet*, 2010, **11**, 60-74.

57. (a) M. E. M. Noble, J. A. Endicott and L. N. Johnson, *Science*, 2004, **303**, 1800-1805; (b) N. Gerits and U. Moens, in *Encyclopedia of Molecular Pharmacology*, eds. S. Offermanns and W. Rosenthal, Springer Berlin Heidelberg, 2008, pp. 1008-1012.

58. (a) J. Zhang, P. L. Yang and N. S. Gray, *Nat. Rev. Cancer*, 2009, **9**, 28-39; (b) J. Singh, R. C. Petter and A. F. Kluge, *Curr. Opin. Chem. Biol.*, 2010, **14**, 475-480; (c) L. Garuti, M. Roberti and G. Bottegoni, *Curr. Med. Chem.*, 2011, **18**, 2981-2994; (d) T. Barf and A. Kaptein, *J. Med. Chem.*, 2012, **55**, 6243-6262; (e) http://www.fda.gov/; (f) S. K. Grant, *Cell. Mol. Life Sci.*, 2009, **66**, 1163-1177.

59. T. A. Haystead, *Curr. Top Med. Chem.*, 2006, **6**, 1117-1127.

60. M. Goto, J. Chow, K. Muramoto, K.-i. Chiba, S. Yamamoto, M. Fujita, H. Obaishi, K. Tai, Y. Mizui, I. Tanaka, et al., *J. Pharmacol. Exp. Ther.*, 2009, **331**, 485-495.

61. F. E. Kwarcinski, C. C. Fox, M. E. Steffey and M. B. Soellner, *ACS Chem. Biol.*, 2012, **7**, 1910-1917.

62. L. A. Honigberg, A. M. Smith, M. Sirisawad, E. Verner, D. Loury, B. Chang, S. Li, Z. Pan, D. H. Thamm, R. A. Miller and J. J. Buggy, *Proc. Natl. Acad. Sci. U. S. A.*, 2010, **107**, 13075-13080.

63. D. Li, L. Ambrogio, T. Shimamura, S. Kubo, M. Takahashi, L. R. Chirieac, R. F. Padera, G. I. Shapiro, A. Baum, F. Himmelsbach, et al., *Oncogene*, 2008, **27**, 4702-4711.

64. N. Yoshimura, S. Kudoh, T. Kimura, S. Mitsuoka, K. Matsuura, K. Hirata, K. Matsui, S. Negoro, K. Nakagawa and M. Fukuoka, *Lung cancer (Amsterdam, Netherlands)*, 2006, **51**, 363-368.

65. T. Zhang, F. Inesta-Vaquera, M. Niepel, J. Zhang, Scott B. Ficarro, T. Machleidt, T. Xie, Jarrod A. Marto, N. Kim, T. Sim, et al., *Chem. Biol.*, 2012, **19**, 140-154.

66. R. Bansal, S. Magge and S. Winkler, *J. Neurosci. Res.*, 2003, **74**, 486-493.

67. J. A. Engelman, K. Zejnullahu, C.-M. Gale, E. Lifshits, A. J. Gonzales, T. Shimamura, F. Zhao, P. W. Vincent, G. N. Naumov, J. E. Bradner, et al., *Cancer Res.*, 2007, **67**, 11924-11932.

68. D. W. Fry, A. J. Bridges, W. A. Denny, A. Doherty, K. D. Greis, J. L. Hicks, K. E. Hook, P. R. Keller, W. R. Leopold, J. A. Loo, et al., *Proc. Natl. Acad. Sci. U. S. A.*, 1998, **95**, 12022-12027.

69. J. C. Henise and J. Taunton, *J. Med. Chem.*, 2011, **54**, 4133-4146.

70. A. Wissner, M. B. Floyd, B. D. Johnson, H. Fraser, C. Ingalls, T. Nittoli, R. G. Dushin, C. Discafani, R. Nilakantan, J. Marini, et al., *J. Med. Chem.*, 2005, **48**, 7560-7581.

71. D. I. Perez, S. Conde, C. Pérez, C. Gil, D. Simon, F. Wandosell, F. J. Moreno, J. L. Gelpí, F. J. Luque and A. Martínez, *Bioorg. Med. Chem.*, 2009, **17**, 6914-6925.

72. M. S. Cohen, C. Zhang, K. M. Shokat and J. Taunton, *Science*, 2005, **308**, 1318-1321.

73. E. Leproult, S. Barluenga, D. Moras, J.-M. Wurtz and N. Winssinger, *J. Med. Chem.*, 2011, **54**, 1347-1355.

74. V. C. Janet, W. F. Frank, M. R. Joshua, L. M. Timothy and J. T. Dennis, *BMC Cancer*, 2007, **7**, 183-183.

75. J. Li, T. S. Kaoud, C. Laroche, K. N. Dalby and S. M. Kerwin, *Bioorg. Med. Chem. Lett.*, 2009, **19**, 6293-6297.

76. C. Carmi, A. Cavazzoni, S. Vezzosi, F. Bordi, F. Vacondio, C. Silva, S. Rivara, A. Lodola, R. R. Alfieri, S. La Monica, M. Galetti, A. Ardizzoni, P. G. Petronini and M. Mor, *J. Med. Chem.*, 2010, **53**, 2038-2050.

77. R. M. Scoggins, A. E. Summerfield, R. A. Stein, C. A. Guyer and J. V. Staros, *Biochemistry (Mosc).* 1996, **35**, 9197-9203.

78. J. Singh, R. C. Petter, T. A. Baillie and A. Whitty, *Nat. Rev. Drug Discov.*, 2011, **10**, 307-317.

79. (a) A. C. Price, K. H. Choi, R. J. Heath, Z. M. Li, S. W. White and C. O. Rock, *J. Biol. Chem.*, 2001, **276**, 6551-6559; (b) F. P. Kuhajda, E. S. Pizer, J. N. Li, N. S. Mani, G. L. Frehywot and C. A. Townsend, *Proc. Natl. Acad. Sci. U. S. A.*, 2000, **97**, 3450-3454; (c) T. M. Loftus, D. E. Jaworsky, G. L. Frehywot, C. A. Townsend, G. V. Ronnett, M. D. Lane and F. P. Kuhajda, *Science*, 2000, **288**, 2379-2381; (d) L. E. Landree, A. L. Hanlon, D. W. Strong, G. Rumbaugh, I. M. Miller, J. N. Thupari, E. C. Connolly, R. L. Huganir, C. Richardson, L. A. Witters, F. P. Kuhajda and G. V. Ronnett, *J. Biol. Chem.*, 2004, **279**, 3817-3827.

80. M. Biel, A. Kretsovali, E. Karatzali, J. Papamatheakis and A. Giannis, *Angew. Chem. Int. Ed.*, 2004, **43**, 3974-3976.

81. (a) M. E. Bakleh, V. Sol, K. Estieu-Gionnet, R. Granet, G. Déléris and P. Krausz, *Tetrahedron*, 2009, **65**, 7385-7392; (b) L. A. Canalle, S. S. van Berkel, L. T. de Haan and J. C. M. van Hest, *Adv. Funct. Mater.*, 2009, **19**, 3464-3470.

82. J. Wang, M. Uttamchandani, L. P. Sun and S. Q. Yao, *Chem. Commun.*, 2006, 717-719.

83. L. B. Poole, C. Klomsiri, S. A. Knaggs, C. M. Furdui, K. J. Nelson, M. J. Thomas, J. S. Fetrow, L. W. Daniel and S. B. King, *Bioconjugate Chem.*, 2007, **18**, 2004-2017.

84. (a) J. N. Li, M. Gorospe, F. J. Chrest, T. S. Kumaravel, M. K. Evans, W. F. Han and E. S. Pizer, *Cancer Res.*, 2001, **61**, 1493-1499; (b) T. S. Ho, Y. P. Ho, W. Y. Wong, L. C. M. Chiu, Y. S. Wong and V. E. C. Ooi, *Biomed. Pharmacother.*, 2007, **61**, 578-587; (c) P. Mera, A. Bentebibelal, E. Lopez-Vinas, A. G. Cordente, C. Gurunathan, D. Sebastian, I. Vazquez, L. Herrero, X. Ariza, P. Gomez-Puertas, G. Asins, D. Serra, J. Garcia and F. G. Hegardt, *Biochem. Pharmacol.*, 2009, **77**, 1084-1095.

85. M. I. Davis, J. P. Hunt, S. Herrgard, P. Ciceri, L. M. Wodicka, G. Pallares, M. Hocker, D. K. Treiber and P. P. Zarrinkar, *Nat. Biotechnol.*, 2011, **29**, 1046-1051.

86. J. J. Fischer, O. Y. Graebner Baessler, C. Dalhoff, S. Michaelis, A. K. Schrey, J. Ungewiss, K. Andrich, D. Jeske, F. Kroll, M. Glinski, M. Sefkow, M. Dreger and H. Koester, *J Proteome Res*, 2010, **9**, 806-817.

87. (a) G. Caravatti, T. Meyer, A. Fredenhagen, U. Trinks, H. Mett and D. Fabbro, *Bioorg. Med. Chem. Lett.*, 1994, **4**, 399-404; (b) S. C. Meyer, C. D. Shomin, T. Gaj and I. Ghosh, *J. Am. Chem. Soc.*, 2007, **129**, 13812-13813.

88. J. Singh, R. C. Petter, T. A. Baillie and A. Whitty, *Nat. Rev. Drug Discov.*, 2011, **10**, 307-317.

89. O. Trott and A. J. Olson, *J. Comput. Chem.*, 2010, **31**, 455-461.

90. (a) F. Hatahet and L. Ruddock, *Antioxid Redox Sign*, 2009, **11**, 2807-2850; (b) L. Ellgaard and L. Ruddock, *Embo Rep*, 2005, **6**, 28-32.

91. in *http://www.uniprot.org/*.

92. V. Nguyen, K. Wallis, M. Howard, A. Haapalainen, K. Salo, M. Saaranen, A. Sidhu, R. Wierenga, R. Freedman, L. Ruddock and R. Williamson, *J. Mol. Biol.*, 2008, **383**, 1144-1155.

93. B. G. Hoffstrom, A. Kaplan, R. Letso, R. S. Schmid, G. J. Turmel, D. C. Lo and B. R. Stockwell, *Nat Chem Biol*, 2010, **6**, 900-906.

94. D. Goplen, J. Wang, P. Enger, B. Tysnes, A. Terzis, O. Laerum and R. Bjerkvig, *Cancer Res.*, 2006, **66**, 9895-9902.

95. R. Freedman, T. Hirst and M. Tuite, *Trends Biochem. Sci*, 1994, **19**, 331-336.

96. A. E. Speers and B. F. Cravatt, *Chem. Biol.*, 2004, **11**, 535-546.

97. B. G. Hoffstrom, A. Kaplan, R. Letso, R. S. Schmid, G. J. Turmel, D. C. Lo and B. R. Stockwell, *Nat. Chem. Biol.*, 2010, **6**, 900-906.

98. J. Ge, C.-J. Zhang, L. Li, L. M. Chong, X. Wu, P. Hao, S. K. Sze and S. Q. Yao, *Acs Chem Biol*, 2013, **8**, 2577.

99. (a) S. B. Bharate, S. D. Sawant, P. P. Singh and R. A. Vishwakarma, *Chem. Rev.*, 2013, **113**, 6761-6815; (b) W. H. Gerwick and B. S. Moore, *Chem. Biol.*, 2012, **19**, 85-98.

100. (a) H. Nagata, H. Yano, K. Sasaki, S. Sato, S. Nakanishi, I. Takahashi and T. Tamaoki, *Biosci., Biotechnol., Biochem.*, 2002, **66**, 501-507; (b) H. Nagata, K. Ochiai, Y. Aotani, K. Ando, M. Yoshida, I. Takahashi and T. Tamaoki, *J. Antibiot.*, 1997, **50**, 537-542; (c) A. Miyanaga, J. E. Janso, L. McDonald, M. He, H. Liu, L. Barbieri, A. S. Eustaquio, E. N. Fielding, G. T. Carter, P. R. Jensen, X. Feng, M. Leighton, F. E. Koehn and B. S. Moore, *J. Am. Chem. Soc.*, 2011, **133**, 13311-13313.

101. C. C. Hughes, J. B. MacMillan, S. P. Gaudencio, P. R. Jensen and W. Fenical, *Angew. Chem. Int. Ed.*, 2009, **48**, 725-727.

102. C. C. Hughes, J. B. MacMillan, S. P. Gaudencio, W. Fenical and J. J. La Clair, *Angew. Chem. Int. Ed.*, 2009, **48**, 728-732.

103. C. N. Carrigan, R. D. Bartlett, C. S. Esslinger, K. A. Cybulski, P. Tongcharoensirikul, R. J. Bridges and C. M. Thompson, *J. Med. Chem.*, 2002, **45**, 2260-2276.

104. P. V. N. Reddy, B. Banerjee and M. Cushman, *Org. Lett.*, 2010, **12**, 3112-3114.

105. Q. Wu, X. Jiao, L. Wang, Q. Xiao, X. Liu and P. Xie, *Tetrahedron Lett.*, 2010, **51**, 4806-4807.

106. K. Tatsuta, K. Imamura, S. Itoh and S. Kasai, *Tetrahedron Lett.*, 2004, **45**, 2847-2850.

107. (a) B. H. Lee, M. F. Clothier and S. S. Johnson, *Bioorg. Med. Chem. Lett.*, 2001, **11**, 553-554; (b) N. Ishida, Y. Nakanishi, T. Moriya and M. Murakami, *Chem. Lett.*, 2011, **40**, 1047-1049.

108. G. S. Krasnov, A. A. Dmitriev, A. V. Snezhkina and A. V. Kudryavtseva, *Expert Opin. Ther. Targets*, 2013, **17**, 681-693.

109. S. Wu and H. Le, *Acta Bioch Bioph Sin*, 2013, **45**, 27-35.

110. J. Dennison, J. Molina, S. Mitra, A. González-Angulo, J. Balko, M. Kuba, M. Sanders, J. Pinto, H. Gómez, C. Arteaga, R. Brown and G. Mills, *Clin. Cancer Res.*, 2013, **19**, 3703-3713.

111. H. S. Choi, H. M. Lee, Y.-J. Jang, C.-H. Kim and C. J. Ryu, *Stem Cells*, 2013, **31**, 2647-2658.

112. J. Zhang, M. Sun, R. Li, S. Liu, J. Mao, Y. Huang, B. Wang, L. Hou, M. Ibrahim and J. Tang, *Biomed. Pharmacother.*, 2013, **67**, 557-560.

113. B. Alberts, A. Johnson, J. Lewis, M. Raff, K. Roberts and P. Walter, *Molecular biology of the cell*, 5th edn., Garland Science, New York, 2008.

114. , http://www.cancer.gov/.

115. A. Mishra and M. Verma, *Cancers*, 2010, **2**, 190-208.

116. S. Jaracz, J. Chen, L. Kuznetsova and I. Ojima, *Biorg. Med. Chem.*, 2005, **13**, 5043-5054.

117. (a) I. Ojima, X. Geng, X. Wu, C. Qu, C. Borella, H. Xie, S. Wilhelm, B. Leece, L. Bartle, V. Goldmacher and R. Chari, *J. Med. Chem.*, 2002, **45**, 5620-5623; (b) X. Wu and I. Ojima, *Curr. Med. Chem.*, 2004, **11**, 429-438.

118. (a) M. Bradley, N. Webb, F. Anthony, P. Devanesan, P. Witman, S. Hemamalini, M. Chander, S. Baker, L. He, S. Horwitz and C. Swindell, *Clinical cancer research : an official journal of the American Association for Cancer Research*, 2001, **7**, 3229-3238; (b) J. Seitz and I. Ojima, in *Drug Delivery in Oncology*, Wiley-VCH Verlag GmbH & Co. KGaA, 2011, pp. 1323-1357.

119. (a) S. Chen, X. Zhao, J. Chen, J. Chen, L. Kuznetsova, S. Wong and I. Ojima, *Bioconjugate Chem.*, 2010, **21**, 979-987; (b) I. R. Vlahov, P. J. Kleindl and F. You, in *Drug Delivery in Oncology*, Wiley-VCH Verlag GmbH & Co. KGaA, 2011, pp. 1283-1322.

120. Z. Xiao, J. Frieder, B. A. Teply and O. C. Farokhzad, in *Drug Delivery in Oncology*, Wiley-VCH Verlag GmbH & Co. KGaA, 2011, pp. 1263-1281.

121. A. Nagy, A. V. Schally, G. Halmos, P. Armatis, R.-Z. Cai, V. Csernus, M. Kovács, M. Koppán, K. Szepesházi and Z. Kahán, *Proceedings of the National Academy of Sciences*, 1998, **95**, 1794-1799.

122. Y. Luo, N. Bernshaw, Z.-R. Lu, J. Kopecek and G. Prestwich, *Pharm. Res.*, 2002, **19**, 396-402.

123. (a) R. Y. Tsien, T. Jiang, E. S. Olson, Q. T. Nguyen, M. Roy and P. A. Jennings, *Proc. Natl. Acad. Sci. U. S. A.*, 2004, **101**, 17867-17872; (b) K. Kurrikoff, J.

Suhorut and ü. Langel, in *Drug Delivery in Oncology*, Wiley-VCH Verlag GmbH & Co. KGaA, 2011, pp. 1187-1217.

124. A. Warnecke, in *Drug Delivery in Oncology*, Wiley-VCH Verlag GmbH & Co. KGaA, 2011, pp. 553-589.

125. A. Schröpfer, U. Kammerer, M. Kapp, J. Dietl, S. Feix and J. Anacker, *BMC Cancer*, 2010, **10**, 553.

126. R. Ramos, B. Manning, A. Aviñó, R. Gargallo and R. Eritja, *Helv. Chim. Acta*, 2009, **92**, 613-622.

127. M. H. Lee, Z. Yang, C. W. Lim, Y. H. Lee, S. Dongbang, C. Kang and J. S. Kim, *Chem. Rev.*, 2013, **113**, 5071-5109.

128. (a) A. Arcaro and M. Wymann, *Biochem. J.*, 1993, **296 (Pt 2)**, 297-301; (b) T. Takac, T. Pechan, O. Samajova, M. Ovecka, H. Richter, C. Eck, K. Niehaus and J. Samaj, *J. Proteome Res.*, 2012, **11**, 3127-3142; (c) R. A. Smith, H. S. Yuan, R. Weissleder, L. C. Cantley and L. Josephson, *Bioconjugate Chem.*, 2009, **20**, 2185-2189; (d) P. Wipf and R. Halter, *Org. Biomol. Chem.*, 2005, **3**, 2053-2061.

129. (a) K. Hamada, T. Sasaki, P. Koni, M. Natsui, H. Kishimoto, J. Sasaki, N. Yajima, Y. Horie, G. Hasegawa, M. Naito, et al., *Genes Dev.*, 2005, **19**, 2054-2065; (b) Ö. H. Yilmaz and S. J. Morrison, *Blood Cells. Mol. Dis.*, **41**, 73-76.

130. Y. Liu, K. R. Shreder, W. Gai, S. Corral, D. K. Ferris and J. S. Rosenblum, *Chem. Biol.*, 2005, **12**, 99-107.

131. (a) M. Wymann, G. Bulgarelli-Leva, M. Zvelebil, L. Pirola, B. Vanhaesebroeck, M. Waterfield and G. Panayotou, *Mol. Cell. Biol.*, 1996, **16**, 1722-1733; (b) E. H. Walker, M. E. Pacold, O. Perisic, L. Stephens, P. T. Hawkins, M. P. Wymann and R. L. Williams, *Mol. Cell*, 2000, **6**, 909-919.

132. W. Dai, Y. S. Liu, N. Jiang, J. Y. Wu and J. S. Rosenblum, *J. Biol. Chem.*, 2007, **282**, 2505-2511.

133. H. Yuan, J. Luo, S. Field, R. Weissleder, L. Cantley and L. Josephson, *Bioconjugate Chem.*, 2005, **16**, 669-675.

134. (a) N. Ihle, R. Williams, S. Chow, W. Chew, M. Berggren, G. Paine-Murrieta, D. Minion, R. Halter, P. Wipf, R. Abraham, L. Kirkpatrick and G. Powis, *Mol. Cancer Ther.*, 2004, **3**, 763-772; (b) J. Holleran, M. Egorin, E. Zuhowski, R. Parise, S. Musser and S.-s. Pan, *Anal. Biochem.*, 2003, **323**, 19-25.

135. P. Wipf, D. J. Minion, R. J. Halter, M. I. Berggren, C. B. Ho, G. G. Chiang, L. Kirkpatrick, R. Abraham and G. Powis, *Org. Biomol. Chem.*, 2004, **2**, 1911-1920.

136. H. Yuan, J. Luo, R. Weissleder, L. Cantley and L. Josephson, *J. Med. Chem.*, 2006, **49**, 740-747.

137. (a) H. Li and Z. Qian, *Med. Res. Rev.*, 2002, **22**, 225-250; (b) L. Bildstein, C. Dubernet and P. Couvreur, *Adv. Drug Del. Rev.*, 2011, **63**, 3-23.

138. (a) S. Weitman, R. Lark, L. Coney, D. Fort, V. Frasca, V. Zurawski and B. Kamen, *Cancer Res.*, 1992, **52**, 3396-3401; (b) G. Toffoli, C. Cernigoi, A. Russo, A. Gallo, M. Bagnoli and M. Boiocchi, *Int. J. Cancer*, 1997, **74**, 193-198; (c) L. Hartmann, G. Keeney, W. Lingle, T. Christianson, B. Varghese, D. Hillman, A. Oberg and P. Low, *Int. J. Cancer*, 2007, **121**, 938-942; (d) P. S. Low and S. A. Kularatne, *Curr. Opin. Chem. Biol.*, 2009, **13**, 256-262.

139. C. Müller and R. Schibli, *J. Nucl. Med.*, 2011, **52**, 1-4.

140. (a) J. N. Hathcock, *Am. J. Clin. Nutr.*, 1997, **66**, 427-437; (b) S. W. Bailey and J. E. Ayling, *Proc. Natl. Acad. Sci. U. S. A.*, 2009, **106**, 15424-15429.

141. C. Leamon and P. Low, *Proc. Natl. Acad. Sci. U. S. A.*, 1991, **88**, 5572-5576.

142. D. Plażuk, J. Zakrzewski, M. Salmain, A. Błauż, B. Rychlik, P. Strzelczyk, A. Bujacz and G. Bujacz, *Organometallics*, 2013, **32**, 5774-5783.

143. J. H. Boyer, R. S. Buriks and U. Toggweiler, *J. Am. Chem. Soc.*, 1960, **82**, 2213-2215.

Chapter 9

Appendix

Chapter 2

The list of proteins identified from LCMS experiments Table S1

#	Accession	Description	Mass	Score	Queries matched	emPAI
1	IPI00007188	Tax_Id=9606 Gene_Symbol=SLC25A5 ADP/ATP translocase 2	33102	691	48	0.95
2	IPI00798387	Tax_Id=9606 Gene_Symbol=- Putative uncharacterized protein ENSP00000319235	48393	672	25	0.39
3	IPI00022462	Tax_Id=9606 Gene_Symbol=TFRC Transferrin receptor protein 1	85274	547	33	0.63
4	IPI00141318	Tax_Id=9606 Gene_Symbol=CKAP4 Isoform 1 of Cytoskeleton-associated protein 4	66097	489	23	1.07
5	IPI00024145	Tax_Id=9606 Gene_Symbol=VDAC2 Isoform 2 of Voltage-dependent anion-selective channel protein 2	30849	442	26	0.85
6	IPI00013871	Tax_Id=9606 Gene_Symbol=RRM1 Ribonucleoside-diphosphate reductase large subunit	90925	430	31	0.48
7	IPI00177817	Tax_Id=9606 Gene_Symbol=ATP2A2 Isoform SERCA2A of Sarcoplasmic/endoplasmic reticulum calcium ATPase 2	111103	427	36	0.46
8	IPI00294779	Tax_Id=9606 Gene_Symbol=VDAC3 Isoform 2 of Voltage-dependent anion-selective channel protein 3	31112	423	32	1.04
9	IPI00011062	Tax_Id=9606 Gene_Symbol=CPS1 Isoform 1 of Carbamoyl-phosphate synthase [ammonia], mitochondrial	165975	396	25	0.24
10	IPI00016610	Tax_Id=9606 Gene_Symbol=PCBP1 Poly(rC)-binding protein 1	37987	389	21	0.65
11	IPI00215965	Tax_Id=9606 Gene_Symbol=HNRNPA1 Isoform A1-B of Heterogeneous nuclear ribonucleoprotein A1	38822	382	10	0.77
12	IPI00303954	Tax_Id=9606 Gene_Symbol=CYB5B cytochrome b5 outer mitochondrial membrane precursor	16798	347	19	0.74
13	IPI00302925	Tax_Id=9606 Gene_Symbol=CCT8 59 kDa protein	60011	340	24	0.31
14	IPI00027497	Tax_Id=9606 Gene_Symbol=GPI Glucose-6-phosphate isomerase	63107	338	13	0.43
15	IPI00479186	Tax_Id=9606 Gene_Symbol=PKM2 Isoform M2 of Pyruvate kinase isozymes M1/M2	58470	336	14	0.39
16	IPI00219018	Tax_Id=9606 Gene_Symbol=GAPDH Glyceraldehyde-3-phosphate dehydrogenase	36201	335	16	0.69
17	IPI00024580	Tax_Id=9606 Gene_Symbol=MCCC1 Methylcrotonoyl-CoA carboxylase subunit alpha, mitochondrial	80935	323	19	0.32
18	IPI00291467	Tax_Id=9606 Gene_Symbol=SLC25A6 ADP/ATP translocase 3	33073	307	31	0.78
19	IPI00016768	Tax_Id=9606 Gene_Symbol=LDHAL6B L-lactate dehydrogenase A-like 6B	41916	301	7	0.26
20	IPI00162563	Tax_Id=9606 Gene_Symbol=RNF40 Isoform 1 of E3 ubiquitin-protein ligase BRE1B	113609	271	8	0.19

21	IPI00396485	Tax_Id=9606 Gene_Symbol=EEF1A1 Elongation factor 1-alpha 1	50109	240	15	1.02
22	IPI00022891	Tax_Id=9606 Gene_Symbol=SLC25A4 ADP/ATP translocase 1	33271	235	24	0.46
23	IPI00011253	Tax_Id=9606 Gene_Symbol=RPS3 40S ribosomal protein S3	26842	225	16	1.02
24	IPI00028031	Tax_Id=9606 Gene_Symbol=ACADVL cDNA FLJ56425, highly similar to Very-long-chain specific acyl-CoAdehydrogenase, mitochondrial	75618	201	15	0.24
25	IPI00299571	Tax_Id=9606 Gene_Symbol=PDIA6 Isoform 2 of Protein disulfide-isomerase A6	54380	194	8	0.19
26	IPI00003881	Tax_Id=9606 Gene_Symbol=HNRNPF Heterogeneous nuclear ribonucleoprotein F	45985	189	7	0.15
27	IPI00554777	Tax_Id=9606 Gene_Symbol=ASNS Asparagine synthetase [glutamine-hydrolyzing]	64899	181	10	0.16
28	IPI00299402	Tax_Id=9606 Gene_Symbol=PC Pyruvate carboxylase, mitochondrial	130293	178	18	0.1
29	IPI00010420	Tax_Id=9606 Gene_Symbol=SLC25A31 ADP/ATP translocase 4	35285	178	10	0.09
30	IPI00027970	Tax_Id=9606 Gene_Symbol=PCBP3 poly(rC) binding protein 3 isoform 1	39725	175	5	0.27
31	IPI00479191	Tax_Id=9606 Gene_Symbol=HNRNPH1 51 kDa protein	51482	175	11	0.2
32	IPI00026781	Tax_Id=9606 Gene_Symbol=FASN Fatty acid synthase	275850	168	12	0.05
33	IPI00298289	Tax_Id=9606 Gene_Symbol=RTN4 Isoform 2 of Reticulon-4	40350	167	13	0.48
34	IPI00009542	Tax_Id=9606 Gene_Symbol=MAGED2 Isoform 1 of Melanoma-associated antigen D2	65085	161	8	0.1
35	IPI00303954	Tax_Id=9606 Gene_Symbol=CYB5B cytochrome b5 outer mitochondrial membrane precursor	16798	157	9	0.74
36	IPI00884896	Tax_Id=9606 Gene_Symbol=TXNRD1 Isoform 1 of Thioredoxin reductase 1, cytoplasmic	72077	156	12	0.25
37	IPI00384051	Tax_Id=9606 Gene_Symbol=PSME2 Putative uncharacterized protein PSME2	28755	154	10	0.55
38	IPI00479217	Tax_Id=9606 Gene_Symbol=HNRNPU Isoform Short of Heterogeneous nuclear ribonucleoprotein U	88924	154	7	0.16
39	IPI00550363	Tax_Id=9606 Gene_Symbol=TAGLN2 Transgelin-2	22377	153	5	0.75
40	IPI00220740	Tax_Id=9606 Gene_Symbol=NPM1 Isoform 2 of Nucleophosmin	29446	153	5	0.38
41	IPI00026824	Tax_Id=9606 Gene_Symbol=HMOX2 Heme oxygenase 2	41928	151	28	0.98
42	IPI00003833	Tax_Id=9606 Gene_Symbol=MTCH2 Mitochondrial carrier homolog 2	33936	150	13	0.75
43	IPI00215637	Tax_Id=9606 Gene_Symbol=DDX3X ATP-dependent RNA helicase DDX3X	73597	148	11	0.09
44	IPI00216592	Tax_Id=9606 Gene_Symbol=HNRNPC Isoform C1 of Heterogeneous nuclear ribonucleoproteins C1/C2	32318	145	8	0.48
45	IPI00216298	Tax_Id=9606 Gene_Symbol=TXN Thioredoxin	11730	144	5	1.16

46	IPI00017334	Tax_Id=9606 Gene_Symbol=PHB Prohibitin	29843	141	10	0.53
47	IPI00008986	Tax_Id=9606 Gene_Symbol=SLC7A5 Large neutral amino acids transporter small subunit 1	54974	141	3	0.06
48	IPI00024804	Tax_Id=9606 Gene_Symbol=ATP2A1 Isoform SERCA1B of Sarcoplasmic/endoplasmic reticulum calcium ATPase 1	111550	137	22	0.12
49	IPI00479185	Tax_Id=9606 Gene_Symbol=TPM3 tropomyosin 3 isoform 4	29024	136	14	0.92
50	IPI00216171	Tax_Id=9606 Gene_Symbol=ENO2 Gamma-enolase	47239	135	5	0.22
51	IPI00873380	Tax_Id=9606 Gene_Symbol=RTN4 Nogo-C	22295	133	10	0.75
52	IPI00409635	Tax_Id=9606 Gene_Symbol=ESYT2 Isoform 2 of Extended synaptotagmin-2	99353	130	12	0.18
53	IPI00006196	Tax_Id=9606 Gene_Symbol=NUMA1 Isoform 2 of Nuclear mitotic apparatus protein 1	236372	130	4	0.04
54	IPI00879148	Tax_Id=9606 Gene_Symbol=- 18 kDa protein	18534	129	5	0.18
55	IPI00010896	Tax_Id=9606 Gene_Symbol=CLIC1 Chloride intracellular channel protein 1	27248	128	5	0.26
56	IPI00216049	Tax_Id=9606 Gene_Symbol=HNRNPK Isoform 1 of Heterogeneous nuclear ribonucleoprotein K	50944	125	6	0.46
57	IPI00000874	Tax_Id=9606 Gene_Symbol=PRDX1 Peroxiredoxin-1	22096	125	8	1.03
58	IPI00419585	Tax_Id=9606 Gene_Symbol=PPIA Peptidyl-prolyl cis-trans isomerase A	18001	124	8	1.36
59	IPI00027350	Tax_Id=9606 Gene_Symbol=PRDX2 Peroxiredoxin-2	21878	122	7	0.33
60	IPI00183968	Tax_Id=9606 Gene_Symbol=TPM3 tropomyosin 3 isoform 1	32987	121	12	0.47
61	IPI00021405	Tax_Id=9606 Gene_Symbol=LMNA Isoform A of Lamin-A/C	74380	121	23	0.24
62	IPI00011200	Tax_Id=9606 Gene_Symbol=PHGDH D-3-phosphoglycerate dehydrogenase	57356	118	8	0.18
63	IPI00024266	Tax_Id=9606 Gene_Symbol=MGST3 Microsomal glutathione S-transferase 3	16734	118	2	0.44
64	IPI00646304	Tax_Id=9606 Gene_Symbol=PPIB Peptidyl-prolyl cis-trans isomerase B	23728	118	5	0.48
65	IPI00011569	Tax_Id=9606 Gene_Symbol=ACACA Isoform 1 of Acetyl-CoA carboxylase 1	267095	117	20	0.09
66	IPI00022314	Tax_Id=9606 Gene_Symbol=SOD2 Superoxide dismutase [Mn], mitochondrial	24707	117	4	0.46
67	IPI00000875	Tax_Id=9606 Gene_Symbol=EEF1G;TUT1 cDNA FLJ56389, highly similar to Elongation factor 1-gamma	56114	113	5	0.19
68	IPI00030255	Tax_Id=9606 Gene_Symbol=PLOD3 Procollagen-lysine,2-oxoglutarate 5-dioxygenase 3	84731	113	7	0.12
69	IPI00922693	Tax_Id=9606 Gene_Symbol=- cDNA FLJ53662, highly similar to Actin, alpha skeletal muscle	38896	112	10	0.09
70	IPI00219217	Tax_Id=9606 Gene_Symbol=LDHB L-lactate dehydrogenase B chain	36900	111	10	0.29

71	IPI00021766	Tax_Id=9606 Gene_Symbol=RTN4 Isoform 1 of Reticulon-4	130250	111	12	0.08
72	IPI00026230	Tax_Id=9606 Gene_Symbol=HNRNPH2;RPL36AP37 Heterogeneous nuclear ribonucleoprotein H2	49517	111	3	0.07
73	IPI00027493	Tax_Id=9606 Gene_Symbol=SLC3A2;LOC442497 Isoform 2 of 4F2 cell-surface antigen heavy chain	58023	111	10	0.18
74	IPI00880053	Tax_Id=9606 Gene_Symbol=- 60 kDa chaperonin	48877	110	9	0.22
75	IPI00171903	Tax_Id=9606 Gene_Symbol=HNRNPM Isoform 1 of Heterogeneous nuclear ribonucleoprotein M	77749	110	13	0.13
76	IPI00337495	Tax_Id=9606 Gene_Symbol=PLOD2 Isoform 2 of Procollagen-lysine,2-oxoglutarate 5-dioxygenase 2	87043	109	4	0.12
77	IPI00376798	Tax_Id=9606 Gene_Symbol=RPL11 Isoform 1 of 60S ribosomal protein L11	20240	108	2	0.17
78	IPI00386755	Tax_Id=9606 Gene_Symbol=ERO1L ERO1-like protein alpha	54358	107	2	0.06
79	IPI00479786	Tax_Id=9606 Gene_Symbol=KHSRP KH-type splicing regulatory protein	73355	106	13	0.04
80	IPI00216691	Tax_Id=9606 Gene_Symbol=PFN1 Profilin-1	15045	106	5	0.84
81	IPI00879148	Tax_Id=9606 Gene_Symbol=- 18 kDa protein	18534	105	6	0.18
82	IPI00163187	Tax_Id=9606 Gene_Symbol=FSCN1 Fascin	54496	105	2	0.06
83	IPI00217966	Tax_Id=9606 Gene_Symbol=LDHA Isoform 1 of L-lactate dehydrogenase A chain	36950	99	11	0.41
84	IPI00008511	Tax_Id=9606 Gene_Symbol=MT-ND5 NADH-ubiquinone oxidoreductase chain 5	67697	98	5	0.05
85	IPI00745125	Tax_Id=9606 Gene_Symbol=SOAT1 Sterol O-acyltransferase 1	65205	98	10	0.16
86	IPI00398795	Tax_Id=9606 Gene_Symbol=RTN3 Isoform 2 of Reticulon-3	111211	97	13	0.09
87	IPI00014053	Tax_Id=9606 Gene_Symbol=TOMM40 Isoform 1 of Mitochondrial import receptor subunit TOM40 homolog	38211	96	13	0.39
88	IPI00000230	Tax_Id=9606 Gene_Symbol=TPM1 tropomyosin 1 alpha chain isoform 2	32715	96	7	0.21
89	IPI00218820	Tax_Id=9606 Gene_Symbol=TPM2 Isoform 3 of Tropomyosin beta chain	28666	96	5	0.25
90	IPI00013991	Tax_Id=9606 Gene_Symbol=TPM2 Isoform 1 of Tropomyosin beta chain	32945	96	5	0.21
91	IPI00005737	Tax_Id=9606 Gene_Symbol=SURF4 Isoform 1 of Surfeit locus protein 4	30374	96	4	0.11
92	IPI00221092	Tax_Id=9606 Gene_Symbol=RPS16 40S ribosomal protein S16	16435	94	2	0.21
93	IPI00396435	Tax_Id=9606 Gene_Symbol=DHX15 Putative pre-mRNA-splicing factor ATP-dependent RNA helicase DHX15	91673	93	6	0.07
94	IPI00015614	Tax_Id=9606 Gene_Symbol=PRSS3 Isoform A of Trypsin-3	32508	93	3	0.1
95	IPI00217966	Tax_Id=9606 Gene_Symbol=LDHA Isoform 1 of L-lactate dehydrogenase A chain	36950	92	12	0.19

96	IPI00297160	Tax_Id=9606 Gene_Symbol=CD44 Isoform 12 of CD44 antigen	39391	92	2	0.17
97	IPI00021326	Tax_Id=9606 Gene_Symbol=SHC1 SHC-transforming protein 1 isoform 3	62854	92	86	0.05
98	IPI00170692	Tax_Id=9606 Gene_Symbol=VAPA Vesicle-associated membrane protein-associated protein A	28103	91	10	0.4
99	IPI00169383	Tax_Id=9606 Gene_Symbol=PGK1 Phosphoglycerate kinase 1	44985	91	14	0.33
100	IPI00550021	Tax_Id=9606 Gene_Symbol=RPL3 60S ribosomal protein L3	46080	89	3	0.15
101	IPI00014424	Tax_Id=9606 Gene_Symbol=EEF1A2 Elongation factor 1-alpha 2	50780	88	14	0.29
102	IPI00329801	Tax_Id=9606 Gene_Symbol=ANXA5 Annexin A5	35971	87	6	0.3
103	IPI00218606	Tax_Id=9606 Gene_Symbol=RPS23 40S ribosomal protein S23	15798	87	3	0.22
104	IPI00006211	Tax_Id=9606 Gene_Symbol=VAPB Isoform 1 of Vesicle-associated membrane protein-associated protein B/C	27439	86	5	0.26
105	IPI00396378	Tax_Id=9606 Gene_Symbol=HNRNPA2B1 Isoform B1 of Heterogeneous nuclear ribonucleoproteins A2/B1	37464	86	2	0.09
106	IPI00394665	Tax_Id=9606 Gene_Symbol=ADAR Isoform 1 of Double-stranded RNA-specific adenosine deaminase	137079	86	10	0.05
107	IPI00014053	Tax_Id=9606 Gene_Symbol=TOMM40 Isoform 1 of Mitochondrial import receptor subunit TOM40 homolog	38211	83	3	0.28
108	IPI00929577	Tax_Id=9606 Gene_Symbol=ABHD2 Similar to Vesicle-associated membrane protein-associated protein A	34492	83	8	0.1
109	IPI00218918	Tax_Id=9606 Gene_Symbol=ANXA1 Annexin A1	38918	82	7	0.39
110	IPI00028888	Tax_Id=9606 Gene_Symbol=HNRNPD Isoform 1 of Heterogeneous nuclear ribonucleoprotein D0	38410	81	3	0.18
111	IPI00289334	Tax_Id=9606 Gene_Symbol=FLNB Isoform 1 of Filamin-B	280188	80	15	0.02
112	IPI00848226	Tax_Id=9606 Gene_Symbol=GNB2L1 Guanine nucleotide-binding protein subunit beta-2-like 1	35511	80	13	0.2
113	IPI00220301	Tax_Id=9606 Gene_Symbol=PRDX6 Peroxiredoxin-6	25133	80	9	0.13
114	IPI00021263	Tax_Id=9606 Gene_Symbol=YWHAZ 14-3-3 protein zeta/delta	27899	79	5	0.4
115	IPI00328354	Tax_Id=9606 Gene_Symbol=MAGED1 Isoform 1 of Melanoma-associated antigen D1	86221	79	6	0.04
116	IPI00013003	Tax_Id=9606 Gene_Symbol=ACACB Isoform Long of Acetyl-CoA carboxylase 2	278375	79	11	0.04
117	IPI00215719	Tax_Id=9606 Gene_Symbol=RPL18 60S ribosomal protein L18	21621	79	4	0.54
118	IPI00106509	Tax_Id=9606 Gene_Symbol=HNRNPAB Isoform 4 of Heterogeneous nuclear ribonucleoprotein A/B	30682	78	2	0.11
119	IPI00025329	Tax_Id=9606 Gene_Symbol=RPL19 60S ribosomal protein L19	23451	78	1	0.14
120	IPI00375339	Tax_Id=9606 Gene_Symbol=ATP1A4 Isoform 1 of Sodium/potassium-transporting ATPase subunit alpha-4	114093	78	67	0.03

121	IPI00396378	Tax_Id=9606 Gene_Symbol=HNRNPA2B1 Isoform B1 of Heterogeneous nuclear ribonucleoproteins A2/B1	37464	77	2	0.09
122	IPI00306369	Tax_Id=9606 Gene_Symbol=NSUN2 tRNA (cytosine-5-)-methyltransferase NSUN2	87214	77	7	0.04
123	IPI00451401	Tax_Id=9606 Gene_Symbol=RCTPI1;TPI1 Isoform 2 of Triosephosphate isomerase	27451	77	2	0.12
124	IPI00299573	Tax_Id=9606 Gene_Symbol=RPL7A 60S ribosomal protein L7a	30148	77	9	0.23
125	IPI00100656	Tax_Id=9606 Gene_Symbol=TECR Isoform 1 of Trans-2,3-enoyl-CoA reductase	36410	76	3	0.19
126	IPI00296337	Tax_Id=9606 Gene_Symbol=PRKDC Isoform 1 of DNA-dependent protein kinase catalytic subunit	473749	74	18	0.01
127	IPI00025491	Tax_Id=9606 Gene_Symbol=SNORA67;EIF4A1 Eukaryotic initiation factor 4A-I	46353	74	5	0.15
128	IPI00794673	Tax_Id=9606 Gene_Symbol=CCT8 Putative uncharacterized protein CCT8	11522	73	4	0.3
129	IPI00879622	Tax_Id=9606 Gene_Symbol=- 18 kDa protein	18042	73	7	0.41
130	IPI00792641	Tax_Id=9606 Gene_Symbol=TKT transketolase isoform 2	59571	72	8	0.06
131	IPI00643920	Tax_Id=9606 Gene_Symbol=TKT cDNA FLJ54957, highly similar to Transketolase	69382	72	8	0.05
132	IPI00010796	Tax_Id=9606 Gene_Symbol=P4HB Protein disulfide-isomerase	57480	72	14	0.32
133	IPI00018248	Tax_Id=9606 Gene_Symbol=KDELR2 Isoform 1 of ER lumen protein retaining receptor 2	24406	72	2	0.29
134	IPI00219153	Tax_Id=9606 Gene_Symbol=RPL22 60S ribosomal protein L22	14778	72	3	0.51
135	IPI00792352	Tax_Id=9606 Gene_Symbol=RAN;RANP1 26 kDa protein	26678	71	4	0.27
136	IPI00220642	Tax_Id=9606 Gene_Symbol=YWHAG 14-3-3 protein gamma	28456	71	6	0.25
137	IPI00000816	Tax_Id=9606 Gene_Symbol=YWHAE 14-3-3 protein epsilon	29326	71	6	0.24
138	IPI00018146	Tax_Id=9606 Gene_Symbol=YWHAQ 14-3-3 protein theta	28032	71	5	0.25
139	IPI00013890	Tax_Id=9606 Gene_Symbol=SFN Isoform 1 of 14-3-3 protein sigma	27871	71	6	0.25
140	IPI00216319	Tax_Id=9606 Gene_Symbol=YWHAH 14-3-3 protein eta	28372	71	5	0.25
141	IPI00328328	Tax_Id=9606 Gene_Symbol=EIF4A2 Isoform 1 of Eukaryotic initiation factor 4A-II	46601	71	5	0.07
142	IPI00025874	Tax_Id=9606 Gene_Symbol=RPN1 Dolichyl-diphosphooligosaccharide--protein glycosyltransferase subunit 1 precursor	72733	71	4	0.09
143	IPI00021129	Tax_Id=9606 Gene_Symbol=AP3B1 Isoform 1 of AP-3 complex subunit beta-1	121815	70	12	0.05
144	IPI00021290	Tax_Id=9606 Gene_Symbol=ACLY ATP-citrate synthase	121674	69	3	0.03
145	IPI00015833	Tax_Id=9606 Gene_Symbol=CHCHD3 Coiled-coil-helix-coiled-coil-helix domain-containing protein 3, mitochondrial	26421	68	2	0.13

146	IPI00217030	Tax_Id=9606 Gene_Symbol=RPS4X 40S ribosomal protein S4, X isoform	29807	68	4	0.37
147	IPI00299000	Tax_Id=9606 Gene_Symbol=PA2G4 Proliferation-associated protein 2G4	43759	67	7	0.34
148	IPI00027626	Tax_Id=9606 Gene_Symbol=CCT6A T-complex protein 1 subunit zeta	57988	66	1	0.06
149	IPI00008530	Tax_Id=9606 Gene_Symbol=RPLP0 60S acidic ribosomal protein P0	34252	66	2	0.2
150	IPI00465361	Tax_Id=9606 Gene_Symbol=RPL13 60S ribosomal protein L13	24247	66	3	0.3
151	IPI00007289	Tax_Id=9606 Gene_Symbol=ALPP Alkaline phosphatase, placental type precursor	59482	65	1	0.06
152	IPI00005107	Tax_Id=9606 Gene_Symbol=NPC1 Niemann-Pick C1 protein	142074	65	2	0.02
153	IPI00019755	Tax_Id=9606 Gene_Symbol=GSTO1 Glutathione S-transferase omega-1	27833	64	3	0.12
154	IPI00028068	Tax_Id=9606 Gene_Symbol=SLC25A19 Mitochondrial thiamine pyrophosphate carrier	35887	63	5	0.19
155	IPI00290142	Tax_Id=9606 Gene_Symbol=CTPS CTP synthase 1	66648	63	1	0.05
156	IPI00027107	Tax_Id=9606 Gene_Symbol=TUFM Tu translation elongation factor, mitochondrial precursor	49843	63	2	0.14
157	IPI00026328	Tax_Id=9606 Gene_Symbol=TXNDC12 Thioredoxin domain-containing protein 12	19194	63	5	0.38
158	IPI00455599	Tax_Id=9606 Gene_Symbol=HSP90AB2P Similar to Heat shock protein HSP 90-beta	49377	63	5	0.07
159	IPI00004584	Tax_Id=9606 Gene_Symbol=KIAA0391 Isoform 2 of Mitochondrial ribonuclease P protein 3	66186	62	2	0.05
160	IPI00553169	Tax_Id=9606 Gene_Symbol=FLNA Putative uncharacterized protein FLNA	248149	61	14	0.01
161	IPI00178352	Tax_Id=9606 Gene_Symbol=FLNC Isoform 1 of Filamin-C	293407	61	8	0.01
162	IPI00216587	Tax_Id=9606 Gene_Symbol=RPS8 40S ribosomal protein S8	24475	61	3	0.14
163	IPI00217975	Tax_Id=9606 Gene_Symbol=LMNB1 Lamin-B1	66368	61	2	0.1
164	IPI00024919	Tax_Id=9606 Gene_Symbol=PRDX3 Thioredoxin-dependent peroxide reductase, mitochondrial	27675	61	2	0.12
165	IPI00220835	Tax_Id=9606 Gene_Symbol=SEC61B Protein transport protein Sec61 subunit beta	9968	61	1	0.35
166	IPI00026241	Tax_Id=9606 Gene_Symbol=BST2 Bone marrow stromal antigen 2	20041	60	6	0.17
167	IPI00030179	Tax_Id=9606 Gene_Symbol=RPL7;RPL7P32 60S ribosomal protein L7	29264	60	3	0.24
168	IPI00008998	Tax_Id=9606 Gene_Symbol=PTPLAD1 Protein tyrosine phosphatase-like protein PTPLAD1	43360	59	5	0.08
169	IPI00549805	Tax_Id=9606 Gene_Symbol=ATP5A1 23 kDa protein	22943	59	3	0.15
170	IPI00178700	Tax_Id=9606 Gene_Symbol=ALG3 Dolichyl-P-Man:Man(5)GlcNAc(2)-PP-dolichyl mannosyltransferase	50835	59	1	0.06

171	IPI00178440	Tax_Id=9606 Gene_Symbol=EEF1B2 Elongation factor 1-beta	24919	59	1	0.13
172	IPI00394896	Tax_Id=9606 Gene_Symbol=RTN3 Isoform 5 of Reticulon-3	26606	58	1	0.13
173	IPI00440493	Tax_Id=9606 Gene_Symbol=ATP5A1 ATP synthase subunit alpha, mitochondrial	59828	58	6	0.11
174	IPI00291006	Tax_Id=9606 Gene_Symbol=MDH2 Malate dehydrogenase, mitochondrial	35937	58	6	0.09
175	IPI00006666	Tax_Id=9606 Gene_Symbol=SLC16A3 Monocarboxylate transporter 4	49437	58	2	0.14
176	IPI00026994	Tax_Id=9606 Gene_Symbol=PRAF2 PRA1 family protein 2	19246	58	1	0.18
177	IPI00418471	Tax_Id=9606 Gene_Symbol=VIM Vimentin	53676	57	8	0.2
178	IPI00909509	Tax_Id=9606 Gene_Symbol=- cDNA FLJ59138, highly similar to Annexin A2	21827	57	6	0.15
179	IPI00418169	Tax_Id=9606 Gene_Symbol=ANXA2 Isoform 2 of Annexin A2	40671	57	6	0.08
180	IPI00025252	Tax_Id=9606 Gene_Symbol=PDIA3 Protein disulfide-isomerase A3	57146	57	8	0.12
181	IPI00298971	Tax_Id=9606 Gene_Symbol=VTN Vitronectin	55069	57	2	0.06
182	IPI00024933	Tax_Id=9606 Gene_Symbol=RPL12 Isoform 1 of 60S ribosomal protein L12	17808	57	3	0.42
183	IPI00290770	Tax_Id=9606 Gene_Symbol=CCT3 chaperonin containing TCP1, subunit 3 isoform b	60424	56	1	0.05
184	IPI00291802	Tax_Id=9606 Gene_Symbol=LMO7 Isoform 3 of LIM domain only protein 7	153589	56	1	0.02
185	IPI00180128	Tax_Id=9606 Gene_Symbol=BZW1 Isoform 2 of Basic leucine zipper and W2 domain-containing protein 1	40513	56	2	0.08
186	IPI00026625	Tax_Id=9606 Gene_Symbol=NUP155 Isoform 1 of Nuclear pore complex protein Nup155	156697	55	8	0.04
187	IPI00892935	Tax_Id=9606 Gene_Symbol=XPO1 Putative uncharacterized protein XPO1	15381	55	1	0.22
188	IPI00298961	Tax_Id=9606 Gene_Symbol=XPO1 Exportin-1	124447	55	6	0.05
189	IPI00654754	Tax_Id=9606 Gene_Symbol=UBC;UBB;RPS27A RPS27A protein	10833	55	2	0.32
190	IPI00220194	Tax_Id=9606 Gene_Symbol=SLC2A1 Solute carrier family 2, facilitated glucose transporter member 1	54049	55	2	0.06
191	IPI00794205	Tax_Id=9606 Gene_Symbol=- 26 kDa protein	25894	54	6	0.27
192	IPI00010810	Tax_Id=9606 Gene_Symbol=ETFA Electron transfer flavoprotein subunit alpha, mitochondrial	35400	54	5	0.31
193	IPI00418813	Tax_Id=9606 Gene_Symbol=- Pseudogene candidate	25309	54	6	0.28
194	IPI00335168	Tax_Id=9606 Gene_Symbol=MYL6;MYL6B Isoform Non-muscle of Myosin light polypeptide 6	16919	54	2	0.44
195	IPI00022624	Tax_Id=9606 Gene_Symbol=GPRC5A Retinoic acid-induced protein 3	40225	54	1	0.08

196	IPI00023001	Tax_Id=9606 Gene_Symbol=FAM162A UPF0389 protein FAM162A	17331	54	2	0.2
197	IPI00306436	Tax_Id=9606 Gene_Symbol=STAT3 Isoform Del-701 of Signal transducer and activator of transcription 3	88723	53	5	0.04
198	IPI00465439	Tax_Id=9606 Gene_Symbol=ALDOA Fructose-bisphosphate aldolase A	39851	53	5	0.17
199	IPI00004534	Tax_Id=9606 Gene_Symbol=PFAS Phosphoribosylformylglycinamidine synthase	144633	53	3	0.05
200	IPI00329389	Tax_Id=9606 Gene_Symbol=RPL6 60S ribosomal protein L6	32708	53	3	0.21
201	IPI00395565	Tax_Id=9606 Gene_Symbol=PTGES2 Putative uncharacterized protein PTGES2	21324	52	2	0.16
202	IPI00024266	Tax_Id=9606 Gene_Symbol=MGST3 Microsomal glutathione S-transferase 3	16734	52	2	0.2
203	IPI00016513	Tax_Id=9606 Gene_Symbol=RAB10 Ras-related protein Rab-10	22755	52	3	0.15
204	IPI00014230	Tax_Id=9606 Gene_Symbol=C1QBP Complement component 1 Q subcomponent-binding protein, mitochondrial	31343	52	1	0.21
205	IPI00003966	Tax_Id=9606 Gene_Symbol=CA9 Carbonic anhydrase 9	49667	52	1	0.07
206	IPI00911004	Tax_Id=9606 Gene_Symbol=P4HB cDNA FLJ59939, highly similar to Protein disulfide-isomerase	25146	51	4	0.28
207	IPI00607576	Tax_Id=9606 Gene_Symbol=C9orf5 Isoform 1 of Transmembrane protein C9orf5	101508	51	4	0.03
208	IPI00022078	Tax_Id=9606 Gene_Symbol=NDRG1 Protein NDRG1	42808	51	1	0.08
209	IPI00031522	Tax_Id=9606 Gene_Symbol=HADHA Trifunctional enzyme subunit alpha, mitochondrial	83688	50	5	0.04
210	IPI00216694	Tax_Id=9606 Gene_Symbol=PLS3 Plastin-3	71279	50	12	0.14
211	IPI00027547	Tax_Id=9606 Gene_Symbol=DCD Dermcidin	11277	50	2	0.3
212	IPI00032304	Tax_Id=9606 Gene_Symbol=PLS1 Plastin-1	70608	49	10	0.1
213	IPI00879622	Tax_Id=9606 Gene_Symbol=- 18 kDa protein	18042	49	1	0.19
214	IPI00029997	Tax_Id=9606 Gene_Symbol=PGLS 6-phosphogluconolactonase	27815	49	5	0.25
215	IPI00017726	Tax_Id=9606 Gene_Symbol=HSD17B10 Isoform 1 of 3-hydroxyacyl-CoA dehydrogenase type-2	27134	49	6	0.12
216	IPI00031420	Tax_Id=9606 Gene_Symbol=UGDH UDP-glucose 6-dehydrogenase	54989	49	1	0.06
217	IPI00293276	Tax_Id=9606 Gene_Symbol=MIF Macrophage migration inhibitory factor	12468	49	1	0.28
218	IPI00179330	Tax_Id=9606 Gene_Symbol=UBC;UBB;RPS27A ubiquitin and ribosomal protein S27a precursor	18296	48	2	0.18
219	IPI00012074	Tax_Id=9606 Gene_Symbol=HNRNPR Heterogeneous nuclear ribonucleoprotein R	70899	48	3	0.09
220	IPI00908791	Tax_Id=9606 Gene_Symbol=LDHA L-lactate dehydrogenase	33970	47	9	0.32

221	IPI00300567	Tax_Id=9606 Gene_Symbol=DCI Isoform 1 of 3,2-trans-enoyl-CoA isomerase, mitochondrial	33080	47	3	0.21
222	IPI00032038	Tax_Id=9606 Gene_Symbol=CPT1A Isoform 1 of Carnitine O-palmitoyltransferase 1, liver isoform	88995	47	2	0.04
223	IPI00185374	Tax_Id=9606 Gene_Symbol=PSMD12 26S proteasome non-ATPase regulatory subunit 12	53270	47	2	0.06
224	IPI00010471	Tax_Id=9606 Gene_Symbol=LCP1 Plastin-2	70815	47	3	0.05
225	IPI00177965	Tax_Id=9606 Gene_Symbol=NT5DC1 5'-nucleotidase domain-containing protein 1	52439	47	6	0.06
226	IPI00643041	Tax_Id=9606 Gene_Symbol=RAN;RANP1 GTP-binding nuclear protein Ran	24408	47	4	0.47
227	IPI00789893	Tax_Id=9606 Gene_Symbol=- Pseudogene candidate	21912	45	4	0.15
228	IPI00246975	Tax_Id=9606 Gene_Symbol=GSTM3 Glutathione S-transferase Mu 3	26998	45	2	0.26
229	IPI00012048	Tax_Id=9606 Gene_Symbol=NME1 Isoform 1 of Nucleoside diphosphate kinase A	17139	45	5	0.43
230	IPI00218570	Tax_Id=9606 Gene_Symbol=PGAM2 Phosphoglycerate mutase 2	28748	45	4	0.25
231	IPI00219525	Tax_Id=9606 Gene_Symbol=PGD 6-phosphogluconate dehydrogenase, decarboxylating	53106	45	1	0.06
232	IPI00739539	Tax_Id=9606 Gene_Symbol=POTEF POTE ankyrin domain family member F	123020	44	8	0.03
233	IPI00479743	Tax_Id=9606 Gene_Symbol=POTEE Isoform 1 of POTE ankyrin domain family member E	122882	44	8	0.03
234	IPI00908506	Tax_Id=9606 Gene_Symbol=DDX3Y cDNA FLJ53122, highly similar to ATP-dependent RNA helicase DDX3Y	44985	44	5	0.07
235	IPI00293616	Tax_Id=9606 Gene_Symbol=DDX3Y ATP-dependent RNA helicase DDX3Y	73564	44	5	0.04
236	IPI00552772	Tax_Id=9606 Gene_Symbol=HM13 Isoform 5 of Minor histocompatibility antigen H13	37018	44	9	0.19
237	IPI00186290	Tax_Id=9606 Gene_Symbol=EEF2 Elongation factor 2	96246	44	6	0.11
238	IPI00026271	Tax_Id=9606 Gene_Symbol=RPS14 40S ribosomal protein S14	16263	44	2	0.46
239	IPI00007423	Tax_Id=9606 Gene_Symbol=ANP32B Isoform 1 of Acidic leucine-rich nuclear phosphoprotein 32 family member B	28941	43	2	0.24
240	IPI00005202	Tax_Id=9606 Gene_Symbol=PGRMC2 Membrane-associated progesterone receptor component 2	26211	43	1	0.13
241	IPI00023779	Tax_Id=9606 Gene_Symbol=NIT1 Isoform 2 of Nitrilase homolog 1	36728	43	2	0.09
242	IPI00902969	Tax_Id=9606 Gene_Symbol=GFER FAD-linked sulfhydryl oxidase ALR	24004	43	1	0.14
243	IPI00302927	Tax_Id=9606 Gene_Symbol=ILK-2;CCT4 T-complex protein 1 subunit delta	57888	43	2	0.12
244	IPI00017297	Tax_Id=9606 Gene_Symbol=MATR3 Matrin-3	95078	42	6	0.03
245	IPI00026089	Tax_Id=9606 Gene_Symbol=SF3B1 Splicing factor 3B subunit 1	146464	42	14	0.02

246	IPI00024067	Tax_Id=9606 Gene_Symbol=CLTC Isoform 1 of Clathrin heavy chain 1	193260	42	11	0.03
247	IPI00465248	Tax_Id=9606 Gene_Symbol=ENO1 Isoform alpha-enolase of Alpha-enolase	47481	42	4	0.07
248	IPI00641829	Tax_Id=9606 Gene_Symbol=BAT1 Isoform 2 of Spliceosome RNA helicase BAT1	50647	42	2	0.07
249	IPI00100858	Tax_Id=9606 Gene_Symbol=SLCO4A1 Isoform 1 of Solute carrier organic anion transporter family member 4A1	77143	42	4	0.04
250	IPI00246058	Tax_Id=9606 Gene_Symbol=PDCD6IP Programmed cell death 6-interacting protein	96590	41	3	0.03
251	IPI00215911	Tax_Id=9606 Gene_Symbol=APEX1 DNA-(apurinic or apyrimidinic site) lyase	35532	41	1	0.09
252	IPI00170436	Tax_Id=9606 Gene_Symbol=MBOAT7 Leukocyte receptor cluster (LRC) member 4	28580	41	1	0.12
253	IPI00796094	Tax_Id=9606 Gene_Symbol=SLC25A11 34 kDa protein	34576	40	5	0.1
254	IPI00797802	Tax_Id=9606 Gene_Symbol=SLC25A11 solute carrier family 25 member 11 isoform 3	28647	40	4	0.12
255	IPI00010720	Tax_Id=9606 Gene_Symbol=CCT5 T-complex protein 1 subunit epsilon	59633	40	1	0.06
256	IPI00012066	Tax_Id=9606 Gene_Symbol=PCBP2 poly(rC) binding protein 2 isoform b	38597	40	8	0.28

NMR Spectra of representative compounds

fe08cxm2
fe08 mat 1.1 yyy7004
2063-1

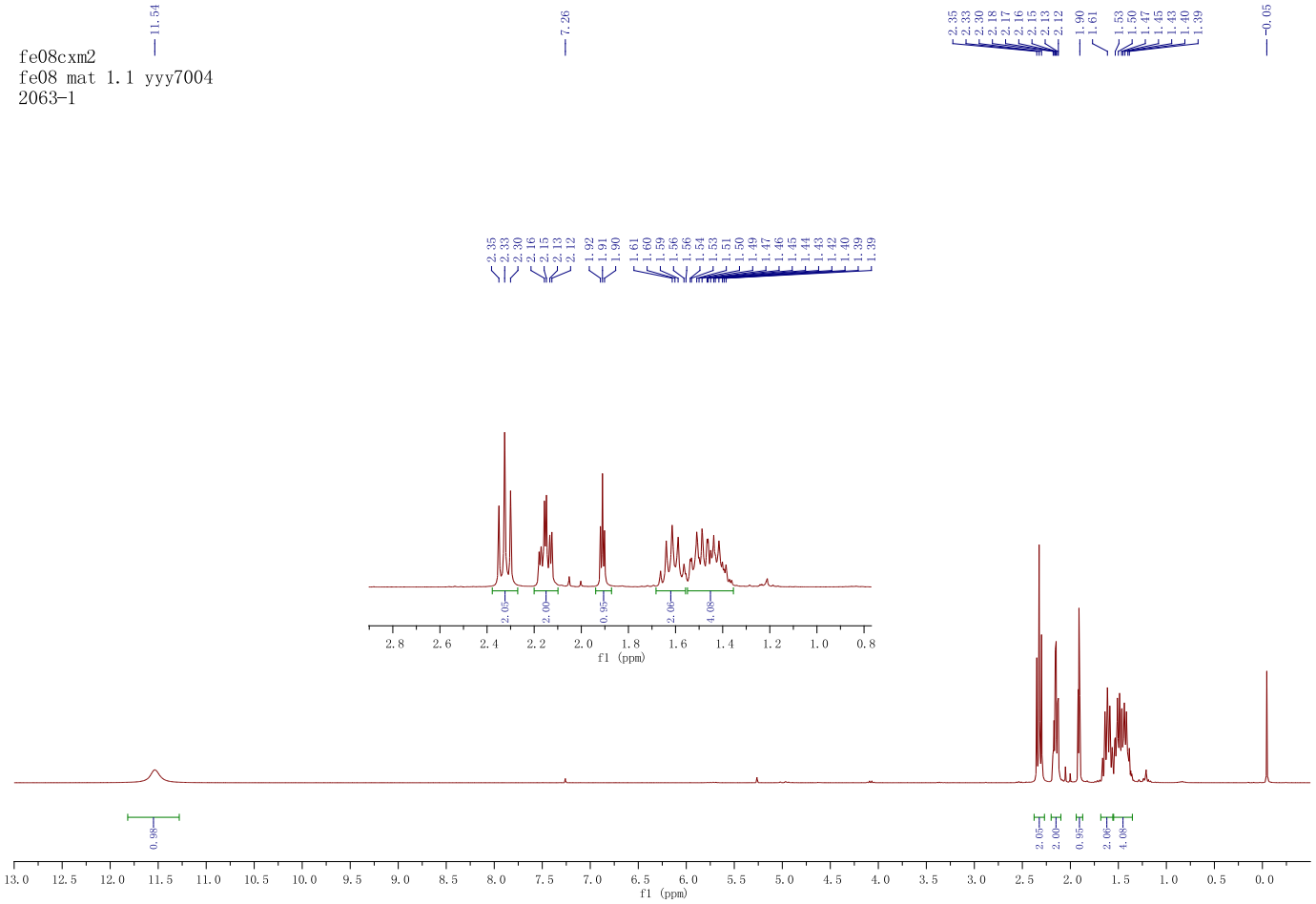

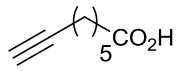

2-6c

fe08cxm2
fe08 mat 1.1 yyy7004
2063-1

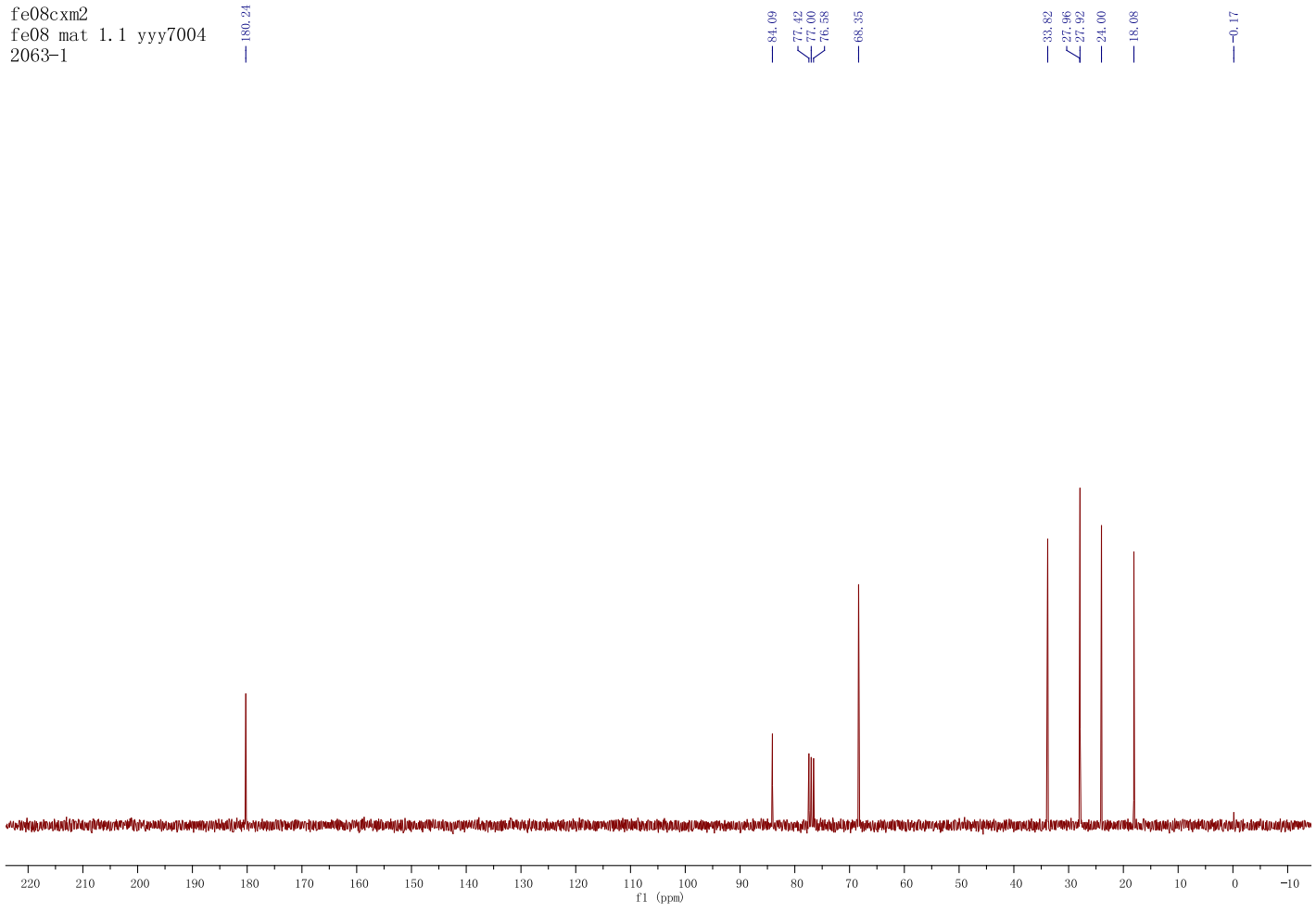

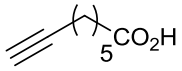

2-6c

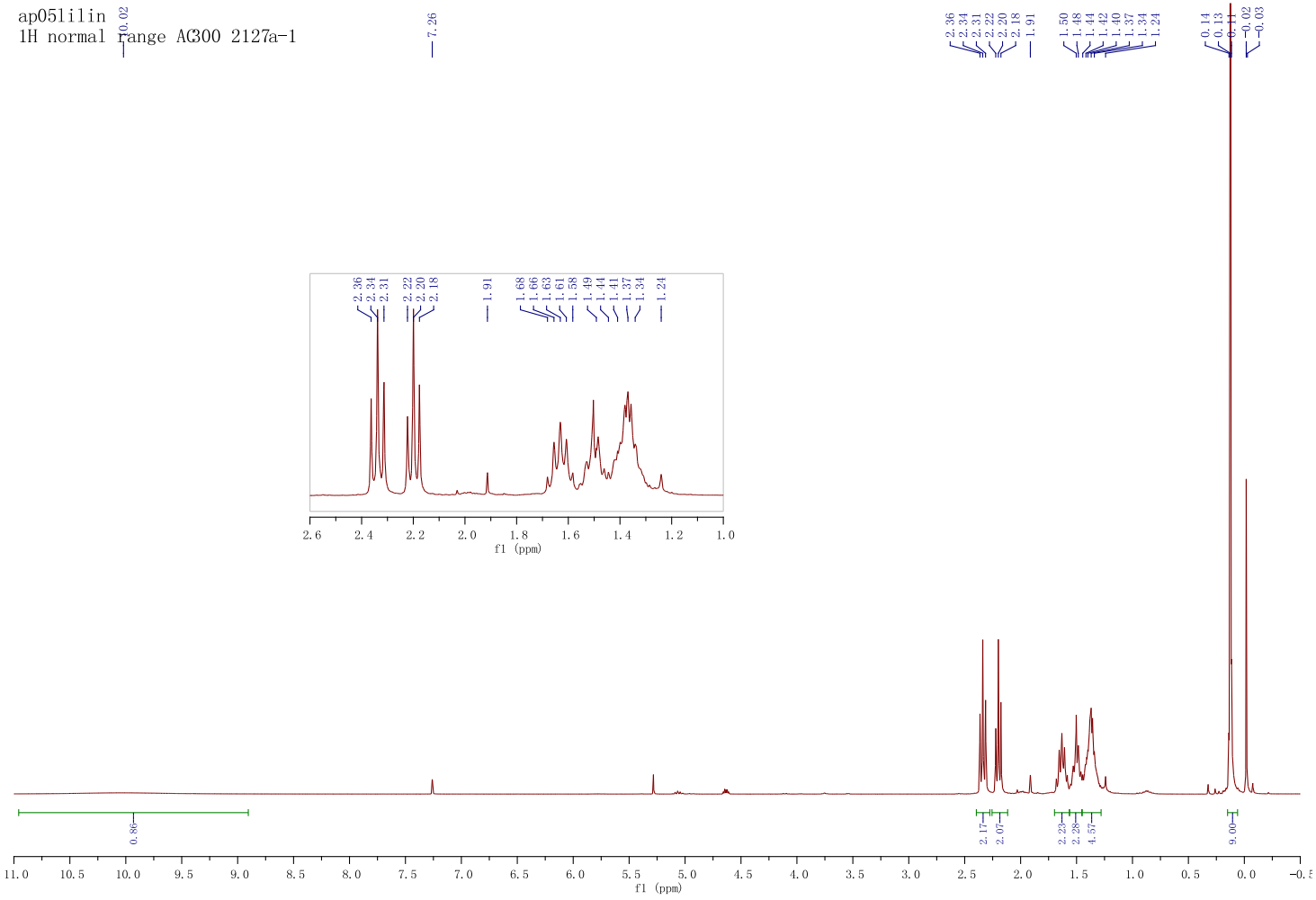
ap05lilin
1H normal range AC300 2127a-1
0.02
7.26
2.36
2.34
2.31
2.22
2.20
2.18
1.91
1.68
1.66
1.63
1.61
1.58
1.50
1.49
1.48
1.44
1.42
1.41
1.40
1.37
1.34
1.24
0.14
0.13
0.11
-0.02
-0.03
f1 (ppm)
0.86
2.17
2.07
2.23
2.26
4.57
9.00

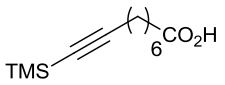
TMS
6
CO2H

2-2d

ap05lilin
1H normal range AC300 2127a-1 c

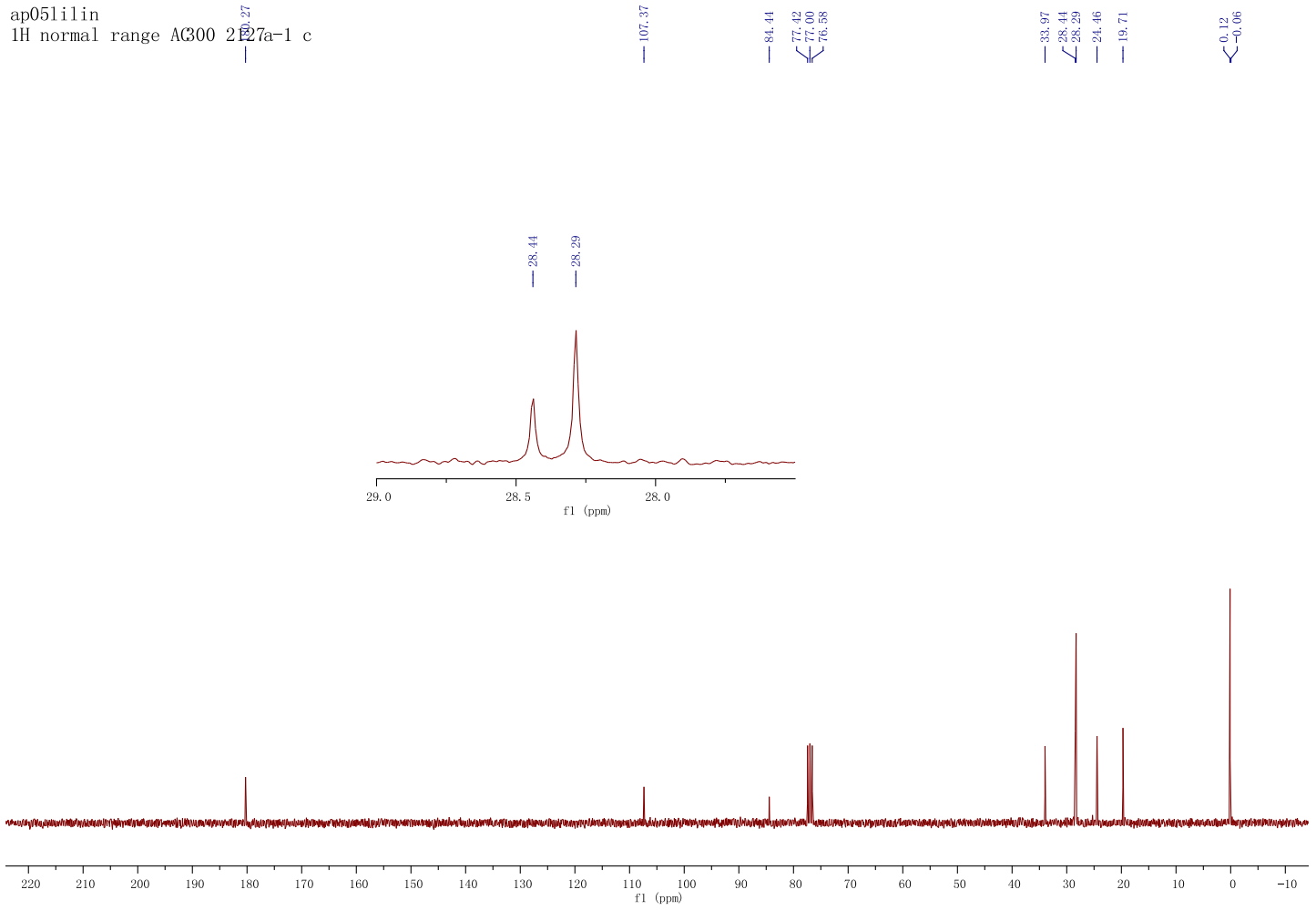

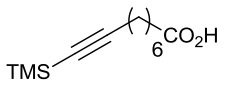

2-2d

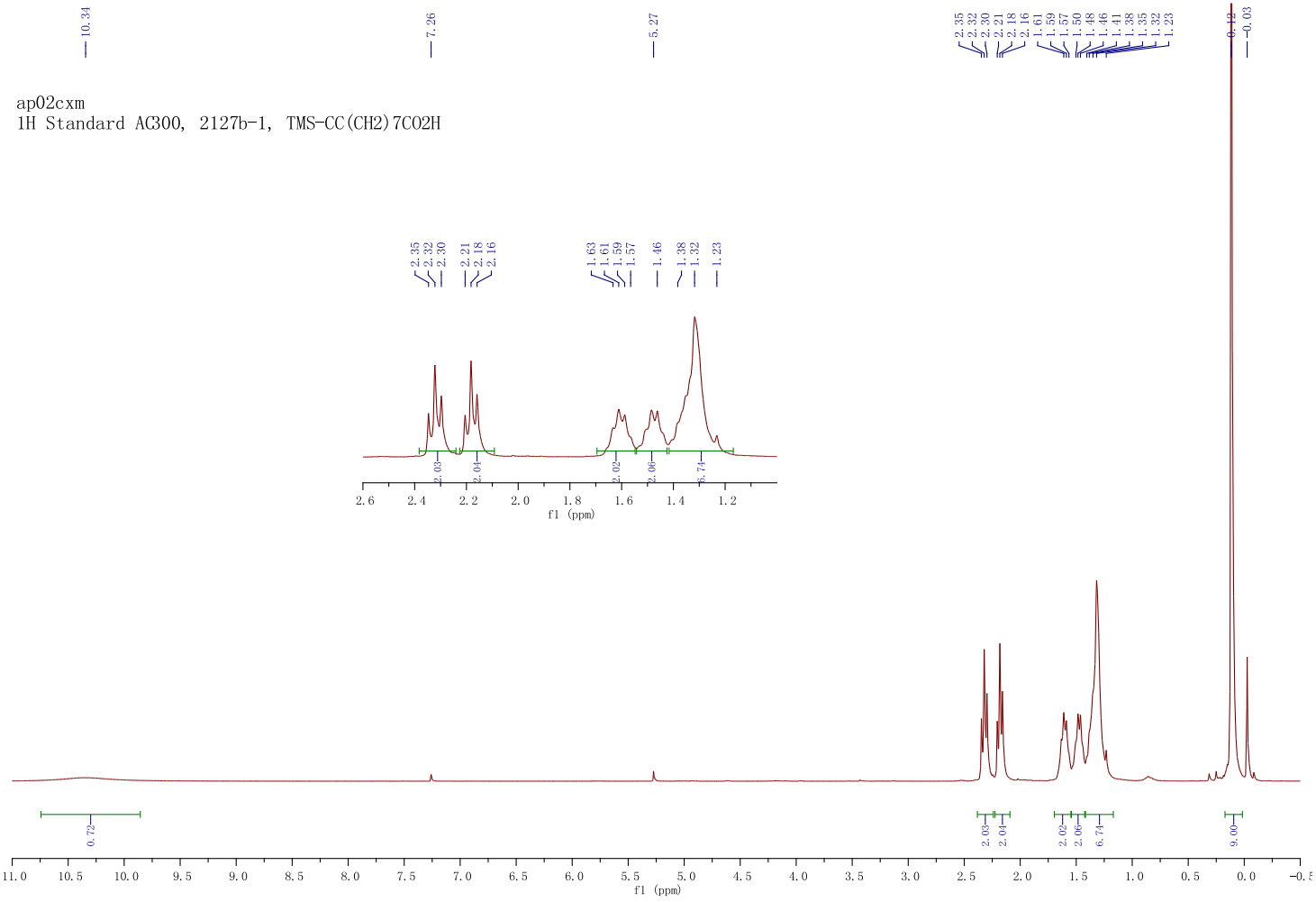
ap02cxm
1H Standard AC300, 2127b-1, TMS-CC(CH2)7CO2H
f1 (ppm)

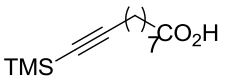
TMS
7
CO2H

2-2e

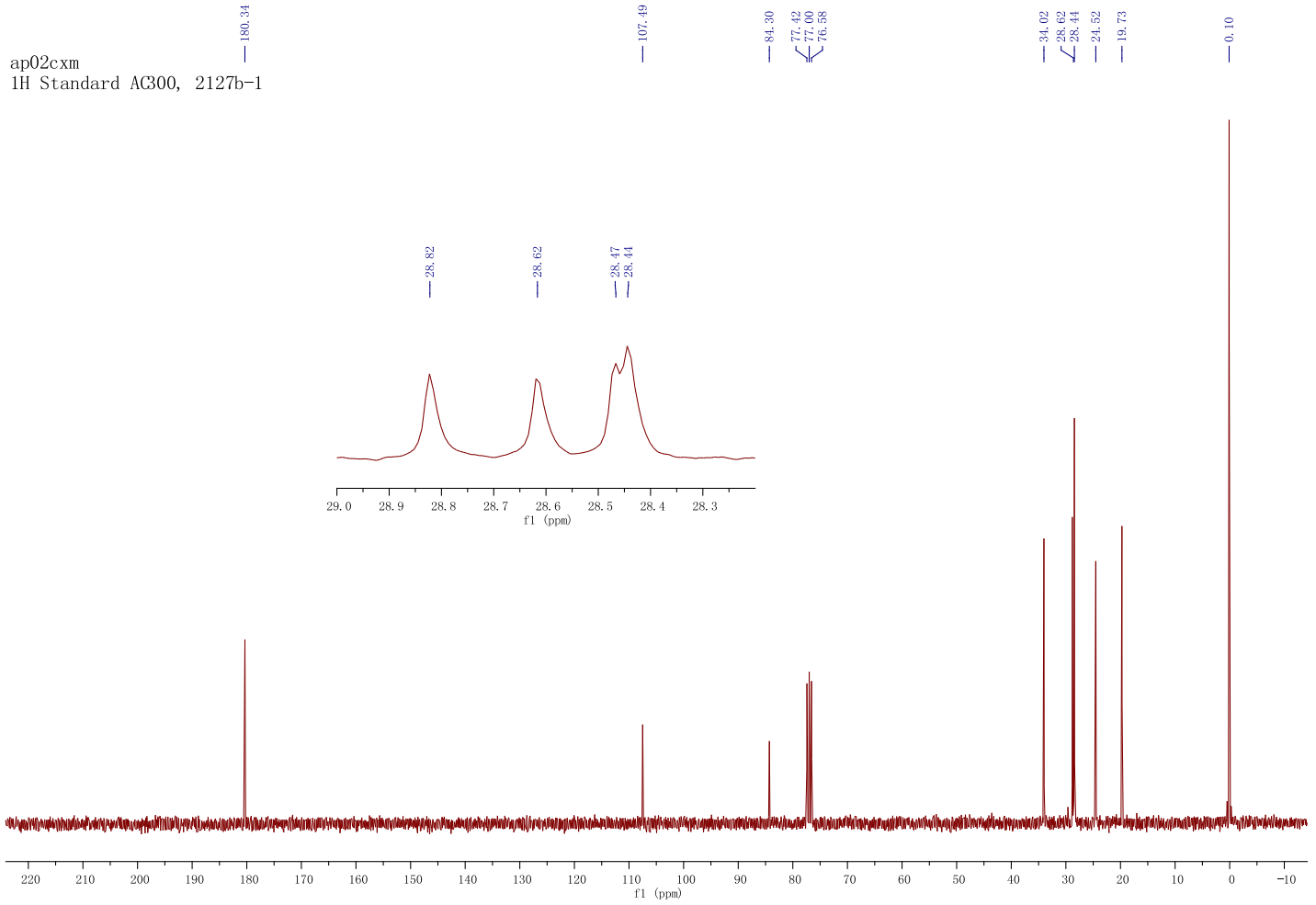
ap02cxm
1H Standard AC300, 2127b-1
180.34
107.49
84.30
77.42
77.00
76.58
34.02
28.62
28.44
24.52
19.73
0.10
28.82
28.62
28.47
28.44
29.0 28.9 28.8 28.7 28.6 28.5 28.4 28.3
f1 (ppm)
220 210 200 190 180 170 160 150 140 130 120 110 100 90 80 70 60 50 40 30 20 10 0 -10
f1 (ppm)

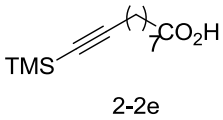
TMS
CO2H
7

2-2e

ja06cxm
1H normal range AC300
1146b2

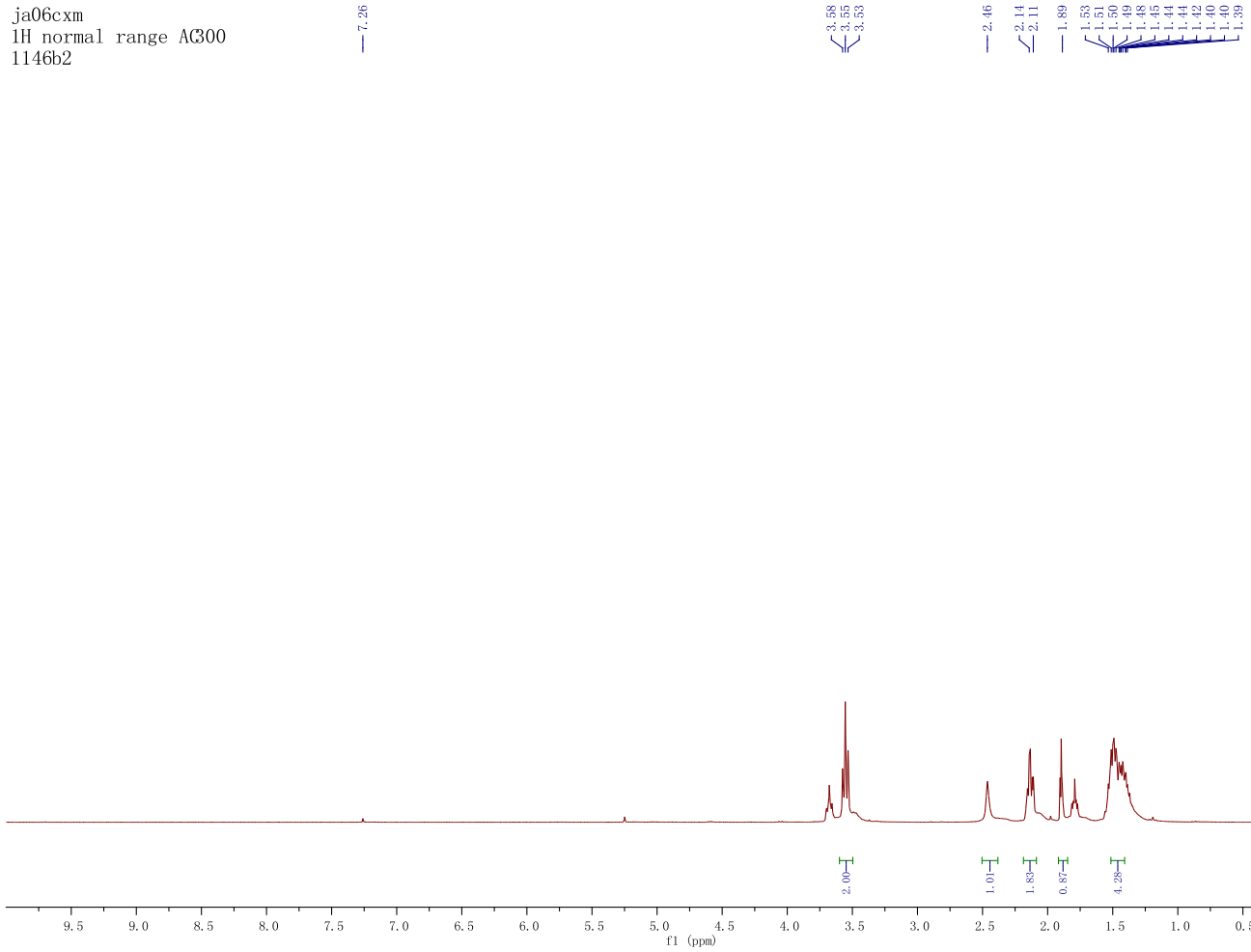

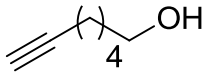

2-4b

ja06cxm
1H normal range AC300
1146b2

84.30
77.42
77.00
76.57
68.20
62.32
31.99
28.09
24.78
18.20

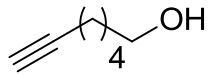

2-4b

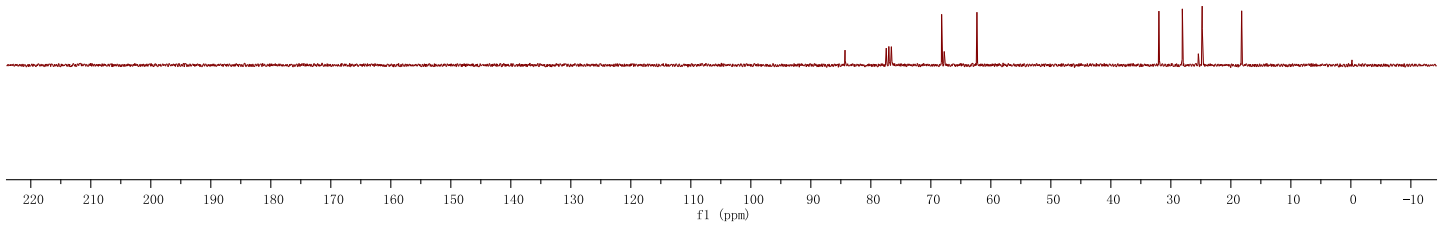

cxm0217
AMX 500, CDCl3, 2065b

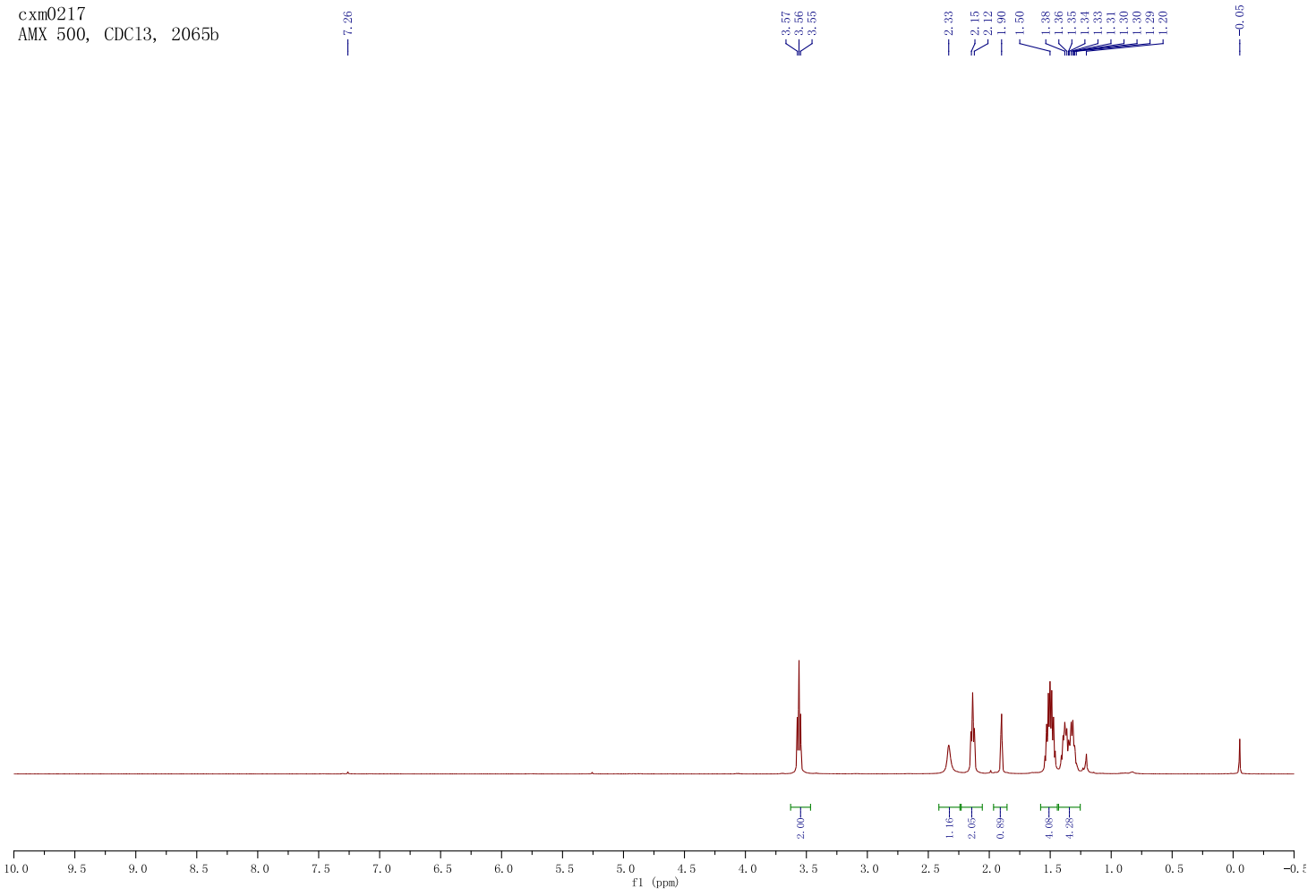

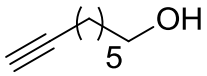

2-4c

cxm0217
AMX 500, CDCl3, 2065b

84.47
77.26
77.00
76.75
68.12
62.50
32.39
31.07
28.25
25.12
18.17
-0.16

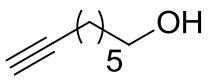

2-4c

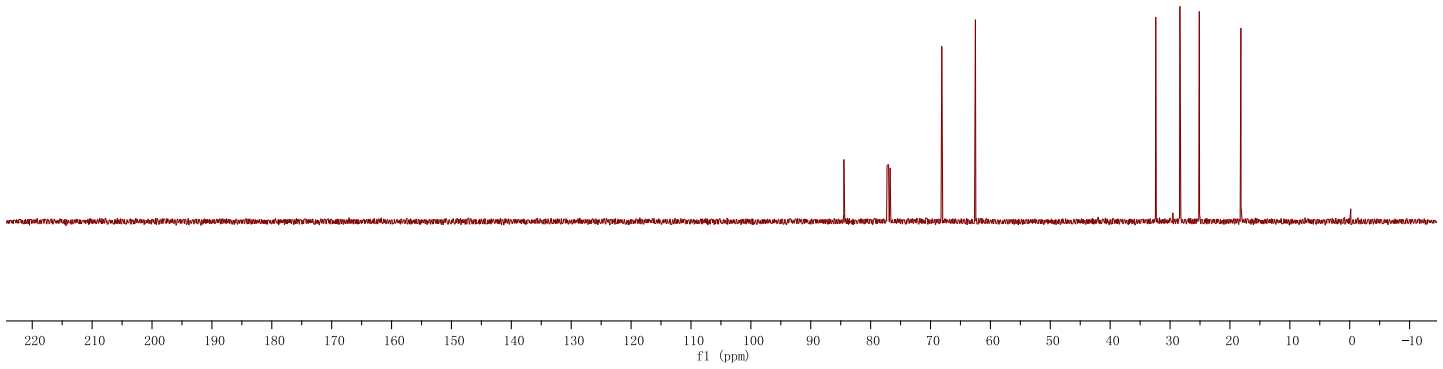

ap07cxm
1H Standard AC300 2131B2

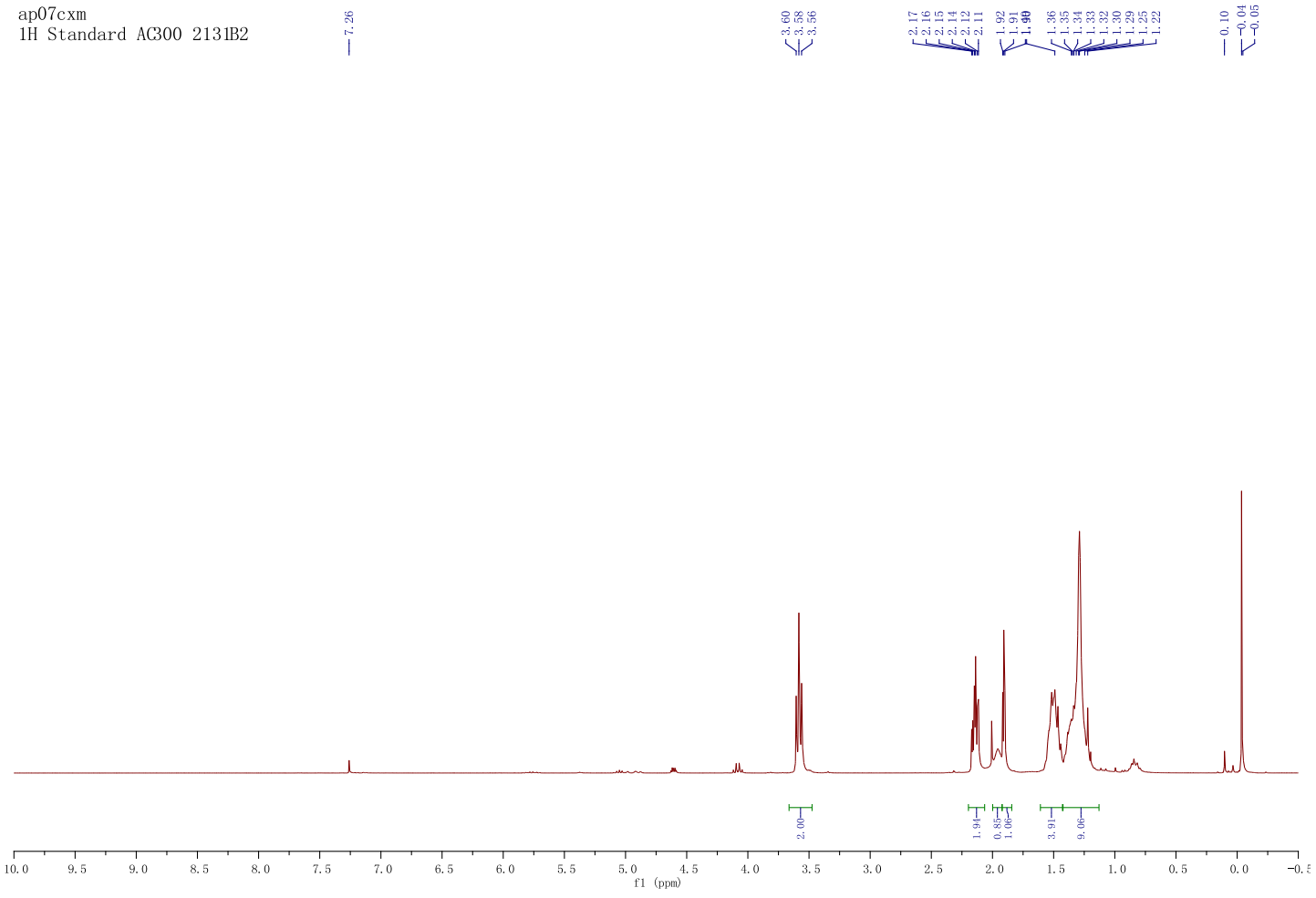

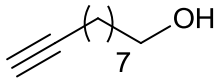

2-4e

ap07cxm
1H Standard AC300 2131B2, C7

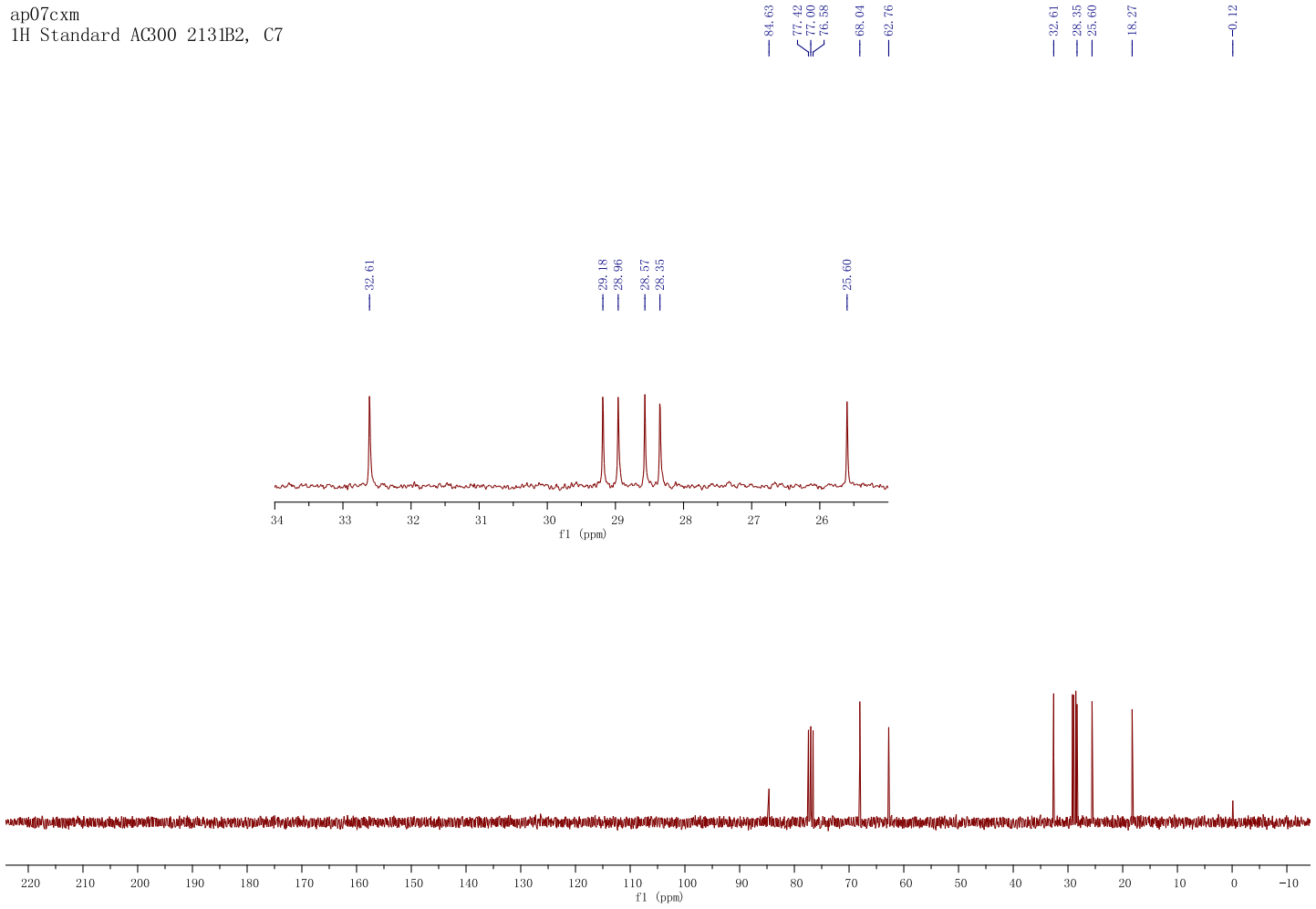

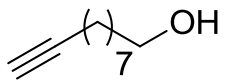

2-4e

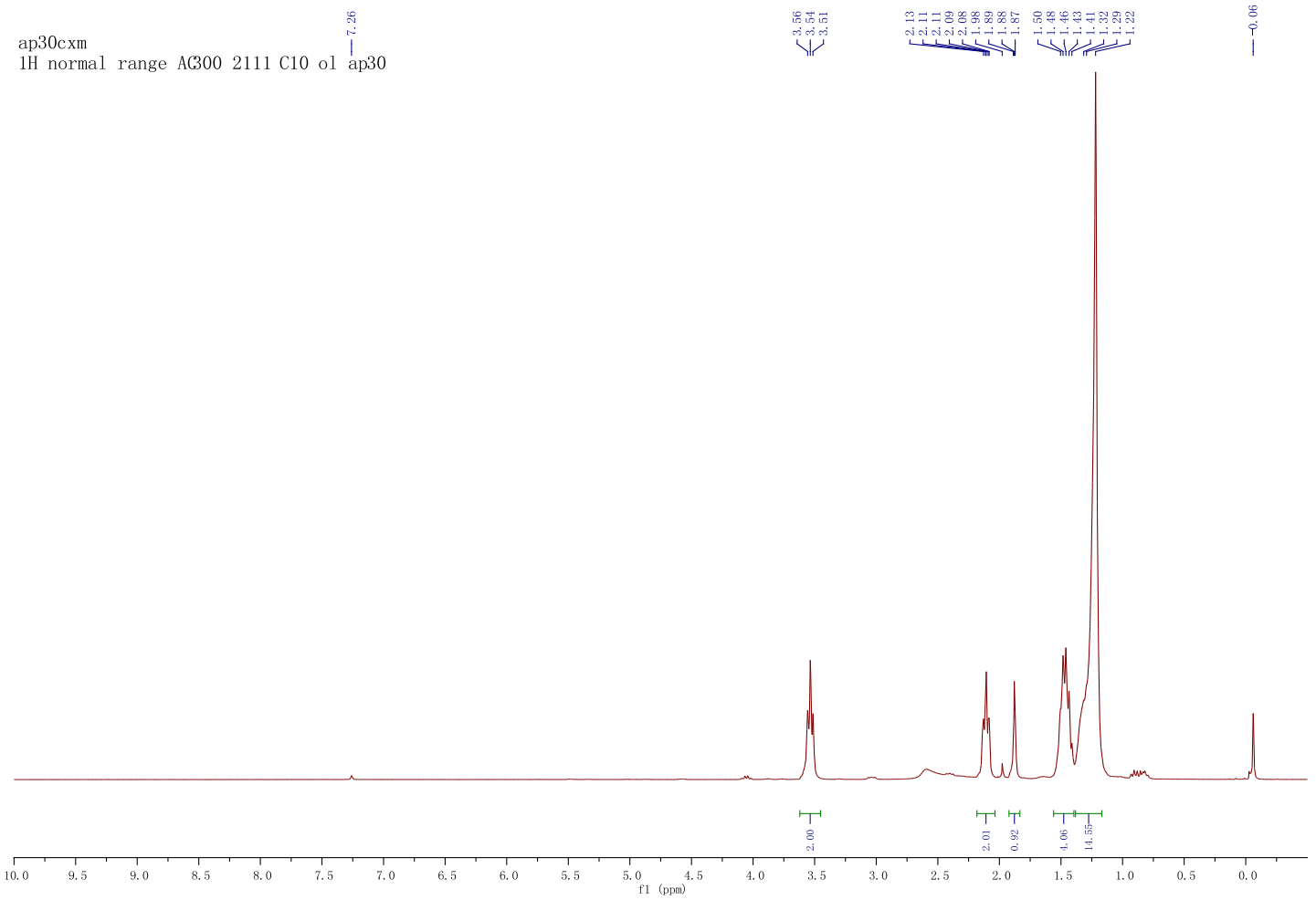
ap30cxm
1H normal range AC300 2111 C10 ol ap30
7.26
3.56
3.54
3.51
2.13
2.11
2.11
2.09
2.08
1.98
1.89
1.88
1.87
1.50
1.48
1.46
1.43
1.41
1.32
1.29
1.22
0.06
2.00
2.01
0.92
4.06
14.55
10.0
9.5
9.0
8.5
8.0
7.5
7.0
6.5
6.0
5.5
5.0
4.5
4.0
3.5
3.0
2.5
2.0
1.5
1.0
0.5
0.0
f1 (ppm)

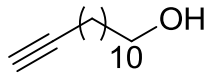
OH
10

2-3g

ap30cxm
13C normal range AC300 2111 C10 ol ap30

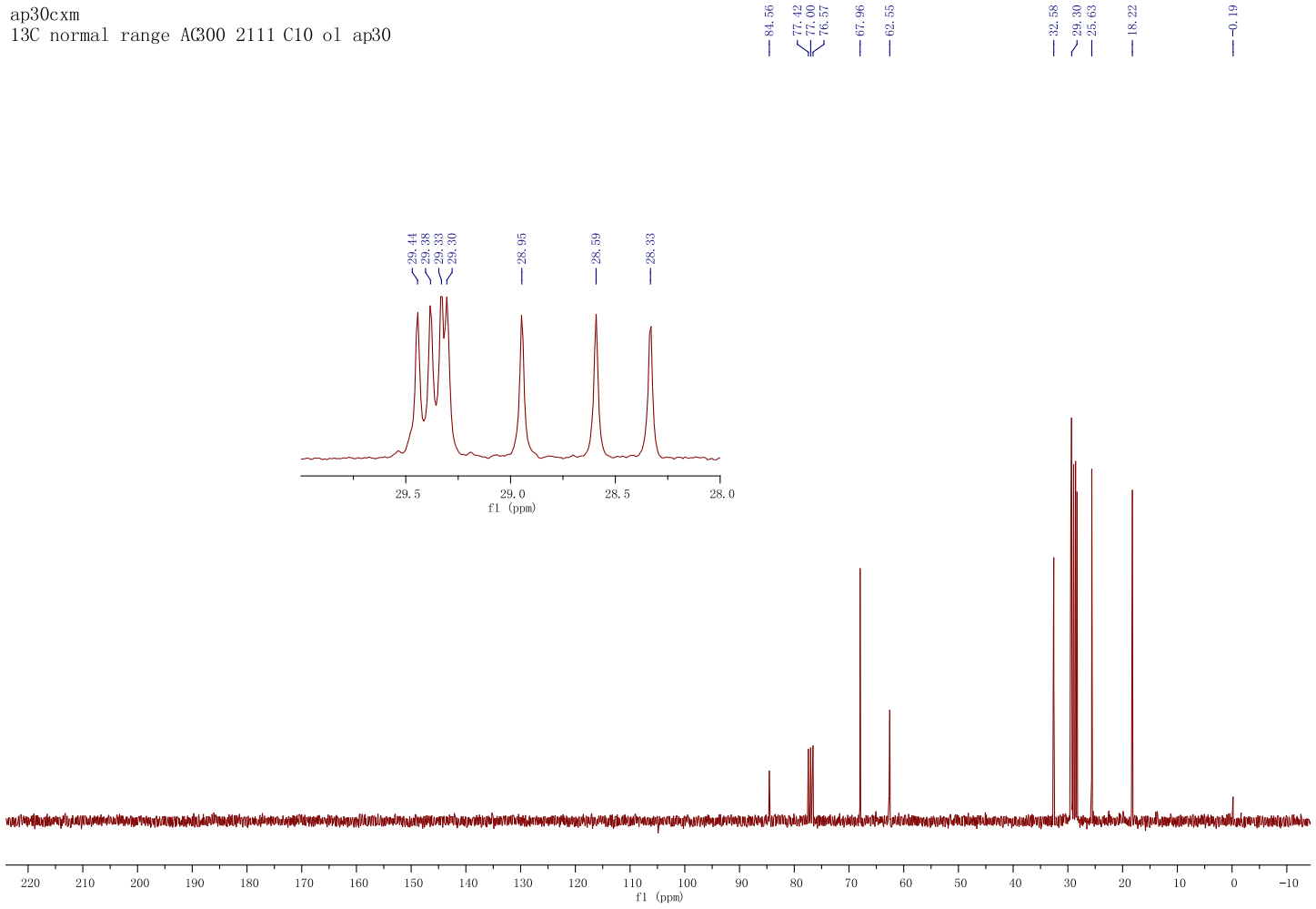

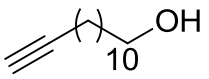

2-3g

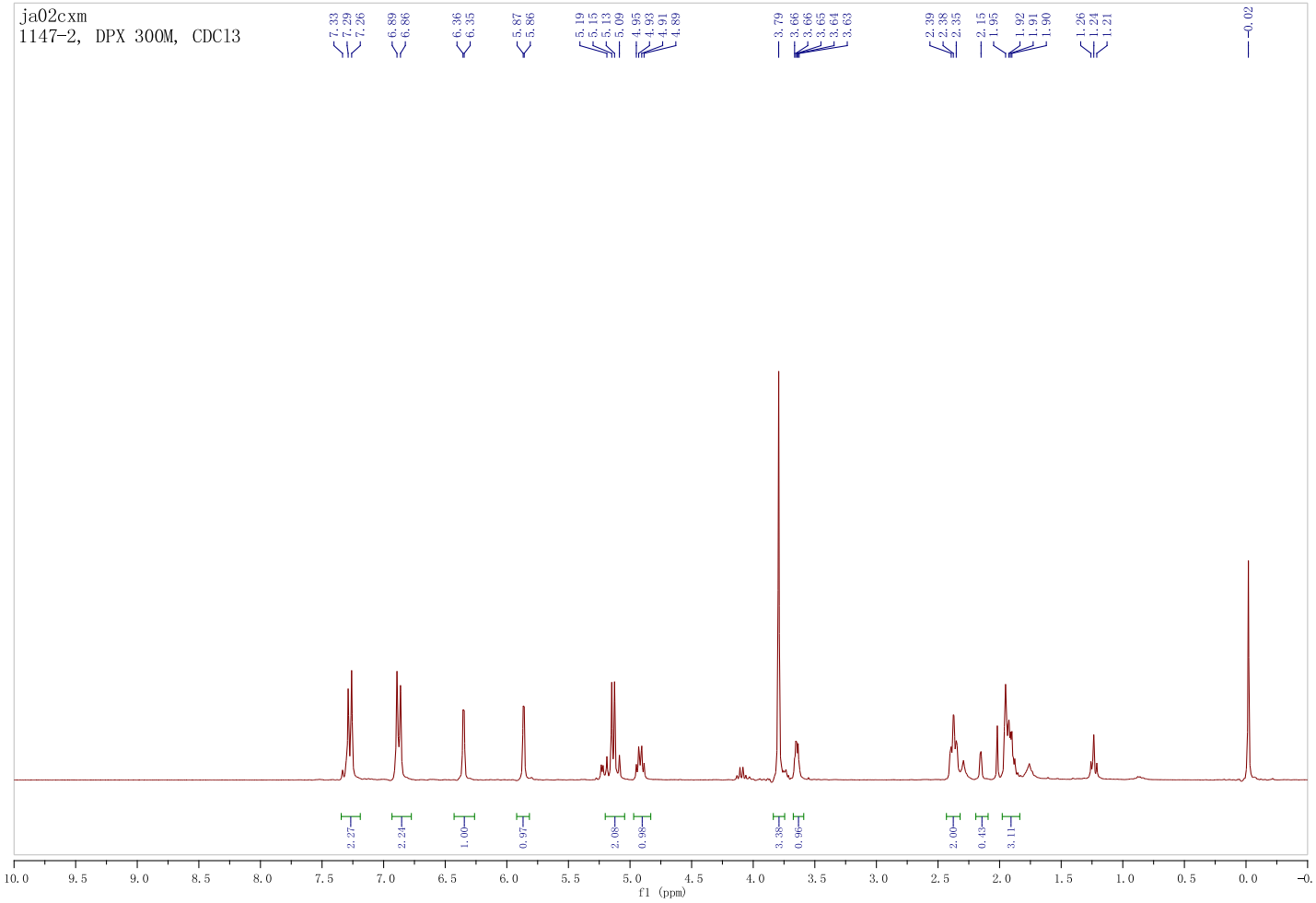
ja02cxm
1147-2, DPX 300M, CDCl3
7.33
7.29
7.26
6.89
6.86
6.36
6.35
5.87
5.86
5.19
5.15
5.13
5.09
4.95
4.93
4.91
4.89
3.79
3.66
3.66
3.65
3.64
3.63
2.39
2.38
2.35
2.15
1.95
1.92
1.91
1.90
1.26
1.24
1.21
0.02
2.27
2.24
1.00
0.97
2.08
0.98
3.38
0.96
2.00
0.43
3.11
10.0
9.5
9.0
8.5
8.0
7.5
7.0
6.5
6.0
5.5
5.0
4.5
4.0
3.5
3.0
2.5
2.0
1.5
1.0
0.5
0.0
f1 (ppm)

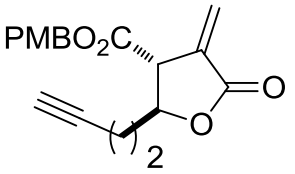
PMBO2C
O
O
2

trans-**2-8a**

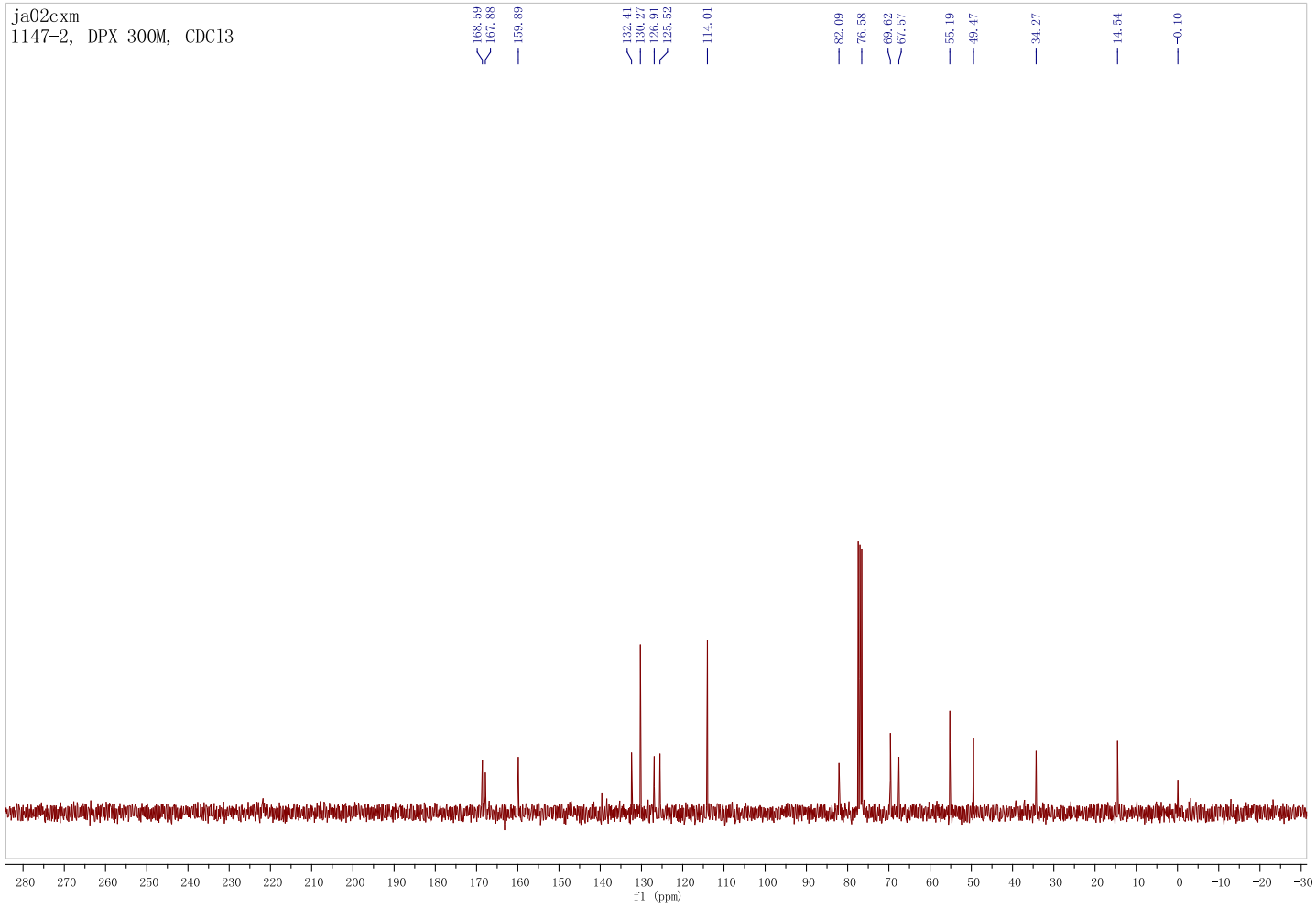
ja02cxm
1147-2, DPX 300M, CDCl3
168.59
167.88
159.89
132.41
130.27
126.91
125.52
114.01
82.09
76.58
69.62
67.57
55.19
49.47
34.27
14.54
-0.10
f1 (ppm)

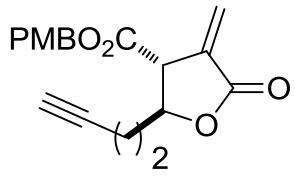
PMBO2C
O
O
2

trans-**2-8a**

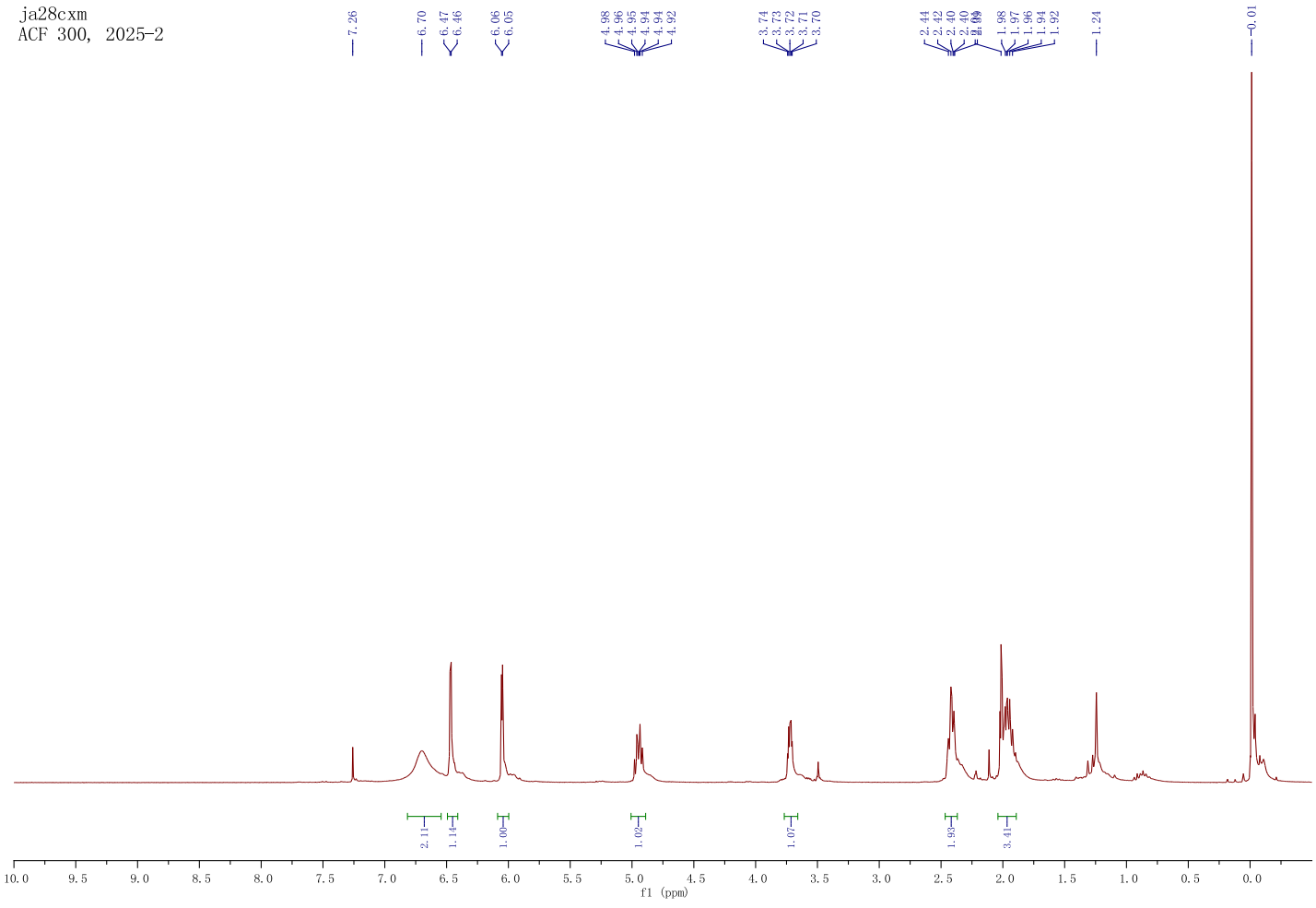
ja28cxm
ACF 300, 2025-2
7.26
6.70
6.47
6.46
6.06
6.05
4.98
4.96
4.95
4.94
4.94
4.92
3.74
3.73
3.72
3.71
3.70
2.44
2.42
2.40
2.40
1.98
1.97
1.96
1.94
1.92
1.24
0.01
2.11
1.14
1.00
1.02
1.07
1.93
3.41
10.0
9.5
9.0
8.5
8.0
7.5
7.0
6.5
6.0
5.5
5.0
4.5
4.0
3.5
3.0
2.5
2.0
1.5
1.0
0.5
0.0
f1 (ppm)

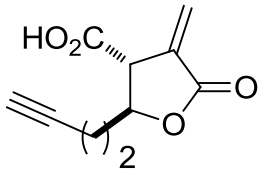
HO2C
O
O
2

trans-**2-9a**

ja28cxm
ACF 300, 2025-2

173.44
168.09
132.01
126.36
82.07
77.42
76.58
69.84
49.30
34.31
14.59
-0.05

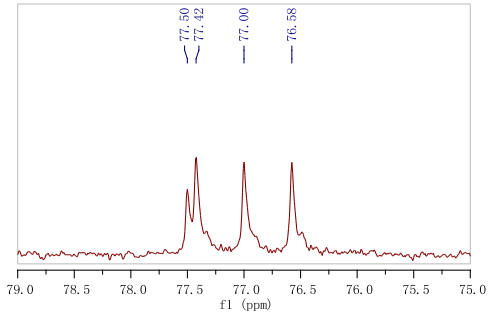

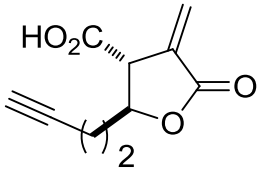

trans-**2-9a**

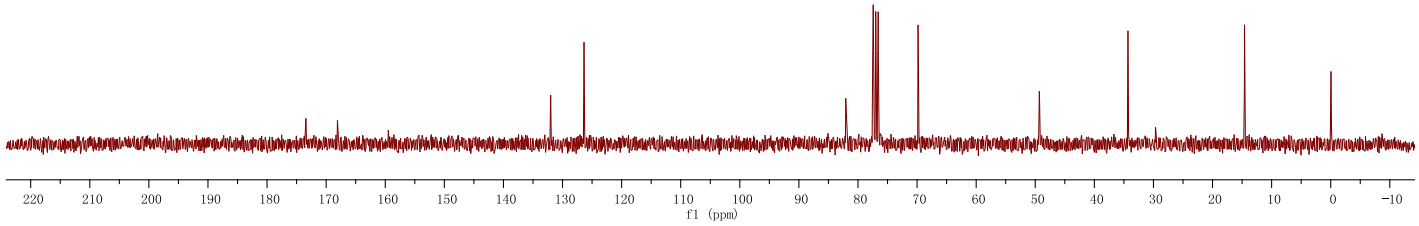

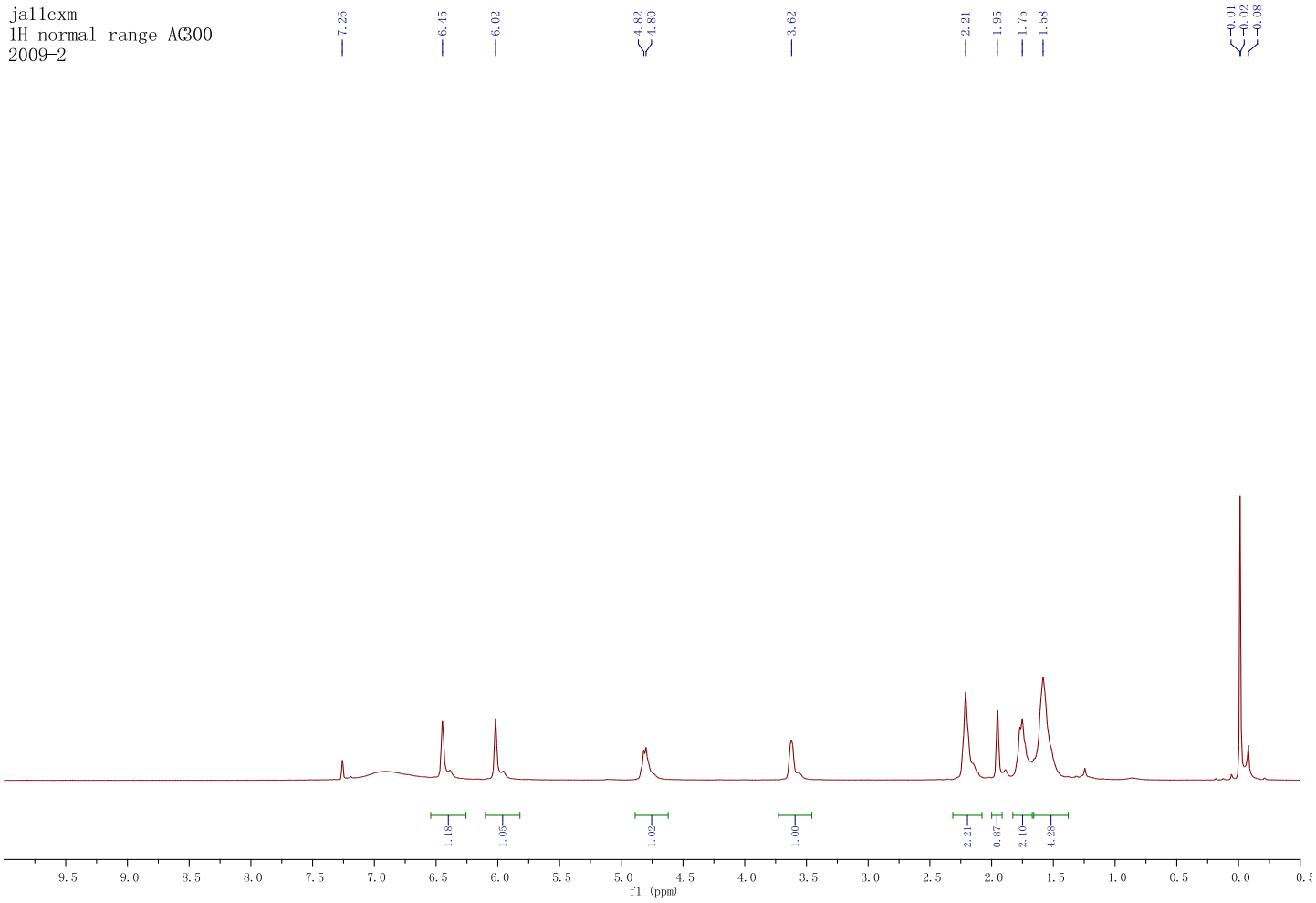
ja11cxm
1H normal range AC300
2009-2
7.26
6.45
6.02
4.82
4.80
3.62
2.21
1.95
1.75
1.58
0.01
0.02
0.08
1.18
1.05
1.02
1.00
2.21
0.87
2.10
4.28
f1 (ppm)

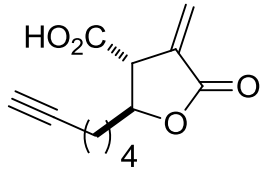
HO2C
O
O
4

trans-**2-9b**

ja11cxm
1H normal range AC300
2009-2

173.97
168.34
132.37
126.03
83.80
78.80
77.42
77.00
76.58
68.78
49.54
35.12
27.79
23.85
18.14
-0.05

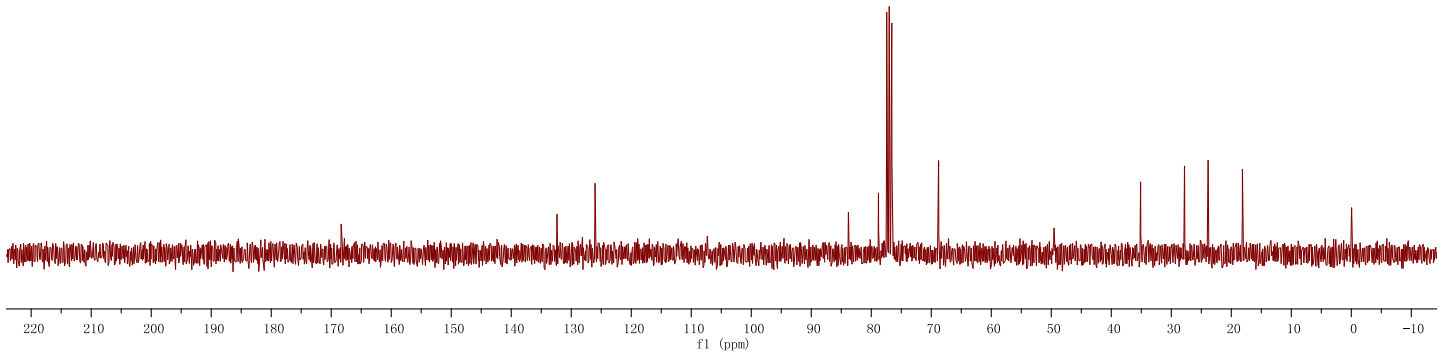

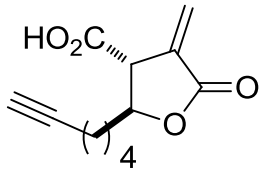

trans-**2-9b**

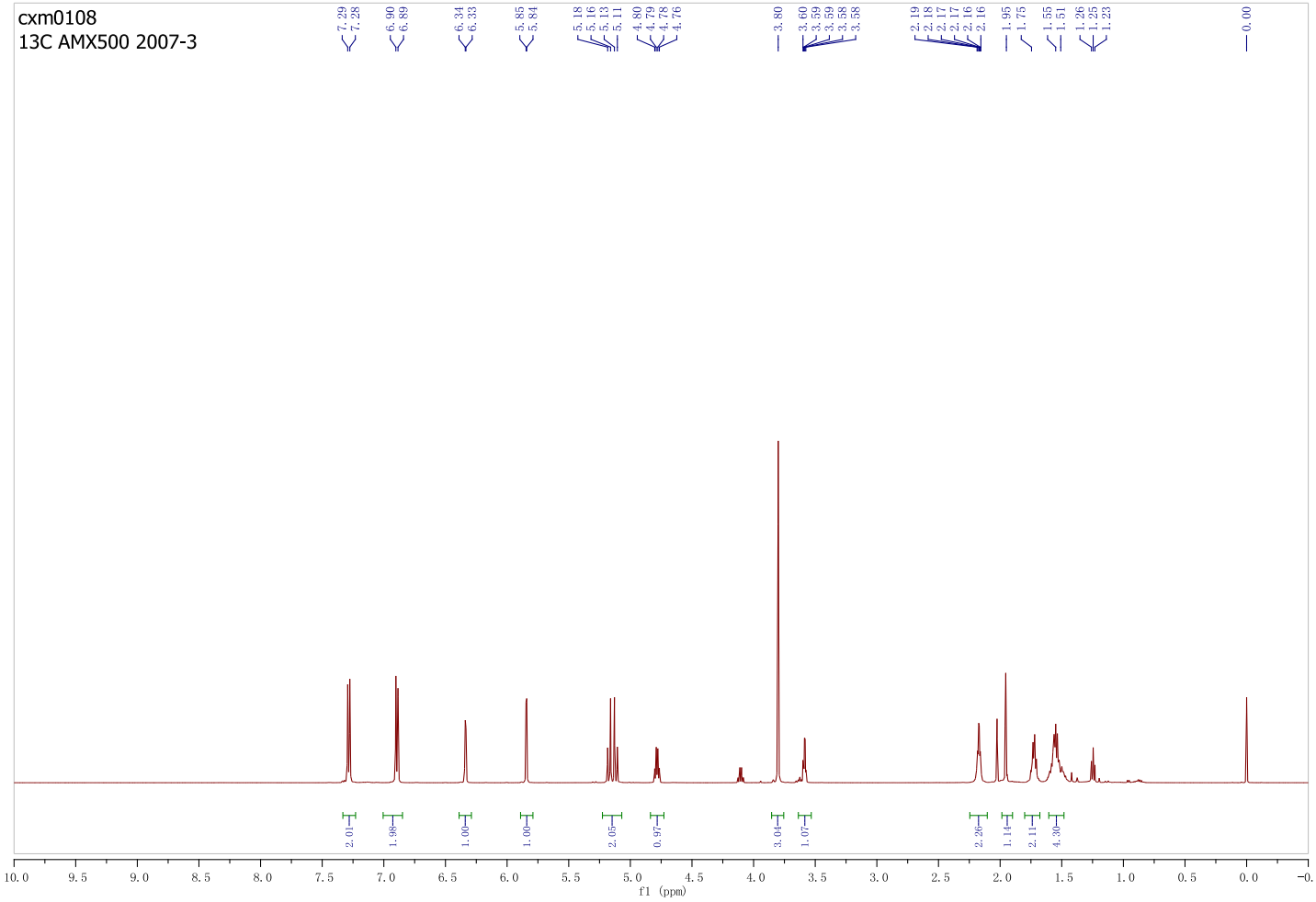
cxm0108
13C AMX500 2007-3
7.29
7.28
6.90
6.89
6.34
6.33
5.85
5.84
5.18
5.16
5.13
5.11
4.80
4.79
4.78
4.76
3.80
3.60
3.59
3.59
3.58
3.58
2.19
2.18
2.17
2.17
2.16
2.16
1.95
1.75
1.55
1.51
1.26
1.25
1.23
0.00
2.01
1.98
1.00
1.00
2.05
0.97
3.04
1.07
2.26
1.14
2.11
4.30
10.0
9.5
9.0
8.5
8.0
7.5
7.0
6.5
6.0
5.5
5.0
4.5
4.0
3.5
3.0
2.5
2.0
1.5
1.0
0.5
0.0
f1 (ppm)

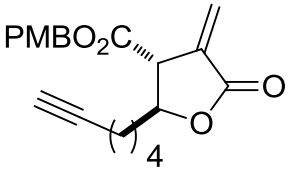
PMBO2C
O
O
4

trans-**2-8b**

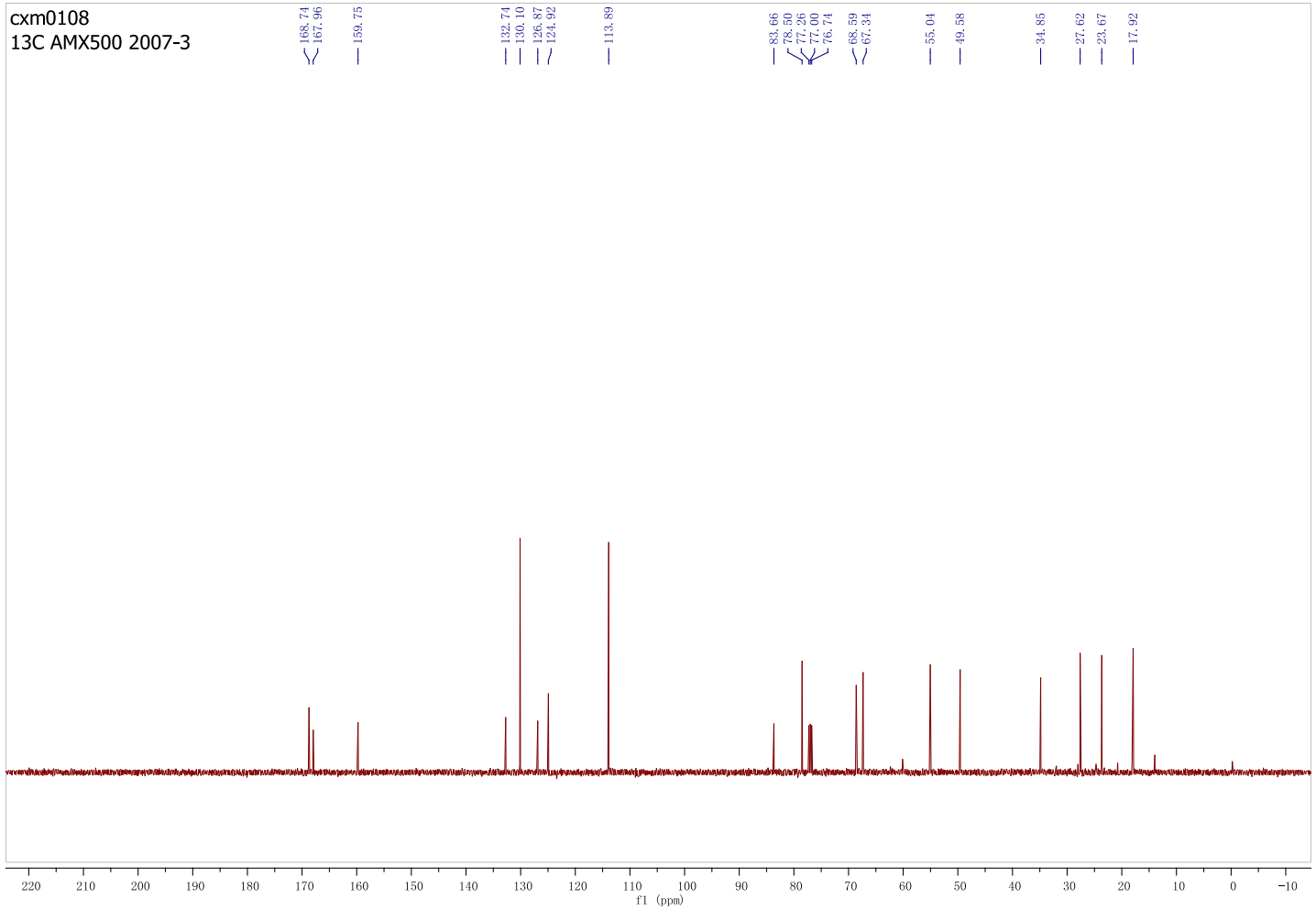
cxm0108
13C AMX500 2007-3
168.74
167.96
159.75
132.74
130.10
126.87
124.92
113.89
83.66
78.50
77.26
77.00
76.74
68.59
67.34
55.04
49.58
34.85
27.62
23.67
17.92
220 210 200 190 180 170 160 150 140 130 120 110 100 90 80 70 60 50 40 30 20 10 0 -10
f1 (ppm)

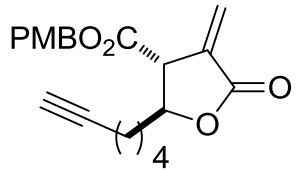
PMBO2C
O
O
4

trans-**2-8b**

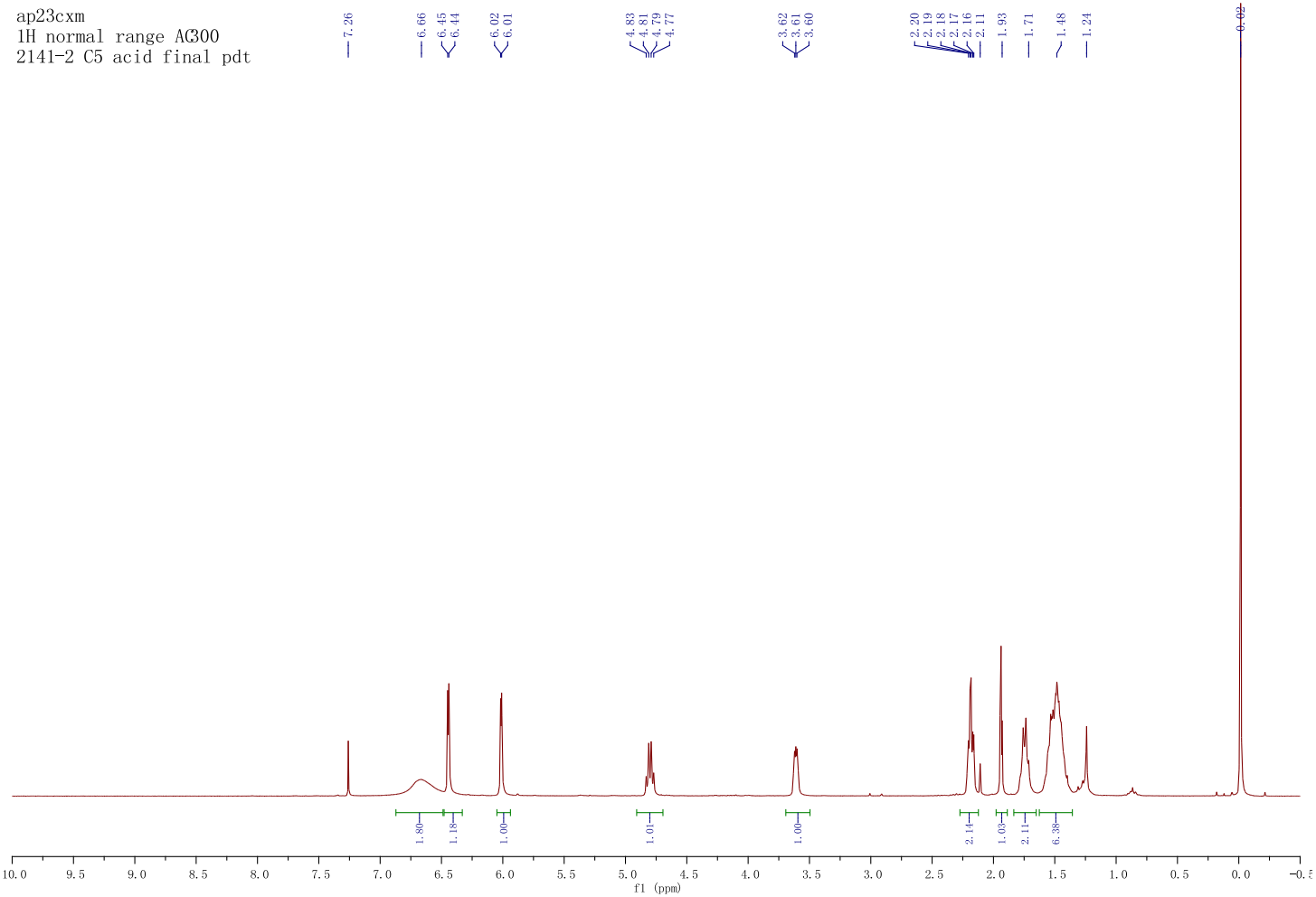
ap23cxm
1H normal range AC300
2141-2 C5 acid final pdt
7.26
6.66
6.45
6.44
6.02
6.01
4.83
4.81
4.79
4.77
3.62
3.61
3.60
2.20
2.19
2.18
2.17
2.16
2.11
1.93
1.71
1.48
1.24
0.02
1.80
1.18
1.00
1.01
1.00
2.14
1.03
2.11
6.38
f1 (ppm)

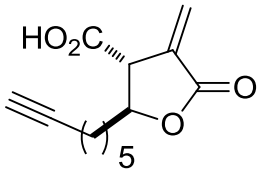
HO2C
O
O
5

trans-**2-8c**

ap23cxm
1H normal range AC300
2141-2 C5 acid final pdt

173.89
168.41
132.39
125.99
84.25
78.89
77.42
77.00
76.58
68.44
49.59
35.54
28.15
28.08
24.30
18.21
-0.06

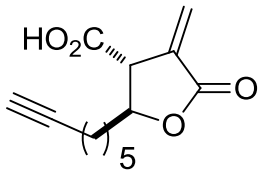

trans-**2-8c**

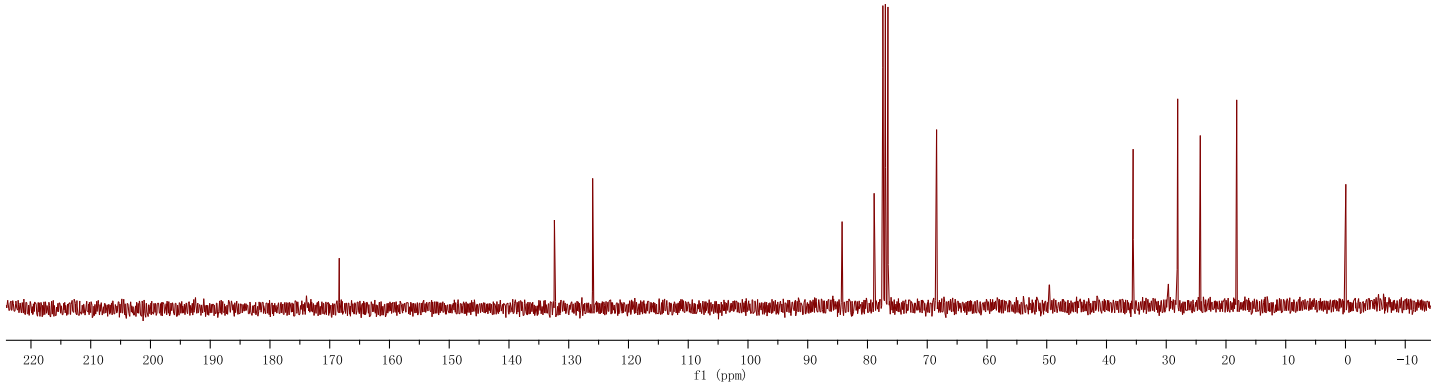

fe28cxm
acf 300, 2069-2 pure

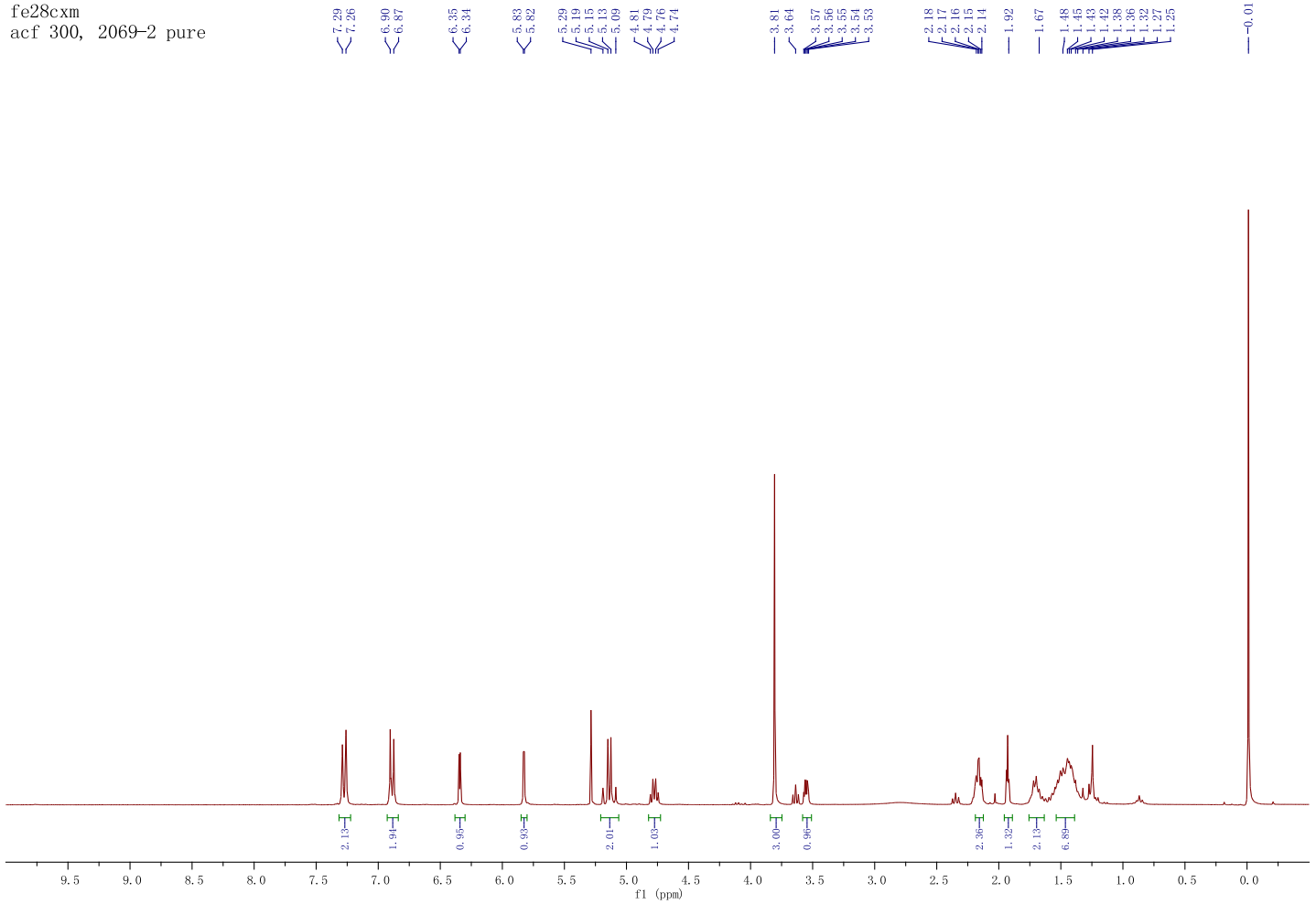

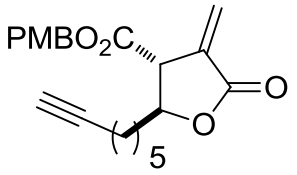

trans-**2-8c**

fe28cxm
acf 300, 2069-2 pure

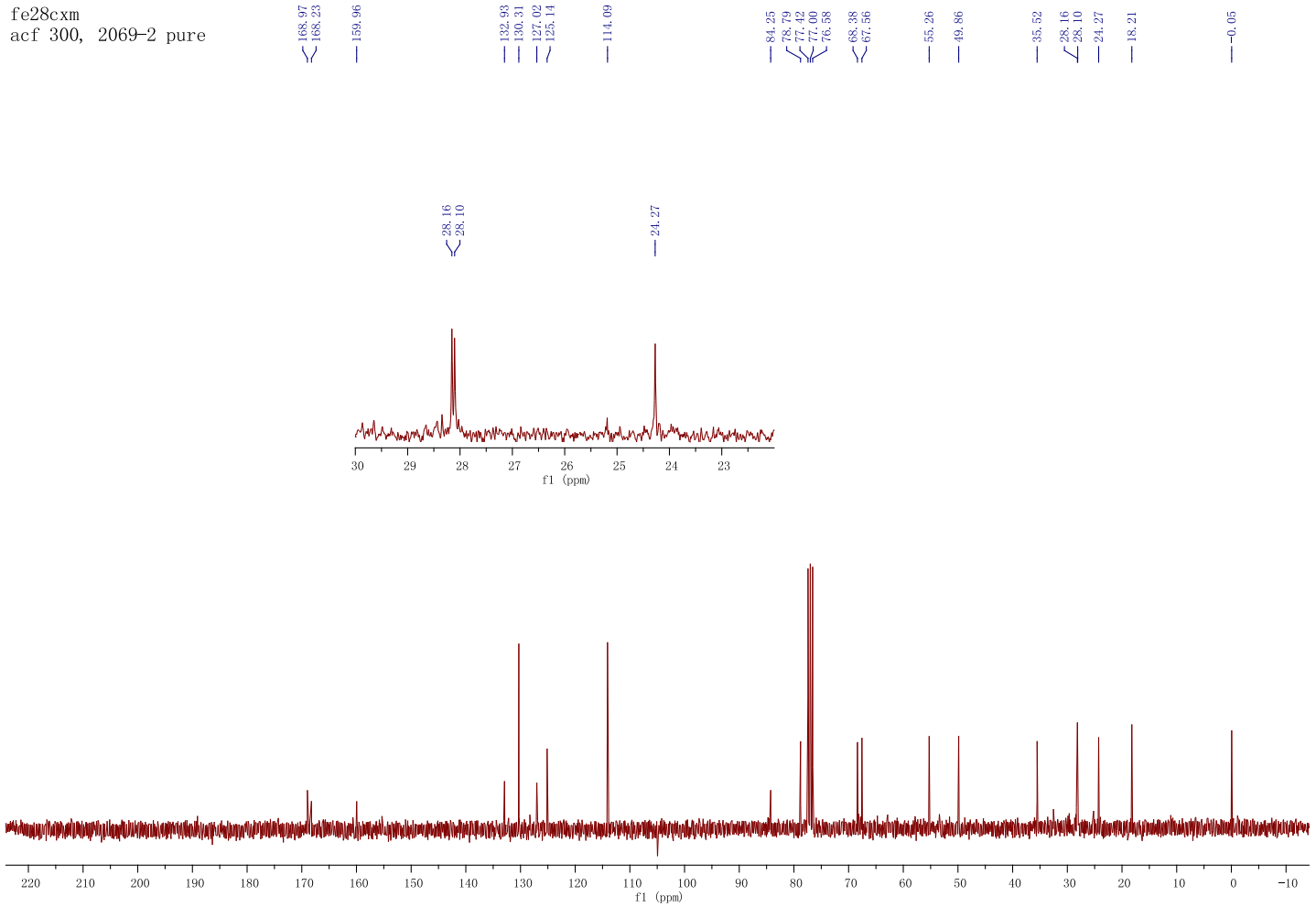

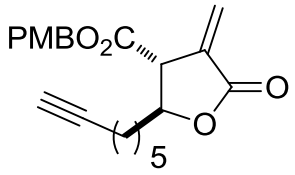

trans-**2-8c**

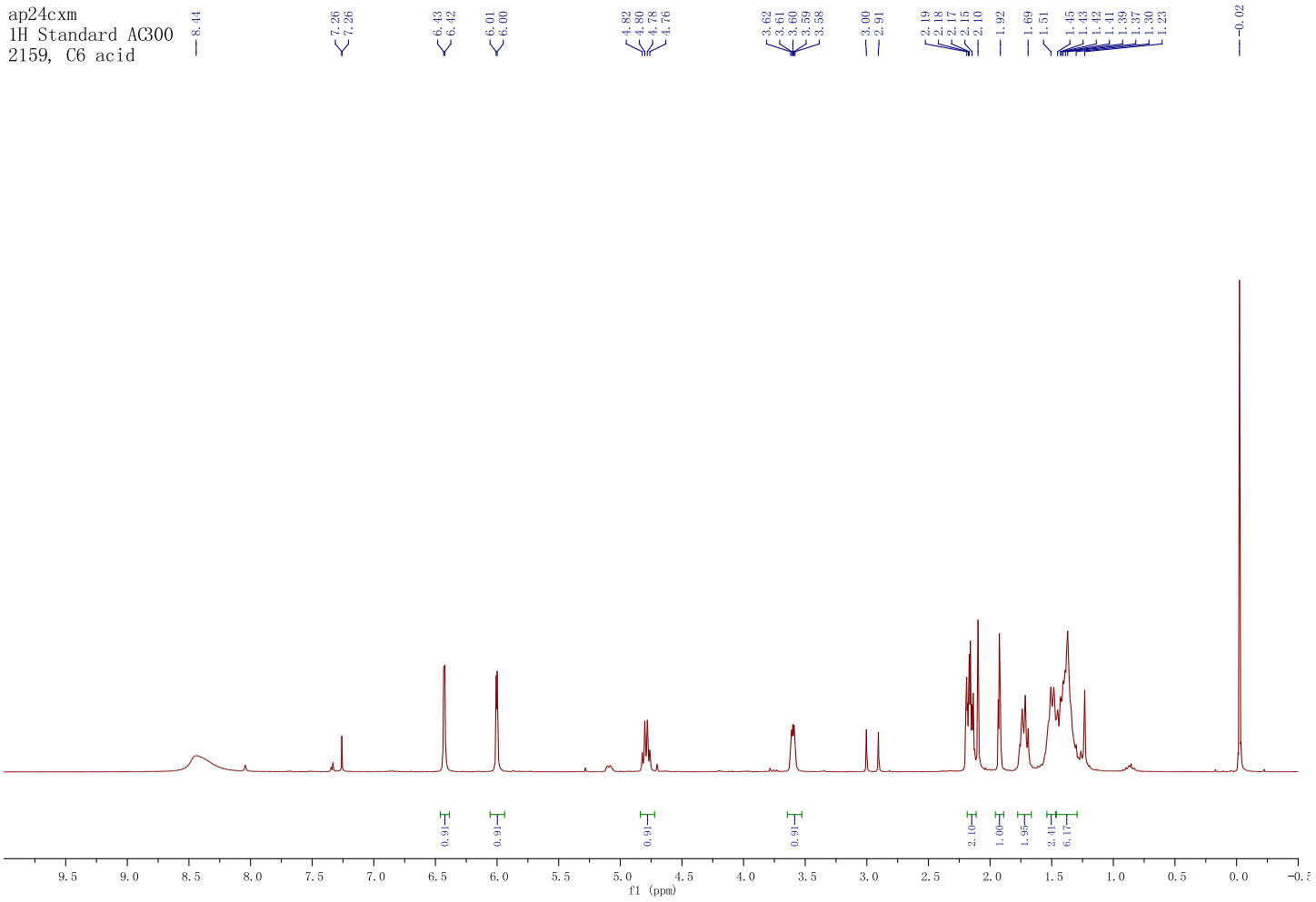
ap24cxm
1H Standard AC300
2159, C6 acid
8.44
7.26
7.26
6.43
6.42
6.01
6.00
4.82
4.80
4.78
4.76
3.62
3.61
3.60
3.59
3.58
3.00
2.91
2.19
2.18
2.17
2.15
2.10
1.92
1.69
1.51
1.45
1.43
1.42
1.41
1.39
1.37
1.30
1.23
0.02
0.91
0.91
0.91
0.91
2.10
1.00
1.95
2.41
6.17
f1 (ppm)

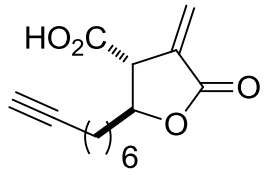
HO2C
O
O
6

trans-**2-9d**

ap24cxm
13C Standard AC300
2159, C6 acid

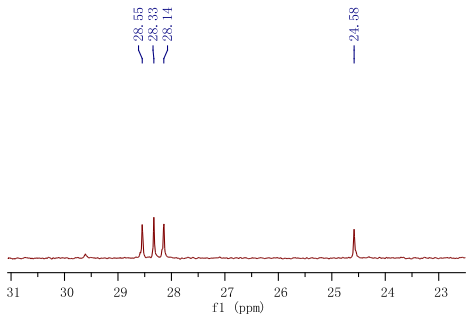

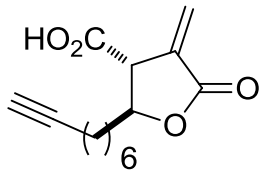

trans-**2-9d**

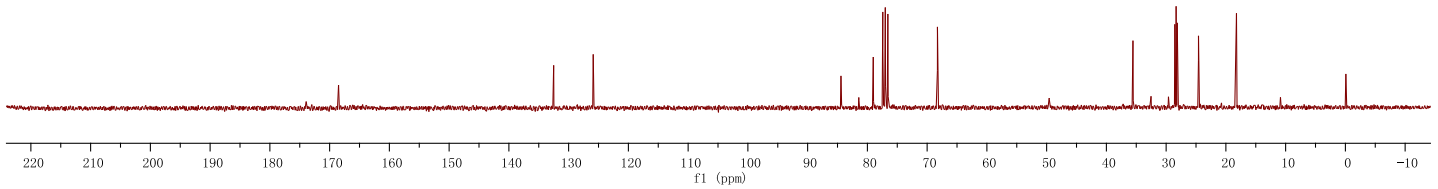

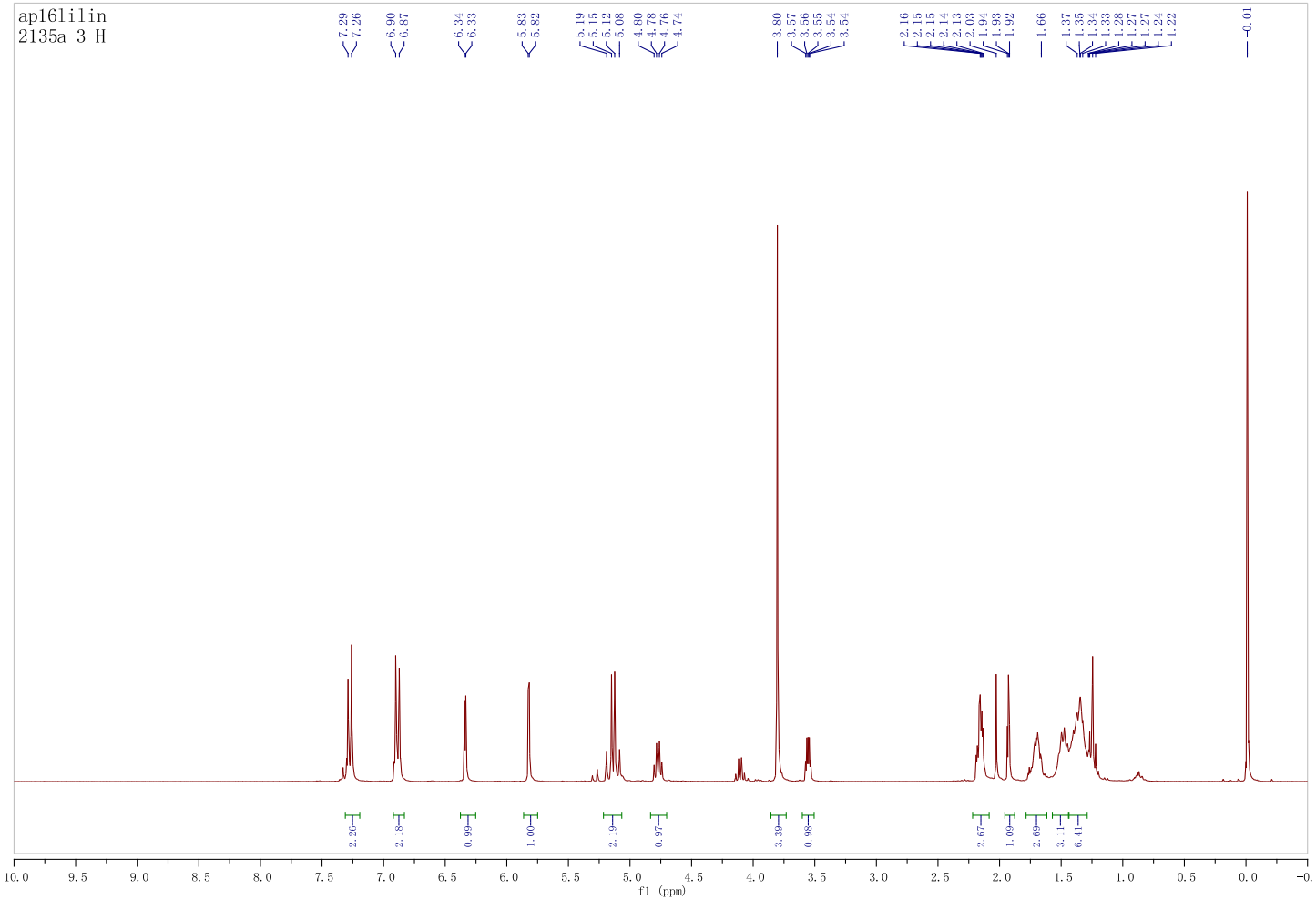
ap16lilin
2135a-3 H
7.29
7.26
6.90
6.87
6.34
6.33
5.83
5.82
5.19
5.15
5.12
5.08
4.80
4.78
4.76
4.74
3.80
3.57
3.56
3.55
3.54
3.54
2.16
2.15
2.15
2.14
2.13
2.03
1.94
1.93
1.92
1.66
1.37
1.35
1.34
1.33
1.28
1.27
1.27
1.24
1.22
-0.01
2.26
2.18
0.99
1.00
2.19
0.97
3.39
0.98
2.67
1.09
2.69
3.11
6.41
f1 (ppm)

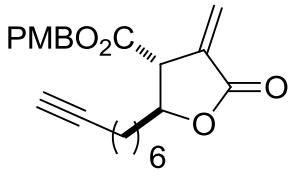
PMBO2C
O
O
6

trans-**2-8d**

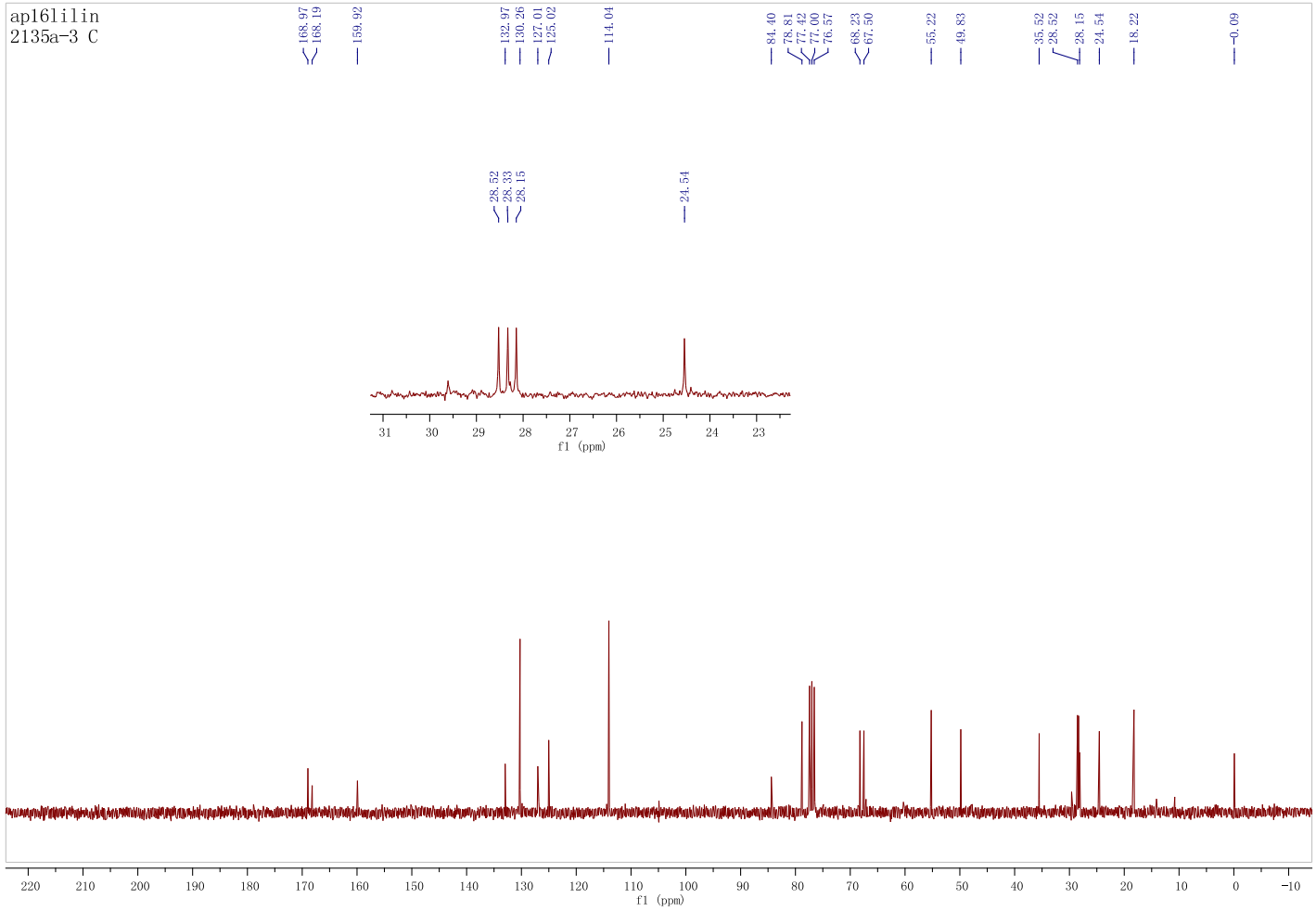
ap16lilin
2135a-3 C
168.97
168.19
159.92
132.97
130.26
127.01
125.02
114.04
84.40
78.81
77.42
77.00
76.57
68.23
67.50
55.22
49.83
35.52
28.52
28.15
24.54
18.22
-0.09
28.52
28.33
28.15
24.54
f1 (ppm)
f1 (ppm)

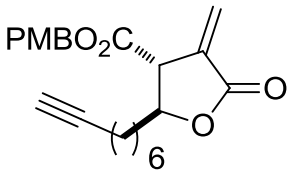
PMBO2C
O
O
6

trans-**2-8d**

ap23cxm
DPX 300, 2143-2, C7 acid

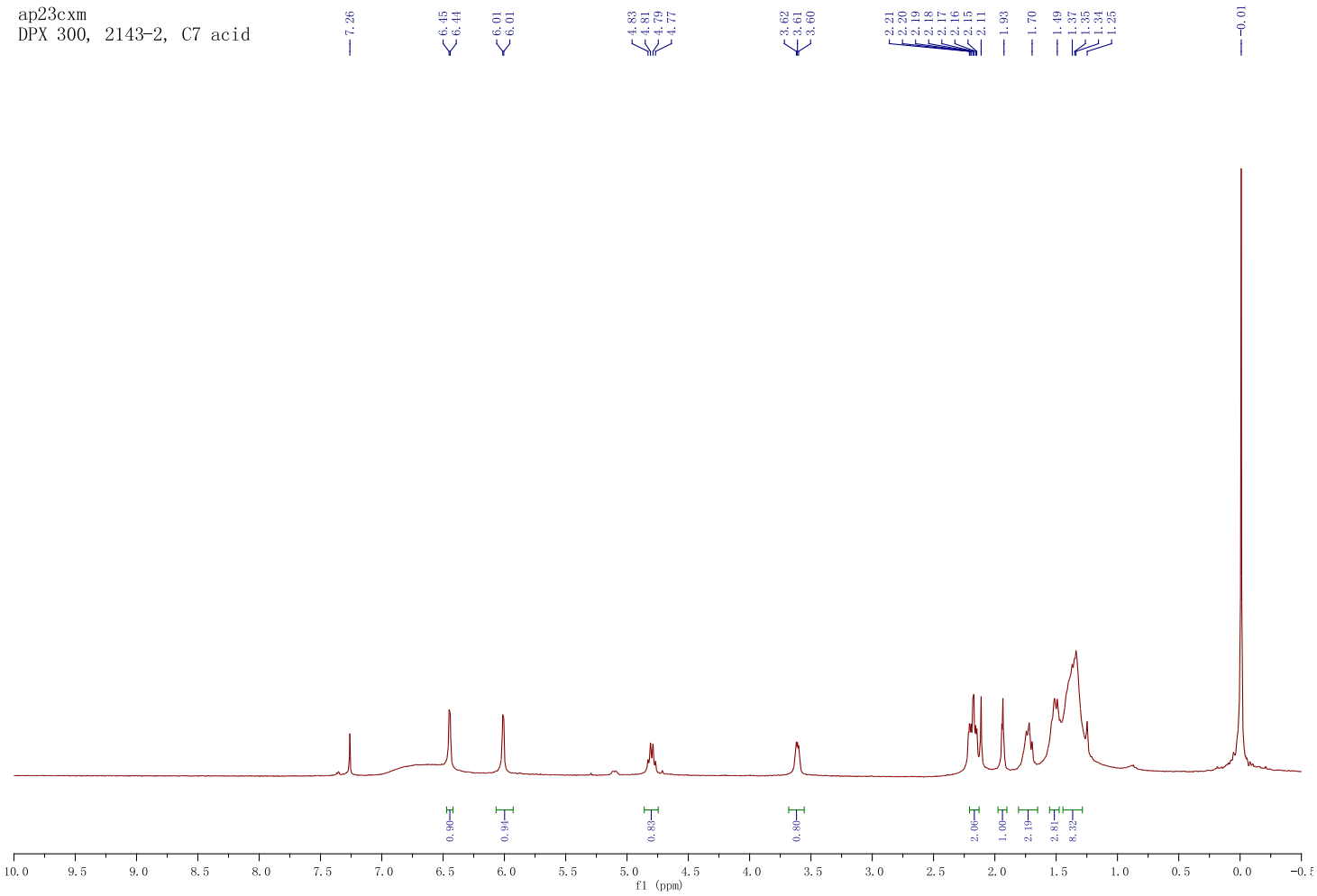

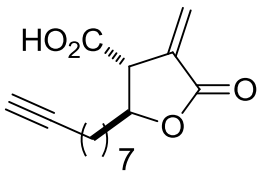

trans-**2-9e**

ap23cxm
DPX 300, 2143-2, C7 acid

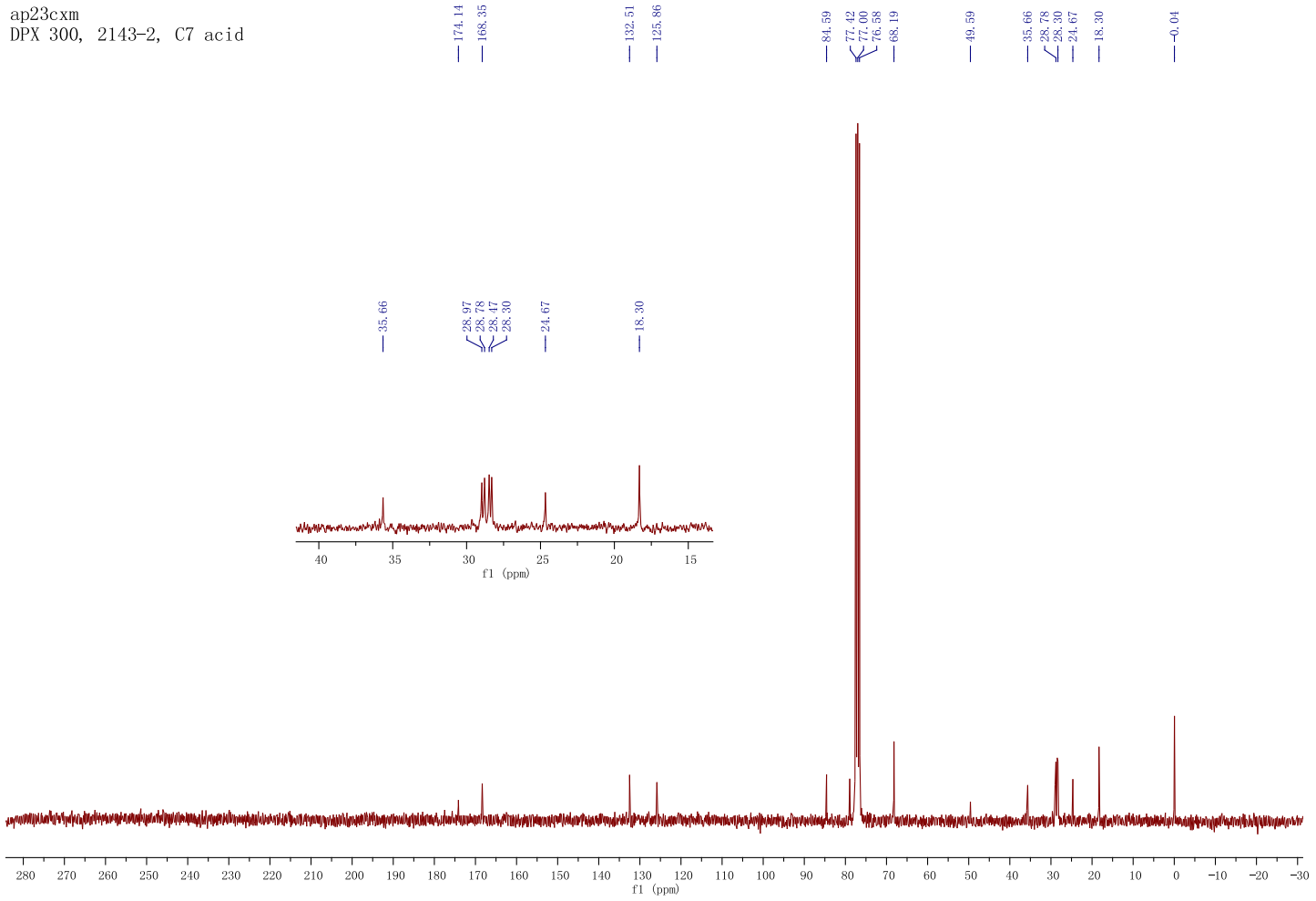

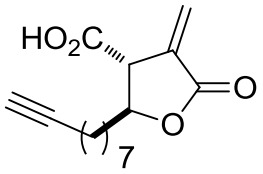

trans-**2-9e**

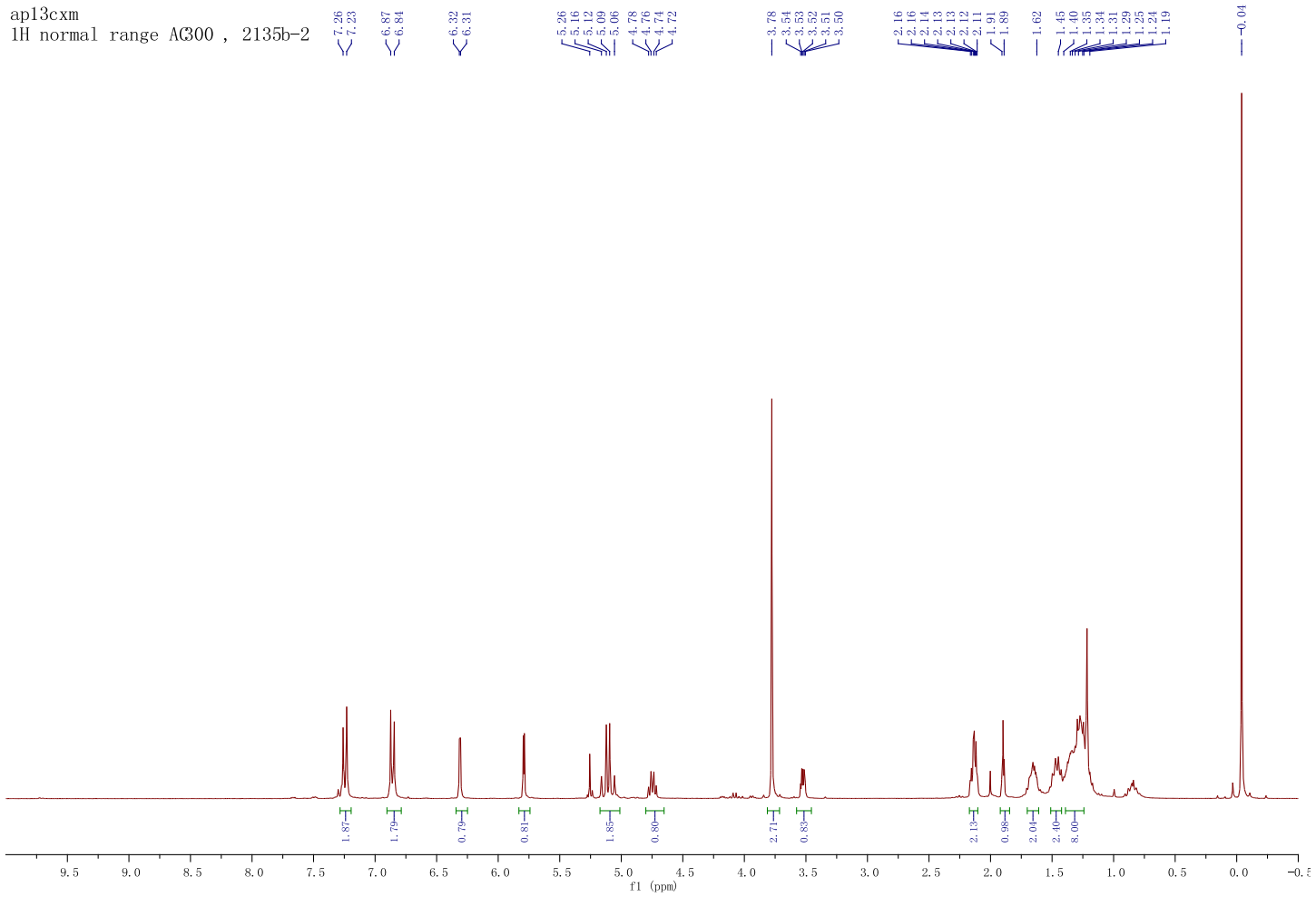
ap13cxm
1H normal range AC300 , 2135b-2
7.26
7.23
6.87
6.84
6.32
6.31
5.26
5.16
5.12
5.09
5.06
4.78
4.76
4.74
4.72
3.78
3.54
3.53
3.52
3.51
3.50
2.16
2.16
2.14
2.13
2.13
2.12
2.11
1.91
1.89
1.62
1.45
1.40
1.35
1.34
1.31
1.29
1.25
1.24
1.19
-0.04
1.87
1.79
0.79
0.81
1.85
0.80
2.71
0.83
2.13
0.98
2.04
2.40
8.00
f1 (ppm)

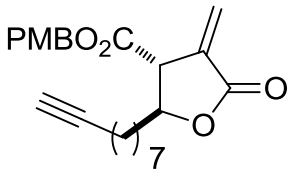
PMBO2C
O
O
7

trans-**2-8e**

ap13cxm
1H normal range AC300 , 2135b-2

169.01
168.25
159.93
132.99
130.29
127.02
125.05
114.06
84.56
78.88
77.42
77.00
76.58
68.15
67.53
55.25
49.85
35.60
28.77
28.30
24.62
18.29
-0.06

29.64
28.94
28.77
28.46
28.30

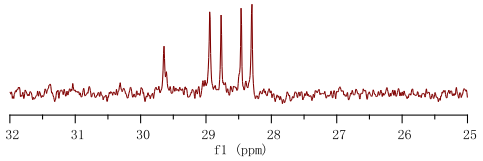

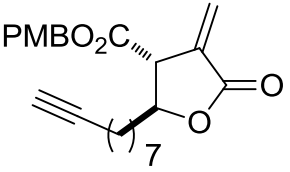

trans-**2-8e**

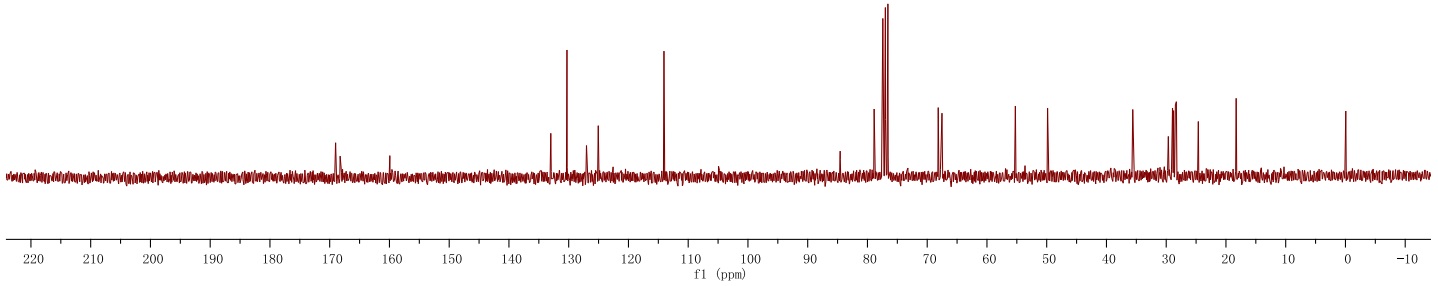

ap28gjy
ACF 300, CDCl3, 2031b-3, cis-C8, PMB

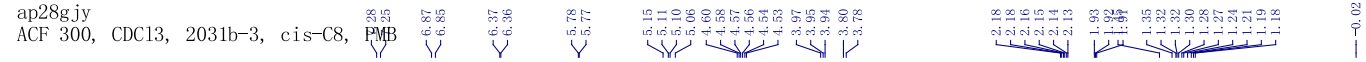

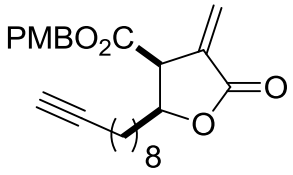

cis-**2-8f**

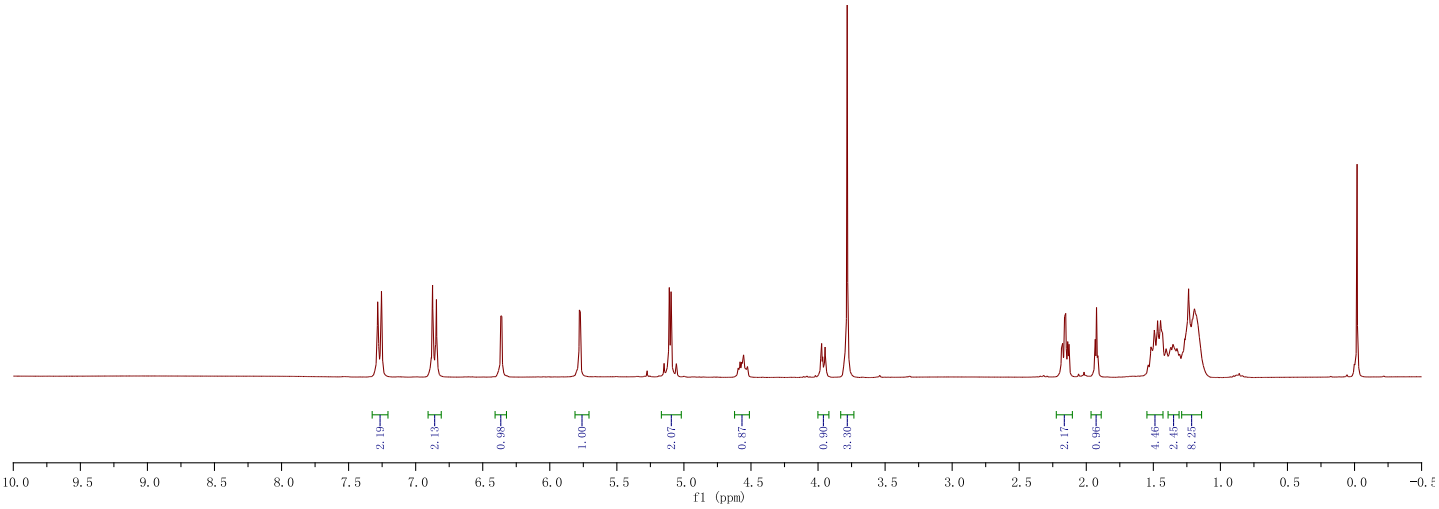

ap28gjy
ACF 300, CDCl3, 2031b-3, cis-C8, PMB

168.74
168.66
159.85
133.57
130.47
127.02
124.88
113.91
84.58
78.26
77.42
77.00
76.58
68.08
66.95
55.16
48.88
29.04
28.97
28.80
28.52
28.33
25.30
18.25
-0.11

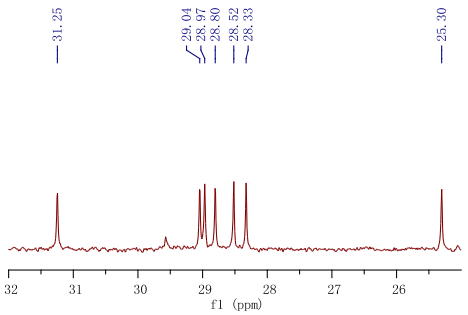

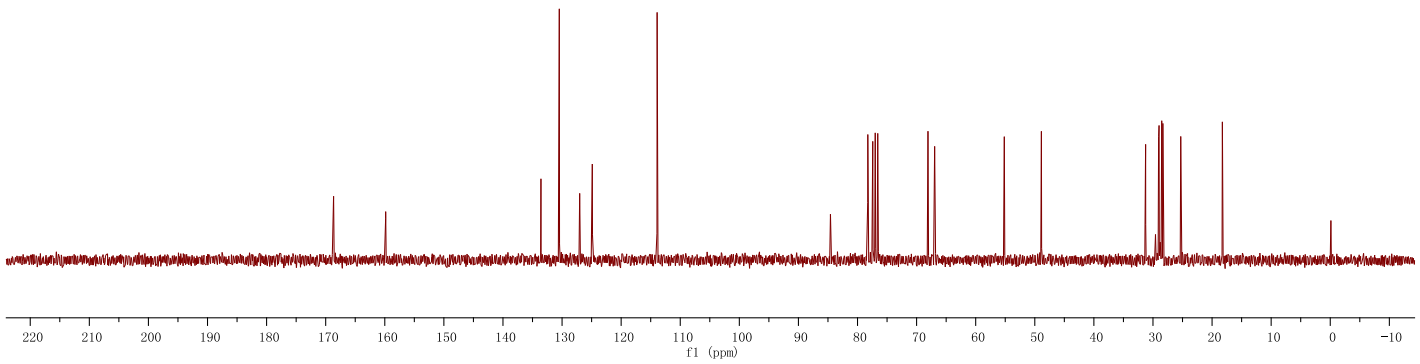

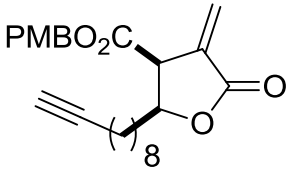

cis-**2-8f**

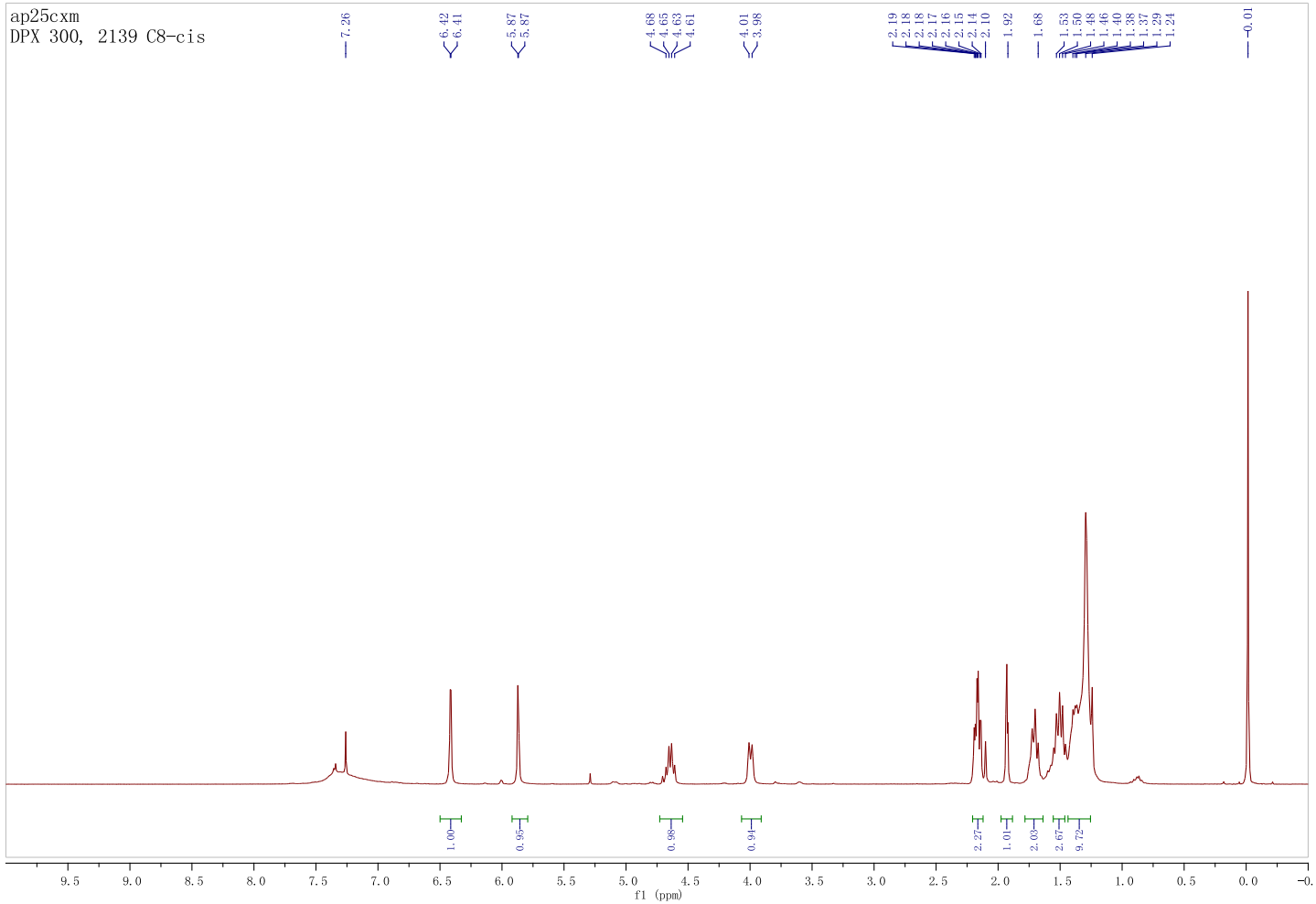
ap25cxm
DPX 300, 2139 C8-cis
7.26
6.42
6.41
5.87
5.87
4.68
4.65
4.63
4.61
4.01
3.98
2.19
2.18
2.18
2.17
2.16
2.15
2.14
2.10
1.92
1.68
1.53
1.50
1.48
1.46
1.40
1.38
1.37
1.29
1.24
-0.01
1.00
0.95
0.98
0.94
2.27
1.01
2.03
2.67
9.72
f1 (ppm)

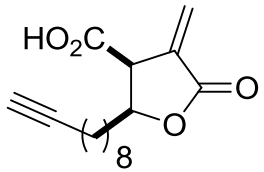
HO2C
O
O
8

cis-**2-9f**

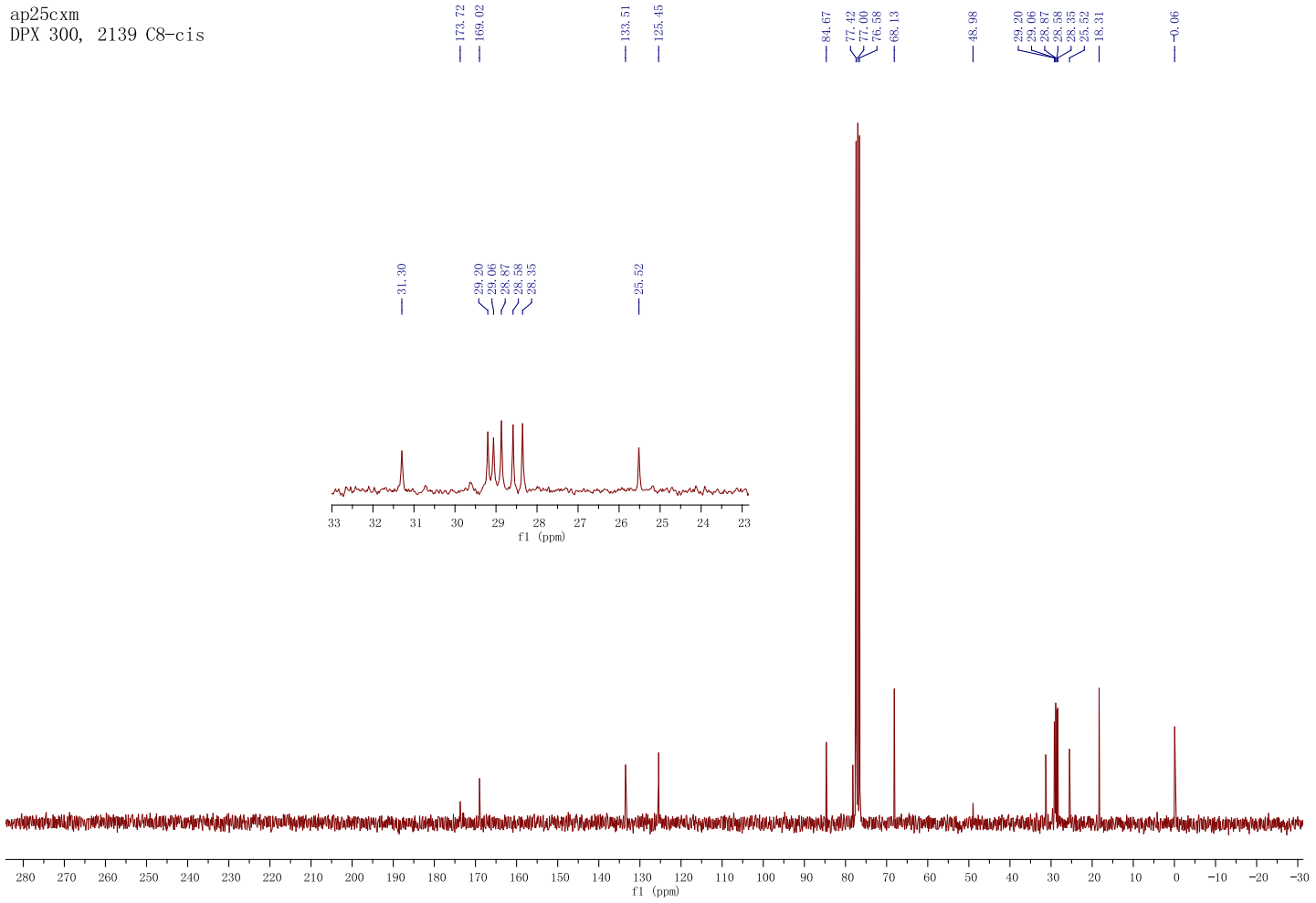
ap25cxm
DPX 300, 2139 C8-cis
173.72
169.02
133.51
125.45
84.67
77.42
77.00
76.58
68.13
48.98
29.20
29.06
28.87
28.58
28.35
25.52
18.31
-0.06
31.30
29.20
29.06
28.87
28.58
28.35
25.52
f1 (ppm)
f1 (ppm)

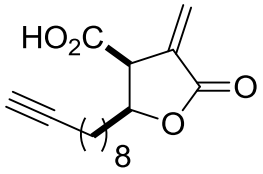
HO2C
O
O
8

cis-**2-9f**

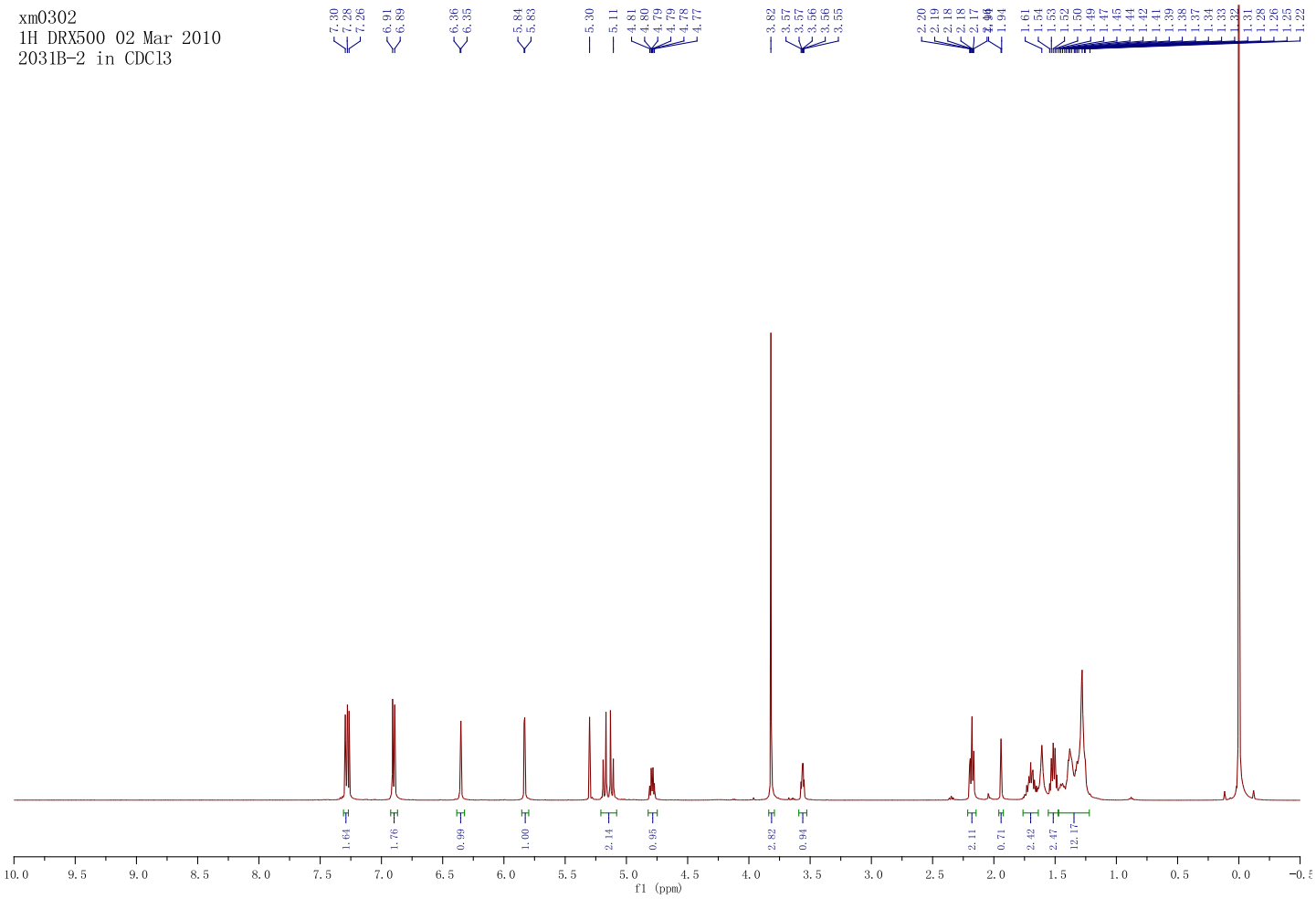
xm0302
1H DRX500 02 Mar 2010
2031B-2 in CDCl3
f1 (ppm)

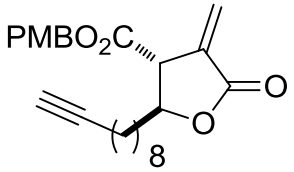
PMBO2C
O
O
8

trans-**2-8f**

fe19cxm
1H normal range AC300 2031b-2

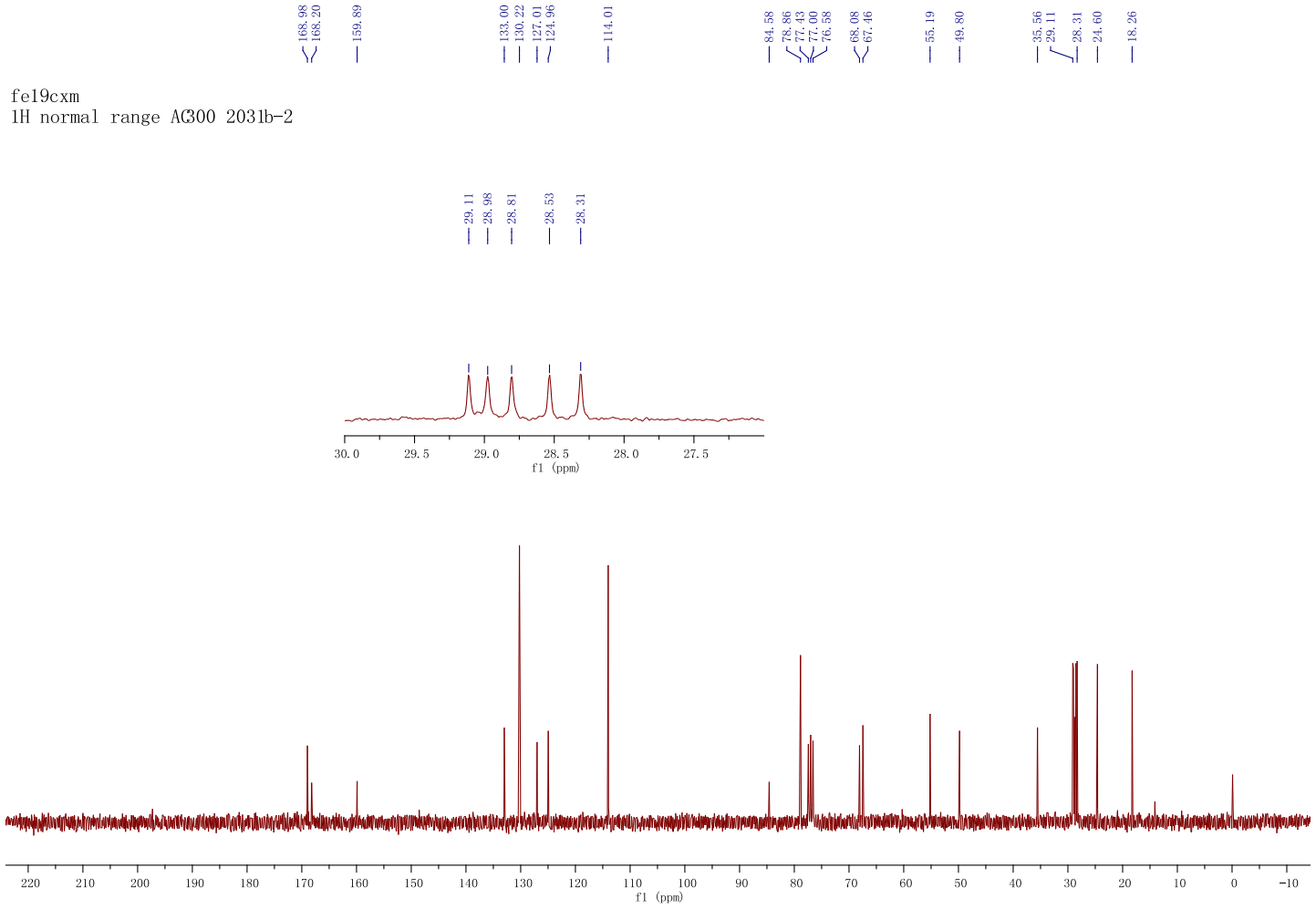

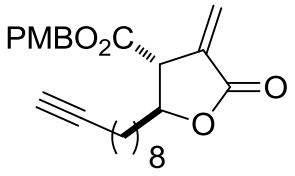

trans-**2-8f**


ap25cxm
DPX 300, 2139 C8=trans
7.66
7.26
6.44
6.43
6.01
6.00
4.82
4.80
4.78
4.76
3.61
3.60
3.59
2.19
2.18
2.16
2.15
2.14
2.13
2.09
1.91
1.68
1.50
1.43
1.39
1.37
1.36
1.34
1.32
1.29
1.23
0.02

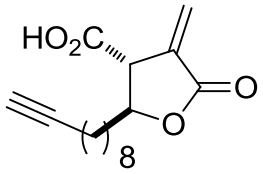
HO2C
O
O
8

trans-**2-9f**

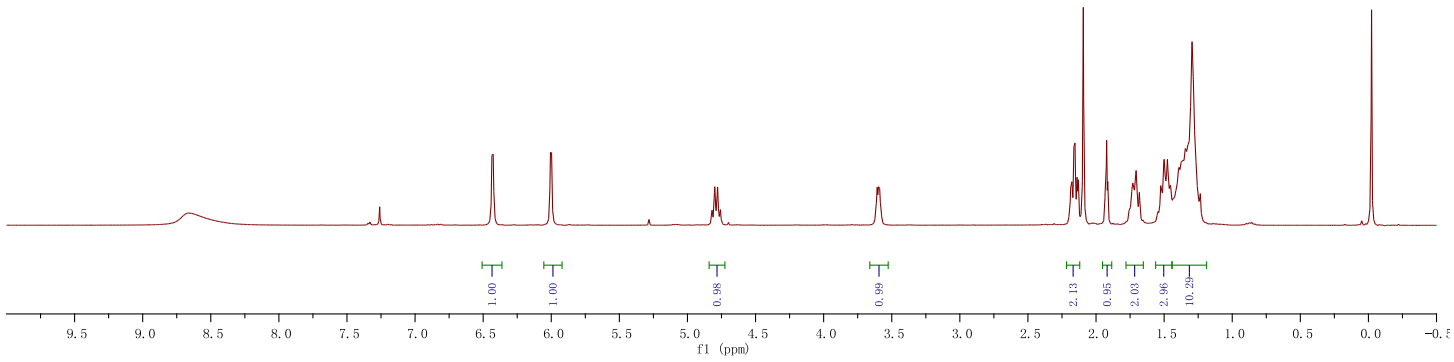
1.00
1.00
0.98
0.99
2.13
0.95
2.03
2.96
10.29
9.5
9.0
8.5
8.0
7.5
7.0
6.5
6.0
5.5
5.0
4.5
4.0
3.5
3.0
2.5
2.0
1.5
1.0
0.5
0.0
f1 (ppm)

ap25cxm
DPX 300, 2139 C8-trans

174.23
168.48
132.49
125.85
84.64
77.42
77.00
76.58
68.10
49.56
35.62
28.83
28.32
24.65
18.28
-0.09

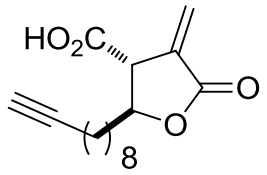

trans-**2-9f**

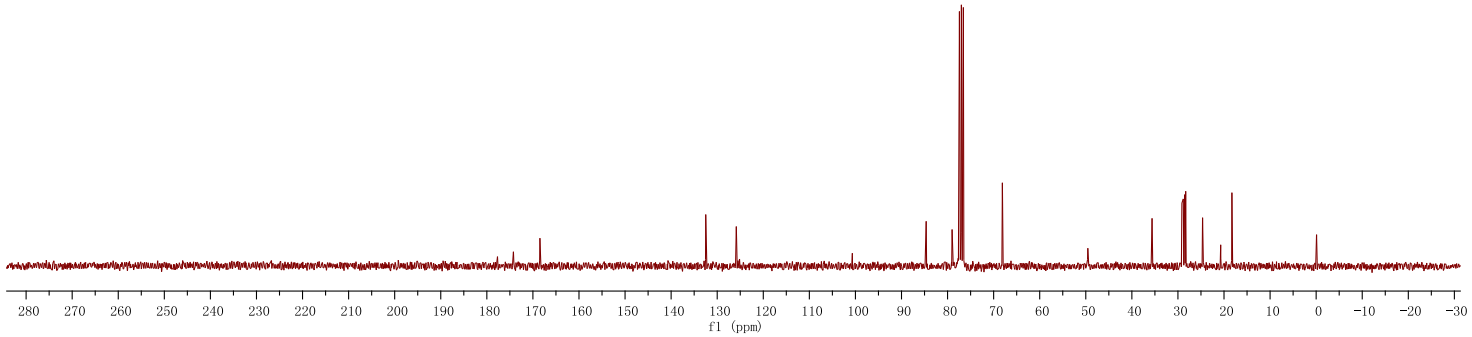

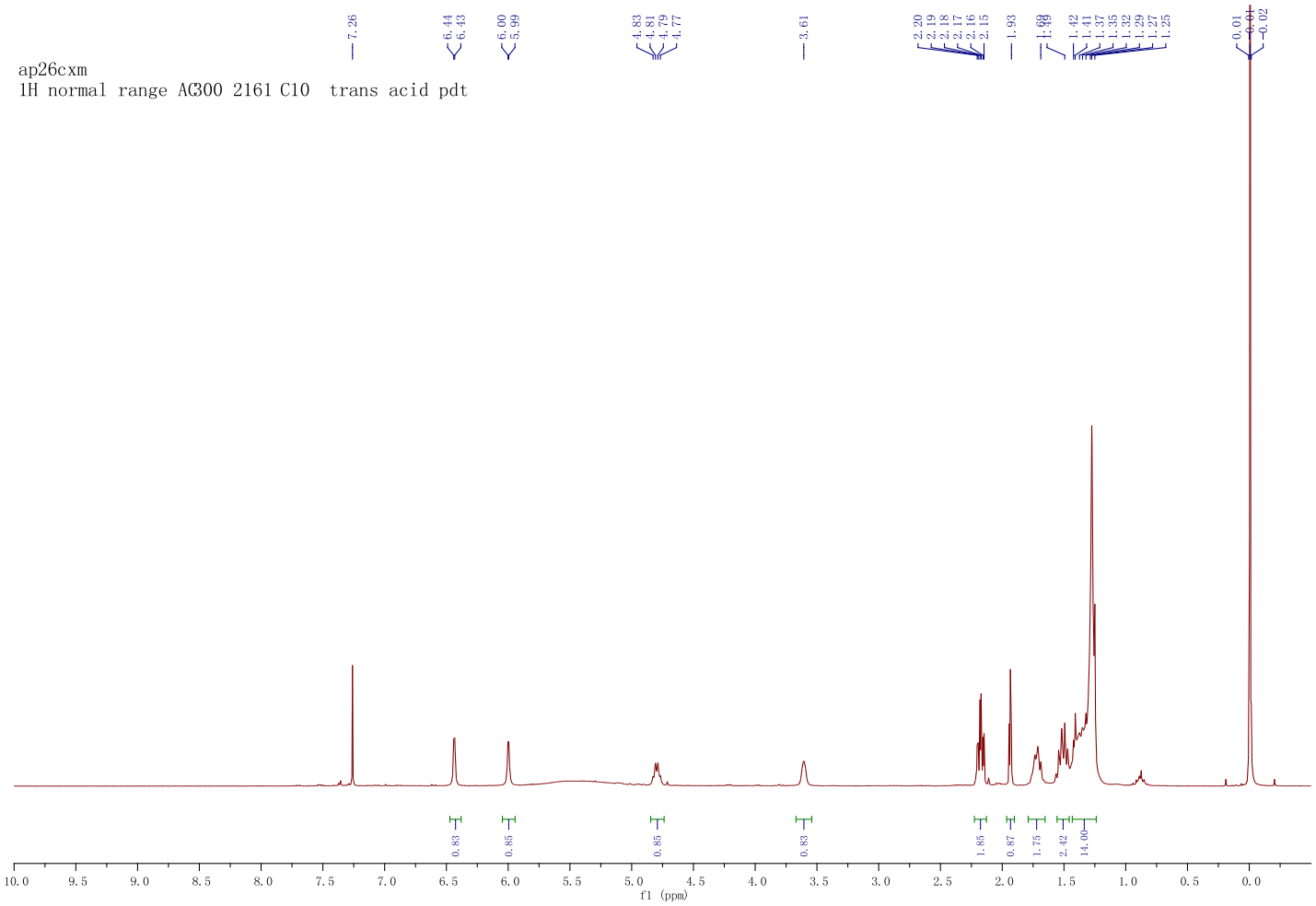
ap26cxm
1H normal range AC300 2161 C10 trans acid pdt
7.26
6.44
6.43
6.00
5.99
4.83
4.81
4.79
4.77
3.61
2.20
2.19
2.18
2.17
2.16
2.15
1.93
1.68
1.42
1.41
1.37
1.35
1.32
1.29
1.27
1.25
0.01
0.01
-0.02
0.83
0.85
0.85
0.83
1.85
0.87
1.75
2.42
14.00
10.0
9.5
9.0
8.5
8.0
7.5
7.0
6.5
6.0
5.5
5.0
4.5
4.0
3.5
3.0
2.5
2.0
1.5
1.0
0.5
0.0
f1 (ppm)

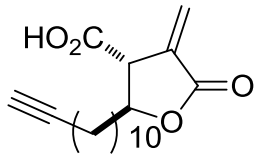
HO2C
O
O
10

trans-**2-9g**

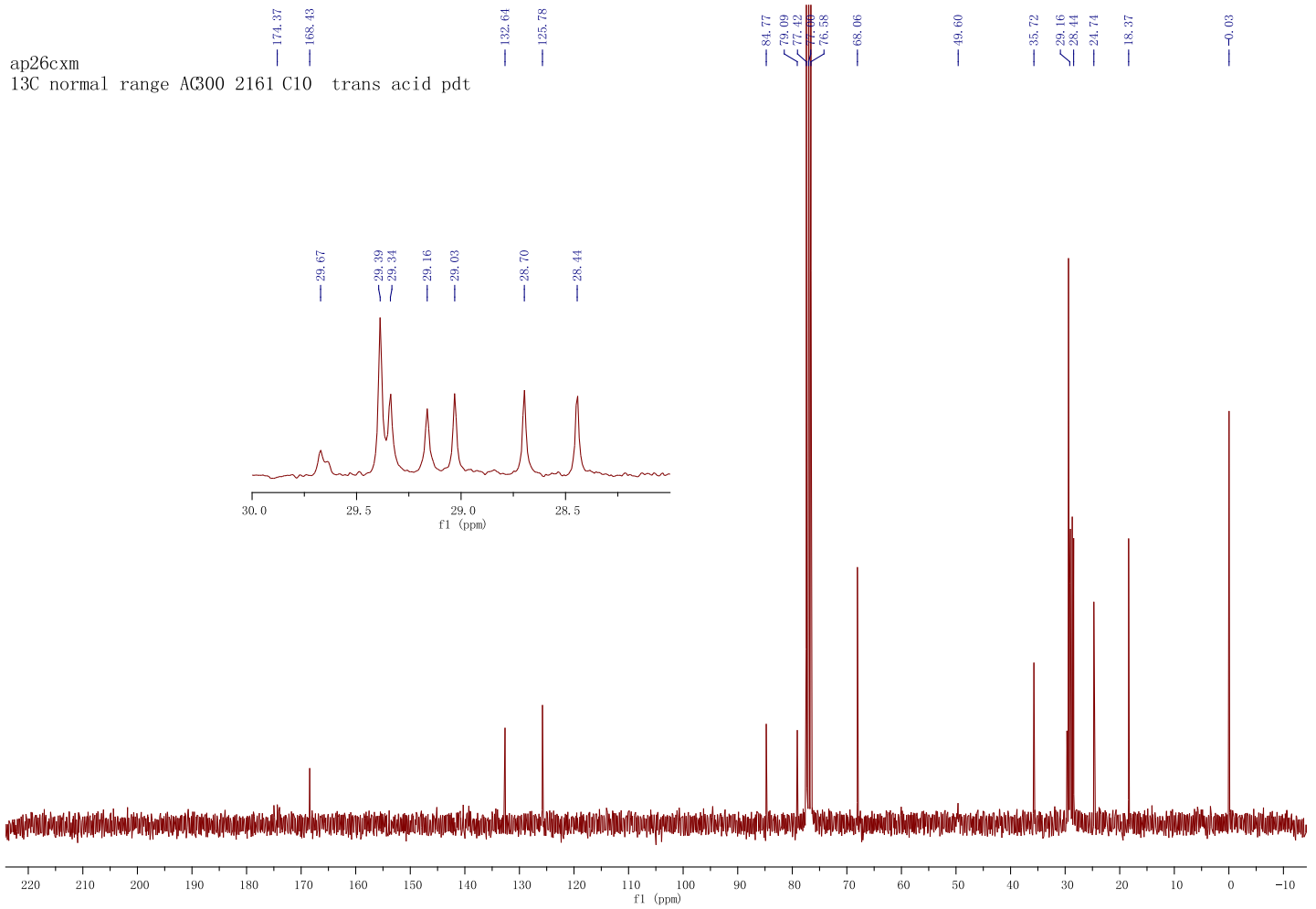
ap26cxm
13C normal range AC300 2161 C10 trans acid pdt
174.37
168.43
132.64
125.78
84.77
79.09
77.42
76.58
68.06
49.60
35.72
29.16
28.44
24.74
18.37
-0.03
29.67
29.39
29.34
29.16
29.03
28.70
28.44
30.0
29.5
29.0
28.5
f1 (ppm)
220
210
200
190
180
170
160
150
140
130
120
110
100
90
80
70
60
50
40
30
20
10
0
-10
f1 (ppm)

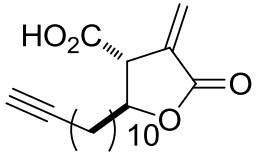
HO2C
O
O
10

trans-**2-9g**

ap19cxm
1H normal range AC300
trans C10-3

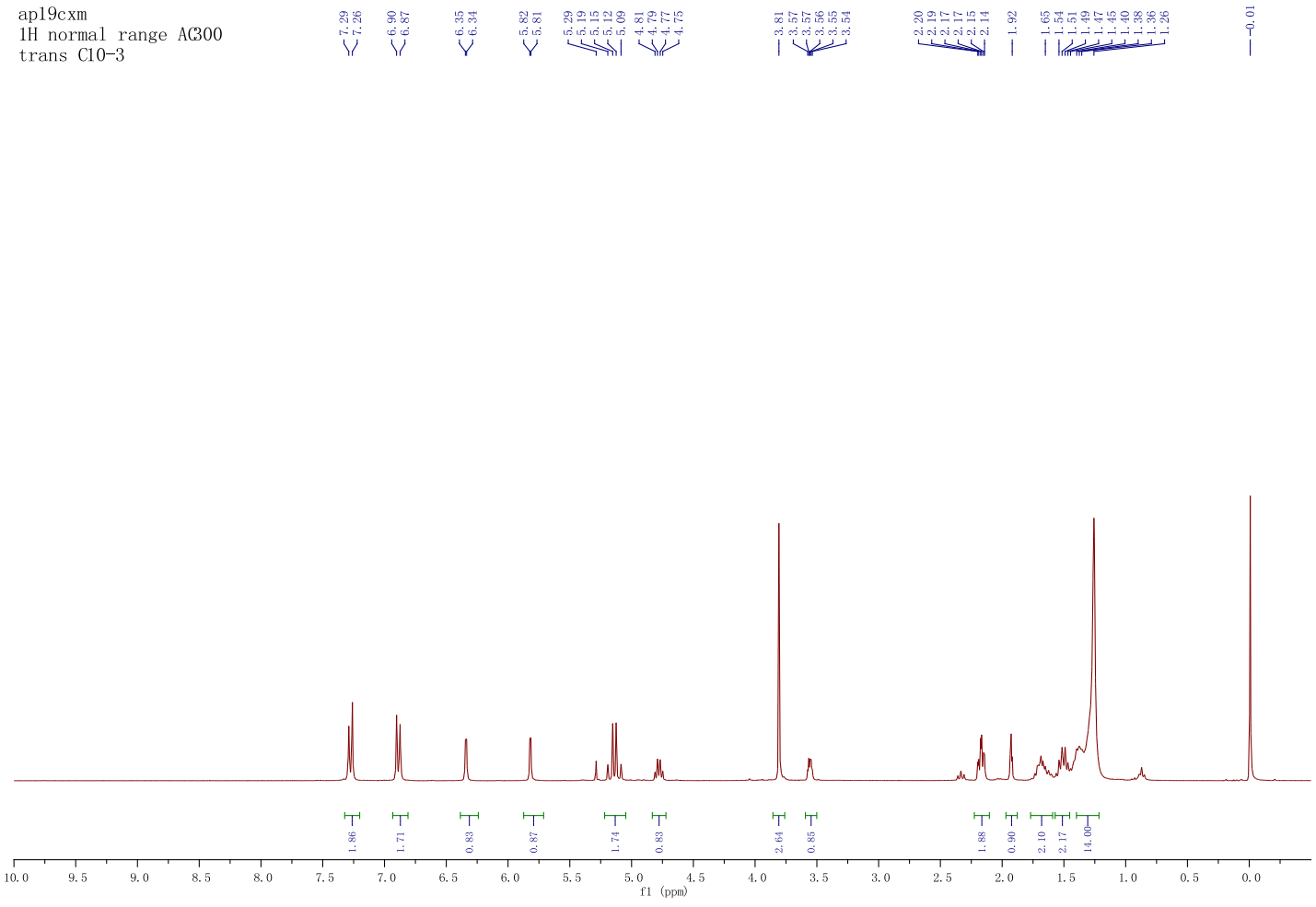

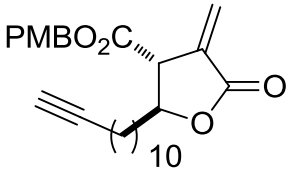

trans-**2-8g**

ap19cxm
1H normal range AC300
trans C10-3

169.04
168.27
159.94
133.05
130.27
127.05
125.01
114.07
84.72
78.94
77.42
77.00
76.58
68.03
67.52
55.24
49.87
35.64
29.10
28.43
24.67
18.34
-0.06

29.35
29.29
29.10
29.01
28.68
28.43

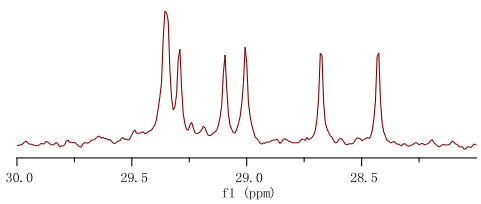

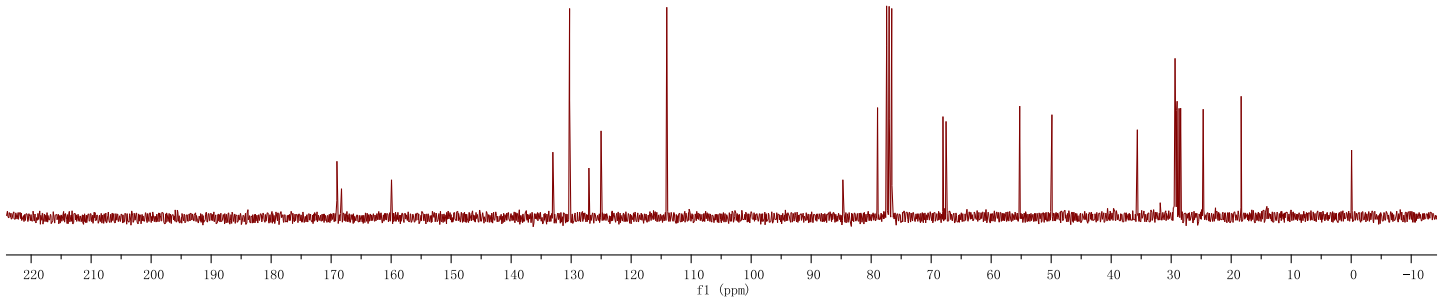

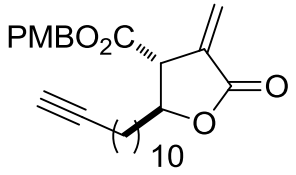

trans-**2-8g**

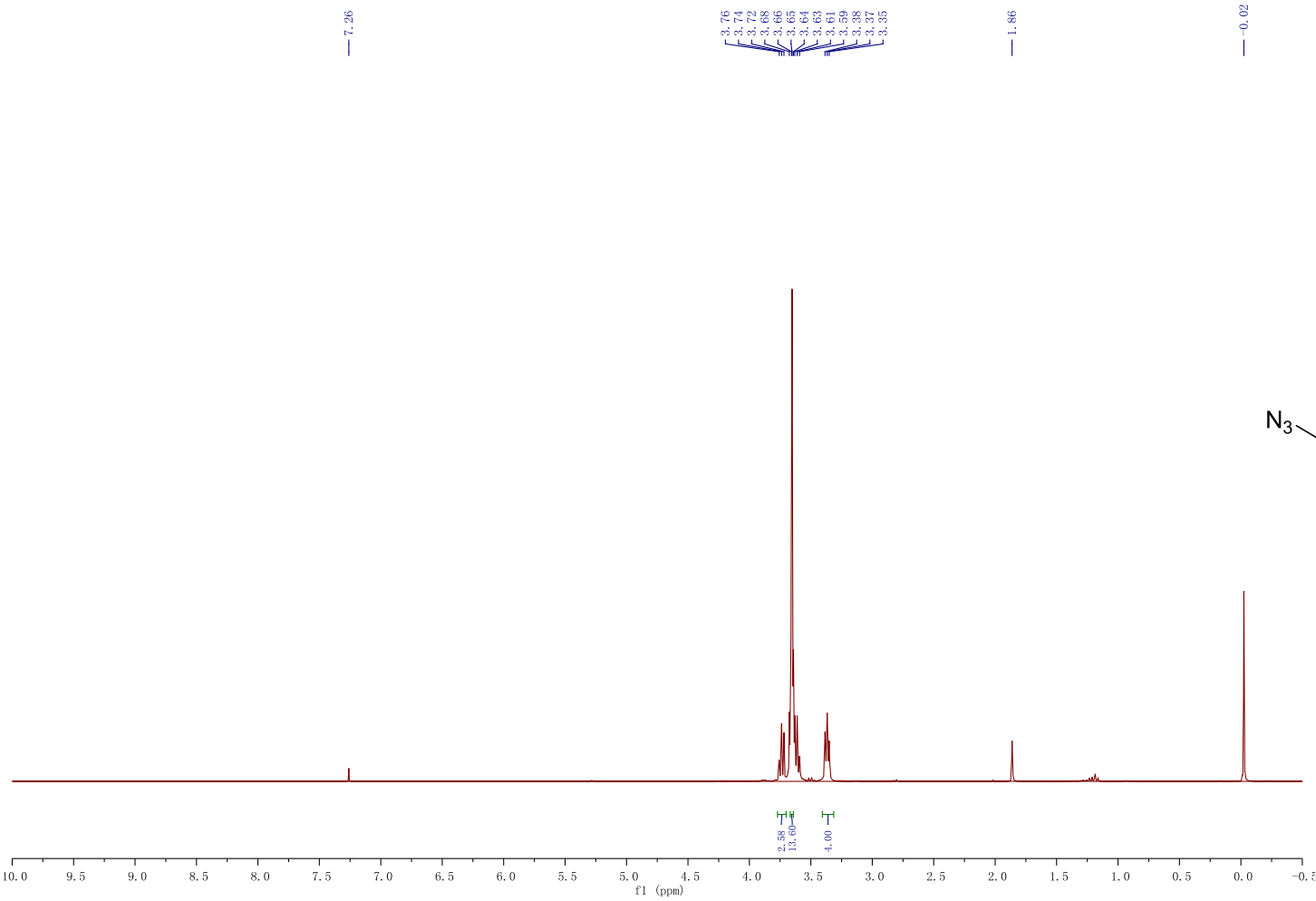
7.26
3.76
3.74
3.72
3.68
3.66
3.65
3.64
3.63
3.61
3.59
3.38
3.37
3.35
1.86
0.02
2.58
13.60
4.00
f1 (ppm)

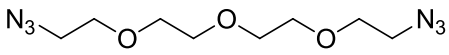
N3
O
O
O
N3

4-12

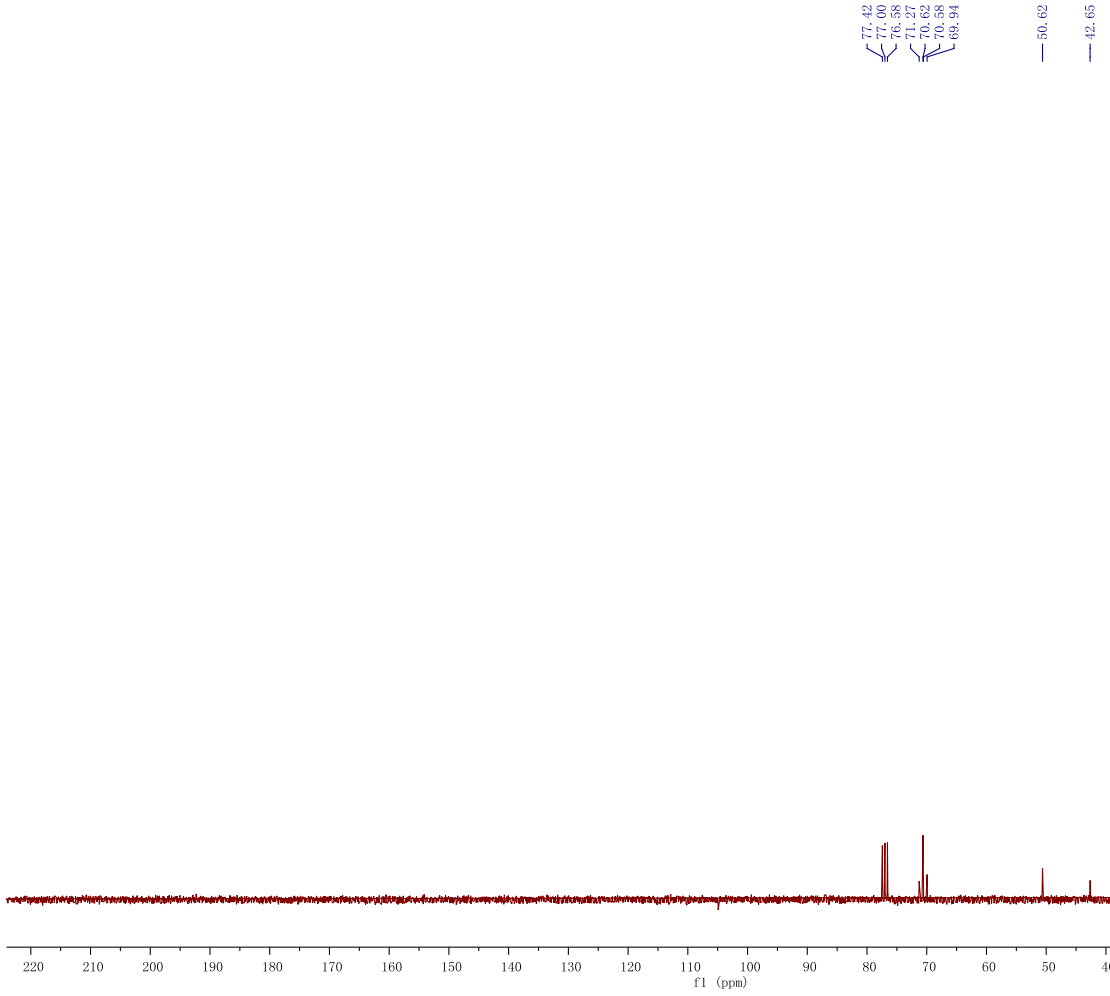
77.42
77.00
76.58
71.27
70.62
70.58
69.94
50.62
42.65
220
210
200
190
180
170
160
150
140
130
120
110
100
90
80
70
60
50
40
30
20
10
0
−10
f1 (ppm)

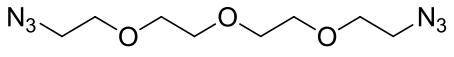
N3
O
O
O
N3

4-12

de10cxm
1H normal range AC300 3148

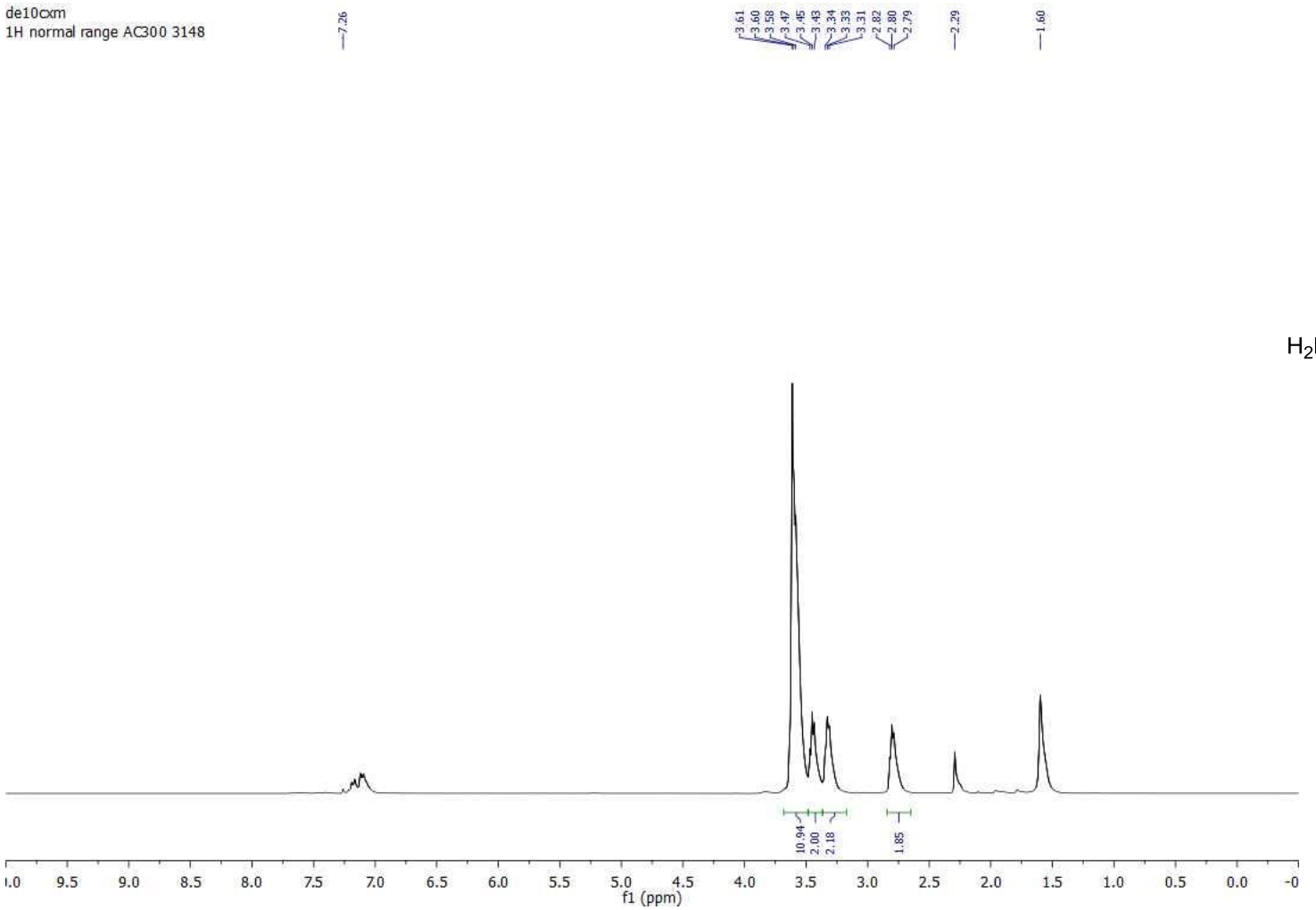

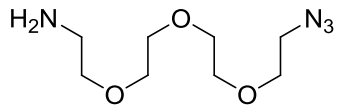

2-13

de10cxm
1H normal range AC300 3148

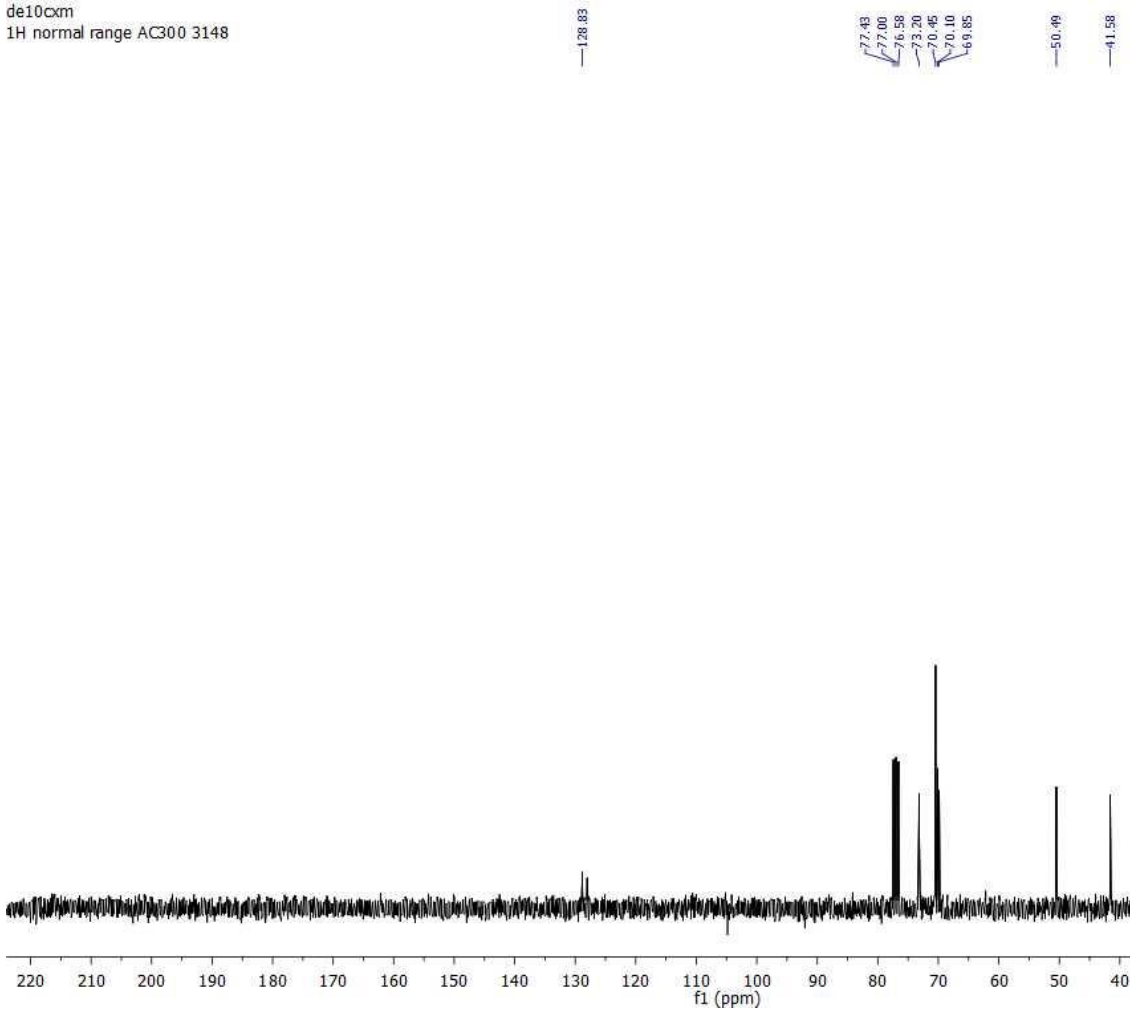

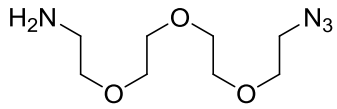

2-13

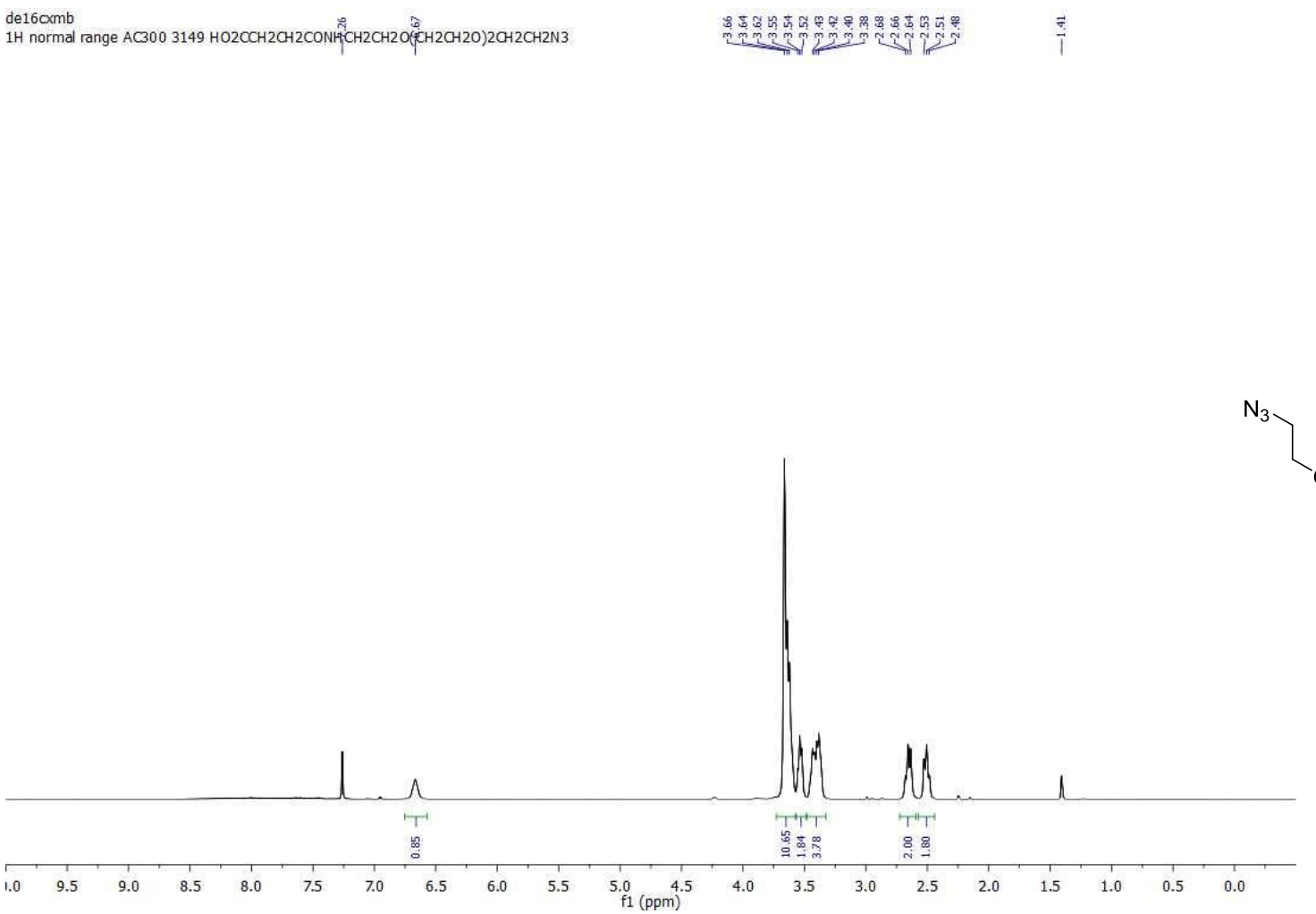
de16cxmb
1H normal range AC300 3149 HO2CCH2CH2CONHCH2CH2O(CH2CH2O)2CH2CH2N3
3.66
3.64
3.62
3.55
3.54
3.52
3.43
3.42
3.40
3.38
2.68
2.66
2.64
2.53
2.51
2.48
1.41
0.85
10.65
1.84
3.78
2.00
1.80
f1 (ppm)

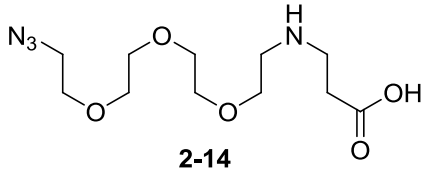
N3
O
H
N
O
O
OH
O

2-14

de16cxmb
1H normal range AC300 3149 HO2CCH2CH2CONHCH2CH2O(CH2CH2O)2CH2CH2N3

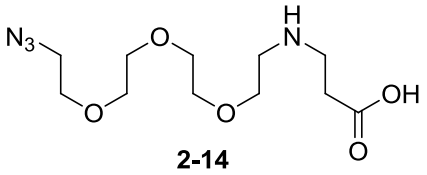

2-14

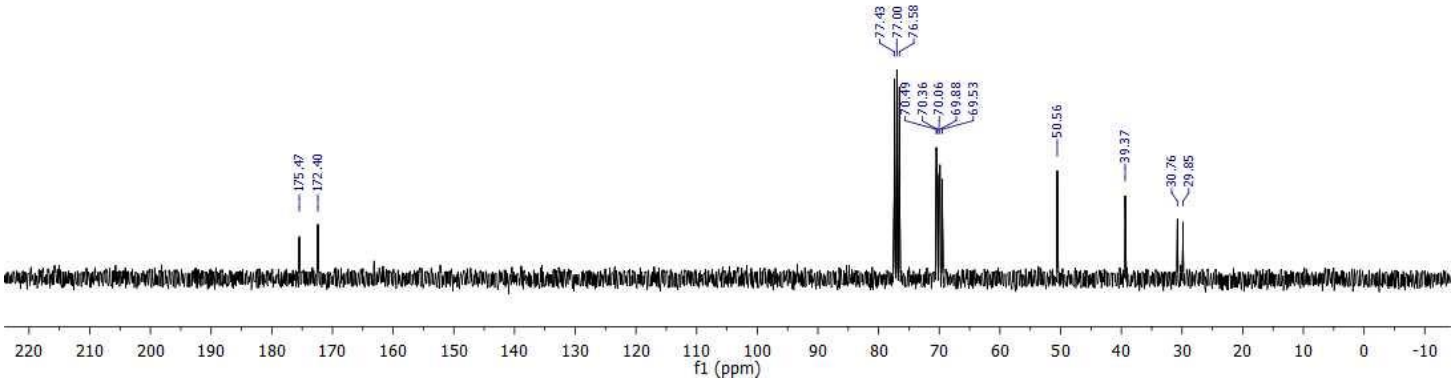

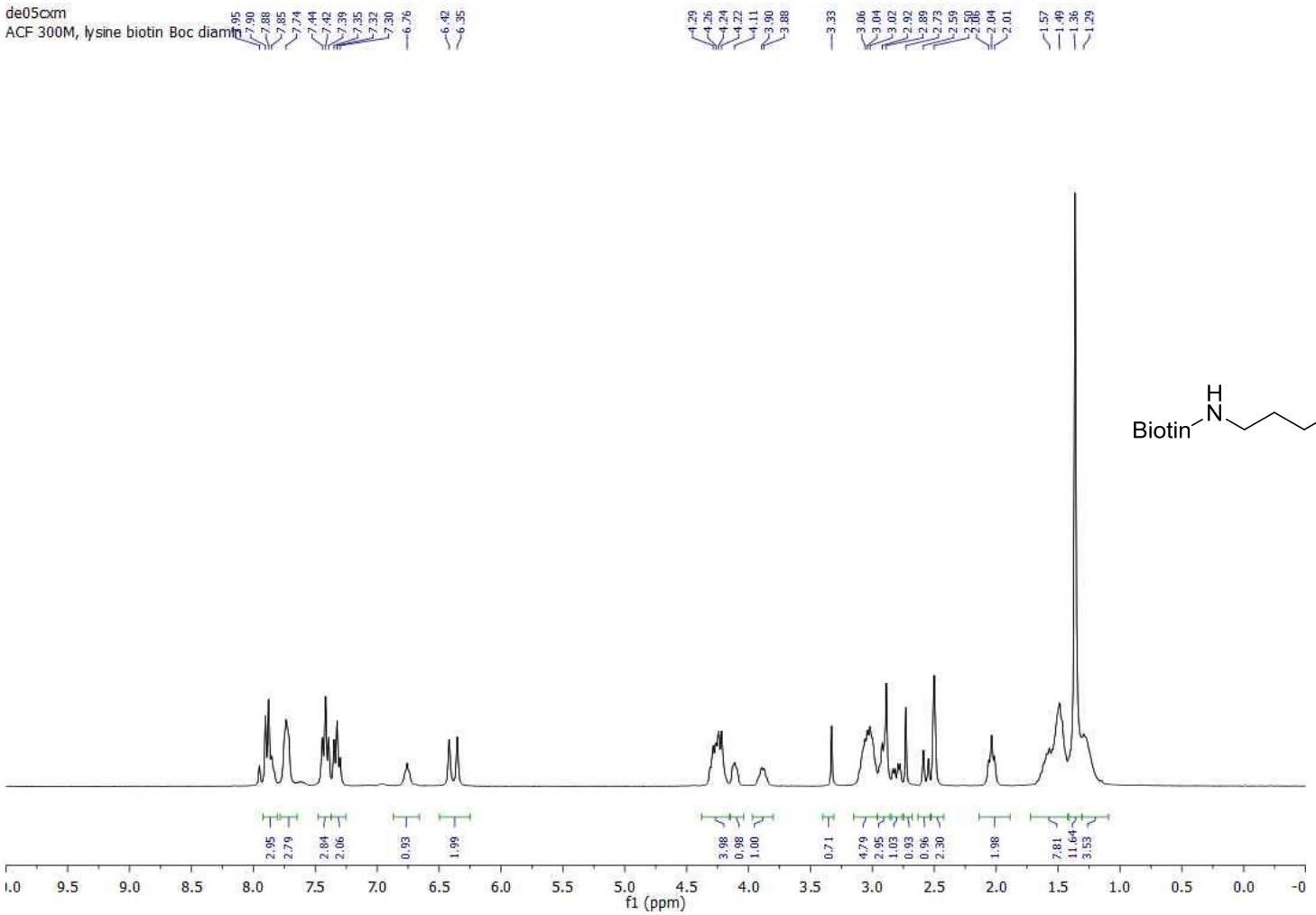
de05cxm
ACF 300M, lysine biotin Boc diamin
f1 (ppm)

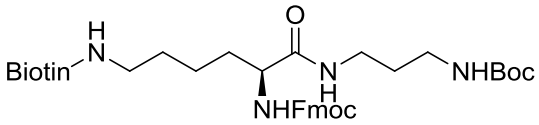
Biotin
H
N
O
N
H
NHBoc
NHFmoc

2-20

de05cxm
ACF 300M, lysine biotin Boc diamin

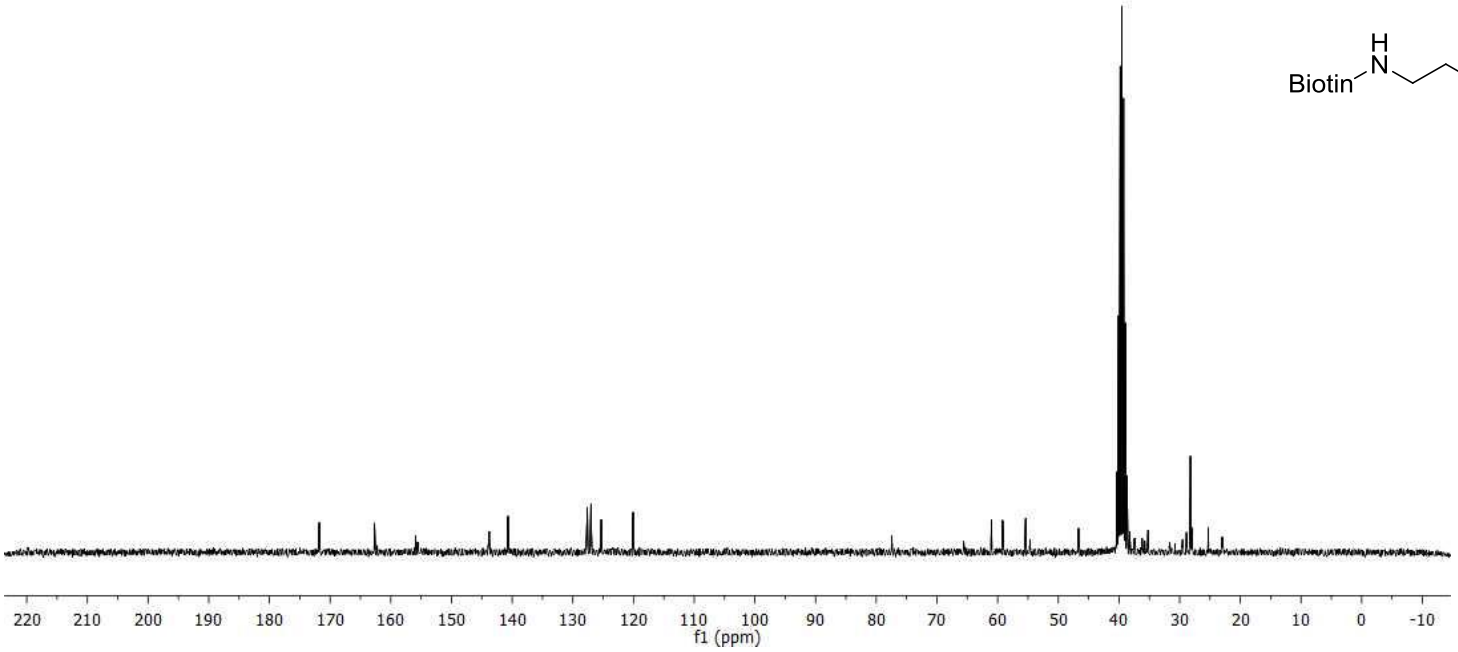

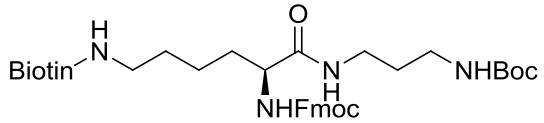

2-20

Chapter 3

The list of some representative proteins identified from LCMS experiments Table S2

				in vitro			***in situ***	
ID	Description	Mass	Score	emPAI	Peptides Matched	Score	emPAI	Peptides Matched
P78527	PRKDC_HUMAN DNA-dependent protein kinase catalytic subunit OS=Homo sapiens GN=PRKDC PE=1 SV=3	473749	431	0.13	22(9)	52	0.04	1(0)
H3BTN5	H3BTN5_HUMAN Pyruvate kinase (Fragment) OS=Homo sapiens GN=PKM PE=2 SV=1	53524	388	0.93	19(11)	127	0.27	6(3)
B2R5T5	B2R5T5_HUMAN Protein kinase, cAMP-dependent, regulatory, type I, alpha (Tissue specific extinguisher 1), isoform CRA_a OS=Homo sapiens GN=PRKAR1A PE=2 SV=1	43183	61	0.08	2(1)	34	0.08	1(0)
P60891	PRPS1_HUMAN Ribose-phosphate pyrophosphokinase 1 OS=Homo sapiens GN=PRPS1 PE=1 SV=2	35325	41	0.29	2(0)	46	0.18	1(0)
G3V5T9	G3V5T9_HUMAN Cyclin-dependent kinase 2 OS=Homo sapiens GN=CDK2 PE=2 SV=1	39553	39	0.17	2(0)	29	0.17	2(0)
Q5R3A8	Q5R3A8_HUMAN Tyrosine-protein kinase Fyn OS=Homo sapiens GN=FYN PE=2 SV=1	55205	25	0.11	4(0)	25	0.05	2(0)
E5RIU6	E5RIU6_HUMAN Cyclin-dependent kinase 1 (Fragment) OS=Homo sapiens GN=CDK1 PE=2 SV=2	21782	23	0.15	3(0)	40	0.33	2(0)

P00558	PGK1_HUMAN Phosphoglycerate kinase 1 OS=Homo sapiens GN=PGK1 PE=1 SV=3	44985	264	1.03	11(4)			
P15531	NDKA_HUMAN Nucleoside diphosphate kinase A OS=Homo sapiens GN=NME1 PE=1 SV=1	15422	100	0.82	3(1)			
B7Z7A9	B7Z7A9_HUMAN Phosphoglycerate kinase OS=Homo sapiens GN=PGK1 PE=2 SV=1	41802	59	0.43	4(0)			
P10398	ARAF_HUMAN Serine/threonine-protein kinase A-Raf OS=Homo sapiens GN=ARAF PE=1 SV=2	68341	55	0.13	2(1)			
H0YFA7	H0YFA7_HUMAN Bifunctional UDP-N-acetylglucosamine 2-epimerase/N-acetylmannosamine kinase OS=Homo sapiens GN=GNE PE=2 SV=2	79555	48	0.04	1(1)			
P13861	KAP2_HUMAN cAMP-dependent protein kinase type II-alpha regulatory subunit OS=Homo sapiens GN=PRKAR2A PE=1 SV=2	45832	47	0.07	4(1)			
B5BU16	B5BU16_HUMAN Mitogen-activated protein kinase kinase 6 OS=Homo sapiens GN=MAP2K6 PE=2 SV=1	37782	43	0.18	2(0)			
A4QPA9	A4QPA9_HUMAN Mitogen-activated protein kinase kinase 1 OS=Homo sapiens GN=MAP2K1 PE=2 SV=1	43753	40	0.08	2(1)			
B4DHB3	B4DHB3_HUMAN Phosphoglycerate kinase OS=Homo sapiens PE=2 SV=1	30258	38	0.11	1(0)			
Q5JT09	Q5JT09_HUMAN Uridine-cytidine kinase 1 OS=Homo sapiens GN=UCK1 PE=2 SV=1	32540	38	0.1	1(1)			
Q14DU5	Q14DU5_HUMAN ROCK2 protein OS=Homo sapiens GN=ROCK2 PE=2 SV=1	82724	36	0.04	1(0)			
Q01813	K6PP_HUMAN 6-phosphofructokinase type C OS=Homo sapiens GN=PFKP PE=1 SV=2	86454	34	0.12	3(0)			

G3V461	G3V461_HUMAN Creatine kinase B-type (Fragment) OS=Homo sapiens GN=CKB PE=2 SV=1	14383	32	0.24	1(0)			
P08237	K6PF_HUMAN 6-phosphofructokinase, muscle type OS=Homo sapiens GN=PFKM PE=1 SV=2	85984	31	0.05	1(0)			
P36507	MP2K2_HUMAN Dual specificity mitogen-activated protein kinase kinase 2 OS=Homo sapiens GN=MAP2K2 PE=1 SV=1	44681	31	0.07	2(0)			
F8WBH4	F8WBH4_HUMAN Interferon-induced, double-stranded RNA-activated protein kinase (Fragment) OS=Homo sapiens GN=EIF2AK2 PE=2 SV=1	11298	30	0.3	1(0)			
Q13131	AAPK1_HUMAN 5~-AMP-activated protein kinase catalytic subunit alpha-1 OS=Homo sapiens GN=PRKAA1 PE=1 SV=4	64596	30	0.1	2(0)			
P19367	HXK1_HUMAN Hexokinase-1 OS=Homo sapiens GN=HK1 PE=1 SV=3	103561	28	0.05	1(0)			
Q15208	STK38_HUMAN Serine/threonine-protein kinase 38 OS=Homo sapiens GN=STK38 PE=1 SV=1	54498	27	0.06	1(0)			
Q7Z7Q6	Q7Z7Q6_HUMAN Hexokinase II (Fragment) OS=Homo sapiens PE=2 SV=1	5875	25	0.61	1(0)			
M0QYH2	M0QYH2_HUMAN Bifunctional polynucleotide phosphatase/kinase OS=Homo sapiens GN=PNKP PE=4 SV=1	54120	23	0.06	1(0)			
F8VTV8	F8VTV8_HUMAN Cyclin-dependent kinase 4 OS=Homo sapiens GN=CDK4 PE=2 SV=1	22238	22	0.32	3(0)			
Q5JQ10	Q5JQ10_HUMAN Adenosine kinase, isoform CRA_a OS=Homo sapiens GN=ADK PE=2 SV=1	39078	20	0.08	1(0)			
Q9Y6E0	STK24_HUMAN Serine/threonine-protein kinase 24	49562	20	0.09	1(0)			

	OS=Homo sapiens GN=STK24 PE=1 SV=1							
J3KPD9	J3KPD9_HUMAN Nucleoside diphosphate kinase B OS=Homo sapiens GN=NME2 PE=3 SV=1	22522	19	0.15	1(0)			
P32298	GRK4_HUMAN G protein-coupled receptor kinase 4 OS=Homo sapiens GN=GRK4 PE=1 SV=3	67738	18	0.05	1(0)			
C1PHA2	C1PHA2_HUMAN Tyrosine-protein kinase receptor OS=Homo sapiens GN=KIF5B-ALK PE=2 SV=1	169283	16	0.02	3(0)			
H3BNI9	H3BNI9_HUMAN Casein kinase II subunit alpha~ (Fragment) OS=Homo sapiens GN=CSNK2A2 PE=2 SV=1	15632	16	0.22	2(0)			
Q05655	KPCD_HUMAN Protein kinase C delta type OS=Homo sapiens GN=PRKCD PE=1 SV=2	78652				39	0.05	1(1)
Q8IWB6	TEX14_HUMAN Inactive serine/threonine-protein kinase TEX14 OS=Homo sapiens GN=TEX14 PE=1 SV=2	169107				36	0.02	1(1)
H7C175	H7C175_HUMAN Serine/threonine-protein kinase LMTK1 OS=Homo sapiens GN=AATK PE=2 SV=2	135361				32	0.02	1(0)
Q4LE51	Q4LE51_HUMAN PIK3CA variant protein (Fragment) OS=Homo sapiens GN=PIK3CA variant protein PE=2 SV=1	126129				16	0.03	1(0)

NMR Spectra of representative compounds

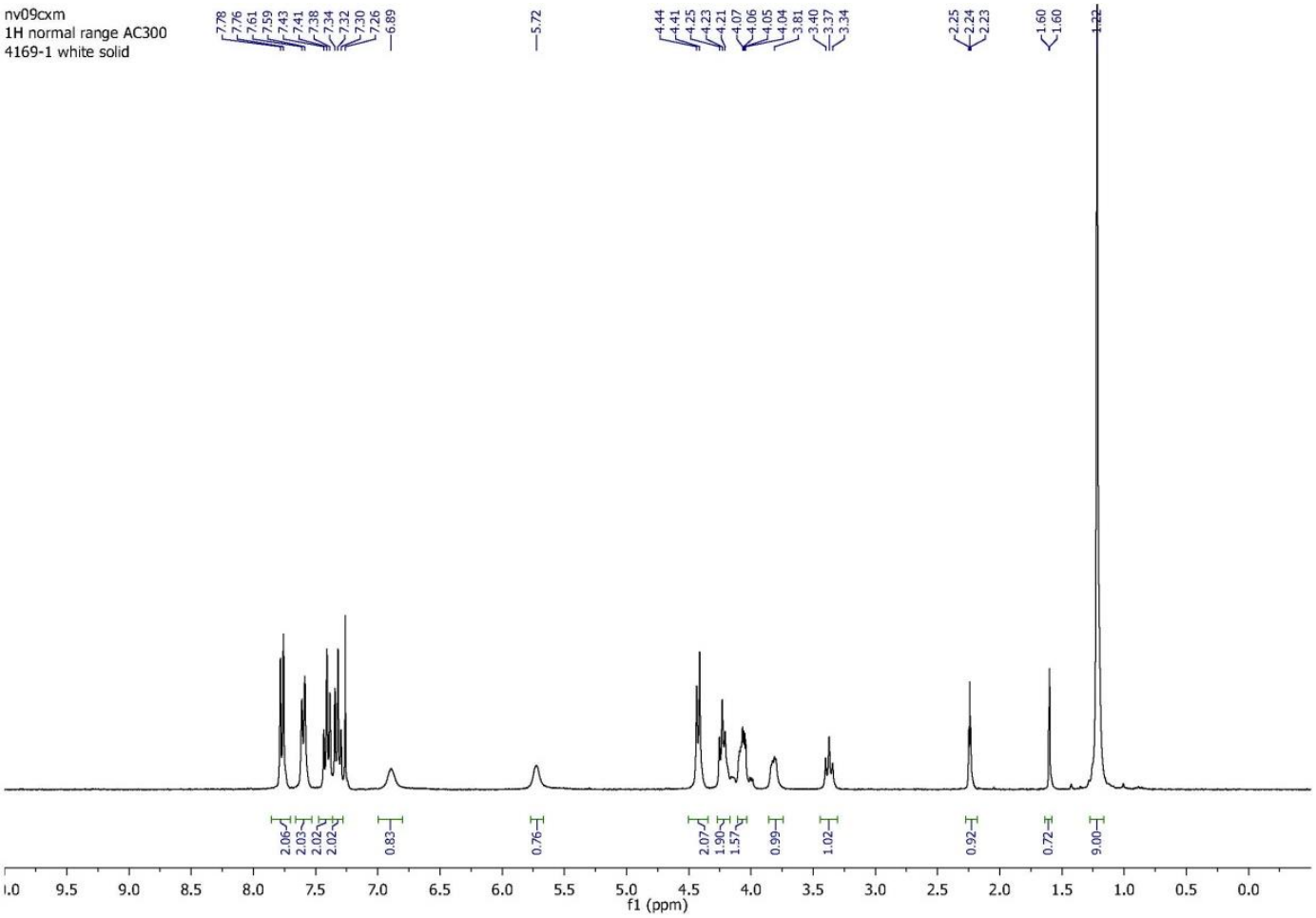
nv09cxm
1H normal range AC300
4169-1 white solid
7.78
7.76
7.61
7.59
7.43
7.41
7.38
7.34
7.32
7.30
7.26
6.89
5.72
4.44
4.41
4.25
4.23
4.21
4.07
4.06
4.05
4.04
3.81
3.40
3.37
3.34
2.25
2.24
2.23
1.60
1.60
1.00
2.06
2.03
2.02
2.02
0.83
0.76
2.07
1.90
1.57
0.99
1.02
0.92
0.72
9.00
f1 (ppm)

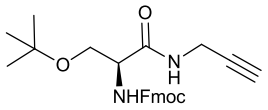
O
O
N
H
NHFmoc

3-2

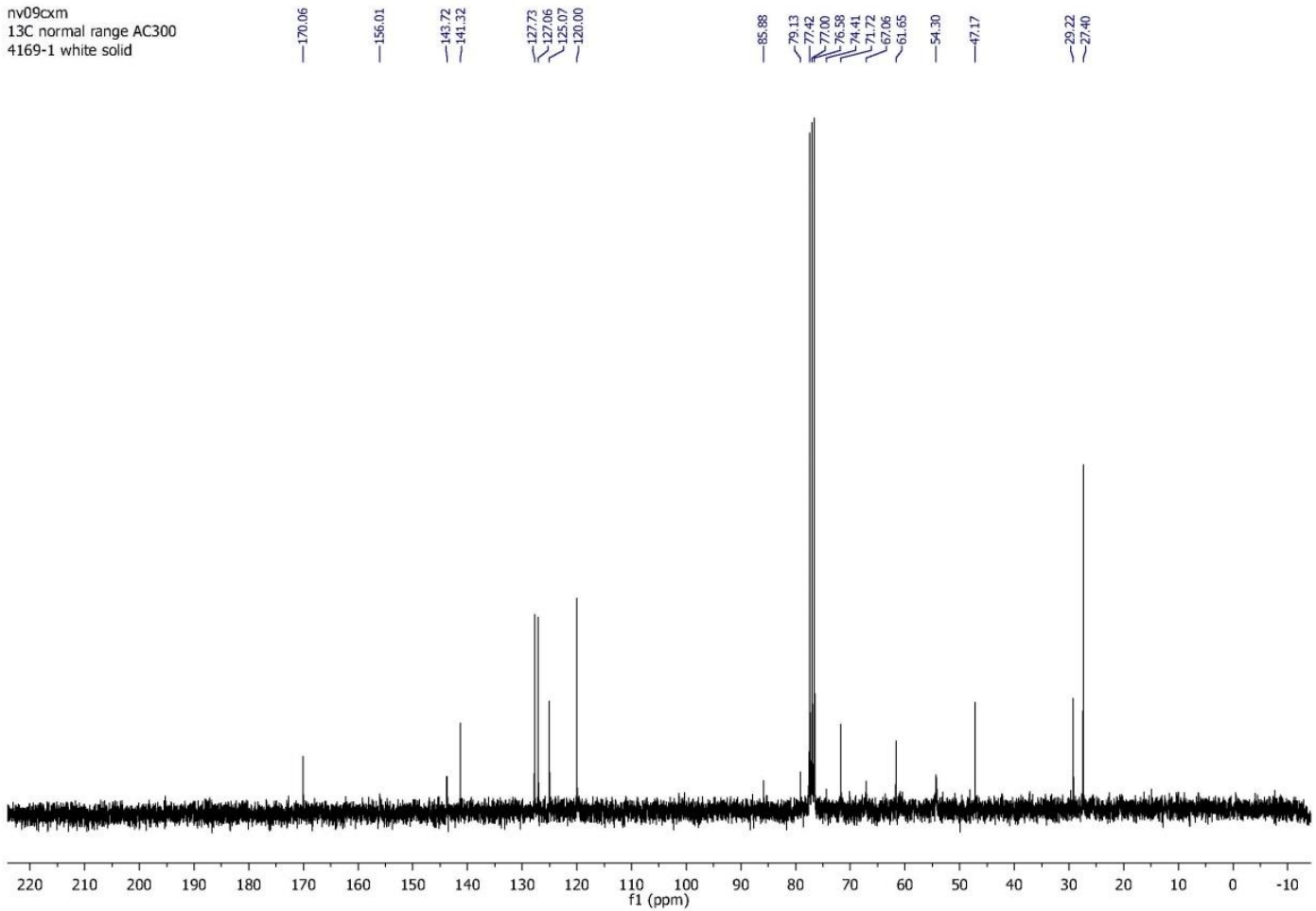
nv09cxm
13C normal range AC300
4169-1 white solid
170.06
156.01
143.72
141.32
127.73
127.06
125.07
120.00
85.88
79.13
77.42
77.00
76.58
74.41
71.72
67.06
61.65
54.30
47.17
29.22
27.40
220 210 200 190 180 170 160 150 140 130 120 110 100 90 80 70 60 50 40 30 20 10 0 -10
f1 (ppm)

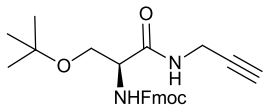
O
O
N
H
NHFmoc

3-2

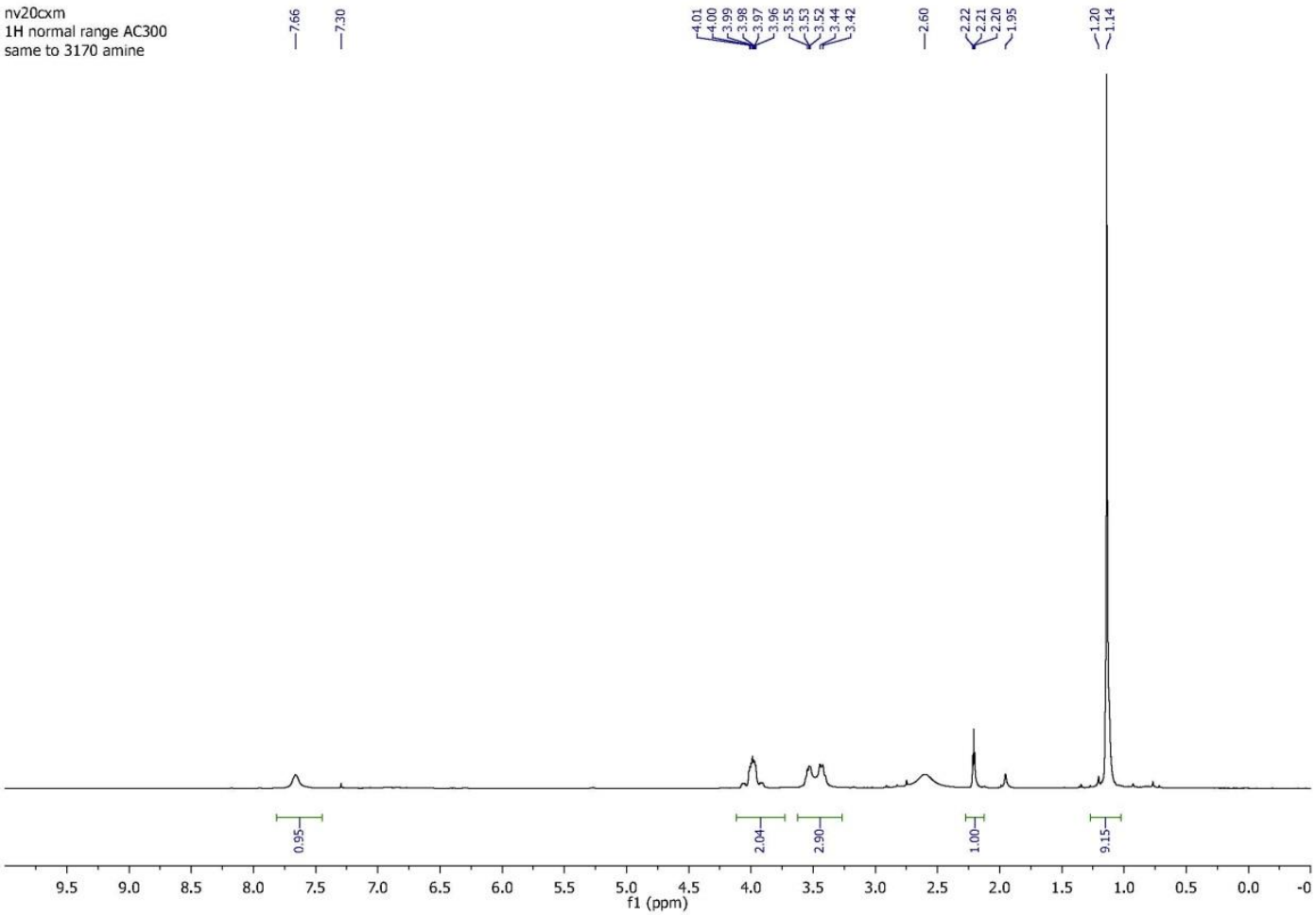
nv20cxm
1H normal range AC300
same to 3170 amine
7.66
7.30
4.01
4.00
3.99
3.98
3.97
3.96
3.55
3.53
3.52
3.44
3.42
2.60
2.22
2.21
2.20
1.95
1.20
1.14
0.95
2.04
2.90
1.00
9.15
9.5 9.0 8.5 8.0 7.5 7.0 6.5 6.0 5.5 5.0 4.5 4.0 3.5 3.0 2.5 2.0 1.5 1.0 0.5 0.0 -0
f1 (ppm)

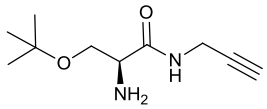
O
O
N
H
NH2

3-3

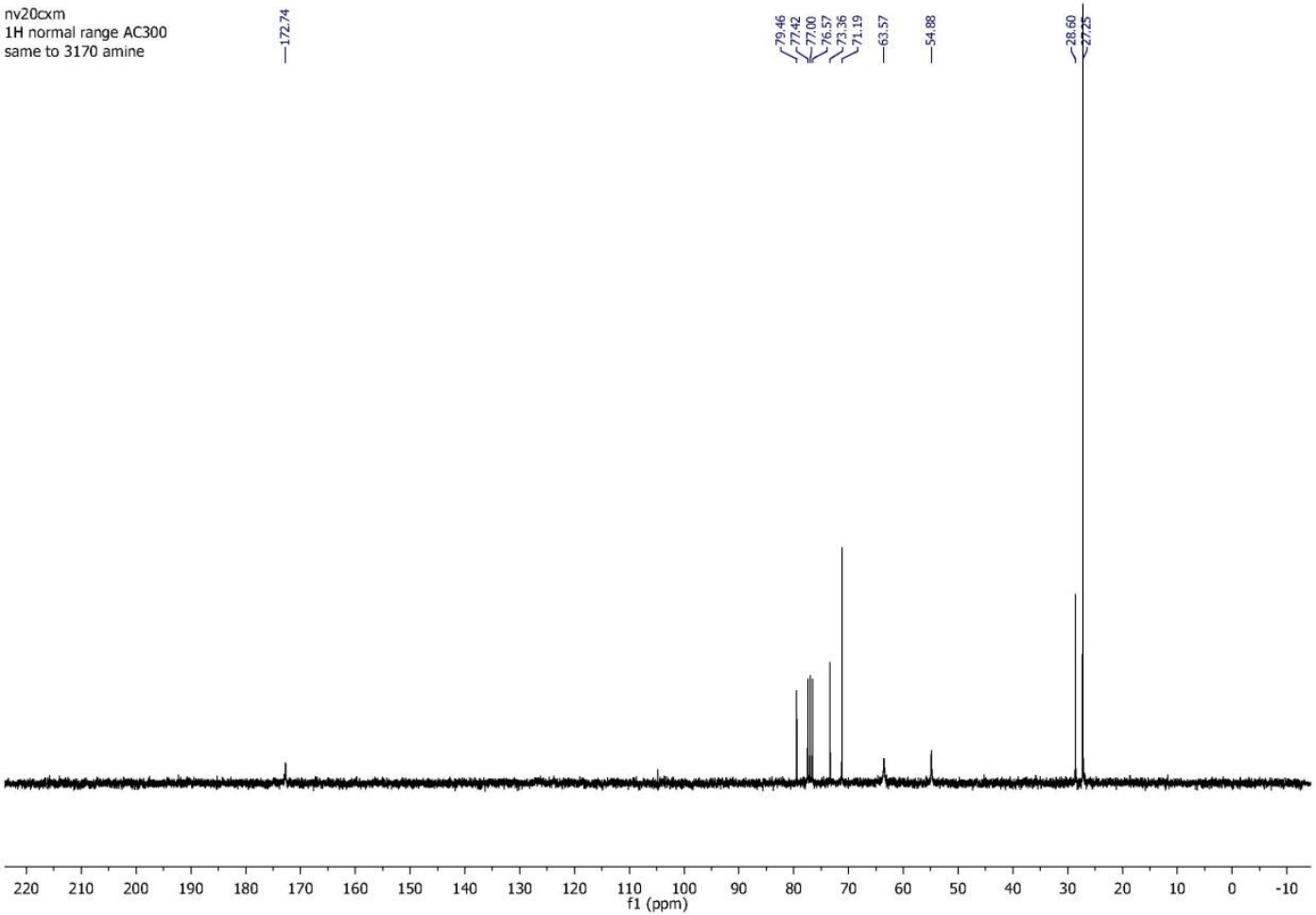
nv20cxm
1H normal range AC300
same to 3170 amine
172.74
79.46
77.42
77.00
76.57
73.36
71.19
63.57
54.88
28.60
27.25
220 210 200 190 180 170 160 150 140 130 120 110 100 90 80 70 60 50 40 30 20 10 0 -10
f1 (ppm)

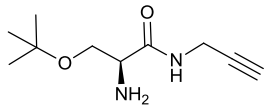
O
O
N
H
NH2

3-3

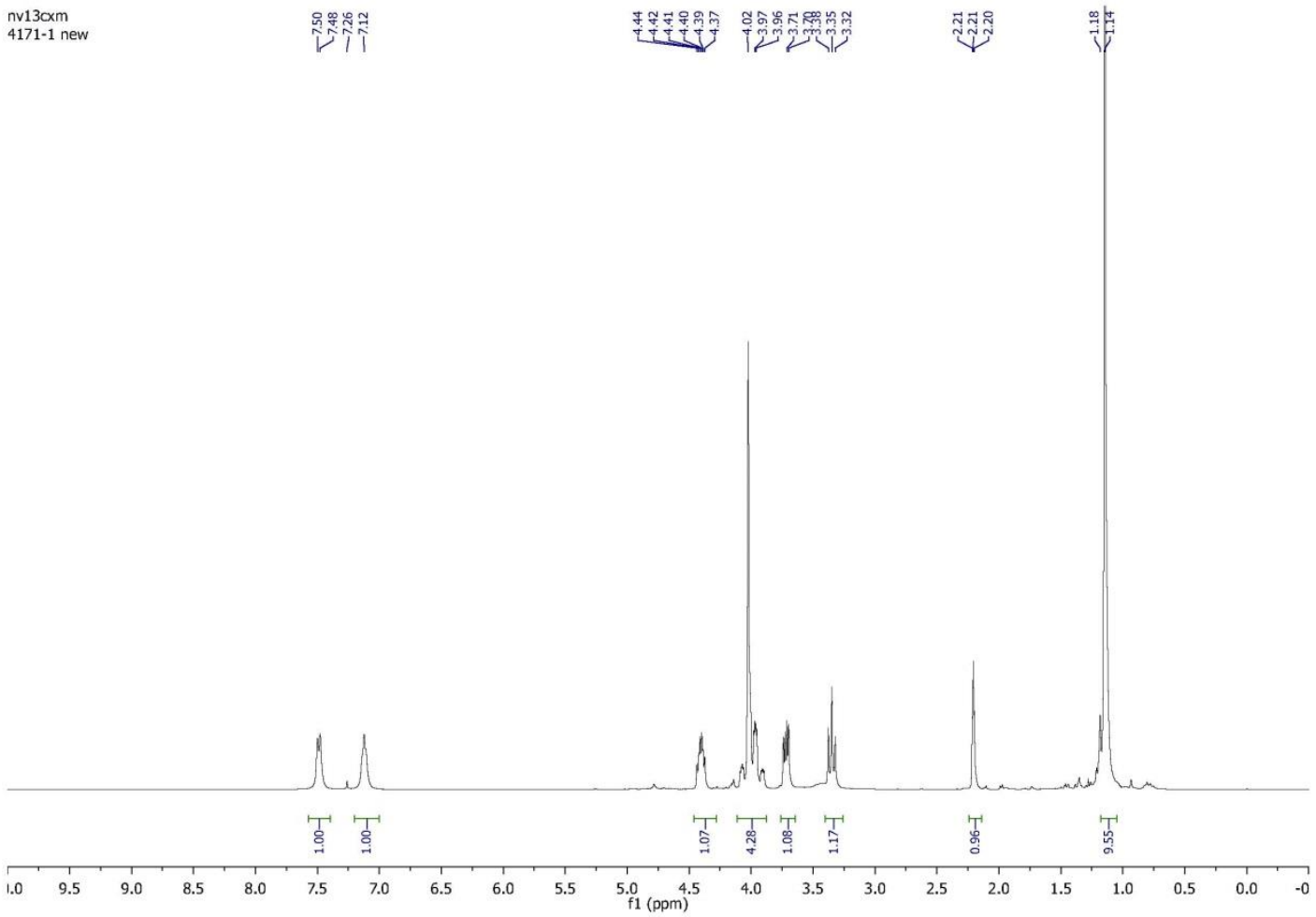
nv13cxm
4171-1 new
7.50
7.48
7.26
7.12
4.44
4.42
4.41
4.40
4.39
4.37
4.02
3.97
3.96
3.71
3.70
3.38
3.35
3.32
2.21
2.21
2.20
1.18
1.14
1.00
1.00
1.07
4.28
1.08
1.17
0.96
9.55
f1 (ppm)

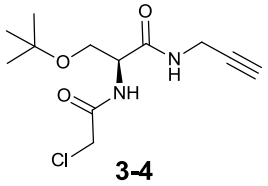
O
O
N
H
O
NH
Cl

3-4

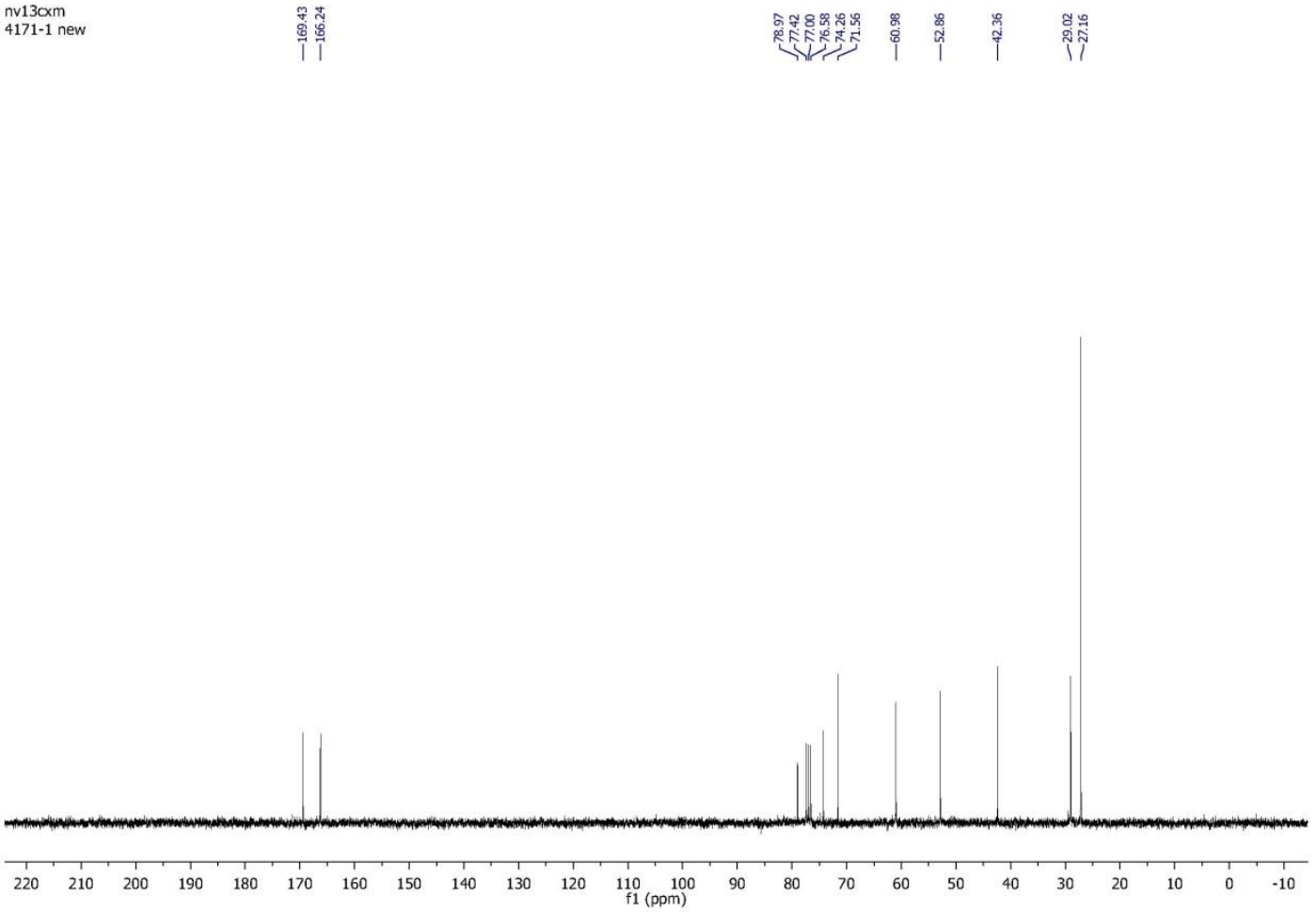
nv13cxm
4171-1 new
169.43
166.24
78.97
77.42
77.00
76.58
74.26
71.56
60.98
52.86
42.36
29.02
27.16
220 210 200 190 180 170 160 150 140 130 120 110 100 90 80 70 60 50 40 30 20 10 0 -10
f1 (ppm)

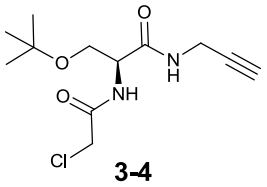
O
O
N
H
O
NH
Cl

3-4

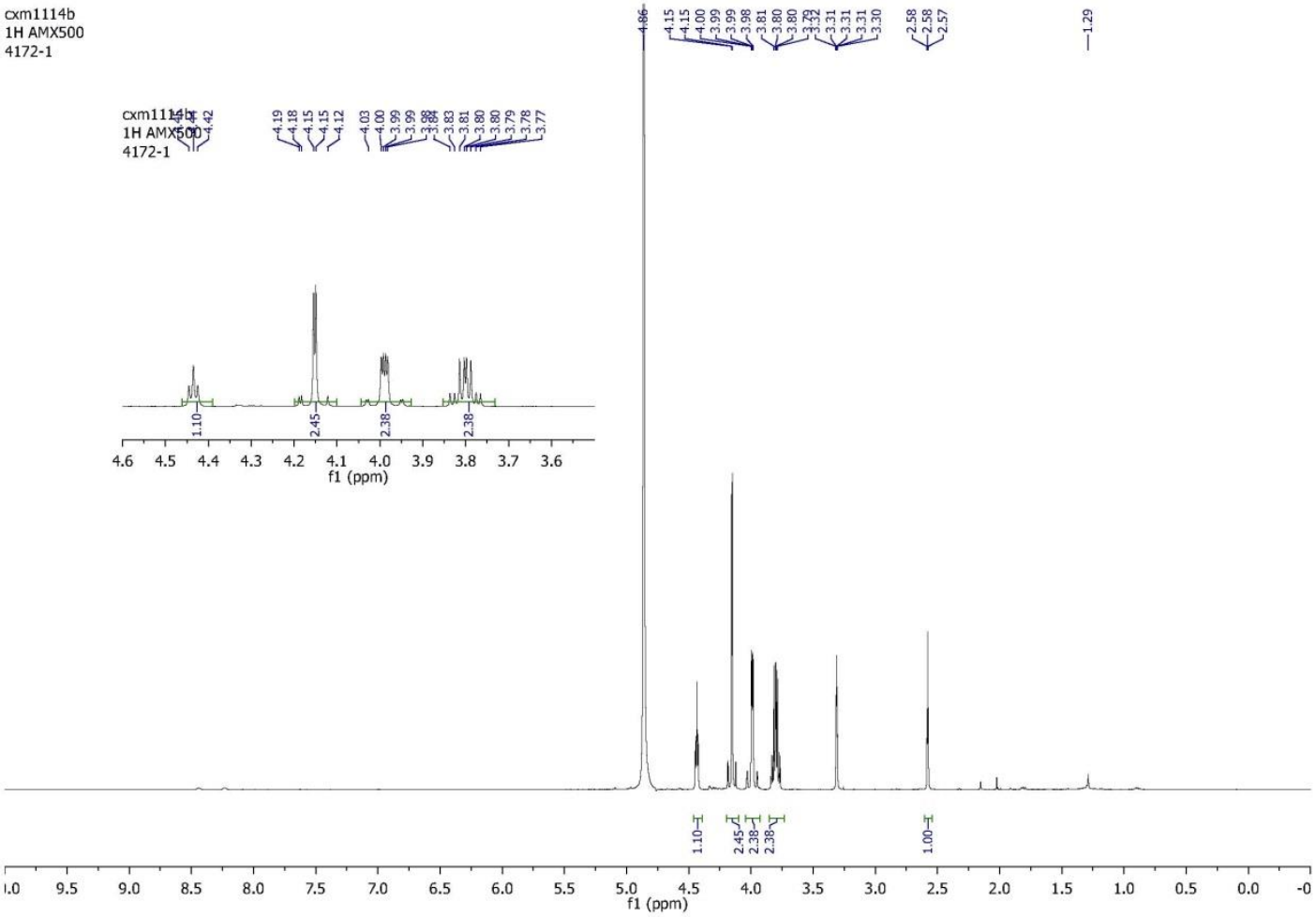

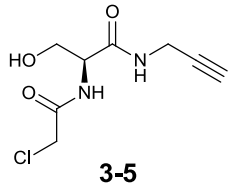

3-5

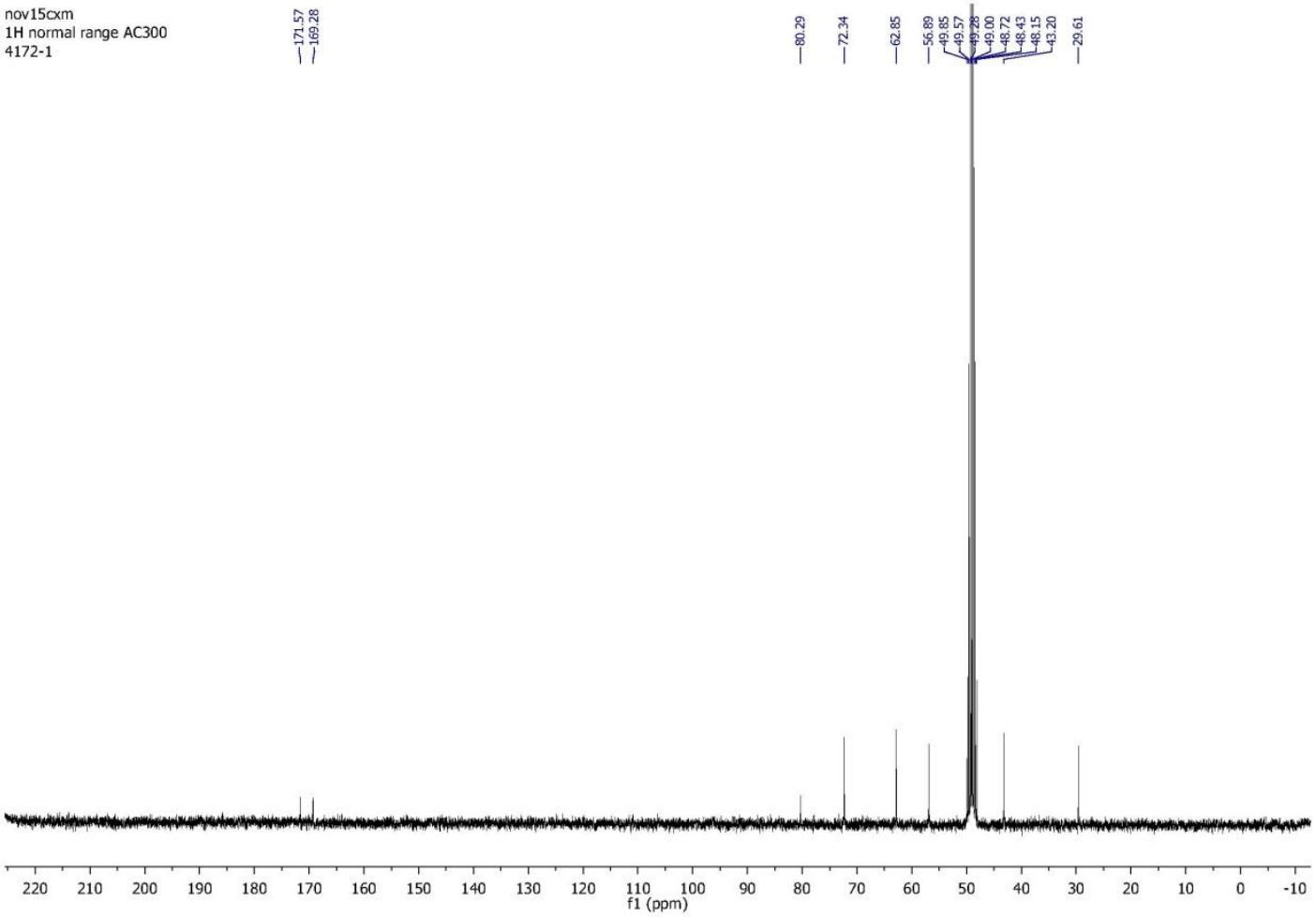
nov15cxm
1H normal range AC300
4172-1
171.57
169.28
80.29
72.34
62.85
56.89
49.65
49.57
49.28
49.00
48.72
48.43
48.15
43.20
29.61
220 210 200 190 180 170 160 150 140 130 120 110 100 90 80 70 60 50 40 30 20 10 0 -10
f1 (ppm)

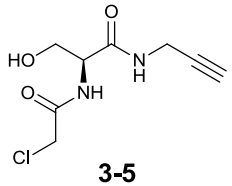
HO
O
N
H
O
NH
Cl

3-5

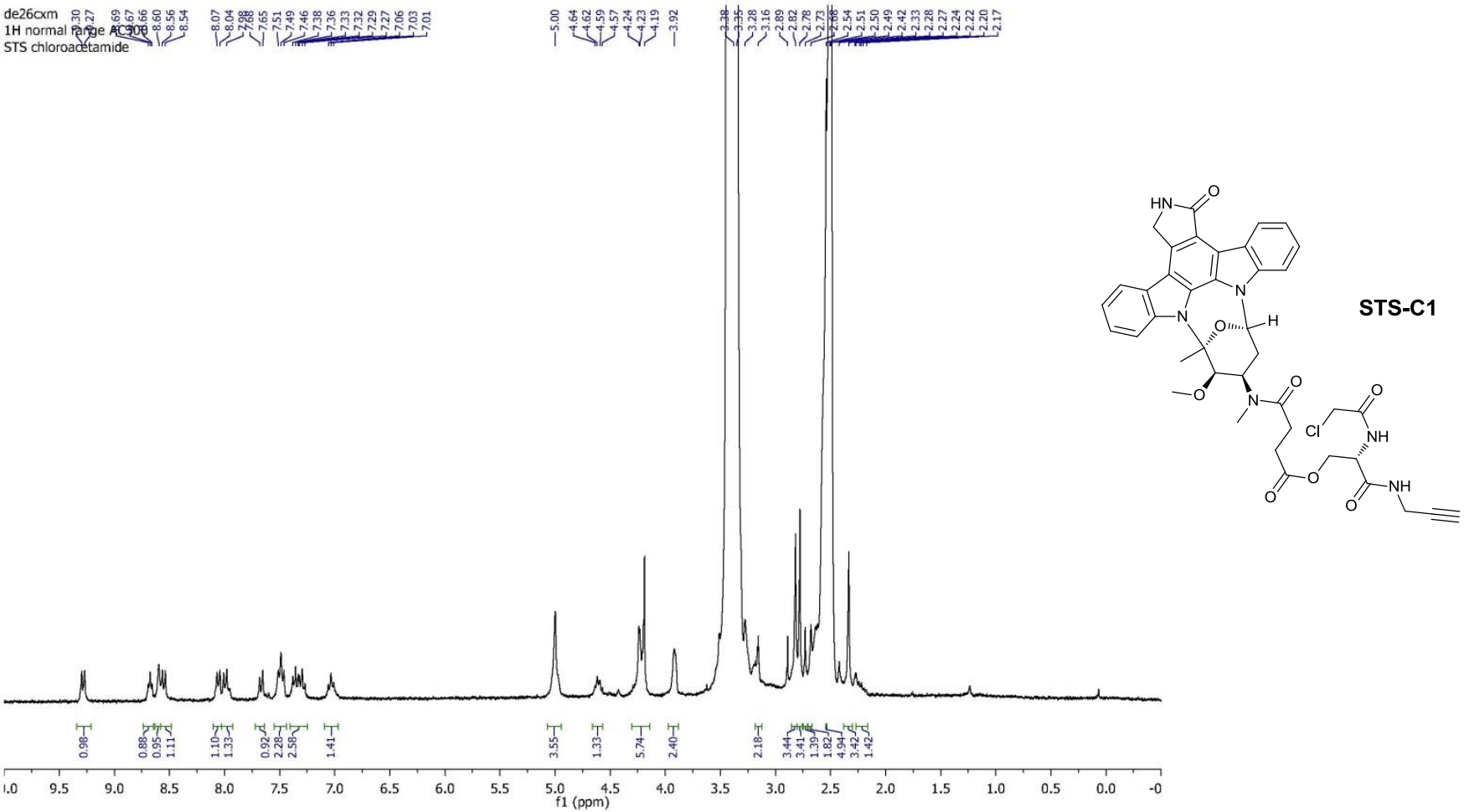
de26cxm
1H normal range AC300
STS chloroacetamide
f1 (ppm)
STS-C1

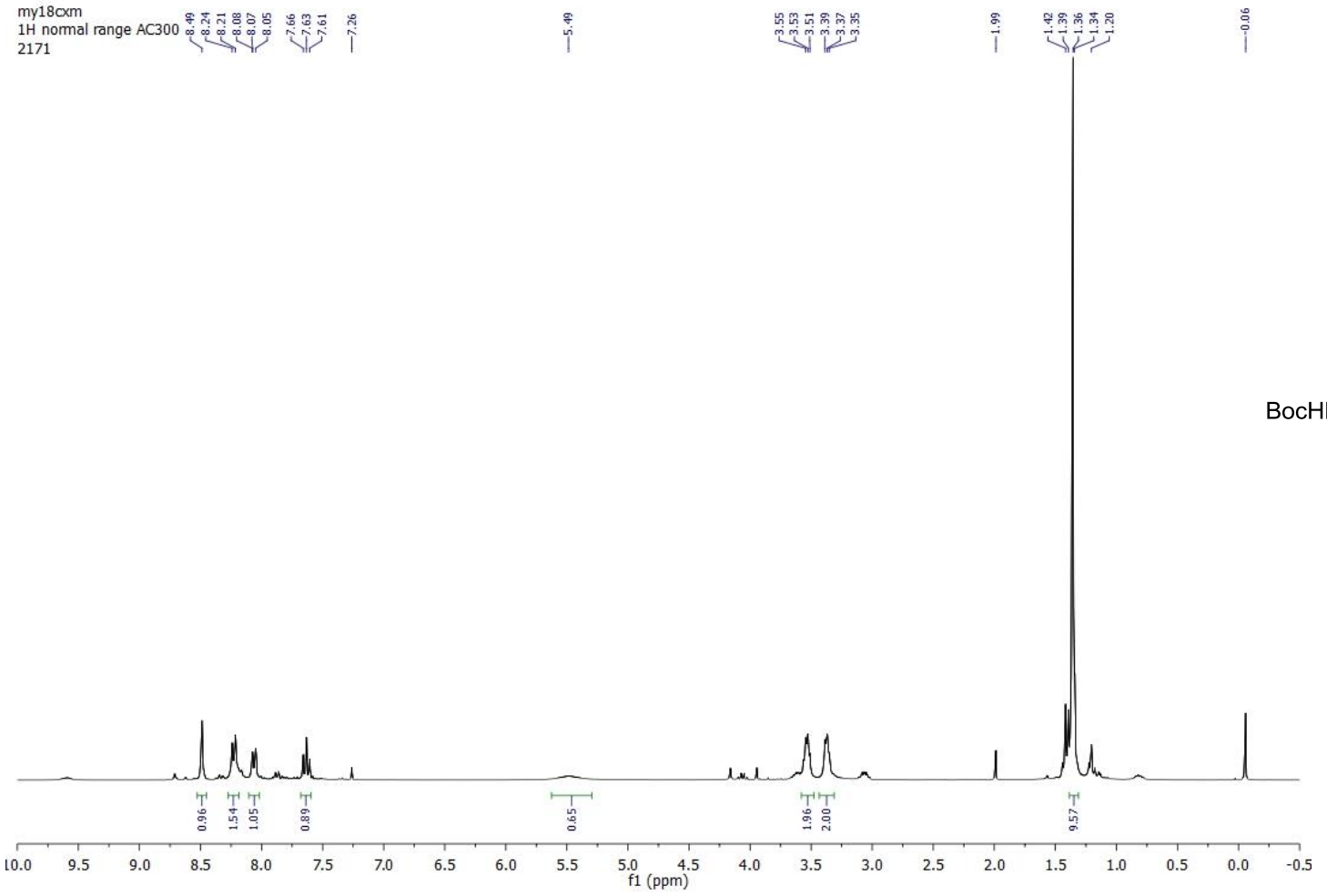
my18cxm
1H normal range AC300
2171
8.49
8.24
8.21
8.08
8.07
8.05
7.66
7.63
7.61
7.26
5.49
3.55
3.53
3.51
3.39
3.37
3.35
1.99
1.42
1.39
1.36
1.34
1.20
0.06
0.96
1.54
1.05
0.89
0.65
1.96
2.00
9.57
f1 (ppm)

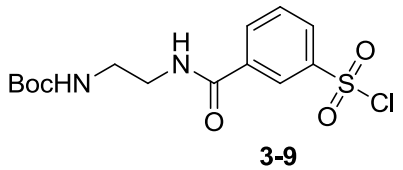
BocHN
H
N
O
O
S
O
Cl

3-9

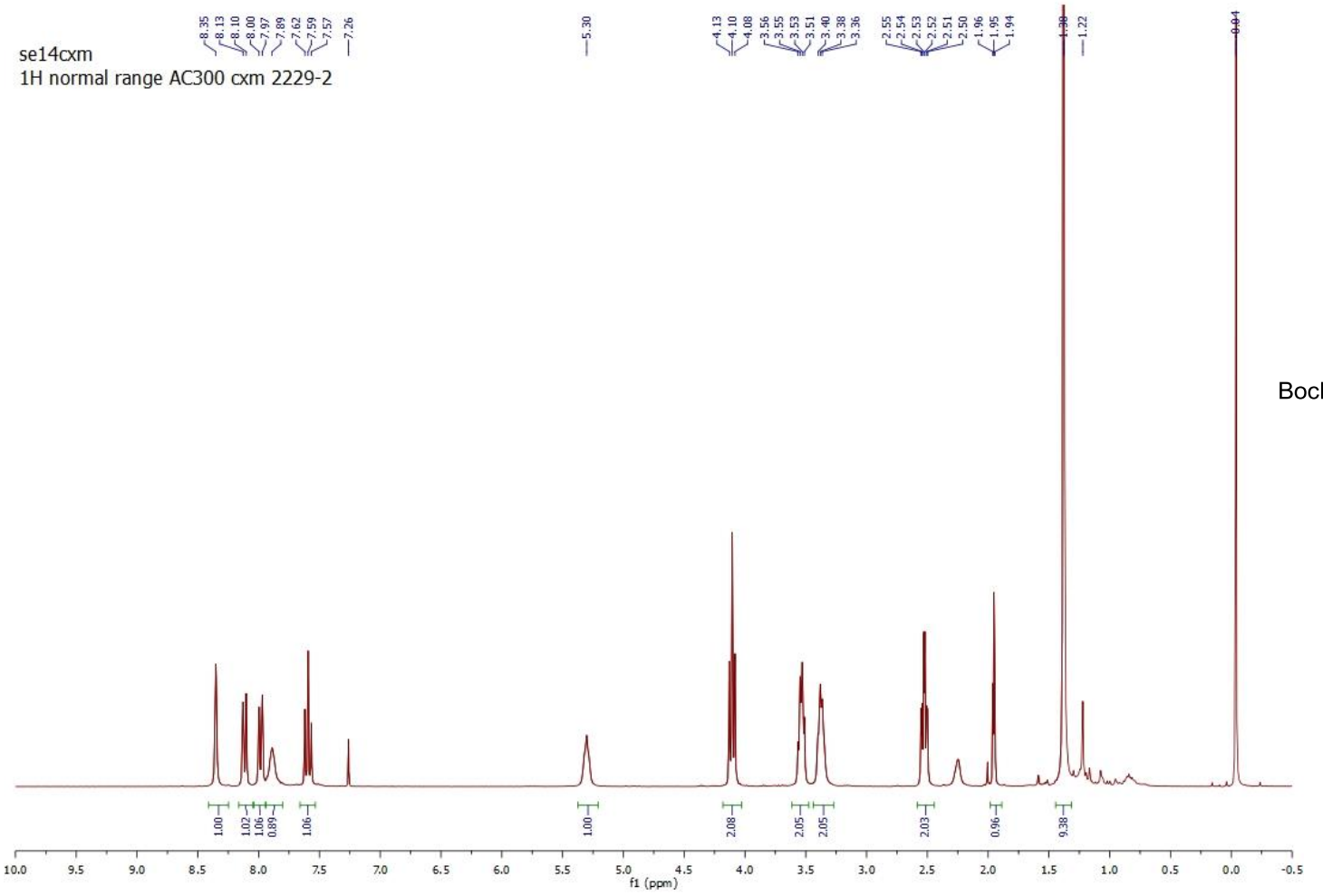
se14cxm
1H normal range AC300 cxm 2229-2
f1 (ppm)

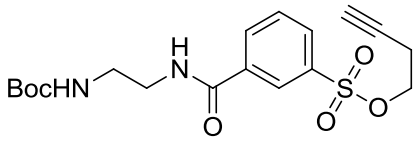
BocHN
H
N
O
O
S
O
O

3-10

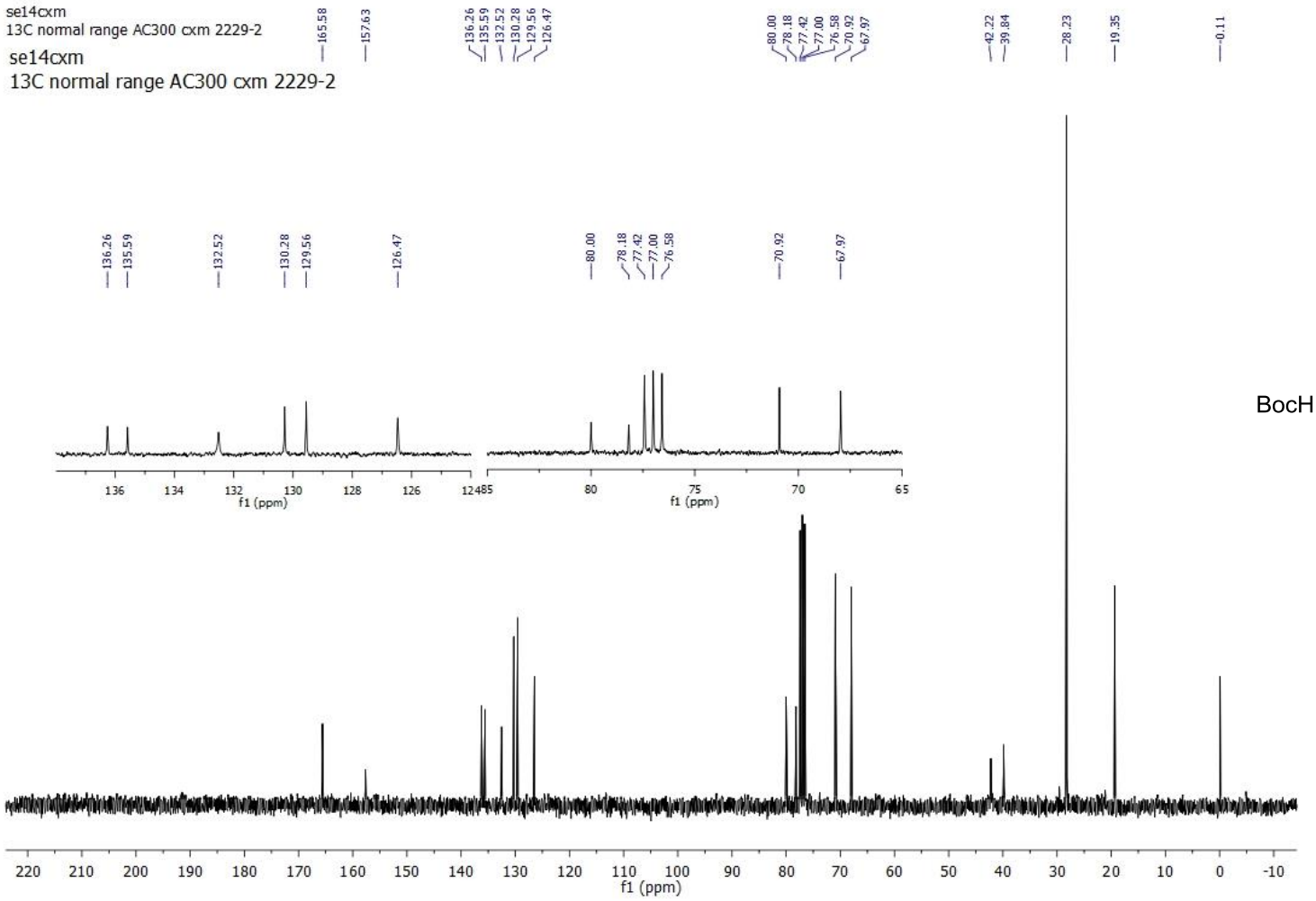
se14cxm
13C normal range AC300 cxm 2229-2
165.58
157.63
136.26
135.59
132.52
130.28
129.56
126.47
80.00
78.18
77.42
77.00
76.58
70.92
67.97
42.22
39.84
28.23
19.35
-0.11
f1 (ppm)

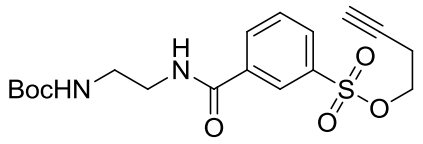
BocHN
H
N
O
O
S
O
O

3-10

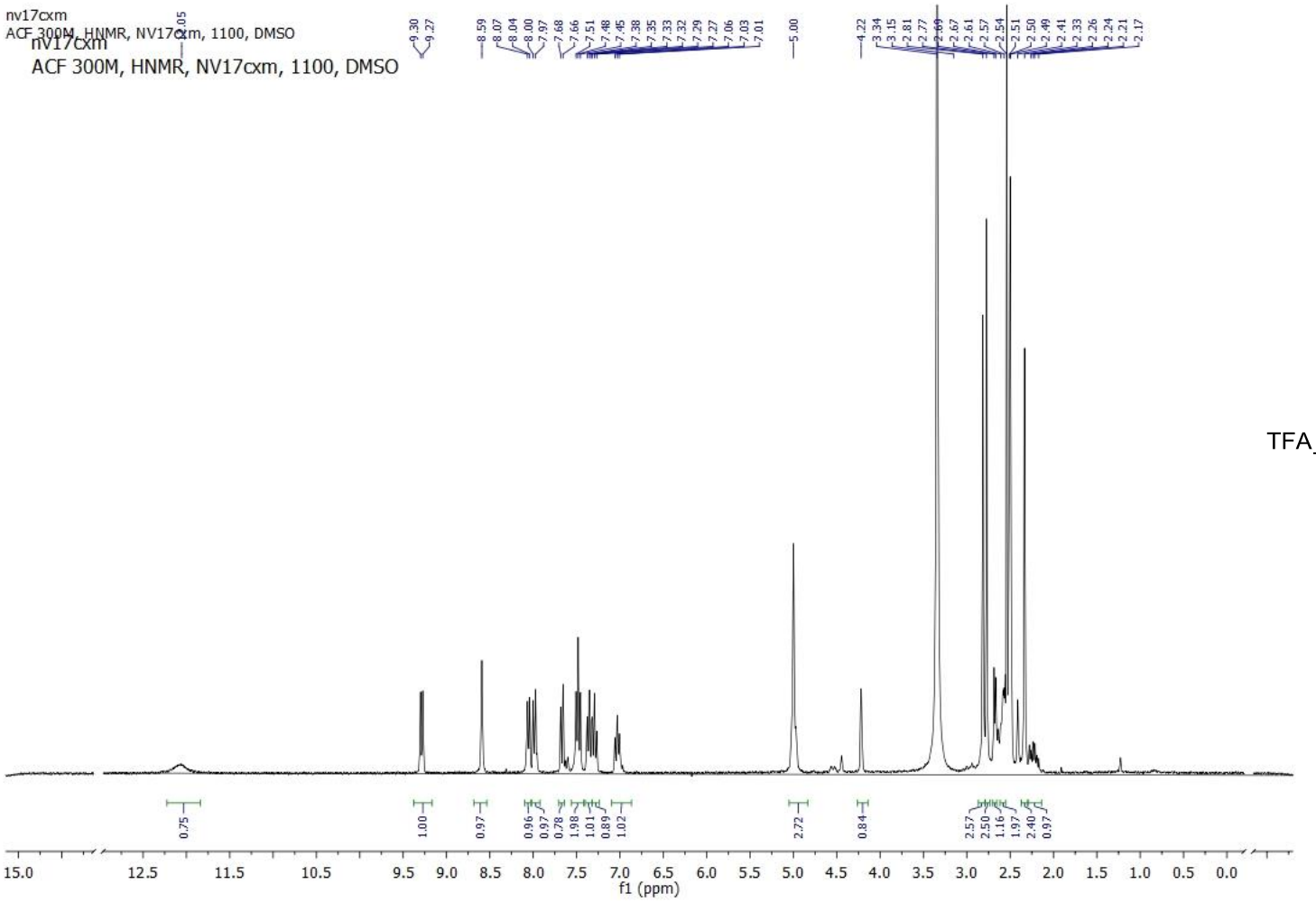
nv17cxm
ACF 300M, HNMR, NV17cxm, 1100, DMSO
f1 (ppm)

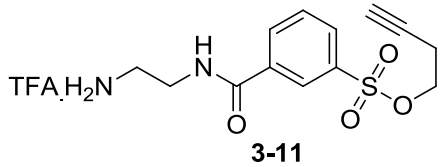
TFA.H2N
H
N
O
O
S
O
O

3-11

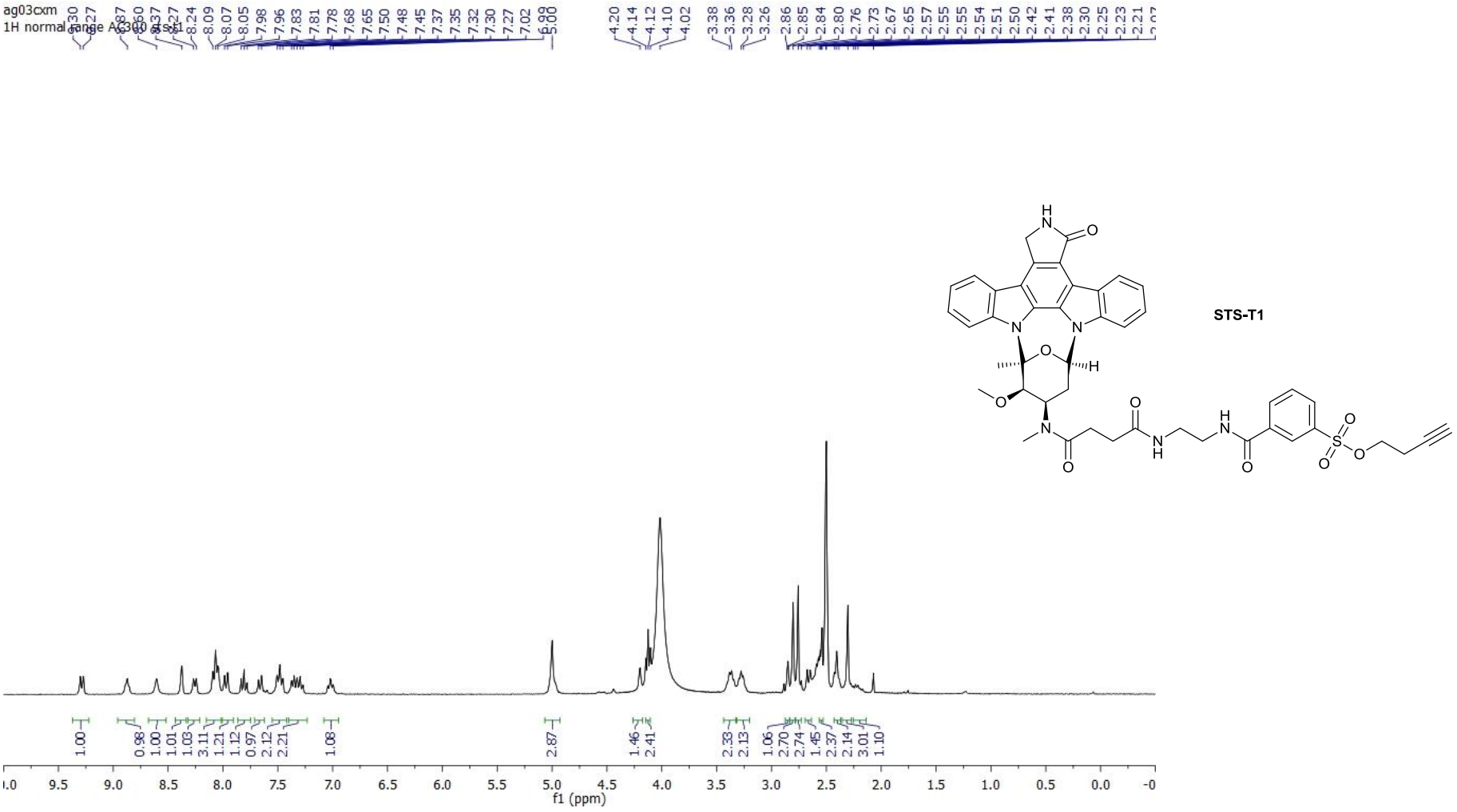
ag03cxm
1H normal range A 360 85 01
STS-T1
f1 (ppm)

ap15cxm 5012, 5017
ACF 300M, 5013 lysine fmoc prpargyl amine

5012

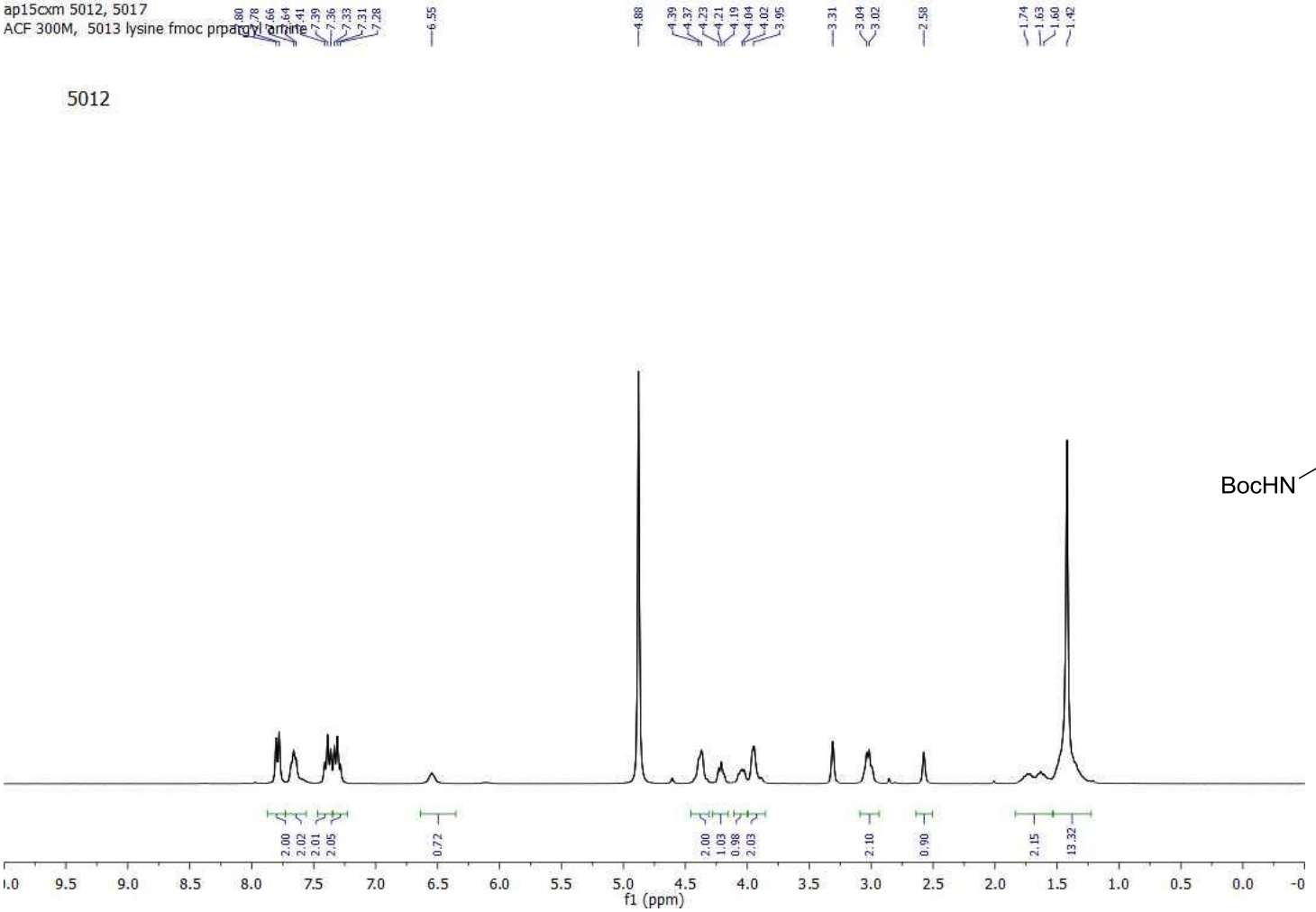

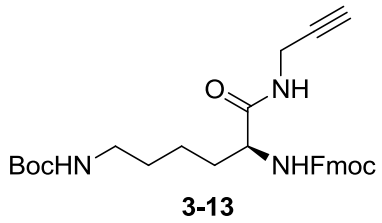

3-13

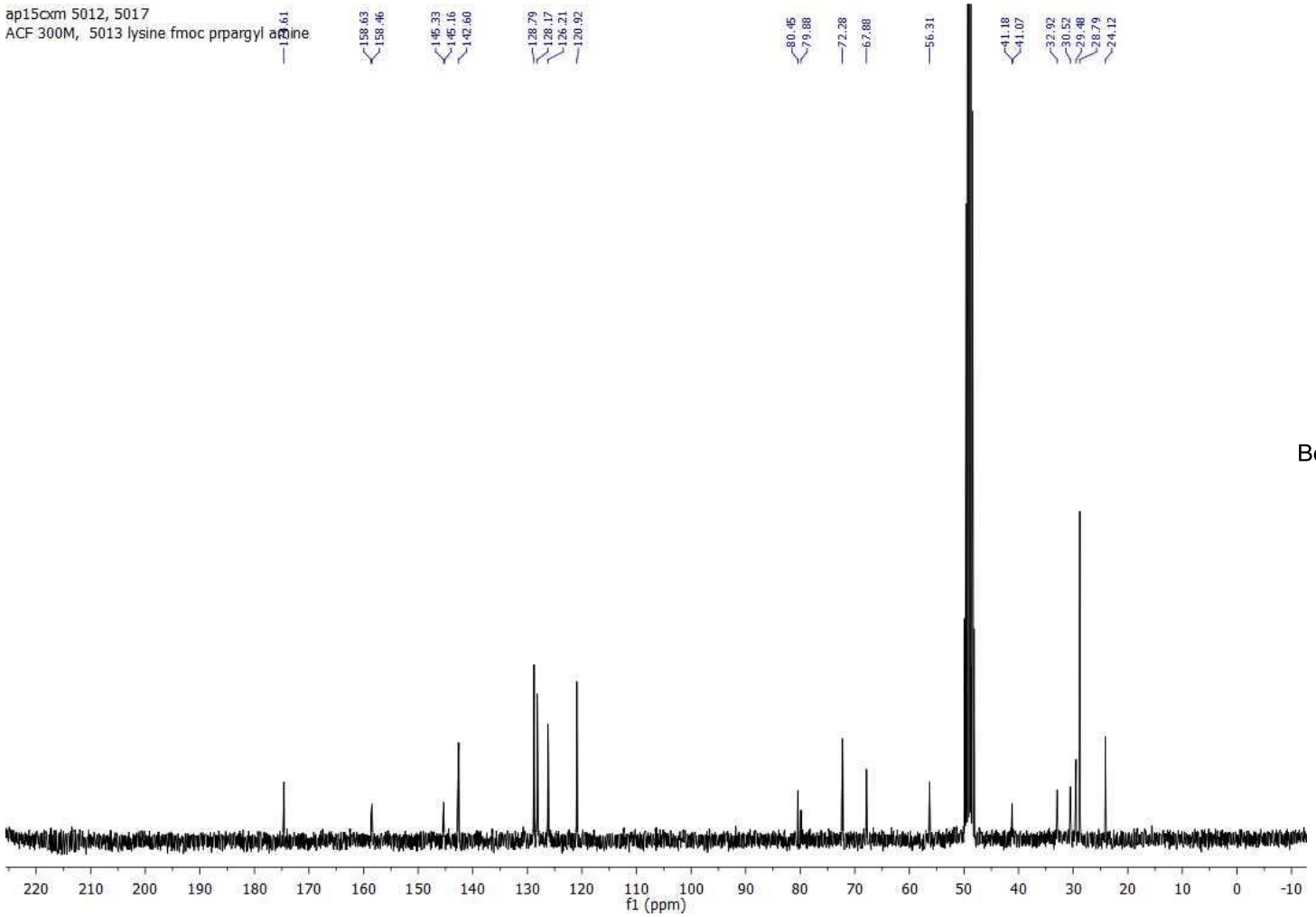
ap15cxm 5012, 5017
ACF 300M, 5013 lysine fmoc prpargyl amine
173.61
158.63
158.46
145.33
145.16
142.60
128.79
128.17
126.21
120.92
80.45
79.88
72.28
67.88
56.31
41.18
41.07
32.92
30.52
29.48
28.79
24.12
220 210 200 190 180 170 160 150 140 130 120 110 100 90 80 70 60 50 40 30 20 10 0 -10
f1 (ppm)

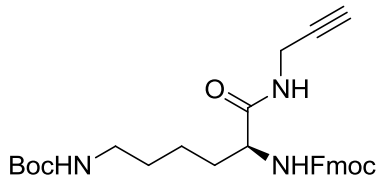
O
NH
BocHN
NHFmoc

3-13


ap06cxm
1H normal range AC300
4012 deboc
7.69
7.66
7.50
7.47
7.35
7.33
7.30
7.26
7.23
6.17
4.32
4.30
4.12
4.10
3.89
2.97
2.85
2.12
1.64
1.34
1.28

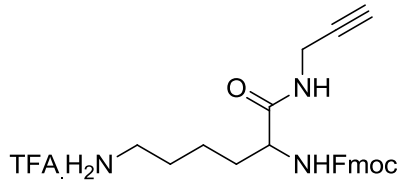
O
NH
TFA·H2N
NHFmoc

3-14

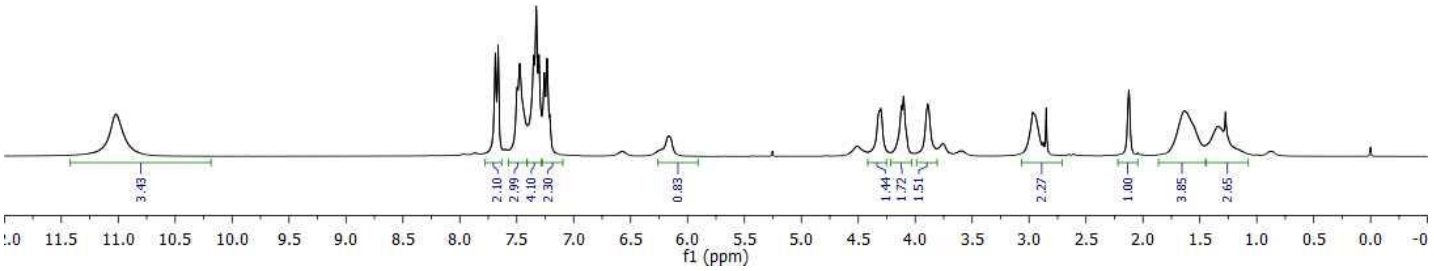
3.43
2.10
2.99
4.10
2.30
0.83
1.44
1.72
1.51
2.27
1.00
3.85
2.65
f1 (ppm)

ap06cxm
13C normal range AC300
4012 deboc

173.07
160.99
160.47
156.98
143.34
143.22
141.18
127.86
127.09
124.85
119.99
77.97
77.42
77.00
76.58
72.00
46.77
39.98
29.33
26.36
21.87

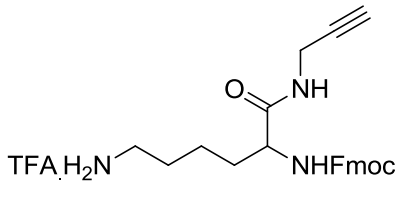

3-14

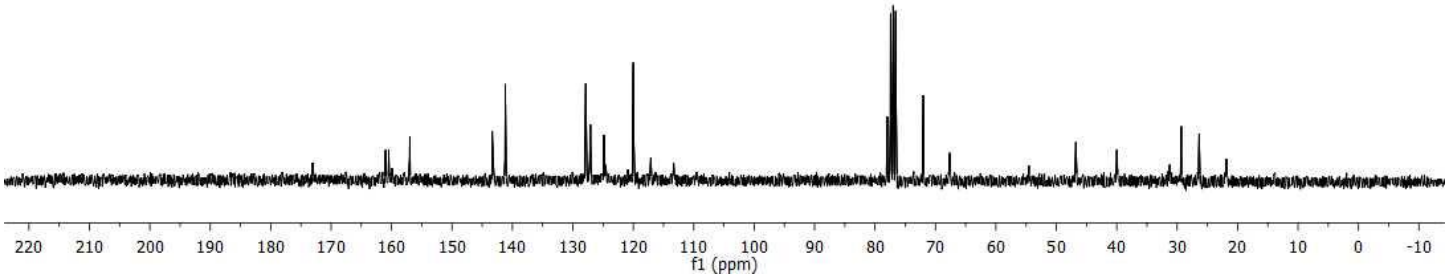

ap17cxm
1H normal range AC300
5020

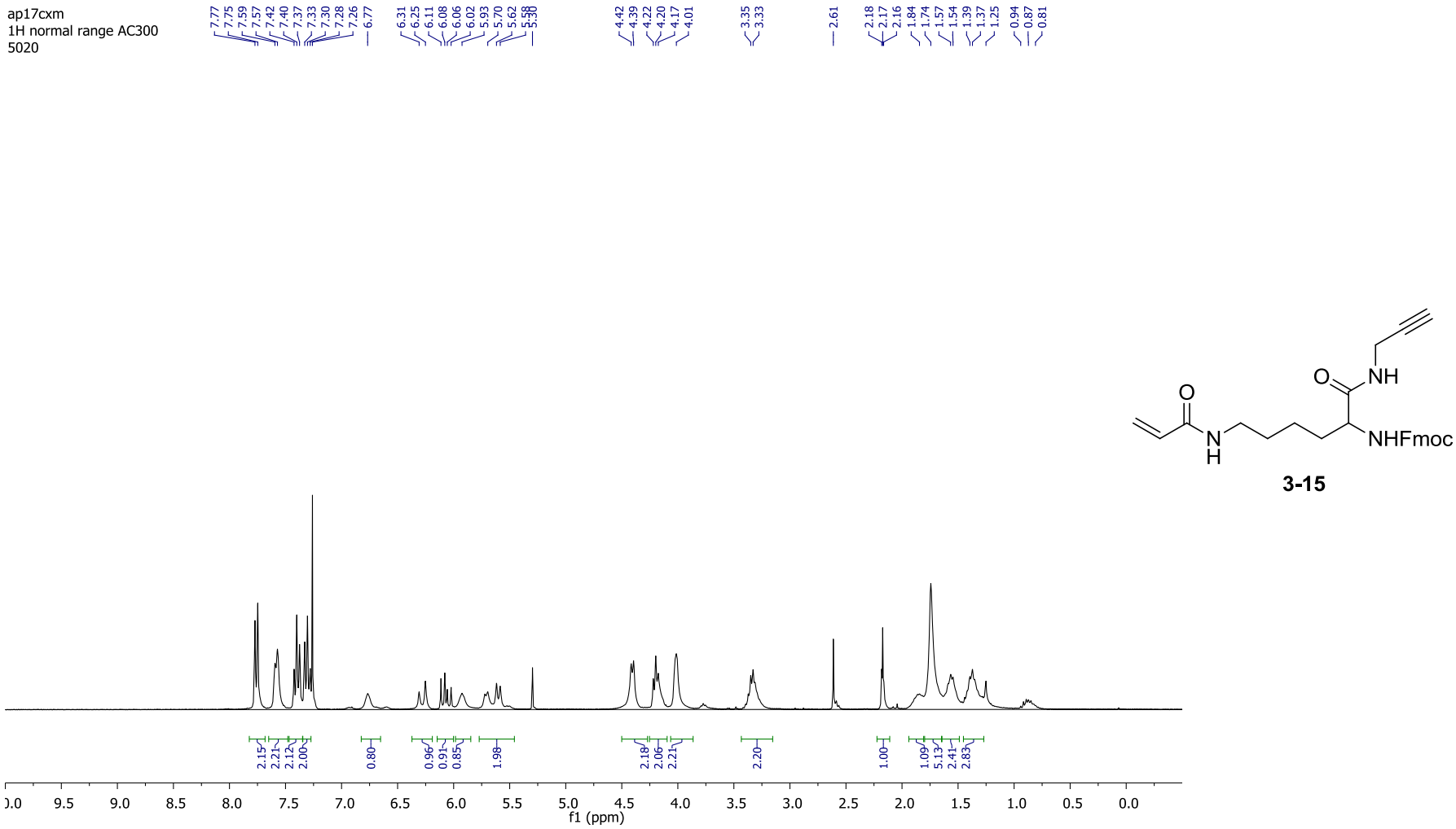

3-15

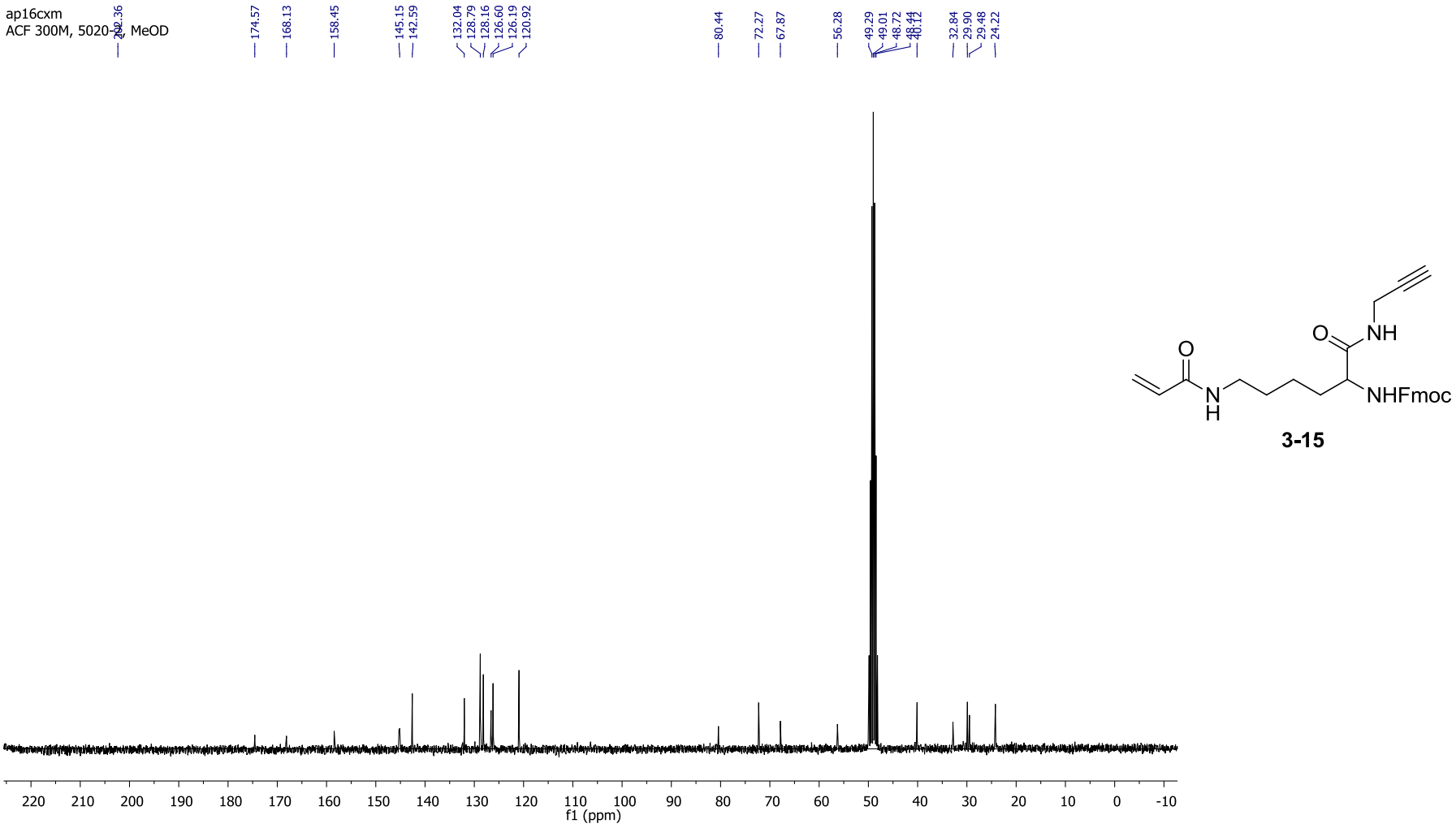
ap16cxm
ACF 300M, 5020-2, MeOD
174.57
168.13
158.45
145.15
142.59
132.04
128.79
128.16
126.60
126.19
120.92
80.44
72.27
67.87
56.28
49.29
49.01
48.72
48.44
48.12
32.84
29.90
29.48
24.22
O
NH
O
N
H
NHFmoc
3-15
220 210 200 190 180 170 160 150 140 130 120 110 100 90 80 70 60 50 40 30 20 10 0 -10
f1 (ppm)

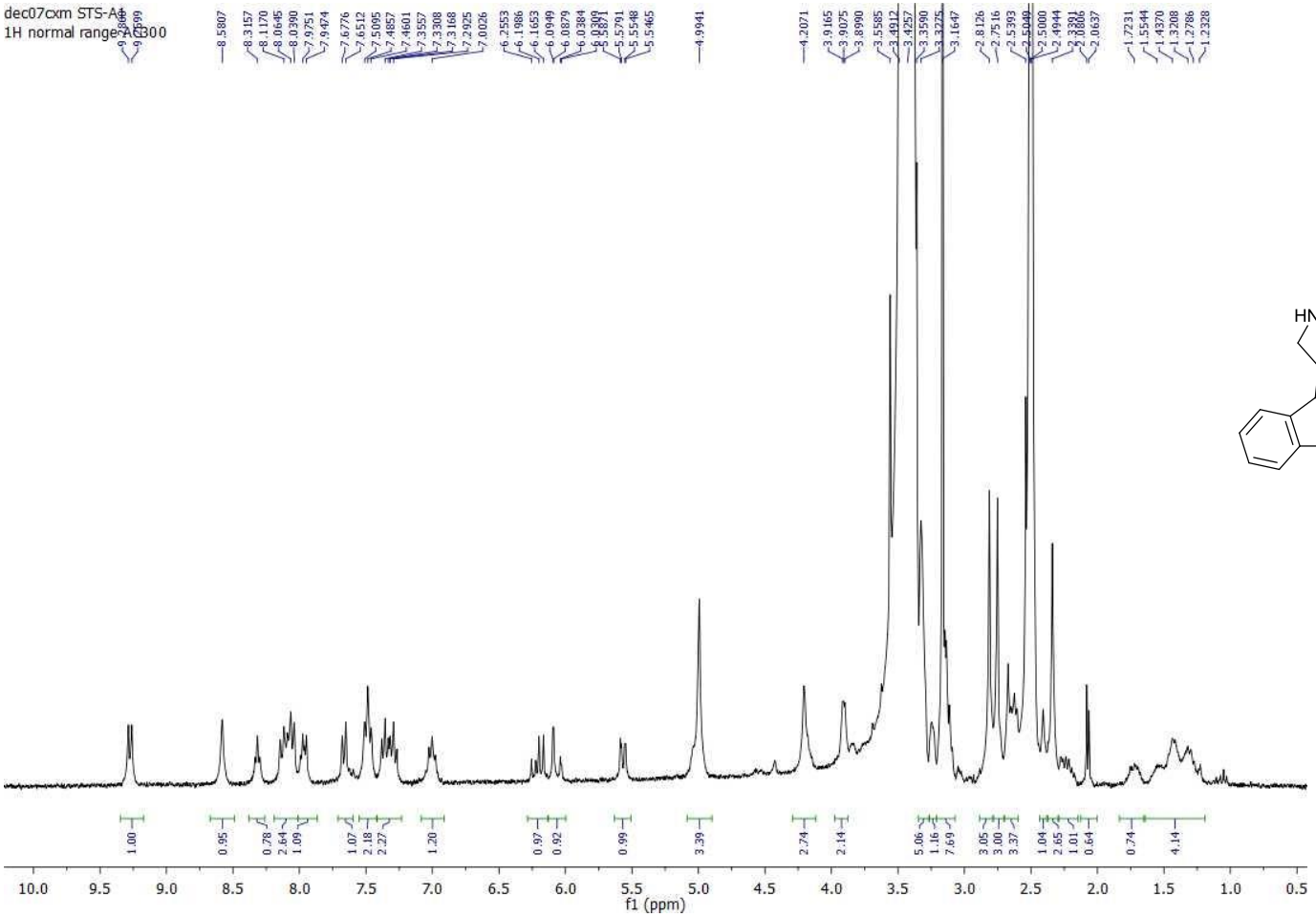

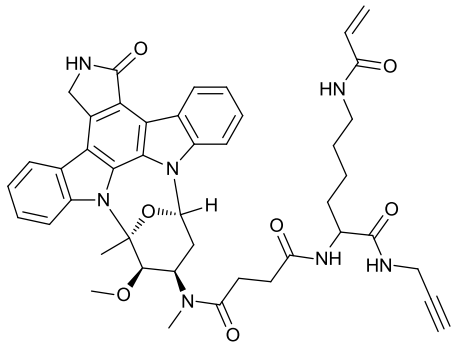

STS-A1

Chapter 4

The list of potential target proteins identified from LCMS experiments Table S3

Entry	Accession	Description	Score	Mass	Peptides Matched	emPAI
1	sp|P00338-3|LDHA_HUMAN	Isoform 3 of L-lactate dehydrogenase A chain OS=Homo sapiens GN=LDHA	373	40097	16	1.04
2	sp|P21796|VDAC1_HUMAN	Voltage-dependent anion-selective channel protein 1 OS=Homo sapiens GN=VDAC1 PE=1 SV=2	190	30868	15	1.27
3	sp|P04406|G3P_HUMAN	Glyceraldehyde-3-phosphate dehydrogenase OS=Homo sapiens GN=GAPDH PE=1 SV=3	189	36201	19	0.85
4	sp|Q6S8J3|POTEE_HUMAN	POTE ankyrin domain family member E OS=Homo sapiens GN=POTEE PE=1 SV=3	134	122882	15	0.08
5	sp|Q9BYZ2|LDH6B_HUMAN	L-lactate dehydrogenase A-like 6B OS=Homo sapiens GN=LDHAL6B PE=1 SV=3	132	42372	10	0.16
6	sp|Q5VTE0|EF1A3_HUMAN	Putative elongation factor 1-alpha-like 3 OS=Homo sapiens GN=EEF1A1P5 PE=5 SV=1	132	50495	20	0.29
7	tr|F8VXY0|F8VXY0_HUMAN	Heterogeneous nuclear ribonucleoprotein A1 OS=Homo sapiens GN=HNRNPA1 PE=4 SV=1	129	32774	11	0.34
8	sp|P07195|LDHB_HUMAN	L-lactate dehydrogenase B chain OS=Homo sapiens GN=LDHB PE=1 SV=2	118	36900	10	0.54
9	sp|P07900-2|HS90A_HUMAN	Isoform 2 of Heat shock protein HSP 90-alpha OS=Homo sapiens GN=HSP90AA1	111	98670	14	0.07
10	sp|P08238|HS90B_HUMAN	Heat shock protein HSP 90-beta OS=Homo sapiens GN=HSP90AB1 PE=1 SV=4	108	83554	12	0.04
11	tr|F5H740|F5H74	Voltage-dependent anion-selective channel protein 3 OS=Homo sapiens	95	31080	8	0.11

	0_HUMAN	GN=VDAC3 PE=4 SV=1				
12	sp|P22626-2|ROA2_HUMAN	Isoform A2 of Heterogeneous nuclear ribonucleoproteins A2/B1 OS=Homo sapiens GN=HNRNPA2B1	91	36041	7	0.3
13	sp|P60842|IF4A1_HUMAN	Eukaryotic initiation factor 4A-I OS=Homo sapiens GN=EIF4A1 PE=1 SV=1	90	46353	7	0.23
14	tr|B4DKM5|B4DKM5_HUMAN	Voltage-dependent anion-selective channel protein 2 OS=Homo sapiens GN=VDAC2 PE=2 SV=1	64	27804	15	0.76
16	tr|B1AN99|B1AN99_HUMAN	Protease, serine, 3 (Fragment) OS=Homo sapiens GN=PRSS3 PE=3 SV=1	64	19674	13	0.37
17	tr|F8W181|F8W181_HUMAN	60S ribosomal protein L6 (Fragment) OS=Homo sapiens GN=RPL6 PE=3 SV=1	43	25876	12	0.44
18	tr|F5GWR2|F5GWR2_HUMAN	60 kDa heat shock protein, mitochondrial OS=Homo sapiens GN=HSPD1 PE=3 SV=1	41	26671	25	0.13
19	tr|H0YG49|H0YG49_HUMAN	Serine/arginine-rich-splicing factor 2 OS=Homo sapiens GN=SRSF2 PE=4 SV=1	41	25372	5	0.13
20	sp|P10809|CH60_HUMAN	60 kDa heat shock protein, mitochondrial OS=Homo sapiens GN=HSPD1 PE=1 SV=2	40	61187	25	0.11
21	tr|E7EQG2|E7EQG2_HUMAN	Eukaryotic initiation factor 4A-II OS=Homo sapiens GN=EIF4A2 PE=3 SV=1	38	41492	7	0.08
22	tr|F5H301|F5H301_HUMAN	Tight junction protein ZO-2 OS=Homo sapiens GN=TJP2 PE=4 SV=1	37	137486	4	0.02
23	sp|Q96RW7-2|HMCN1_HUMAN	Isoform 2 of Hemicentin-1 OS=Homo sapiens GN=HMCN1	36	609525	6	0.01
24	sp|Q8NCM8-2|DYHC2_HUMAN	Isoform 2 of Cytoplasmic dynein 2 heavy chain 1 OS=Homo sapiens GN=DYNC2H1	36	496587	10	0.01
25	sp|Q6P1J9|CDC73	Parafibromin OS=Homo sapiens GN=CDC73 PE=1 SV=1	36	60653	5	0.05

	_HUMAN					
26	sp|P00387-2|NB5R3_HUMAN	Isoform 2 of NADH-cytochrome b5 reductase 3 OS=Homo sapiens GN=CYB5R3	36	31836	7	0.1
27	sp|P12755|SKI_HUMAN	Ski oncogene OS=Homo sapiens GN=SKI PE=1 SV=1	35	81209	6	0.04
28	tr|H3BQ34|H3BQ34_HUMAN	Pyruvate kinase isozymes M1/M2 OS=Homo sapiens GN=PKM2 PE=4 SV=1	34	30929	7	0.11
29	tr|A2RRB2|A2RRB2_HUMAN	ZNF608 protein OS=Homo sapiens GN=ZNF608 PE=2 SV=1	33	46929	10	0.07
30	tr|G3XAL0|G3XAL0_HUMAN	Malate dehydrogenase OS=Homo sapiens GN=MDH2 PE=3 SV=1	33	24921	5	0.29
31	tr|E9PBX6|E9PBX6_HUMAN	Transmembrane protein C5orf28 OS=Homo sapiens GN=C5orf28 PE=4 SV=1	32	13393	5	0.25
32	tr|H0YKE0|H0YKE0_HUMAN	WD repeat-containing protein 72 OS=Homo sapiens GN=WDR72 PE=4 SV=1	30	126837	6	0.03
33	tr|G3V161|G3V161_HUMAN	Kelch repeat and BTB (POZ) domain containing 3, isoform CRA_a OS=Homo sapiens GN=KBTBD3 PE=4 SV=1	30	61834	6	0.05
34	sp|Q96PE2|ARHGH_HUMAN	Rho guanine nucleotide exchange factor 17 OS=Homo sapiens GN=ARHGEF17 PE=1 SV=1	30	223645	4	0.01
35	sp|Q99741|CDC6_HUMAN	Cell division control protein 6 homolog OS=Homo sapiens GN=CDC6 PE=1 SV=1	30	63650	4	0.05
36	sp|Q13011|ECH1_HUMAN	Delta(3,5)-Delta(2,4)-dienoyl-CoA isomerase, mitochondrial OS=Homo sapiens GN=ECH1 PE=1 SV=2	30	36136	7	0.19
37	tr|F8WDZ3|F8WDZ3_HUMAN	CKLF-like MARVEL transmembrane domain-containing protein 7 OS=Homo sapiens GN=CMTM7 PE=4 SV=1	29	16390	24	0.21
38	sp|Q6PHW0|IYD1_HUMAN	Iodotyrosine dehalogenase 1 OS=Homo sapiens GN=IYD PE=1 SV=2	29	33510	15	0.1

40	tr|H3BP27|H3BP27_HUMAN	tRNA-specific adenosine deaminase 1 (Fragment) OS=Homo sapiens GN=ADAT1 PE=4 SV=1	28	13669	10	0.25
41	sp|A6NKP2|D42E2_HUMAN	Putative short-chain dehydrogenase/reductase family 42E member 2 OS=Homo sapiens GN=SDR42E2 PE=3 SV=3	27	47125	4	0.07
42	tr|A8MQ54|A8MQ54_HUMAN	Protein SOGA2 OS=Homo sapiens GN=SOGA2 PE=4 SV=1	27	188697	10	0.02
43	sp|Q8N5R6-2|CCD33_HUMAN	Isoform 2 of Coiled-coil domain-containing protein 33 OS=Homo sapiens GN=CCDC33	26	114508	8	0.03
44	tr|A6NJU0|A6NJU0_HUMAN	Heat shock 70 kDa protein 14 OS=Homo sapiens GN=HSPA14 PE=2 SV=2	26	29744	15	0.11
45	sp|P12004|PCNA_HUMAN	Proliferating cell nuclear antigen OS=Homo sapiens GN=PCNA PE=1 SV=1	25	29092	4	0.11
46	tr|H0YEN5|H0YEN5_HUMAN	40S ribosomal protein S2 (Fragment) OS=Homo sapiens GN=RPS2 PE=3 SV=1	24	21426	4	0.16
47	tr|G3V151|G3V151_HUMAN	HCG1782642, isoform CRA_a OS=Homo sapiens GN=TATDN3 PE=4 SV=1	23	31331	7	0.11
48	tr|E7ENS5|E7ENS5_HUMAN	Uncharacterized protein OS=Homo sapiens GN=SEPT5 PE=3 SV=1	22	42835	4	0.08
49	sp|P01880-2|IGHD_HUMAN	Isoform 2 of Ig delta chain C region OS=Homo sapiens GN=IGHD	22	47827	6	0.07
50	tr|D6RGD1|D6RGD1_HUMAN	Unconventionnal myosin-X (Fragment) OS=Homo sapiens GN=MYO10 PE=4 SV=1	17	96861	3	0.03

NMR Spectra

Chapter 4
NMR Spectra of representative compounds

ma03cxm
1H normal range AC300
3174 MeO2CCH2CH2COCO2Me

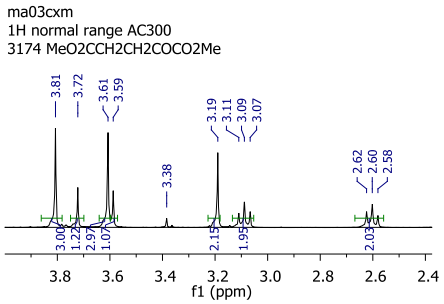

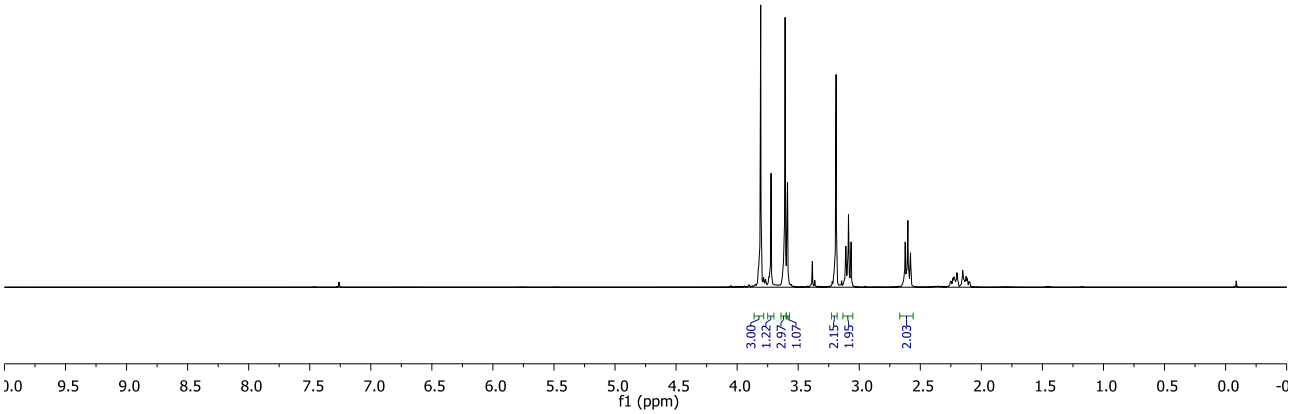

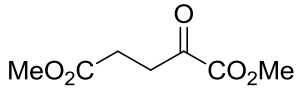

4-2

ma07cxm
1H normal range AC300

MeCO2CHCHCOCO2Me

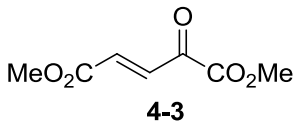

4-3

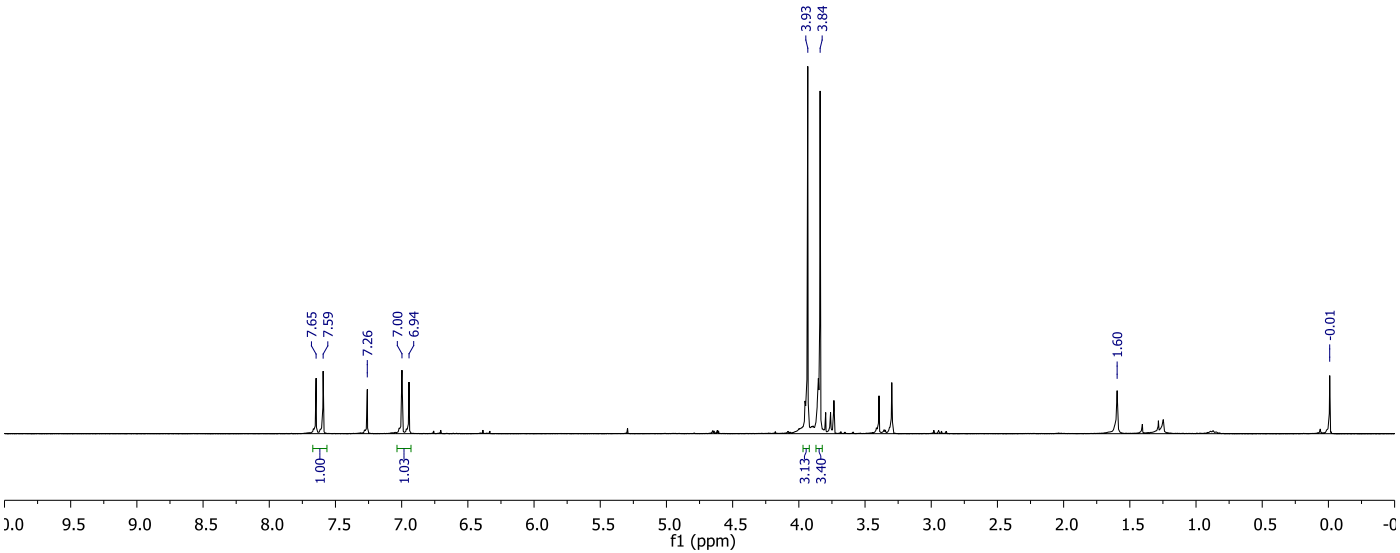

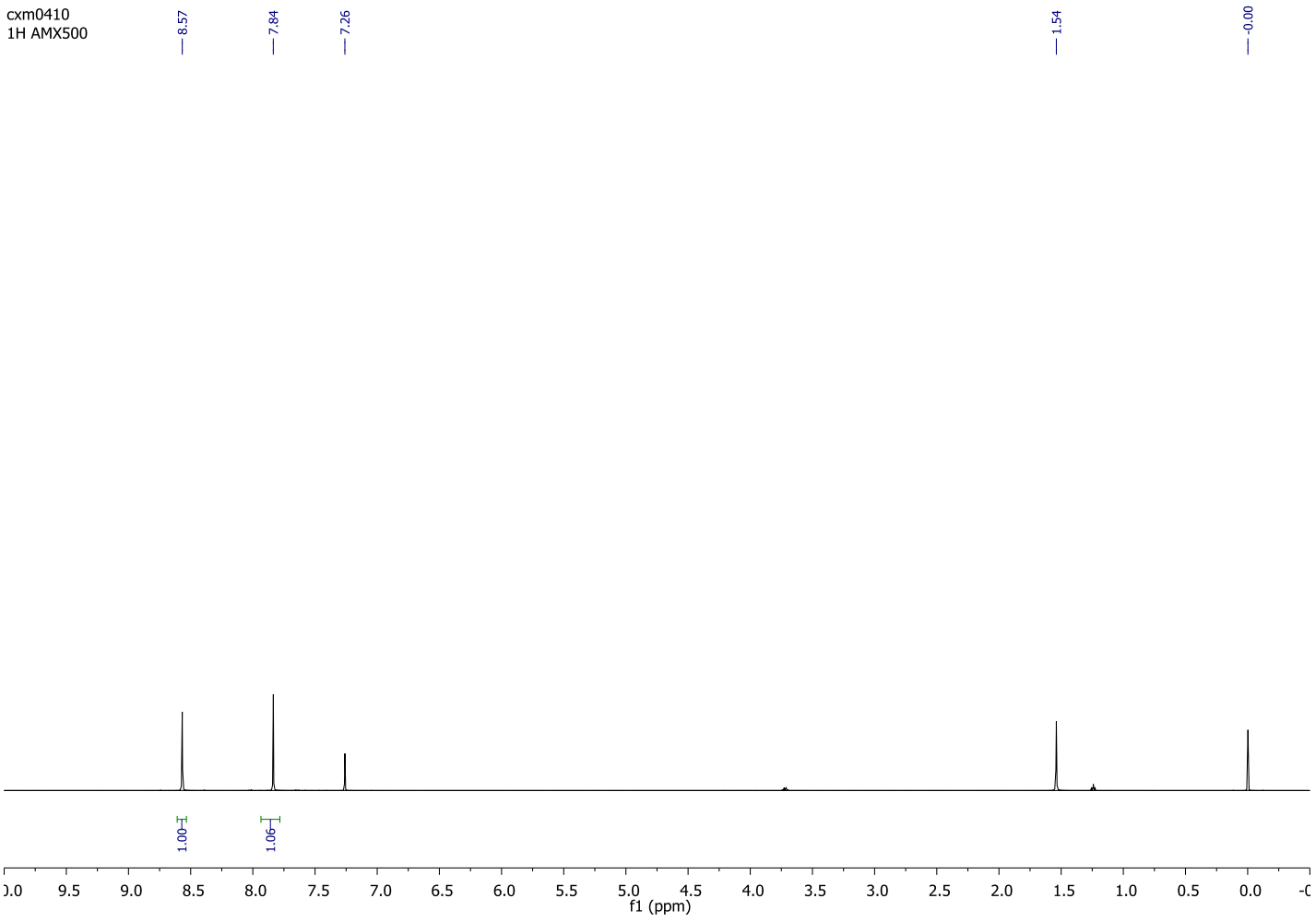
cxm0410
1H AMX500
8.57
7.84
7.26
1.54
-0.00
1.00
1.06
f1 (ppm)

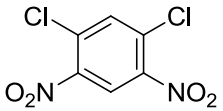
Cl
Cl
O2N
NO2

4-5

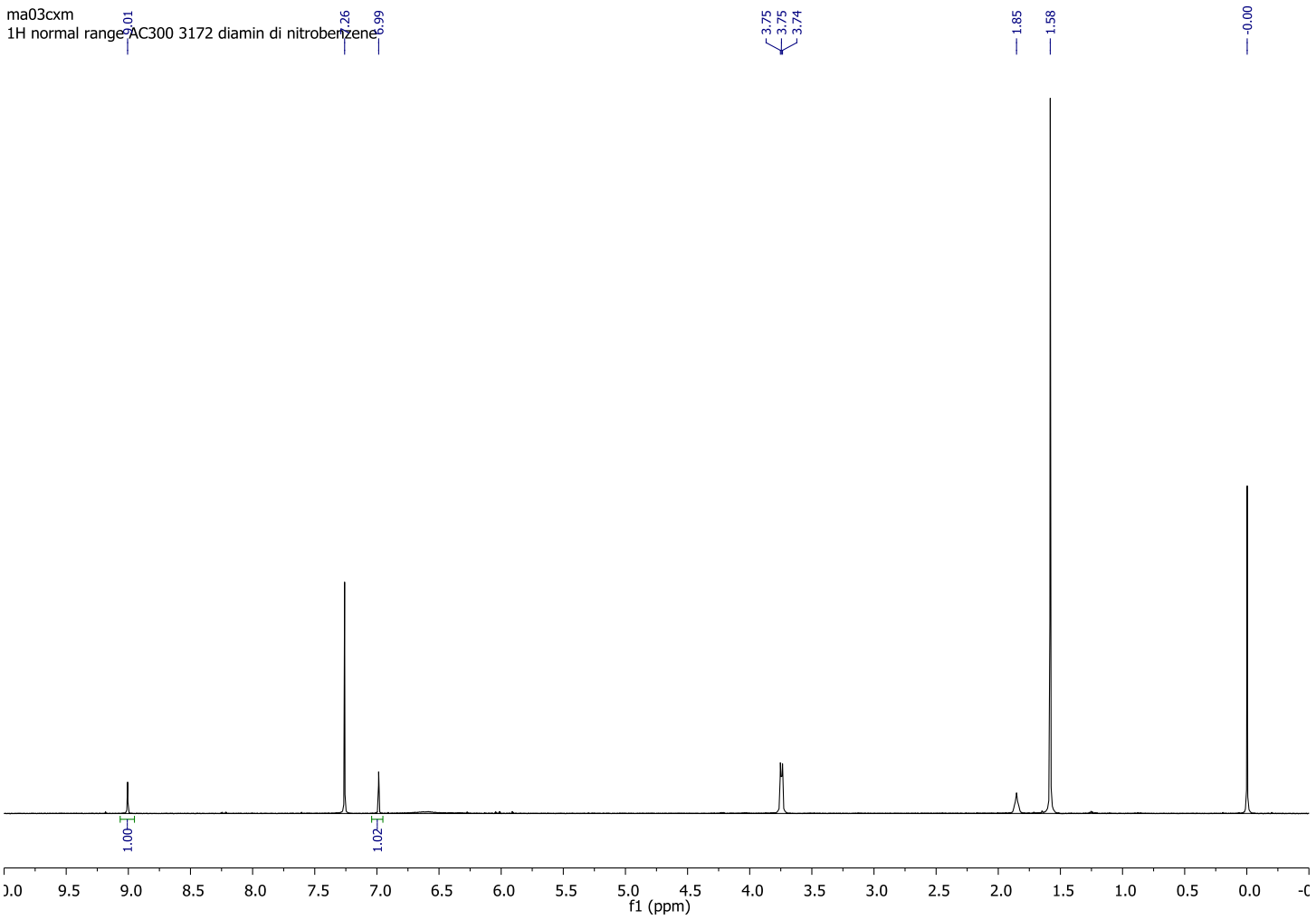
ma03cxm
1H normal range AC300 3172 diamin di nitrobenzene
9.01
7.26
6.99
3.75
3.75
3.74
1.85
1.58
-0.00
1.00
1.02
f1 (ppm)

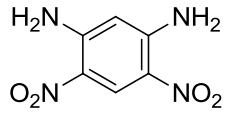
H2N
NH2
O2N
NO2

4-6

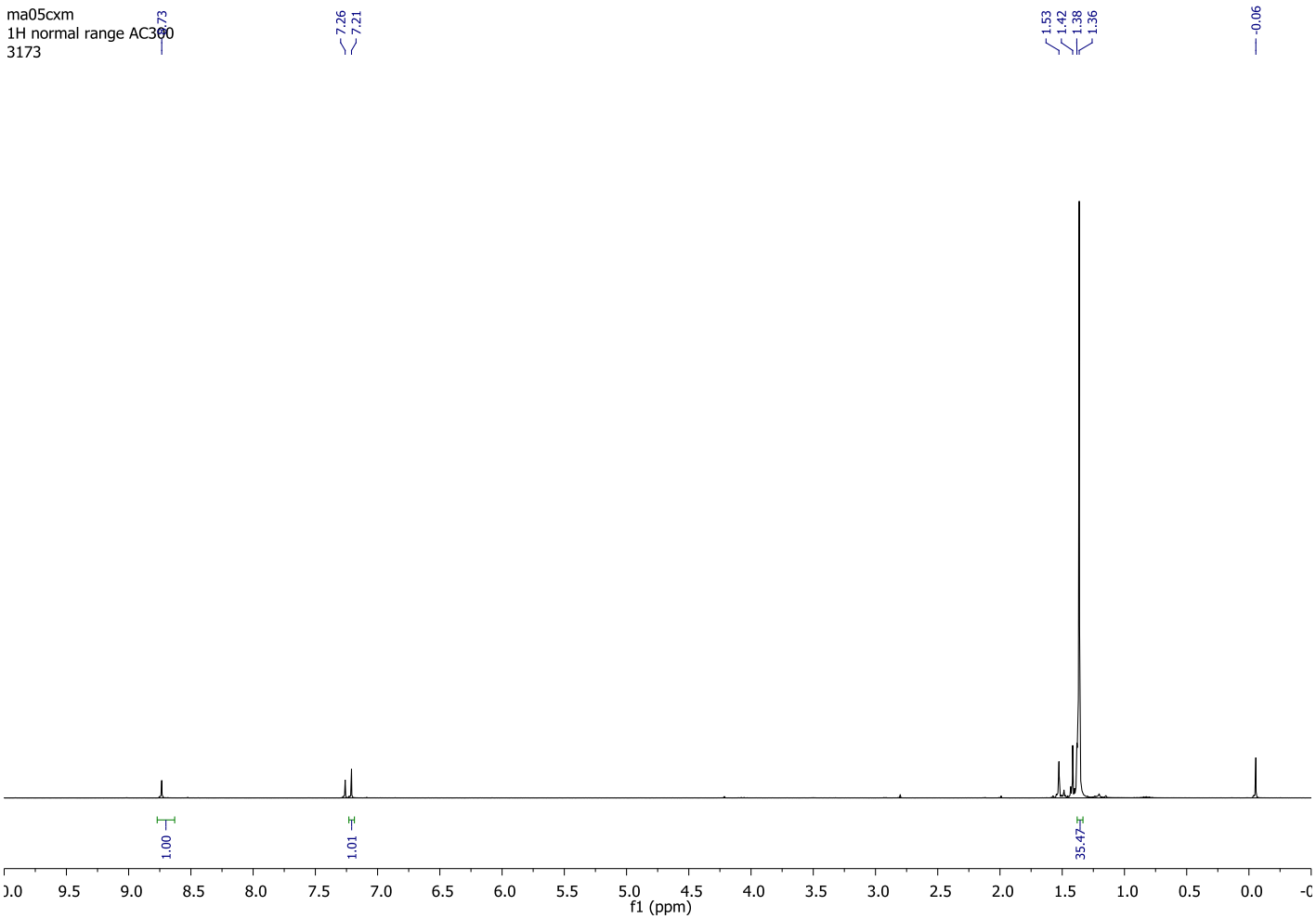
ma05cxm
1H normal range AC300
3173
8.73
7.26
7.21
1.53
1.42
1.38
1.36
-0.06
1.00
1.01
35.47
f1 (ppm)

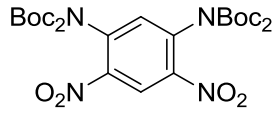
Boc2N
NBoc2
O2N
NO2

4-7

ma05cxm
1H normal range AC300
3173

148.99
143.91
137.49
134.70
122.04
84.99
77.42
77.00
76.58
27.71

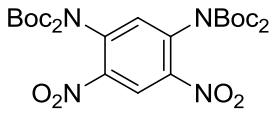

4-7

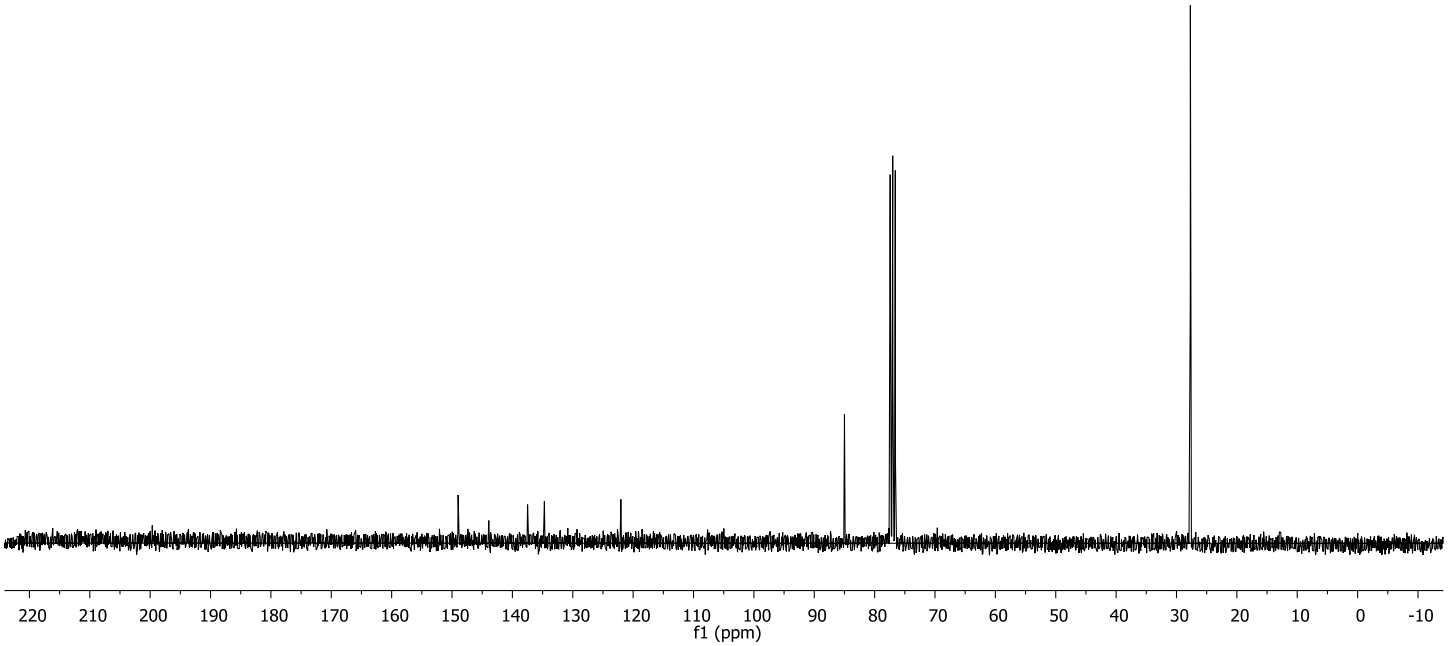

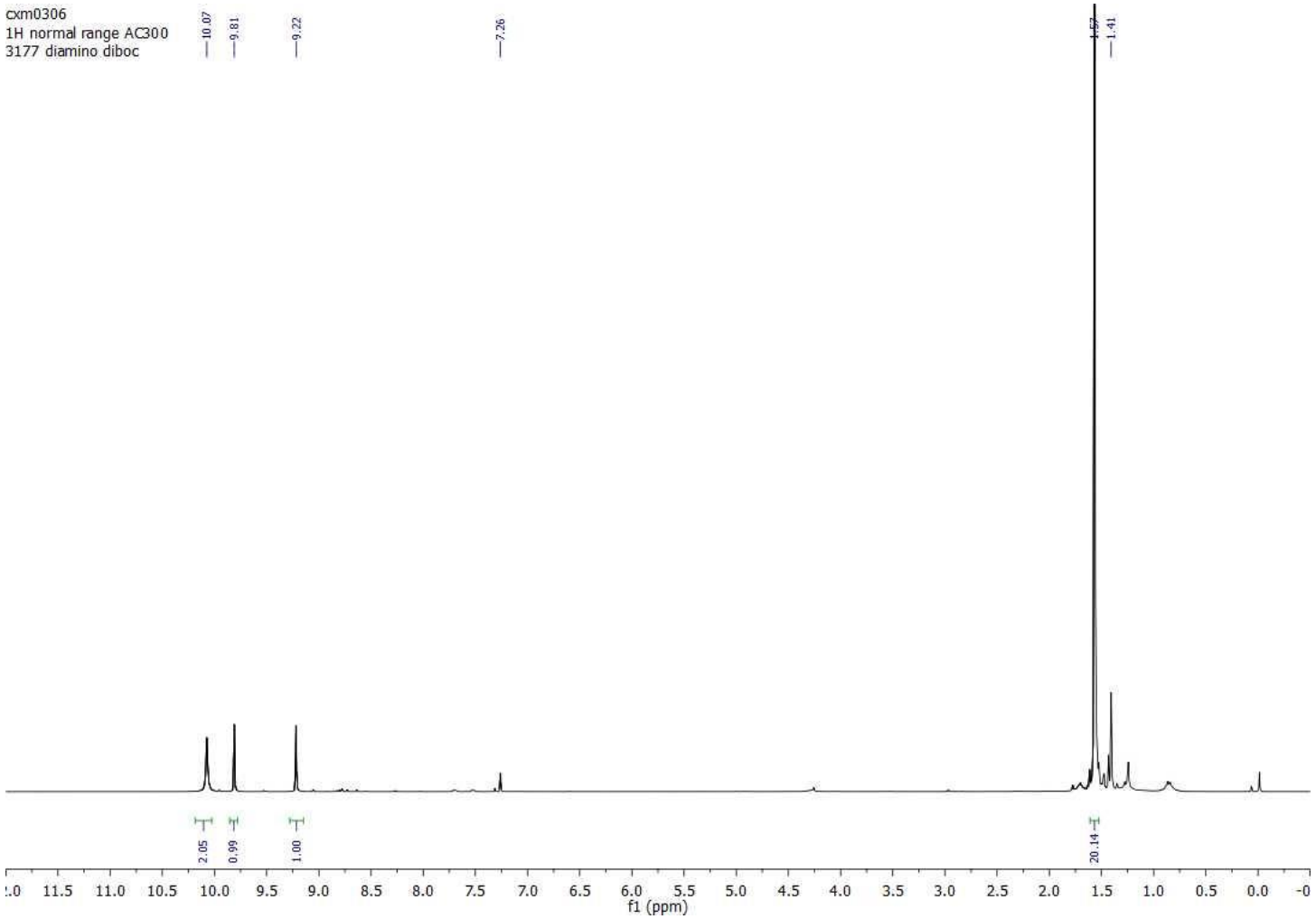
cxm0306
1H normal range AC300
3177 diamino diboc
10.07
9.81
9.22
7.26
1.57
1.41
2.05
0.99
1.00
20.14
f1 (ppm)

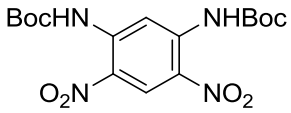
BocHN
NHBoc
O2N
NO2

4-8

cxm0306
1H normal range AC300
3177 diamino diboc

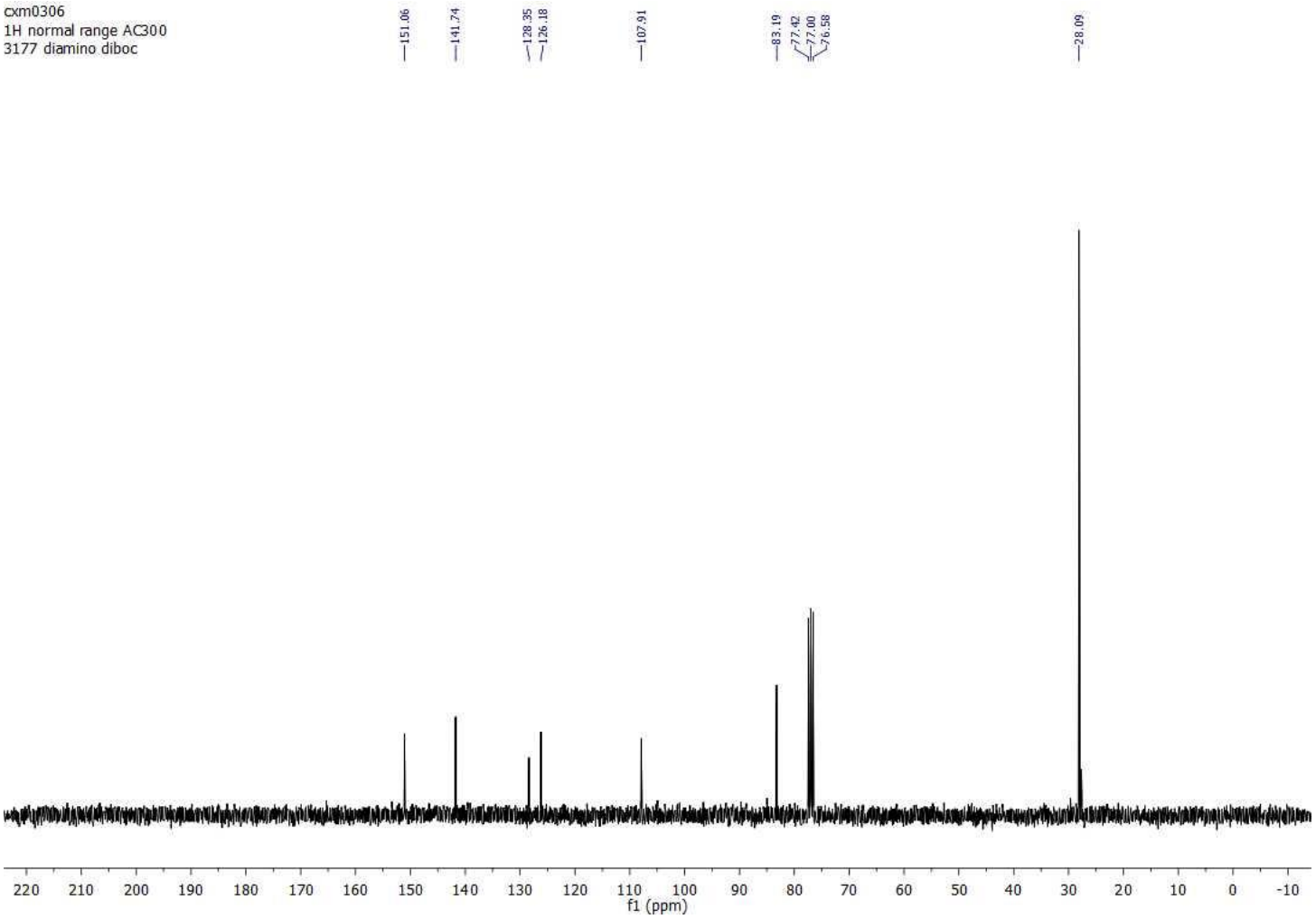

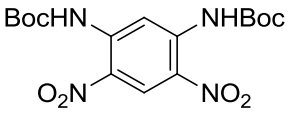

4-8

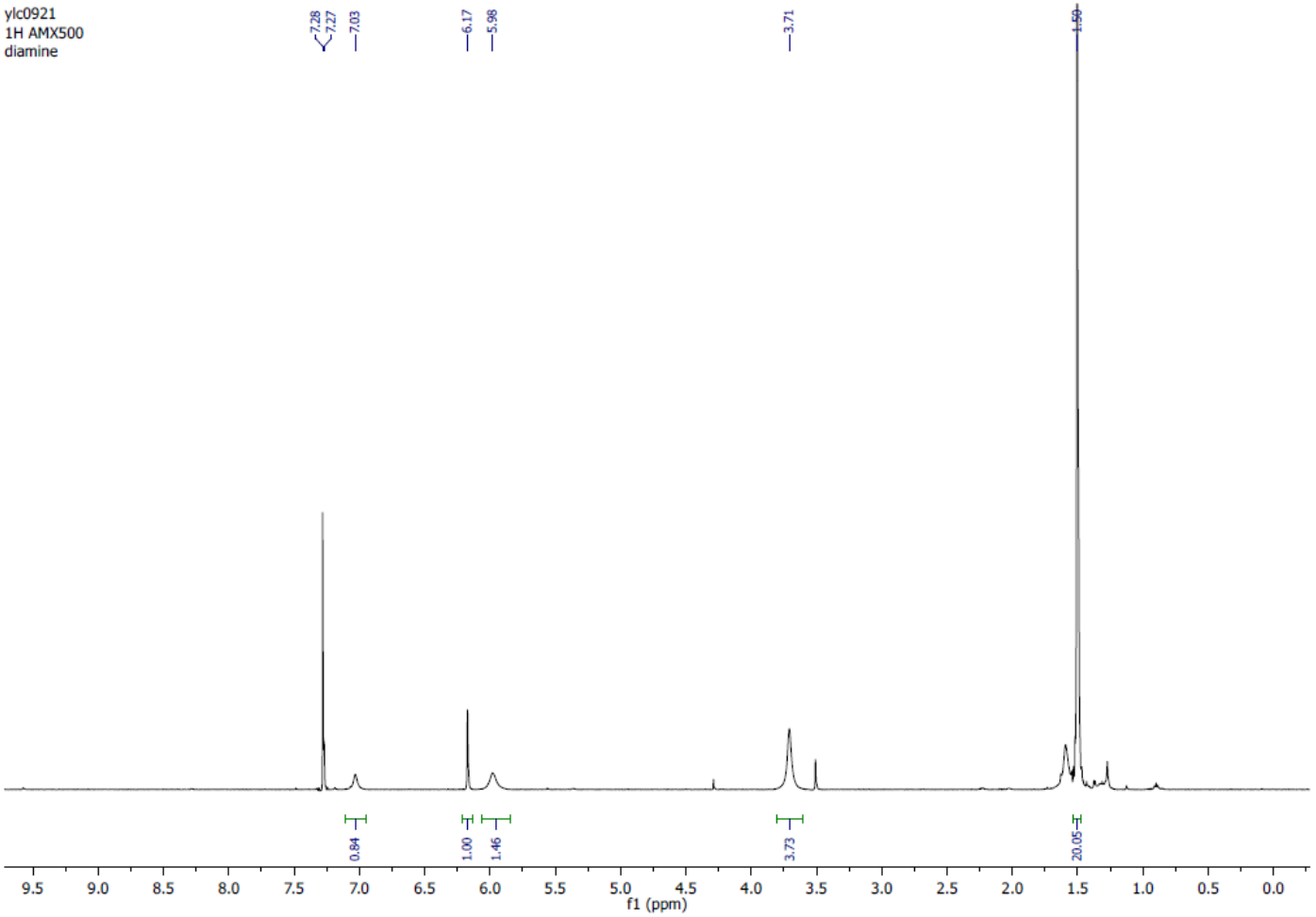
ylc0921
1H AMX500
diamine
7.28
7.27
7.03
6.17
5.98
3.71
1.59
0.84
1.00
1.46
3.73
20.05
9.5 9.0 8.5 8.0 7.5 7.0 6.5 6.0 5.5 5.0 4.5 4.0 3.5 3.0 2.5 2.0 1.5 1.0 0.5 0.0
f1 (ppm)

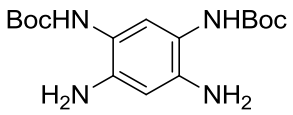
BocHN
NHBoc
H2N
NH2

4-9

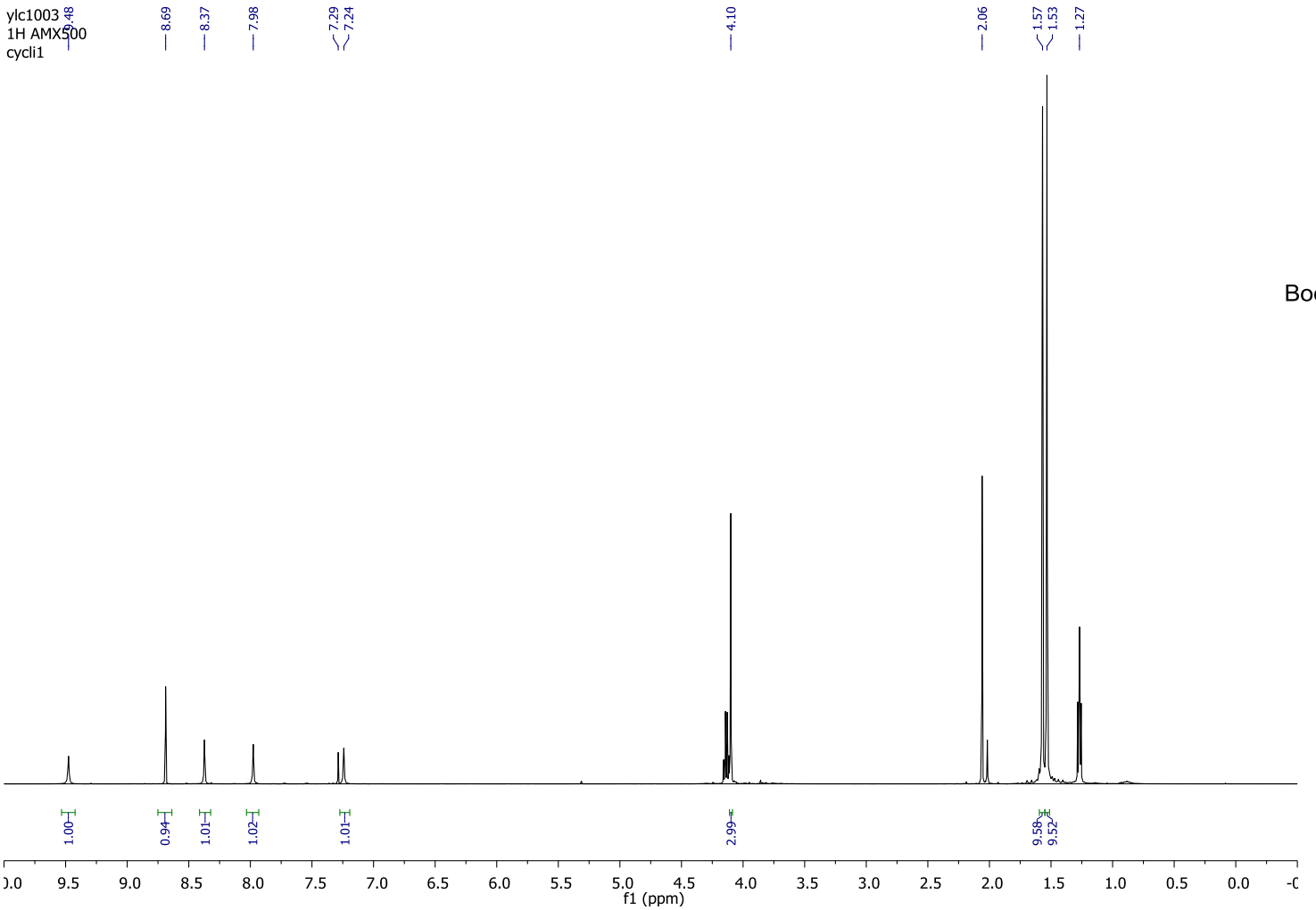
ylc1003
1H AMX500
cycli1
9.48
8.69
8.37
7.98
7.29
7.24
4.10
2.06
1.57
1.53
1.27
1.00
0.94
1.01
1.02
1.01
2.99
9.58
9.52
f1 (ppm)

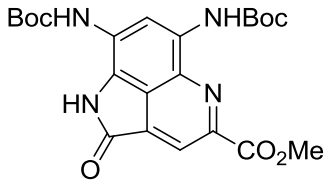
BocHN
NHBoc
HN
N
O
CO2Me

4-10

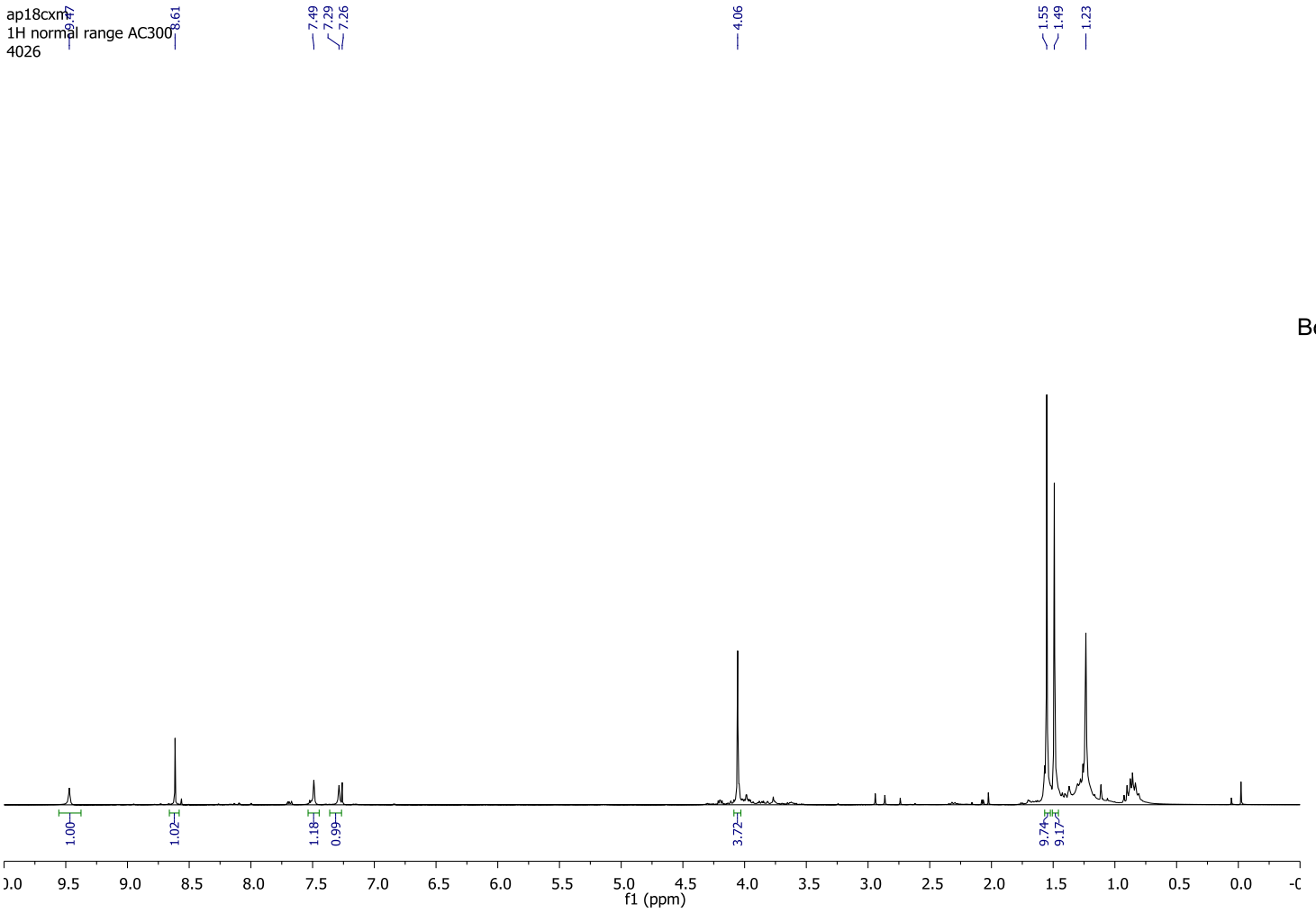
ap18cxm
1H normal range AC300
4026
9.47
8.61
7.49
7.29
7.26
4.06
1.55
1.49
1.23
1.00
1.02
1.18
0.99
3.72
9.74
9.17
f1 (ppm)

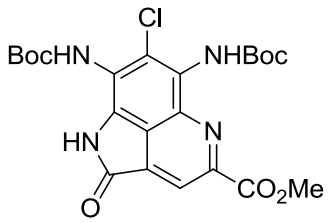
Cl
BocHN
NHBoc
HN
N
O
CO2Me

4-11

ap18cxm
13C normal range AC300
4026

165.75
164.97
152.82
152.27
149.29
138.55
135.05
129.12
127.62
122.02
121.85
119.21
117.98
83.51
81.54
77.42
77.00
76.58
53.26
28.09
28.04

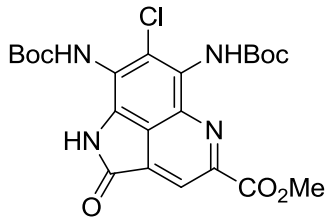

4-11

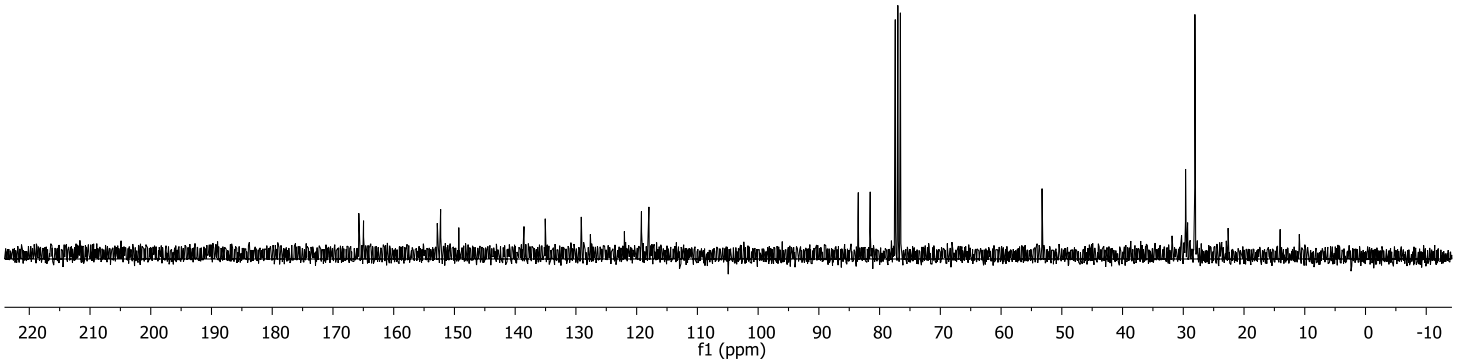

apr30cxm
1H normal range AC300
4037-2 pd pure

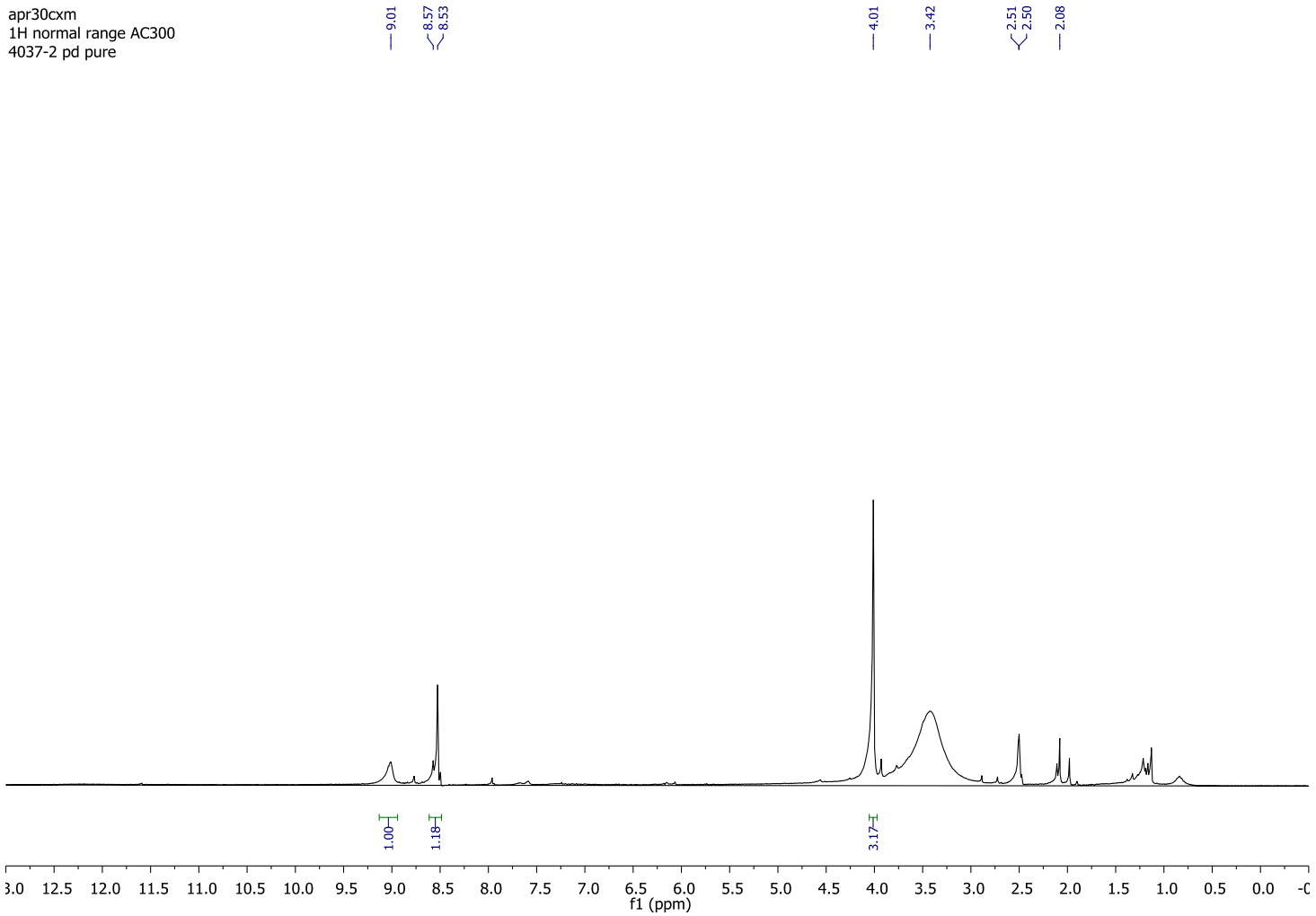

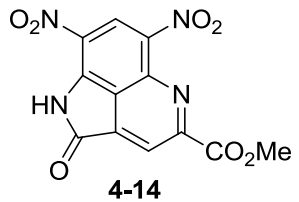

4-14

may25cxm
1H AC300
4057

9.03
8.64
8.59
8.57
4.02
4.00
3.52
3.51
3.32
2.51
2.51
2.50
2.49
2.08
1.33
1.23
1.22

4056

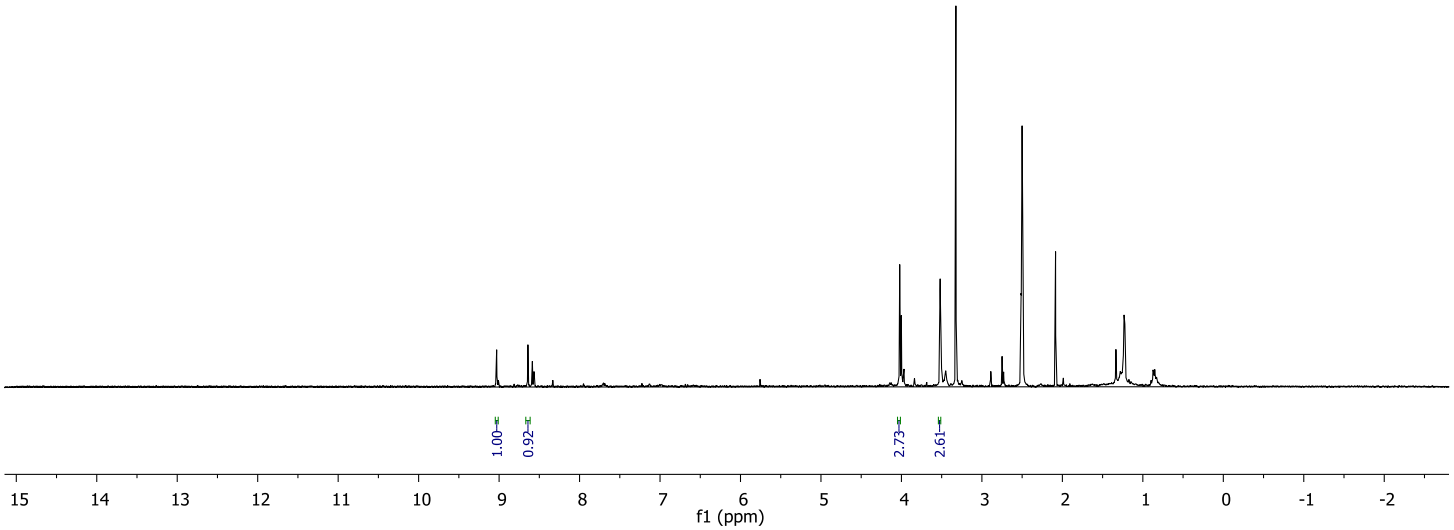

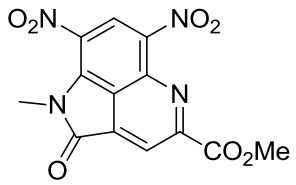

4-15

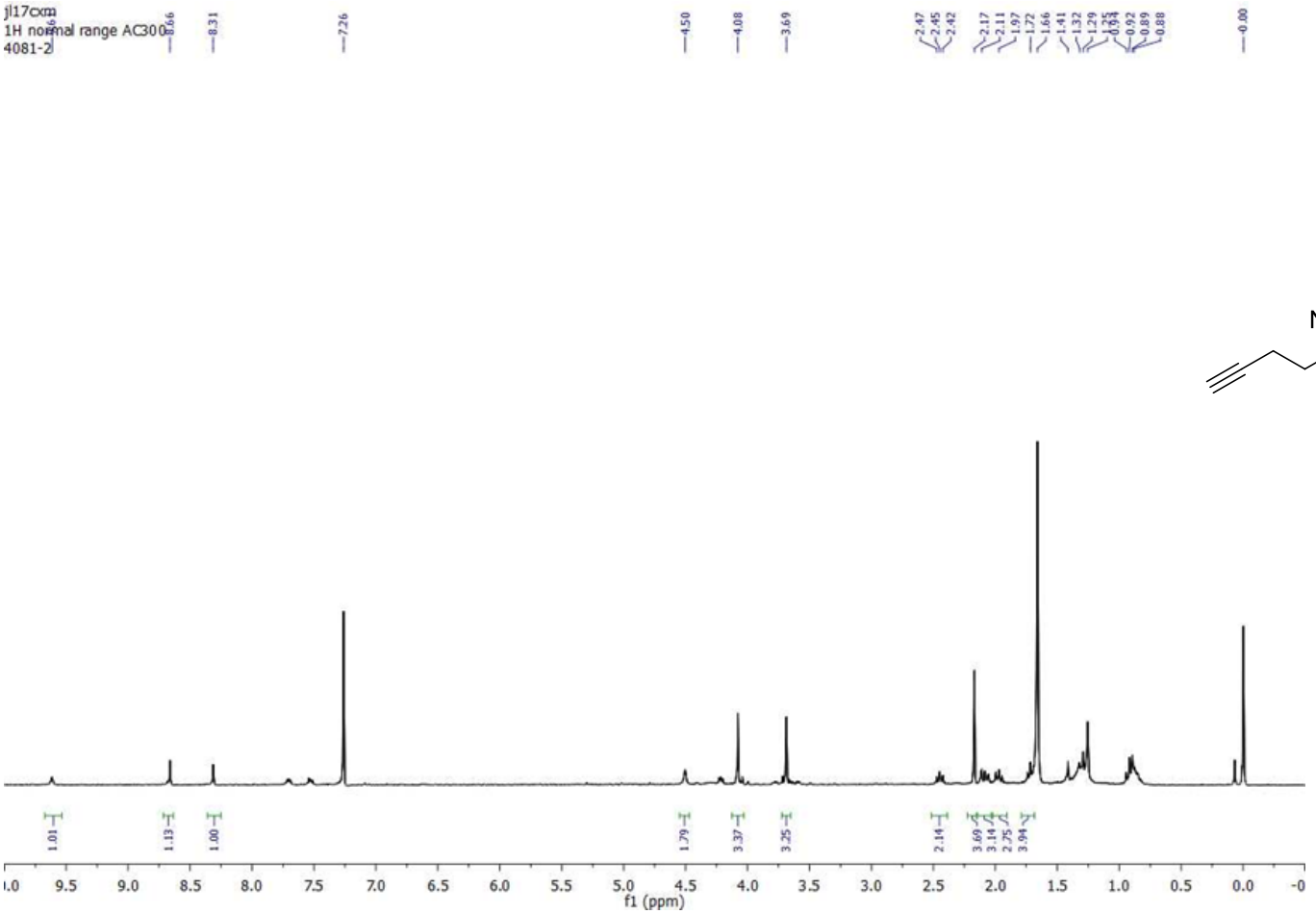
jl17cxm
1H normal range AC300
4081-2
8.66
8.31
7.26
4.50
4.08
3.69
2.47
2.45
2.42
2.17
2.11
1.97
1.72
1.66
1.41
1.32
1.29
0.92
0.89
0.88
0.00
1.01
1.13
1.00
1.79
3.37
3.25
2.14
3.69
3.14
2.75
3.94
f1 (ppm)

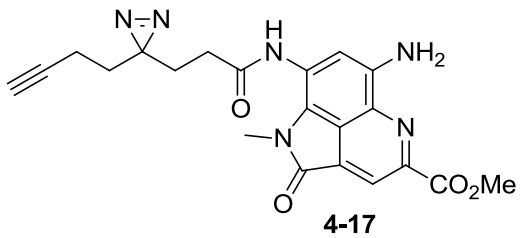
N
N
H
N
O
NH2
N
N
O
CO2Me

4-17

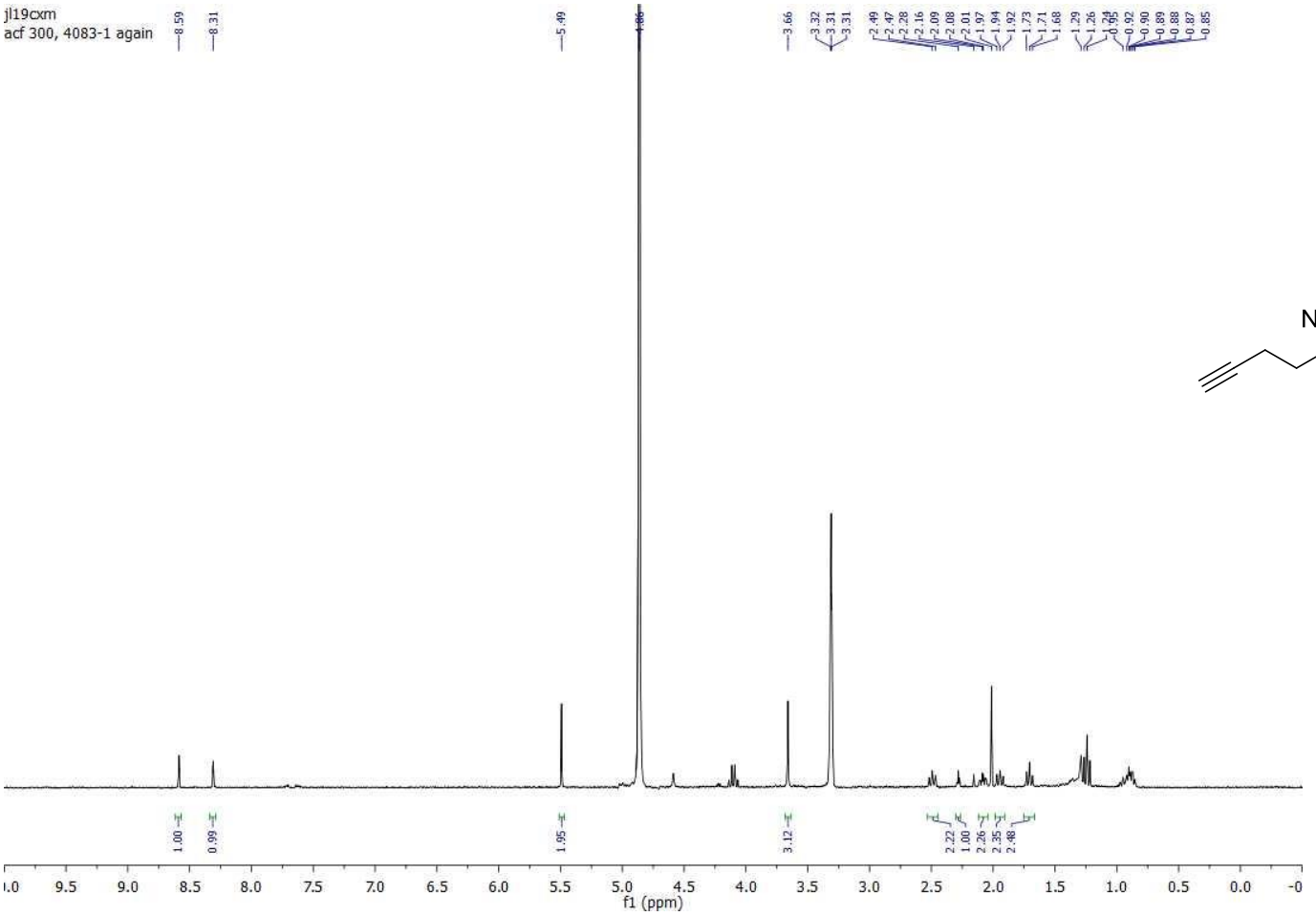
jl19cxm
acf 300, 4083-1 again
8.59
8.31
5.49
1.86
3.66
3.32
3.31
3.31
2.49
2.47
2.28
2.16
2.09
2.08
2.01
1.97
1.94
1.92
1.73
1.71
1.68
1.29
1.26
0.92
0.90
0.89
0.88
0.87
0.85
1.00
0.99
1.95
3.12
2.22
1.00
2.26
2.35
2.48
f1 (ppm)

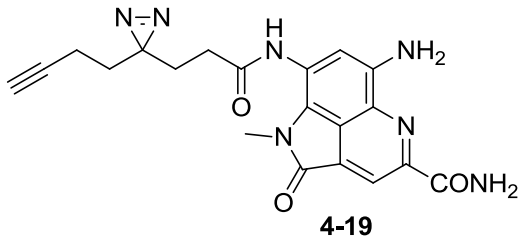
N
N
H
N
NH2
O
N
N
CONH2
O

4-19

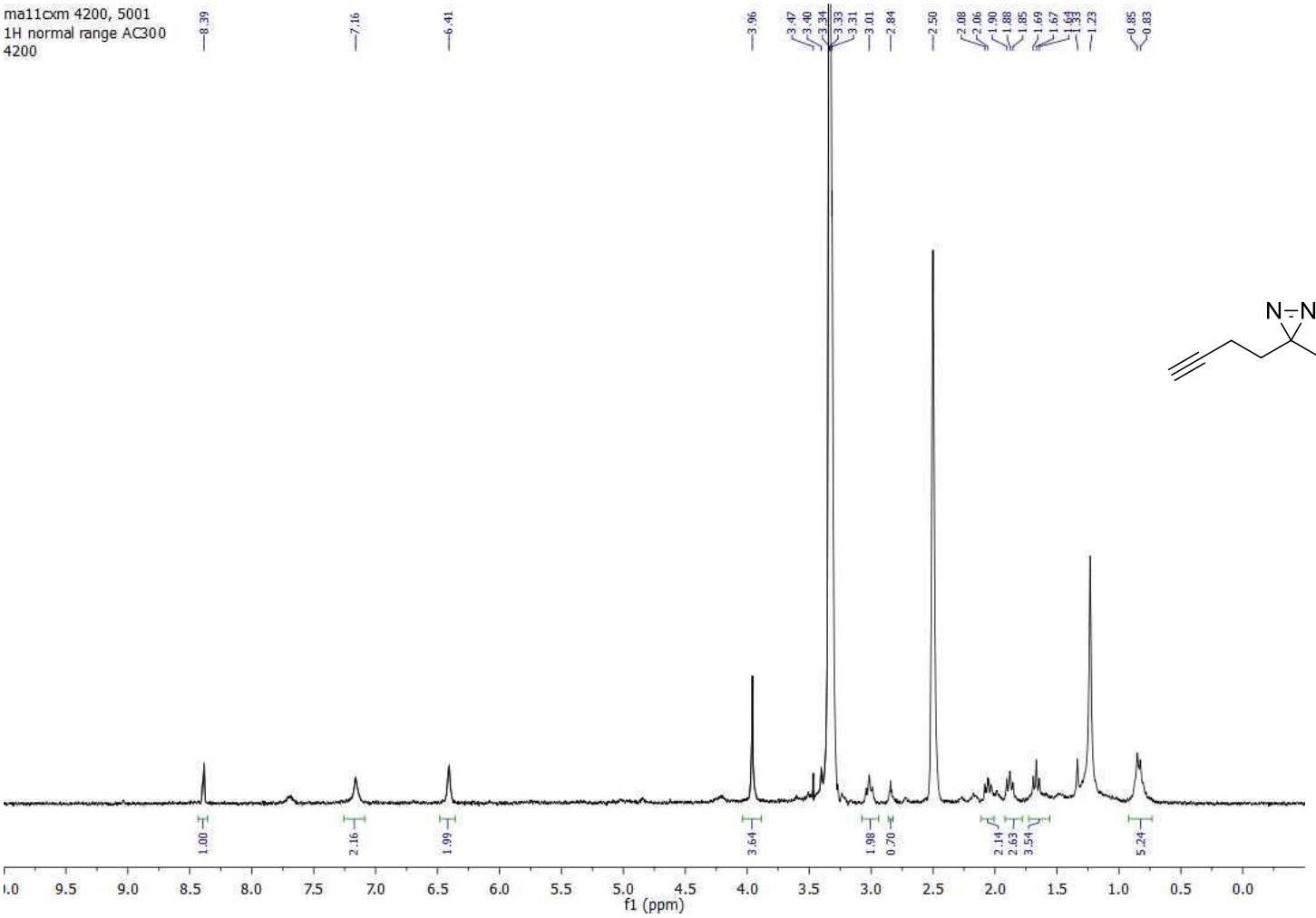
ma11cxm 4200, 5001
1H normal range AC300
4200
8.39
7.16
6.41
3.96
3.47
3.40
3.34
3.33
3.31
3.01
2.84
2.50
2.08
2.06
1.90
1.88
1.85
1.69
1.67
1.64
1.33
1.23
0.85
0.83
1.00
2.16
1.99
3.64
1.98
0.70
2.14
2.63
3.54
5.24
f1 (ppm)

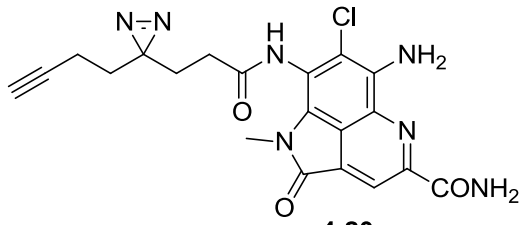
N=N
H
N
Cl
NH2
O
N
N
O
CONH2

4-20

Chapter 5

nv28cxm
1H normal range AC300
C3

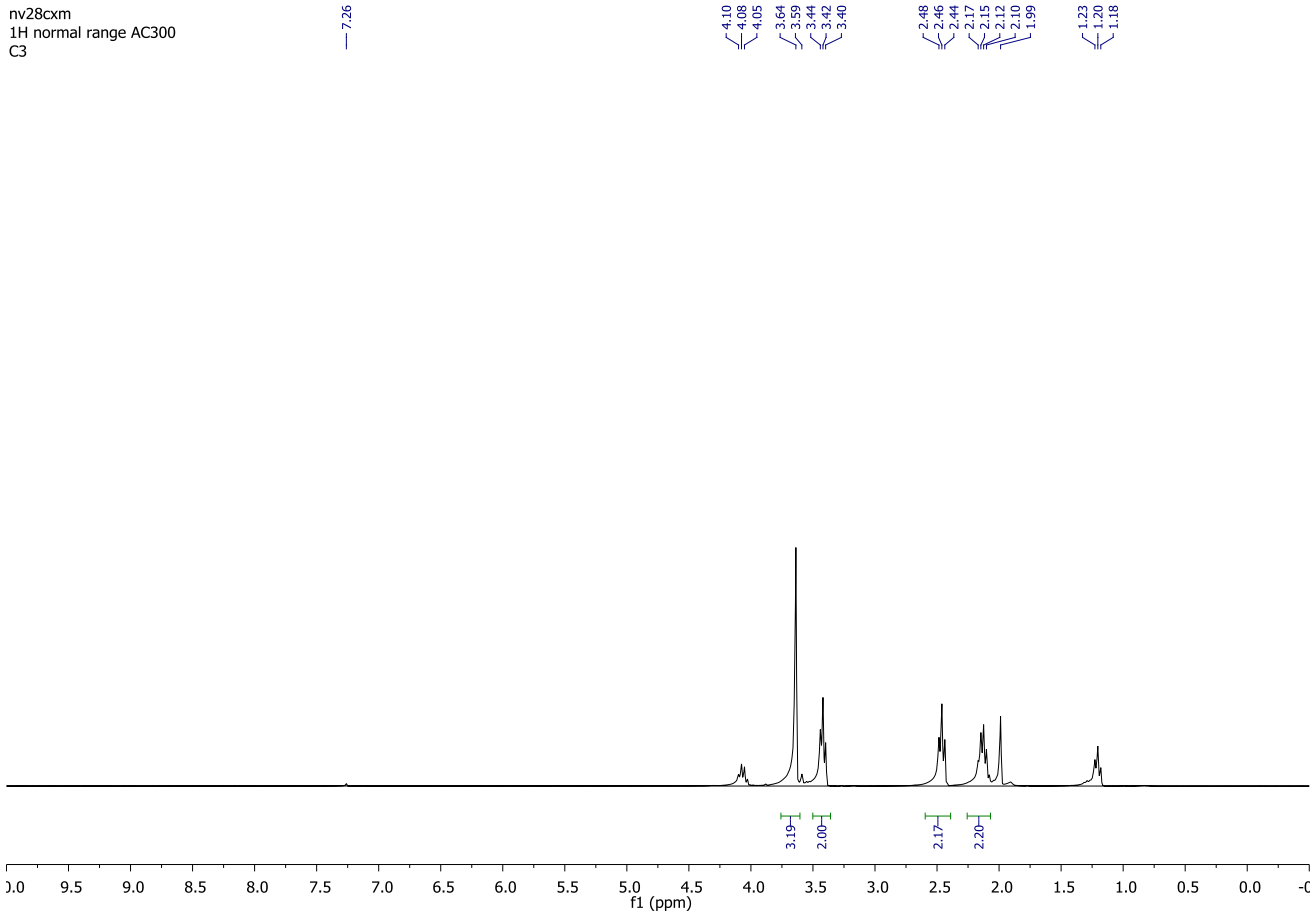

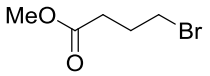

nv28cxm
1H normal range AC300
C3

172.82
77.43
77.00
76.58
51.56
32.56
32.05
27.60

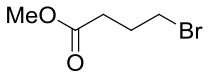

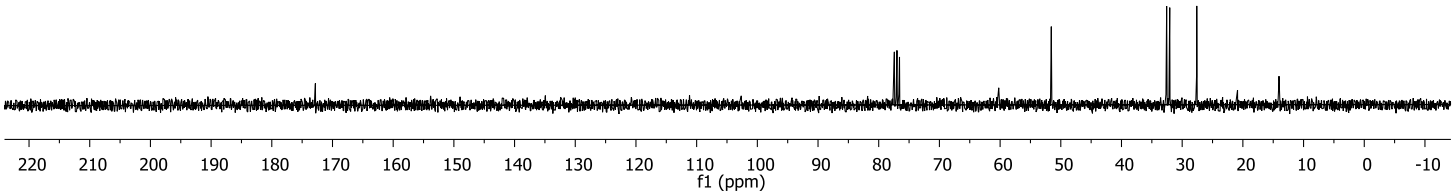

nv28cxm
1H normal range AC300
C3 N3

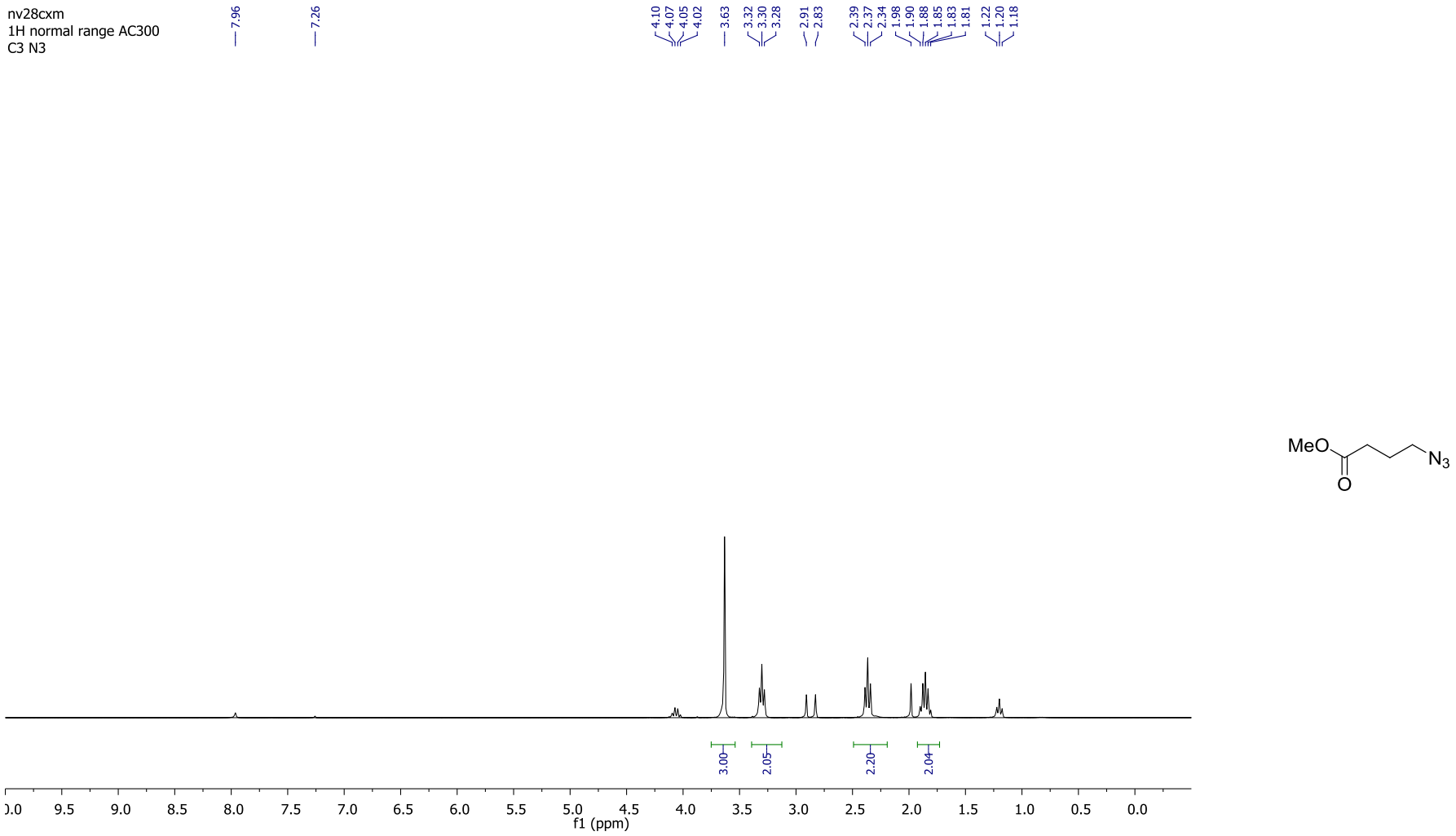

nv28cxm
1H normal range AC300
C3 N3

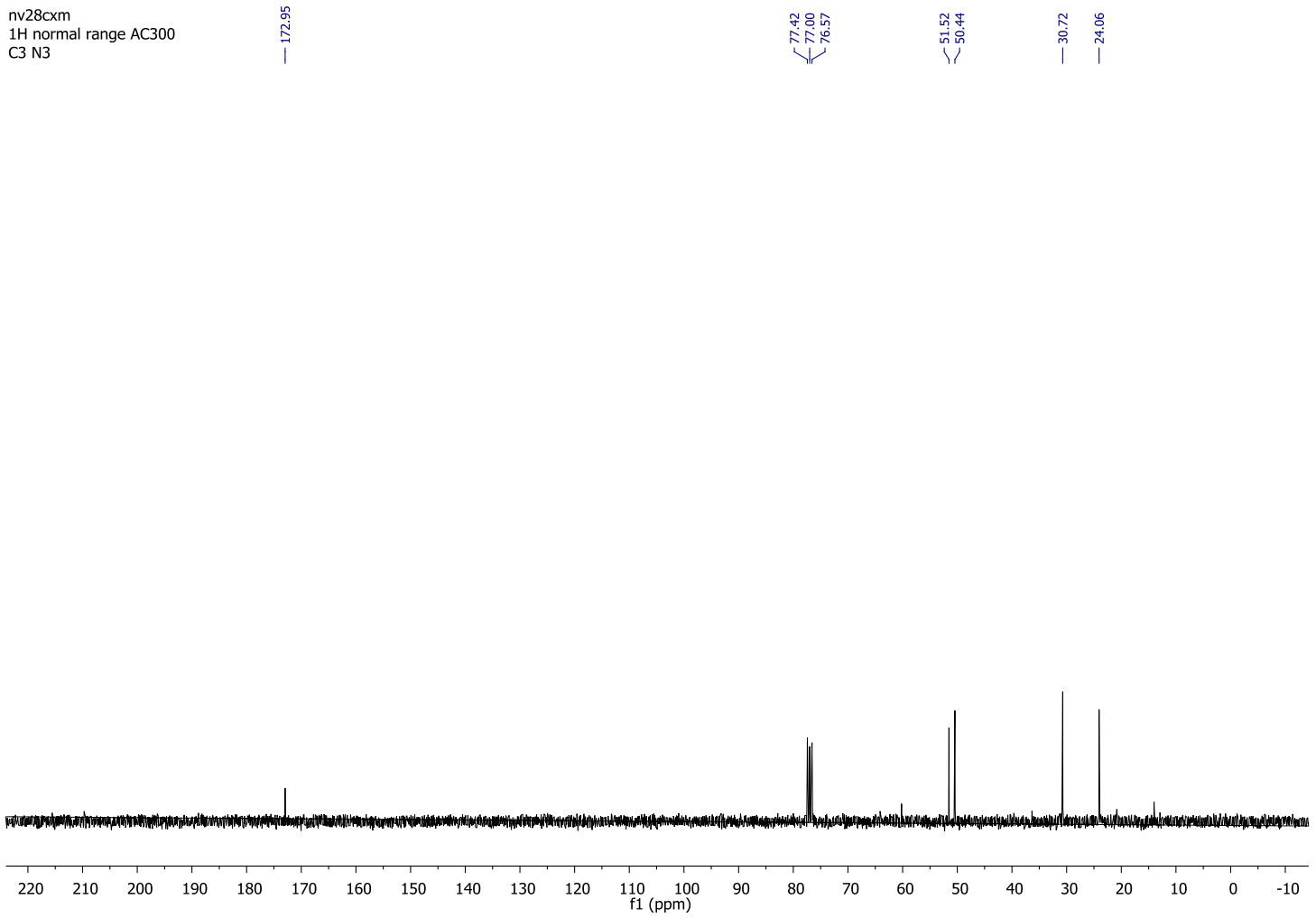

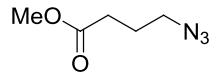

cxm1124
DRX 500M, CO2HCH2CH2CH2N3

7.97
7.26
5.46
4.74
4.33
4.31
4.30
3.33
2.93
2.91
2.90
2.84
2.47
2.46
2.44
2.25
2.23
1.88
1.87

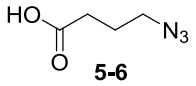

5-6

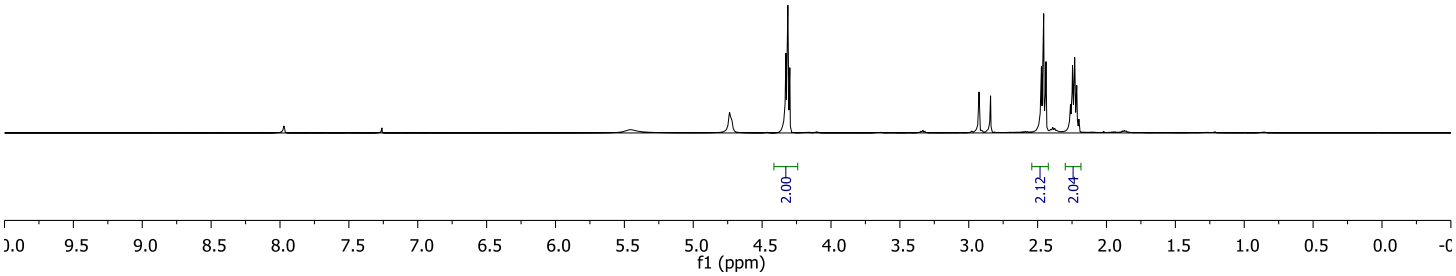

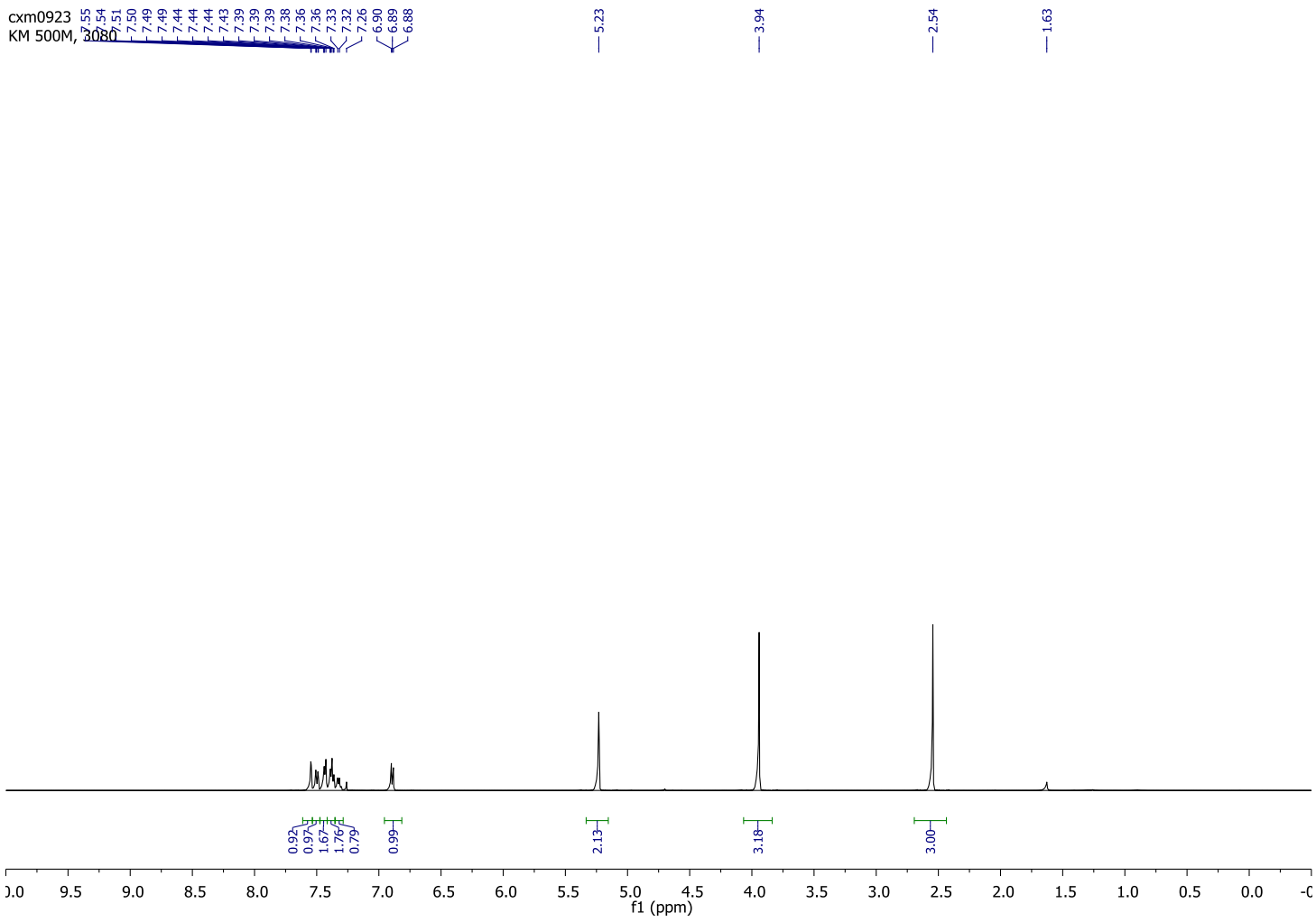
cxm0923
KM 500M, 3080
7.55
7.54
7.51
7.50
7.49
7.49
7.44
7.44
7.44
7.43
7.39
7.39
7.39
7.38
7.36
7.36
7.33
7.32
7.26
6.90
6.89
6.88
5.23
3.94
2.54
1.63
0.92
0.97
1.67
1.76
0.79
0.99
2.13
3.18
3.00
f1 (ppm)

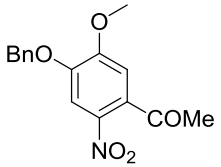
O
BnO
COMe
NO2

5-9

se03cxm 4117
1H normal range AC300
4117 nitrophenol

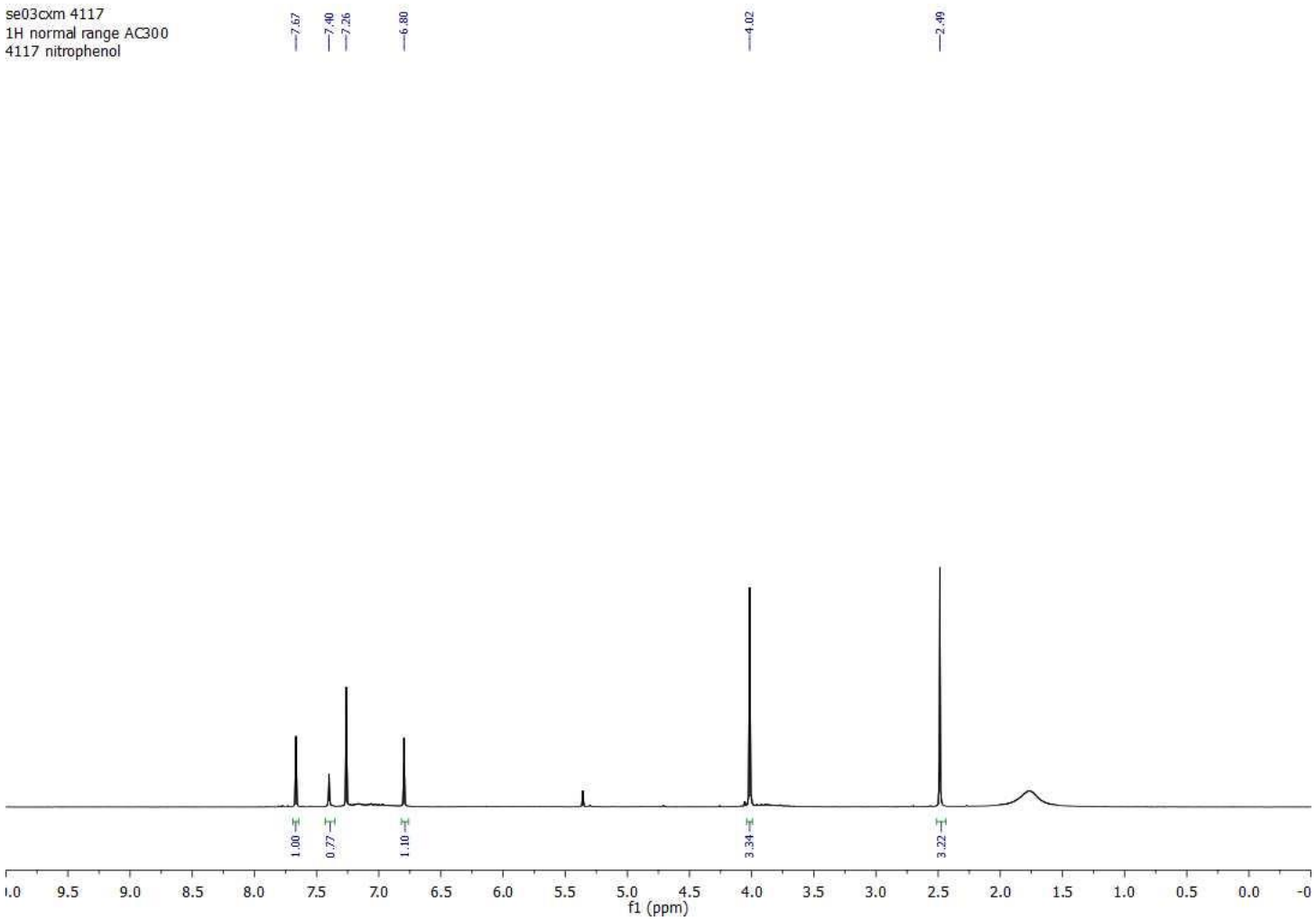

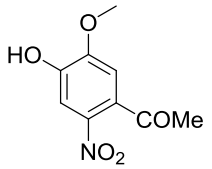

5-10

sep17cxm
ACF 300M, HNMR
4127 nitrobenzene methyl ester ketone

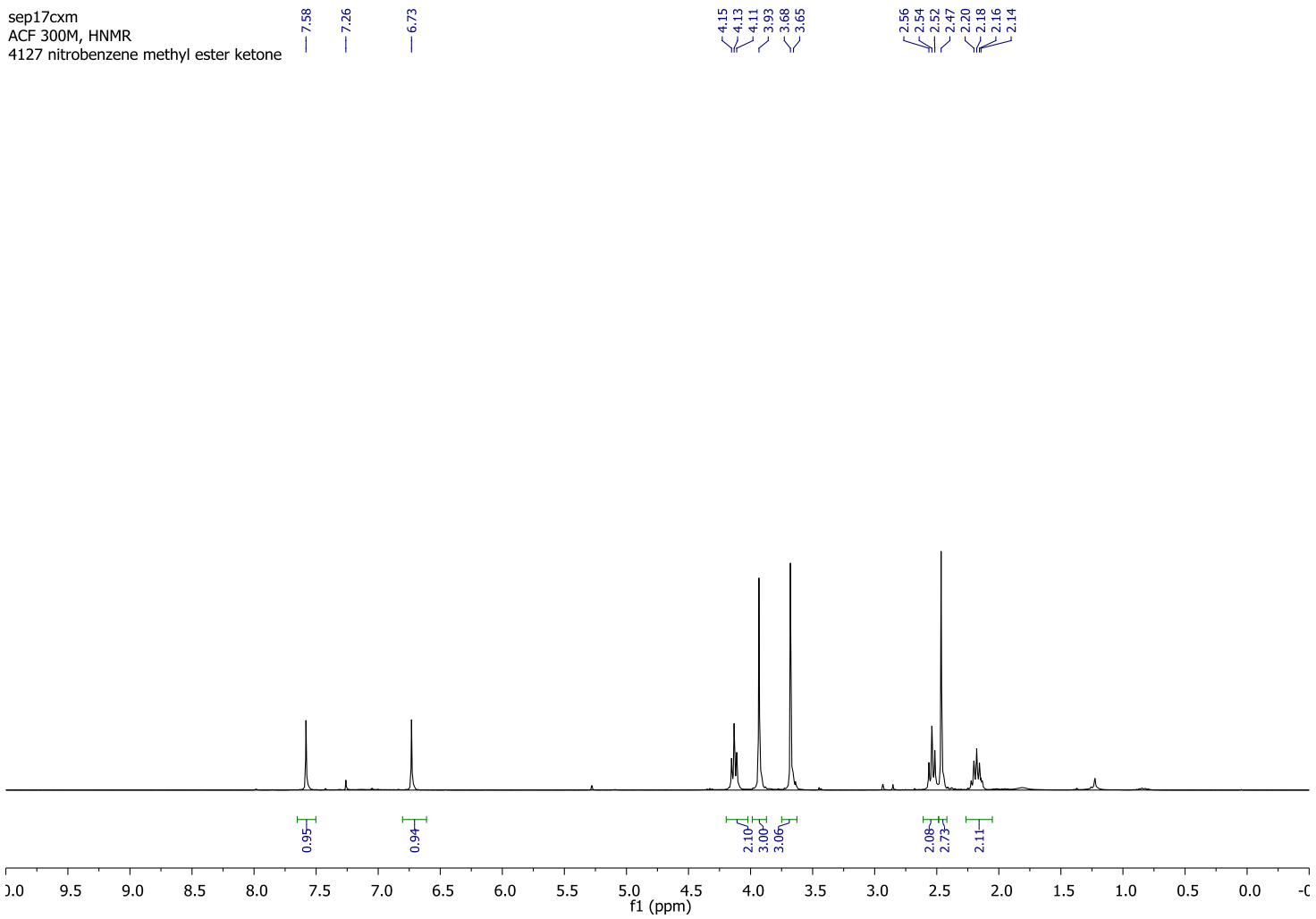

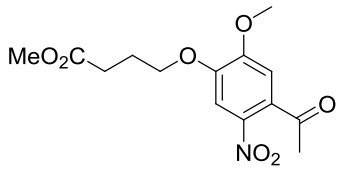

5-11

ag22cxm 4102, 4104
1H normal range AC300
4104 nitrobenzen methyl ester alcohol

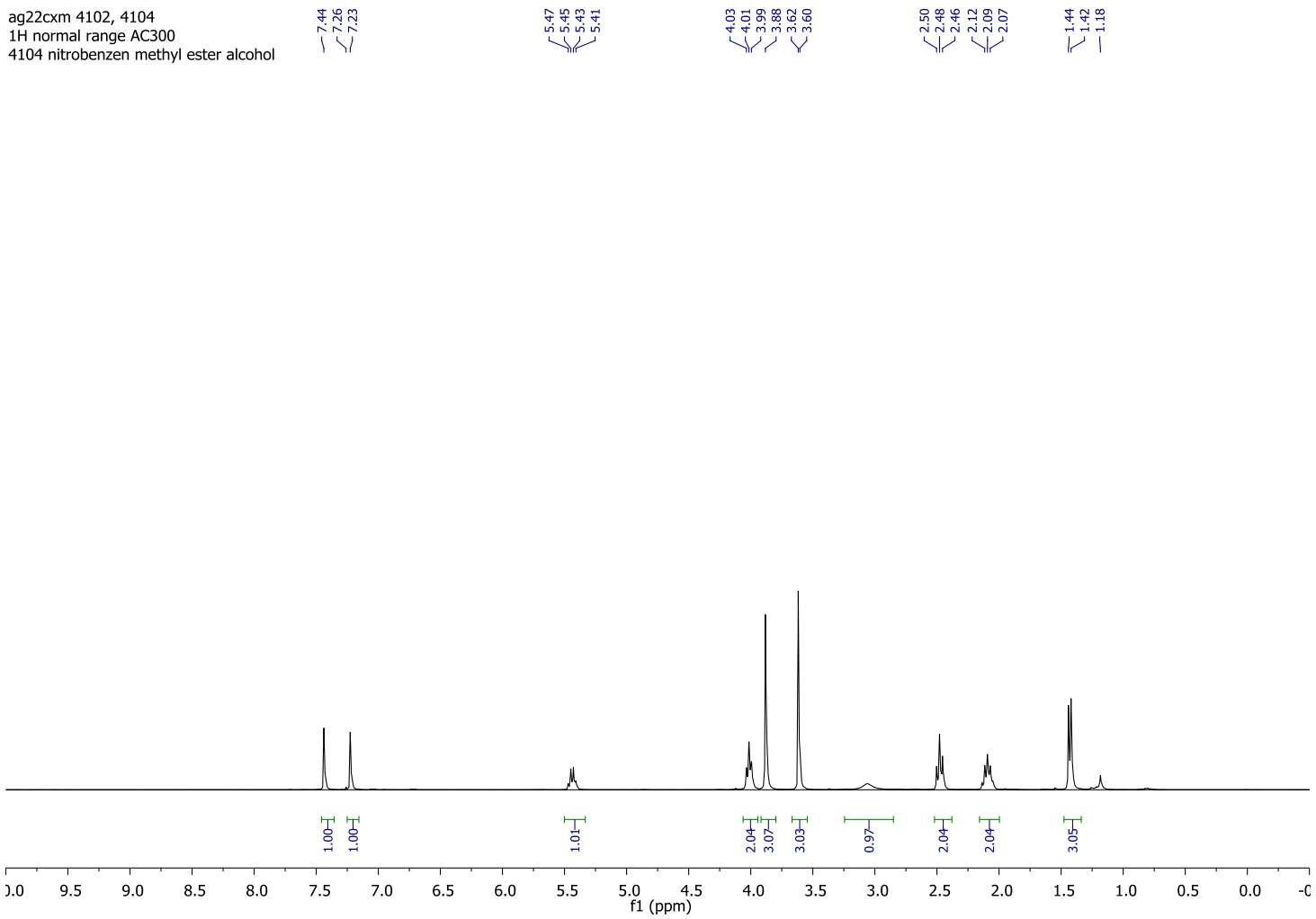

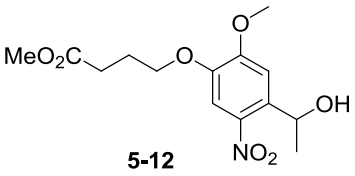

5-12

ag22cxm 4102, 4104
13C normal range AC300
4104 nitrobenzen methyl ester alcohol

173.32
153.87
146.53
139.06
137.23
108.75
108.51
77.43
77.00
76.58
68.00
65.35
56.08
51.52
30.18
24.22
24.05

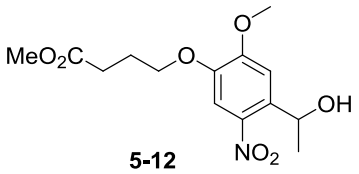

5-12

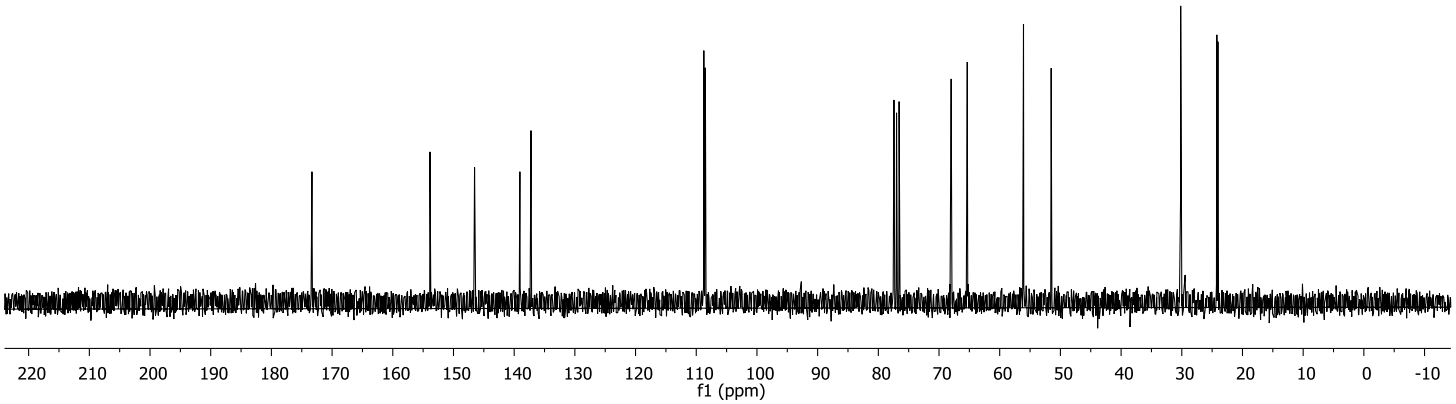

cxm0910
1H AMX500
4121-3

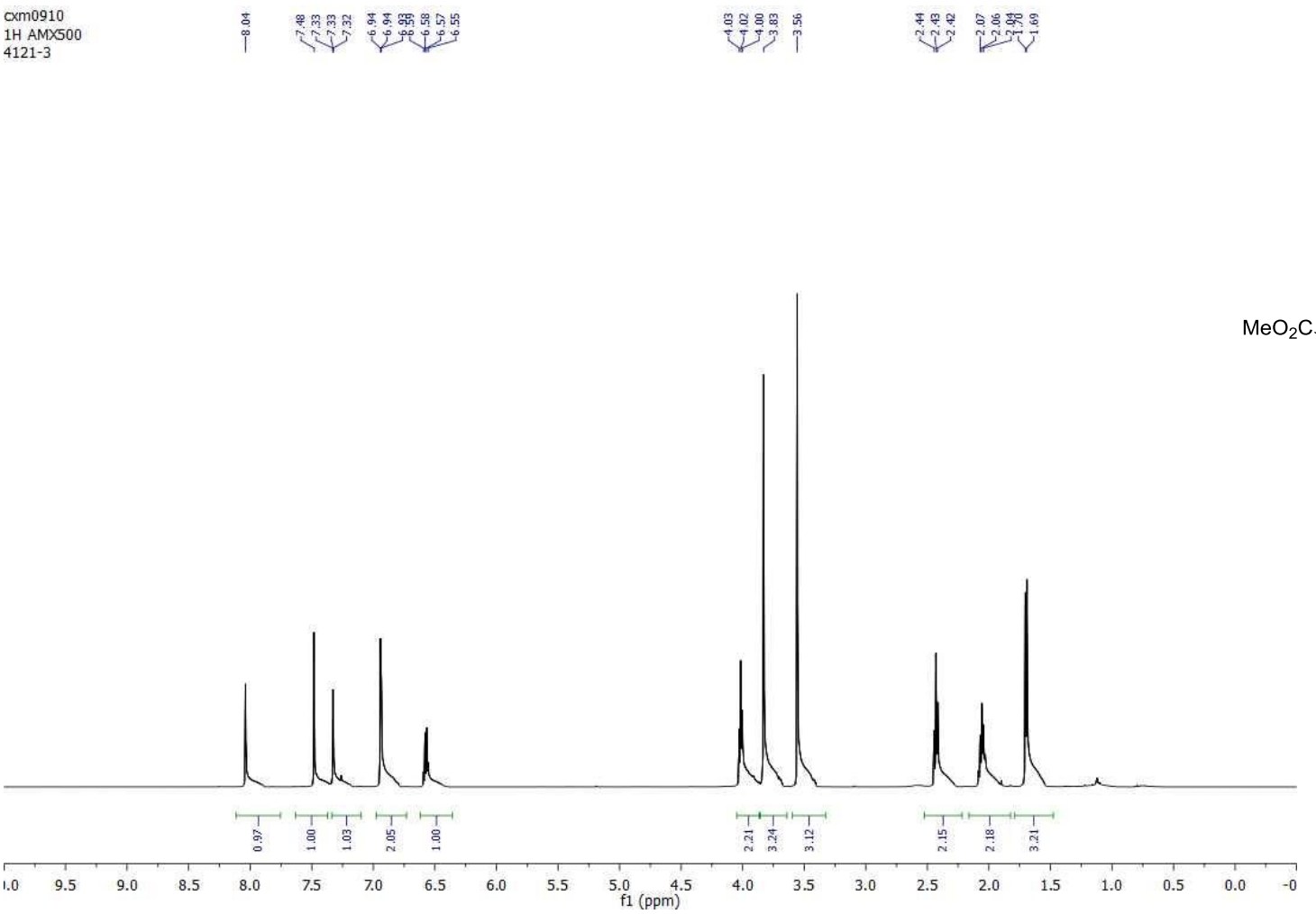

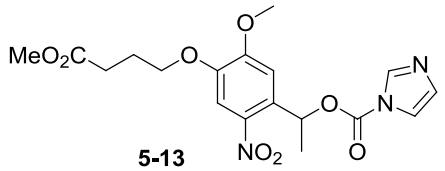

5-13

cxm0910
13C AMX500
4121-3

172.85
153.79
147.47
147.21
139.59
136.56
130.42
130.41
116.69
108.61
107.63
77.26
77.00
76.74
72.48
67.89
56.01
51.26
29.88
23.81
21.38

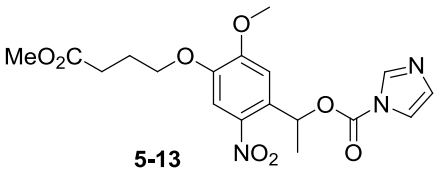

5-13

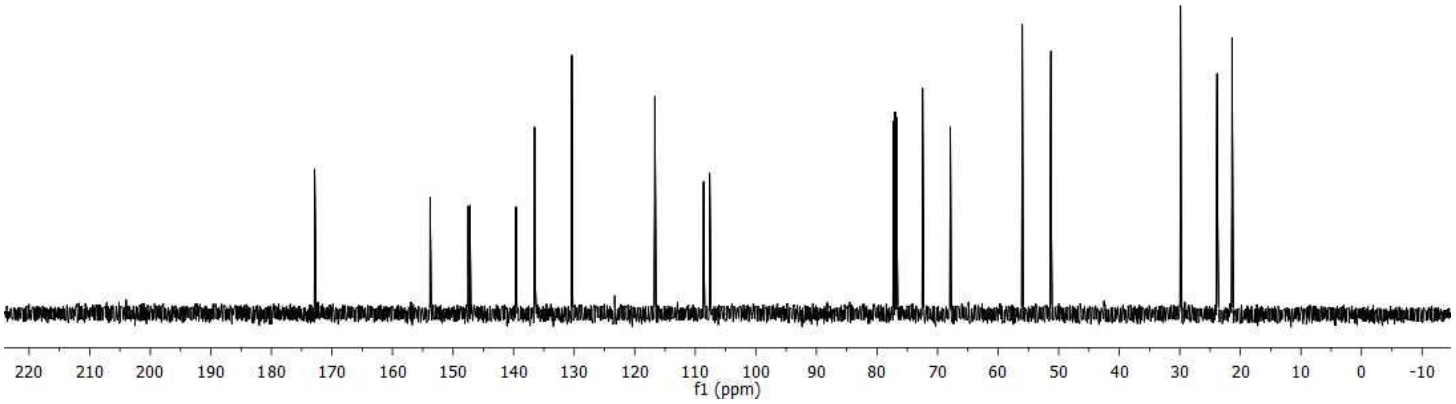

cxm1030
4135 nitro bezene methyl ester

7.55 7.04 6.32 6.31 5.51 4.08 4.08 3.92 3.67 3.65 3.25 3.24 3.22 3.10 3.09 2.53 2.52 2.41 2.15 2.13 2.01 2.00 1.55 1.47 1.39 1.38 1.34 1.24 1.23 1.21

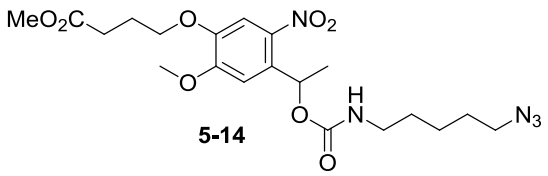

5-14

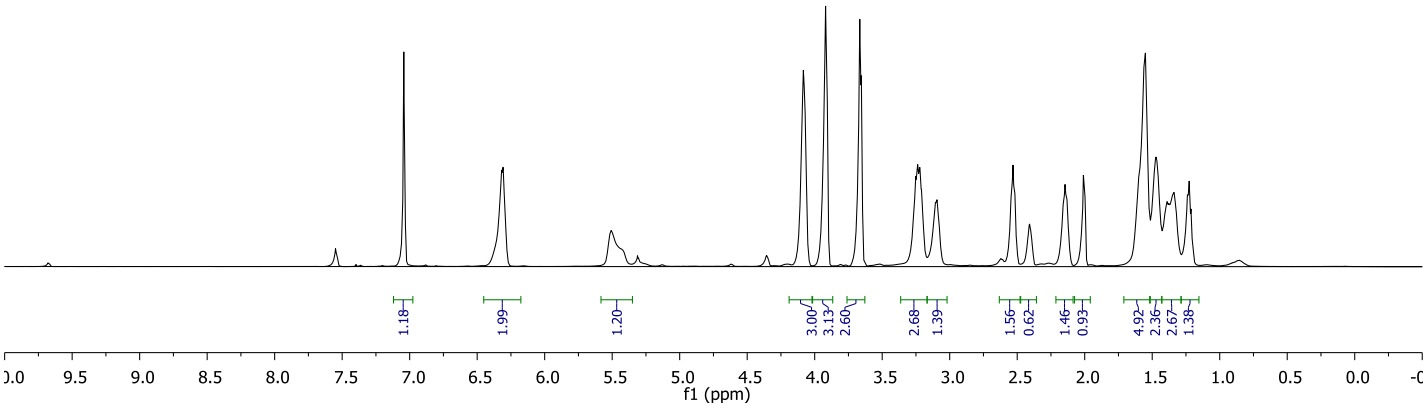

cxm1030

172.79
170.48
154.97
153.63
146.55
139.00
133.89
108.54
107.73
77.26
77.00
76.74
74.03
67.99
67.70
59.76
55.70
51.89
51.03
50.81
50.69
40.13
29.77
28.92
28.15
27.90
24.05
23.78
23.29
21.56
13.60

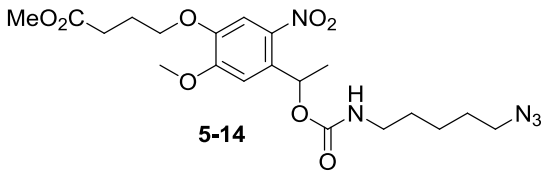

5-14

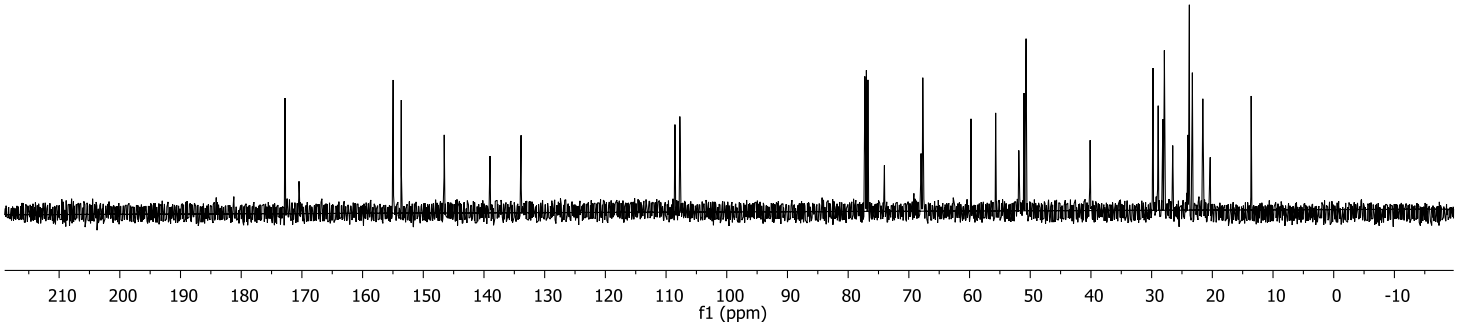

se07cxm
1H normal range AC300
4118 nitrobenzene acid

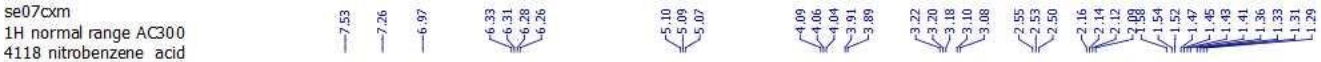

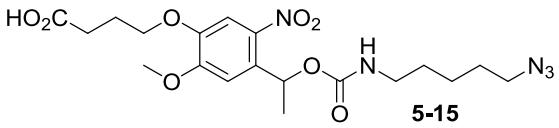

5-15

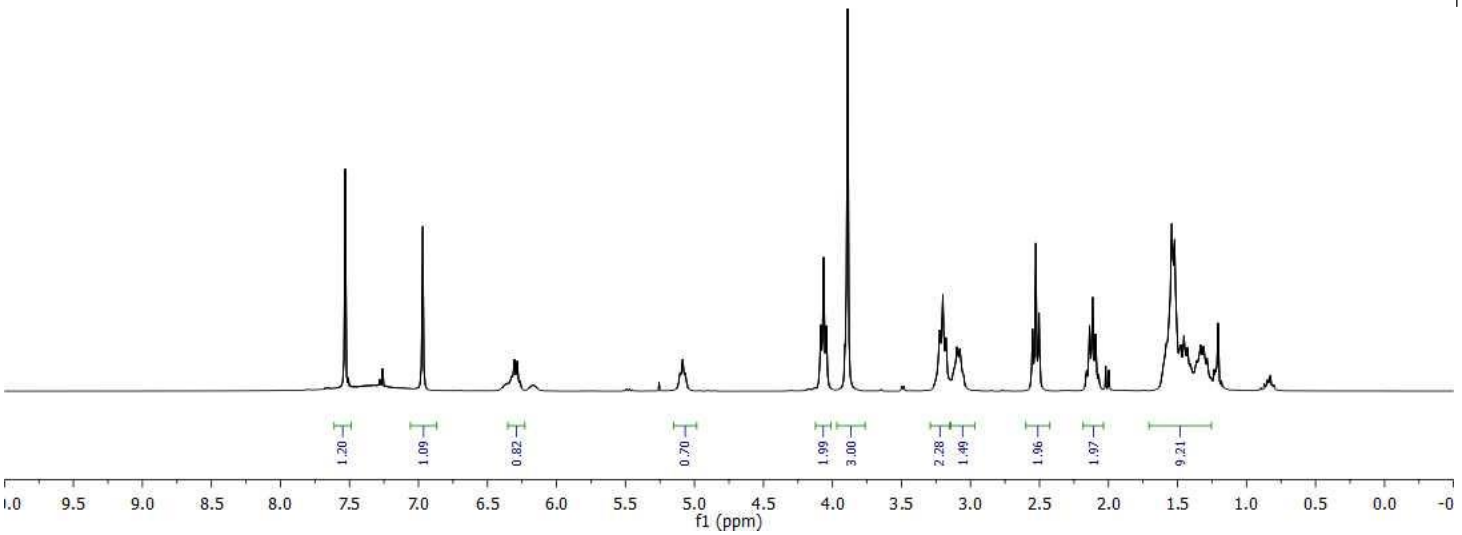

se07cxm
13C normal range AC300
4118 nitrobenzene acid

177.64
155.35
153.83
146.82
139.33
134.00
108.82
107.94
77.42
77.00
76.58
68.63
67.88
56.07
51.01
40.51
30.04
29.22
28.21
23.80
23.60
21.95

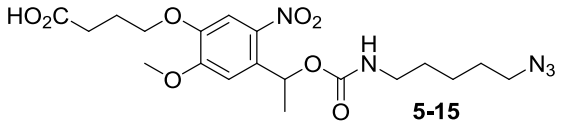

5-15